A MODERN GEODETIC REFERENCE SYSTEM FOR NEW ZEALAND
Options and implications of changing from NZGD49

MERRIN B. PEARSE

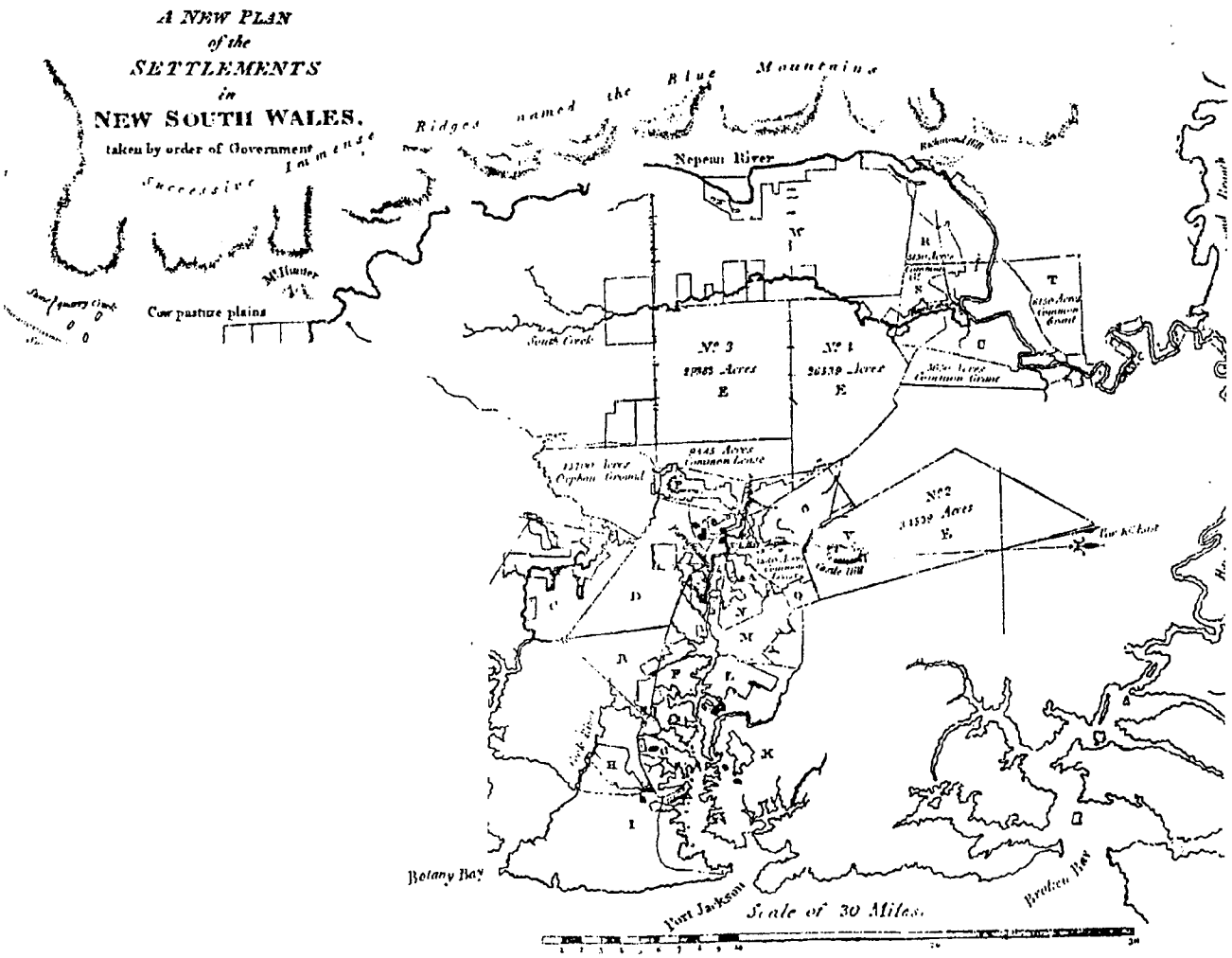

UNISURV S-52, 1998

Reports from

SCHOOL OF GEOMATIC ENGINEERING

THE UNIVERSITY OF NEW SOUTH WALES SYDNEY NSW 2052 AUSTRALIA

UNISURV REPORT S-52, 1998

A MODERN GEODETIC REFERENCE SYSTEM FOR NEW ZEALAND
Options and implications of changing from NZGD49

MERRIN B. PEARSE

Received: December, 1996
Accepted: December, 1997

SCHOOL OF GEOMATIC ENGINEERING
UNIVERSITY OF NEW SOUTH WALES
SYDNEY NSW 2052
AUSTRALIA

National Library of Australia

Card No. and ISBN 0 7334 1641 1

Abstract

New Zealand possesses a horizontal geodetic datum, established in 1949 (NZGD49), and a number of distinct vertical datums. NZGD49 coordinates remain fixed at their originally defined values despite the fact that New Zealand is subjected to crustal deformation. This deformation is due to the collision of the Australian and Pacific tectonic plates at a rate of approximately 50 mm/yr.

It is proposed that New Zealand requires a new consistent three dimensional geocentric reference system which possess the following features:

i) a dynamic reference system, to account for deformation, having a defined relationship to an ITRF.
ii) a nationwide velocity model to allow combining of different epoch data.
iii) a gravimetric geoid to convert between ellipsoidal heights and orthometric heights.
iv) coordinate transformation parameters between NZGD49 and the new system.

To address the geodetic options and implications related to the establishment of such a reference system the following research was undertaken.

GPS can be used to monitor crustal deformation and also provide three dimensional geocentric coordinates in terms of a global reference system. A new three dimensional geocentric reference system for New Zealand was realised through a set of station coordinates for the 1993 New Zealand wide GPS network. This thesis used the GAMIT/GLOBK software suite to produce coordinates in terms of the dynamic ITRF93 at the mean observation epoch of 1993.200, with formal uncertainties of 2cm (1σ).

GPS-derived ellipsoidal heights need converting to orthometric heights to be of practical use. This conversion theoretically requires geoid heights. The capabilities and efficiency of the UNSW RINT software was significantly enhanced as part of this thesis. A gravimetric geoid (0.05° resolution) was computed using RINT for a test region of New Zealand. These gravimetric geoid heights were shown to be superior to those

derived from the evaluated global geopotential models and met New Zealand's third order levelling specifications.

Transformation parameters are required to allow the conversion between NZGD49 and any new reference system. This thesis analysed existing transformation parameters between NZGD49 and global reference systems and developed new transformation parameters which incorporated a velocity model to account for the deformation. The new transformation parameters produced smaller coordinate residuals than the existing parameters but the maximum residuals were still approximately 2.0 m.

Acknowledgments

This study has involved both the active and passive participation by a number of people who together have helped bring this thesis to fruition. I am not only indebted to those people and organisations who have directly contributed their resources but also to those people who offered their time and wisdom to my often persistent discussions and inquiries.

I would like to thank my two supervisors, Bill Kearsley and Peter Morgan, who both operated an open door policy, with almost 24 hour access to their precious time. This provided me with the luxury of being able report exciting results as they occurred or obtain valuable assistance and alternative options during times of subdued progress. My visit's to the University of Canberra were both successful and enjoyable due to the support from Peter and his staff (particularly Russell Tiesler, Barry McDowall, Gail Ransom and Daniel Garrard).

I am indebted to the New Zealand Department of Survey and Land Information (DOSLI) and since July 1996, Land Information New Zealand (LINZ), for providing the study scholarship which made this research possible. I hope that the skills I have obtained during my research, along with this thesis, are justification for the confidence they have in me and look forward to applying these skills on my return to Wellington. There are a few of my fellow colleagues of the former DOSLI (now split into Terralink and LINZ) that deserve special mention for their assistance during my research. They are George Williamson, Graeme Blick, Chris Crook, Brent George, Jim Hall, Geoff Linnell, Glen Rowe and Kelvin Tait. I am particularly indebted to Don Grant for his assistance in my application for the original Masters based scholarship, support in my application to have the scholarship upgraded to a PhD and for his valuable comments on my research and final thesis.

Chris Rizos and the Satellite Navigation and Positioning Group (SNAPpers) for their hospitality, especially during the initial months of settling into a new city. Bernie

Hirsch and Brian Donnelly for their computer support, which shed light on how a computer worked and why I was trying to make it perform the near impossible.

David Lemon for insuring that I try to justify the relevance of my research from the GIS perspective, and who along with Catherine Ticehurst and Jeffrey Forrest guided, both myself and my partner Louise Taylor into the Australian bush to enjoy the flora and fauna. This often involved searching for snakes and orchids during the day, then wombats and flying foxes at night (one day we all will see a Koala in the wild!). Paul Tregoning for encouraging me into rock-climbing (as a means to relieve the stress of GPS processing), one highlight of which was standing on top of the Three Sisters in the Blue Mountains.

Matthew Higgins and Niraj Manandhar who between them introduced me to extreme gravity fields. The complexity of the Australian geoid investigated by Matt was often unexpected considering the surrounding terrain, however there was no doubts in what a terrain correction was when investigating the Nepalese geoid with Niraj. While trying to develop a better understanding of the GAMIT/GLOBK software suite and the theories of plate tectonics, Kim Mobbs was always available to discuss my queries.

Finally and in no way the least important is Louise, who has been a great source of support and friendship, through out my research, especially during the final stages. She was always keen to discuss my daily progress (over a glass of wine) and convince me that my day had been successful. Louise possess the great skill, when you are trying to generate diagrams for a thesis, of being a Cartographer and to her the credit for the more complicated diagrams must go. Also, Louise's faith in me completing my research was a tremendous source of strength and I thank her dearly.

Contents

List of Tables

List of Figures

List of Acronyms

AHD	Australian Height Datum of 1971
BIH	Bureau International de l'Heure
BMs	Levelling Benchmarks
CIO	Conventional International Origin
CIGNET	Cooperative International GPS Network
CIRS	Conventional Inertial Reference System
CTP	Conventional Terrestrial Pole
CTRS	Conventional Terrestrial Reference System
DEM	Digital Elevation Model
DMA	Defense Mapping Agency
DoD	Department of Defense
DORIS	Doppler Orbit determination and Radio-positioning Integrated on Satellite
DOSLI	Department of Survey and Land Information, New Zealand
DOY	Day of year
EGM96	NASA GSFC and DMA joint Earth Geopotential Model of 1996
FAGS	Federation of Astronomical and Geophysical Data Analysis Services
FFT	Fast Fourier Transform
FHT	Fast Hartley Transform
GGM	Global Geopotential Model
GIS/LIS	Geographic Information System / Land Information System
GPS	NAVSTAR Global Positioning System
GRS 80	Geodetic Reference System 1980
IAU	International Astronomical Union
ICSM	Inter-governmental Committee on Surveying and Mapping
IERS	International Earth Rotation Service
IGS	International GPS Service for Geodynamics
IGSN71	International Gravity Standardisation Network 1971
IPMS	International Polar Motion Service
ITRF92 / 93	IERS International Terrestrial Reference Frame 1992 / 1993

ITRS	IERS International Terrestrial Reference System
IUGG	International Union of Geodesy and Geophysics
LINZ	Land Information New Zealand (formerly part of DOSLI)
LLR	Lunar Laser Ranging
LSC	Least Squares Collocation
MIT	Massachusetts Institute of Technology
MRE	Multiple Regression Equations
MSL	Mean Sea Level
NAD27 / 83	North American horizontal Datum of 1927 / 1983
NAVD88	North American Vertical Datum of 1988
NGVD29	USA National Geodetic Vertical Datum of 1929
NZGD49	New Zealand Geodetic Datum 1949
NZMG	New Zealand Map Grid
OSU91A	Ohio State 1991 geopotential and SST harmonic coefficient model
RINEX	Receiver Independent Exchange Format
RINT	Ring Integration
SIO	Scripps Institution of Oceanography
SLR	Satellite Laser Ranging
SST	Sea Surface Topography
UNSW	The University of New South Wales
UTC	Coordinated Universal Time
VLBI	Very Long Baseline Interferometry
WGS72	World Geodetic System 1972
WGS84	World Geodetic System 1984, Doppler derived
WGS84(G730)	World Geodetic System 1984, GPS derived
gpu	geopotential units, 1 gpu = 1 kGal m
mGal	milliGal, a unit of acceleration, 1 mGal = 10^{-3} Gal = 10^{-5} ms^{-2} $\cong$ 3m in N
ppm	parts per million ($x10^{-6}$)
rms	Root Mean Square = $\sqrt{\sum x^2/n}$
sd	standard deviation = $\sqrt{\sum (x-\bar{x})^2/n}$

Chapter 1

Introduction

1.1 Background

New Zealand, like many countries, possesses a post 1940 geodetic datum in which the horizontal (or surface component) is distinct from the vertical component. While this separation of horizontal and vertical components has been traditional, it has been mandated by the different systems used in the two components.

In New Zealand, the horizontal geodetic datum (referred to as the New Zealand Geodetic Datum of 1949 - NZGD49) was established in 1949 from first-order geodetic triangulation observations that spanned the period 1923 to 1949. NZGD49 utilises the International (Hayford) ellipsoid oriented to approximate the geoid only across New Zealand and consequently NZGD49 is not a geocentric datum.

Unlike many other countries, such as Australia, Canada and the United States of America, no unified vertical datum has been established in New Zealand. Rather a number of discrete normal orthometric networks exist around local tide gauges in both the North and South Islands. In several instances these discrete networks, built upon first-order spirit levelling, utilise common stations however no attempt has been made to adjust these networks to form a single unified system.

A common problem for both the horizontal and vertical datums is that New Zealand is situated across the active Australian and Pacific tectonic plate boundary. This boundary is converging at approximately 50 mm/yr. The continuing and pervasive effect of this crustal deformation has altered the relative positions of the first-order horizontal and vertical stations; however, these first order coordinates remained fixed at their originally defined values. The fixing of the first order coordinates is of particular concern to the horizontal component as defined by NZGD49. With the advent of new positioning

technologies (eg. the NAVSTAR Global Positioning System - GPS) it is relatively easy to measure the combined effect of crustal deformation and errors in the observations and adjustment of NZGD49. Bevin and Hall (1994) have shown that these combined effects have introduced distortions of up to 6 m into NZGD49. Users of NZGD49 are becoming increasingly aware of these distortions due to their own use of the new positioning technologies. As a result there is a growing demand for either a new consistent datum to be established or at least suitable methods be made available to convert GPS-derived positions into NZGD49.

1.2 Thesis Aim

The aim of this research was to investigate the geodetic implications of defining a new three dimensional, homogeneous and geocentric reference system for New Zealand based on GPS data. The economic, cadastral and mapping implications are beyond the scope of this thesis. This investigation into a GPS compatible reference system is warranted when considering the increasing popularity of the GPS technology for the positioning of physical features and transportation vehicles, both nationally and globally. By establishing a set of coordinates in terms of a global geocentric reference frame (the type used by GPS) it would be possible to investigate how the new global reference frame and NZGD49 can be mathematically related to enable data, referenced to either system, to be transformed between these systems. However, the ellipsoidal heights generated by processing GPS data bear no relationship to the direction fluids will flow due to the influence of gravity. It is therefore necessary to investigate the determination of a geoid model for New Zealand to allow the ellipsoidal heights to be converted to the more meaningful orthometric heights. Orthometric heights are used extensively in the design of engineering projects (ie. road design and gravity assisted transportation of fluids for drainage, irrigation and electricity generation).

The main aims of this thesis are:

- determine the geodetic requirements of modern geodetic reference system for New Zealand.
- establish a set of coordinates for New Zealand stations in terms of a global geocentric dynamic reference system.

- establish a suitable method for calculating a gravimetric geoid for New Zealand.
- improve the capabilities and efficiency of the University of New South Wales (UNSW) gravity computation software suite known as GRAV.
- investigate the transformation of coordinates between global references frames and NZGD49.

1.3 Thesis Method

The methods used to meet the above stated aims are:

i) summarise the current status of the national horizontal and vertical datums in New Zealand; outline weaknesses in both the horizontal and vertical datums that may warrant the expense and disruption of establishing and adopting a) a new horizontal datum, b) a unified vertical datum, or c) a combined horizontal and vertical datum; with an improved understanding of the current status of the national horizontal and vertical datums, consider what features a new reference system should have so as to meet the requirements of new positioning and data management technologies (ie. GPS and digital databases, respectively).

ii) establish a set of station coordinates for New Zealand in terms of the most accurate available global reference frame. This would expose any difficulties that may be peculiar to New Zealand (or other countries) which has small global extents, is located on a tectonically active plate boundary, and whose national network of GPS data has not been attached to a global geocentric reference frame.

iii) investigate the computation of geoid heights using global geopotential models (GGM) and the enhancement of these GGM by using local New Zealand gravity data.

iv) having established ellipsoidal heights and geoid heights, derive orthometric heights from this data. These derived orthometric heights can then be compared with the spirit levelled (tide gauge constrained) orthometric heights at common stations, to allow the investigation into the quality of the three heights (ellipsoidal, geoidal and orthometric).

v) compare the currently available transformation parameters, and those derived as part of this research, to convert between global geocentric reference frames and NZGD49.

1.4 Thesis Overview

The findings of this research have been organised into the following chapters. Chapter 2 begins by outlining the geodynamics in New Zealand, as a background to discussion on the requirements of a modern geodetic reference system for New Zealand. A brief history of the current horizontal geodetic datum and the multiple vertical datums are presented. Discussion focuses on the fact that New Zealand has multiple vertical datums and considers the establishment of a single consistent nationwide vertical datum. The datum demands of future developments of the New Zealand survey system are then outlined.

The establishment of a set of coordinates for New Zealand, in terms of a global geocentric dynamic reference system are described in Chapter 3. The GPS data used is from the 1st Order 2000 Datum Investigation campaign of March 1993, undertaken by the Department of Survey and Land Information (DOSLI). A brief outline is given of the major terrestrial reference frames used by GPS. A review of the problems encountered and benefits obtained from processing the GPS data in the GAMIT/GLOBK software suite and its resulting attachment to the International Earth Rotation Service (IERS) Terrestrial Reference Frame of 1993 (ITRF93).

Chapter 4 contains the research into the computation of geoid heights using GGM and the enhancement of these GGM by the use of local New Zealand gravity data. A brief outline of the theory of computing geoid heights from gravity anomalies is given along with the gravity data available for New Zealand. An area in the lower North Island was selected for the testing of the enhancements to the GGM using the UNSW, Ring Integration (RINT) based geoid software suite. Also described are improvements to the capabilities and efficiency of the RINT software. Based on the tests a method is proposed for the computation of a New Zealand wide gravimetric geoid. Possible

difficulties testing a national geoid model, due to the multiple vertical datums, are raised.

The problem of relating coordinates derived in terms of a three dimensionally consistent ITRF93 with New Zealand's horizontal geodetic datum (NZGD49) and multiple vertical datums is investigated in Chapter 5. A summary of the primary coordinate systems in geodesy is given before outlining the theory of different transformation methods. The currently available sets of transformation parameters to convert between global reference systems and NZGD49 are presented, along with the transformation method and parameters developed as part of this research. Investigations then focus on the accuracy of the coordinates obtained by applying these transformation parameters. Alternative methods to transform coordinates between NZGD49 and global reference systems or a new national reference system for New Zealand are discussed.

The conclusions and recommendations of this research are presented in Chapter 6.

Chapter 2

Geodetic Setting of New Zealand

2.1 Introduction

This chapter begins by summarising the geodynamics in New Zealand, as a background to discussion on the requirements for a modern geodetic reference system in New Zealand. The variety of horizontal and vertical surveys that have been carried out in New Zealand to establish the nation's current horizontal geodetic datum and the multiple vertical datums are outlined. Discussion then focuses on some of the obstacles and benefits of developing a consistent vertical datum for New Zealand.

2.2 Geodynamics in New Zealand

New Zealand is located across the boundary between the Australian and Pacific plates (Figure 2-1). The North Island is at the southern end of the Tonga-Kermadec-Hikurangi oblique subduction zone. This subduction zone terminates at the northern end of the South Island and dips westward from the Hikurangi Trench (ie. the Pacific plate is subducting beneath the Australian plate). In the far south of the South Island, the plate boundary is an opposed subduction zone dipping eastward from the Puysegur Trench (ie. the Australian plate is subducting beneath the Pacific plate). Between these two subduction zones, two largely submerged continental fragments, the Challenger Plateau and the Chatham Rise, collide obliquely.

Each of the two main islands therefore have distinct tectonic features that reflect the complex temporal and spatial interactions between subduction and strike-slip regimes along the New Zealand portion of the Australian - Pacific plate boundary. See Cox and Hart (1986) or Park (1988) for principles of plate tectonics.

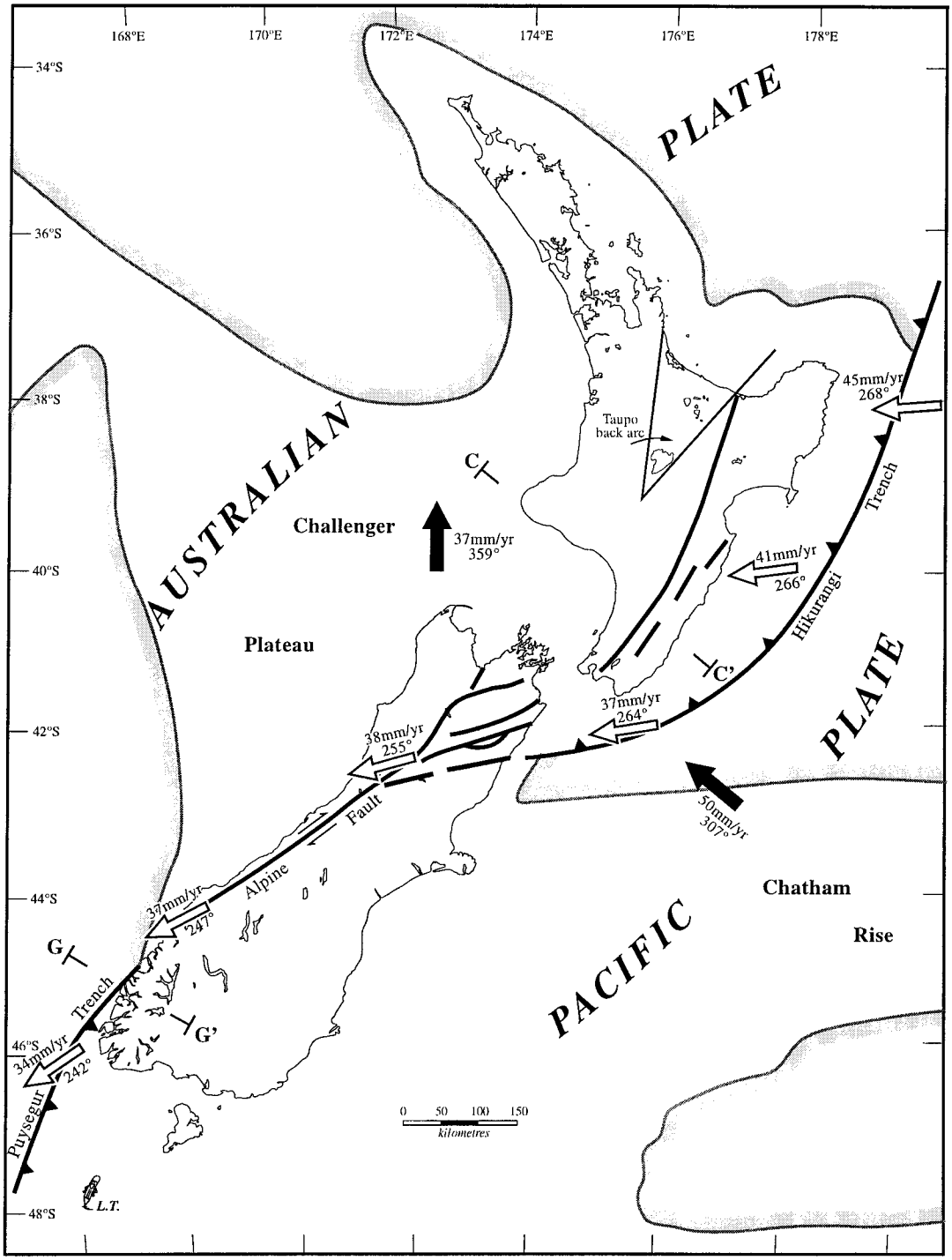

Figure 2 - 1 : Location of the Pacific and Australian plate boundary in the New Zealand region (adapted from Cole 1990; and Anderson and Webb 1994). The solid arrows represent the absolute plate motion (in terms of Nuvel1A) at Wellington, if Wellington was located only on the Australian or Pacific plates, based on DeMets *et al.* (1994). The hollow arrows represent the relative plate motion between the Australian (fixed) and Pacific plates, based on DeMets *et al.* (1994). Shading represents the Rise/Plateau boundaries.

The Taupo back arc region in the centre of the North Island is an area of back arc spreading that is occurring on land. This is one of the few occurrences in the world of back arc spreading on land and it experiences a principle extension rate of $0.21 \pm 0.09 \times 10^{-6}$/yr ($1\sigma$) at an azimuth of $124 \pm 13°$, which corresponds to 8 ± 4 mm/yr extension over 40 km across the Taupo Volcanic Zone (Darby and Meertens, 1995). This back arc region also has volcanic activity, which along with the spreading, is a feature associated with back arc spreading.

The No Net Rotation NUVEL-1A (DeMets *et al.*, 1990, 1994) plate motion model, which is based on geophysical data, predicts that the relative plate motion between the Pacific plate and the Australian plate is 45 mm/yr to the north of New Zealand, and diminishes further south to 34 mm/yr (Figure 2-1). These rates are in agreement with results from the analysis of terrestrial geodetic observations, such as those by Reilly (1990) who reported rates between the Australian and Pacific plates of up to 58 mm/yr in the north, and 39 mm/yr in the south of New Zealand.

For the lower half of the South Island the Alpine fault gives the appearance of being a relatively simple collision plate boundary. However, Pearson *et al.* (1995) report that there is some debate in the literature as to the proportion of the relative plate motion accommodated by the Alpine fault. Estimates vary between 25% and 100% of the relative motion, although there is general agreement that any remaining motion is accommodated over a broad area mainly to the east of the Alpine fault. The northern part of the South Island contains the transition zone between continental collision and subduction on the Hikurangi Trench. In this region the plate boundary broadens from the Alpine fault into a series of northeast-southwest trending strike-slip faults that accommodate most of the relative plate motion (Berryman *et al.*, 1992).

The seismicity associated with subduction zones is one of their most characteristic features (Park, 1988). The dipping zone of earthquake foci, widely known as the Benioff zone, constitutes one of the most important pieces of evidence for the hypothesis of subduction of oceanic lithosphere. Benioff zones for the New Zealand region have been reported by Reyners (1989), Anderson *et al.* (1993) and Anderson and

Webb (1994). Figure 2-2 contains two examples of Benioff zones, one across the Hikurangi Trench and one across the Puysegur Trench, for earthquakes between January 1, 1990 and February 28, 1993. The difference in the angle of the dipping zone is indicating the variation in subduction rates at the plate boundaries. The direction shows that for Figure 2-2A the Pacific plate is subducting under the Australian plate, while Figure 2-2B shows the Australian plate is subducting under the Pacific plate.

In Figure 2-3 it is clear that there are lower levels of seismicity in the region of the Alpine fault. This highlights that the Alpine fault is undergoing a different tectonic process to regions on either side for the period 1964 to 1991. The North Island region of the deformation between the Pacific and Australian plates is marked by a diffuse band of earthquakes 200-300 km in width (Figures 2-2A and 2-3). This is typical of regions where plate boundaries cross continental lithosphere, and is in contrast to the relatively narrow bands of seismicity that mark plate boundary zones in oceanic lithosphere, such as that to the south of the South Island (Anderson *et al.*, 1993) (Figures 2-2B and 2-3).

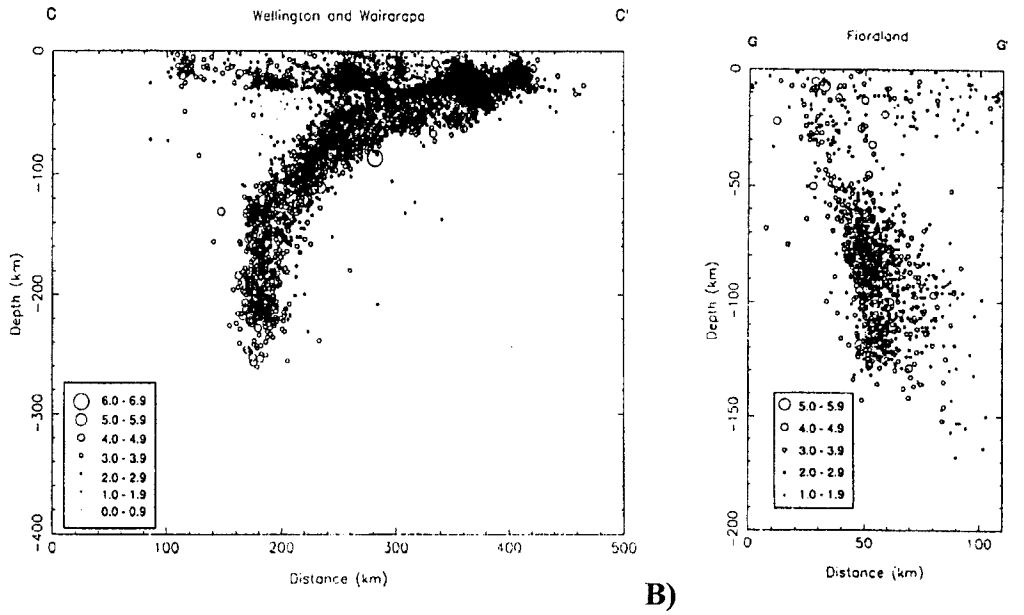

A) B)

Figure 2 - 2 : Cross-sections of Benioff zones for earthquakes between January 1, 1990 and February 28, 1993, across: A) the Hikurangi Trench, and B) the Puysegur Trench (Anderson and Webb, 1994). See Figure 2-1 for cross-section locations. The symbol size is scaled to magnitude in unit steps of M_L.

Figure 2-3 shows that for the period from 1964 to 1991 most regions of New Zealand experienced shallow earthquakes (<40 km) of magnitude ≥4.0 on the Richter scale. Only a small number of these earthquakes would have caused rupturing of the Earth's surface, however, they still indicate that deformation due to tectonics is occurring across New Zealand. In support of the seismic evidence of deformation across New Zealand, Wellman (1955), Walcott (1984), Reilly (1990) and Bevin and Hall (1994) have all reported the existence of deformation from the analysis of geodetic measurements, without there being any specific earthquakes causing the surface to rupture.

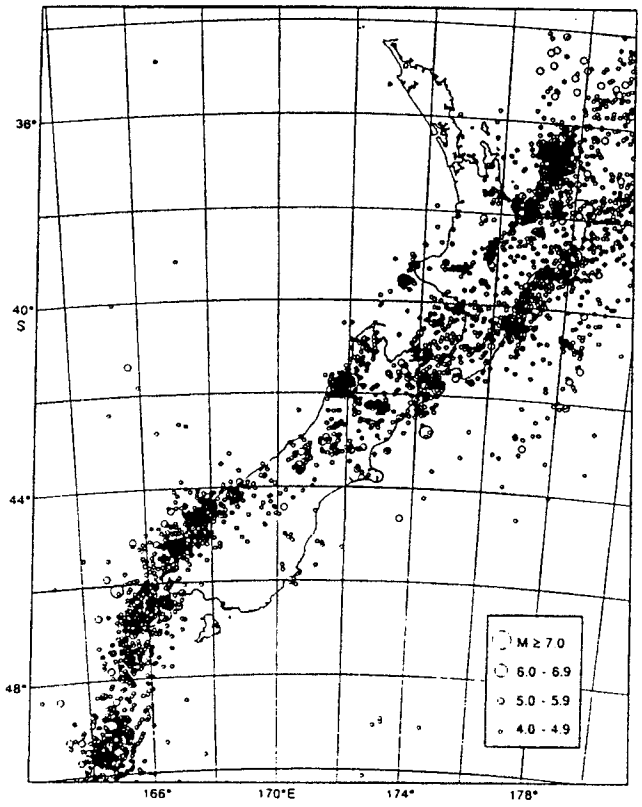

Figure 2 - 3 : Shallow earthquakes (<40 km) of magnitude ≥4.0 on the Richter scale reported by the New Zealand Seismological Observatory from 1964 to 1991 (Anderson *et al.*, 1993)

The results from seismicity, geodetic analysis and geological studies, show that New Zealand experiences a variety of forms of deformation. These deformations need to be considered in the maintenance of any new geodetic datum for New Zealand. Beavan *et al.* (1996) have shown that these deformations are easily detectable within two years using modern geodetic observing techniques (ie. GPS receivers) (see Figure 2-4).

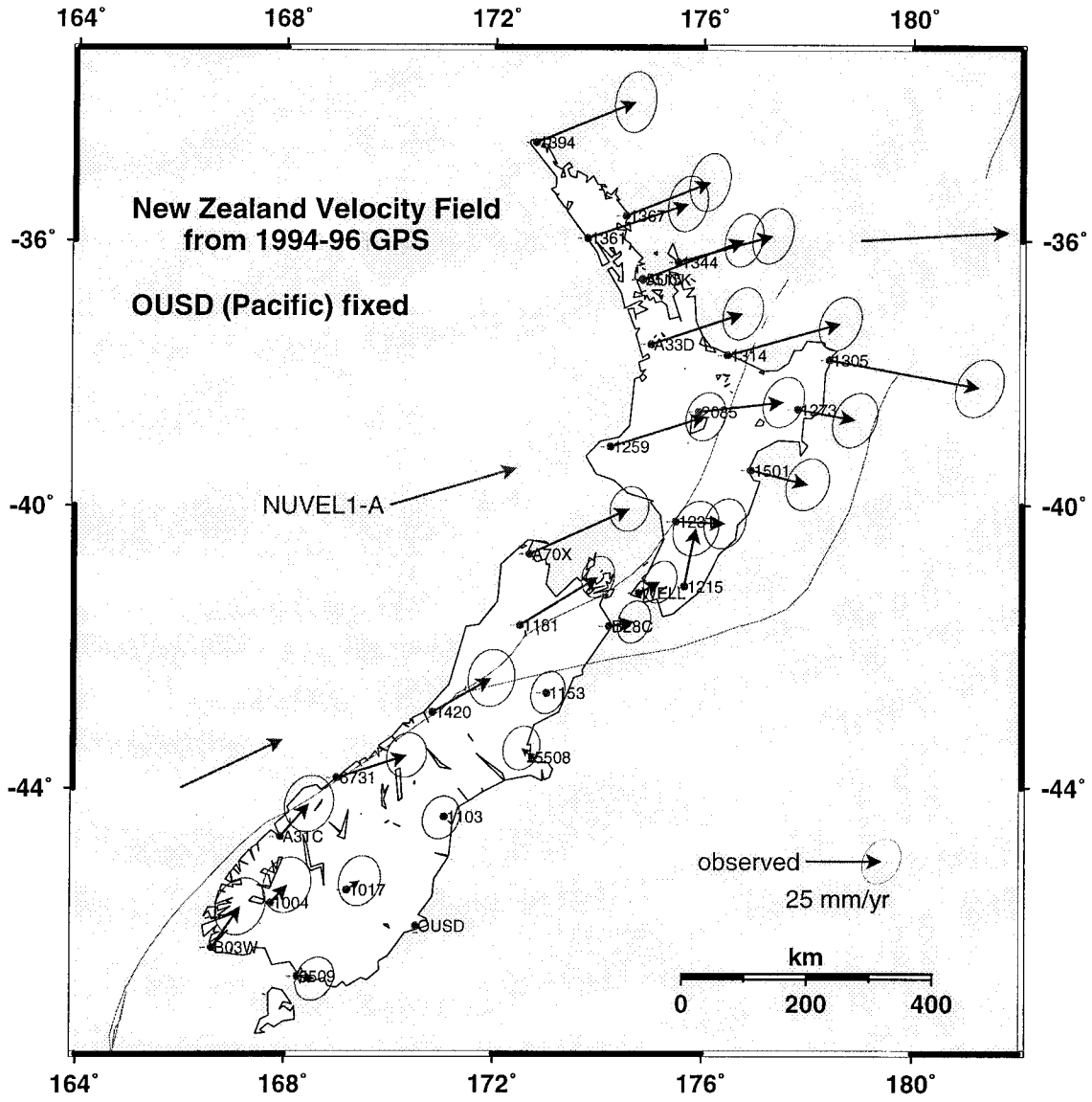

Figure 2 - 4 : Velocity field of the New Zealand GPS sites that were observed in February 1994, 1995 and 1996 (see Appendix I) with the Otago University site (OUSD) fixed to the NUVEL1-A pacific plate rate. Arrows without 1 sigma error ellipses are NUVEL1-A rates. Light grey lines running from the SW to NE indicate the approximate position of the plate boundary. Mercator projection drawn using GMT (Wessel and Smith, 1991). (Beavan *et al.*, 1996).

From Figure 2-4 it is clearly seen that all stations on either the North Island or the South Island do not experience the same deformations. Stations near the plate boundary (approx. 100 km) are undergoing different deformation rates to those located further away. Figure 2-4 demonstrates that using simple velocity field models such as: i) all North Island or all South Island stations have the same deformation rates, or ii) all stations on one side of the plate boundary have the same deformation rates, is not valid. Velocity field models involving greater complexity are therefore required to predict New Zealand's deformation.

2.3 Roles of a Modern Geodetic Reference System

Conventional geodetic datums have been established in the past, as was the case for NZGD49 (Jones 1981 and Section 2.4.2.3), by defining :

i) the size and shape of the reference ellipsoid,
ii) the relationship between a physical point on the Earth's surface (Geodetic Origin) and the centre of the reference ellipsoid,
iii) the direction of the minor axis of the reference ellipsoid, and
iv) the origin of the longitude measurement.

These conventional geodetic datums had no observation methods available to enable the relationship between the centre of the reference ellipsoid and the centre of mass of the Earth to be determined. However, since the advent of space based observation techniques, such as Doppler, Satellite Laser Ranging and GPS, it is now possible to determine the relationship between the centre of the reference ellipsoid (Cartesian coordinate origin) and the centre of mass of the Earth.

As a result of being able to determine the location of the centre of mass of the Earth, reference systems have been developed which place the centre of the reference ellipsoid at the Earth's centre of mass (eg. World Geodetic System 1984 - WGS84). These "geocentric" reference systems (Section 5.2.3) allow for consistent global reference frames to be established which allow navigation and positioning, be it on land, water, or in the air, to be undertaken in terms of a single reference frame, irrespective of location in the world.

As New Zealand has no common land boundaries with other countries, the problem of common stations having different geographic coordinates has not been a significant issue. However, with the increasing importance being placed on defining New Zealand's continental shelf boundary the difference between nationally defined geodetic datums is likely to become an issue for New Zealand.

There are a number of issues that need to be considered before an old datum is replaced by a new reference system (See Section 2.3.1). The age of the datum is irrelevant,

however, if the national datum is not geocentric there are increasing demands from users of geocentric positioning technologies, such as GPS, that transformation parameters be established to allow the conversion between the national datum and global geocentric reference frames (ie. between NZGD49 and WGS84 or ITRF, see Chapter 5).

New positioning technologies, such as GPS and electronic total stations, are able to measure between stations with a higher accuracy than the technology that was used to establish NZGD49. As a result of this improvement in technology, and the continuing effects of earth deformation in New Zealand, distortions in NZGD49 of up to 6.0 m have been reported by Bevin and Hall (1994). Some users of NZGD49, who have purchased these new positioning technologies, are frustrated that their surveys with higher internal consistency than NZGD49 have to be distorted to fit this datum (GMS, 1996). Consequently, they are requesting that a new consistent datum be established in New Zealand so that they are able to obtain the benefits of improved accuracy offered by the new technologies.

2.3.1 Considerations for defining a geodetic reference system

Each geodetic reference system, whether it be of national, continental or global extent, will be required to meet different user requirements, such as accuracy and consistency with adjoining datums. As a starting point for defining a new geodetic reference system for New Zealand, it is worth analysing the criteria that Gubler and Schneider (1994) list as part of the establishment of the European Terrestrial Reference System (ETRS). They are:

i) Coordinates of geodetic points determined in a particular reference system should not vary more than inevitable over time spans of one to several decades.

ii) The realisation of the system, the so-called reference frame (namely the geodetic points and a set of coordinates), should have a sufficiently long lifetime in order to guarantee criterion i).

iii) If the area concerned is subject to deformation, due eg. to deformation of the earth's crust, the reference system should provide a suitable functionality to model the kinematics.

iv) A national reference system (frame) should not differ more than absolutely necessary from continental or global reference systems (frames).

v) On one hand, regular mathematical transformation formulae should be provided to transform coordinates defined in the national system into continental and global systems such as ITRS.

vi) On the other hand, it must be assured that a sufficient number of identical points will be known in the old as well as in the new system (and frame) in order to allow transformations between the old national system (respectively frame) and the new one.

Gubler and Schneider (*ibid.*) note that some of the criteria may be in conflict with each other and that it is important to discuss the importance of the criteria carefully before deciding on a reference system.

Analysing the first criteria of Gubler and Schneider for its suitability to New Zealand, it is true that prolonging the time spans between varying the coordinates of geodetic points in a particular reference frame, does have benefits for paper-based databases. The major benefit is that to update an entire paper-based database involves a considerable amount of time (eg. months or years) However, with digital databases, there is no longer a need to maintain the coordinates at fixed values for long periods of time.. If the database has been designed to accommodate time-varying coordinates, and suitable velocity models are available updates can be performed automatically by computers within a small fraction of the time (eg. minutes or hours).

For the second criteria, if the reference system is designed to accommodate variation of the coordinates of geodetic points (ie. be dynamic as ITRF is; Section 3.4.1), then the reference frame can realise the reference system for as long as the reference system is deemed appropriate by its users. If a new geocentric reference frame is established for New Zealand with out the ability to accommodate deformation then the new reference frame will not only be distorted over time, like NZGD49, but will also not remain geocentric.

In Section 2.2 it was shown that New Zealand is subjected to Earth deformation, that can reach 50 mm/yr in magnitude. Therefore, as described in criteria three, a new reference system should provide a suitable functionality to model the kinematics of New Zealand.

Criteria four can be met, as suggested by Grant and Pearse (1995), by developing a method so that a dynamic national reference system (frame) can be steered to remain within specified limits of the global reference system (frame). An analogy is how GPS time is steered so as to maintain a close relationship to Coordinated Universal Time (UTC).

The transformation formulae in criteria five and six are important in New Zealand because users of the current datum, NZGD49, will require a method for converting their databases to any new reference system. Even if no new reference system is adopted in New Zealand, there are growing needs for users of NZGD49 to be able to easily convert their data into global reference frames, such as WGS84, without ambiguity or significant loss of accuracy. Currently the only transformation parameters available for converting between NZGD49 and WGS84 are based on Doppler derived WGS72 coordinates of NZGD49 sites (see Section 5.4.2) (These transformations are of low accuracy and do not model local distortions).

Earthquakes can cause distortions in localised areas of the national reference frame (geodetic network). Often in New Zealand the area affected by an earthquake is resurveyed and adjusted back into the geodetic network holding the first-order control station coordinates fixed at their original NZGD49 values. As a result the new survey is distorted to fit the continually distorting first-order network. Grant (1995) proposes a dynamic national reference system which would allow the coordinates to be changed. This would enable a consistent reference system to be maintained more easily and be able to accommodate earth deformation.

2.4 The New Zealand Horizontal Datum

The establishment of a National Datum in New Zealand was driven partly by the necessity to provide both Government and new settlers with reliable plans and descriptions to enable the safe issue of titles to land. Lee (1978) provides an extensive description of the Geodetic Triangulation of New Zealand from settlement until 1974. Early geodetic surveys were localised and no serious attempt at connecting these surveys was undertaken until 1909. A summary of early geodetic surveys as reported by Lee (*ibid.*) is contained in Section 2.4.1. Geodetic triangulation designed to connect the early isolated geodetic surveys began in 1921. This geodetic triangulation was not completed until 1949, at which time the first geodetic datum for New Zealand was established and called New Zealand Geodetic Datum 1949 (NZGD49) (Figure 2-5). Lee (*ibid.*) provides a comprehensive description of this geodetic triangulation which is summarised in Section 2.4.2. Geodetic surveys undertaken in New Zealand since the establishment of NZGD49, through to early 1993, are outlined in Section 2.4.3.

2.4.1 Settlement and Provincial Surveys

From settlement until 1852, land surveys in New Zealand were only undertaken to assist in the production of a plan to accompany the sale of land to settlers. These settlement surveys did not claim to have used scientific methods or to have achieved great accuracy. Often these surveys were inaccurate. There was no real attempt to place them in their correct relative position or, in some cases, even to orient them. Lee (1978) notes that bearings were often magnetic bearings and positions were often scaled from nautical charts with no comprehensive control surveys being undertaken. Due to gaps or overlaps in the surveys there was frequent litigation over land boundaries.

Between 1853 and 1876 New Zealand was administered by Provincial Governments - initially six and later nine. Each Provincial Government had its own Survey Department which was given the task of introducing some form of order to the survey records, to at least provide security of tenure to the land purchasers. The Provinces of Auckland, Hawke's Bay and Wellington made successful attempts to bring order to the survey records through the use of triangulation schemes. Unfortunately these competently

performed triangulation surveys suffered from the errors in the standard of length. In other Provinces triangulation was either avoided or, when performed, was undertaken in an inefficient manner that made it unreliable.

Rather than using triangulation, the Province of Otago introduced a system to control the orientation of surveys. This system was introduced in 1856 by J.T. Thomson and divided the Province into four large districts called "meridional circuits". Within each circuit an initial station was selected and the true meridian was determined by astronomical observation. Bearings, but not distances, were carried outwards by traverse from the initial station to the boundaries of the circuit, following the valleys that were suitable for settlement. As later surveys linked these valley traverses there was no attempt to adjust out the discrepancies. This system satisfied the immediate needs of the time but not of the future.

In 1872 the Secretary for Crown Lands, W.S. Moorhouse, recommended that all surveys be placed under the control of the Central Governments Surveyor-General and that general triangulation be carried out.

In 1876 the Provincial Governments were abolished. J.T. Thomson was appointed by the General Government as Surveyor-General. The Chief Surveyors of the Provincial Districts remained in control of their local surveys, but were now under the direction of the Surveyor-General. At the time of Thomson's appointment there was a large backlog in land purchases awaiting the demarcation of boundaries. There was therefore an urgent need for a system that would rapidly bring all surveys under a reasonably correct system of control. Thomson therefore rejected the general triangulation and introduced for all districts of the colony the meridional circuit system which he had earlier used in Otago. Twenty eight meridional circuits were established, nine in the North Island and nineteen in the South Island.

The meridional circuit bearings were sufficient for orientation of any survey but alone could not provide accurate coordinates. Triangulation was required for this purpose. This was being undertaken by Provincial Districts without any specific regulation by the

Surveyor-General. By the mid-1880s a continuous network of triangles extended for 1500 km from North Cape to Stewart Island. This network was primarily to link the settlement surveys and was conducted to low geodetic standards.

In 1901 new second order triangulation was commenced to bring uniformity to all the different nets of minor triangles, which had spread inland from the coastal network in advance of the settlement surveys in the Wellington and Taranaki districts. For the secondary triangulation two baselines were selected. These were the Eltham and Wairarapa bases (Figure 2-5). The secondary triangulation was never intended to replace the need for national triangulation, though the two baselines were observed to sufficient accuracy to enable their use in the national triangulation.

2.4.2 New Zealand Geodetic Datum 1949

2.4.2.1 Field Surveys

In 1921, the work needed to provide a national geodetic control network for New Zealand commenced.

Between 1921 and 1923 reconnaissance, network design and station marking was conducted. In 1923 the first angle observations finally began at the Kaingaroa baseline (Figure 2-5) and were carried to the coast northward and eastward. The sides of the triangles averaged about 30 km in length. Until 1927, angular observations were made in daylight using a Troughton and Simms 200 mm transit micrometer theodolite reading to 1". A minimum of 12 sets of horizontal angle observations and 2 sets of vertical angle observations were observed. As the work progressed larger triangles were trialed, resulting in an optimum length of sight of 50 km being adopted. By the end of the field observations, latitude had been determined by astronomical observations at what amounted to one in every three stations in the North Island and one station in every six in the South Island, a total of 67 stations. Astronomic azimuth had been observed at 40 stations, being one in every seven stations in both islands.

Some of the errors of triangle closure in the part of the network observed in the first few years were large, occasionally reaching 5", although the majority were less than 1". In 1929, a Wild T3 geodetic theodolite, reading to 0.2" replaced the transit theodolite. In 1930, observations were made at night to lamps instead of to the opaque beacons formerly used for daytime observations. As a result of the improved triangle closures obtained, the method of observing to beacon lamps at night was adopted. This resulted in improved progress and triangle closures rarely exceeding 2".

The observation of vertical angles was performed during daylight hours, as with all observations of the early period. Vertical observations were generally observed between midday and 2 pm, but if conditions prevented observations during the daylight hours they were performed as close as possible to midnight.

Progress was halted in February 1931 due to the Napier earthquake and the subsequent fires that destroyed all survey records of the Hawke's Bay District. Once the urgent work required to establish new survey control in the Hawke's Bay had been completed, further geodetic triangulation work was suspended for financial reasons during the depression of the early 1930s.

In 1936 the first-order triangulation resumed. Observations in the form of a quadrilateral across Cook Strait were completed in 1938. During the observation of the South Island, the mountainous areas to the west were avoided.

The outbreak of the Second World War did little to impede progress of the survey. This was mainly due to the fact that the threat of invasion increased the need for topographical maps for military use. The production of "provisional" topographic maps made the value of geodetic triangulation clear, as it allowed survey data from different districts and different degrees of reliability to be combined.

From 1940 to 1942 the network was spread down the South Island, and across Foveaux Strait to Stewart Island (Figure 2-5).

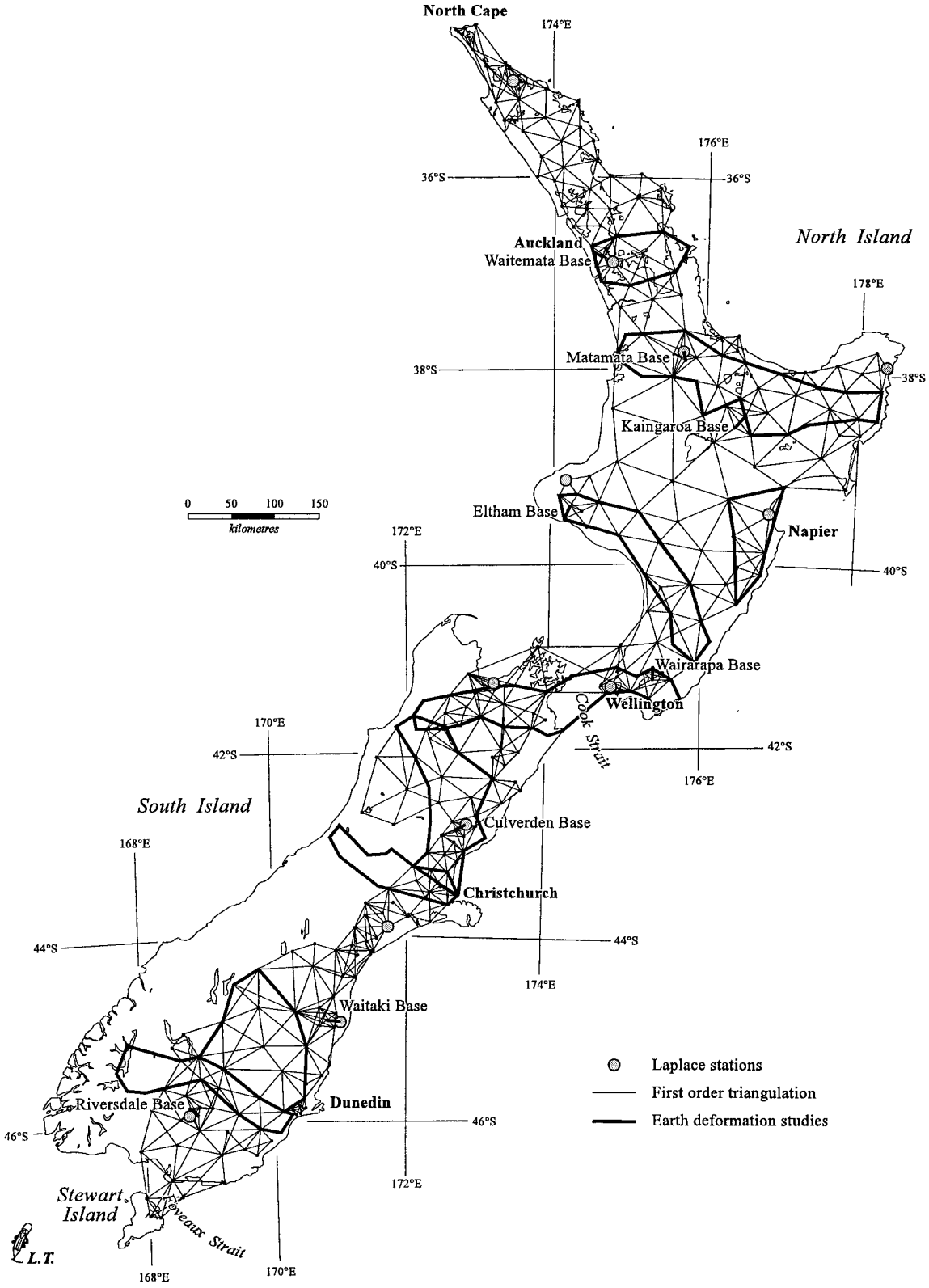

Figure 2 - 5 : Combined First-Order Triangulation Network used in the establishment of NZGD49; the 1973 extension of the First-Order network to include the north-western part of the South Island; plus the EDS surveys up until 1990 (adapted from NZNCGG, 1991). NZMG Projection.

Due to the War, restrictions on the availability of baseline measuring equipment meant that the three South Island baselines were not measured until 1947. At the same time, two of the five North Island baselines were re-observed to allow comparison with earlier measurements. The difference between the 1947 and 1911 measurements at the Matamata baseline indicated the more recent determination was 12.2 ppm shorter, while the Waitemata baseline was 7.3 ppm shorter. The mean of these two determinations, 9.7 ppm, was used to correct the other North Island baselines.

The heights of the primary triangulation stations were determined by adjusting the vertical observations. The primary purpose of determining the height of the stations was to reduce the horizontal observations to the ellipsoid. The heights used to reduce the observations to the ellipsoid were actually orthometric heights - not ellipsoidal heights which were unknown. Therefore it was implicitly assumed that the geoid and the ellipsoid were coincident (Chapter 4 indicates that this is not necessarily the case). The height adjustment was controlled by using the heights of eight tide gauges (four in each island) that had been determined from different 3 year observation periods (refer to Section 2.5 for further discussion on the vertical datum).

In 1948 twelve Laplace stations were observed, with observations being completed in early 1949. This marked the completion of the field work which had spanned 40 years (counting the secondary triangulation baselines).

The primary triangulation was broken down to give networks of smaller triangles being referred to secondary and tertiary networks. These three levels of triangulation were given the terminology of first-, second- and third-order networks and originally had the specifications as contained in Table 2-1.

	Triangle Closure		Length Closure	Average Length of side
	Average	Maximum		
First-order	1"	3"	1 in 25000	50 km
Second-order	3"	5"	1 in 10000	15 km
Third-order	5"	8"	1 in 5000	5 km

Table 2 - 1 : Original NZGD49 horizontal classification for triangulation surveys (Lee, 1978, p. 21)

2.4.2.2 Adjustment

The adjustment of the geodetic network observations was done with the aid of electro-mechanical calculating machines and by the then usual method of condition equations. For the adjustment of the observations, each of the eight base networks was regarded as a separate figure and adjusted independently. The remainder of the network was divided into four figures, two in each island. The part of the eastern North Island network that had been observed to the lower accuracy using the micrometer theodolite was one of the North Island figures. The South Island was already divided into two, with the northern figure including the connection across the Cook Strait.

Following the final adjustment, it was possible to establish the "Geodetic Datum 1949", and to express all the triangulation in terms of a homogeneous system over the whole country. Stations were coordinated on the National Grids, as the North and South Islands had independent transverse Mercator projections. The International (Hayford) spheroid (ellipsoid) was adopted as the figure that best approximated the geoid for New Zealand surveys. The Hayford ellipsoid had been defined by the International Geodetic and Geophysical Union in 1924 by specifying the semi-major axis (a) and the flattening (f) as:

$a = 6378388$ m $\qquad f = 1/297$

All measurements of length in surveys and on plans affecting land titles in New Zealand were required in 1935 to be in terms of a chain of 100 links, having a length of 66 imperial feet. The conversion from metres to links was therefore carried using the Sears(1927) metre-foot relationship (also known as the Sears ratio) of:

1 metre = 39.370147 inches (Sutherland, 1994)

and resulted in the value adopted in New Zealand for the semi-major axis being:

$a = 31706827.42$ links

When New Zealand adopted the metric system in 1973, the S.I. metric-imperial ratio was used and this ratio differs from the Sears ratio by 1.7 ppm. This introduced a systematic scale error into NZGD49.

In 1973, when maps and surveys were metricated in New Zealand, one-projection coordinate system (New Zealand Map Grid - NZMG; Reilly, 1973) was adopted for topographical maps, but for cadastral surveys the meridional circuits were retained with only minor amendment of boundaries in some places.

A scheme for the extension of the first-order triangulation network was undertaken in the north-western part of the South Island during 1973. This area, like the entire west coast of the South Island, had not been covered by the original survey (Figure 2-5).

2.4.2.3 Origin of NZGD49

When NZGD49 was established, no station was specifically designated as the Geodetic Origin. However, Lee (1978) describes how Papatahi, near Wellington, was designated the Initial Station as follows:

> "The final solution of the triangles gave the final spherical angles and lengths of sides, and from these the final latitudes, longitudes and azimuths could be computed, beginning at some initial station of defined position. The station chosen as the initial station was Papatahi, a centrally situated station of the main net and one of the corner stations of the subsidiary net containing Kelburn. The differences between astronomic and geodetic latitude at 65 stations and the differences between astronomic and geodetic azimuths at 39 stations from the first adjustment were known, and the latitude and azimuth at Papatahi were chosen so as to make the means of these differences equal to zero. The longitude adopted was that derived from Kelburn. The rounded-off values are :
>
> | | |
> |---|---|
> | South latitude | 41° 19' 08.9000" |
> | East longitude | 175° 02' 51.0000" |
> | Azimuth to Kapiti No. 2 | 347° 55' 02.500" |
>
> and these define the Geodetic Datum 1949, on which all subsequent computation of horizontal position has been based."

The datum for heights was described above in Section 2.4.2.1.

Jones (1981) outlines that it was obvious that it was intended that Papatahi be the Origin since geodetic latitude, longitude and azimuth were defined there when it was

designated the Initial Station. However, only astronomic latitude was observed at Papatahi and thus it is not possible to determine if Laplace's equation (5.3) is satisfied at the station. Since the height of Papatahi was determined by trigonometrical levelling, as opposed to spirit levelling, the relationship between geoidal and ellipsoidal height is indeterminate or at best ill-defined. Jones (*ibid.*) also shows that Kelburn has a strong case to be considered as the Geodetic Origin of NZGD49, since it satisfies all the criteria which are prescribed for an origin (Section 2.3). That is, the Laplace equation is satisfied and the relationship between the Origin and the centre of the reference ellipsoid is uniquely and unambiguously defined.

With Kelburn designated as the Origin of NZGD49 the full statement on NZGD49 is given by Jones (*ibid.*) as:

Reference Ellipsoid : International (Hayford) a = 6378388 m; f = 1/297
Origin : Kelburn

ϕ =	geodetic latitude	=	41° 17' 10.1916" S
λ =	geodetic longitude	=	174° 46' 05.0263" E
α =	geodetic azimuth to Island Bay No.2	=	172° 07' 02.95"
h =	ellipsoidal height	=	126.66 m

The mean observed values of the above quantities are:

Φ =	astronomic latitude	=	41° 17' 03.50" S
Λ =	astronomic longitude	=	174° 45' 59.19" E
A =	astronomic azimuth to Island Bay No.2	=	172° 07' 06.80"
H =	orthometric height	=	126.66 m

The following quantities may be derived from the above values:

$\Phi - \phi$	=	-6.69"	
$\Lambda - \lambda$	=	-5.84"	
$A - \alpha$	=	3.85"	
H - h	= N =	0.00m	(This is an implicit assumption rather than an explicit constraint and was actually assumed for all stations as noted earlier).

NZGD49 is realised through the (approximately) 290 first order stations that have been coordinated with respect to the Initial Station.

2.4.3 Post 1949 Geodetic Datum for New Zealand

Besides the sporadic second, third and fourth order densification surveys of the NZGD49 network, there has been no specific attempt to resurvey the first order network until the mid 1990s (Section 2.6). However, there have been geodetic surveys

undertaken to either determine the relationship between NZGD49 and the Earth's geocentre or to monitor earth deformation across the country.

The determination of transformation parameters between NZGD49 and WGS72 has been reported by Mackie (1982, 1983). These have been analysed in Chapter 5. The parameters were developed using 18 well distributed stations (which had Satellite Doppler-derived WGS72 coordinates) and were connected to the first order network. The TRANSIT Doppler data was collected between 1975 and 1979 with coordinates having an accuracy of 1.5 m in each axis (90% confidence limit). Rowe (1981) describes the survey data used by Mackie (*ibid.*) along with other Doppler surveys undertaken in New Zealand prior to 1981.

Mackie (*ibid.*) also proposed that a redefinition of NZGD49, based on the Doppler positions, be adopted for scientific use in New Zealand. This new proposed datum, referred to by Mackie as the New Zealand Geodetic Datum 1981, appears (from the lack of literature on the topic) to have received little support from the scientific community and has not been widely adopted.

The Earth Deformation Study (EDS) surveys initiated by the Royal Society of New Zealand were, as their name implies, designed primarily for detecting earth deformation using geodetic surveys. Bevin *et al.* (1984) describe these EDS surveys that, where appropriate, were designed to occupy first order stations. However, the survey data from these networks has not been used in a readjustment of the first order stations, even though a significant portion of the country has been reoccupied (Figure 2-5).

2.5 The New Zealand Vertical Datums

New Zealand does not have a single consistent height datum. Rather a collection of individual datums, each based on Mean Sea Level (MSL) determined at a tide gauge. This section summarises the historical development of these MSL datums and reports on their internal and relative consistency.

Due to the well established and documented principles of precise levelling, details will not be included in this thesis (see, eg., Bomford, 1980; Bannister and Raymond, 1984; or Vanicek and Krakiwsky, 1986).

2.5.1 Historical Development

This section on the historical development of the vertical datums is a summary of the work by Gilliland (1987) unless specifically referenced.

In 1930-31 the Department of Lands and Survey purchased equipment suitable to undertake precise levelling. The first recorded precise levelling was carried out by the Department in 1932, in cooperation with the Wellington City Council. However, this work does not form part of the national precise levelling network. The oldest records forming part of the national system of precise levelling are from a survey in 1937 between the Lyttelton and Timaru tide gauges (Figure 2-6). The primary purpose of the work was to coordinate the various systems of levels that had been undertaken for drainage, irrigation and road construction on the Canterbury Plains.

Between 1940 and 1948 there were only 35 miles (56 km) of precise levelling completed due to the more urgent mapping requirements for the war and the subsequent land surveying demands. From 1948 until 1990 there was a continuous effort to increase the coverage of the precise levelling networks in both the North and South Islands. The earlier work during this period was mainly to support engineering and mapping projects, though in 1973 the emphasis was changed to undertake the Royal Society of New Zealand's Earth Deformation Studies program (Section 2.4.3). The state of the precise levelling networks at 1990 for the North and South Islands is illustrated in Figure 2-6. Since 1990 there has been little emphasis placed on extending or even resurveying the precise levelling network.

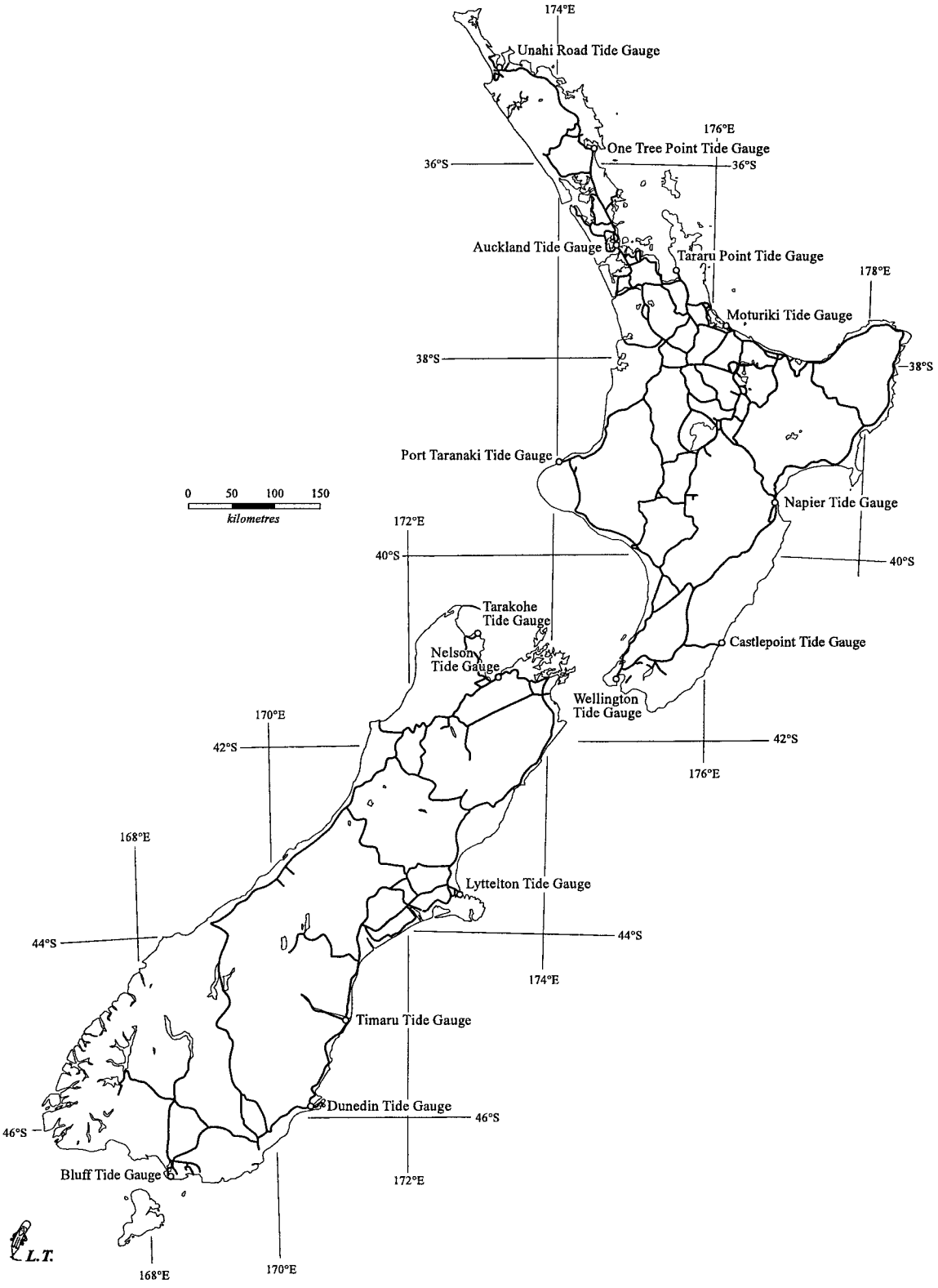

Figure 2 - 6 : New Zealand Precise Levelling network as at 1990 (adapted from NZNCGG, 1991). NZMG Projection.

The first instructions on how precise levelling should be performed in New Zealand were issued by the Surveyor General in 1948. These instructions were slightly modified in 1972 to accommodate the introduction of automatic levelling instruments and electronic data recording. They detail the methods and procedures required for the placement of bench marks (BMs), field observation techniques, limits of error and other relevant technical information.

There are two types of BMs. The first are Fundamental BMs being placed every 35-40 km. These are carefully located on solid ground, preferably rock, in substantially constructed sub-surface concrete chambers. The second type, Standard BMs, are placed between Fundamental BMs at intervals of about 1.5 km. Each Standard BM is generally a stainless steel pin set in a concrete block.

There are a series of local height datums used for the levelling networks which are defined by MSL, as determined at various locations from tide gauge observations over a varying range of time intervals and epochs. The description of the datum for heights for the first-order triangulation (Section 2.4.2) stations is reported by Lee (1978) as follows:

> "The heights of stations are measured from mean sea level as established by tide gauge record at the principal ports. The datum itself has usually been derived from the records over a period of at least three years, often a random selection of years from amongst those available. Connections between tide gauges and the triangulation network have been made by precise levelling. For the first computation of the heights of first-order stations, eight starting points were available, four in the North Island and four in the South Island".

The dates of tidal observation that were used to determine these eight stations, where known, and also the determination of other height datums are given by Gilliland (1987) (Table 2-2). It is important to note that the tide gauges of the principal ports used to determine the eight datums are all in sub-optimal locations such as harbours or river mouths rather than at the open-coast.

Datum Name	Connected to Triangulation at	Approximate Latitude (S)	Approximate Longitude (E)	Observation Period of MSL
Auckland	Mt Eden	36° 52'	174° 47'	1909 - 1923
Bluff	The Bluff	46° 34'	168° 24'	1918 - 1934
Dunedin	Flagstaff	45° 54'	170° 28'	unknown
Gisborne		38° 39'	178° 02'	1926
Lyttelton	2nd order station	43° 38'	172° 42'	1918 - 1933
Moturiki		37° 38'	176° 10'	1949 - 1953
Napier	Bluff Hill No. 2	39° 28'	176° 55'	unknown
Nelson	Botanical Hill	41° 15'	173° 16'	1939 - 1942
One Tree Point		35° 52'	174° 30'	1960 - 1963
Tararu		37° 06'	175° 31'	1922 - 1923
Taranaki	3rd order station	39° 03'	174° 02'	1918 - 1921
Wellington	Kelburn	41° 17'	174° 47'	1909 - 1946

Table 2 - 2 : Mean Sea Level (MSL) datum used for the precise levelling networks. Compiled from Gilliland (1987) and Lee (1978)

All BMs within the levelling network have a reduced height referenced to a particular datum. In some cases a BM may have its height referenced to more than one datum (Section 2.5.2).

2.5.2 Specifications and reduction of field observations

The accuracy requirements for precise levelling are specified in terms of the maximum allowable difference between the forward and backward measurement. The original specifications for precise levelling set down by the Surveyor General were, when expressed in metric units, $\pm 3\text{mm}\sqrt{l}$, where l is the length of the levelling run in kilometres. Since 1975, when the Royal Society's Earth Deformation Study programme began, the specifications were changed to $\pm 2\text{mm}\sqrt{l}$ when using the Zeiss Ni 002 automatic level.

As with the horizontal triangulation, so too the levelling networks have different orders. The specifications for the levelling networks to fourth order are contained in Table 2-3.

Gilliland (1987) states that the "Orthometric heights of each BM are determined successively from selected datum or existing BM of known orthometric height

referenced to the datum by summing the orthometrically corrected height differences" (Appendix L). "These heights so derived are actually normal orthometric heights and not orthometric heights since normal gravity rather than observed gravity has been used in the correction formulae and thus no account is taken of the local variation in the gravity field". Section 3 of Appendix L describes the differences in the computation of orthometric and normal orthometric heights.

Network order	Specification
first	spirit levelling with a maximum close error of ± 2 mm$\sqrt{l}$, where l is the distance in km.
second	spirit levelling with a maximum close error of ± 7 mm$\sqrt{l}$, where l is the distance in km.
third	spirit levelling which does not meet 1st or 2nd order specifications, trigonometric levelling that is well controlled with short or low elevation observations
fourth	trigonometric levelling that is poorly controlled with long or high elevation observations

Table 2 - 3 : Specifications for New Zealand Levelling Networks (Glen Rowe, pers. comm., 1996)

If the difference between the normal and observed gravity is 10 mGal then there is an error of only 0.001 m between the orthometric and normal orthometric heights per 100m in measured height difference (Bomford, 1980). An extreme hypothetical case of the difference between orthometric and normal orthometric heights for the lower North Island test area (Section 4.4) is now presented. From Table 4-2 we take the maximum residual gravity anomaly of 200 mGal and assume this residual occurs at the summit of Mount Ruapehu (2800 m). Applying Bomford's approximation results in there being an error of 0.56 m between the orthometric and normal orthometric heights of a point at sea level and another at the summit of Ruapehu. A more realistic hypothetical example would be between a BM at Waiouru (950 m) and another at Bulls (50 m), with a residual gravity anomaly of 15 mGal. In this example the difference in height between methods would be only 0.014 m. Considering the distance of approximately 150 km between the marks this is less than half the allowable observational errors for first order levelling.

As was mentioned in Section 2.5.1, it is possible for some BMs to have heights defined in terms of more than one datum. Gilliland (1987) reported that discrepancies between these various datums, as witnessed at common BMs (ie. a BM connected to more than one datum) is less than 0.25 m.

During the first half of 1996 a search of DOSLI's Geodetic Database revealed that the largest discrepancy of a first order BM was 0.48m. Further investigation revealed that three first-order BMs had discrepancies over 0.44 m and were all located in the Taranaki area. When these three points were removed the largest discrepancy on a first-order BM was 0.23 m. As there has been no direct attempt, due to practical limitations, to connect levelling networks between the North and South Islands, investigation of discrepancies of both islands was undertaken separately. The maximum discrepancy in the North Island was 0.23 m from a total of 473 possible comparisons. The maximum discrepancy in the South Island was 0.13 m. However, for the South Island all but 6 of the possible 176 comparisons in the South Island were between the Lyttelton and Nelson tide gauges. Considering the extent of the precise levelling network along the west coast of the South Island, a maximum discrepancy of only 0.13 m should be approached with caution until further investigations into the South Island height networks are undertaken.

2.5.3 Future Developments

Before outlining some of the possible future developments of New Zealand's vertical datums it is worthwhile summarising their current state and the different user requirements for vertical datums.

The primary intention of a vertical datum is to provide a network of points that have their heights determined with respect to an equipotential surface. For engineering projects concerned with the transportation of fluids or the monitoring of localised deformations, a relative height in terms of a local vertical datum is often sufficient except in coastal areas, where height in terms of sea level may be more important. These users require a high relative accuracy but are not often concerned with the accuracy of absolute MSL height. For topographic maps to meaningfully represent the elevations of features on the Earth's physical surface, the height of topographic features

need to be known with respect to a physically meaningful surface, such as that approximated by MSL. Therefore topographic map users expect that maps have relative and absolute height accuracy. The most demanding requirements for a vertical datum come from users wanting to monitor small vertical changes in sea level. They require highly accurate heights in both absolute and relative terms, to enable the detection of small (often sub-centimetre) variations in the height of their monitoring points.

New Zealand currently has vertical datums (levelling traverses) that have high internal relative accuracy due to the tight specifications for differences between levelling runs (Table 2-3). It has been shown in Section 2.5.2 that comparisons between the various vertical datums at first order benchmarks can reach 0.48 m. The majority of this discrepancy is probably due to the different procedures for determining MSL, different observation periods, possible variation in MSL (ie. sea surface topography) and the sub-optimal location of the tide gauges.

From the perspective of using New Zealand's tide gauge data to monitor sea level variations Goring and Bell (1996) are very critical. They state, "To grace the motley collection of tide gauge recorders around the New Zealand coast with the term 'network' is an exaggeration, for it wrongly implies that there is some overall plan for the collection of tidal and sea level data."

If New Zealand is to establish a consistent nationwide vertical datum reliably related to MSL, existing tide gauge recording facilities need to be maintained especially at sites which have been used in the determination of a MSL datum for precise levelling networks. This will allow future determinations of MSL at these tide gauges to be related to earlier determinations, and will allow investigations of long term variations. However, one needs to be able to determine whether a detected change in MSL is in fact due to variation in the sea level or instability of the tide gauge BM. To eliminate (or reduce) the latter, it is desirable to monitor the position of the tide gauge BM by means of changes in absolute gravity, ellipsoidal height, or both.

MSL is not an equipotential surface due to the effects of tides, weather patterns, and location specific features. Each tide gauge is likely to determine MSL as a unique equipotential surface. If an adjustment of all levelling traverses for either the North or South Island is performed holding only one tide gauge BM fixed, non zero MSL heights at the other tide gauge BMs for that island are likely to exist. One has to then decide whether to cope with the fact that the unconstrained tide gauges will have a non-zero height or whether to constrain the height of all tide gauges to zero in an adjustment, thus introducing distortion to the levelling datum which will no longer represent a single physical equipotential surface.

The current vertical datum of the United States of America is the North American Vertical Datum of 1988 (NAVD88), which was realised by a minimum-constraint adjustment of Canadian-Mexican-USA levelling observations, holding fixed the height of one primary tidal benchmark in Quebec, Canada (Zilkoski *et al.* 1992). Therefore, NAVD88 has not been distorted to give zero heights at tide gauge benchmarks. For the USA, the NAVD88 replaced the National Geodetic Vertical Datum of 1929 (NGVD29). NGVD29 was realised by constraining, in the adjustment of Canadian and USA levelling observations, the heights of 26 tide gauge benchmarks in both Canada and the USA. A minimal constraint adjustment of NGVD29 when compared to the constrained adjustment results show differences exceeding 0.5 m (Zilkoski *et al.* 1992).

Another example of a large continental wide vertical datum is that for Australia. The Australian Height Datum of 1971 (AHD) was realised by a constrained adjustment which held fixed 30 tide gauge benchmarks (Roelse *et al.* 1975). The AHD was designed primarily as a mapping datum, though differences between the constrained adjustment and a minimum constraint adjustment are of the order of 1.5 m along the East Australian coast (Morgan, 1992).

The NGVD29 and AHD examples show the magnitude of distortions in the levelling network that result from constraining more than one tide gauge height to zero. The land masses of New Zealand cover a considerably smaller portion of the Earth's surface than either the USA or Australia. New Zealand does have a reasonable geographical extent

(approx. 13° in latitude and longitude) one could expect different tide gauges to experience different sea surface topography (SST) effects. The tide gauges used to determine the MSL around New Zealand have often been located poorly, such as within harbours or river mouths, and consequently realise a MSL on different equipotential surfaces due to these local effects on sea level. The adjustment of levelling data in New Zealand by constraining more than one tide gauge to zero in each island is likely to distort the datum from an equipotential surface, unless this SST is modelled.

Despite the number of stations constrained in the adjustment and the distortion that can be introduced into the datum, both the USA and Australia have a single nationwide vertical datum. This avoids the confusion that can exist in New Zealand, with its multiple vertical datums.

If the SST cannot be modelled, then the MSL height of the tide gauge and corresponding BMs will deviate from the geoid by the magnitude of the SST effect. Consequently, gravimetrically determined geoid heights (Chapter 4) will not be able to convert between orthometric and ellipsoidal heights to better than the magnitude of the SST effect.

If New Zealand is to develop a single national vertical datum then the distortion introduced by constraining different tide gauges to zero is only one of a number of considerations that need to be taken into account. Other considerations include, but are not limited to:

i) whether the national vertical datum should have a known relationship to a global reference system.
ii) which method of conversion between national and regional vertical datum heights should be applied.
iii) which design specifications for precision and accuracy of the national datum heights should be adopted.
iv) what will be the impact on users of changing from (and not changing from) the current regional vertical height datums to a single national vertical datum.
v) what type of height system is to be adopted (See Appendix L for options).

vi) whether to incorporate vertical deformation rates.

For (i), the relationship between a national vertical datum and a global reference system is required and can be achieved by collecting GPS data at BMs which have been assigned heights in terms of the national vertical datum. Once the GPS data has been processed in terms of an ITRF (Section 3.4.1) solution then the relationship between the national vertical datum and a global reference system will be known at these common stations.

Consideration (ii), of converting between old regional datum heights and a national vertical datum, can be addressed by developing transformation parameters (Chapter 5).

The method used to realise the national vertical reference system will be influenced by the consideration (iii), while considerations (iv), (v) and (vi) will dictate the type of reference system adopted. There are a number of different vertical reference systems available, with some being able to detect which direction water will flow due to defining the height in terms of equipotential surfaces, while others are simply mathematical approximations of the Earth. A brief summary of different vertical reference systems that are commonly used in geodesy is contained in Appendix L.

2.5.3.1 Determining the Geoid position

The problem with all the heights commonly used in geodesy (Appendix L), except ellipsoidal height, is that the position of the geoid is not directly measurable.

The geoid has conventionally been determined by observations of MSL at tide gauges, although tide gauges only measure the relative motion between the sea surface and the land. As was discussed earlier in Section 2.5.3, each tide gauge is likely to determine MSL as a unique equipotential surface.

With the advent of Satellite Altimetry, it is possible to measure the instantaneous sea surface with high spatial resolution, as opposed to tide gauges which can measure the instantaneous sea surface with high temporal (but low spatial) resolution. Once the Satellite Altimetry data has had the effects of the open ocean SST removed, there is still

the uncertainty in the geoid position at the coast as the altimeter loses lock near the coast (see Figure 4-16), and therefore is not able to measure the effects of sea bed topography or river discharge.

Combining GPS measurements of the tide gauge position with the tide gauge measurements of the instantaneous sea surface allows the absolute determination of the instantaneous sea surface at the tide gauge. If the satellite altimeter orbits were computed in terms of a GPS reference frame, then the combination of the high spatial resolution satellite altimetry derived geoid, with the high temporal resolution tide gauge determination of the position of the geoid, could result in an improved estimate of the geoid position. However, the effects of coastal sea bed topography and river discharge will remain. Zilkoski *et al.* (1992) report that realistic models to compute the sea surface topography at the tide gauge sites to required accuracy were unavailable in 1992. This still remains the case for most of the world, including New Zealand.

Several techniques for determining a regional vertical datum have been put forward by various authors in recent years (see Groten and Muller, 1990; Rizos et al., 1991; and Vanicek, 1991). The general consensus was that the establishment of a regional vertical datum needs to consider the potential differences derived from a combination of spirit levelling and gravity data, precise altimeter data, and the tide gauge records at primary tide gauge stations, all in a combined adjustment solution (Balasubramania, 1994).

2.5.3.2 Summary

The three dimensional dynamic reference system discussed in Section 2.6 and Chapter 3, is primarily going to be established using GPS data. The heights from processing the GPS data in terms of a global reference frame will be ellipsoidal. As discussed in Appendix L, ellipsoidal heights bear no relationship to the geoid (ie. MSL), which is the surface the general public expects heights to refer to.

Orthometric heights do meet the general requirements for heights and can be determined from ellipsoidal heights if the geoid height is known to sufficient accuracy (see Chapter 4). However, geoid heights are not yet known to sufficient accuracy to combine with ellipsoidal heights and match the spirit levelled heights for high precision projects.

The development of a single New Zealand wide vertical datum is warranted due to the limitations, for general use, of the ellipsoidal height determined as part of the three dimensional dynamic reference system. Any attempt to establish a single national vertical datum for New Zealand, should consider including the potential differences derived from a combination of levelling and gravity data, precise altimeter data, and the tide gauge records at primary tide gauge stations. These data should be combined in an adjustment which is consistent with the development of any scientific global vertical datum, such as that proposed by Rapp and Balasubramania (1992) and the first iteration by Balasubramania (1994).

2.6 Development of the New Zealand Survey System

New Zealand's current cadastral survey methods have ensured that property boundaries move generally in concert with the landowners' assets, and therefore by spatial definition the cadastre is currently dynamic (Grant, 1995). With the establishment of a digital cadastral database (DCDB) in New Zealand coordinates have been assigned to the cadastral boundaries. The current spatial accuracy of the DCDB is not sufficiently high enough to be significantly affected by the dynamics of the cadastre (Grant, 1995). However, with the passing of time and the expected improvement in the spatial accuracy of the cadastral coordinates, the situation will arise that these coordinates will not represent the physical location of the landowners' boundaries and assets. This is, of course, undesirable for both the landowners and the government, as the cadastre is intended to record the landowners rights of the land and avoid litigation over disputed boundaries.

If the coordinates held in a future cadastral survey database are going to become and remain definitive, then the cadastre, and the geodetic datum to which the cadastre is related, need to be able to account for the spatial dynamics of the physical monumentation and landowners' assets. The problems arising from a dynamic digital coordinated cadastre will not be canvassed in this thesis, these matters are canvassed in Grant (1995). This thesis concentrates on the issues affecting the incorporation of

coordinate dynamics into the establishment of a modern geodetic reference system for New Zealand.

Before dynamics can be incorporated into a geodetic datum, it is necessary to determine the quality of the current geodetic datum (NZGD49) and whether or not a new datum needs to be established. In New Zealand, the 1st Order 2000 March 1993 GPS survey was the first campaign undertaken specifically by DOSLI for datum investigations. These datum investigation studies have been continued by DOSLI (and since July 1996, by Land Information New Zealand - LINZ) with further GPS campaigns as summarised in Appendix I. Analysing the results of the March 1993 campaign, Bevin and Hall (1994) have shown that distortions of up to 6.0 m exist in NZGD49.

The study by Bevin and Hall (*ibid.*) was primarily concerned with establishing the magnitude of distortions within NZGD49. However, the March 1993 GPS data provided an opportunity to coordinate the stations occupied in a global dynamic reference system, such as ITRS. Chapter 3 reports on the establishment of coordinates in terms of ITRF93 at the epoch of 1993.200 for these GPS stations.

It is anticipated that a new geodetic datum for New Zealand will be a geocentric reference system tied to ITRS. However, it is still being debated whether or not the reference system will be 'fixed' or 'dynamic' (Grant, 1995). Irrespective of this decision, a velocity model to monitor the motion of the ground marks will be required. This will enable observations collected over several years (Appendix I) to be adjusted in terms of a common epoch.

Any new horizontal, vertical or three dimensional geocentric geodetic reference system should not ignore the fact that points on the surface of the Earth are moving. The general public is likely to assume that coordinates and the associated features are fixed, while in reality the feature changes position while the coordinate remains unchanged. Therefore, it is better to begin educating people about the reality of changing coordinates. The user community should be educated to accept that if coordinates are defined as having an associated date, then conversion to common epochs can be accommodated (where required) by means of kinematic models. If a new geocentric

reference system is fixed rather than dynamic (ie. does not account for crustal movement) then it will slowly become non-geocentric, out of terms with global reference systems and thus degraded. As computer technology is still developing rapidly, there is no reason to doubt that the computational problems of maintaining a dynamic reference system will be quite manageable in the future.

2.7 Summary

New Zealand is located across the active boundary between the Australian and Pacific tectonic plates. This pervasive deformation provides a challenge to the maintenance of a national geodetic datum. The current horizontal geodetic datum (NZGD49) ignores the fact that this deformation is distorting the network. Bevin and Hall (1994) have shown that distortion of up to 6 m is present in NZGD49 due to the original observation and adjustment methods, combined with the deformation effect when compared to the GPS results. LINZ is undertaking GPS campaigns in New Zealand to further investigate NZGD49 distortions and the possible establishment of a new dynamic reference system.

A new GPS derived national reference system would be consistent in the horizontal and vertical but the vertical component would produce ellipsoidal heights. As ellipsoidal heights bear no relationship to the geoid, it was argued that a consistent orthometric height datum should also be established for New Zealand. This new vertical datum would replace New Zealand's current collection of individual datums.

The establishment of a single nationwide vertical datum, based on orthometric heights, will still result in users of the GPS technology wanting to be able to convert their ellipsoidal heights into orthometric heights. For this conversion the geoid height is required. Investigations into the determination of the geoid height for New Zealand are contained in Chapter 4.

As part of the investigations into the possible establishment of a dynamic reference system for New Zealand, the data from the GPS campaign used by Bevin and Hall (1994) was processed in terms of the dynamic ITRF. Discussion on processing this data and results are contained in Chapter 3.

Chapter 3

Dynamic Coordinates for New Zealand from GPS data

3.1 Introduction

New Zealand's original, and only, national geodetic datum, New Zealand Geodetic Datum 1949 (NZGD49) is the result of terrestrial geodetic surveys undertaken from 1930 to 1946. A full description on NZGD49 can be found in Lee (1978) which was summarised in Section 2.4.2. Since the time of these surveys, the land mass of New Zealand has continued to be subjected to earth deformation, primarily a result of the collision between the Pacific and Australian tectonic plates, which has a rate of about 50 mm/yr (Section 2.2). It can therefore be expected that between 1949 and 1995 there will have been deformation of up to 2.5 m between the east coast and the west coasts of New Zealand.

The NZGD49 coordinates, which form the datum for cadastral surveys in New Zealand, have been held fixed at the values determined in 1949. Due to the improvement in the accuracy and precision of survey techniques and the continued deformation of the New Zealand crust, surveys carried out today do not fit with the coordinates of the primary NZGD49 stations. When NZGD49 is replaced, the new reference system should attempt to take into account the effects of earth deformation (ie. have a velocity model), to ensure that large step changes are infrequent in the case of a static reference system, and in the case of a dynamic reference system the velocity model will be an integral part of the whole reference system definition (Section 2.6).

This chapter will look at the role GPS can play in providing coordinates for stations in New Zealand. These coordinates are in terms of the global dynamic reference system, ITRS (International Earth Rotation Service (IERS) Terrestrial Reference System). A summary will be presented of ITRF93 coordinates obtained by processing, using the

GAMIT / GLOBK software suite, a set of nationwide GPS data collected by the Department of Survey and Land Information (DOSLI) in March 1993.

The results and discussions presented in this chapter are an extension to those contained in Pearse and Morgan (1995) and Morgan *et al.* (1996). These two references should be consulted for general information on the processing of the GPS data in the GAMIT/ GLOBK software suite, while this chapter will describe details of the NZ GPS data (Section 3.2) and processing (Section 3.5).

As the GPS theory and technology is now well advanced there is numerous literature available to the reader requiring comprehensive details on GPS. Therefore it is not necessary to provide a detailed description of GPS in this thesis. Readers requiring further details are directed to one of the following texts (which is not intended to be a comprehensive list): King *et al.*(1985), Wells *et al.* (1986), Seeber (1993) or Kaplan (1996). Another useful source of information is Morgan *et al.* (1996).

3.2 New Zealand GPS data

In March 1993 DOSLI undertook a 13 day GPS campaign across New Zealand. The GPS network was designed for the six Ashtech LM-XII GPS receivers, which DOSLI had available at the time of the campaign. The network design was influenced, firstly by the requirement to occupy at least one first or second order station (Table 2-1) in each of the 28 meridional circuits (Section 2.4.1), which also had relatively easy access. The second influence was the intended GPS post processing software, the Ashtech proprietary software GPPS, that DOSLI had available in early 1993. GPPS's main restriction was that a 24 hour data session could not be processed unless broken into sub-sessions where at least one satellite was present for the entire sub-session. Thus the observations were chosen to consist of two four-hour sessions per day.

For the period 8th through 20th March (DOY 067 to 079), 1993, the best satellite constellations for two four-hour observation sessions was from 0700 to 1100 and 1200 to 1600 Coordinated Universal Time (UTC) (Figure 3-4). This nine hour time span

(0700-1600) in terms of New Zealand local summer time (UTC + 13 hours) was from 2000 to 0500. Thus GPS observations could be taken during, what was considered to be, the more stable ionospheric conditions of the evening and early morning, allowing the transportation of the GPS equipment during the daylight hours.

Three New Zealand fiducial sites were chosen to form the common sites between observation sessions. These local fiducial sites were Whangaparaoa (D045) in the Auckland area, Three Sisters (D474) near Invercargill and Heaphy House (WELL = D475) in Wellington (Figure 3-1). As the four roving receivers were moved each day to new sites in the South Island, the two local fiducial sites D474 and WELL were operated. When the roving receivers were in the North Island, the local fiducial sites D045 and WELL were operated. The local fiducial sites were operated continually throughout the nine hours of observing each day (0700 to 1600 UTC). The four new sites for each day were operated for the first four hours (0700 to 1100 UTC) after which they were switched off for an hour, during which time the antenna was set up at a new height. They were then switched on for the second four hour session (1200 to 1600 UTC). The reason for altering the antenna height was to try to detect incorrect height of instrument measurements through having a second occupation at each site. The procedure of altering the antenna height was also adopted in the 'TREX' campaigns in Southern California but has subsequently been abandoned (Peter Morgan, pers. comm., 1996). The altering of the antenna height created some processing problems in the GAMIT software (Section 3.5.1). It is no longer the recommended procedure (see Appendix I). Another problem associated with the switching off the receiver is that the clock characteristics had to be re-established.

For the original design of the March 1993 campaign, the reader is directed to Bevin and Hall (1994). These authors processed the data in Ashtech's GPPS software for the purpose of detecting distortions in NZGD49 rather than establishing a set of dynamic coordinates. A summary of the GPS data available from the March 1993 New Zealand observation campaign is contained in Appendix A.

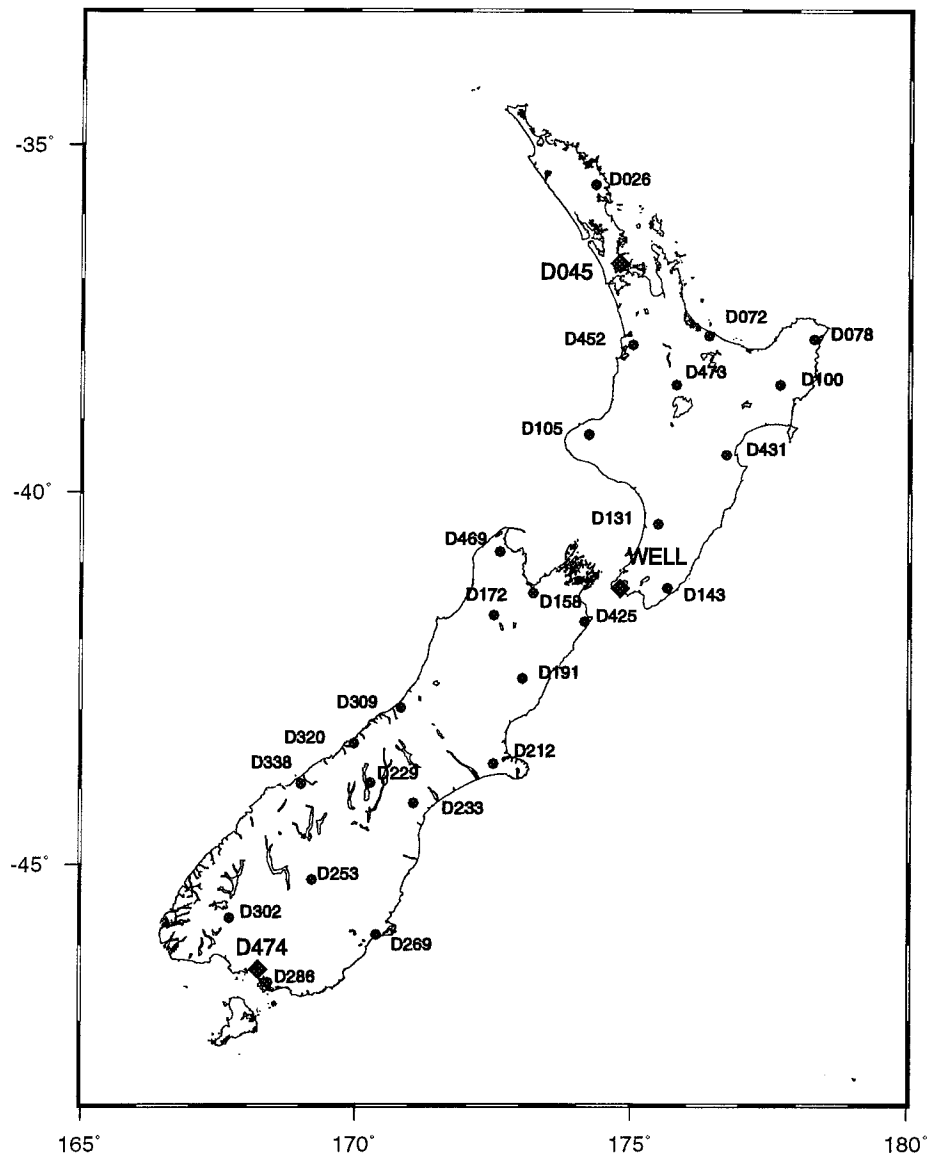

Figure 3 - 1 : Distribution of New Zealand GPS sites having data available for processing in GAMIT from the March 1993 Campaign. The 3 local fiducial sites (D045, D474 and WELL) are shown as diamonds, while the local sites are shown as circles. The following sites also had receivers on eccentric marks: at WELL was D482, D483 and D485; at D072 was D484; and at D473 was D481. Mercator projection drawn using GMT (Wessel and Smith, 1991).

Due to the remoteness of most of the sites, field processing of the data was not able to be undertaken to verify the quality of the data being collected each day. The data was therefore posted to DOSLI's Geodetic Branch in Wellington for rapid quality control processing. With delays in getting the data to a Post Office and the mail delivery time, it was normally about a week before all the data from one day's observations could be

processed with GPPS to check the quality. As a result of the delay in receiving the data at the central site and the logistics of distributing replacement receivers to the remote sites, it was ten days before one faulty receiver (alias Ashtech number 4) was replaced.

Unfortunately none of the data collected by the Ashtech number 4 receiver was able to be processed due to the poor quality of the data. Section 3.5.3.1 outlines the unsuccessful processing of this data in GAMIT, with graphical examples of the data given in Appendix E. The replacement receiver was a Leica Wild GPS-System 200. However, at the time of the campaign no data from a Leica receiver had been processed in the Ashtech GPPS software by DOSLI. Therefore a second Leica receiver was set up eccentric to the WELL site and operated for the last three days of the campaign as a base site for the roving Leica receiver. Subsequently it was established that the Leica data was able to be combined with the Ashtech data and processed successfully in GPPS. This is also the case for processing in the GAMIT / GLOBK software suite (see Appendix D).

On day 069 the receiver (alias Ashtech number 1) which was stationed at WELL for the entire campaign, had a poor signal to noise ratio detected for all satellites. The pre-amp was replaced before observations began on day 070. Unfortunately none of the data collected by the Ashtech number 1 receiver was able to be processed for DOY 067, 068 or 069 (Section 3.5.3.1).

At the time of the campaign, the GPS constellation consisted of a total of 22 operational satellites, consisting of 4 Block I satellites (PRN 03, 11, 12, 13) and 18 Block II satellites (PRN 01, 02, 14 to 29), all of which were observed.

The data from the Ashtech receivers were converted from the Ashtech format to RINEX (Receiver Independent Exchange Format) using the Ashtech software, ASHTORIN. The Leica data was converted to RINEX using the conversion module in the Leica SKI software. This RINEX data was then imported into the GAMIT software for processing (Section 3.5).

3.3 Global GPS data

The GAMIT software used to process the GPS data (Section 3.5) allows the estimation of three-dimensional relative positions of ground stations and satellite orbits for each session, normally 24 hours. For the estimation of satellite orbits, the network of GPS sites needs to cover a significant portion of the earth's surface, ideally the whole globe. The New Zealand network alone was too small so additional GPS data from four sites, one in Tahiti (PAMA), two in Australia (DS42, HOB1) and one in Antarctica (MCMU), were included to give a coverage of about 1/12 of the earth's surface (Figure 3-2). These four additional sites, referred to as regional fiducial sites, allowed for orbit estimation in the processing of the New Zealand data (Section 3.5). Additionally and perhaps more importantly, they also enable the New Zealand network to be correctly placed in terms of the global reference frame thereby overcoming all relative and origin issues. The raw RINEX data for the four additional New Zealand regional fiducial GPS sites was obtained from CDDIS, which is one of the global data centres of IGS (International GPS Service for Geodynamics, refer Section 3.4.2).

GAMIT is essentially a relative processing system dependant on *a priori* values for station coordinates and earth rotation parameters as well as the mode of defining the geocentre. These dependencies are controlled or solved by referencing the GAMIT solution to an external framework. The most efficient way to establish the origin is to adjust the daily GAMIT solutions (generated in a loosely constrained system where the network strength is maintained) together in GLOBK where the coordinates of stable reference frame sites are constrained.

The attachment process requires at least one station, though in order to minimise errors at this single attachment station it is usual for 3 or 4 stations to be used (Morgan *et al.*, 1996). To attach the New Zealand network (Figure 3-1) to an ITRF, the closest IGS core site (Table 3-3) of DS42 was included in the daily New Zealand GAMIT solutions, along with the MCMU and PAMA sites, which form part of the Scripps Institution of Oceanography (SIO) global daily solution. Since these stations were adjusted simultaneously with the IGS core stations they can be assumed to be in the same system but with increased uncertainty. The Cooperative International GPS Network (CIGNET)

site at Hobart (HOB1) was also included to increase the regional network strength, through the additional double difference observations between the New Zealand regional fiducial sites, local fiducial sites and local sites.

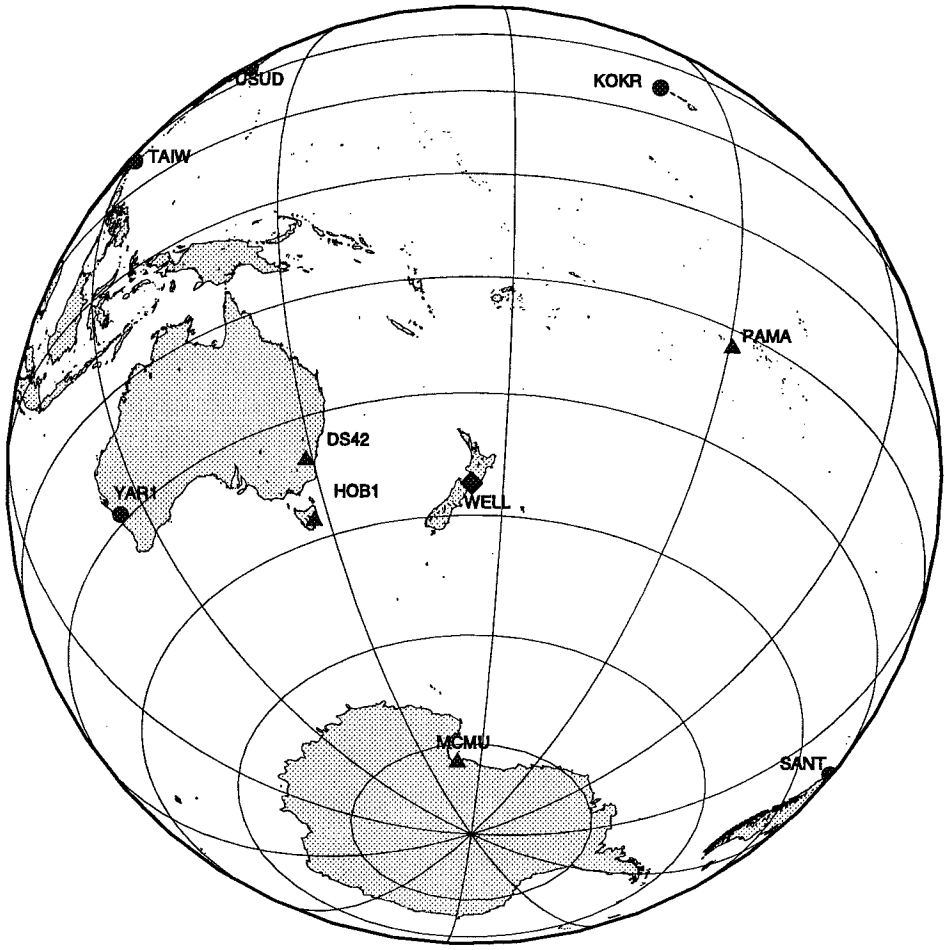

Figure 3 - 2 : The four regional fiducial sites, shown with triangles (PAMA, DS42, HOB1 and MCMU), needed to allow orbit estimation and attachment to the global reference frame for the March 1993 campaign. The sites shown with circles form part of the SIO global network of GPS sites, while WELL (the diamond) is a local fiducial site. Orthographic Azimuthal projection drawn using GMT (Wessel and Smith, 1991).

As daily global GAMIT solution files, which included all 13 core IGS sites plus additional global GPS sites (Figure 3-3), were available from SIO, this global framework was used to attach the New Zealand network to an ITRF realisation. The data for these

additional Global GPS sites from SIO were not in the RINEX format but in the processed GAMIT output H-file format, and as such were combined with the New Zealand regional network during the network adjustment using GLOBK (Section 3.5.2).

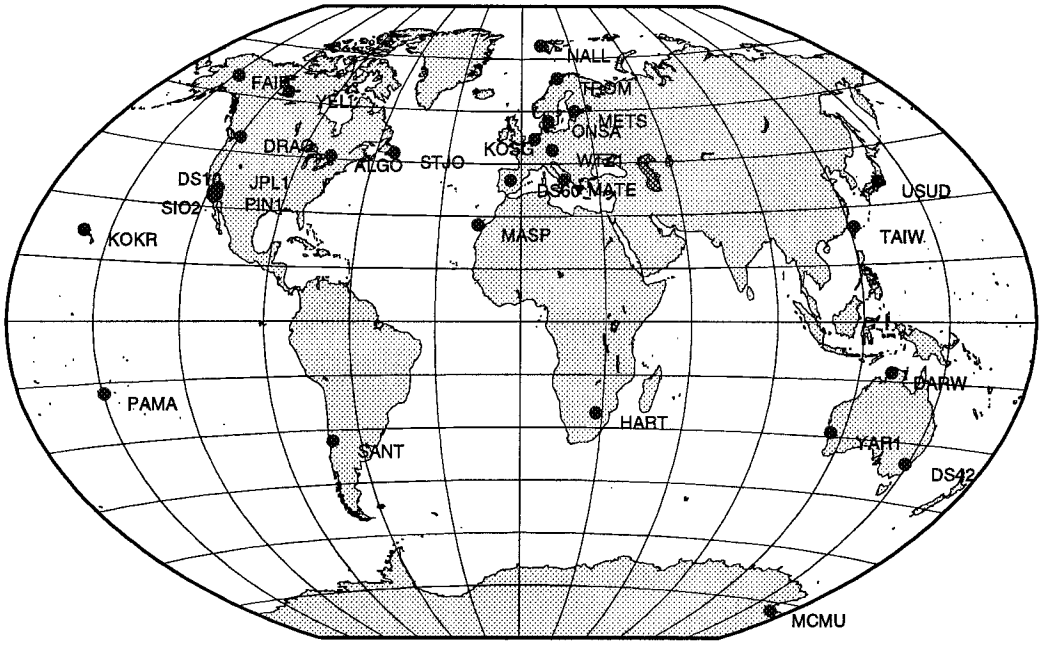

Figure 3 - 3 : Distribution of SIO's global network of GPS stations at 1993, which include the 13 core IGS stations. Notice the bias towards northern hemisphere stations. Winkel Tripel projection drawn using GMT (Wessel and Smith, 1991).

3.4 International Terrestrial Reference Frame Coordinates

The determination and maintenance of a Conventional Terrestrial Reference System (CTRS) (Section 5.2.2) requires extensive collaboration between different international organisations operating various high-precision techniques in space geodesy. In order to coordinate the work of the various international organisations, a central organisation has been established, which currently is the International Earth Rotation Service (IERS). Section 3.4.1 summarises the work of IERS in determining and maintaining a CTRS. With the rapid rise in the use of GPS for geodynamic studies a separate organisation has been established to coordinate global GPS activities and is called the International GPS

Service for Geodynamics (IGS). A brief summary of IGS activities to assist in maintaining a CTRS is contained in Section 3.4.2.

Neither Section 3.4.1 nor 3.4.2 are intended to be a comprehensive description of all the activities performed by IERS and IGS. They merely provide an outline of the necessary information required in subsequent sections of this thesis to understand how the New Zealand GPS data has been coordinated in terms of a CTRS. Detailed information is given in the annual reports of each organisation and the special publications of each service. These two summary sub-sections were compiled from IERS (1996) and Zumberge *et al.* (1995), respectively.

With the extensive use of GPS, a commonly used realisation of a CTRS is that of WGS84. This CTRS is different from the ITRF series and must not be confused with it. Section 3.4.3 outlines briefly the WGS84 reference frame, which is maintained primarily to support the US Department of Defense use of GPS for navigation.

Transformation parameters required to convert between ITRF and WGS84 realisations are included in Section 5.4.1.

3.4.1 International Earth Rotation Service (IERS)

IERS was established during 1987 by the International Astronomical Union (IAU) and the International Union of Geodesy and Geophysics (IUGG). IERS commenced operation on January 1, 1988. The IERS centralised the distinct and different services offered by the International Polar Motion Service (IPMS) and the Earth Rotation Section of the Bureau International de l'Heure (BIH) (Yokoyama, 1991).

One of the responsibilities of IERS is the definition and maintenance of a CTRS, based on observing stations that use high-precision techniques in space geodesy (IERS, 1996). The CTRS maintained by the IERS is known as the IERS Terrestrial Reference System (ITRS). Since 1988, IERS has realised the ITRS by producing a yearly set of global coordinates and velocities (ie. X, Y, Z, $\dot{X}$, $\dot{Y}$, $\dot{Z}$). These coordinates are obtained by

combining various SLR, LLR, VLBI and more recently DORIS and GPS solutions to obtain an IERS International Terrestrial Reference Frame (ITRF) which is qualified by a year (for example: ITRF88 and ITRF89).

For each space geodetic technique (ie. SLR, LLR, VLBI, DORIS and GPS; see Seeber, 1993) there are a number of analysis centres around the world. These process the data using their own choice of software but comply with the standard reference system as defined by the IERS Standards (McCarthy 1989, 1992, and 1996). These individual realisations are adjusted by IERS Terrestrial Frame Section (ITFS), using a least-squares technique, to obtain station coordinates and an associated velocity field at an epoch. The reference epoch varies between ITRF solutions, though it is common for a second set of coordinates and velocities to be defined for each ITRF at the epoch of 1988.0.

Prior to ITRF91, no velocity field had been derived so the AMO-2 model (Minister and Jordan, 1978) was used to account for the time evolution of ITRS. ITRF91 was the first realisation of ITRS to derive a global velocity field by combining site velocities estimated by SLR and VLBI analysis centres (Boucher and Altamimi, 1993). To ensure the condition of no-net-rotation of ITRS with respect to the earth's crust, NNR-NUVEL1 (DeMets *et al.*, 1990) was selected as the reference motion model of ITRF92. For ITRF93 the more recent geophysical reference motion model, NNR-NUVEL1A (DeMets *et al.*, 1994) was used instead of NNR-NUVEL1. This was due to the recent re-calibration of the geomagnetic time scale which resulted in the two NUVEL models being different by a factor of 0.9562. NNR-NUVEL1A, like NNR-NUVEL1, is a horizontal motion model only. For consistency of the three-dimensional nature of ITRS, the vertical velocity is set to zero with an assumed error of 1 cm/year (Boucher *et al.*, 1994). Further details on specific ITRF solutions are given in the appropriate IERS technical notes (ie. for ITRF93 refer Boucher *et al.* 1994).

For the determination of a station's position in an ITRF, the station is assigned to a specific tectonic plate. The point position of the station at time, t, on the surface of the solid earth is given by McCarthy (1996) as:

$$\vec{X}(t) = \vec{X}_o + \vec{V}_o(t - t_o) + \sum_i \Delta\vec{X}_i(t) \qquad (3.1)$$

where

$\Delta\vec{X}_i$ = corrections due to various time changing effects, ie. residual solid Earth tide displacement, ocean loading, post glacial rebound and atmospheric loading. These effects are assumed to be zero in this research due to both their periodic nature and the level of modelling adopted in GAMIT.

$\vec{X}_o$ = position at epoch t_o .

$\vec{V}_o$ = velocity at epoch t_o .

t_o = initial reference epoch (ie. 1988.0).

New Zealand's ITRF92 station Wellington (WELL) is assigned to the Australian plate (Boucher *et al.*, 1993) but is clearly not consistent with this assumption (Morgan *et al.*, 1996). The Wellington station, like most of New Zealand, is located within the deforming zone between the Australian and Pacific tectonic plates (Section 2.2). Assigning Wellington to either plate is likely to be incorrect, as shown by Morgan *et al.* (*ibid.*). Current ITRF's accommodate the horizontal velocity of sites on plate boundaries by assigning a larger *a priori* standard deviation (10 cm/year) to the site's velocity than for sites located on the rigid part of a tectonic plate (3 mm/year) (Boucher *et al.*, 1994). Therefore to improve the reliability of a New Zealand station's connection to an ITRF solution when processing multiple campaigns, a specific plate motion or earth deformation model for New Zealand needs to be developed.

However, as the March 1993 New Zealand GPS campaign only spanned 13 days and coordinates were determined at the mid-observation epoch of 1993.200, reliable velocity estimates were required only for those ITRF sites used to attach the New Zealand network to ITRF93. Additionally, the attachment to sites such as PAMA and DS42 on rigid tectonic plate interiors ensures the correct placement of the New Zealand epoch solution without reference to WELL.

3.4.2 International GPS Service for Geodynamics (IGS)

The International GPS Service for Geodynamics (IGS) began formal operation on January 1, 1994. This formal operation followed testing and pilot phases that commenced in June 1992 and formal establishment of IGS in 1993 by the International Association of Geodesy (IAG). IGS, like IERS, is a member of the Federation of Astronomical and Geophysical Data Analysis Services (FAGS) and it operates in close

cooperation with IERS. This brief history on the establishment of IGS and the following extracts of IGS operations were obtained from Zumberge *et al.* (1995).

The primary objective of IGS is to provide a service to support, through GPS data products, geodetic and geophysical research activities. To help meet this objective IGS collects, archives and distributes GPS observational and product data sets from a broad spectrum of international GPS activity. To enable the successful and timely delivery of these products IGS has a number of components which include data collection, archive and analysis centres.

The data provided by IGS and IERS and their close cooperation greatly facilitated the determination of ITRF coordinates for New Zealand sites (Section 3.5). This was primarily because SIO is an analysis and data collection centre for IGS. Therefore SIO, through IGS, deduces coordinates and velocities for the 13 core IGS sites which are supplied to IERS. The SIO GPS realisation of an ITRF is combined with other IGS analysis centres realisations, which are then analysed by IERS along with the SLR, LLR, VLBI and DORIS data. This analysis by IERS provides a check on how well GPS realisations of an ITRF compare with other high-precision techniques in space geodesy. The SIO daily global GAMIT solutions, which were considered by IERS as part of their realisation of the ITRF, were available for the period of the New Zealand campaign. Their adjustment with the daily GAMIT solutions for local New Zealand network provided an efficient and consistent connection to the chosen ITRF (Section 3.5.2).

3.4.3 World Geodetic System 1984 (WGS84)

The United States Defense Mapping Agency (DMA) has been involved in the development of World Geodetic Systems since 1960. The World Geodetic System that was established in 1984 (WGS84) used Doppler data from the US Navy Navigation Satellite System (NNSS). WGS84 was primarily developed to support the US DMA's mapping, charting and geodetic products and includes in its definition a geocentric coordinate system, a reference ellipsoid, a consistent set of fundamental constants, and an Earth Gravitational Model and associated global geoid (DMA, 1991).

The WGS84 reference frame constitutes a mean or standard earth rotating at a constant rate around a mean pole of rotation fixed in time. Its origin is at the earth's centre of mass, and the axes are coincident with the Conventional Terrestrial System as defined by BIH for the epoch of 1984.0. The fundamental parameters and reference ellipsoid of WGS84 are the same as the IUGG's defined Geodetic Reference System 1980 (GRS80), as described by Moritz (1980a), except for one parameter, $\overline{C}_2$. WGS84 defines the normalised second degree zonal harmonic coefficient of gravitational potential constant, $\overline{C}_2$ (= $-J_2/\sqrt{5}$), instead of the dynamical form factor, J_2, of GRS80. The indirect use of $\sqrt{5}$ thus introduced a truncated difference (after the eighth digit) in the flattening, *f*, for the WGS84 ellipsoid from the *f* of GRS80 ellipsoid (Kumar, 1993). DMA (1991) gives the full list of adopted constants for WGS84, while further information on GRS80 is given in Section 4.2.1.

The WGS84 reference frame, now over a decade old, was designed only to have an accuracy of 1-2 metres (1 sigma), which is more than adequate even for large scale mapping (DMA 1991). However recent geodetic requirements of the Department of Defense (DoD) has required accuracy at the decimetre level. By comparing the four defining parameters (*a*, GM, J_2 and ω; Section 5.2.3) of WGS84 with the more recently adopted scientific community values of IERS (McCarthy, 1992), it was established that the GM value was the only parameter warranting revision. The main reason for updating the original WGS84 GM value was to reduce the 1.3 metre radial error (bias) in all DoD GPS orbit fits. The GM value of the IERS standards was adopted as the new WGS84 GM (Malys and Slater, 1994).

At the time of redefining the GM parameter for WGS84, the coordinates of the five Air Force and five DMA GPS monitor stations were updated. This was achieved by simultaneously processing GPS data from the Air Force, DMA and selected IGS sites during the 1992 global IGS campaign. The adjustment of these Air Force and DMA sites was performed while constraining a selection of the IGS sites to their ITRF91 values. This resulted in a new realisation of WGS84 through the adoption of new coordinates for the 10 DoD GPS tracking stations. The new realisation of WGS84 is reported by Swift (1994) to be coincident with ITRF91 at the order of 10 cm. This

refined WGS84 reference frame, along with the improved GM value, have been given the designation WGS84 (G730), and was placed into DMA's orbit processing from the first day of GPS week 730 which corresponds to 2 January 1994 (Malys and Slater, 1994).

3.5 GPS data processing with the GAMIT / GLOBK suite

The processing of the GPS data reported in this thesis used the GAMIT component of the suite (Section 3.5.1) to generate daily solutions. These daily solutions were then combined to obtain the final station coordinates in terms of ITRF93 by using the GLOBK component (Section 3.5.2).

The March 1993 New Zealand GPS data was processed using strategies consistent with those of Morgan *et al.* (1996). This led to the data being incorporated with the work of Morgan *et al.* (*ibid.*) and resulted in coordinates being published in terms of ITRF92 at the epoch of 1994.0, in accordance with their contract with the Inter-governmental Committee on Surveying and Mapping (ICSM). However during the time the New Zealand data was being processed ITRF93 was established and it was decided that it was more appropriate to determine coordinates in terms of this new reference frame at the mean observation epoch of 1993.2 (DOY 073). A summary of this determination of ITRF93 coordinates has been reported by Pearse and Morgan (1995).

The following sub-sections contain a detailed description of how the results reported by Pearse and Morgan (*ibid.*) were generated and the necessary variations to the strategies of Morgan *et al.* (*ibid.*) due to the nature of the New Zealand data.

3.5.1 GAMIT processing of daily solutions

The GAMIT software (King and Bock, 1994) is a comprehensive GPS analysis package, jointly developed at the Massachusetts Institute of Technology (MIT) and Scripps Institution of Oceanography (SIO), University of California at San Diego. This suite of software was used to compute the daily network solutions reported in this thesis.

When the processing of New Zealand data began in GAMIT, the associated daily solution adjustment software GLOBK, ver. 3.0 (Section 3.5.2), did not allow the adjustment of multiple occupations of the one station in a 24 hour period, if the heights of the antenna varied. This unfortunately meant that the initial processing in GAMIT had to be done using two sessions per day. As satellite orbits, which need as long a span of data as possible, were being estimated, the cutting of the 24 hour global data sets into approximately two, 12 hour sessions, was less than ideal. Figure 3-4a shows the splitting of the data with two sessions per day for processing. This method was aimed at combining the solutions from the two sessions using GAMIT, but required three GAMIT runs. One run was required for each of the sessions and the third run joined the sessions. Days 067, 070 and 078 were processed as 2 sessions.

In the release of GLOBK version 3.2 a new feature to account for sites affected by an earthquake was included. This earthquake file appeared to allow sites to be renamed in the same session and for the height of the receiver to change. Thus the remaining 10 days were processed in GAMIT as single 24 hour sessions. The second session of a site in New Zealand was given a new name in GAMIT. For example, D309 was called E309 for the second session. Figure 3-4b shows the continuous data within one session and two names for each local site. This method required only one GAMIT run and meant no observations were broken during the days observations, resulting in longer data spans which increased cycle-slip detection and strengthened the orbit estimation. However, during the adjustment of the data in GLOBK, it was discovered that the earthquake file could only be used with separate session data. To overcome the problem of joining the two sets of local site coordinates the GLORG option of GLOBK was used (Section 3.5.2).

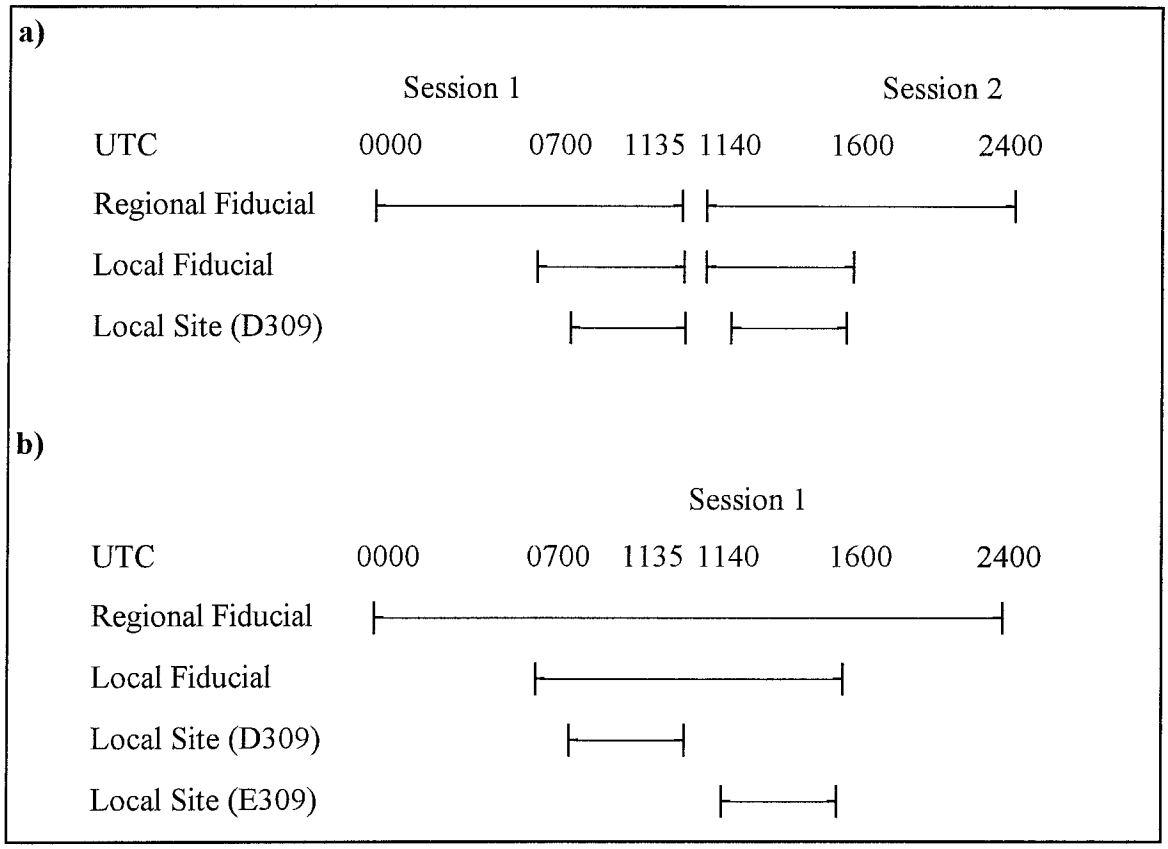

Figure 3 - 4 : The different methods for processing the data in GAMIT. a) has two sessions with the Regional and Local Fiducial data being split. b) has one session with no splitting of the observed data. Examples of sites for each category are :- Regional Fiducial = DS42, MCMU; Local Fiducial = WELL, D045, D474; Local Site = D072, D309, E309.

During the processing of the GPS data, GAMIT's automatic data editing module (AUTCLN) was developed to an operational level. Initially, days were processed using SINCLN, which operates on one-way residuals. AUTCLN operates on both single and double differenced residuals. AUTCLN is able to detect cycle slips and questionable data more reliably than SINCLN, due to its use of all combinations of the available phase and pseudo-range data. The use of AUTCLN in the processing of the data significantly reduced the amount of time required to manually edit cycle slips in the data using CVIEW. This meant that it became possible to generate a list of the worst cycle slips, rather than searching all combinations producing double difference observations to find the cycle slips.

CVIEW is the interactive editing module of GAMIT. CVIEW can display on the screen almost all combinations of phase and pseudo-range residuals, as well as showing clock

behaviour and satellite sky tracks. The main feature of CVIEW is that it allows interactive editing of data. That is cycle slips can be repaired and questionable data unweighted. The combinations of data primarily used to edit the data were:

L1 = L1 phase or carrier beat phase of the 1575.42 MHz signal (f1)

L2 = L2 phase or carrier beat phase of the 1227.60 MHz signal (f2)

LC = Ionospheric free combination = L3 = 2.546 L1 - 1.984 L2

LG = Geometry free combination = L4 = L2 - 0.779 L1

WL = Wide-lane combination = L2 - L1 + (P1 + P2)(f1 - f2)/(f1 + f2),
where P1 and P2 are the precise (P-code) pseudo-range of both the GPS frequencies, f1 and f2 respectively.

The LC combination has the benefit of almost completely eliminating the effects of the ionosphere for long baselines but results in an increase in the effect of other error sources (ie. a larger noise on the generated signal since adding noise : $\sqrt{(2.546\,L1)^2 + (1.984\,L2)^2}$). The LG combination cancels all the geometrical and other non-dispersive delays (ie. tropospheric) so leaving the ionospheric variations. The WL combination has the advantage, if the P-code is available, of determining the difference in integer ambiguities for L1 and L2, as it is free of both ionospheric and geometric effects.

Examples of various combinations of the available GPS signal with real data are contained in Appendix E, along with discussion of the features displayed in the data. The examples are in the form of CVIEW plots, which show the L1, L2, LC, LG and WL combinations for a selection of sites and satellites.

Days 067 and 070 were cleaned using SINCLN, while days 068, 069 and 071 - 079 were cleaned using AUTCLN. However, for all days, all combinations of double difference observations were checked in CVIEW manually to ensure no cycle slips or questionable data remained. The manual editing also removed any small segments of data, usually less than 10 minutes, that either preceded or followed the main data. This is now part of the AUTCLN process. The rationale for removing this data was that there was no strength in such data sets as a new bias flag was needed.

The data on DOY 067 for DS42, HOB1, MCMU and PAMA to satellite PRN 25 shows that WL is available, due to all four sites having Rogue receivers, which can track the P-code (Figures E-2 through E-7). It is interesting to note that the standard deviation on the WL for the DS42 and HOB1 receivers is approximately 75% and 30% that of the MCMU and PAMA receivers, respectively. This is probably due to the DS42 and HOB1 receivers having lower internal noise levels and experiencing lower tropospheric and ionospheric effects at these sites during this period. The major effect is probably due to the ionosphere (Figure E-6). When the standard deviation of the LG combination is compared at the plot scale, the DS42, HOB1 and PAMA data is smooth. This indicates very small ionospheric delay for these three sites when compared to the significantly noisier LG data at MCMU (Figure E-6).

When a receiver is performing poorly, it can become very obvious in the CVIEW plots. Appendix E also contains examples of the Ashtech receivers that were operating at D253, D269, D474 and WELL on DOY 067. One can clearly see that data from D269 (Figure E-10) and WELL (Figure E-12) have larger noise in comparison to the data at D474 (Figure E-8) and D253 (Figure E-9). The data from D474 and D253 are more typical of other Ashtech and Leica receivers that were operated during the March 1993 New Zealand GPS campaign.

The strategy adopted while cleaning the data was to constrain the size of the adjustments to the *a priori* coordinates of the sites and satellites, at a precision level to which the sites were considered known in a relative sense. The site constraints used are shown in Table 3-1, and were obtained from Morgan *et al.* (1996) experience which suggests that the constraints should be an order of magnitude larger than the formal errors from the GLOBK output.

Site Code	Name	Latitude (m)	Longitude (m)	Radius (m)
DS42	Tidbinbilla (Canberra) [1]	0.020	0.020	0.100
WELL	Wellington CIGNET [2]	0.050	0.050	0.200
HOB1	Hobart CIGNET [2]	0.050	0.050	0.500
MCMU	Mc Murdo [3]	0.250	0.250	0.250
PAMA	Tahiti [3]	0.250	0.250	0.250
Dxxx	New site in NZ	100.0	100.0	100.0

Table 3 - 1 : *A priori* coordinate constraints used in GAMIT. Notes: [1] - best knowledge due to being an IGS core site; [2] - reliably connected to global frame; [3] - poorly connected to global frame.

The IGS core site, DS42, was considered to be known the best, while the new local sites in New Zealand were known least. *A priori* coordinates for the New Zealand sites, Dxxx, were taken from the results obtained by Bevin and Hall (1994) through processing the GPS data in the Ashtech GPPS software and converted from WGS84 to ITRF92 using the transformation parameters of IERS as described in Section 5.4.1. Transformation was to ITRF92 as ITRF93 had not been established when processing began. Due to the small difference between ITRF92 and ITRF93 (refer Table 5-2) these coordinates were still suitable as *a priori* values considering the size of the *a priori* constraints.

The constraints on the Keplerian *a priori* orbital errors and force parameters are shown in Table 3-2. The *a priori* satellite positions were obtained from SIO solutions for each day. These solutions are generated by SIO through processing a global network of GPS sites that have well determined coordinates from which high quality satellite orbits can be determined (Figure 3-3). As local orbits were being generated the SIO orbits only provided a more reliable *a priori* orbit, thus saving one iteration in GAMIT. This would otherwise have been required if the lower quality broadcast orbits had been used. When undertaking a local survey of (say) less than 250 km in extent, the SIO orbits would be held fixed, as the local network would not have sufficient strength to solve the coordinates of the satellite orbit.

Keplerian *a priori* orbital errors (ppm)					
Semi-axis	Eccentricity	Inclination	Ascending Node	Perigee	Mean Anomaly
5.0	5.0	5.0	5.0	5.0	5.0
Force Parameters (%)					
Solar Radiation Force 1 (x)		Solar Radiation Force 2 (y)		Solar Radiation Force 3 (z)	
10.0		0.01		0.01	

Table 3 - 2 : *A priori* satellite orbit constraints.

The data in the New Zealand regional solution was processed at an interval of 30 seconds and a satellite cut-off elevation of 15 degrees above the horizon.

The following models and default constants were used in GAMIT for the meteorological parameters:

Atmospheric propagation delay model

Dry and Wet Zenith delay : Saastamoinen (1972)

Dry and Wet mapping function : CfA-2.2 (Davis *et al.*, 1985)

Default Meteorological data

Pressure : 1013.25 mbars

Temperature : 20.0° C

Humidity : 50.0 %

Clock modelling (KLOCK) : option 3, which estimates the receiver clock offset epoch-by-epoch using the pseudo-range, was used for all receivers. However, the Leica receiver keeps its clock synchronised with the GPS time, so option 1 could have been used as this assumes zero offset, though the difference between the clock models is negligible at the level.

GAMIT release 9.28 has an Antenna Phase Centre variation modelling option. This option was in the development stage when processing the March 1993 GPS data, so was not incorporated. The modelling of the antenna phase centre variation is likely to improve results and should be investigated in future data processing. Additional improvements to GAMIT since the data was processed include full Earth and Ocean Tide Loading models, improved orbit modelling by including once per revolution terms

and the fixing of small but important satellite elevation effects, and stochastic atmospheres.

The GAMIT manual describes weighted constraints as a way of taking account of ionospheric effects so that for short baselines the algorithm uses L1 and L2 independently, while for long baselines the algorithm uses the linear combination, LC. The processing of the NZ data used the LC option for all baselines irrespective of the baseline length. This was primarily necessitated by the need to have baselines in excess of 200 kms to network the local sites (Dxxx) to the local fiducial stations (D045, D474, WELL).

The results from processing a day of GPS data in GAMIT are in the form of vectors from the Earth's centre of mass to the stations and satellites, along with the associated covariance matrix. The actual parameters solved for in GAMIT were :

i) The three components of the station vector, (X,Y,Z)
ii) One 24 hour mean zenith delay parameter for each site
iii) The six conventional components of the satellite state vector (X, Y, Z, $\dot{X}$, $\dot{Y}$, $\dot{Z}$)
iv) Three non-gravitational corrections to the satellite state vector
v) Biases (cycle slips) as appropriate
vi) estimates of the integer phase ambiguities

GAMIT release 9.28 did not have the capability to solve for more than the one 24 hour mean zenith delay parameter for each site. The zenith delay parameter is used to account for tropospheric errors. More recent GAMIT releases now support multiple zenith delay parameters per site, and therefore for future processing it is recommended that multiple zenith delay parameters be solved for at each site (ie. every 2 hours solve for a new mean zenith delay parameter). These extra zenith delay parameters are likely to improve the results, especially in the height component.

The daily GAMIT solutions then need to be adjusted together using GLOBK. As a final step in GAMIT the constraints as listed in Tables 3-2 and 3-3 are loosened by

approximately two orders of magnitude to obtain what is basically a free-net adjustment for use in GLOBK.

3.5.2 GLOBK adjustment of daily GAMIT solutions

GLOBK is a Kalman filter which analyses solution vectors and their associated covariance matrices generated in the GPS analysis program, GAMIT. The basic algorithms and a description of Kalman filtering is given in Herring *et al.* (1990).

Once daily solutions have been cleaned (cycle slips removed) in GAMIT, the separate daily solutions can be adjusted together, with the coordinates of fiducial stations constrained or held fixed. This forces the results to comply with the defined reference frame.

To improve the degree to which the final coordinates would be in terms of ITRF93 the daily GAMIT solutions (H-files) from SIO were combined with the New Zealand GAMIT solutions. The inclusion of the SIO solutions is an important step, as these solutions contain approximately 30 stations which are distributed around the world, these stations having been observed in a number of campaigns to determine their ITRF coordinates. Unfortunately all but 7 of the stations in the 1993 SIO solutions are in the northern hemisphere (Figure 3-3).

GLOBK begins the adjustment using data from the GAMIT solution file which has the earliest mean epoch for the satellite ephemeris. Due to the New Zealand network being processed in two sessions of approximately 12 hours for the first day of the campaign (DOY067), the first session had a mean epoch earlier than the SIO 24 hour session. The GLOBK subroutine unify_svs was used to make the satellite ephemeris files consistent, though large prefit chi-squared values were still encountered. To provide a more appropriate GAMIT solution file for initialisation of the adjustment of the New Zealand and SIO networks, an extra SIO solution at either end of the New Zealand campaign was obtained from SIO (ie. SIO solutions obtained were DOY 066 through 080).

Both Tregoning (Section 4.4, 1996) and Morgan *et al.* (Chapter 9, 1996) have reported inconsistencies between southern hemisphere dominated GPS data sets and the ITRF92 values for the 13 core IGS sites. Similar inconsistencies have been found while trying to attach the March 1993 New Zealand GPS data to ITRF93. To minimise these discrepancies while still endeavouring to fit to ITRF93 as best as possible, the positions and velocities of only some core IGS stations were used to define the reference frame (Table 3-3). These sites were chosen after testing various combinations and analysing the results so as to minimise the adjustments to the less constrained IGS Core sites. The coordinates and velocities for the IGS Core stations that were held fixed were obtained from Boucher *et al.* (1994).

As discussed in Section 3.2 and depicted in Figure 3-4, the New Zealand local sites had two occupations of the same station within one 24 period, where only the height of the instrument was changed. GLOBK required two names for the two independent occupations with a 24 hour session. Therefore, GLOBK generated an output file containing two sets of station coordinates and the associated VCV for these dual occupation sites. The GLORG option of GLOBK was then used to equate the two sets of coordinates. This equating of the coordinates was only required for the sites which had two 4-hour sets of data processed in GAMIT using a single session. Herring (1994) describes GLORG as the origin (translation and rotation) fixing program for the data analysis. Essentially GLORG allows the translation and rotation values and velocities to be determined by a minimisation of the deviations between horizontal positions and velocities given in the *a priori* station position file.

The final coordinates are in terms of ITRF93 at a mean observation epoch of 1993.200 (Appendix B).

STATION	CODE	N position	E position	N velocity	E velocity
Algonquin	ALGO	held	held	held	held
Fairbanks	FAIR	held	held	held	held
Goldstone	DS10				
Hartebeesthoek	HART				
Kokee Park	KOKR	held	held	held	held
Kootwijk	KOSG	held	held		
Madrid	DS60				
Santiago	SANT				
Tidbinbilla	DS42	held	held	held	held
Tromso	TROM	held	held		
Wettzell	WTZ1				
Yaragadee	YAR1			held	held
Yellowknife	YELL				

Table 3 - 3 : List of the 13 IGS core sites and those stations used to define the March 1993 GPS reference frame and attachment to ITRF93. Refer to Figure 3-3 for station locations. Note : some of the codes used are not the official IGS codes but are local codes of the equivalent station; the Up (local vertical) component for both position and velocity were not held fixed.

3.5.3 Analysis of results

As the processing of the GPS data progressed through GAMIT and GLOBK, different inconsistencies within the data became apparent. The next two sub-sections describe inconsistencies that can be attributed to a particular receiver or satellite. The last sub-section (3.5.3.3) contains general comments on the analysis of the results.

3.5.3.1 Problem Receivers

Prior knowledge of GPS receivers which had performed poorly during the New Zealand GPS campaign was obtained from Bevin and Hall (1994). However, it was decided that an attempt to process all the collected data should be undertaken in case the GAMIT software was able to process data which had to be rejected when using the Ashtech GPPS software. With the interactive visual data editing facilities of GAMIT it was envisaged that there was a better chance of cleaning this previously rejected data. However, as explained below, the data rejected by Bevin and Hall (*ibid.*) was not able to be processed in GAMIT, though the remaining data was able to be cleaned in GAMIT

more reliably, due to the ability to visually check the data, than using the Ashtech GPPS software.

Initially data rejected by Bevin and Hall (*ibid.*) was accepted by GAMIT. However, problems were encountered when attempting to combine the daily GAMIT solutions in GLOBK as the network was clearly distorted from day to day. The largest adjustments to the *a priori* coordinates clearly indicated those sites whose receivers had performed poorly were at fault. GAMIT solutions were re-computed without the faulty receiver sites. This improved the statistics on both the daily GAMIT solutions and the GLOBK adjustment. These improved statistics clearly indicated that significant contamination was being introduced by this noisy data.

The sites which were not able to be processed had been observed by one of two receivers. Both these receivers (alias Ashtech number 1 and 4) had pre-amps which were faulty. After the pre-amp was replaced in receiver number 1 (located at WELL - before DOY 070 observations began, see Section 3.2) there were no further problems in processing data collected by this receiver. Unfortunately receiver number 4 was not diagnosed during the campaign as having a faulty pre-amp, and this resulted in no data collected by this receiver being processable. Appendix E contains CVIEW examples of both receiver 1 (located at WELL, Figure E-13) and receiver 4 (located at D269, Figure E-11) for DOY 067. It is obvious from these CVIEW plots that both these receivers, when separately combined with DS42 and satellites (PRN 15 and 25) to form the two-way combination have many cycle slips, especially when compared with other sites observing the same satellites.

3.5.3.2 Problem Satellites

The data from DOY 076 was not processable in GAMIT when PRN 18 data was included, as it caused adjustments in the order of metres to site *a priori* coordinates. According to the NANU (Notice Advisory to NAVSTAR Users) message number 059-93077, PRN 18 was switched unusable from 1515 UTC on day 076 to 0554 UTC on day 077. It is suspected that PRN 18 was performing poorly before being switched unusable, thus affecting the data collected earlier on DOY 076. There was no noticeable

deterioration in the solution for DOY 076 with the exclusion of PRN 18 when compared with coordinate repeatability plots of other days (Appendix D).

3.5.3.3 General comments

Appendix D contains figures showing the consistency between the daily solutions of GAMIT for the local North, East and Up components of each site. To help the following discussion on the quality of the results, the D474 repeatability plot is also included in this section (Figure 3-5). As can be seen from the figures in Appendix D, the daily solution components are generally within 3σ confidence level of the D474 standard deviations given in Figure 3-5.

Analysing the site repeatabilities between different days was difficult due to the variations in the network geometry and processing techniques. However, a few comments are worth making and generally can be confirmed through Figure 3-5 when references to the figures in Appendix D are not given.

i) DOY 070 generally had the largest variation in site coordinates and uncertainties, especially for the second session (when compared with other daily solutions of the same site). However, the cause of these larger residuals is unclear. DOY 070 was processed using SINCLN with 2 sessions. The first session had data from 00:00 to 07:00 UTC for DS42, which did not coincide with data from the New Zealand sites. The second session had no data from DS42. The loss of DS42 from the network may indicate the reason for the poorer results for the second session on DOY 070. To establish if varying the network geometry caused the large uncertainties for DOY 070, the following days were investigated. DOY 067 was the other day that was processed with the same approach as DOY 070, ie. using two sessions and SINCLN. However, only one site, D474, was suitable to make comparisons between these two days (Appendix A). From this unfortunately small sample of one, it would appear that DOY 070, when compared with DOY 067, has been affected adversely by the lack of data at the regional fiducial site, DS42, especially for the second session which contained no DS42 data. This example of the deterioration in the quality of the session solution when data from DS42 was

not available shows the extra network strength obtained by including well known IGS core sites in the network.

ii) Site repeatabilities are generally superior when at least 2 of the 3 New Zealand local fiducial sites are operating in conjunction with all 4 regional fiducial sites (ie. DOY 071, 074 and 075); this is confirmed at WELL (Figure D-6).

iii) Having established that variations in the fiducial network can affect the site uncertainties, a careful choice of days is required to determine the effect of using two processing sessions with SINCLN as opposed to one session with AUTCLN. DOY 078 had been processed using AUTCLN with 2 sessions, so these provided the only opportunity to distinguish between results processed using SINCLN and AUTCLN. Unfortunately DOY 078 had only HOB1 and DS42 as fiducial sites, which are both located to the west of New Zealand and separated by only approximately 830 km (Figure 3-2). As a consequence it was not possible to distinguish between the effect of varying the number of processing sessions, from the effect of changing the data editing software.

iv) To compare the combined effect of using either SINCLN on two sessions or AUTCLN on one session, DOY 067, 068 and 069 were investigated as these days had a consistent fiducial network. For D474 there is no discernible difference between DOY 067 which used SINCLN with two sessions or DOY 068 and 069 which both used AUTCLN with one session. Making the same comparison at D253 (Figure D-21) shows that DOY 067 has smaller uncertainties than both DOY 068 and 069. The only significant difference between sites D474 and D253 is that D474 collected data continuously for 9 hours while D253 collected two sets of 4 hours of data which were separated by 1 hour. One reason that could explain this is that breaking continuous data into two sessions can cause sites with 4 hour data spans to have reduced formal uncertainties, though without an improvement in their overall accuracy.

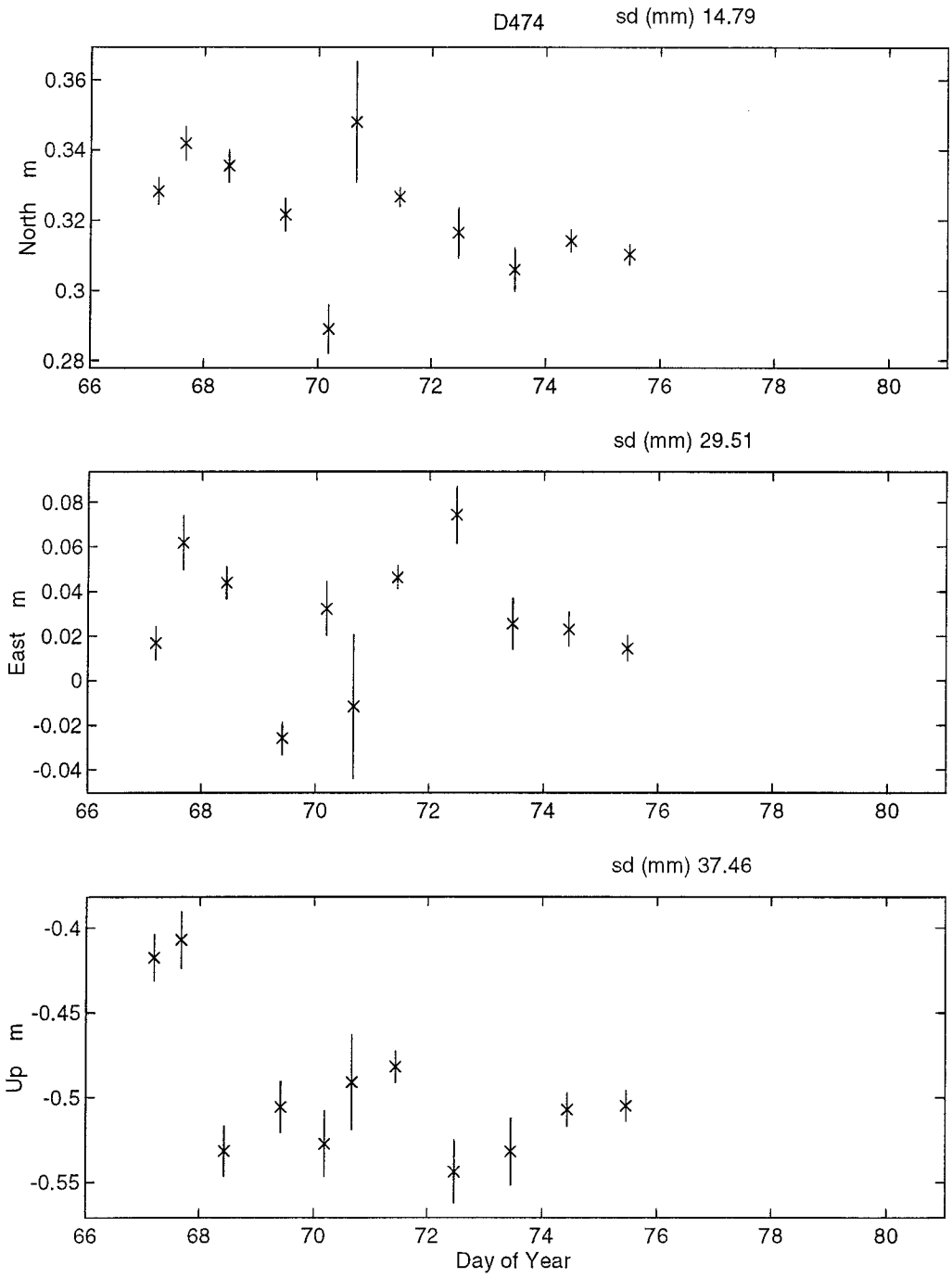

Figure 3 - 5 : D474 site repeatabilities between daily GAMIT solutions after performing a backward adjustment in GLOBK. The variation plotted is the daily solutions correction to the *a priori* coordinate value for each of the three components. sd is the standard deviation of each component in millimetres. The error bars are the formal one sigma values. Note that DOY 067 and 070 were processed using 2 sessions (Figure 3-4a).

v) Because the New Zealand regional network was adjusted in GLOBK with the SIO global network, three of the regional fiducial sites (DS42, MCMU and PAMA) were contained in both solutions. The small number of duplicate baselines between these three regional fiducial sites was thought to have no adverse impact on the solution. The benefit of these sites being contained in both networks was that a comparison could be made between the New Zealand network estimates of their position and those of the SIO network. Appendix D contains the site repeatabilities for MCMU (Figure D-1) and PAMA (Figure D-2). From these diagrams it is clear from the standard deviations that the New Zealand network determinations for these sites were consistent with those of SIO.

vi) If the southern hemisphere sites of MCMU and PAMA are compared with the northern hemisphere sites of DS60 (Figure D-3) and YELL (Figure D-4), it is clear that the northern hemisphere sites' standard deviations are almost an order of magnitude smaller. This improved quality of the northern hemisphere sites is mainly the consequence of the denser network of permanent tracking sites (Figure 3-3).

To summarise the analysis of the site repeatability diagrams (Appendix D) the following comments can be made.

i) It is inconclusive that the results of processing the days with two sessions and using SINCLN were inferior to those days that used a single session and AUTCLN.

ii) There is a noticeable decrease in the quality of results for days which are missing one or more regional or local fiducial sites. This could be less noticeable if one was not estimating local orbit parameters, though this was not tested.

iii) The repeatability of common site coordinates, between the SIO and New Zealand networks, were in agreement.

The output of GLOBK gives the formal uncertainties of the sites estimated coordinates in the X, Y and Z components. A comparison of these uncertainties was undertaken to establish whether there is an improvement in the uncertainty by re-occupying sites. This was achieved by calculating the magnitude of the vector formed by each sites X, Y and Z

formal uncertainty components (σ_x, σ_y, σ_z), summing up the magnitudes of those sites that had been observed for the same number of days (n) and then taking the average for each number of site occupations.

$$\text{uncertainty} = \sum_{i=1}^{n} \left\| \begin{matrix} \sigma_x \\ \sigma_y \\ \sigma_z \end{matrix} \right\| \Big/ n \qquad (3.2)$$

Table 3-4 contains the results from grouping site uncertainties together based on the number of days occupied. From this table it is clear that the formal uncertainty of a site is improved by increasing the number of days occupied. This is as one would expect.

It should be noted that the hours of data collection per 24 hours varied between sites. The results for one to three days occupation in Table 3-4 are based on two four-hour data sets per 24 hour period in contrast to sites with 12 and 13 occupations which had a single 24 hour data set.

Number of days occupied n	Number of Sites	Hours of data per day	Mean Uncertainty (metres)	Calculated Uncertainty ($0.0189/\sqrt{n}$)	Observed minus Calculated (metres)
1	10	2 x 4hr	0.0189	0.0189	0.0000
2	12	2 x 4hr	0.0112	0.0134	-0.0022
3	3	2 x 4hr	0.0093	0.0109	-0.0016
5	1	9hr	0.0089	0.0085	0.0004
9	2	9hr; 24hr	0.0056	0.0063	-0.0007
10	1	9hr	0.0075	0.0060	0.0015
12	2	24hr	0.0047	0.0055	-0.0008
13	1	24hr	0.0037	0.0052	-0.0015

Table 3 - 4 : Formal uncertainty of site coordinates with respect to the number of days the site was occupied. The mean formal uncertainty is quoted at the one sigma level.

What is of more use from generating the results in Table 3-4 is that in planning further campaigns one is able to obtain an estimate of the quality a site is likely to obtain based on the number of days the site is occupied. To help in this planning a power series was determined so as to model the mean uncertainty. It was found that the simple relationship of $0.0189/\sqrt{n}$, where n is the number of days the site is occupied, suitably modelled the uncertainties (Table 3-4 and Figure 3-6).

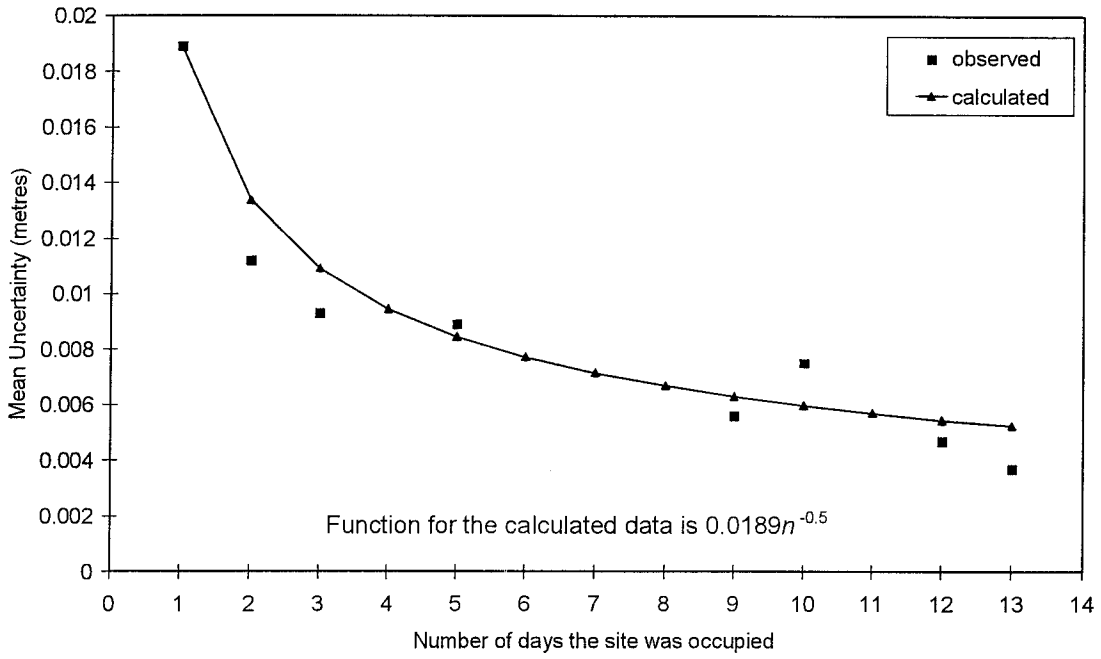

Figure 3 - 6 : Formal uncertainty of site coordinates with respect to the number of days the site was occupied. Note: amount of data collected varied between sites (see Table 3-4).

With an increase in GPS data available at the 13 core sites, due to the passing of time, one would expect to be able to monitor a site position with improved precision. The IERS 1994 realisation of ITRF92 stated the formal uncertainties for the XYZ components as 5-11 mm (IERS 1994, p61) for the core sites. For the IERS 1995 realisation of ITRF93 the formal uncertainties had been reduced to 2-5 mm (*ibid.*, p 66). These formal uncertainties reported by IERS represent the minimum uncertainty attainable in attaching GPS data to an ITRF. Therefore the formal uncertainties in Table 3-4 would appear to be realistic, considering the relatively small amount of data used in the New Zealand network.

If the coordinates in Appendix B were transformed to another epoch besides 1993.200, then the New Zealand sites whose velocities are uncertain would have significantly degraded results at the new epoch.

3.6 Summary

The processing of the March 1993 New Zealand GPS data in GAMIT and GLOBK has resulted in a set of coordinates for the New Zealand sites which are in terms of ITRF93 with a formal uncertainty of 2 cm (1σ). The results are at the mid-observation epoch of March 14, 1993 (1993.200), with the Cartesian coordinates contained in Appendix B, while the ellipsoidal coordinates are in Appendix C.

With the experience gained from processing this New Zealand GPS campaign data in the GAMIT/GLOBK suite it is recommended that future GPS data collected for use in establishing high precision networks (such as national primary control networks) should: occupy sites for a minimum of 3 days collecting 24 hour data sets (ie. 3 x 24hr). Future processing of GPS data for datum maintenance or development in New Zealand should investigate the effects of antenna phase centre modelling, full Earth and Ocean Tide Loading models, improved orbit modelling by including once per revolution terms and the fixing of small but important satellite elevation effects, and stochastic atmospheres.

Chapter 4

Gravimetric Geoid Computation

4.1 Introduction

With the increased use of satellite based methods, such as GPS, for determining position in 3-dimensions with relative accuracy of better than 0.1 part per million (ppm), gravimetric geoid computation methods need to be developed further to maintain this accuracy through the conversion of ellipsoidal heights obtained from GPS to orthometric heights. Orthometric heights are required for most engineering and surveying applications, especially those dealing with the dynamics of water and other fluids, since differences in orthometric heights closely represent differences in equipotential surfaces. As was described in Section 2.5.2, with examples of the effect, New Zealand heights are normal orthometric heights rather than orthometric heights due to the use of normal gravity instead of observed gravity. For the remainder of this thesis the term orthometric height will be used to described New Zealand heights due to the small difference between the two heights below 1000 m. The difference between the ellipsoidal height and the orthometric height of a point is called the geoid height (N). This difference results from the fact that ellipsoidal heights are referenced to a mathematical model of the earth's surface while the orthometric heights refer to the geoid (heights are discussed in Appendix L). The geoid is an equipotential surface that approximates mean sea level and its theoretical continuation under the continents (see Figure 4.2). The purpose of this chapter is to outline a method to determine the geoid height with sufficient accuracy to allow the transformation of ellipsoidal heights to orthometric heights, so as to meet 3rd, 2nd or perhaps even 1st order levelling specifications in New Zealand (Table 2-3).

There are a number of techniques to convert ellipsoidal heights to orthometric heights. Three of these methods are outlined below. Each has advantages depending on the nature of the survey site and the accuracy required for the project.

i) The first method of determining orthometric heights from the ellipsoidal heights from GPS, is to include in the GPS network, connections to spirit levelled marks within and at the limits of the survey area. Then, by assuming that the geoid height can be represented by some mathematical surface, eg. a plane between those spirit levelled points, the GPS network can be adjusted into approximate orthometric heights. The method involves holding the orthometric heights fixed while also estimating three dimensional transformation parameters. The resulting parameters effectively incorporate a plane geoid height function and the adjustment results in the application of this function to the new stations. This method may work for surveys of small extents over flat terrain, but is unlikely to produce suitable results anywhere that the geoid departs significantly from a simple geometric surface, such as in mountainous areas or where large gravity anomalies occur. Gilliland (1986) reports geoid height variations of > 0.1 m in 25 km for areas of Australia where the terrain varied by only 300 m. Featherstone *et al.* (1995) have shown that in areas of Australia the gravity field is not always correlated with the terrain. Another disadvantage of this method is that orthometric heights of suitable accuracy need to be available around the extents of the survey. Also, any error (other than gross error unless using only 3 stations) in the control orthometric height maps directly into the interpolated height, with no independent means of checking the value of N. Thus there is no effective redundancy in the control heights.

A variation on this first method is to calculate the differences between the orthometric and ellipsoidal heights at all possible stations within the survey area. From these differences a contour map can be generated and local geoid heights scaled off the map for stations that only have ellipsoidal heights, thus allowing the determination of the orthometric height (see Collins and Leick, 1985 and Holloway, 1988). A modification of this method was used for mapping control purposes in the rugged Fiordland area of New Zealand and is believed to have achieved the required height accuracy specifications of ± 1.0 metre (Tait, 1991). Once again, there is no method of testing the correctness of control heights except against gross errors.

ii) The second method is to compute geoid heights from Global Geopotential Model (GGM) coefficients. Depending on the degree and order of the model, the complexity of the local geoid and the amount of local terrestrial gravity data used in developing the specific GGM, geoid height accuracy can vary widely between project locations. As a GGM is a finite expansion of potential coefficients, it has limited resolution. Current GGM are complete up to degree and order 360, which means that features of only 0.5° or larger in size (approximately 55 km) can be modelled (see Section 4.2.5).

iii) The third method of determining the geoid height at a point is based on the use of a GGM and local gravity observations to define smaller geoid features than the resolution of the GGM. This method produces a gravimetric geoid and is the method on which the remainder of this chapter will focus. As can be see from Figure 4-1, New Zealand has reasonably dense gravity data coverage on land which is about 1 station per 7.5 km^2 (Gilliland, 1988). Therefore it seems reasonable to take advantage of this asset, and to use this gravity in the determination of a New Zealand geoid model.

This is not the first attempt to compute a gravimetric geoid for New Zealand. Gilliland (1990) produced a gravimetric geoid for New Zealand on a 0.25° grid by combining gravity data and the OSU81 (Rapp, 1981) GGM to degree and order 180. However without any ellipsoidal heights from GPS no comparison using equation 4.1 below could be made.

Mackie (1982) determined geoid heights at 18 stations, distributed across New Zealand, by comparing Doppler derived WGS72 ellipsoidal heights with spirit levelled orthometric heights.

Mackie's work did not use local gravity data, though when Gilliland (*ibid.*) compared his results with the results of Mackie (*ibid.*), after reduction to a common datum and the removal of biases, a Root Mean Square (rms) of geoid heights of less than 1.3 m was obtained. At the time this was a reasonable result given observation error in Doppler

height, but with present day techniques it should be possible to obtain results at least an order of magnitude better.

The possibility of increased accuracy has come about with the improvement in GGM's and the accuracy of ellipsoidal heights, primarily from GPS, at which geoid heights can be tested. With these improvements and the demand from GPS users to be able to convert the GPS ellipsoidal heights to orthometric heights, it is appropriate to develop a high resolution, national geoid model for New Zealand.

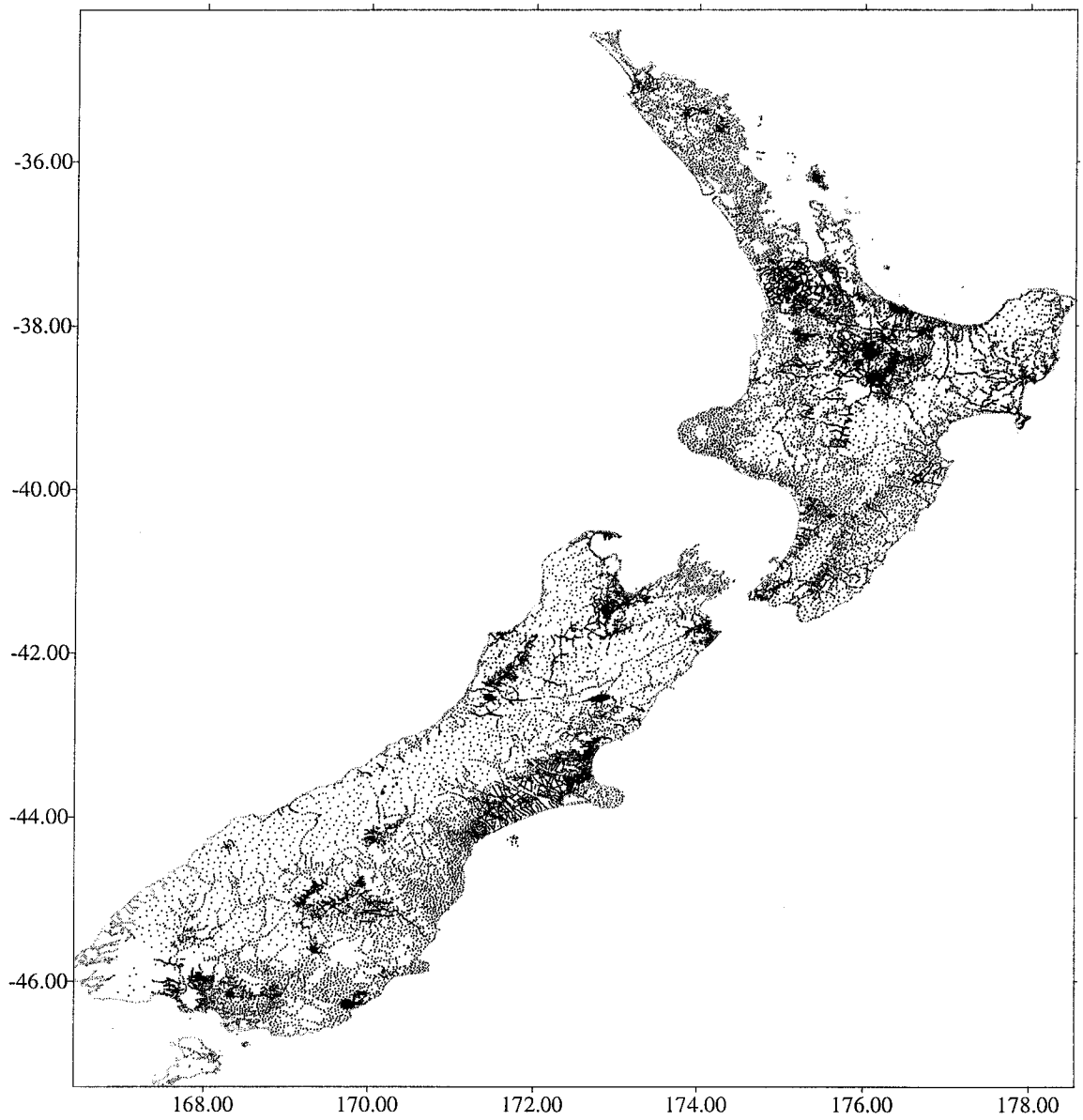

Figure 4 - 1 : Distribution of Land Gravity data available for New Zealand. Rectangular projection

The lower North Island was selected as the test area for the development of a gravimetric geoid model for New Zealand for three main reasons :

i) both land and sea gravity data was available

ii) approximately 100 points had both ellipsoidal height from GPS and orthometric height from spirit levelling (control stations)

iii) the region encompasses rugged terrain which is typical for New Zealand, varying from sea level to 1500 metres

Having both ellipsoidal heights (h) obtained by GPS, and orthometric heights (H) from spirit levelling one can check on the quality of the geoid height (N) obtained by using the new gravimetric geoid model. This check uses the well-known algebraic relationship of (4.1) which is illustrated in Figure 4-2.

$$h = H + N \tag{4.1}$$

The value of N obtained by subtracting the orthometric height from the ellipsoidal height at each of the control stations is known as the geometric geoid height (N_{GEO}).

$$N_{GEO} = h_{GPS} - H_{Levelling} \tag{4.1a}$$

From (4.1) it is clear that identifying the source of any errors in the determination of one or more of the height components will not be possible.

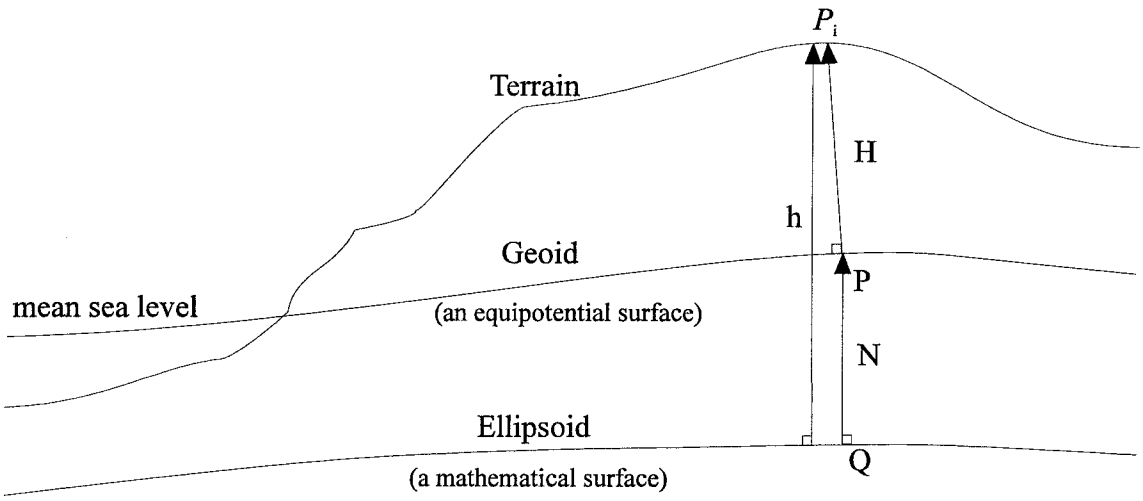

Figure 4 - 2 : Relationship between Geoid, Ellipsoid and Orthometric heights

Through processing gravity data using the RINT (Ring Integration) based software (see Section 4.3) in the lower North Island, a procedure is developed to expand the gravimetric geoid model to cover the whole of New Zealand. This New Zealand specific geoid model can then be used to convert ellipsoidal heights (GPS) to orthometric heights.

4.2 Theoretical Background

This section outlines the theory of determining geoid heights from gravity data. As was described in Section 4.1 the geoid height is required to convert ellipsoidal heights from GPS to orthometric heights which are required for most surveying and engineering applications.

4.2.1 Normal Gravity

The use of an ellipsoid of revolution to approximate the shape of the earth allows, amongst other applications, the computation of gravity on the ellipsoid. The currently accepted international reference ellipsoid is the Geodetic Reference System 1980 (GRS80). The four conventional constants adopted by the XVII General Assembly of the International Union of Geodesy and Geophysics (IUGG) to define GRS80 are (Moritz, 1980a) :

equatorial radius of the Earth :

$a = 6\ 378\ 137$ m

Geocentric gravitational constant of the Earth (including the atmosphere) :

$GM = 3.986005 \times 10^{14}\ m^3 s^{-2}$

dynamical form factor of the Earth, excluding the permanent tidal deformation :

$J_{20} = 1.08263 \times 10^{-3}$

angular velocity of the Earth :

$\omega = 7.292115 \times 10^{-5}$ rad s^{-1}

Moritz (*ibid.*) went on to state that from a given ellipsoid of revolution it is possible to define an equipotential surface, $U = U_0 =$ constant, of a certain potential function, U, called the normal gravity potential. Using geodetic coordinates (ϕ, λ, h) the normal

gravity at the surface of the ellipsoid, $\gamma_Q = |\text{grad } U|$, can be evaluated rigorously using Somigliana's closed formula (Heiskanen and Moritz, 1967, eqn. 2-78).

$$\gamma_Q = \frac{a\gamma_a \cos^2\phi + b\gamma_b \sin^2\phi}{\sqrt{a^2\cos^2\phi + b^2\sin^2\phi}} \tag{4.2}$$

where: γ_a is the equatorial normal gravity on the ellipsoid

γ_b is the polar normal gravity on the ellipsoid

a is the semimajor axis

b is the semiminor axis

Equation (4.2) can also be expressed as a series. The conventional abbreviated series (*ibid.*, eqn. 2-116) describing the variation of normal gravity on the ellipsoid with geodetic latitude (ϕ), and after substituting the constants for GRS80 is

$$\gamma_Q = 9.780327(1+0.0053024 \sin^2\phi - 0.0000058 \sin^2 2\phi) \quad \text{ms}^{-2} \tag{4.3}$$

and has an accuracy of 1 μms^{-2} = 0.1 mGal.

The derived values for normal gravity at the equator and pole, in terms of the GRS80 ellipsoid are respectively (Moritz, *ibid.*) :

$\gamma_a = 9.7803267715$ ms^{-2}

$\gamma_b = 9.8321863685$ ms^{-2}

The unit of acceleration in the SI-system is ms^{-2}, though the cgs-system unit of acceleration, the "Gal" = cm s^{-2}, is still widely used in geodesy and geophysics. The following example shows γ_a expressed in terms of different units of acceleration.

$\gamma_a = 9.7803267715$ ms^{-2}

$\gamma_a = 978.03267715$ Gal

$\gamma_a = 978032.67715$ mGal where 1 milligal = 10^{-3} Gal = 10^{-5} ms^{-2}

4.2.2 The Boundary Value Problem in Physical Geodesy

The natural reference system - the geoid - is the equipotential surface, W_o, that is chosen so as to approximate MSL without the effects of ocean currents, weather and tides and is

also the theoretical continuation of MSL under the land. A point (x,y,z) is on the geoid if the potential of the point, $W_{(x,y,z)} = W_0$.

The mathematical reference system is normal gravity (γ_Q) (see Section 4.2.1). The potential of the normal gravity field being denoted by $U_{(x,y,z)} = U_0$ = constant and therefore exactly corresponds to the geoid defined by the surface $W_{(x,y,z)} = W_0$ = constant.

Heiskanen and Moritz (1967, Section 2-13) state that the small difference between the actual gravity potential W and the normal gravity potential U at the geoid is called the disturbing or anomalous potential T

$$T_{(x,y,z)} = W_{(x,y,z)} - U_{(x,y,z)} \tag{4.4}$$

If the x,y,z position is on the geoid at point P, as shown in Figure 4-3, then the disturbing potential on the geoid becomes

$$T_P = W_P - U_P \tag{4.5}$$

where W_P is the Earth's gravity potential at the geoid and U_P is the normal gravity potential at the geoid. Thus at the geoid, $W_P = W_0 = U_Q = U_0$.

The gravity anomaly vector ($\Delta\mathbf{g}$) is the difference between the gravity vector **g** at P and the normal gravity vector γ at Q.

$$\Delta\mathbf{g} = \mathbf{g}_P - \gamma_Q \tag{4.6}$$

The difference in the magnitude component of the gravity anomaly vector is the gravity anomaly (Δg), while the difference in direction is the deflection of the vertical. There are two components to the deflection of the vertical, one is the north-south component (ξ) and the other is the east-west component (η) (see Torge, 1980, Chapter 5).

It is also possible to obtain the difference between the gravity vector **g** and the normal gravity vector γ at the same point P. The difference in the direction gives the gravity disturbance vector

$$\delta = \mathbf{g}_P - \gamma_P \tag{4.7}$$

while the difference in the magnitude gives the gravity disturbance

$$\delta g = g_P - \gamma_P = -\frac{\partial T_P}{\partial n} \tag{4.8}$$

As the elevation is determined along the geoid normal, n, rather than the ellipsoid normal, n', then ∂n can be approximated by ∂h to determine the gravity disturbance (Figure 4-3).

The gravity disturbance can in theory be used instead of the gravity anomalies for computing geoids, though practical methods have not been developed.

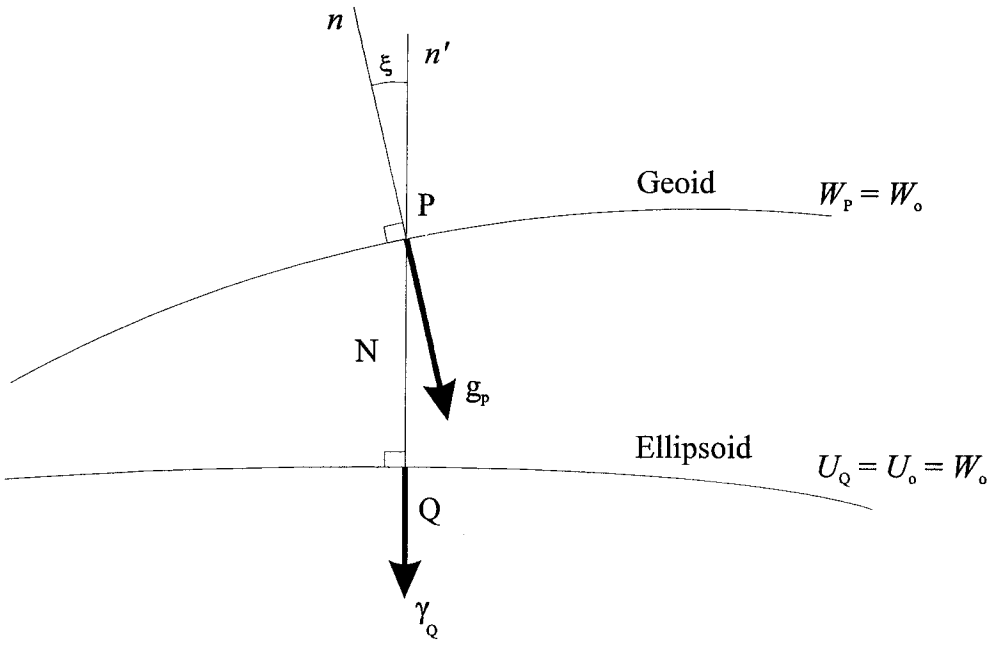

Figure 4 - 3 : Relationship between the Ellipsoid and the Geoid (adapted from Heiskanen and Moritz, 1967, Fig. 2-12)

From Figure 4-3, when the deflection of the vertical ξ is small, one can express the normal gravity potential at the geoid, U_P, as a function of the normal gravity potential on the ellipsoid, U_Q, and the geoid height, N, by (Heiskanen and Moritz, 1967, eqn. 2-143)

$$U_P = U_Q + \left(\frac{\partial U}{\partial n}\right)_Q \mathrm{N} = U_Q - \gamma_Q \mathrm{N} \tag{4.9}$$

where $\left(\frac{\partial U}{\partial n}\right)_Q$ is the derivative of U_Q with respect to the geoid normal. By inserting (4.9) into (4.5), Brun's generalised formula is obtained

$$T_P = W_P - U_P = W_P - U_Q + \gamma_Q \mathrm{N} \tag{4.10}$$

Because the reference ellipsoid is assumed to have the same potential as the geoid

$$W_P = U_Q = W_0 \tag{4.11}$$

Brun's formula simplifies to

$$T_P = \gamma_Q N \tag{4.12}$$

which relates the geoid height to the disturbing potential.

4.2.2.1 The Fundamental Equation of Physical Geodesy

The relationship between the gravity anomaly Δg and the unknown disturbing potential T will now be developed. With analogies to (4.9) the normal gravity γ at P can be written as

$$\gamma_P = \gamma_Q + \frac{\partial \gamma_Q}{\partial h} N \tag{4.13}$$

combining (4.8) and (4.13) results in

$$\delta g = g_P - \gamma_Q - \frac{\partial \gamma_Q}{\partial h} N = -\frac{\partial T_P}{\partial h} \tag{4.14}$$

and applying the gravity anomaly component of (4.6), then Brun's simplified formula (4.12), the following equivalent equations are obtained

$$\frac{\partial T_P}{\partial h} + \Delta g - \frac{\partial \gamma_Q}{\partial h} N = 0 \tag{4.15a}$$

$$\frac{\partial T_P}{\partial h} + \Delta g - \frac{1}{\gamma_Q}\frac{\partial \gamma_Q}{\partial h} T_P = 0 \tag{4.15b}$$

where (4.15b) is referred to as the **Fundamental Equation of Physical Geodesy** as it relates the desired quantity T_P, to the measured quantity Δg. T_P is desired because it allows N to be computed from (4.12).

To be complete it should be noted that the first derivative with respect to the normal height, h, on the left hand side of (4.15), should be the geoidal normal, n, while the second occurrence should be the ellipsoidal normal, n'. However, in reality due to the small magnitude of deflection of the vertical values, this difference is insignificant.

Assuming that the effect of masses outside the geoid have been removed (refer to Section 4.2.4 to see how this is achieved in practice), that is the density ρ is zero outside the geoid, the anomalous potential T is harmonic there and satisfies Laplaces' equation (Heiskanen and Moritz, 1967, p. 86)

$$\Delta T \equiv \frac{\partial^2 T}{\partial x^2} + \frac{\partial^2 T}{\partial y^2} + \frac{\partial^2 T}{\partial z^2} = 0 \tag{4.16}$$

By i) taking the spherical approximation of the normal gravity on the ellipsoid,

ii) assuming that the geoidal and ellipsoidal normals can be approximated by the radius vector (r),

iii) introducing the mean radius of the Earth (R),

the spherical approximation of the fundamental equation of geodesy is obtained as follows (Heiskanen and Moritz, *ibid.*, eqn. 2-151f)

$$\frac{\partial T_P}{\partial r} + \frac{2T_P}{R} + \Delta g = 0 \tag{4.17}$$

As (4.17) is a boundary condition the following assumptions are made to enable it to be solved on the geoid:

i) mass of the reference ellipsoid equals the mass of Earth.

ii) centre of the reference ellipsoid coincides with the Earth's geocentre.

iii) no mass exist outside the geoid.

iv) gravity anomalies are available over the entire surface of the Earth and refer to the geoid.

These assumptions are never fully met in reality. In an attempt to satisfy these assumptions various terrain and gravity reductions are applied to the gravity anomalies. Heiskanen and Moritz (1967, Chapter 3) give detailed descriptions of these various reductions, and these are briefly summarised in Section 4.2.4.

4.2.3 Gravimetric techniques for solving the Geodetic Boundary Value Problem

In this section a brief review is given of the different ways of solving Laplace's equation (4.16) subject to the boundary condition (4.17). These are fundamental to the computation of geoid heights from observed gravity anomalies.

4.2.3.1 Stokes' Method

Solving (4.16) under the condition of (4.17) results in the spherical Stokes' formula (4.18), which enables the disturbing potential T_P to be found as a function of the gravity anomalies Δg on the geoid.

$$T_P = \frac{r}{4\pi}\iint_{\sigma} \Delta g\, S(\psi)\, d\sigma \tag{4.18}$$

where $d\sigma$ is an element of the unit sphere. $S(\psi)$ is known as the spherical Stokes' function and is given in closed form by

$$S(\psi) = \operatorname{cosec}\left(\frac{\psi}{2}\right) - 6\sin\left(\frac{\psi}{2}\right) + 1 - 5\cos\psi - 3\cos\psi \ln\left(\sin\frac{\psi}{2} + \sin^2\frac{\psi}{2}\right) \tag{4.19}$$

where ψ is the surface spherical distance. By applying Brun's simplified formula (4.12) to (4.18) the geoid height can be obtained

$$\mathrm{N} = \frac{r}{4\pi\gamma_Q}\iint_{\sigma} \Delta g\, S(\psi)\, d\sigma \tag{4.20}$$

Both (4.18) and (4.20) are equivalent and are referred to as Stokes' formula or Stokes' integral. Using the spherical approximation it is possible to set $r = R$ and $\gamma_Q = G$, and neglecting quantities of the order of $3\text{x}10^{-3}$ N (Heiskanen and Moritz, *ibid.*, section 2-16).

$$\mathrm{N} = \frac{R}{4\pi G}\iint_{\sigma} \Delta g\, S(\psi)\, d\sigma \tag{4.20a}$$

To solve Stokes' formula, the surface integral can be approximated by a double summation. The surface elements $d\sigma$ are replaced by small but finite compartments q, which are obtained by suitably subdividing the surface of the Earth. Heiskanen and Moritz (1967, Section 2-24) describe two methods for this subdivision, which are summarised in sections 4.2.3.2(i) and 4.2.3.3.

Before moving on, a few comments should be made about Stokes' function (4.19). There exists a singularity when $\psi = 0$. As $\psi \to 0$, $S(\psi) \to \infty$ (see Figure 4-7). Therefore, as the compartment q approaches the point of computation, Stokes' function can not be assumed linear across the extent of the compartment. A common approach to overcome this non-linearity near the point of computation is to reduce the size of the compartments when near the point of computation, though other mathematical techniques are available.

4.2.3.2 Solving Stokes' Integral using Geographical Coordinates

(i) *Quadratures*

If grid lines forming a fixed coordinate system, such as geographical coordinates, ϕ and λ, are chosen to subdivide the surface of the Earth, the compartments are a series of blocks or quadratures (Figure 4-4).

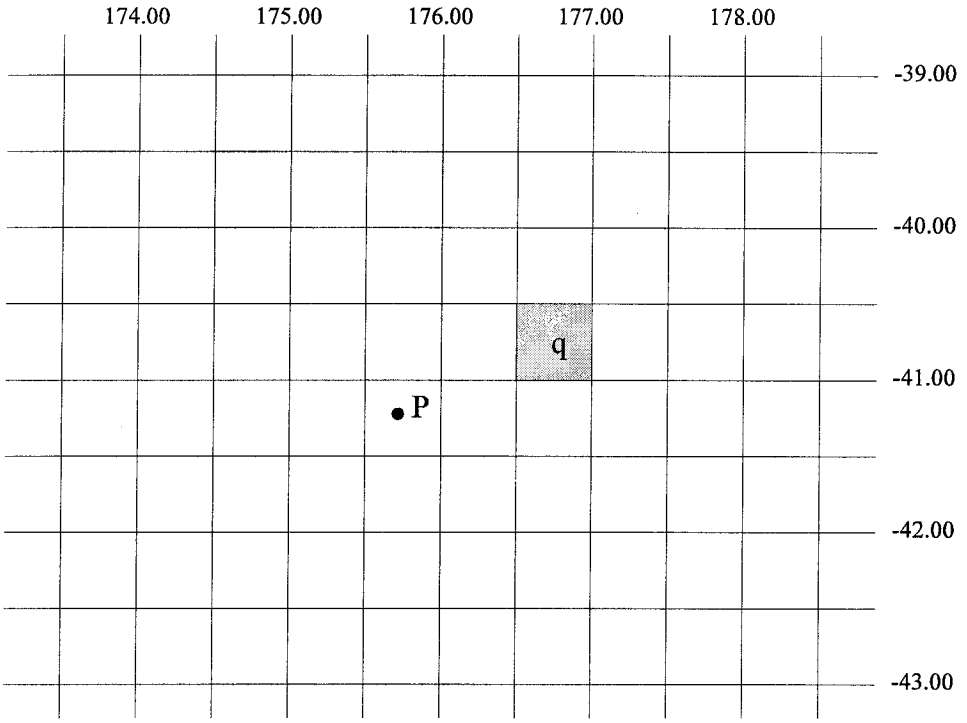

Figure 4 - 4 : Quadratures formed from a grid of geographical coordinates

By numerical summation of all the compartments it is possible to calculate the geoid height. This summation should in theory be performed over the entire Earth - an impossibility because such a global data set does not exist. By using a GGM to compute the long wavelength contribution to the geoid height the summation can be limited to a cap of a few degrees around the point of computation. By limiting the integration to a cap one introduces a truncation error that can be reduced by modifying Stokes' function. The original idea was that of Molodenskii *et al.* (1962), with many authors developing different approaches, some of which have been compared in Featherstone (1992). For further details on the technique of numerical summation of quadratures the reader is directed to Engelis *et al.* (1984) or Gilliland (1994). The use of a GGM for the long wavelength component is described in further detail in Section 4.2.6.

(ii) *Fast Fourier Transforms*

Rather than numerical summation of the quadratures it is possible to use the fact that Stokes' integral (4.20), when using geographical coordinates, is in the form of a convolution integral. Thus (4.20) can be evaluated using fast Fourier transform (FFT) techniques provided that the gravity data are given on regular grids. Sideris (1994) states that FFT overcomes the problem of slow computation speed experienced by numerical summation. More importantly FFT provides homogeneous coverage of results and it seems that it is not necessary to modify Stokes' function, especially when using a GGM for the long wavelength features of the geoid. For information on the theory of FFT see Bracewell (1986). While for the practical application of FFT there are many papers, though Tsuei *et al.* (1994) is given as starting point due to the inter-comparison of techniques to evaluate geoid heights in the frequency domain (FFT) and the space domain (Least-Squares Collocation, Section 4.2.3.4).

Spectral techniques for geoid computations are not restricted to the FFT. Recently the fast Hartley transform (FHT) has grown in popularity due to the reduction in computation time and computer memory requirements when compared to the FFT (Tziavos, 1996). Li and Sideris (1995) reported that numerical computations indicate that for the computation of three 2-D convolutions with size 1024 by 1024, the use of FHT instead of FFT can reduce the required computer memory by 44% and reduce the computer time by 33%.

One final comment on techniques that use geographical coordinates, is that the randomly spaced gravity observations have to be regularised onto a grid for use by FFT or FHT. Care needs to be taken during the griding procedure so as to maintain a fair representation of the random input data. Also some numerical summation techniques often pre-compute mean compartment gravity anomaly values to reduce the computation time. Errors can be introduced in the pre-processing stage which propagate into N, especially for small ψ.

4.2.3.3 Solving Stokes' Integral using Polar Coordinates

In section 4.2.3.2 the compartments chosen to subdivide the surface of the Earth were defined by a fixed coordinate system. By choosing a coordinate system that varies for each computation point it is possible to overcome the problem of Stokes' function

having a singularity at $\psi = 0$ (Section 4.3.1). Instead of using geographical coordinates, local polar coordinates can be used at each point of computation to subdivide the surface of the Earth.

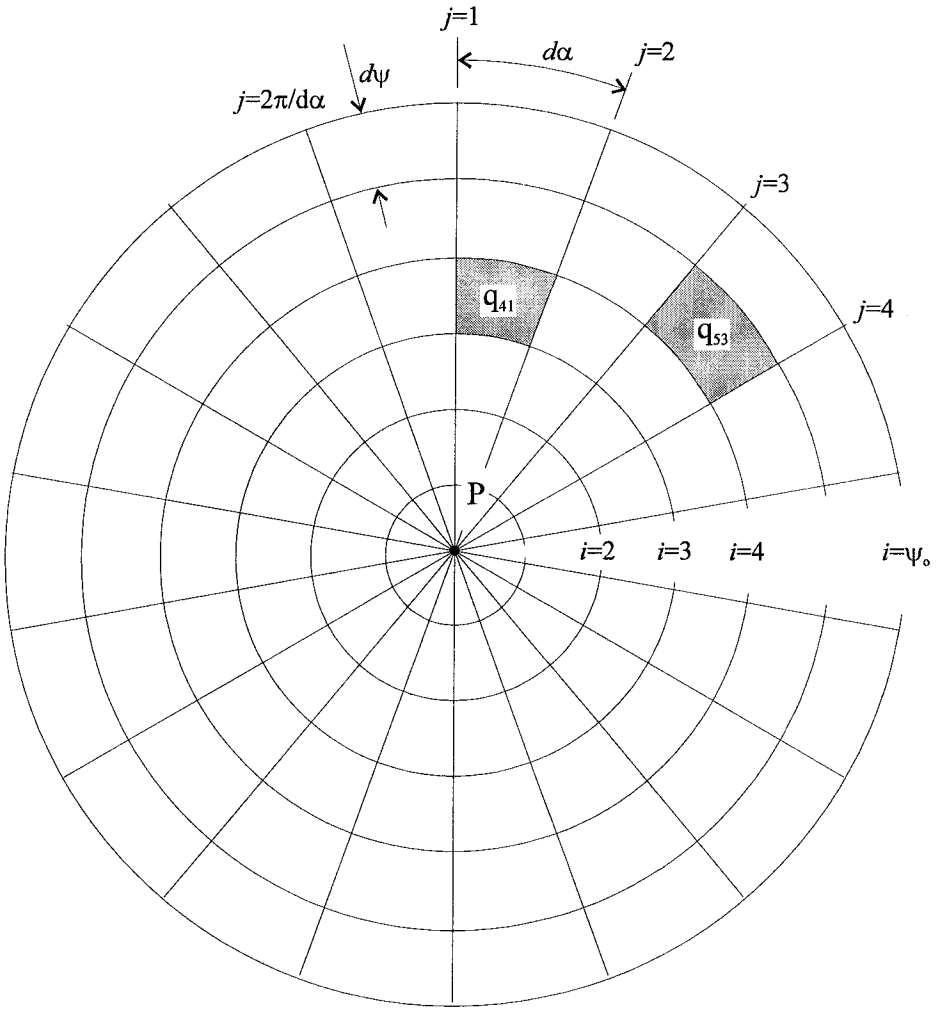

Figure 4 - 5 : Compartment structure using Polar coordinates

The compartments generated from using local polar coordinates are formed by concentric circles and radial lines centred on the point of computation (Figure 4-5). This method is called Ring Integration (RINT). The theory for RINT was originally developed by Lambert and Darling (1936), which is outlined in Heiskanen and Moritz (1967, Section 2-24), and has been developed for electronic computation by Kearsley (1986b). The RINT technique has been used in all the gravimetric solutions presented in this thesis and is described in further detail in Section 4.3. One of the features of RINT worth noting at this point is that the randomly spaced gravity data is used as input, eliminating the need to preprocess the raw gravity data onto a regular grid. The

'processing' to estimate mean gravity anomalies for the compartment is done in the computation of N. RINT also propagates the formal errors in the short wavelength geoid height (Section 4.3.2) from error estimates of the mean compartment gravity anomaly.

4.2.3.4 Least Squares Collocation

An alternative to numerical integration is least squares collocation (LSC). The main advantage of the LSC prediction method is that it can be used to predict any parameter describing the earth's gravity field from other observed parameters, using the statistical relationship which exists between these parameters. That is the auto- and cross-covariance functions need to be known. Other advantages of LSC is that the method can use randomly distributed data, with non-uniform noise associated with the data (Tscherning and Forsberg, 1992) and estimates of the error of the predicted quantities are readily obtainable (Lahmeyer, 1988).

The general formula for the geoid height at a point N(P) using LSC is given by Moritz (1980b, eqn. 14-27) as

$$N(P) = C^{Ng} (C^{gg} + C^{nn})^{-1} \Delta g_i \qquad (4.21)$$

where C^{Ng} is the cross covariance function of geoid heights and gravity anomalies. C^{gg} and C^{nn} are the auto covariance functions of the residual gravity anomalies and the noise respectively, and Δg is the point (rather than mean block) residual gravity anomalies (Section 4.3.4.1). As can be seen from (4.21) the choice of the covariance function is critical in the final results obtained from LSC.

For information on the theory of LSC see Moritz (1980b); for the practical application of LSC Tscherning and Forsberg (1992) and de Min (1995) are useful starting points, because they give inter-comparisons of LSC with numerical integration techniques.

4.2.3.5 Molodenskii's Problem

This section briefly outlines the approach of Molodenskii *et al.* (1962) to overcome some of the assumptions made in solving Stokes' integral. As land gravity observations are generally taken on the physical surface of the Earth (as compared with marine

gravity observations which are taken on or close to the geoid), an approximation of the density of the masses between the geoid and the terrain surface has to be assumed to allow the reduction of the gravity observations from the terrain surface down to the geoid. Molodenskii *et al.* (*ibid.*) proposed that instead of solving the boundary condition at the geoid, solve it at the terrain surface and thus eliminate the need to apply the terrain effect corrections as outlined in Section 4.2.4.

To apply Stokes' method at the terrain surface Molodenskii *et al.* (*ibid.*) had to introduce the concepts of the height anomaly (ζ), normal height (H^N) and a new surface called the telluroid (Σ) (Heiskanen and Moritz, 1967, Section 8-3). Unfortunately the height anomalies computed by the method of Molodenskii *et al.* are related to the quasi-geoid which is not a level surface and has no physical meaning whatever. However the quasi-geoid mapped on the ellipsoid is a close approximation to the geoid.

4.2.4 Terrain Effects

In applying Stokes' method (Section 4.2.3.1) to solving the geodetic boundary value problem it is assumed that no masses exist outside the geoid. As the observed gravity g is normally measured on or above the terrain surface these observations have to be reduced to the geoid surface before Stokes' formula (4.18) can be solved.

There are a number of methods available to correct the observed gravity for the effects of the terrain above the geoid. However there are basically two approaches. The first is the Bouguer reduction which attempts to completely remove the effect of mass between the terrain and the geoid. The second is based on some model of isostasy and is called Isostatic reduction. Instead of removing the mass above the geoid, the mass is shifted into the interior of the geoid in order to make up the mass deficiencies that exist under the continents (Heiskanen and Moritz, 1967, Section 3-5).

The remainder of this section will only describe methods to remove the mass effect that are based on the Bouguer reduction method, either as it was applied to the data described in Section 4.4.1, or variations recommended for use in future geoid model computations in New Zealand.

It is worth noting that there appears to be some inconsistency in the literature with regard to the terminology and symbols used to describe the corrections to the observed gravity due to the effects of the terrain above the geoid. The terminology used in this section is a combination from many sources; any differences in terminology will be noted when they occur.

4.2.4.1 Bouguer Plate Reduction

The first step in removing the topographic mass (mass between the geoid and the terrain surface) is called the Bouguer plate reduction (also referred to as the incomplete or simple Bouguer reduction). With the assumption that the terrain around the gravity observation point (S) is completely horizontal and the topographic mass has a constant density (ρ), the attraction of a plate of infinite radius and a thickness equal to the orthometric height of S (H_S) (see Figure 4-6) is obtained by (Torge, 1980, eqn. 5.70)

$$\delta g_{bpr} = 2\pi G\rho H_S = 0.0419 \times 10^{-5}\ \rho H_S = 0.1119 H_S \times 10^{-5}\ (ms^{-2}) \qquad (4.22)$$

where δg_{bpr} is the Bouguer plate reduction

G is the Newtonian gravitational constant, $6.67259 \times 10^{-11}\ kg^{-1}\ m^3\ s^{-2}$ (Cohen and Taylor, 1990)

ρ is the Bouguer or mean crustal density, ie assumed density within the plate. The value of $\rho = 2.67 \times 10^3\ kg\ m^{-3}$ is commonly used.

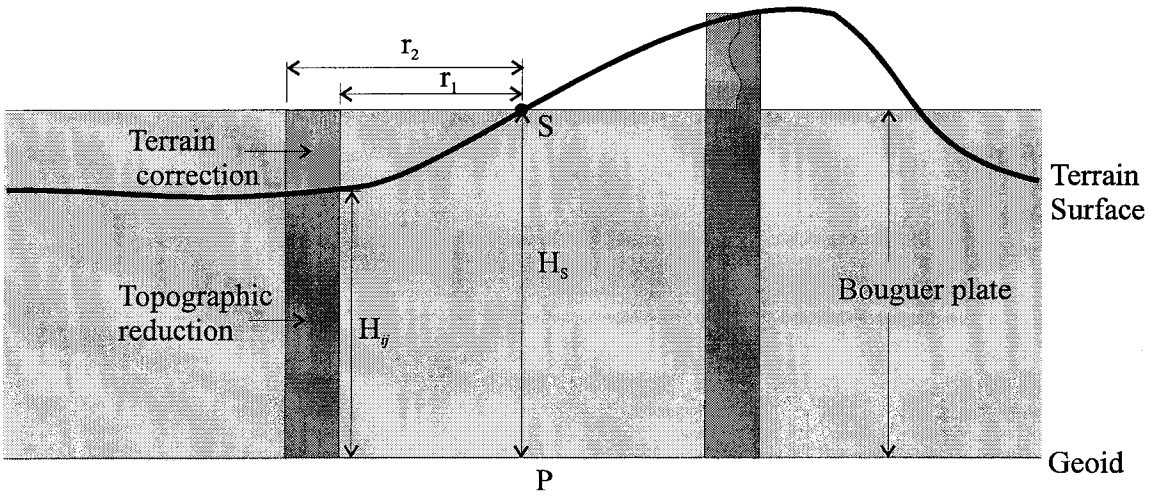

Figure 4 - 6 : Bouguer reduction and Terrain Correction

4.2.4.2 Terrain correction

The Bouguer plate reduction does not take into account the variation of the terrain surface with respect to the Bouguer plate surface (see Figure 4-6). The variation of the terrain from the Bouguer plate is accounted for by the terrain correction δg_{tc} and if a plane is assumed for the Bouguer plate reduction, δg_{tc} is always positive.

Using the law of gravitation the terrain is divided into vertical columns using concentric rings and radii centred at the point of observed gravity (similar to the division using polar coordinates in Section 4.2.3.3). The vertical component of gravitation for each compartment is computed using (Torge, 1980, eqn. 5.71)

$$\delta g_{ctc} = G\rho\Delta\alpha\left(r_2 - r_1 + \sqrt{\Delta H^2 + r_1^2} - \sqrt{\Delta H^2 + r_2^2}\right) \qquad (4.23)$$

where δg_{ctc} is the vertical component of gravitation for compartment *ij*

$\Delta\alpha$ is the angle between the radial lines centred on the gravity point. ie. $2\pi/n$, where n is the number of compartments per ring (r_1, r_2 pair).

r_1, r_2 are the inner and outer radii for the compartment.

ΔH is the difference between the mean-compartment height and the point of computation, ie. $H_S - H_{ij}$. (see Figure 4-6)

i, j are the radial position of the appropriate ring and position of the compartment within the ring, respectively.

By summing the contributions from each compartment the terrain correction is obtained for the point of observed gravity, ie.

$$\delta g_{tc} = \sum_{i=1}^{n_{max}} \sum_{j=1}^{J} \delta g_{ctc} \qquad (4.24)$$

where J is the total number of compartments per ring

Hammer (1939) developed a method of calculating the terrain correction using (4.23) that tried to maintain nearly square compartments. The method is referred to as Hammer Zones and applies a constraint on the selection of compartment size by insisting that $r_2/r_1 = (n+\pi)/(n-\pi)$. This constraint results in both a larger number of compartments per ring, and an increase in the size of the radial component of the compartment, with increasing distance from the point of gravity observation.

With the number of gravity observations increasing and the availability of DEM's, FFT approaches to calculating the terrain correction have become popular due to their superior computation speed over numerical integration methods such as (4.24). The original development of the 2D FFT to calculate the terrain correction using a DEM was by Sideris (1984). This work applied a linear approximation using the first-order term of the series expansion of the rigorous formula for terrain corrections. Sideris (1990) developed a 2D FFT method for any order but the 2D FFT cannot be applied when the density in the z-direction varies or there are large terrain inclinations (Peng *et al.*, 1995). To overcome the limitations of the 2D FFT method Peng *et al.* (*ibid.*) have developed a 3D FFT method to calculate the terrain correction using density values on a 3D grid.

4.2.4.3 Topographic Reduction

The Topographic reduction δg_{Topo} is the combination of the Bouguer plate reduction (4.22) with the terrain correction (4.24)

$$\delta g_{Topo} = \delta g_{bpr} - \delta g_{tc} \tag{4.25}$$

The main source of error in the topographic reduction comes from the assumed density ρ of the topographic mass, used in both the Bouguer plate reduction and the terrain correction. However, Smith (1992, p. 64) reported that varying the density in Hawaii from 2.67×10^3 kg m^{-3} to 2.9×10^3 kg m^{-3}, which is a large physical variation, made little practical difference to the N values (less than 0.01m).

4.2.4.4 Free-air Reduction

Applying the topographic reduction alone to the observed gravity only removes the mass. The gravity station must also be reduced to the geoid and as the point is not moved through any mass (because the mass has already been accounted for in the topographic reduction) the correction is referred to as the free-air reduction. The rigorous free-air reduction is (Heiskanen and Moritz, 1967, eqn. 2-124)

$$\gamma_h - \gamma = -\frac{2\gamma_a}{a}\left[1 + f + m + \left(-3f + \frac{5}{2}m\right)\sin^2\phi\right]h + \frac{3\gamma_a}{a^2}h^2 \tag{4.26}$$

where γ_h is the normal gravity for a point at latitude ϕ, situated at height h.

γ is the normal gravity (4.2) at the ellipsoid for the same latitude as γ_h

f is the oblate flattening of the reference ellipsoid

m is the ratio of centrifugal force and gravity at the equator of the reference ellipsoid, $m = \frac{\omega^2 a}{\gamma_a}$ (*ibid.*, eqn. 2-100)

An alternative form of (4.26) is (*ibid.*, p. 78), though as h is often unknown it is common to replace h with H, thus giving

$$\gamma_h - \gamma = \frac{\partial \gamma}{\partial h} H + \frac{1}{2!}\frac{\partial^2 \gamma}{\partial h^2} H^2 + \ldots \qquad (4.27)$$

It should be noted that in (4.27) since $\partial g/\partial H$ is unknown it is approximated by $\partial \gamma/\partial h$. Rather than using (4.27), it has been common practise to use a simplified free-air reduction, which neglects the dependence on latitude and omits terms non-linear in H. The linear or simplified free-air reduction is (Torge, 1980, eqn. 5.66)

$$\delta g_{sfa} = -\frac{\partial g}{\partial H} H \cong -\frac{\partial \gamma}{\partial h} H \cong +0.3086 \ H \ (\text{mGal}) \qquad (4.28)$$

Pavlis (1988), Heck (1990) and Featherstone (1992) have all shown that applying only the simplified free-air reduction is not adequate for precise gravity studies. The second term on the right hand side of (4.27) can reach about 4 mGal in the Himalayas (Pavlis, *ibid.*, p. 59) and 0.5 mGal in mountainous regions of the British Isles (Featherstone, *ibid.*, p. 100).

Combining the simple free-air reduction (4.28) with the correction term associated with GRS80 of Heck (*ibid.*, eqn. 3-8) results in the second-order free-air reduction δg_{fa}.

$$\delta g_{fa} = \delta g_{sfa} + (-1.69\text{x}10^{-4} + 4.4\text{x}10^{-4}\sin^2\phi)H + 7.21\text{x}10^{-8} H^2 \quad (\text{mGal}) \qquad (4.29)$$

The use of (4.29) should be restricted to cases when only the simple free-air reduced gravity observations are available. When the raw gravity observations are available then (4.26) should be used with H replacing h (Featherstone, *ibid.*, section 5.1.1) as follows

$$\delta g_{fa} = -\frac{2\gamma_a}{a}\left[1 + f + m + \left(-3f + \frac{5}{2}m\right)\sin^2\phi\right]H + \frac{3\gamma_a}{a^2}H^2 \qquad (4.30)$$

$$= (-0.308769 + 4.40\text{x}10^{-4}\sin^2\phi)H + 7.21\text{x}10^{-8} H^2 \quad (\text{mGal}) \quad \text{for GRS80}$$

4.2.4.5 Bouguer reduction

The Bouguer reduction δg_{br} is the combination of the Bouguer plate reduction, Terrain reduction and the Free-air reduction

$$\delta g_{br} = -\delta g_{bpr} + \delta g_{tc} + \delta g_{fa} \qquad (4.31)$$

When the Bouguer reduction is applied to the observed gravity, Bouguer gravity g_B is obtained on the geoid.

$$g_B = g + \delta g_{br} = g - \delta g_{bpr} + \delta g_{tc} + \delta g_{fa} = g - \delta g_{Topo} + \delta g_{fa} \quad (4.32)$$

Other terminology used for the Bouguer reduction include the refined Bouguer reduction and the complete Bouguer reduction.

4.2.4.6 Gravity anomalies

Since the Bouguer gravity g_B in (4.32) refers to the geoid (actually co-geoid, see Section 4.2.4.7) it is possible to obtain gravity anomalies as defined in Section 4.2.2 by subtracting the normal gravity γ_Q (4.2) referred to the ellipsoid (Heiskanen and Moritz, 1967, eqn. 3-19)

$$\Delta g_B = g_B - \gamma_Q \quad (4.33)$$

where Δg_B is called the Bouguer anomaly.

Any of the terrain reductions in the preceding sections can also be converted to their anomaly component by applying the appropriate terrain reduction to the observed gravity and subtracting the normal gravity $\gamma_{Q.}$, ie the Free-air anomalies Δg_{fa} would be obtained by using

$$\Delta g_{fa} = g + \delta g_{fa} - \gamma_Q \quad (4.34)$$

The Faye anomaly (Δg_{Fy}) is obtained by applying the terrain correction and the Secondary Indirect Effect (δg_{SI}) (Section 4.2.4.7), to the free-air anomaly.

$$\Delta g_{Fy} = \Delta g_{fa} + \delta g_{tc} + \delta g_{SI} \quad (4.35)$$

Since the terrain reductions described so far only relate to the gravity observations they are also referred to as gravity reductions.

4.2.4.7 Indirect Effect and the Secondary Indirect Effect

By removing the topographic masses outside (above) the geoid in, say, the Bouguer reduction, the gravitational potential of the earth has been changed. As the geoid was originally defined by the equipotential surface, W_o, the effect of removing the topographic mass means that a point originally on the geoid will have experienced a change in gravity potential of δW. The new equipotential surface that the point lies on is called the co-geoid. Hence if any of the gravity anomalies outlined in Section 4.2.4.6

were used in Stokes' integral then the values of N computed would refer to the co-geoid rather than the geoid. Each of the different gravity reductions results in a different co-geoid being generated.

The difference in the height between the geoid and the co-geoid is called the indirect effect on the geoid undulation, δN_I, and can be computed via Brun's formula as

$$\delta N_I = \delta W / \gamma_Q \tag{4.36}$$

Different methods of computing the indirect effect have been investigated by, amongst others, Wichiencharoen (1982a) and Sideris (1990). The simplest, though least accurate way of computing δN_I is that of Grushinsky's formula.

$$\delta N_I = \frac{-\pi G \rho H^2}{\gamma_Q} \tag{4.37}$$

The computation of the geoidal height can then be computed using (Torge, 1980, eqn. 5.63)

$$N = N^C + \delta N_I \tag{4.38}$$

where N^C is the co-geoidal height.

A secondary effect of this approach is the effect of N^C on the gravity anomalies. Since the co-geoid lies above the geoid, and no masses exist between the surfaces, the reduction of gravity anomalies from the geoid to the co-geoid can be applied as a free-air reduction (δg_{SI}). This is referred to as the Bowie reduction or the secondary indirect effect on the gravity anomalies, and is computed using (Heiskanen and Moritz, 1967, eqn. 3-51)

$$\delta g_{SI} = +0.3086\ \delta N_I \tag{4.39}$$

Including the two indirect effects caused by the gravity reductions, (4.20) is rewritten as

$$N = \frac{r}{4\pi\gamma_Q} \iint_\sigma (\Delta g + \delta g_{SI})\ S(\psi)\, d\sigma + \delta N_I \tag{4.40}$$

4.2.4.8 Atmospheric Effect

In Stokes' solution of the geodetic boundary value problem, one of the assumptions is that no mass remains outside the geoid. In previous sections the removal of the topographic mass has been considered but there still remains the effect that the mass of

the atmosphere has on the gravity observations taken on the Earth's surface. This is known as the Atmospheric Effect, δg_A.

Besides the removal of the masses outside the geoid, other reasons for requiring δg_A to be calculated are: i) that GRS80 is defined including the mass of the atmosphere and ii) that geopotential coefficients include the mass of the atmosphere due to its effect on the satellite orbits. Therefore to ensure consistency between data types δg_A should be calculated.

The precise calculation of δg_A is difficult due to the constantly changing atmospheric densities. However, due to the small magnitude of the atmospheric mass in relation to the Earth's mass, δg_A is small (under 1 mGal). This can be seen from (4.41) and (4.42) which are models of δg_A by Wichiencharoen (1982b) and Featherstone (1992) respectively.

$$\delta g_A = 0.8658 - 9.727\text{x}10^{-5}\, H + 3.482\text{x}10^{-9}\, H^2 \tag{4.41}$$

$$\delta g_A = 0.871 - 1.0298\text{x}10^{-4}\, H + 5.3105\text{x}10^{-9}\, H^2 - 2.1642\text{x}10^{-13}\, H^3 + 9.5246\text{x}10^{-18}\, H^4 - 2.2411\text{x}10^{-22}\, H^5 \tag{4.42}$$

where δg_A is in mGal and H is the orthometric height in metres.

4.2.4.9 Summary of Terrain and Atmospheric Effects on Stokes' integral

To enable N to be solved by using (4.20) the effects of the terrain above the geoid have to be removed. The result of these reductions when combined with (4.20) results in

$$\mathbf{N} = \frac{r}{4\pi\gamma_Q} \iint_{\sigma} (\Delta g_{Fy} + \delta g_{SI} + \delta g_A)\, S(\psi)\, d\sigma + \delta N_I \tag{4.43}$$

where Δg is the gravity anomaly (either Bouguer, Free-air or Faye) and the Indirect effects are appropriately computed depending on which gravity anomaly is used.

4.2.5 Global Geopotential Models

Torge (1980, p. 28) shows that the gravitational potential of the Earth (V) can be fully expressed in spherical harmonics as

$$V = \frac{GM_E}{r}\left(1 + \sum_{n=1}^{\infty}\sum_{m=0}^{n}\left(\frac{a}{r}\right)^n \left(\overline{C}_{nm}\cos m\lambda + \overline{S}_{nm}\sin m\lambda\right)\overline{P}_{nm}(\cos\vartheta)\right) \tag{4.44}$$

where G is the Newtonian gravitational constant

M_E is the mass of the Earth

a is the equatorial radius of the Earth

r is the geocentric radial distance to the computation point

n,m are the degree and order respectively

$\overline{C}_{nm}$ is the normalised zonal Stokes' harmonic coefficients

$\overline{S}_{nm}$ is the normalised tesseral Stokes' harmonic coefficients

$\overline{P}_{nm}$ is the normalised associated Legendre polynomial

λ, ϑ are the geocentric longitude and colatitude

When $n = 0$, the potential of the spherically symmetric Earth's mass M_E is concentrated at the centre of mass. The term $n = 0$ has been removed from (4.44) and by setting the origin of the coordinates at the centre of mass of the Earth the first degree terms are forced to zero, ie $C_1=C_{1,1}=S_{1,1}=0$ (Torge, *ibid.*, eqn. 2.57).

The harmonic coefficients, $\overline{C}_{nm}$ and $\overline{S}_{nm}$, can be explicitly determined for the earth's gravity field using spherical harmonic analysis, though Featherstone (1992, Section 3.1) points out that amongst other limitations the density distribution within the Earth is not well defined, so (4.44) can only be determined by a limited series ($n_{\max}$) as follows (Featherstone, *ibid.*, eqn. 3.1)

$$V_{GGM} = \frac{GM_{GGM}}{r}\left(1 + \sum_{n=2}^{n_{\max}}\sum_{m=0}^{n}\left(\frac{a_{GGM}}{r}\right)^n \left(\overline{C}_{nm}\cos m\lambda + \overline{S}_{nm}\sin m\lambda\right)\overline{P}_{nm}(\cos\vartheta)\right) \quad (4.45)$$

When (4.45) is solved complete to degree and order $n_{\max}$ it will be referred to as a Global Geopotential Model (GGM). The subscript *GGM* has been used to highlight the fact that values of *GM* and *a* associated with a GGM sometimes differ from those of GRS80, and the unknown true values of the Earth.

The practical determination of the Earth's gravity potential is achieved through the use of satellite and/or surface information. Since the early 1960's there have been numerous GGM developed. Nerem *et al.* (1995) give a review of recent progress in the representation of the Earth's gravitational potential. To date GGM have been computed up to $n_{\max} = 360$ (see Rapp *et al.*, 1991 and Gruber and Anzenhofer, 1993). Improved

n_{max} = 360 GGM are being developed using different data sets and weighting procedures (eg. Rapp and Nerem, 1994), and GGM to n_{max} = 720 are being considered (Rapp, 1995).

The maximum resolution of a GGM is in theory directly proportional to n_{max} by the relationship π/n_{max}. Therefore a GGM with n_{max} = 360 should be able to recover geoidal features with half wavelengths of 0.5° ≅ 55 km.

For the optimisation of the RINT technique in the lower North Island test area of New Zealand (Section 4.5) only four GGM were used, as shown in Table 4-1. It should be noted that in Table 4-1 GRS80 is not a GGM but is included to highlight the different *GM* and *a* values used in its definition.

GGM name	Reference	n_{max}	GM_{GGM} (m^3s^{-2})	a_{GGM} (m)	data
GEM-T2	Marsh *et al.*, 1990	36	$3.98600436 \times 10^{14}$	6378137	st
OSU81	Rapp, 1981	180	$3.98600436 \times 10^{14}$	6378137	st, sa, tg
OSU91A	Rapp *et al.*, 1991	360	$3.98600436 \times 10^{14}$	6378137	st, sa, tg
EGM96	Lemoine *et al.*, 1996	360	$3.986004415 \times 10^{14}$	6378136.5	st, sa, tg
GRS80	Moritz, 1980a	--	3.986005×10^{14}	6378137	--

Table 4 - 1 : Global Geopotential Models used in analysis (adapted from Featherstone, 1992). Note: st - satellite orbit perturbation information; sa - satellite altimeter derived information; tg - observed terrestrial gravity anomalies

Once the harmonic coefficients ($\overline{C}_{nm}$ and $\overline{S}_{nm}$) have been determined it is then possible to calculate values for the geoid height and the gravity anomaly. The geoidal height from the GGM (N_{GGM}) can be computed using (Torge, 1980, eqn. 5.55b)

$$N_{GGM} = R\sum_{n=2}^{n_{max}}\sum_{m=0}^{n}\left(\overline{C}_{nm}\cos m\lambda + \overline{S}_{nm}\sin m\lambda\right)\overline{P}_{nm}(\cos\vartheta) \qquad (4.46)$$

where R is the mean radius of the Earth. The gravity anomaly from the GGM (Δg_{GGM}) can be computed using (Torge, 1980, eqn. 5.54a)

$$\Delta g_{GGM} = \frac{GM}{R^2}\sum_{n=2}^{n_{max}}\sum_{m=0}^{n}(n-1)\left(\overline{C}_{nm}\cos m\lambda + \overline{S}_{nm}\sin m\lambda\right)\overline{P}_{nm}(\cos\vartheta) \qquad (4.47)$$

4.3 Ring Integration Technique

The Ring Integration Technique (RINT) is basically the solving of Stokes' formula (4.20) by numerical integration using polar coordinates and scaling Stokes' function (4.19) by sin(ψ) to overcome the singularity at ψ = 0. See Section 4.2.3 for a summary of other Gravimetric techniques to solving the Boundary Value Problem. A flow diagram of the School of Geomatic Engineering, UNSW, gravity computation software is contained in Appendix F, with software enhancements undertaken as part of this research described in Section 4.3.6.

The theory for RINT was originally developed by Lambert and Darling (1936) and is outlined in Heiskanen and Moritz (1967, Section 2-24). A number of authors have developed this theory further and produced geoid heights (Section 4.3.3). Kearsley (1984, 1985, 1986a, 1988) has been the main proponent of RINT. Kearsley's work forms the basis of the method that has been used to determine a procedure to develop a gravimetric geoid for New Zealand and is described in the remainder of this chapter.

4.3.1 Non-linearity of Stokes' Function

As was outlined in Section 4.2.3.1 Stokes' function tends to infinity when the spherical distance approaches zero. Due to the rapid change in S(ψ) below 2° (Figure 4-7), S(ψ) can not be assumed to be linear across the compartment. To overcome this non-linearity Lambert and Darling (1936) suggested the use of the F(ψ) function.

Taking (4.20) and setting $d\sigma = \sin\psi\, d\psi\, d\alpha$, Stokes' Integral can be written as (Kearsley, 1985, eqn. 2.5)

$$N = \frac{r}{4\pi\gamma_Q}\int_{\psi=0}^{\pi}\int_{\alpha=0}^{2\pi}\Delta gS(\psi)\,\sin\psi\, d\psi\, d\alpha \qquad (4.48)$$

where $d\psi$ is the increment in the spherical radial distance centred upon the computation point.

$d\alpha$ is the increment in the direction of the radial line.

with F(ψ) defined as S(ψ) sinψ (4.48) can be rewritten as

$$N = \frac{r}{4\pi\gamma_Q} \int_{\psi=0}^{\pi} \int_{\alpha=0}^{2\pi} \Delta g \, F(\psi) \, d\psi \, d\alpha \tag{4.49}$$

F(ψ) in closed form is obtained by multiplying (4.19) by sinψ, resulting in

$$F(\psi) = 2\cos\left(\frac{\psi}{2}\right) - \sin\psi\left[6\sin\left(\frac{\psi}{2}\right) - 1 + \cos\psi\left\{5 + 3\ln\left(\sin\frac{\psi}{2} + \sin^2\frac{\psi}{2}\right)\right\}\right] \tag{4.50}$$

From Figure (4-7) it can be seen that F(ψ) does not have a singularity at ψ = 0 and is also a flatter function than its parent S(ψ). Closer examination (see Figure 4-8) shows that in the range 0° < ψ < 2°, which encompasses common spherical cap sizes (Section 4.3.2), F(ψ) can safely be considered linear.

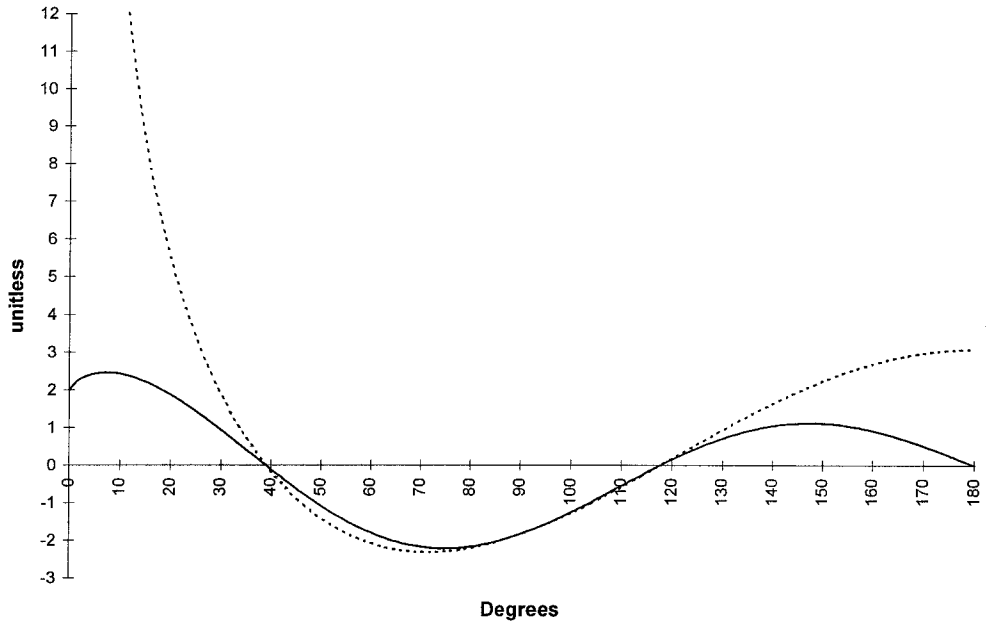

Figure 4 - 7 : Plot of the S(ψ) and F(ψ) functions for 0° < ψ ≤ 180°. Where S(ψ) is the pecked line and continues to infinity at 0°, F(ψ) is the solid line.

4.3.2 Global Geopotential Model and Stokes' Integral

Stokes' integral (4.20) requires that the gravity anomalies Δg be available over the whole of the earth's surface so the integration can be performed globally. This is neither feasible or required as has been shown by many authors, including Rapp and Rummel

(1975) and Kearsley (1988). Through the use of a GGM to provide the medium to long wavelength features of N, the integration of Stokes' integral can be restricted to a spherical cap of, at most, a couple of degrees. This method of using a GGM is common in modern geoid determinations and is not restricted to the RINT approach (see Torge, 1980 and Heiskanen and Moritz, 1967).

By incorporating the GGM with Stokes' integral the gravimetric geoid height is computed by

$$N_{GRAV} = N_{GGM} + N_{RINT} \tag{4.51}$$

where N_{GGM} is the longer wavelength features of the gravity field represented by the GGM and computed using (4.46).

N_{RINT} is the short wavelength features of the gravity field integrated by Stokes' integral (4.49) out to the spherical cap of ψ_O.

$$N_{RINT} = \frac{r}{4\pi\gamma_Q} \int_{\psi=0}^{\psi_0} \int_{\alpha=0}^{2\pi} \Delta g \, F(\psi) \, d\psi \, d\alpha \tag{4.52}$$

In it's present form (4.51) has introduced two errors because:

i) Stokes' integral has been truncated at a spherical cap of ψ_0. This truncation error results in the values for the integration of (4.52) in the range of $\psi_0 < \psi \leq \pi$ being neglected (Jekeli, 1981). Further discussion of methods to reduce the truncation error are contained in Section 4.3.2.1, and

ii) the gravity anomalies in (4.52) contain the long wavelength features so (4.51) includes these long wavelengths features twice. To avoid this the gravity anomaly (Δg) is reduced by the gravity anomaly of the GGM (Δg_{GGM}), to the same degree and order that N_{GGM} was computed, before the integral is solved (Kearsley, 1988). The new gravity anomalies produced from Δg-Δg_{GGM}, are called residual gravity anomalies, Δg_r. Thus applying this update to (4.52) results in the equation that forms the foundation of the Ring Integration technique

$$N_{RINT} = \frac{r}{4\pi\gamma_Q} \int_{\psi=0}^{\psi_0} \int_{\alpha=0}^{2\pi} (\Delta g - \Delta g_{GGM}) \, F(\psi) d\psi \, d\alpha \tag{4.53}$$

where Δg_{GGM} is computed using (4.47). In (4.53) the integration reference surface has changed from the reference ellipsoid (n = 2) to the GGM geoid solution ($n = n_{max}$) (Vanicek and Sjoberg, 1991).

The technique of combining Stokes' integral and a GGM by way of (4.51) is referred to as the Remove - Restore technique. This is because the GGM gravity anomaly (Δg_{GGM}) is removed from the gravity anomaly (Δg) before integration and restored after integration by the GGM geoid height (N_{GGM}).

4.3.2.1 Kernel modification to reduce truncation error

In applying (4.53) to a limit of ψ_0 the contribution of Δg_r in the range $\psi_0 < \psi \leq \pi$ is neglected from the determination of N_{RINT}. This neglected component is referred to as the truncation error (N_{Trunc}) and can be computed by

$$N_{Trunc} = \frac{r}{4\pi\gamma_Q} \int_{\psi=\psi_0}^{\pi} \int_{\alpha=0}^{2\pi} (\Delta g - \Delta g_{GGM})\, F(\psi)\, d\psi\, d\alpha \qquad (4.54)$$

It is common for the truncation error not to be computed in geoid computations. However, a simple way to overcome the computation of (4.54) while reducing the effects of N_{Trunc} is to modify Stokes' integration kernel so that the effect of Δg_r outside ψ_0 is minimised.

Numerous researchers have proposed different modification's to Stokes' integral to minimise the truncation error but only four will be investigated for use with RINT. The four modifications are based on Wong and Gore (1969), Meissl (1971), Vanicek and Sjoberg (1991), and Featherstone and Evans (1996). All four modifications were originally developed for use with the $S(\psi)$ function, however they can easily be converted to a $F(\psi)$ function suitable for use in RINT by appropriately multiplying by $\sin\psi$.

A brief summary of each modification will now be given, though for further details the reader is referred to Featherstone (1992) along with the respective original authors.

i) Wong and Gore (1969) reduce the truncation error by suppressing the low degree Legendre coefficients in $S(\psi)$ using

$$F_{wg}^{N_{mod}}(\psi) = F(\psi) - \sum_{n=2}^{N_{mod}} \frac{(2n+1)}{(n-1)} P_n(\cos\psi)\sin\psi \qquad (4.55)$$

where N_{mod} is the degree of modification to the integration kernel. This integer number can be different to the maximum degree of expansion of the geopotential model (n_{max}). The choice of a large kernel modification has to be approached with caution as it behaves as a filter and removes all corresponding wavelengths below this degree, thus not allowing errors in the GGM to be corrected by the terrestrial gravity data (Featherstone, 1992, Section 6.3). N_{mod} was restricted to 36 for this investigation.

ii) Meissl (1971) proposed reducing the truncation error by subtracting the value of Stokes' kernel at ψ_0 from the kernel itself :

$$F_{me}(\psi) = F(\psi) - S(\psi_o)\sin\psi_o = F(\psi) - F(\psi_o) \tag{4.56}$$

iii) Vanicek and Sjoberg (1991) reduce the truncation error by applying similar theory to that of Molodenskii *et al.* (1962) in the generalised Stokes scheme for a higher than second degree reference surface :

$$F_{vs}^{N_{\text{mod}}}(\psi) = F_{wg}^{N_{\text{mod}}}(\psi) - \sum_{n=2}^{N_{\text{mod}}} \frac{(2n+1)}{2} t_k(\psi_0) P_n(\cos\psi)\sin\psi \tag{4.57}$$

The Molodenskii-like ellipsoidal truncation coefficients (t_k) are given by :

$$\sum_{n=2}^{N_{\text{mod}}} \frac{(2n+1)}{2} t_k(\psi_0) e_{nk}(\psi_0) = Q_n(\psi_0) - \sum_{n=2}^{N_{\text{mod}}} \frac{(2n+1)}{2} e_{nk}(\psi_0) \tag{4.58}$$

where the Molodenskii truncation coefficients (Q_n) are easily computed using the algorithms of Paul (1973), and

$$e_{kn}(\psi) = \int_{\psi_O}^{\pi} P_k(\cos\psi) P_n(\cos\psi)\sin\psi d\psi \tag{4.59}$$

As was the case for the Wong and Gore approach ($F_{wg}^{N_{\text{mod}}}(\psi)$) the higher the degree of kernel modification the larger the filtering effect, so N_{mod} is also restricted to 36 for this research.

iv) Featherstone and Evans (1996) applied the theory of Meissl (*ibid.*) to the Vanicek and Sjoberg (*ibid.*) modification. Thus when (4.56) is applied to (4.57) the modification is :

$$F_{fe}^{N_{\text{mod}}}(\psi) = F_{vs}^{N_{\text{mod}}}(\psi) - F_{vs}^{N_{\text{mod}}}(\psi_o) \tag{4.60}$$

The form of the original $F(\psi)$ and the four modified kernels for $\psi_0 = 0.3°$ ($\cong$ 30 km) and $\psi_0 = 1.5°$ ($\cong$ 150 km) can be seen in Figure 4-8. As the $F(\psi)$ values were computed at the mid compartment rather than outer ring edge (the full ψ_0), values for the Meissl, and the Featherstone and Evans modifications approach but do not equal zero. At ψ_0 these two modifications do equal zero.

The evaluation of these four modifications to reduce truncation error using gravity data is contained in Section 4.5.5. Algorithms for the kernel modifications were generously supplied by Will Featherstone, Curtin University of Technology, Western Australia.

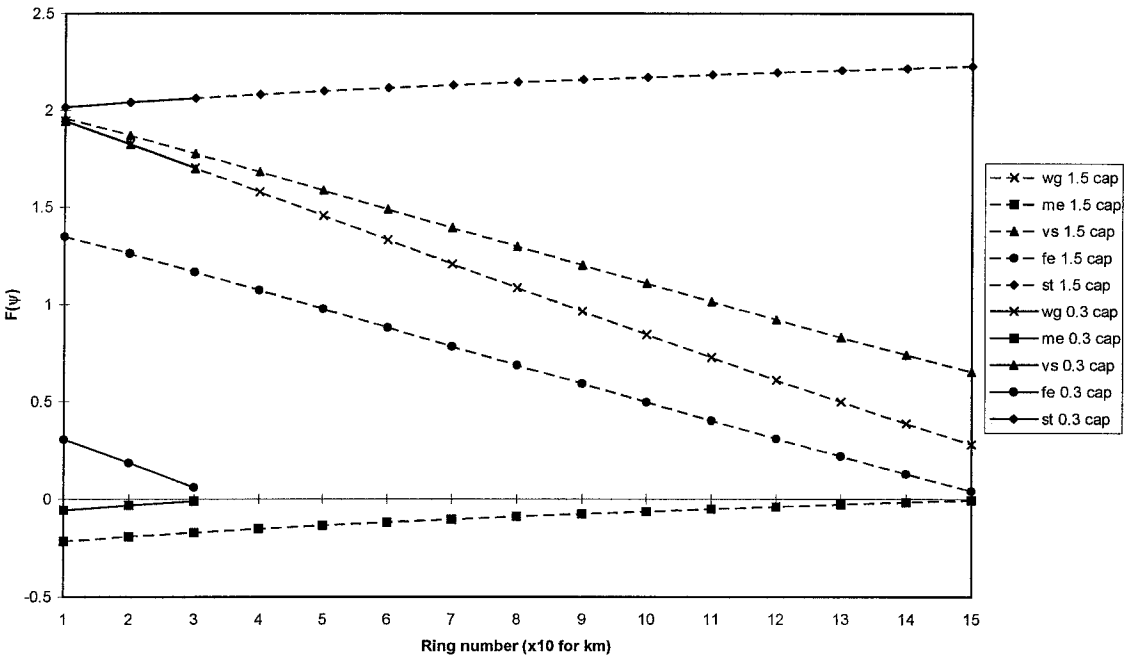

Figure 4 - 8 : Modified kernels to minimise truncation error at $\psi_0 = 0.3°$ and 1.5°. The abbreviations are : Wong and Gore (wg), Meissl (me), Vanicek and Sjoberg (vs), Featherstone and Evans (fe), and Stokes (st). Note at plot scale wg and vs are equivalent for $\psi_0 = 0.3°$.

4.3.3 Computational refinements to the RINT technique

Other authors to use the RINT technique in association with their own modifications are Stewart (1990) and Tsen (1992). Both these authors use the RINT technique to compute

the inner zone (short wavelength) contribution to the geoid (as does Kearsley) and rely on a GGM to provide the outer zone (long wavelength) contribution (see Section 4.3.2 for the combining of GGM and gravity data).

Kearsley develops the rings so that each compartment makes the same contribution per mGal to N at the computation point, obviating the need to compute the area of each compartment in the ring structure.

The work by Stewart was based on the algorithms described in Kearsley (1986b). Stewart chose to use a fixed compartment size so that the mean gravity anomaly for each compartment could be pre-computed. This technique was designed to overcome the computational effort of having to recompute the mean gravity anomaly for each compartment around each point requiring a geoid height.

Tsen (*ibid.*), like Kearsley, uses varying compartment sizes around each computation point. However, Tsen breaks the inner zone into three sub-zones, each having a different number of compartments per ring, with zones further from the computation point having a larger number of compartments.

4.3.4 Practical evaluation of Ring Integration

The practical evaluation of the equation that forms the foundation of the Ring Integration technique, (4.53), will be briefly outlined in this section. For the full development of this approach see Kearsley (1985, 1986a), and from which the following derivations have been taken.

The modified Stokes' integral (4.53) can be used to produce a pattern of compartments, bounded by rings concentric to the computation point and by lines radiating from these points (Figure 4-5). By setting $d\alpha$ to a constant it is possible to vary the ring radii (ψ_j) so that each compartment contributes equally (per mGal) to the geoid height at the computation point.

Defining C_N as the contribution to N_{RINT} for one compartment bounded by $d\alpha$, ψ_i and ψ_j (where j=i+1), one can write

$$C'_N = K_1 \int_{\psi_i}^{\psi_j} \Delta g_r \, F(\psi)\, d\psi \tag{4.61}$$

where $K_1 = \dfrac{r}{4\pi\gamma_Q}\, d\alpha$ and C'_N is in meters. However, C'_N is more convenient if expressed in units of meters per mGal (m/mGal) of the gravity anomaly, thus (4.61) becomes

$$C_N = K_1 \int_{\psi_i}^{\psi_j} F(\psi)\, d\psi \tag{4.62}$$

It should be noted that due to the change in the normal gravity at the surface of the ellipsoid (γ_Q) for each computation point the ring radii (ψ_i and ψ_j) are unique to that computation point.

From (4.53) and (4.62) the integral can be reduced to a double summation.

$$N_{RINT} = C_N \sum_{i=1}^{I} \sum_{j=1}^{J} \Delta\hat{g}_{ij} \tag{4.63}$$

where $\Delta\hat{g}_{ij}$ is the residual mean free-air gravity anomaly (Section 4.3.2) assumed in practice to equal the value at the mid point of compartment *i,j*.

i is the index for the rings.

I is the upper limit of the index for the rings ($I \equiv \psi_0$).

j is the index for the sectors, apex angle $d\alpha$.

$J = 2\pi/d\alpha$, ie. maximum number of compartments per ring.

From (4.63) it can be seen that solving the short wavelength component of the gravity by using RINT is mainly concerned with determining the value of the residual free-air gravity anomaly at the mid-point of each compartment. Then it is a simple matter of summing all such values and scaling by C_N.

One of the advantages of RINT is that the compartment size can be varied to match the average density of the irregularly distributed gravity observations. Also the area, $d\sigma$, of

each compartment does not have to be computed for each ring since this has been accounted for in the evaluation of C_N.

4.3.4.1 Mid-compartment gravity anomaly

When computing the gravity anomaly for each compartment there is a choice between determining the mean or the mid compartment value. RINT computes the mid compartment value by interpolating on the Δg_B surface rather than the Δg_{fa} surface, as this is theoretically a smoother surface (Heiskanen and Moritz, 1967 and Nettleton, 1976). Analysis on the use of Δg_B and Δg_{fa} in New Zealand is contained in Section 4.5.3.

The interpolation uses a plane fit to 7 points and a weighting based on the distance of the point from the mid compartment. The 7 points are chosen so as to select the 3 closest points to the compartment middle, then the next closest point from each of the 4 quadrants to give a well conditioned figure for the interpolation.

4.3.4.2 Mean residual free-air anomaly for the compartment

Once the mid compartment residual Bouguer anomaly has been computed (Section 4.3.4.1) it needs to be converted back to a residual free-air anomaly for use in (4.63). RINT has the option to use either the height information of the gravity stations or a DEM to determine the mean height of the compartment to be used in (4.28) to reconstruct the residual free-air anomaly.

If a DEM is available then the mean height is computed by taking the mean of all the heights which are contained in the compartment.

If no DEM is available, a mean of the heights of the 7 points chosen to interpolate the mid compartment residual Bouguer anomaly is used.

4.3.5 Analysis techniques of the RINT solution

The RINT technique has parameters which can be varied so as to optimise the geoid heights that are computed. These parameters include the ability to: **a)** vary the maximum radius of the integration cap; **b)** vary the size of the compartments; and **c)** use the DEM data. To find which parameter settings are optimum for a specific project area, two techniques are primarily used to evaluate the results. These two techniques will be described in further detail in the following two sub sections, though in summary the first uses the absolute point comparison of the N_{GRAV} and N_{GEO} at each control station, while the second uses the relative line comparison of N_{GRAV} and N_{GEO} between each control station. An alternative analysis technique is investigated in Appendix M.

4.3.5.1 Absolute Point Comparison (δN)

From (4.1) it is possible to compare the gravimetric height of the geoid (N_{GRAV}), computed using RINT, with the geometric height of the geoid (N_{GEO}) once all three heights (h, H, N) are known at the control stations. The difference in the geoid heights (δN) is computed by subtracting N_{GRAV} from N_{GEO}, ie.

$$\delta N = N_{GEO} - N_{GRAV} = (h_{GPS} - H_{Levelling}) - N_{GRAV} \tag{4.64}$$

The use of δN to analyse the N_{GRAV} results has to be approached with caution. One has to assume that there is no bias between any one of the three height datums used (h, H or N). This bias could be in the form of a constant offset and/or a slope between the datums. As δN values would have an expected value of zero if there existed no errors in any of the three heights, analysis of δN can highlight gross errors in the height data. However, identifying which of the three height data has the error is not possible without further information.

4.3.5.2 Relative Line Comparison (δΔN)

To reduce the effects that biases in any of the three height datums can have on the ΔN analysis the relative line comparison is used. The magnitude of δΔN gives an indication of the accuracy of orthometric heights obtained from combining ellipsoidal and geoidal heights using relative heighting methods. By biases in a height datum one means any assumptions that introduce error in the data reductions and adjustment procedures for obtaining the respective height. Instead of calculating the difference in geoid heights at

each control station, the difference between pairs of control stations is calculated using the following formula

$$\delta\Delta N = \Delta N_{GEO} - \Delta N_{GRAV} \quad (4.65)$$

where $\Delta N_{GEO} = h_b - h_a - H_b + H_a$

$\Delta N_{GRAV} = N_{GRAV\,b} - N_{GRAV\,a}$

subscripts *a* and *b* identify the two control stations used for the differencing

The statistical analysis of the $\delta\Delta N$ values can be affected by the choice of control station pairs, ie. *a* to *b* or *b* to *a*. To minimise this effect, the same combination of pairs of control stations should be used through out the analysis, along with the root mean square (rms) of the $\delta\Delta N$ since it is insensitive to the direction of the control station pairing.

4.3.6 Enhancements to the UNSW gravity computation software

The UNSW gravity computation software suite, known as GRAV, was enhanced in a number of areas during this research. This section briefly describes the major enhancements that improved both the capabilities and performance of the GRAV suite.

Prior to 1994 the UNSW copy of the GRAV suite was only compiled on the universities VAX central computer. The first enhancement was therefore to rewrite VAX specific code as standard fortran to enable the compilation of the code on other computing platforms (primarily PC and UNIX). During the testing rounding errors in the original code were discovered for some variables that were only declared as real*4. These rounding errors were more significant for larger cap sizes, amounting to approximately 0.01 m in N per 10 km of cap size.

The input commands for each component of the GRAV suite (see Appendix F) were incorporated into a batch file instead of requiring keyboard input at run-time. This modification to the GRAV suite was undertaken as a joint project with Matt Higgins. The use of batch files enabled the geoid computation process to be automated, thus allowing different tests to be combined in a single batch file and run sequentially over night. In addition example batch files, and help files, were included in the software to

provide users with batch file templates. During this project an error in the search routine for extracting a subset of gravity data around the computation point was found. Instead of exiting a search loop after sufficient data was obtained the remainder of the file was still read. As the GRAV suite stores data by latitude from south to north the effect on large datasets, such as the Australian wide file, was that considerable processing time was wasted in reading unwanted data for southern sites. Removal of this error improved the computation speed significantly at southern sites (eg. Hobart) but the improvement was reduced the further north the site was. For a northern site (eg. Darwin) there was no improvement.

Inspired by the improvement at southern sites another project to improve the searching of data was undertaken by the author. This resulted in the format of the residual gravity file being changed to a fixed record type, unformatted file so as to allow direct access binary reading. A simple "halving" search routine was then implemented to further improve the time required to search for the desired data. The combined effect of changing the file format and adding the search routine was that at most six records needed to be read to get to the start of the desired data irrespective of the computation points location with respect to the start of the file. The time savings for this change depended on the extent of the data files, though now the computation time for a site was independent of the data file extents, consequently there is no need to have a number of smaller data files containing overlapping data.

The residual gravity data used to be stored as real*8 and when dealing with the Australian wide data set this was almost a 100 Mbyte file. To reduce the hard disk requirements for the GRAV suite the residual gravity data storage format was changed to integer*4 which resulted in approximately a 50% file size reduction.

The GRAV suite was also updated to allow the use of DEM's in the computation of geoid models (see Higgins *et al.*, 1996) and a version developed to test kernel modifications (Section 4.3.2.1) designed to reduce truncation errors due to the integration limit.

4.4 Data - Sources and Validation

4.4.1 Terrestrial Gravity data

The original gravity data supplied by DOSLI for this investigation was derived from a research contract described in Gilliland (1988). The two files supplied were MEANAN.DAT and NZGRAV.DAT. A description of how these two files were generated can be found in Gilliland (1988, 1990) and Woodward (1982).

The MEANAN.DAT file contained mean gravity anomalies for every 1/10 th of a degree block over New Zealand (Latitude S32° - S50°, Longitude E164° - E181°). This file was not used as the RINT based software can directly use the randomly distributed gravity anomalies (Section 4.2.3.3).

The NZGRAV.DAT file contained both land and sea gravity data from Latitude S24.05° - S57.95°, Longitude E162.69° - E191.5°. This data file, as described in Gilliland (1988), contained free-air gravity anomalies in μms^{-2} referenced to the International Gravity Standardisation Network 1971 (IGSN71) and the Geodetic Reference System 1980 (GRS80), being corrected for atmospheric effects (land and sea data) and terrain correction (land data only). The latitude and longitude of the gravity data was in terms of NZGD49 which is not a geocentric datum and uses the International Hayford spheroid as the Figure of the Earth (refer to Section 2.4 or Lee, 1978, p57). The conversion of the NZGD49 latitude and longitude of the gravity data to WGS84 was performed using the Mackie based seven parameter similarity transformation parameters (Table 5-5). The orthometric heights of the gravity stations are in metres and generally were obtained by barometric levelling, although some heights were obtained by spirit levelling or trigonometric heighting. Reilly (1972) states that the accuracy of the barometric levelling varies largely with the degree of control of pressure variation. For surveys under favourable conditions heights could vary between 2-5 m while in windy conditions in mountainous areas variations could attain 10-20 m. The atmospheric effect was calculated as per the recommendations in the GRS80 system. The inner and outer terrain correction was applied out to a radius of 21.94 km (Woodward, 1982) using Hammer's (1939) method. The use of Hammer's method is outlined in Section

4.2.4.2 along with modern techniques of applying the terrain correction. Due to the format of the gravity data supplied to DOSLI, it was not possible to extract the size of the terrain correction that had actually been applied to the observations. An indication of the terrain corrections applied to the data could have been obtained by applying (4.24) or the Hammer (1939) method, however this would not have given original corrections due to the original DEM not be available.

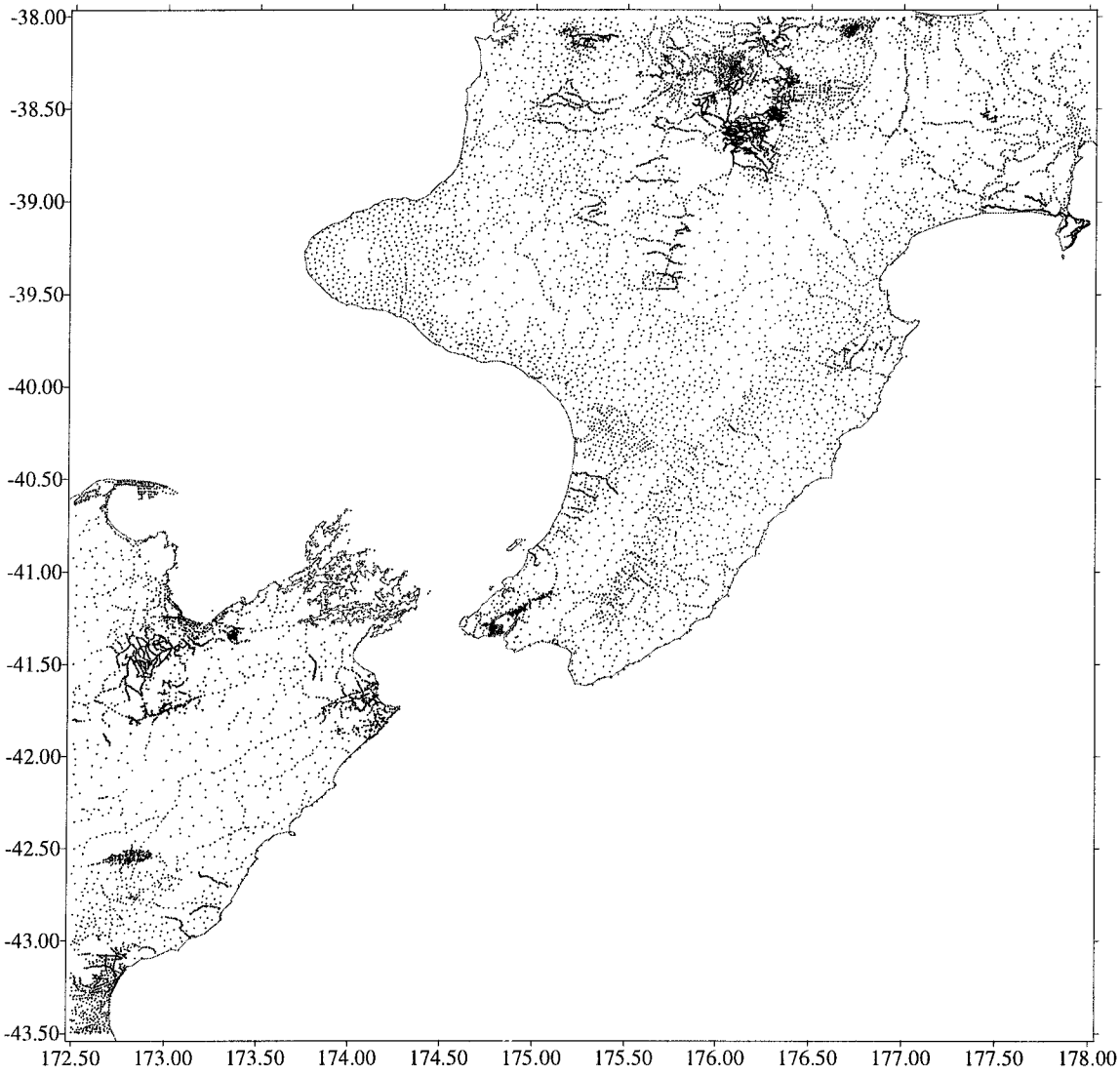

Figure 4 - 9 : Land gravity data for the lower North Island test area. Rectangular projection

The land data for the lower North Island test area (Lat. S38.00° - S43.50°, Long. E172.50° - E178.00°) (Figure 4-9) was extracted from NZGRAV.DAT. There were 15748 records for this land area of approximately 100,000 km^2, which averages out at a

station density of approximately 1 per 6.5 km^2 that is marginally denser than the national average of 7.5 km^2 (Section 4.1).

As can be seen from Figure 4-9, all the land stations for the lower North Island test area appear to fall on land. The gravity stations at approximately S40.7°, E175.0° are on islands. However, if we look back to Figure 4-1 there appears to be a cluster of land stations off the east coast of the South Island (approximately S44.3°, E171.8°) where no islands exist. Irregularities such as this have not been investigated beyond the limit of the lower North Island test area.

4.4.2 Off-shore Gravity data

The ship-borne gravity data for the lower North Island test area (Lat. S38.00° - S43.50°, Long. E172.50° - E178.00°) was extracted from NZGRAV.DAT, which is described in Section 4.4.1. Unlike the land gravity there was (obviously) no need to apply the terrain correction. Figure 4-10 shows the location of the off-shore data, and clearly shows stations on land and a distinct grid pattern.

After holding discussions with Gilliland, University of South Australia and Crook, DOSLI, it was concluded that the original off-shore gravity data that was supplied for use by Gilliland (1988) was read incorrectly during the processing. The grid pattern apparent in Figure 4-10 can be explained as follows: coordinates that had blanks rather than zeros after the decimal place were read ignoring the blanks (ie. 41°.0015 was in the file as 41__15 so was read as 41°.15) and consequently all points between 0.0 and 0.1 of a degree were read incorrectly.

The impact of this error is that if the normal gravity was calculated using the incorrectly read latitude and longitude then the free-air anomalies will be in error due to the observations being at one point and the normal gravity at another which could have been up to 0.9 degrees away.

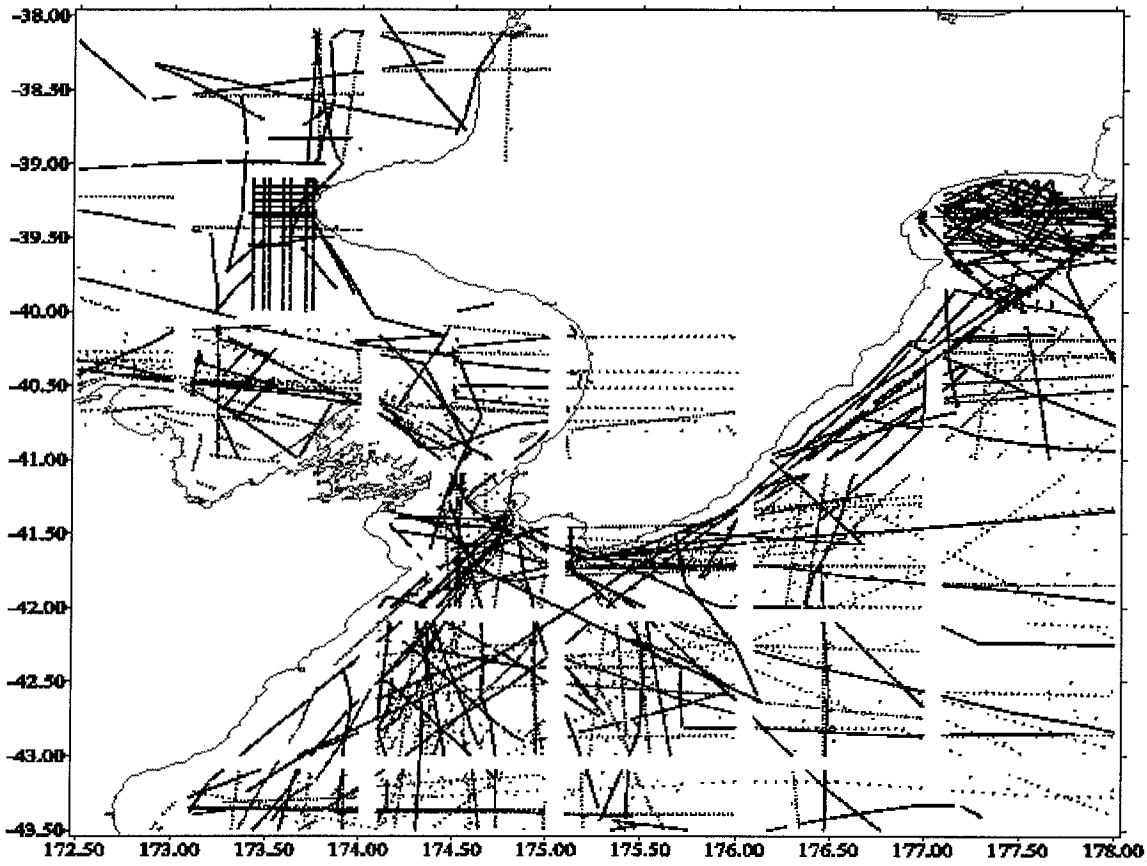

Figure 4 - 10 : Original Off-shore gravity data for the lower North Island test area. Rectangular projection

It was decided that due to the time restrictions the original data, as supplied to Gilliland (*ibid.*) which DOSLI still had on tape, would not be reprocessed. Instead Crook inferred the corrections applied by Gilliland (*ibid.*) by seeking identical points in the NZGRAV.DAT file and in the data read directly from the tape (avoiding the points which were affected by errors reading the tape). For these common points the corrections were determined by fitting a polynomial function of latitude to the data.

The polynomial function fitted all the test points to within the numerical accuracy of the data (ie 0.1 μms^{-2}). This polynomial function was then used to correct all the data read from the tape. The corrected off-shore data was stored in MDBGRAV3.DAT and the points in the lower North Island test area (67,582 records) are shown in Figure 4-11.

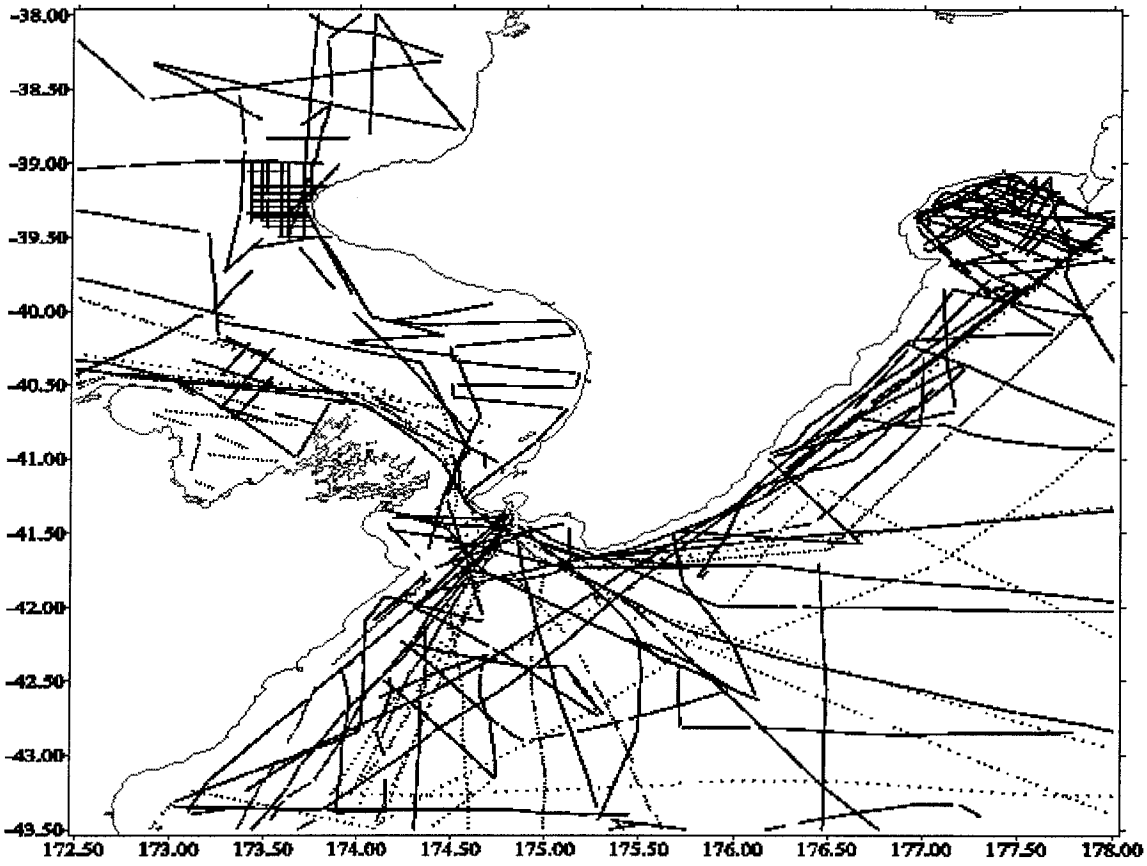

Figure 4 - 11 : Corrected Off-shore gravity data for the lower North Island test area. Rectangular projection

The Institute of Geological and Nuclear Sciences in New Zealand (IGNS), who are responsible for the New Zealand gravity data, were approached for any additional gravity data that had been collected since DOSLI last obtained a copy of the gravity data. This resulted in additional off-shore data being made available. As this new data was in the same format as the original tape data that DOSLI had, the new data was converted using the same latitude function as had been used to create the MDBGRAV3.DAT, and was stored in NEWGRAV.DAT. Figure 4-12 shows this additional off-shore gravity data for the lower North Island test area which consists of 53,072 records.

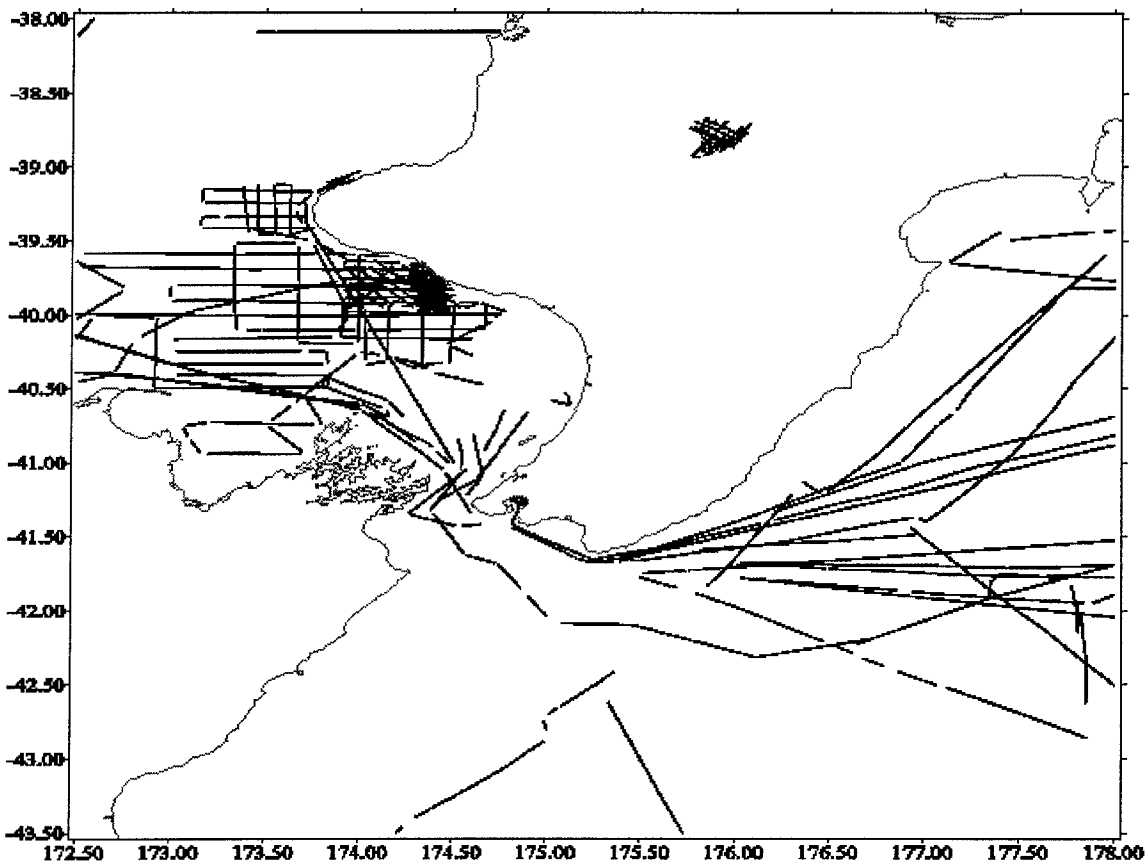

Figure 4 - 12 : Additional Off-shore gravity data from IGNS for lower North Island test area. Rectangular projection

A point to be noted is that Figure 4-12 shows that gravity data observed on Lake Taupo (S38.7, E176.0) is included as off-shore data. The orthometric height of the data observed on the lake is given as 0.0 m in the NEWGRAV.DAT file. The lake surface is approximately 600 m above sea level and by plotting the gravity data in the vicinity of Lake Taupo, confirmed that the gravity observations on the lake have had the free-air correction applied.

The combined off-shore data extracted from the NEWGRAV.DAT and MDBGRAV3.DAT files for the lower North Island test area resulted in 120,654 records for an area of approximately 140,000 km^2, which averages out at a station density of approximately 1 per 1.1 km^2. As can been seen from Figures 4-11 and 4-12 most of the ship-borne gravity has been observed at a high density along the ships track, but the distance between ship tracks can easily be 20 km apart. No attempt was made to thin

the off-shore gravity data in the along track direction to be comparable to the track spacing. It was assumed that this did not affect the final gravimetric geoid computation.

4.4.3 Combined Gravity data and preprocessing

The combined off-shore and land data extracted from the NEWGRAV.DAT, MDBGRAV3.DAT and NZGRAV.DAT files for the lower North Island test area resulted in 136,402 records and was stored as MNTHSORT.DAT (Figure 4-13). For the test area of approximately 240,000 km^2 this averages out at a station density of approximately 1 per 1.7 km^2 when including the effect of the dense along track ship-borne gravity.

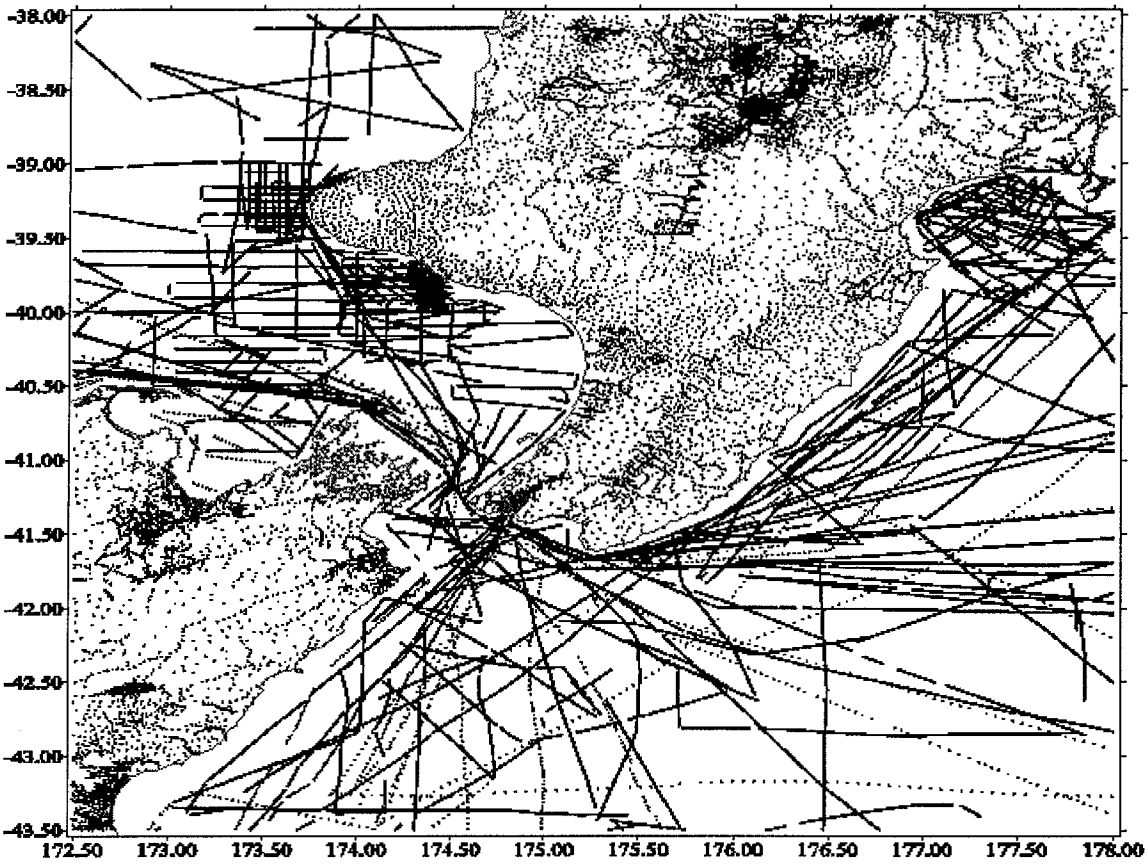

Figure 4 - 13 : Distribution of the combined Off-shore and Land free-air gravity anomalies for the lower North Island test area. Rectangular projection

The free-air gravity anomalies, within the lower North Island test area (Figure 4-13), have the following statistics (units : μms^{-2}): maximum = 2042.0, minimum = -1681.4, mean = -184.9, and standard deviation = 457.2 (Figure 4-14).

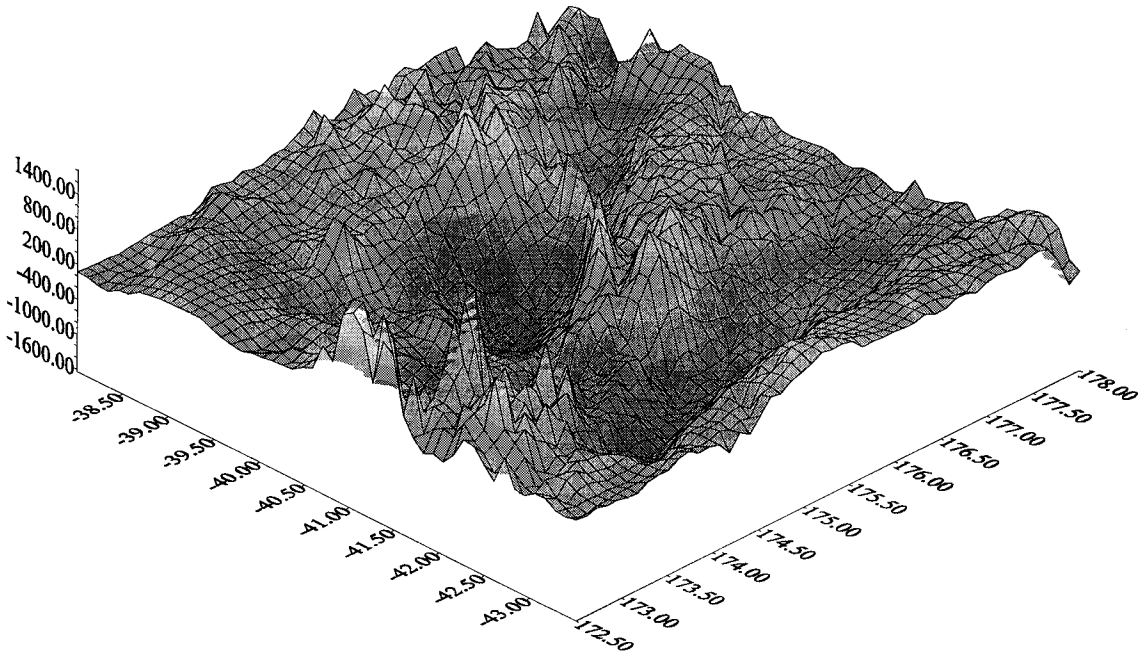

Figure 4 - 14 : Surface plot of the Free-air gravity anomalies of the lower North Island test area (units = μms^{-2})

As was explained in Section 4.3.2, the GGM value for the gravity anomaly is removed from the observed gravity anomaly before the Ring Integration is performed. This removal of the GGM gravity anomaly is performed in the RESIDGRV program, which also checks for duplicate points in the input observed gravity anomaly file. A point is classified as being duplicate if it has, at the fifth decimal place of a decimal degree, the same Latitude and Longitude as another point (approximately 1 metre or less difference in position).

When the combined Off-shore and Land gravity file (consisting of 136,402 records) was run through RESIDGRV there were 15,185 duplicate points. These points can be seen in Figure 4-15, and shows that most duplicate points occur when data is collected from boats, ie. sea or lake areas, and often represent cross-over points.

When the positions of the remaining 121,217 residual free-air gravity anomalies are plotted, there is no visual difference to Figure 4-13, so no new figure has been included.

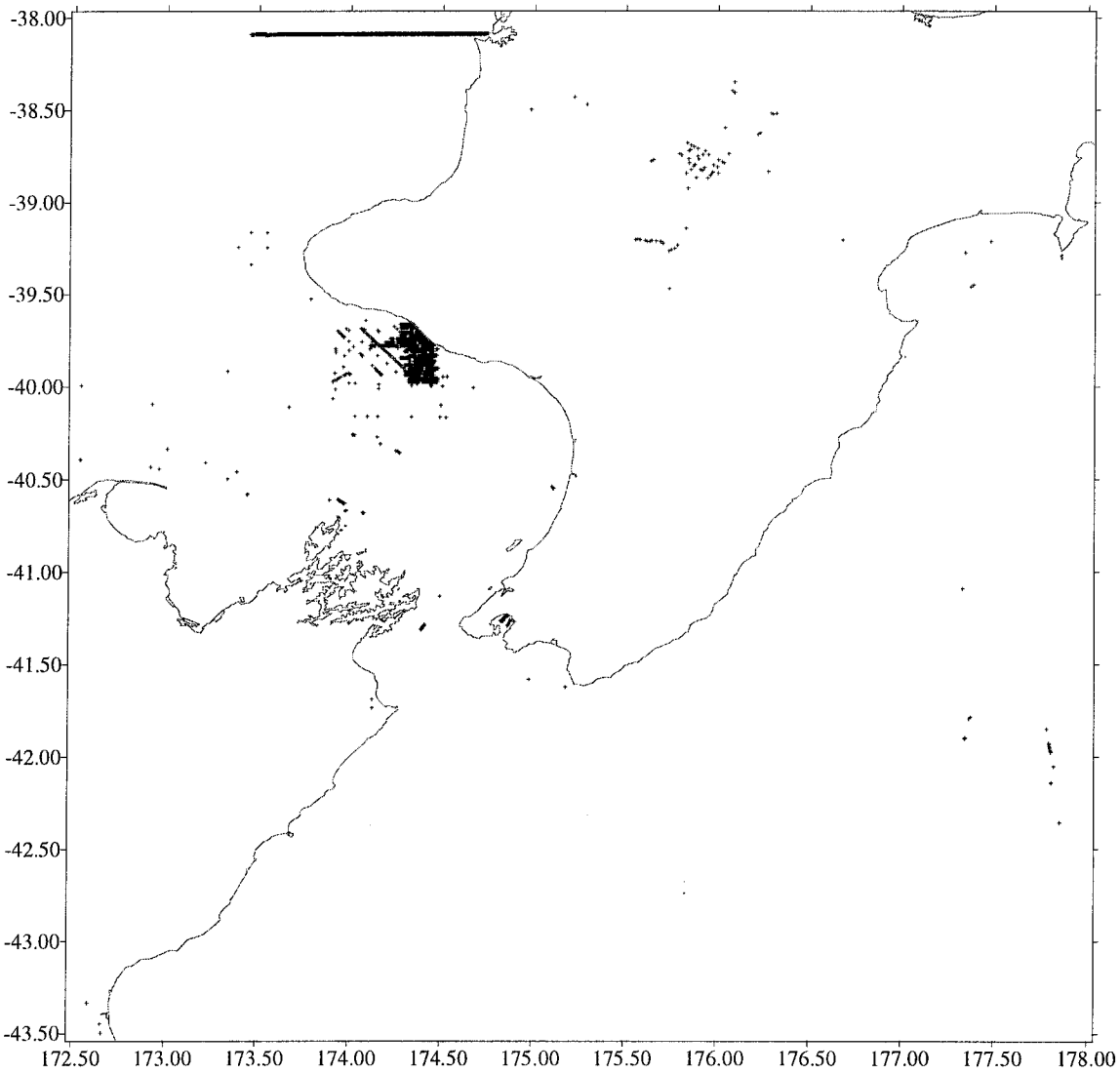

Figure 4 - 15 : Duplicate points from combined Off-shore and Land gravity data. Rectangular Projection

4.4.4 Satellite Altimetry gravity data

The Satellite Altimetry gravity data was obtained from Scripps Institution of Oceanography, La Jolla, California, USA by anonymous ftp to baltica.ucsd.edu. The file downloaded was titled world_grav.img.4 and consists of a global 3 minute grid of off-shore gravity anomalies on a Mercator projection. The associated README file states that the grid was derived from the following data sources:

Seasat	- Used in areas north of 30 S latitude. Profiles within 10 km of a Geosat Exact Repeat Mission (Geosat/ERM) track were excluded.
Geosat/ERM	- Average of 62 Geosat/ERM profiles.
Geosat/GM	- Declassified Geosat Geodetic Mission (Geosat/GM) data south of 30 S.
ERS-1	- ERS-1 Ocean Products (OPR) Geophysical Data Records (GDR's). The first 16 repeat cycles of the 35-day repeat orbit were averaged to improve their accuracy and resolution.
ERS-1	- ERS-1 fast delivery profiles from the first 200 days of the ERS-1/GM.

The following overview of the gridding method used to generate world_grav.img.4 is based on Sandwell (1992).

Satellite altimetry uses a pulse-limited radar to measure the altitude of the satellite above the closest sea surface point. Global precise tracking coupled with orbit dynamic calculations provide an independent measurement of the height of the satellite above the ellipsoid. The difference between these two measurements is equal to the instantaneous sea surface height which, after removal of tides, is a good approximation of the marine geoid (neglecting oceanographic effects).

To avoid a multi-satellite crossover adjustment, which would become enormous due to the small spacing between the satellite tracks, another method was developed for using the sea surface topography profiles. The method begins with both the ascending and descending altimeter profiles being differentiated once in the along-track direction resulting in geoid slopes or along track vertical deflections. This differentiation suppresses the long wavelength radial orbit error to well below the noise level of the altimeter. The ascending and descending slope profiles are then interpolated onto separate Mercator grids. These two grids are summed and differenced to form comparable grids of east and north vertical deflection.

Using Laplace's equation, the vertical gravity gradient can be calculated directly from the vertical deflection grids without any assumptions. However, Fourier analysis is required to construct gravity anomalies from the two vertical deflection grids. A GGM (complete to degree 40) is used to limit the effective range of the implied convolution associated with the vertical deflection to gravity anomaly conversion, so a flat-earth approximation can be used as long as data are gridded on a map projection. This is achieved by removing the GGM from the profiles before gridding and construction of east and north vertical deflections. The GGM is later added back to the gridded gravity anomaly data.

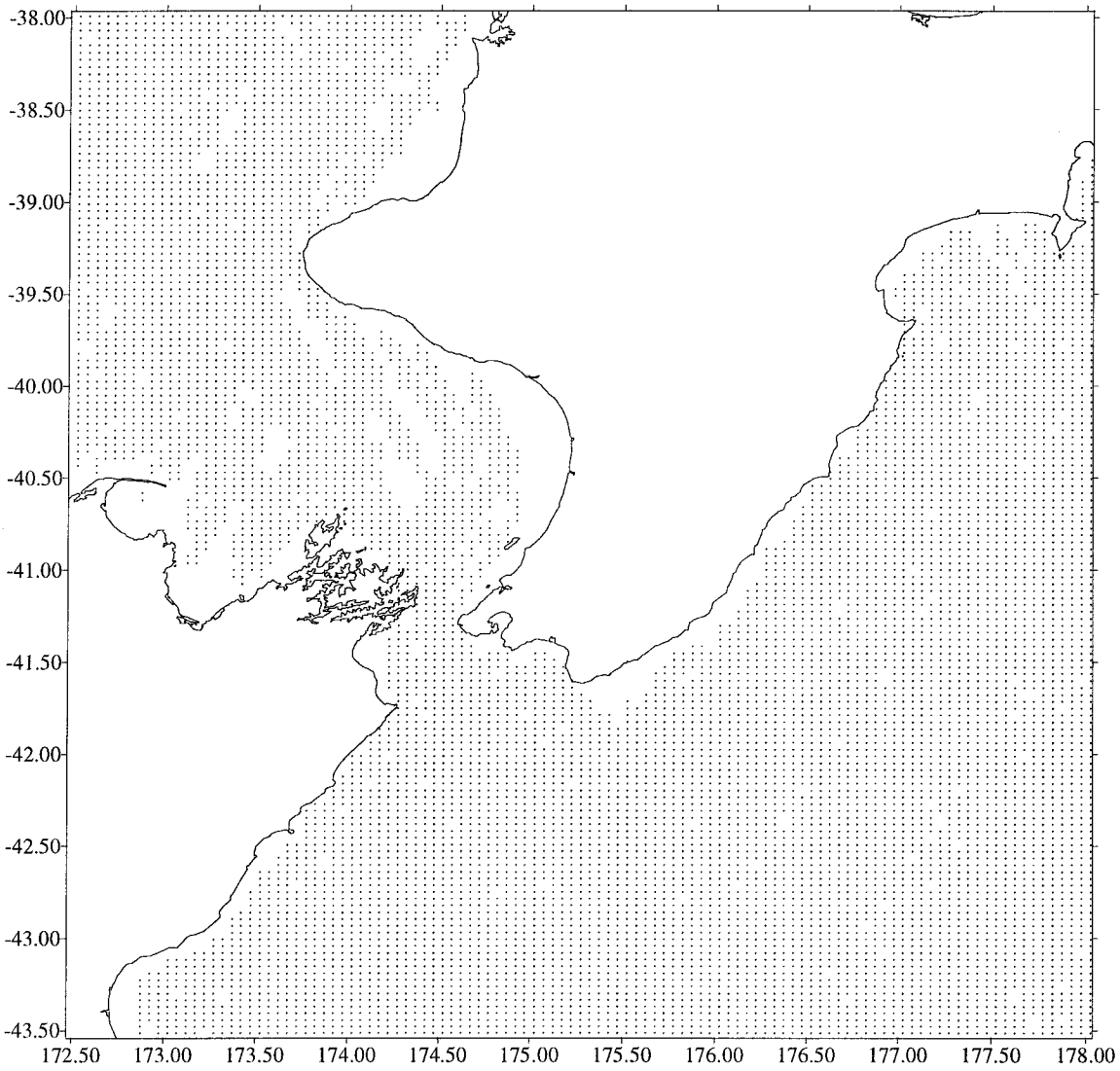

Figure 4 - 16 : Distribution of the Satellite Altimetry data for the lower North Island test area. Rectangular projection

From world_grav.img.4 the data for the lower North Island test area was extracted (Figure 4-16). As can be seen the Satellite Altimeter provides regular and consistent data at sea, but near the coastline there can be considerable data loss. This data loss is due to radar reinitialisation problems after crossing land.

4.4.5 Digital Elevation Model

A digital elevation model (DEM) was generated to cover (Lat. S37.74° - S43.82°, Long. E171.76° - E178.52°) the Lower North Island test area using DOSLI's in-house software. The elevations ranged from 0 to 2855 m. The portion of this DEM immediately surrounding the RINT optimisation points (Section4.4.6) is represented by a surface plot in Figure 4-17. The elevations in this portion ranged from 0 to 1570 m.

The DOSLI software derives the spot heights at the grid points, rather than average cell heights, from the 20m contours on the 1:50000 topographic map series. The interpolation used to generate the spot heights is based on constructing profiles across the grid in E-W, N-S, SE-NW and SW-NE directions. The contours are intersected with each profile and heights then interpolated from the contour intersection points onto the grid points.

This gives four elevations at each location. A weighted mean is derived from these values. Weighting is according to the proximity of the nearest contour - if one profile intersects a contour near a grid point then the corresponding height will be given greater weight than that from a profile which does not intersect a contour near the grid point.

The DEM consists of a set of values which are exactly consistent with the contours but which may contain significant artefacts relating to the directions of the profiles. In an effort to reduce these artefacts a smoothing algorithm is applied to the DEM elevations. The algorithm attempts to remove abrupt changes in slope and rate of change of slope.

The northing and easting coordinates for the spot heights were then converted from the New Zealand Map Grid (NZMG) to latitude and longitude in terms of GRS80 to give an

approximate grid spacing of 0.004°. Full information on NZMG is given in Reilly (1973).

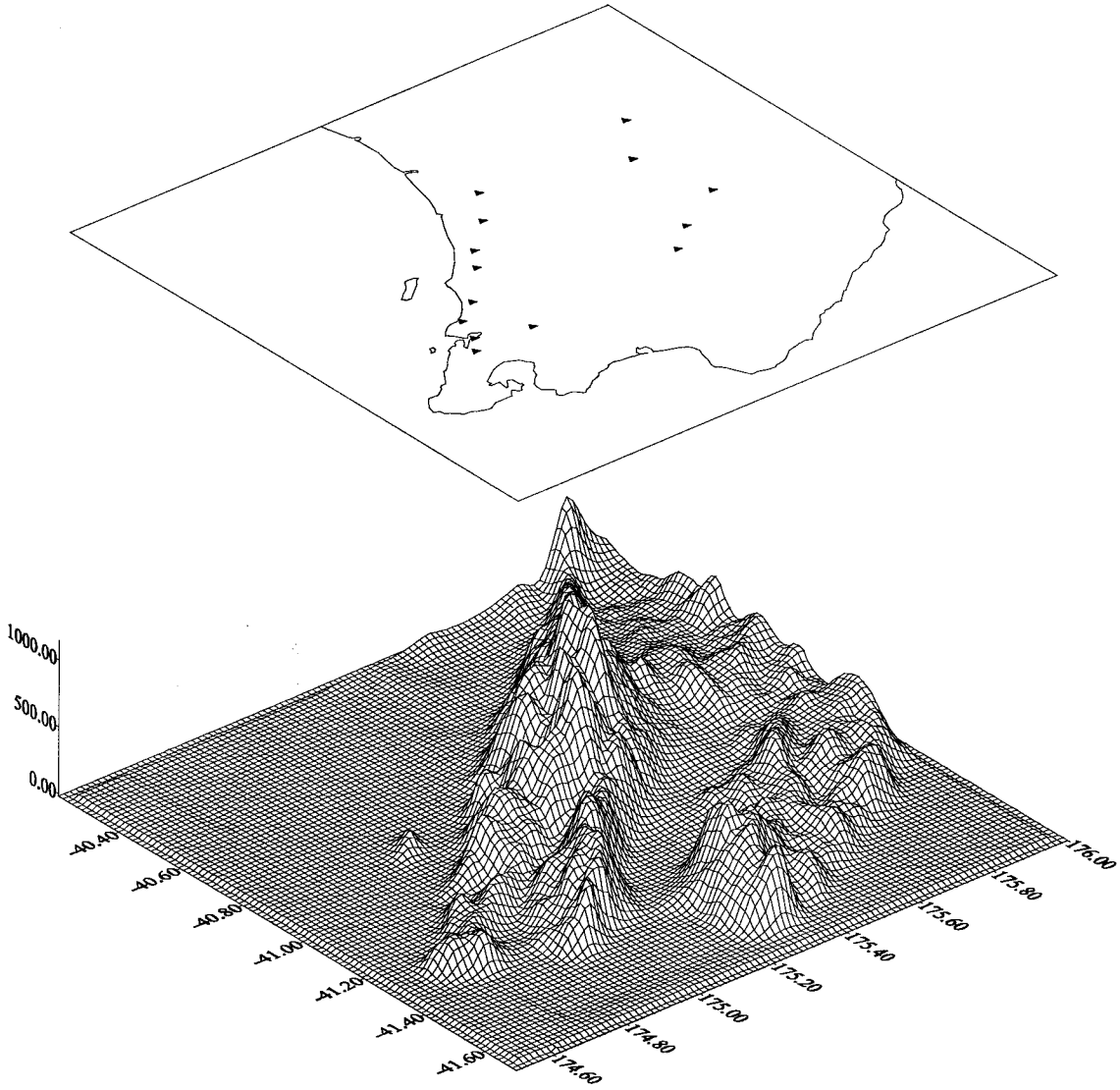

Figure 4 - 17 : Terrain for the lower North Island test area. Top: Coastline with the 14 first order control stations. Bottom: Smoothed terrain surface with heights in metres

4.4.6 GPS data

During 1994 there were a number of GPS campaigns undertaken by DOSLI to improve the horizontal control network between Wellington and Palmerston North. These different GPS campaigns were combined in a single adjustment using the SNAP software (Crook, 1995). The adjustment held the WGS84 latitude, longitude and ellipsoidal height of the Heaphy House GPS Pillar fixed in a minimally constrained

adjustment (Jim Hall, pers. comm., 1995). The coordinates and station names for these 108 GPS stations are contained in Appendix G, with their distribution shown in Figure 4-18.

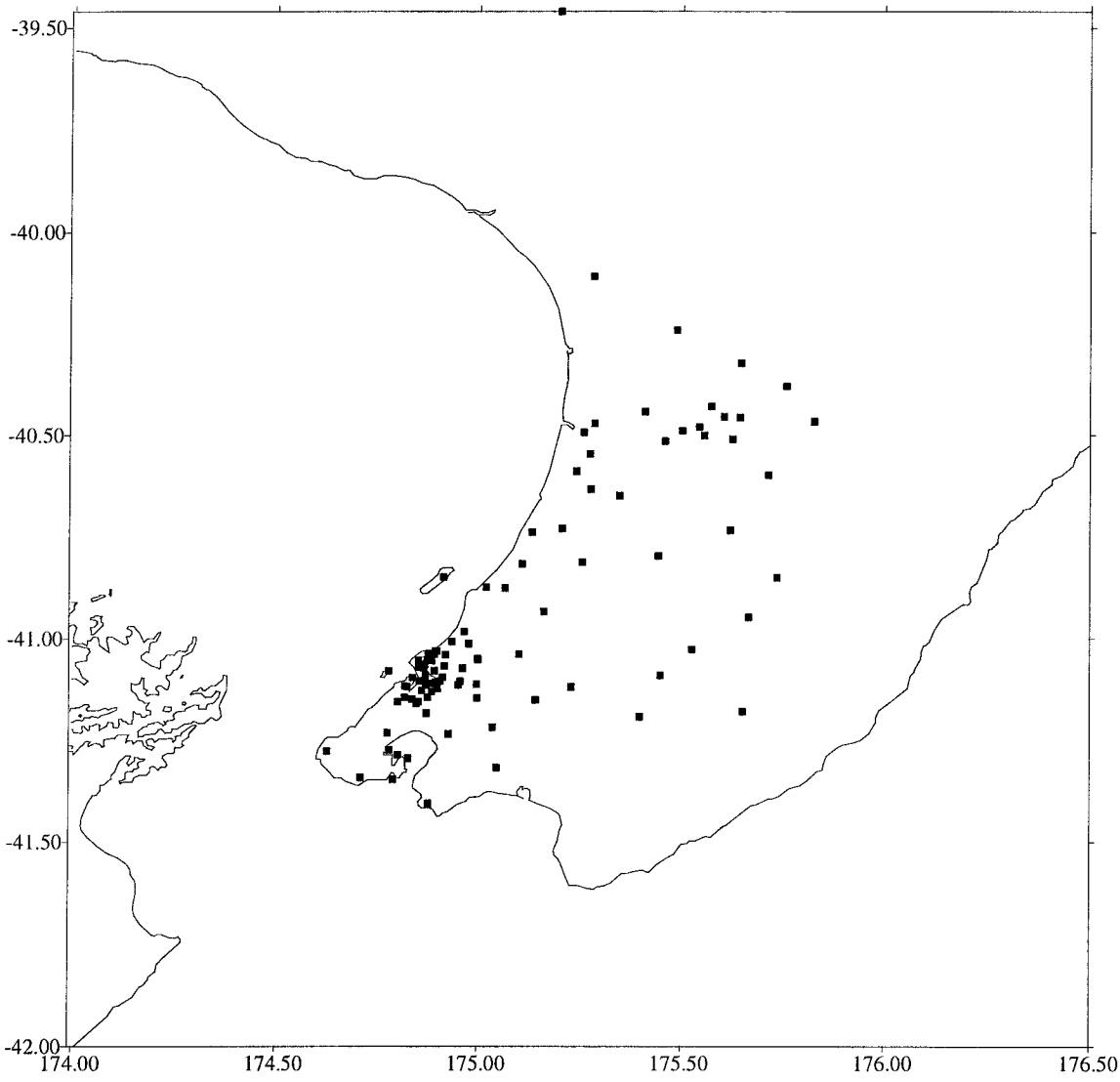

Figure 4 - 18 : Distribution of the 108 GPS stations for the lower North Island test area. Rectangular projection

The optimisation of RINT for the lower North Island test area (Section 4.5) was undertaken using a subset of the available GPS stations. The subset of stations were selected using primarily two criteria. The first criteria was to reduce the biasing in the optimisation results due to densely occupied regions (ie. S41°, E174.4°), while still maintaining a well distributed set of stations. The second criteria was designed to allow

results obtained at first order orthometric height stations (which are normally located in valleys) to be checked against results at stations located in regions with more rugged terrain. Therefore, a selection of third order orthometric height stations were chosen, as these sites were located on ridge lines. This subset consisted of 33, out of the original 108, stations and was comprised of 14 first order (max. height = 334.232m) and 19 third order stations (max. height = 1545.99m) (Figure 4-19).

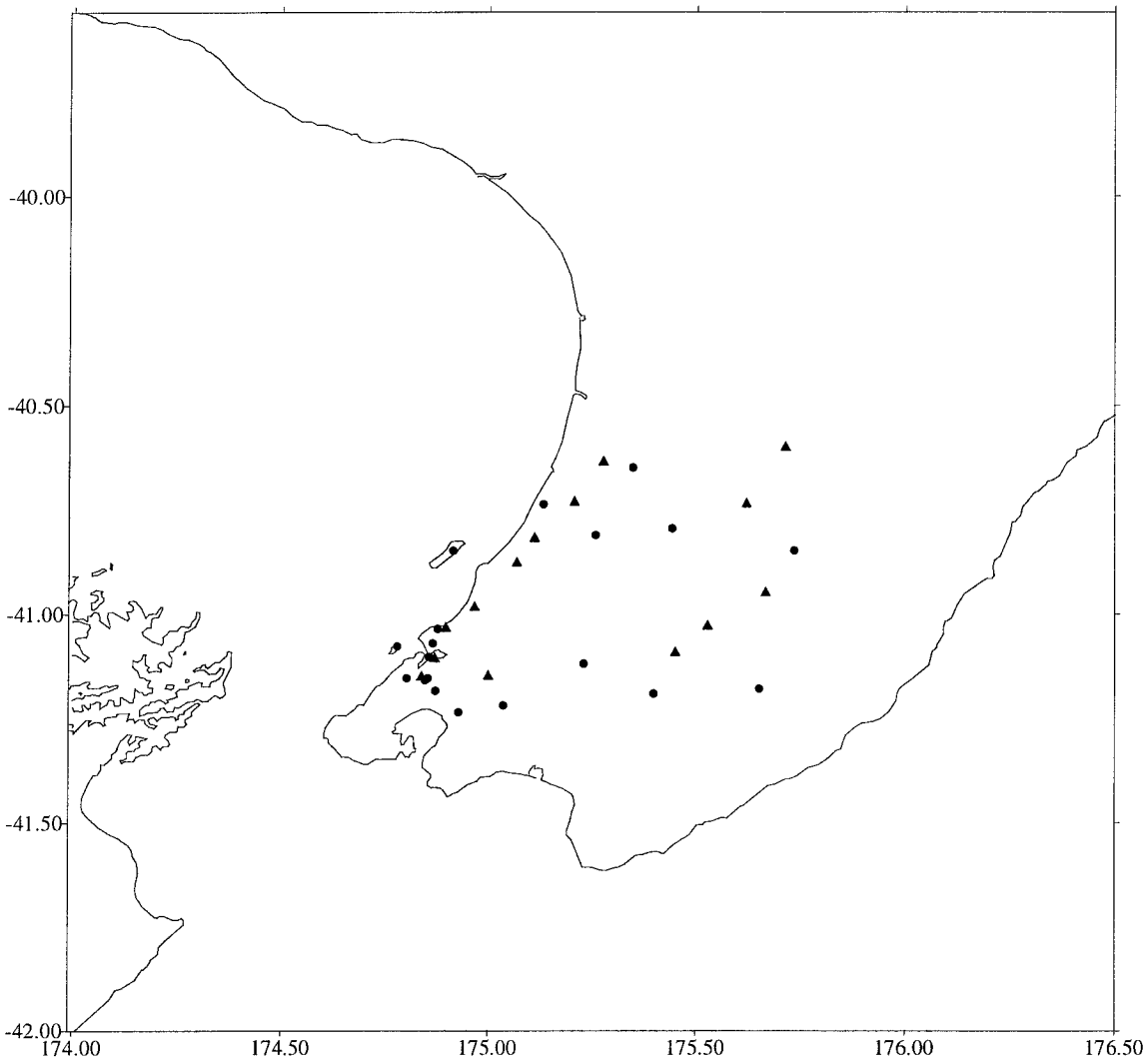

Figure 4 - 19 : Distribution of the selected 33 GPS stations, with 1st order (triangles) or 3rd order (circles) orthometric heights, for optimisation of RINT in the lower North Island test area. Rectangular projection

4.4.7 Orthometric Height data

The orthometric height for the 108 control stations in the lower North Island test area were extracted from the DOSLI Geodetic Database. These extracted heights are listed in Appendix H, along with an indication of their height order. Section 2.3 describes the history of New Zealand levelling network and outlines the height order specifications.

4.5 Method of optimisation on test area of New Zealand

A test area covering the lower North Island has been chosen to trial different configurations of the Ring Integration technique (Section 4.3). This section presents the results of these trials in a progressive nature where the previous optimum result has further smaller corrections applied.

The three main reasons for choosing the lower North Island as the test area are :

- **i)** both land and sea gravity data was available (Figure 4-13)
- **ii)** approximately 100 points (control stations) had both ellipsoidal height from GPS and orthometric height from spirit levelling (Figure 4-18)
- **iii)** the area consists of rugged terrain which is typical for New Zealand, varying from sea level to 1500 metres (Figure 4-17)

Restricting the test to a small part of New Zealand also reduced the pressure on the limited computer resources available for the project.

In October 1996, a new GGM was released through a joint project between the NASA Goddard Space Flight Centre (GSFC) and the U.S. Defense Mapping Agency (DMA), being referred to as the Earth Geopotential Model of 1996 (EGM96) (Lemoine *et al.*, 1996). Due to the late release of EGM96, with respect to the completion of this thesis, analysis of EGM96 with respect to the other GGM listed in Table 4-1, has been restricted to Sections 4.5.1 and 4.5.6.

4.5.1 Comparing Global Gravity Models by residual gravity anomalies

As RINT uses residual free-air gravity anomalies (Section 4.3.2) the first test was to determine which GGM best represented the gravity data of the region. As stated above the gravity data available for this project were free-air gravity anomalies that had been terrain corrected using Hammer's method out to 21.94 km and which had had the atmospheric correction applied (Section 4.4.1).

The procedure for the test was to take the gravity data and reduce them by the gravity anomalies of each GGM (Δg_{GGM}) listed in Table 4-1. The statistics of these residual gravity anomalies (Δg_r) were then calculated to assess which model best represented the physical data. The results are contained in Table 4-2.

GGM	Reference	Mean	Standard Deviation	Minimum	Maximum
GEM-T2	Marsh *et al.*, 1990	-14.5	44.7	-168.9	202.8
OSU81	Rapp, 1981	-2.3	29.7	-119.7	188.8
OSU91A	Rapp *et al.*, 1991	-8.6	20.6	-97.0	193.7
EGM96	Lemoine *et al.*, 1996	-6.5	19.4	-112.9	193.6

Table 4 - 2 : Comparing GGM by residual gravity anomalies. (Units are mGal, Standard Deviation is given at 1 sigma)

The model which performed worst was GEM-T2. GEM-T2 was derived from satellite orbit analysis only and has a maximum resolution of only about 5° which is basically the extent of the test area, so this poor result was not unexpected.

Prior to the inclusion of EGM96 (n_{max} = 360, resolution 0.5°) in Table 4-2, OSU81 (n_{max} = 180, resolution 1°) had the mean which was closest to zero but OSU91A (n_{max} = 360, resolution 0.5°) had the smallest standard deviation. The large mean for the OSU91A model could indicate that there is an inconsistency between the datum of the model and the datum of the gravity data. However, as OSU91A gave an improvement of 30% in the standard deviation over OSU81, OSU91A was considered the better model to represent the test area's gravity data. Further trials still use both OSU91A and OSU81 to provide a means to identify results which may be influenced by the choice of GGM.

With the inclusion of EGM96 (n_{max} = 360, resolution 0.5°) in Table 4-2, it is clear that the mean residual gravity anomaly of EGM96 for the test area is a 24% improvement over OSU91A. Though the large mean for EGM96 still indicates that there could be an inconsistency between the datum of the model and the datum of the gravity data. The standard deviation of the residual gravity anomalies using EGM96 has improved slightly (by 5%) over the OSU91A value. The conclusion from analysing the mean and standard deviation is that this test area's observed gravity is better represented by EGM96 than OSU91A.

4.5.2 Optimum cap size for RINT

Determining the integration radius for RINT is an important step. The inclusion of too little local gravity data will result in the higher frequency geoid features missed by the model still being unaccounted for by the local gravity data. However, if too large a radius is chosen to include the local data, information contained in the model will be unnecessarily duplicated. As well the computation time will increase for no further improvement and, as will be shown, can for certain cap sizes degrade the results. RINT allows the compartment sizes to vary through the choice of the parameters $d\alpha$ (4.48) and C_N (4.61). For the following sub-sections the values of $d\alpha$ = 10° and C_N = 0.0003 m/mGal were used. The effect of varying these parameters was tested and it was found that features in the results, such as the amplitude and wavelength of the W-curve (Section 4.5.2.1), were not significantly altered. The choice of $d\alpha$ = 10° and C_N = 0.0003 m/mGal were chosen so compartments were approximately square in shape and this meant the radii of the rings incremented by about 10 km.

4.5.2.1 Effect of varying GGM

The purpose of this section is to test the effect of the reference GGM on determining the optimum cap size for RINT.

The two GGM tested were OSU81 (n_{max} = 180) and OSU91A (n_{max} = 360). The results for the δN (4.64) analysis of the 14 first order stations (Section 4.4.6) for a cap size from ring 0 out to ring 20 (ie. 0° to 2.0°, or approx 0 km to 200 km) are contained in Figure 4-20. From this figure it is obvious that the mean δN varies with respect to both the

GGM and the ring number. This is because any gravimetric determination of the geoid is deficient in the zero- and first-degree terms.

The standard deviation of the δN for each model have common minima and maxima for ring numbers, though the amplitude varies. OSU81 has the larger standard deviations, which is to be expected since OSU91A has a resolution that is 50% finer than OSU81 (see Section 4.2.5 for model resolution).

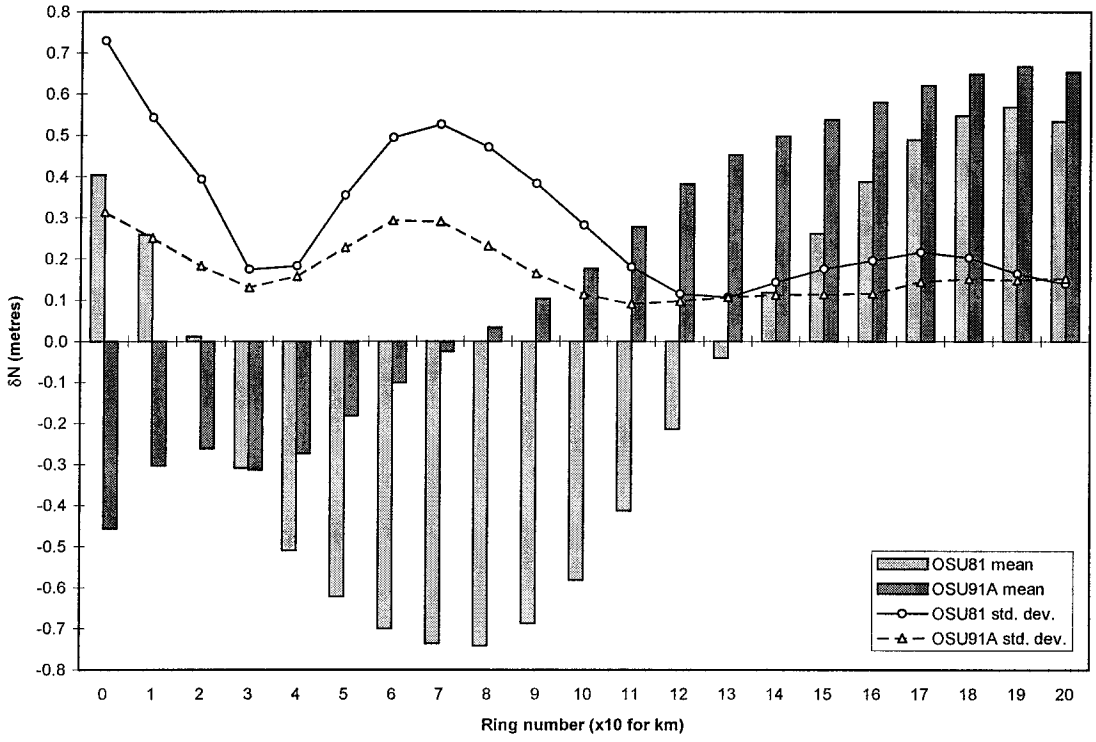

Figure 4 - 20 : δN values at the 14 first order control stations when varying the reference GGM between OSU81 and OSU91A.

To reduce the effects of datum inconsistencies it is necessary to use relative line comparison (Section 4.3.5.2). The results from analysing the 91 baselines formed between the 14 first order control points are contained in Figure 4-21. These 91 baselines have an average length of 42.9 km, with a minimum of 5.6 km and a maximum of 95.8 km. The first point to note is that ring number zero (model only) performs worst for both models. Therefore including local gravity in the computation of the geoid height by using RINT will improve the results. For example, ring 1 gives a 25% improvement in rms over ring 0. Thus by including local gravity within 10 km, a significant improvement occurs.

A problem with comparing the δΔN directly is that they could be biased by the length or the orientation of the line. To investigate whether a length bias existed, it was removed by dividing the δΔN values by the length of the line and expressing the result in parts per million (ppm). The mean and root mean square (rms) of the ppm values were then calculated using 4-66 and 4-67.

$$\delta\Delta N_{mean}^{ppm} = \frac{\sum_{i=1}^{n} \left| \frac{\delta\Delta N_i}{s_i} \right|}{n} \times 10^6 \tag{4.66}$$

$$\delta\Delta N_{rms}^{ppm} = \frac{\sum_{i=1}^{n} \left(\frac{\delta\Delta N_i}{s_i} \right)^2}{n} \times 10^6 \tag{4.67}$$

where $\delta\Delta N_{mean}^{ppm}$ is the mean of the relative line comparison expressed as a ppm in terms of the line length.

$\delta\Delta N_{rms}^{ppm}$ is the rms of the relative line comparison expressed as a ppm in terms of the line length.

$\delta\Delta N_i$ is the relative difference in ΔN for the i^{th} baseline.

s_i is the length of the i^{th} baseline.

n is the number of baselines.

By comparing the OSU81 and OSU91A results for either δΔN or ppm (Figures 4-21 and 4-22) it is clear that there are two distinct groups of ring numbers that produce optimum results (rings 3-4 and 11-14). OSU91A performs the best in both rms and mean for all rings. If there does exist a correlation between the δΔN values and baseline length it is not significant as indicated by the similarity between the figures.

The bi-modal or W-curves, as first noted by Kearsley (1988), clearly exist in this analysis. Kearsley (*ibid.*) noted that the wavelength of the curve approximates the half wavelength recovered in theory by the GGM when summed to n_{max} (ie. $180/n_{max}$). This does not seem to occur in the analysis performed with the New Zealand data. Varying of n_{max} from 180 (OSU81) to 360 (OSU91A) does not significantly affect the wavelength of the W-curve but the amplitude is reduced with higher values for n_{max}

(Figure 4-22). Further tests aimed at understanding the mechanisms that generate the W-curve have been conducted and are contained in Appendix J.

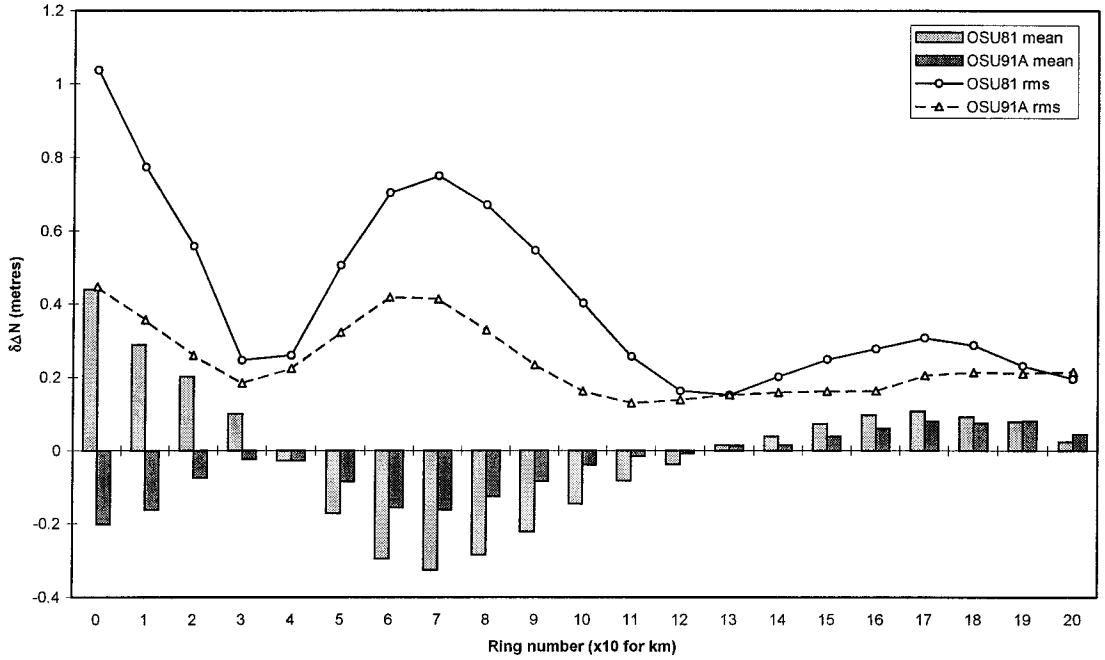

Figure 4 - 21 : δΔN values at the 14 first order control stations when varying the reference GGM between OSU81 and OSU91A.

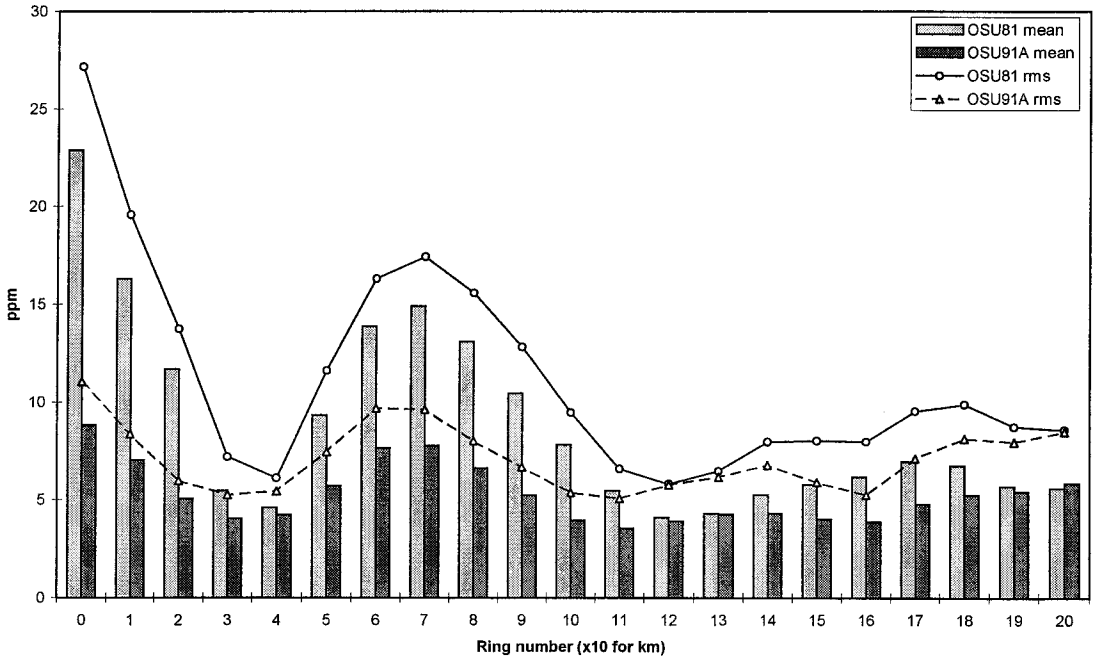

Figure 4 - 22 : Investigation of a baseline length bias by comparing OSU81 and OSU91A in an relative sense at the 14 first order control stations.

From the results of comparing OSU81 and OSU91A, at the 14 control stations, OSU91A was chosen as the superior GGM. This confirms the earlier results in Section 4.5.1 (pre EGM96) and therefore OSU91A has been chosen as the GGM to be used as the reference model.

As was described in Section 4.3.4.1 the use of the analysis of absolute N differences needs to be undertaken with caution due to the effects of datum inconsistencies. However, plotting δN for each control station can identify control stations which have gross errors in one or more of their heights. Figure 4-23 illustrates how easy it is to detect gross errors by plotting the third order control stations δN values for each ring calculated with respect to OSU91A with a DEM used to calculate the mean compartment height. As can be seen from Figure 4-23 the points labelled D136 and D510 follow the general upward trend with increasing ring number but are significantly offset from the other control points.

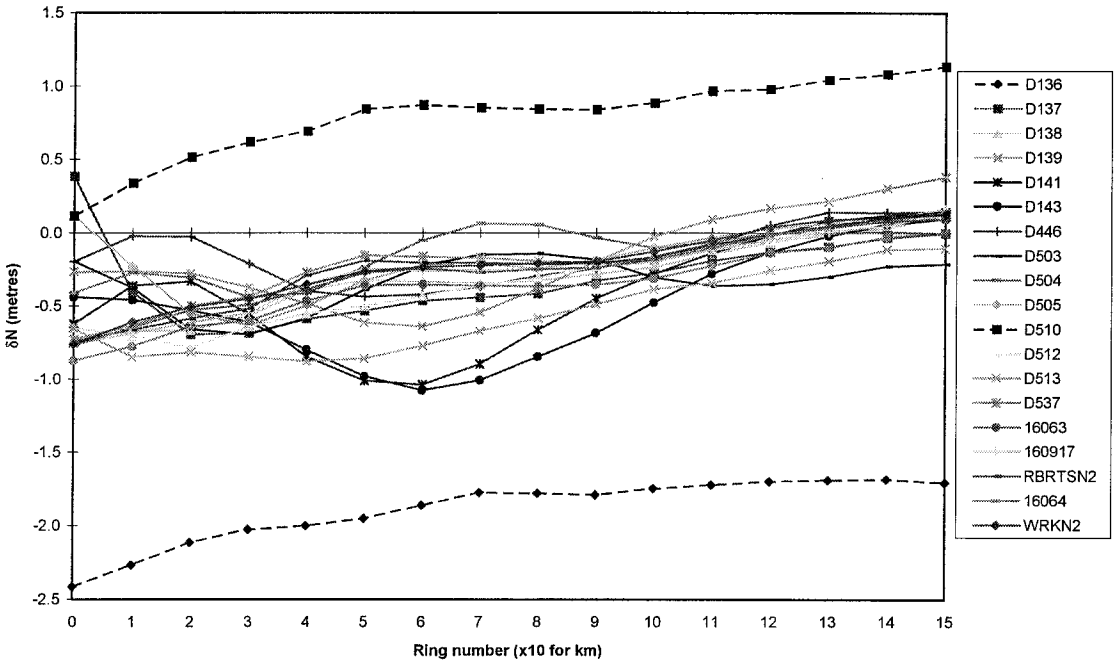

Figure 4 - 23 : Absolute point comparison of the 19 individual 3rd order control stations using OSU91A and a DEM for compartment heights.

There is no way of determining which height element (h, H or N) may be causing the error. However, the error is likely to be in the orthometric height since D136 and D510 are both located on different islands (Kapiti and Mana, respectively) to the remainder of

the control stations. It is possible that the gravimetric geoid height is in error due to the combination of land and off-shore gravity observations, but this is discounted because, if it were, one would expect to see jumps in the lines when the cap changes from including land data to off-shore data. The ellipsoidal height has been established in a homogeneous GPS campaign, and it would be most unlikely that both small island sites had their antenna heights incorrectly measured. This leaves the orthometric height as the probable source of error. This view is reinforced when one remembers that the orthometric heights of the two control stations (D136 and D150) were determined by trigonometric levelling across water.

For the remainder of the analysis using the third order control stations, both D136 and D510 were removed.

Once the control stations with gross errors have been removed it is then possible to properly analyse the relative line comparisons (Section 4.3.5.2).

4.5.2.2 Mean compartment height from gravity station information or a DEM

The RINT based software had the option to use the height of the seven gravity stations, chosen as described in Section 4.3.4.1, to calculate the mean height of the compartment. This mean height is used to reconstruct the residual free-air anomaly from the residual Bouguer anomaly (Section 4.3.4.2). This section shows the results from using both these seven gravity points and a DEM to obtain the mean height of the compartment and the effect this has on determining the optimum cap size for the integration. For further information on the development and testing of the benefits of using a DEM to generate the mean height of the compartment see Higgins *et al.* (1996).

Using OSU91A to n_{max} = 360 as the reference GGM, the δN values for the first order control stations were computed using both the DEM and the gravity station heights only (no DEM) to calculate the mean compartment height (Figure 4-24). It is clear from the results that the δN mean is significantly affected by the use of the DEM, whereas the standard deviation of the δN sees only a marginal change (max 0.02m). The wavelength of the W-curve remains unchanged but the amplitude is increased slightly when the DEM is used. At the optimum cap (ring numbers 3 and 11) the standard deviation of

the δN from using the DEM has improved by approximately 15%, however at the sub-optimum ring (number 6) the standard deviation has deteriorated by 6%. The reasoning behind the increase in the amplitude of the W-curve is not understood. To try to understand this amplitude change the following approach was taken.

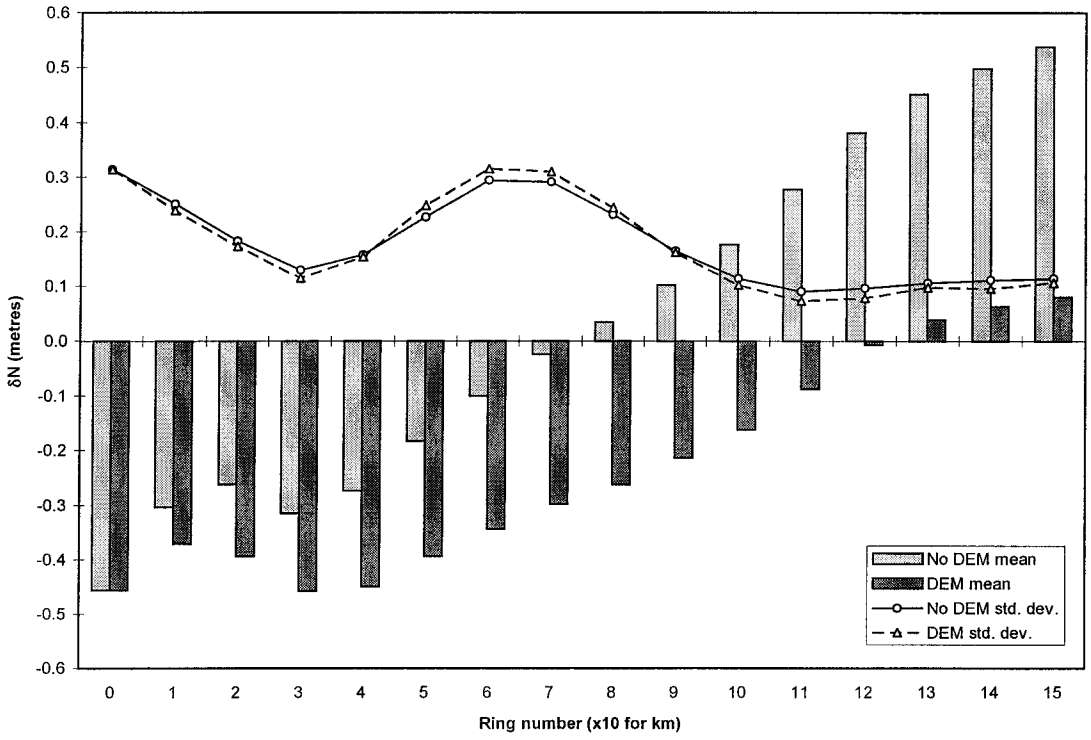

Figure 4 - 24 : δN values for the first order control stations computed using the DEM or gravity station heights to calculate the mean compartment height.

Since the first order control stations are generally located on valley floors, because of the difficulties of undertaking spirit-levelling along ridge tops, it was decided to compare the results of the first order stations with those of third order control stations. The third order control stations are more likely to be located in areas of difficult topography, but as a consequence have lower quality orthometric height determinations. It should also be noted that the third order control stations orthometric height would have been adjusted in terms of the first order stations, thus containing the same height datum errors.

As was the case with the 14 first order control stations, the 19 third order control stations results for the δN mean is significantly affected by the use of the DEM (Figure

4-25). On average the δN standard deviations for the third order control stations is 10% worse than the first order control stations. This could be due to the expected precision's of the 1st and 3rd order levelling alone (Section 2.5.2). It is also clear again that when using the DEM, the amplitude of the δN standard deviation W-curve increases. For the two optimum rings (numbers 3 and 11) the improvement (over the non DEM solution) was 17% and 19%, respectively. The sub-optimum ring (number 6) deteriorated by 8%. It is worth noting that ring number 11 is only considered as one of the optimum rings at this stage of the analysis because it is the first of a series of rings at which the inclusion of further gravity data does not significantly affect the δN results. Further discussion on selecting the optimum ring for generating a geoid model is contained in Section 4.5.2.3.

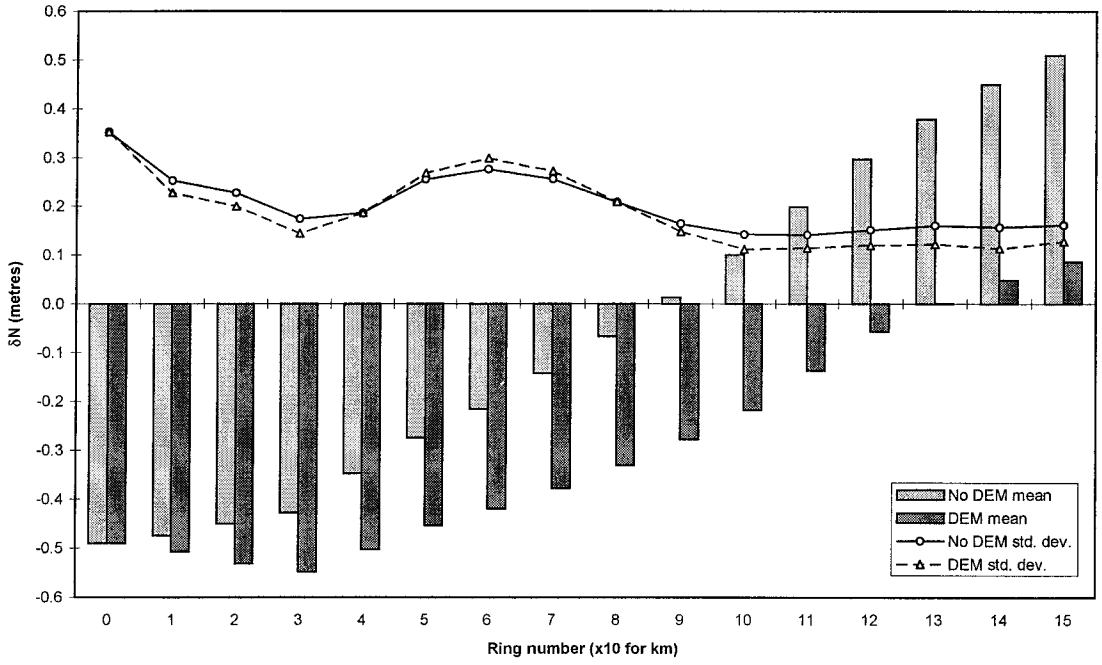

Figure 4 - 25 : δN values for the third order control stations computed using the DEM or gravity station heights to calculate the mean compartment height.

Considering that any datum inconsistencies could be affecting the δN analysis, relative line comparisons (δΔN) are now analysed to further highlight the benefits of using a DEM to calculate the mean compartment height. As the δΔN results expressed as straight differences could be influenced by the length of the baseline, the analysis will be done using δΔN expressed as ppm values.

The 17 third order control stations have 136 independent baselines with an average length of 40.7 km with a minimum of 0.6 km and a maximum of 85.5 km.

Analysing the ppm results for both the first and third order control stations we see that for rings number 1 to 3 and 6 to 15 the use of the DEM improves the solution, however the DEM solution is degraded for rings number 4 to 8 (Figures 4-26 and 4-27). The concern about this degradation is highlighted at ring number 6 (ie. a spherical cap of approximately 0.6°) where the inclusion of the gravity data has no significant improvement over the OSU91A model only solution, for the first order control stations and produces a poorer result than the model for the third order control stations. This degradation has been significantly reduced when using EGM96 as the reference GGM (Section 4.5.6).

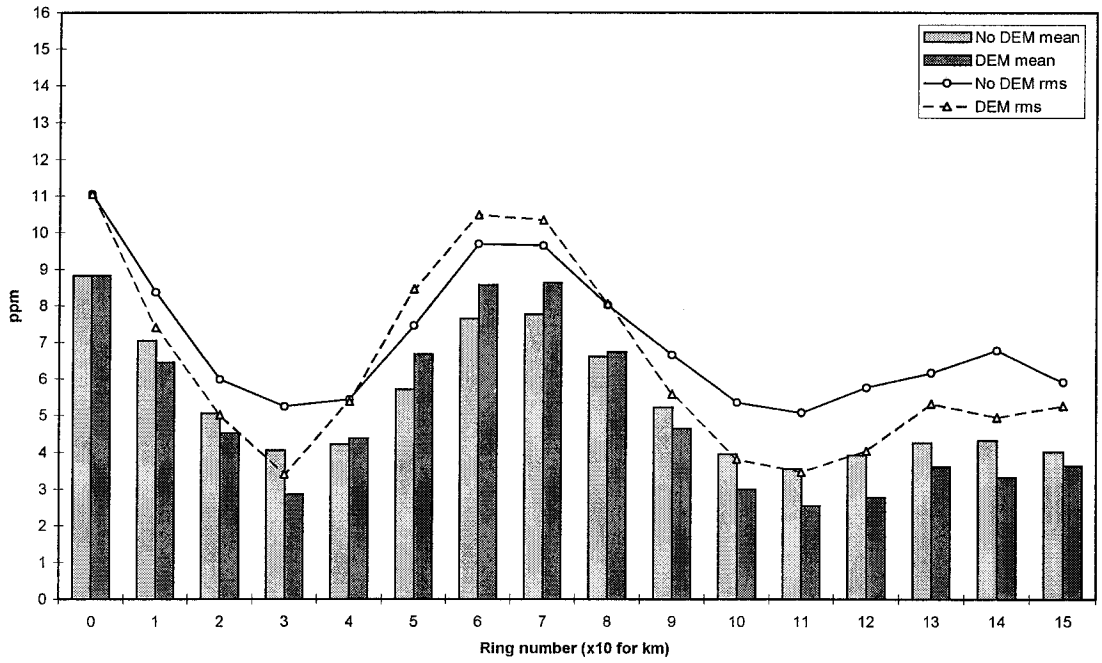

Figure 4 - 26 : $\delta\Delta N$ values (expressed in ppm) for the first order control stations computed using the DEM or gravity station heights to calculate the mean compartment height.

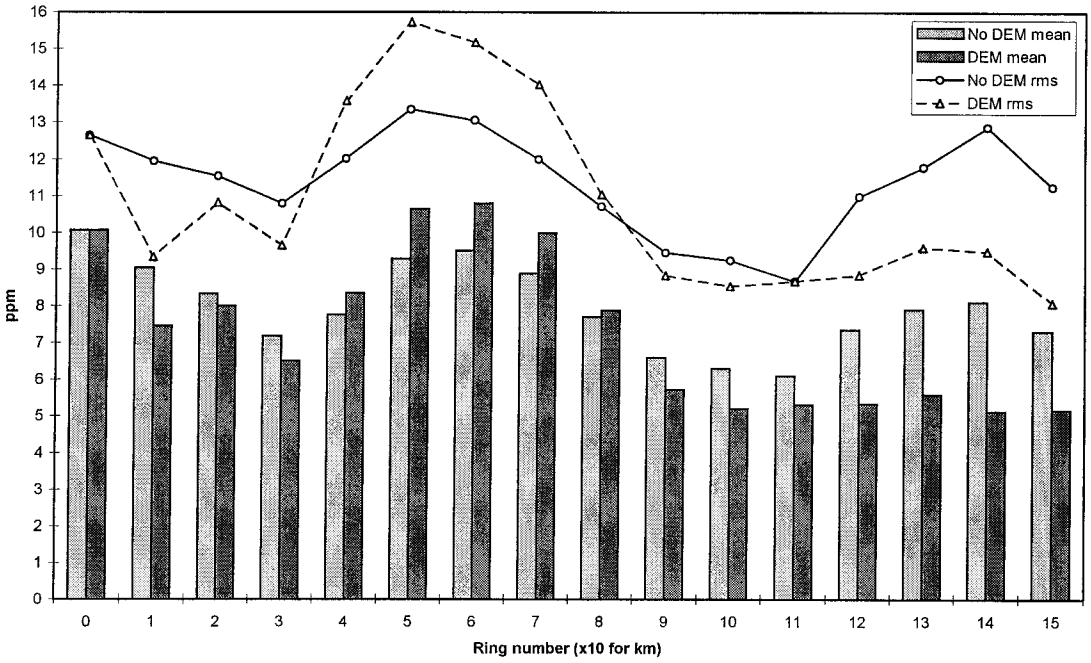

Figure 4 - 27 : $\delta\Delta N$ values (expressed in ppm) for the third order control stations computed using the DEM or gravity station heights to calculate the mean compartment height.

4.5.2.3 Considerations when selecting optimum cap size for RINT

Through the use of local gravity observations in the RINT technique it is predicted that N_{GRAV} values obtained will be closer to the true N value than the N_{GGM} values. From the results presented in Sections 4.5.2.1 and 4.5.2.2 the varying of the GGM or the method of obtaining the mean compartment height can change the accuracy of the solutions. What was also shown to be true was that these variations did not alter the optimum or sub-optimum ring numbers.

Due to the presence of the W-curve, especially in the $\delta\Delta N$ and ppm results, a choice has to be made between the two local minimum ring numbers 3 and 11.

The advantage of ring number 11 is that the ring numbers either side of 11 generally vary less with respect to 11, than the ring numbers either side of ring 3 vary with respect to ring number 3. The disadvantage of ring number 11 is that the spherical cap required for RINT has a radius of approximately 110km as opposed to ring number 3 having a radius of approximately 30km. Assuming that the gravity data has a constant coverage

across the extent of the project then ring number 3 will only require 7.5% of the data that ring number 11 requires for each computation point. In other words, if the compartments are generated from radial lines with apex angles of 10°, and the radii of the concentric circles increase by 10.0°, then ring 3 will need 288 fewer compartments than ring 11 for the summation for each computation point. The use of ring number 3 as the limit of integration will not only save considerable computer processing time but also will reduce the amount of gravity and DEM data that needs to be stored on-line while generating the geoid heights, resulting in a further time saving.

However, as the computation of a national geoid model is performed only once in a number of years the processing time is not a major concern. The primary concern is generating the best possible model.

From Figure 4-26 we can see that the results from ring 3 are only 0.3 ppm worse that those from ring 11. In terms of the rms of the ppm, integration to rings 3 and 11 are not significantly different.

The variability of the results near ring number 3 was noted above. However, it was considered that the benefits of reduced on-line data requirements outweighed the disadvantages, and therefore ring number 3 was chosen as the optimum ring for calculating a relative geoid in the lower North Island test area. The choice of ring number 3 means that the optimum spherical cap size is approximately 31 km (≅ 0.3°). This optimum spherical cap size has also been chosen for geoid computations in the Philippines (Kearsley, 1993, p11) and Australia (Higgins *et al.*, 1996).

4.5.3 Bouguer or Free-air anomalies for interpolation in RINT

When interpolating a gravity anomaly at the compartment mid-point (Section 4.3.4.1) the surface used should be smooth to enable a reliable estimate to be obtained. Geophysical texts such as Dobrin (1976) and Nettleton (1976), as well as the geodesy text of Heiskanen and Moritz (1967), state that the residual Bouguer anomaly surface should be smoother than the residual free-air anomaly surface.

Featherstone *et al.* (1995) compared δg_B and δg_{fa} across Australia and concluded that it was unclear which anomaly was the smoothest for interpolation. This section investigates the effect of using δg_{fa} and δg_B as the interpolation surface for the lower North Island test area. The test involved using the same seven gravity stations to estimate the mean Δg_{fa} for that compartment. However, in this test the free-air anomalies were used directly for interpolation.

The test was performed at the first order control stations. The results (Figure 4-28) show that there is no practical difference between using the free-air anomalies or the Bouguer anomalies in this lower North Island test area. However, as was shown in Section 4.5.2.2, using a DEM (rather than the seven gravity stations) to calculate the mean compartment height to reconstruct the free-air anomaly from the Bouguer anomaly does significantly improve the results. Therefore it is recommended that interpolation be undertaken using the Bouguer anomalies, and a DEM used to estimate the mean compartment height in the lower North Island test area.

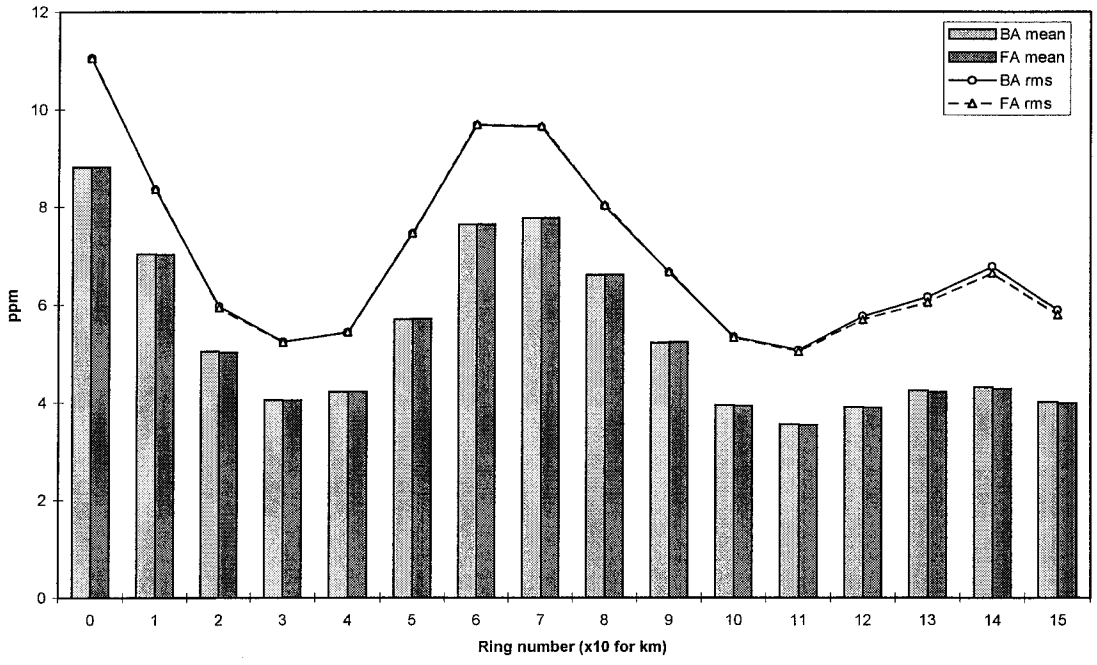

Figure 4 - 28 : $\delta\Delta N$ values (expressed in ppm) for the first order control stations computed using Bouguer Anomalies (BA) and Free-air Anomalies (FA) for the mid compartment interpolation.

4.5.4 Satellite Altimeter or Ship-borne gravity data

The effect of using the satellite altimeter gravity data (Section 4.4.4) instead of ship-borne gravity data is compared in this section. The residual free-air gravity anomalies were computed in terms of OSU91A and no DEM was used to calculate the mean compartment height. The decision not to use a DEM was based on the assumption that as only the source of the off-shore gravity data was being varied, the relative difference between the results would reflect this source - the on-shore data being the same for both solutions.

From Figures 4-29 and 4-30 it is clear that the use of the satellite altimetry data instead of the ship-borne data results in an apparent lower quality solution at all cap sizes tested. However, the choice of optimum cap size has not been affected (ie. Ring number 3, see Section 4.5.2.3). It is also interesting to note that the W-curve (Section 4.5.2.1) is still present with only the amplitude changing.

The lower North Island test area contains dense ship-borne gravity data (Section 4.4.2). If the test area contained no ship-borne gravity data at all, then the use of satellite altimetry data to supplement the land gravity data in a RINT solution (Ring 3) would still be a 20% improvement over OSU91A, ie. Ring 0 (Figure 4-30).

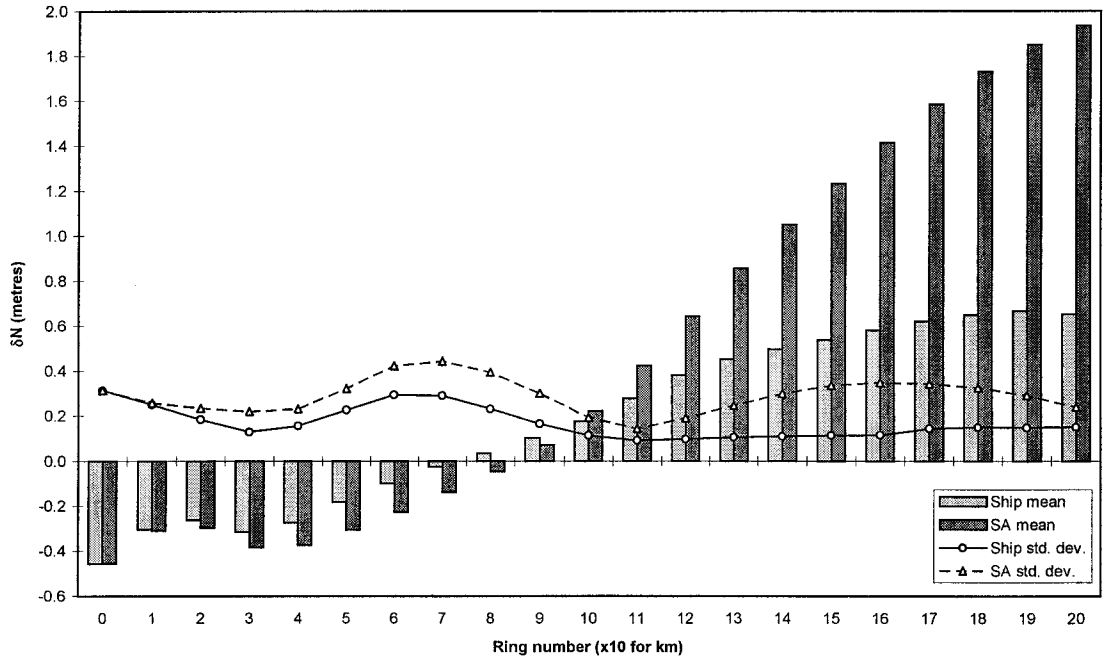

Figure 4 - 29 : δN values computed using Ship-borne or Satellite Altimeter (SA) gravity data for marine areas around the first order control stations.

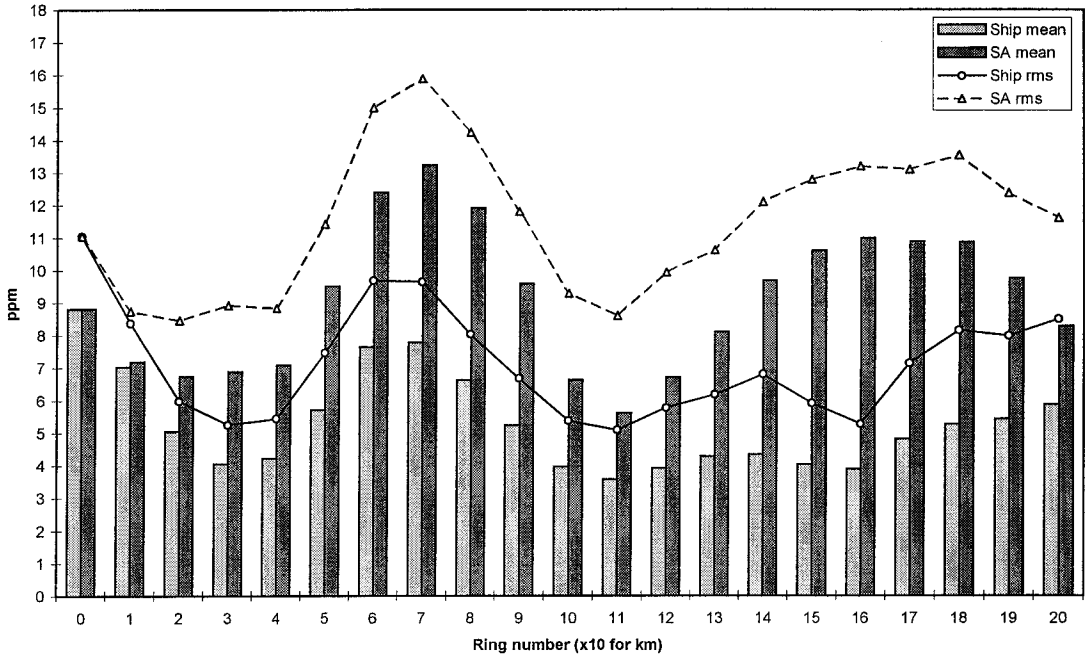

Figure 4 - 30 : $\delta\Delta N$ values (expressed in ppm) computed using Ship-borne or Satellite Altimeter (SA) gravity data for off-shore areas around the first order control stations.

At the time the Satellite Altimetry gravity anomaly test was undertaken, world_grav.img.4 was the latest file available. However, more recent files such as world_grav.img.7.2 have been generated with a 2 minute grid (Sandwell *et al.*, 1995). These denser grid files may produce improved results over the tested grid. Also, there may be a datum style shift between the terrestrially observed (land and ship-borne) gravity and the satellite altimetry derived gravity which may be able to be modelled in future research.

4.5.5 Evaluation of Kernel Modifications using gravity data

The theory of modifying the Stokes integration kernel to reduce truncation error was introduced in Section 4.3.2.1. This section evaluates each of the four proposed modifications against the standard RINT kernel, $F(\psi)$, by analysing the differences to the computed N values within each integration limit (ring number).

The degree of kernel modification (N_{mod}) was fixed at 36 for all the tests. OSU91A was the GGM used to generate the residual free-air gravity anomalies (Δg_r) to degree and order 360 and a DEM provided the mean compartment heights.

As it has been shown in previous sections that the absolute point comparison (δN) can contain biases due to the likes of datum errors and gravity reduction assumptions, only the relative line comparison considering the length of the baselines (ppm) will be used to investigate the modified kernels.

The ppm mean value of the 14 first order control stations for spherical cap sizes of 0.1° increments up to 1.5° is contained in Figure 4-31. The first point that needs clarification is the reason behind the small differences between the Stokes ppm mean in Figure 4-31 and that of Figure 4-26 (section 4.5.2.2). To simplify the incorporation of the modified kernels in the RINT software the increment between rings was fixed at 0.1° rather than being varied to give equal contribution to N_{RINT} per compartment as is normally the case (Section 4.3.4). This results in $\psi_o = 1.5°$ at ring number 15 rather than $\psi_o = 1.34°$ (if equal per mGal contribution to N_{RINT} per compartment is enforced) and therefore slightly different gravity data is used in each compartment. However, as the tests were primarily concerned with relative differences between the respective kernels this difference in the data used was not considered significant.

From Figure 4-31 it is clear that the different kernel modifications affect the final geoid results. The Meissl kernel modification gives the poorest agreement, with results deteriorating as further local gravity data is incorporated. All other kernel modifications, except Stokes' at ring 6 perform better than the OSU91A model only solution. The Featherstone and Evans kernel modification appears to be still improving at the maximum cap size tested (Ring number 15).

Larger cap sizes were not able to be tested as the limit of the DEM was reached at ring 15. It was considered best to use a DEM so that the errors in the computed N values were minimised, thus enabling a more critical analysis of the relationship between the kernel and its result.

Featherstone and Evans performs considerably worse than Wong and Gore, and Vanicek and Sjoberg (approximately a factor of 2 and 1.6 respectively), at ring numbers 3 and 10.

The familiar W-curve of Stokes' kernel has disappeared from the results when the Meissl or Featherstone and Evans kernel modifications are used. Both these kernels have values close to zero for small cap sizes (Figure 4-8), therefore, the long wavelength component (N_{GGM}) of N_{GRAV} dominates the result at small cap sizes. This may indicate that the W-curve is an artefact of errors in the residual gravity rather than the choice of kernel.

There is practically no difference between Wong and Gore, Stokes or Vanicek and Sjoberg kernel modifications at the optimum cap size of ring number 3 (Section 4.5.2.3). Of these three kernel modifications Stokes has the largest W-curve amplitude. Both Vanicek and Sjoberg and Wong and Gore give slightly better results however the simplicity of Stokes still makes it attractive to use.

The rms values expressed in ppm for the modified kernels are contained in Figure 4-32. These rms results are very similar to the mean results in Figure 4-31. The same comments therefore hold as for the analysis of the means, and reinforce the point that ring number 3 using either Stokes, Wong and Gore, or Vanicek and Sjoberg kernel modifications produce the optimum solution. Given the simplicity of Stokes kernel there appears to be no advantage in applying any kernel modification to reduce truncations errors in this lower North Island test area.

The Featherstone and Evans modified kernel has the attractive feature of eliminating the W-curve for cap sizes smaller than ring 15. However, further tests at larger cap sizes are required to investigate where the Featherstone and Evans kernel modification based solution reaches a minimum. It should be remembered that other errors in the gravity reduction and conversion to geoid height may be masking truncation errors. Therefore

as improvements are made to other assumptions in determining geoid height the effects of truncation errors may become significant.

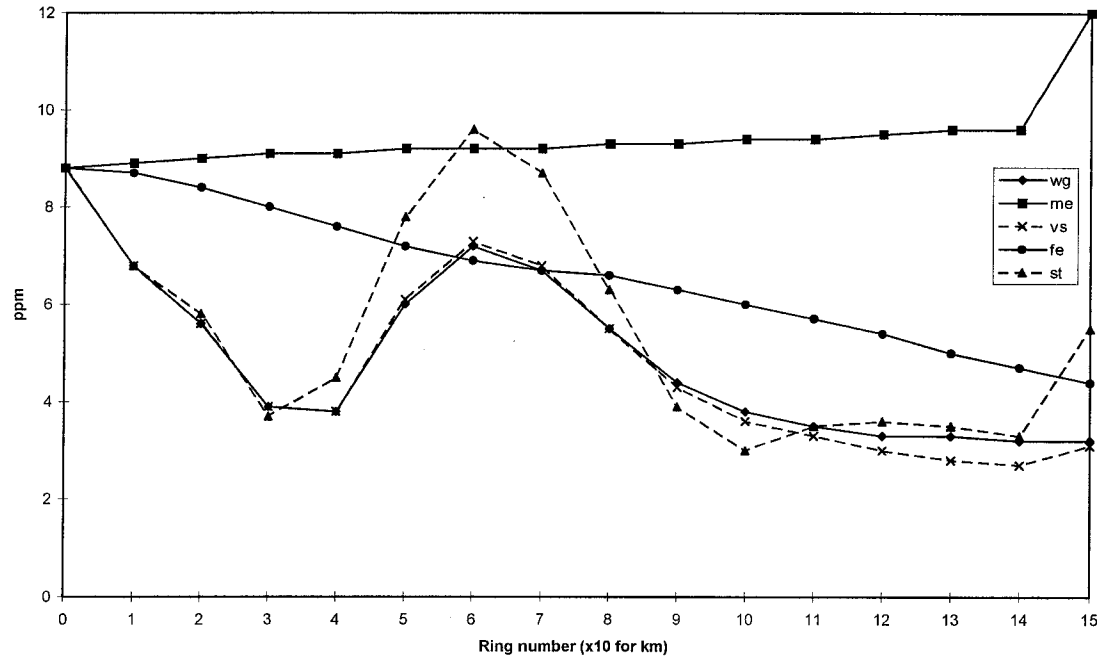

Figure 4 - 31 : mean values (expressed in ppm) computed using modified kernels at the first order control stations. The abbreviations are : Wong and Gore (wg), Meissl (me), Vanicek and Sjoberg (vs), Featherstone and Evans (fe), and Stokes (st).

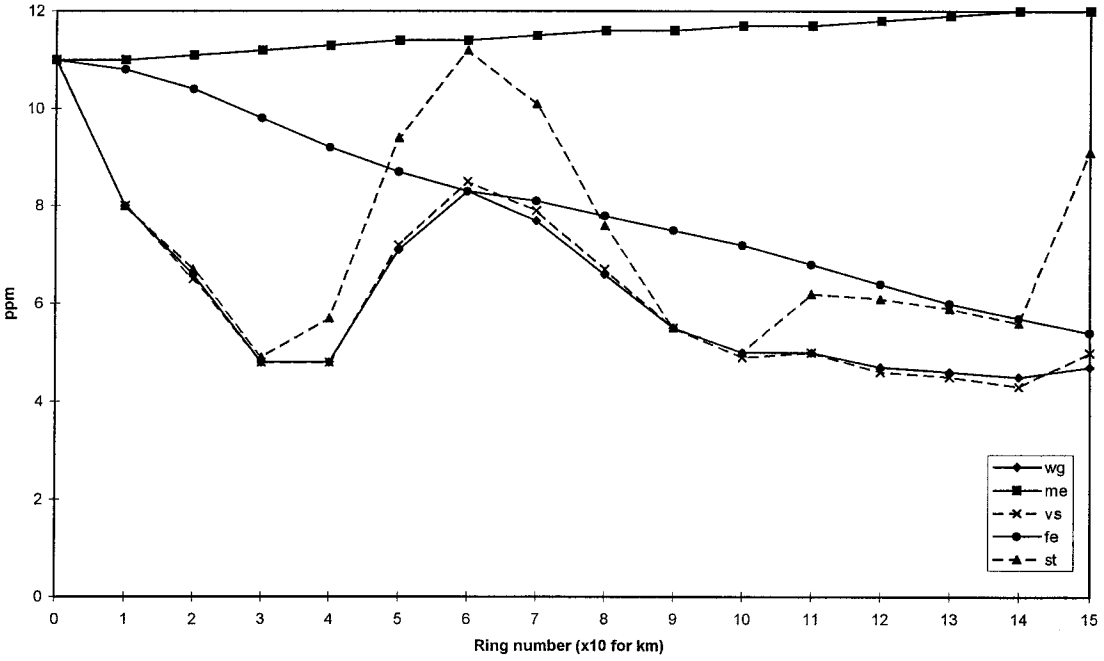

Figure 4 - 32 : rms values (expressed in ppm) computed using modified kernels at the first order control stations. Abbreviations as per previous figure.

4.5.6 Comparison of OSU91A and EGM96 as the reference GGM

Section 4.5.2.1 investigates the differences between using OSU81 or OSU91A as the reference GGM for RINT, and showed that OSU91A was superior. This section compares the effect of using the new GGM, EGM96 (n_{max} = 360), as the reference GGM for RINT against OSU91A (n_{max} = 360).

As was shown in Section 4.5.2.1, the use of absolute comparisons of N (δN) are affected by datum inconsistencies, while relative line comparisons ($\delta\Delta N$) can be biased by the length of line, therefore this section will only present results using $\delta\Delta N$ values expressed in ppm, using (4.66) and (4.67), to minimise these influences.

Comparing the OSU91A and EGM96 based N value results (Figure 4-33), at the first order control stations, computed using a DEM to determine the mean compartment height, it can be clearly seen that EGM96 is generally superior to OSU91A in terms of both mean and rms. However, it is interesting to note that at ring zero (ie. model only) OSU91A produces the better results, while at ring 3 both models have practically identical results and beyond ring 9 the difference in the results is basically insignificant. An appealing feature of Figure 4-33 is the reduction in the amplitude of the W-curve for both the mean and rms when using EGM96. This is especially true in the vicinity of the previously determined optimum cap size of ring 3 (0.3°) (Section 4.5.2.3), as now the differences between using rings 2, 3 or 4 are practically negligible.

To check this apparent improvement with EGM96 over OSU91A at the first order control stations, a comparison using the third order control stations was performed (Figure 4-34). The difference between the rms from the different GGM are insignificant, except for rings 4 through 8, where EGM96 is superior. It is interesting to note that by using the local gravity data in RINT with ring 5 as the cap size produces rms results that are inferior to using either of the GGM on their own. The mean difference for all rings below ring 9, except rings 2 and 3, have improved with the use of EGM96. However, rings 2 and 3, and ring 9 and above show no significant difference between the choice of reference GGM.

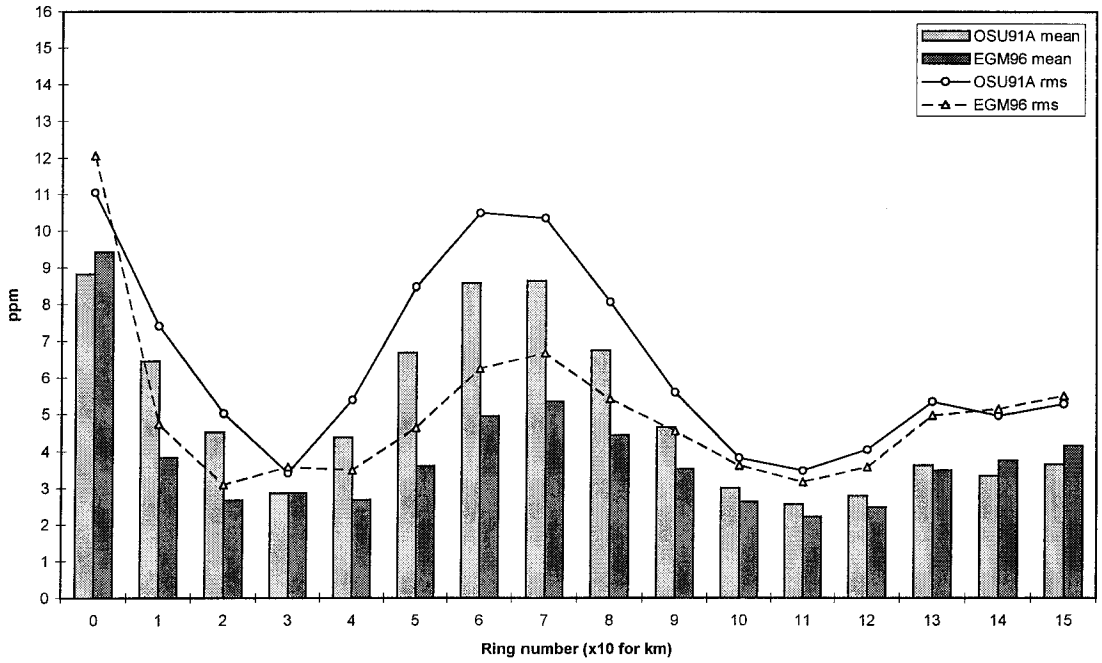

Figure 4 - 33 : δΔN values (expressed in ppm) for the first order control stations computed using EGM96 or OSU91A as the reference GGM and the DEM to calculate the mean compartment height.

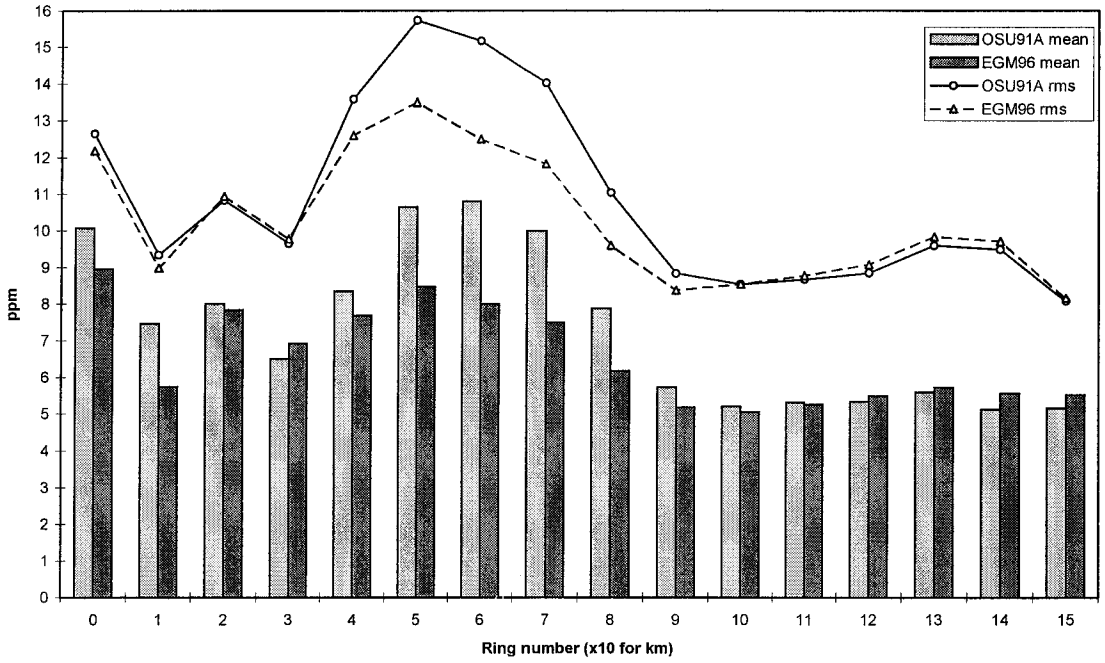

Figure 4 - 34 : δΔN values (expressed in ppm) for the third order control stations computed using EGM96 or OSU91A as the reference GGM and the DEM to calculate the mean compartment height.

It can be concluded from these results in Figures 4-33 and 4-34 that using EGM96 as the reference GGM in RINT (for the lower North Island test area) will produce results that are superior, or at least equivalent, to using OSU91A. The choice of ring 3 for the optimum cap size (Section 4.5.2.3) still is valid when using EGM96 as the reference GGM in RINT, however from the results at the third order control stations (Figure 4-34) it could be argued that ring 1 is optimum.

To check the conclusion from Section 4.5.2.2, that the use of a DEM to determine the mean compartment height improves the results (except for rings 4 to 8), was not biased by the use of OSU91A, the comparison of the evaluations using the gravity station heights only with the DEM was repeated for the first order control stations using EGM96 as the reference GGM (Figure 4-35). From Figure 4-35 it is clear that the use of the DEM to estimate the mean compartment height improves the results at all rings, except rings 5 to 7 which are practically equivalent to using the gravity station heights.

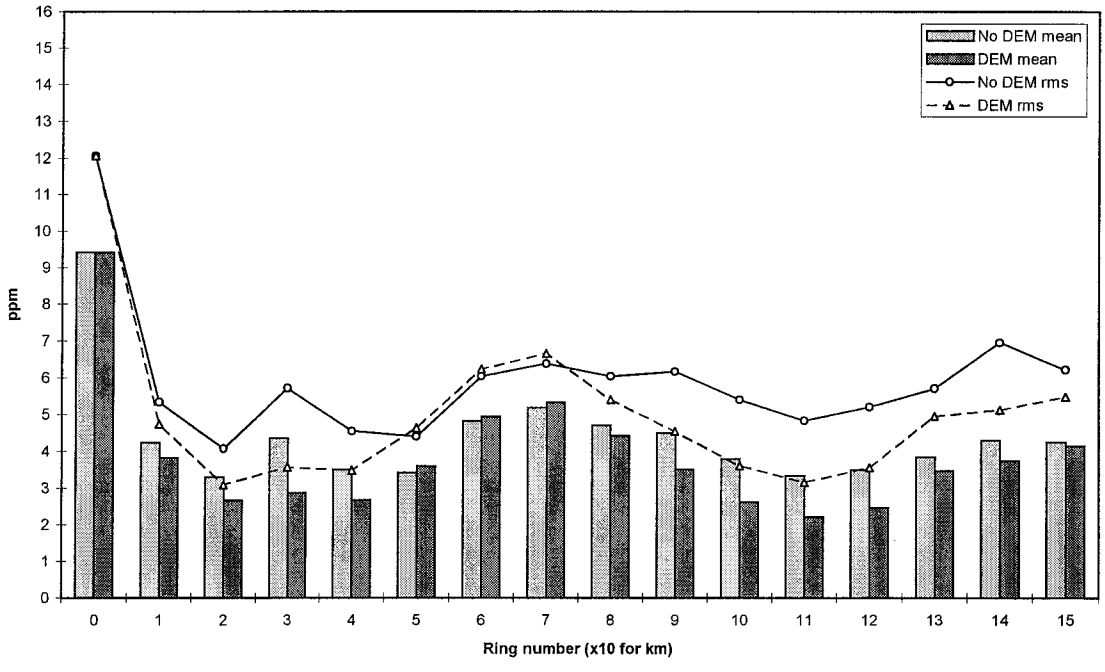

Figure 4 - 35 : $\delta\Delta N$ values (expressed in ppm) for the first order control stations computed using the DEM or gravity station heights to calculate the mean compartment height with EGM96 as the reference GGM.

4.6 Lower North Island Gravimetric Geoid

The practical requirements of a gravimetric geoid, for use in the field, are not likely to need or require the rigorous point computation which RINT offers for some of the following reasons:

i) the computing resources required to store the large gravity data and DEM files, which for the lower North Island test area were 1.94 Mb and 5.14 Mb, respectively,
ii) time and/or accuracy requirements may necessitate pre-computing geoid heights,
iii) electronic data processing facilities may not be available and therefore paper based products may be required (ie. tables of values or contour plots).

These field requirements can be met by pre-computing a grid of N values using RINT at an appropriate density for a specific region (ideally the whole country - as was done in Australia; Steed and Holtznagel, 1994). This grid of N values could be stored electronically for automated interpolation of N values at points of interest or contour plots generated to allow manual interpolation.

A grid was generated for a portion of the lower North Island test area to illustrate the benefits of this approach. The grid had extents of S40.05° to S41.50° and E174.55° to E175.85°, and an interval of 0.05° which resulted in 30 rows and 27 columns, to give a total of 810 grid nodes. Two different methods were used to compute the N values at these grid nodes and then contour plots generated for each. The first method used the EGM96 model only (ie N_{GGM} from eqn. 4.46) (Figure 4-36a), while the second method used the RINT solution with EGM96 as the reference GGM (ie N_{RINT} from eqn. 4.51), a DEM for estimating the mean compartment height and a cap size of ring 3 (≅0.3°) (Figure 4-36b). Each of these grid files of N values only required 0.03 Mb of disk space. If the grid (with the same density) had covered the same area as the entire DEM and gravity files, the gridded N value files would have occupied approximately 0.45Mb (stored as ascii), compared to the combined gravity and DEM file requirements of 7.08 Mb (stored in a compressed binary format).

From the contour plots the RINT based solution (Figure 4-36b) appears to show more of the finer geoid features than the EGM96 model only solution (Figure 4-36a), as expected. Comparing the associated statistics, for each of the contour plots, confirms that the RINT based solution contains finer geoid features (due to the large sd), and also highlights that the RINT based solution determined smaller N values than the EGM96 model only solution.

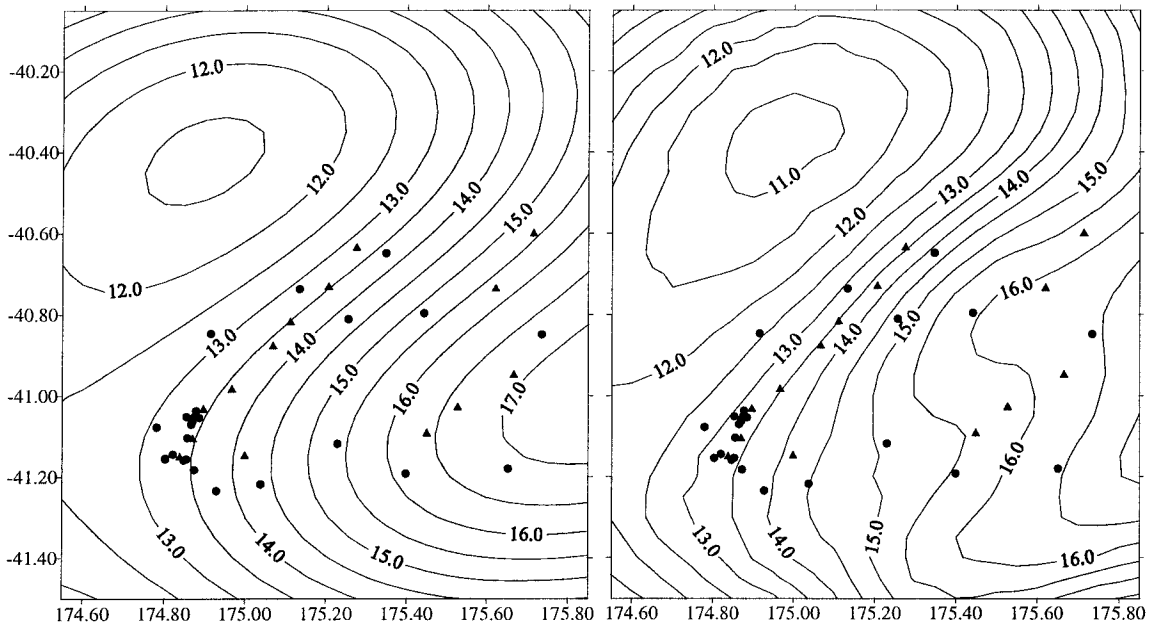

a) (min: 11.392m, max: 17.327m mean: 13.818m, sd: 1.643m)

b) (min: 10.774m, max: 17.139m, mean: 13.676m sd: 1.810m)

Figure 4 - 36 : Lower North Island geoid contour plots in terms of GRS80. Where a) is the EGM96 model only N values, and b) is the RINT generated N values for ring 3, the DEM for compartment heights and using EGM96 as the reference GGM. (units = metres). The selected GPS control stations with first order (triangles) and third order (circles) orthometric height are also shown.

To test that the RINT based solution generated more realistic N values than the EGM96 model only solution, N values were interpolated for each GPS station shown in Figure 4-36 (excluding D136 and D510, see Figure 4-23) and a δN comparison (4.64) performed. From Table 4-3, the standard deviation for both the first and third order stations is lower when using the RINT based solution. It is interesting to note that both solutions have a mean of approximately 0.5 m. This indicates that there may be a datum bias in one, or more, of the three heights (h, H, N).

Height order (No. stations)	Solution type	min. (m)	max. (m)	mean (m)	sd (m)
First order (14)	EGM Only	-1.109	0.064	-0.528	0.354
	RINT	-0.584	-0.267	-0.402	0.091
Third order (17)	EGM Only	-0.969	0.079	-0.530	0.229
	RINT	-0.783	-0.167	-0.474	0.154

Table 4 - 3 : δN analysis of lower North Island geoid grid representation generated either using the EGM96 GGM or RINT with EGM96 as the reference GGM, a DEM for estimating the mean compartment height and a ring 3 cap size (≅0.3°)

4.7 New Zealand wide Geoid investigations

The determination of a gravimetric geoid using the RINT technique has been limited to the lower North Island test area. The main reason that a nationwide gravimetric geoid was not computed for New Zealand was that suitable DEM were not yet available for most of the country. It is envisaged that in the near future a dense (say 1 to 5 km grid) nationwide gravimetric geoid will be required to be generated for New Zealand and it would be appropriate for the national geodetic agency of New Zealand, LINZ, to compute this geoid. It has been shown above that the RINT technique provides a viable method in the lower North Island test area. This was able to be proven through there being available suitable ellipsoidal and orthometric heights to allow checking using (4.64) and (4.65).

If one begins to look at validating a New Zealand wide gravimetric geoid, once established, there are likely to be some difficulties arising from the fact that New Zealand does not have a single consistent height datum (Section 2.5). It should also be noted that the lower North Island test area had an average gravity data spacing on land of 1 station per 6.5 km^2, which is slightly denser than the national average of 7.5 km^2, however the density can be significantly lower in some parts of the country, ie Fiordland in the south-west of the South Island (Figure 4-1). The lower North Island test area also had reasonably well distributed marine gravity data, though other New Zealand coastal regions have significantly sparser gravity data.

To begin to understand whether not having a consistent nationwide height datum is going to significantly influence the validating of a nationwide gravimetric geoid the following analysis was performed. The nationwide GPS stations from Chapter 3 were used as control for absolute point comparison (δN, where $N_{GRAV} = N_{GGM}$). The GPS stations for this analysis as those as shown in Figure 3-1 (excluding D172 and D269 due to data processing problems). The analysis was originally done using N_{GGM} computed from OSU91A, though with the release of EGM96 these tests were repeated.

The initial δN results indicated that the North and South Island were performing in significantly different ways. Therefore, a separate analysis of each island was undertaken and results are shown in Tables 4-4 and 4-5. It should be noted that unfortunately in the North Island there was only one GPS station (D131) having a first order orthometric height, while the South Island had no first order and only one second order orthometric height station (D286). When the standard deviation of the δN results between the islands is compared, it was not unexpected that the North Island stations showed better comparisons than the South Island stations, due in part to the different quality of the orthometric heights. What was interesting to see was that, irrespective of which GGM was used, the δN mean was different between the Islands by approximately 1.0 m.

Station ID	h	H	Order of H	OSU91A N	EGM96 N	OSU91A δN	EGM96 δN
D026	174.519	136.090	3	38.224	38.316	0.205	0.113
D045	141.907	106.700	2	35.802	35.104	-0.595	0.103
D072	95.930	66.600	4	29.319	29.218	0.011	0.112
D078	360.584	338.690	3	21.265	21.267	0.629	0.627
D100	323.545	301.360	3	21.313	21.738	0.872	0.447
D105	263.238	240.600	2	22.383	22.955	0.255	-0.317
D131	143.727	131.380	1	12.897	13.139	-0.550	-0.792
D143	590.954	575.200	3	16.396	16.809	-0.643	-1.056
D431	119.396	101.080	2	18.463	18.151	-0.147	0.165
D452	319.113	287.000	4	31.864	31.684	0.249	0.429
D473	760.488	733.280	3	26.585	27.404	0.623	-0.196
WELL	37.820	24.980	2	13.649	13.086	-0.809	-0.246
					minimum	-0.809	-1.056
					maximum	0.872	0.627
					mean	0.008	-0.051
					std. dev.	0.561	0.500

Table 4 - 4 : δN comparison between OSU91A and EGM96 at the North Island GPS stations coordinated in terms of ITRF93 (units = metres).

To try and resolve whether the apparent bias in the South Island stations was due to the poor orthometric heights or from another source, it was decided to evaluate how well each of the two GGM's were able to represent the land only gravity data.

Station ID	h	H	Order of H	OSU91A N	EGM96 N	OSU91A δN	EGM96 δN
D158	791.897	775.700	4	15.495	15.002	0.702	1.195
D191	405.657	392.100	4	13.035	13.261	0.522	0.296
D212	510.526	498.560	3	11.820	11.915	0.146	0.051
D229	1005.888	995.600	3	8.367	8.854	1.921	1.434
D233	397.352	388.400	4	8.381	8.491	0.571	0.461
D253	1681.042	1673.000	4	6.481	6.746	1.561	1.296
D286	269.062	265.150	2	3.184	3.611	0.728	0.301
D302	411.445	405.500	4	3.840	4.479	2.105	1.466
D309	919.511	905.320	3	11.696	11.345	2.495	2.846
D320	114.831	103.860	3	8.501	8.966	2.470	2.005
D338	14.639	7.160	3	5.716	5.893	1.763	1.586
D425	254.693	243.000	4	12.011	11.25	-0.318	0.443
D469	169.677	150.800	4	19.859	18.634	-0.982	0.243
D474	176.531	172.550	3	3.386	3.802	0.595	0.179
					minimum	-0.982	0.051
					maximum	2.495	2.846
					mean	1.020	0.986
					std. dev.	1.056	0.833

Table 4 - 5 : δN comparison between OSU91A and EGM96 at the South Island GPS stations coordinated in terms of ITRF93 (units = metres).

The evaluation involved the statistical analysis of the residual gravity anomalies (Δg_r, Section 4.3.2) for each island separately (Table 4-6). As the South Island has greater topographic variations than the North Island, it is not surprising that the Δg_r standard deviation in the South Island is larger than in the North Island. As is also clearly seen from Table 4-6 the Δg_r mean is significantly larger for the South Island than the North Island. The reason for this bias in the residual gravity anomalies for the South Island is not fully understood, though is likely to be in part due to both GGM not having sufficient resolution to be able to represent the abrupt change in the geoid near the Southern Alps.

	North Island		South Island	
	OSU91A	EGM96	OSU91A	EGM96
No. Stations	17467	17467	17296	17296
Minimum	-96.994	-112.903	-83.208	-78.279
Maximum	146.787	143.194	193.732	193.639
Mean	-0.171	-1.877	-8.700	-9.091
Std. Dev. (1σ)	21.138	20.527	34.261	34.295

Table 4 - 6 : North and South Island Land Only residual free-air gravity anomalies with respect to the OSU91A and EGM96 GGM's (units = mGal).

From an analysis of the δN and Δg_r results (Tables 4-4 through 4-6) it is unclear as to whether the South Island bias is a result of the poor orthometric height control or insufficiencies in the GGM's, though it is probably a combination of both. If GPS stations in the South Island had first order orthometric heights then at least the control height uncertainty could be reduced. Therefore, it is recommended that first order orthometric height stations need to be occupied by GPS, in both islands, so as to provide control stations to evaluate any future nationwide gravimetric geoid. If tide gauge benchmarks were also occupied with GPS, this would provide information not only useful to evaluating a gravimetric geoid but also the vertical datums of New Zealand.

From Table 4-4 and 4-5 it was surprising to see that the differences in N_{GGM} values between OSU91A and EGM96 could vary from basically 0.0m (D078) up to 1.2m (D469). To investigate the size and location of the maximum difference between the two N_{GGM} values across New Zealand, a 0.1° x 0.1° grid of N values were generated from each GGM. The difference between these two surfaces (Figure 4-37, sense OSU91A minus EGM96) revealed that variations ranged from -2.357 m (S39.5°, E175.0°) to 1.233m (S40.5°, E173.0°), with a mean of -0.024 m and a standard deviation of 0.341m.

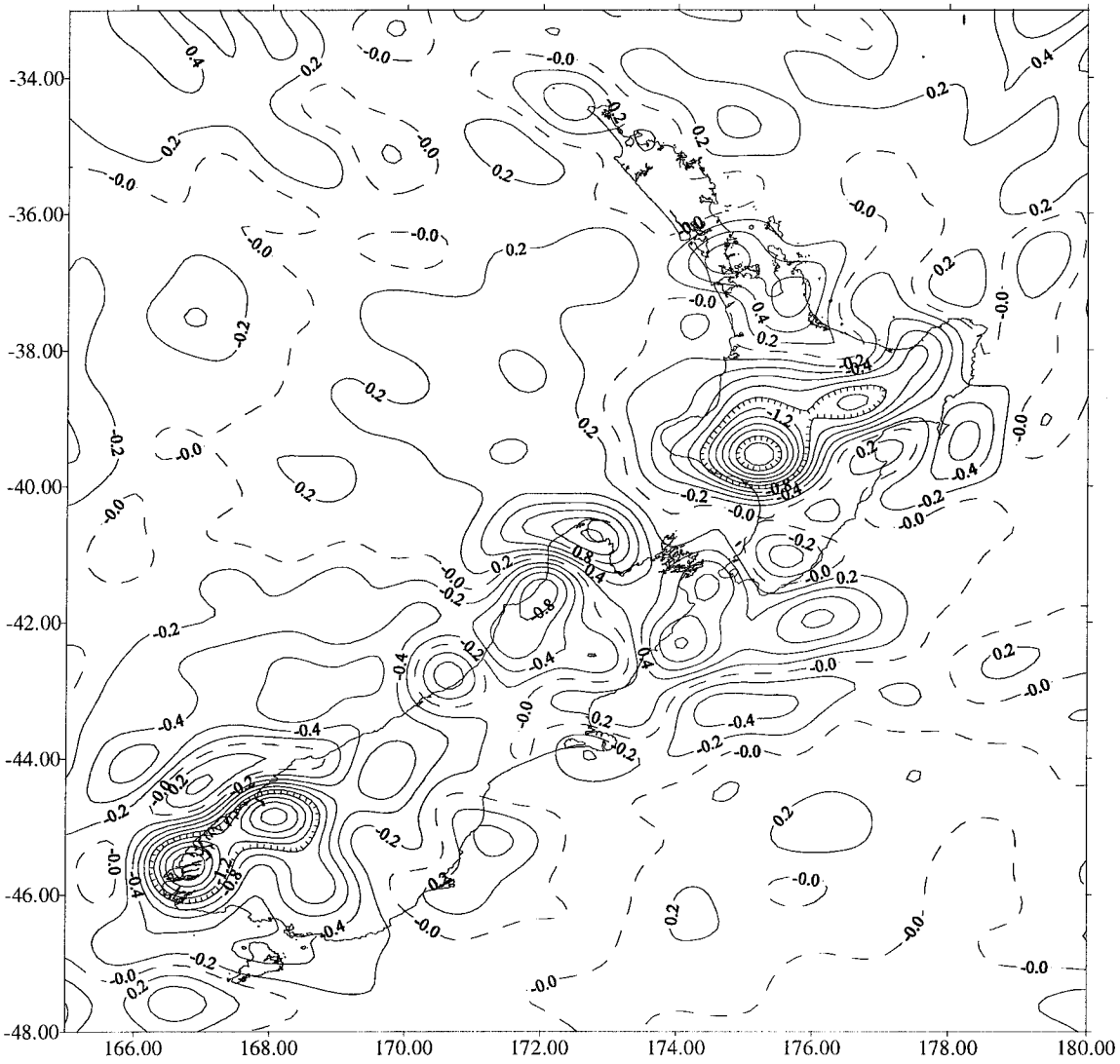

Figure 4 - 37 : Geoid height differences across New Zealand generated by subtracting EGM96 from OSU91A for a 0.1° x 0.1° grid.

The probable reason for the high frequency variations, since they are located primarily on land, is the application of different power law constraints to the satellite only solutions (Rene Forsberg, pers. comm., 1996). OSU91A used Kaula's power law, divided by the square root of two, which underestimates the power in the Earth gravity field, as determined from surface gravity observations (Lemoine *et al.*, 1996). Lemoine *et al.* (*ibid.*) state that EGM96 used a power law constraint derived from the signal of the surface gravity data to spectrally constrain the coefficients of the EGM96 satellite only solution. As the satellite only solution is the foundation of the high degree

quadrature solution, it important that the spectrum of the errors in the satellite only model be consistent with the signal observed by surface gravity data. Another reason for the variations is that EGM96 contains terrain corrections.

From the use of a more appropriate power law constraint, EGM96 is able to represent smaller scale variations in the geoid than OSU91A.

4.8 Summary

This chapter summarised the theory behind the determination of gravimetric geoids and outlined some of the practical methods applied to solving the geodetic boundary problem. The RINT technique was used to compute a gravimetric geoid for a test area in the lower North Island of New Zealand. From analysing geoid heights computed from the gravimetric geoid, and also a selection of global geopotential models, against the available geometric control the following comments can be made.

i) EGM96 produced geoid heights which had better agreement than OSU91A, against the geometric control, in the lower North Island test area.
ii) The use of local gravity observations in the determination of geoid heights using the RINT technique produced further improvement compared with the geometric control, than those computed using the EGM96 model only geoid heights.
iii) The RINT generated geoid heights, in the test area, are optimised when both a DEM is used for the computation of the mean compartment height and a spherical cap radius of 0.3° (≅ 30 km) is set.
iv) From the analysis at the first order stations the best comparison between a geometrically-determined ΔN and a ΔN from an optimised RINT gravimetric geoid is approximately 4 ppm for line lengths over 6 km. This meets the New Zealand second order levelling specifications.
v) Tests on modifications to the Stokes' kernel to reduce truncation error indicate that for the test area these modifications appear to be insignificant. Any change is probably below the noise levels in the control data.

The lower North Island gravimetric geoid could possibly be refined further by applying the second order free-air correction, and the terrain correction beyond the current radius

of 21.94 km, to the currently available free-air gravity anomalies. In applying further corrections to the gravity data, one should not forget to consider the magnitude of the correction with respect to the raw gravity data observation accuracy.

With the realisation of a dense nationwide gravimetric geoid for New Zealand, whether computed using RINT or another proven technique, surveys undertaken using GPS will be able to convert the ellipsoidal heights into orthometric heights with improved accuracy than is currently available using global geopotential models. With the improved geoid heights being available from a gravimetric geoid, transformation parameters between GPS derived reference frames and NZGD49 will be able to be computed more rigorously. These datum transformation issues are investigated in Chapter 5.

Chapter 5

Transformations

5.1 Introduction

In New Zealand, as in many other countries such as Australia, there are legal requirements for land titling work to be performed in terms of the current geodetic system, despite any shortcomings. As other important information about the land is related to the legal title the geodetic system can often become an integral part of most Geographic Information Systems (GIS) and Land Information Systems (LIS). The absolute nature of the geodetic coordinates though may be relaxed to 1 or 2 meters for many applications.

The operational efficiency, especially today with hand held GPS receivers, of directly determining positions from satellites in a three dimensional reference system has necessitated the development and generation of transformation procedures. This is especially true for those transformation procedures that operate from three dimensional space to the combined two dimensional space of NZGD49 and the multiple New Zealand levelling networks.

A general (and somewhat arbritary) classification of transformations accuracy are the three following levels which can be considered as application based:

i) the 1~5 metre level. This level would be used by most practical GIS/LIS users to ensure the uniformity and homogeneity of their digital products and systems.
ii) the sub-metre level. This level would be used by surveyors, and other professions, who need to maintain property boundaries.
iii) the sub-decimetre level. This level would currently be used by scientific users. While this level is desirable, it is normally achieved by recomputing data in terms of uniform and homogeneous three dimensional reference systems.

It will be shown in this chapter that, at the present time, only item (i) can be achieved. However, since this represents a considerable use of GPS and NZGD49, and with a new reference system for New Zealand still to be defined, it is an important aspect of transformations. It will also be shown that the literature on transformations, as determined for New Zealand, has significant deficiencies.

5.2 Coordinate Systems

There are a number of different terrestrial (earth-fixed) and inertial (space-fixed) reference systems used in geodesy. This section gives a summary of only those reference systems which were of primary importance to this thesis. For further details on those reference systems presented below, and coordinate systems in general, see Mueller (1969), Bomford (1980), Vanicek and Krakiwsky (1986), Lambeck (1988) and IERS special publications (ie. Boucher *et al.*, 1994 and McCarthy, 1996).

A reference system is the realisation of a detailed model that is used in the relationship between the configuration of the basic structure and its coordinates. At this point the coordinates are fully defined but not necessarily accessible. The system is usually realised by the determination of a set of conventionally chosen parameters and coordinates (eg. star positions, station positions or pole coordinates) that define the reference frame (Mueller, 1985). A terrestrial reference frame is realised through the coordinates of stations which are fixed to the surface of the Earth and hence rotate with the Earth's rotation, whereas an inertial reference frame is realised through the coordinates of stellar objects and other sources for which their rotation can be highly modelled thereby reducing the system to one which is free of accelerations.

The following definitions of coordinate systems have been adopted from Lambeck (1988) and Soler and Hothem (1988).

5.2.1 Conventional Inertial Reference System (CIRS)

An inertial reference system can be defined in terms of stellar objects or sources fixed in space, or dynamically by the motion of a planet or satellite. It is a system in which there

are, by definition, no accelerations and hence no rotations. This is usually achieved by modelling the rotation.

i) Celestially based CIRS

The fundamental, or primary, plane of a celestial reference system can be either the equatorial plane or the ecliptic (Earth's mean orbital plane about the Sun). The intersection of these two planes defines the line of nodes. The principal (Z) axis is perpendicular to the fundamental plane and defined by the cross product of any two vectors in the fundamental plane. The secondary plane contains the vernal equinox (the point where the Sun appears to cross the Earth's equator from the southern to northern hemisphere. ie. at the intersection of the ecliptic and equatorial planes) and the principal (Z) axis. The third (Y) axis is chosen to make the system right-handed (the cross product of the Z axis and the line of nodes). The origin is implicitly defined once the stellar bodies are assigned coordinates. The coordinates of bodies can be specified by the declination (δ, analogous to ϕ) and right ascension (RA, analogous to λ) (Figure 5-1) or by Cartesian coordinates.

The Conventional Inertial Reference System (CIRS) is normally realised by assigning coordinates to extragalactic celestial radio sources, and some collocated optical positions, and serves as a reference for the motion of the Conventional Terrestrial Reference System (CTRS) (Section 5.2.2).

ii) Satellite based CIRS

This is an earth-centred spatial Cartesian system, whose origin is at the earth's centre of mass *CM* (the geocentre, the centre of mass including the mass of the atmosphere). The defining planes are the orbit of the satellite and the equator of the Earth (fundamental plane). These two planes intersect along the line of nodes. The principal (Z) axis is perpendicular to the fundamental plane and defined by the cross product of any two vectors in the fundamental plane. The secondary (X) axis is the line of nodes with the positive end being through the point where the satellite appears to cross the Earth's equator from South to North. The third (Y) axis is chosen to make the system right-handed. The position of an orbiting satellite can also be described by its declination and

right ascension, although it is more common to describe its position and velocity in Cartesian coordinates.

5.2.2 Conventional Terrestrial Reference System (CTRS)

The CTRS is the closest practical approximation of the geocentric natural system and probably the most important system in geodesy (Vanicek and Krakiwsky, 1986, p. 296).

It is an earth-fixed spatial Cartesian system, $(X\ Y\ Z)_{CT}$, whose origin is at the earth's centre of mass *CM*. The conventional terrestrial Z axis (Z_{CT}) coincides with the mean rotational axis of the earth at an epoch, known as the Conventional Terrestrial Pole (CTP). The mean equatorial plane perpendicular to the Z_{CT} axis forms the XY-plane. The XZ-plane is generated by the mean meridian which contains the Z_{CT} axis and the "mean" observatory of Greenwich. The X_{CT} axis is the intersection of the XY- and XZ-planes, with positive being through the mean Greenwich observatory meridian. The Y_{CT} axis is selected to make the system right-handed (Figure 5-1).

The CTP was for many years realised by the Conventional International Origin (CIO), which was defined by the mean position of the Earth's instantaneous pole during the period 1900 to 1905. However in recent years the BIH reference pole of epoch 1984.0 has been adopted to realise the CTP.

There are a number of different terrestrial coordinate systems that have been established to realise the CTRS. Some of the most rigorously defined realisations are those produced yearly by IERS, being referred to as ITRF (Section 3.4), as they combine globally distributed observations from different techniques (ie. GPS, LLR, SLR, DORIS and VLBI). In addition to these combination solutions it is common for the different techniques to produce their own realisations, with WGS84(G730) being an example of a GPS realised CTRS.

The connection between the CTRS and CIRS frames by tradition is through the conventional rotations expressed as (Mueller, 1969):

$$\mathbf{X}_{CTRS} = \mathbf{S}\,\mathbf{N}\,\mathbf{P}\,\mathbf{X}_{CIRS} \qquad (5.1)$$

Where **P** is the matrix of rotation for precession, **N** for nutation matrix, and **S** for earth rotation matrix (polar motion and sidereal time).

5.2.3 Geodetic Reference Surface (Datum)

The choice of a geodetic reference surface (geodetic datum) is often based on the best-fitting ellipsoid of the entire earth surface or any portion of it. If the ellipsoid is chosen to represent the entire Earth a global geocentric datum is established, while if the ellipsoid is defined to only represent a portion of the Earth's surface then a regional usually non-geocentric datum is established (Soler and Hothem, 1988). In both cases there is a minimisation, usually in the vertical direction.

The "ideal" global datum is defined by the ellipsoid which best approximates MSL globally. Because the Earth is rotating and has mass, its best physical approximation is given through the four parameters of a geodetic reference system (GRS), specifically (Soler and Hothem, 1988):

i) a equatorial radius
ii) GM geocentric gravitational constant
iii) J_{20} dynamical form factor, and
iv) ω earth's angular velocity

Note that the flattening is not one of the adopted constants, but is inferred through J_{20}. GRS80, as its name suggests, is an example of a GRS (Section 4.2.1)

However, due to the observational limitations imposed by early conventional geodesy, two different types of datums have been historically implemented:

A two-dimensional (surface) datum realised by geodetic curvilinear coordinates (ϕ,λ) referred to a prescribed ellipsoid and determined through the adjustment of geodetic measurements (eg. directions, distances, astronomic azimuth's, latitudes and longitudes), which are unable to define the geocentre. Examples are NZGD49 (Section 2.4.2) and the North American Datum of 1927 (NAD27). These datums are frequently called horizontal as they rarely consider the vertical component.

A vertical datum, completely separated from the horizontal datum, which in essence is a physical datum (ie. ellipsoid independent) based on the adjustment of levelling observations and the heights of selected tide gauge stations. Examples of continent wide vertical datums are the Australian Height Datum of 1971, AHD71 (Roelse *et al.*, 1975), and the American National Geodetic Vertical Datum of 1929 (NGVD29). New Zealand has a number of separate vertical datum that have not been adjusted together to form a consistent nationwide vertical datum (Section 2.5).

Even though the early horizontal datums were unable to be geocentric, the ellipsoidal axes were able to be defined so as to be approximately parallel to the CTRS axis by geometric means. The Laplace equation (condition) attempts to achieve this for classical triangulation.

A point on the Earth's surface with a geodetic azimuth, α, and a geodetic zenith distance, ζ, to a second point, are related to the astronomical azimuth, A, and astronomical zenith distance, z, between the same points, by (Heiskanen and Moritz, 1967, p. 186):

$$A - z = \eta \tan\phi + (\xi \sin\alpha - \eta \cos\alpha) \cot z \qquad (5.2)$$

Where ξ and η are deflection of the vertical components expressed in the local north-south and east-west directions, respectively, or latitude and the prime vertical.

As first-order triangulation networks have lines of sight which are almost horizontal, $z \cong 90°$, then (5.2) can be simplified to get Laplace's equation in its simplified form:

$$A - z = \eta \tan\phi = (\Lambda - \lambda) \sin\phi \qquad (5.3)$$

Where Λ is the astronomical longitude and λ is the geodetic longitude.

A Laplace station is a site for which astronomic azimuth and longitude have been measured and geodetic azimuth and longitude have been computed. A single Laplace station can be used to for orienting the reference ellipsoid so as its axes are parallel to the CTRS, however it is common for conventional horizontal datums to be realised

using more than one Laplace station so as to reduce the effect of measurement errors by performing a combined adjustment.

The use of the simplified Laplace equation, different time origins, different star catalogues and/or errors in the astronomic azimuths can introduce non-parallelism between geodetic systems and the CTRS. This often necessitates the introduction of small rotations about the axes (ε_x, ε_y, ε_z) for transforming between geodetic systems (Figure 5-2).

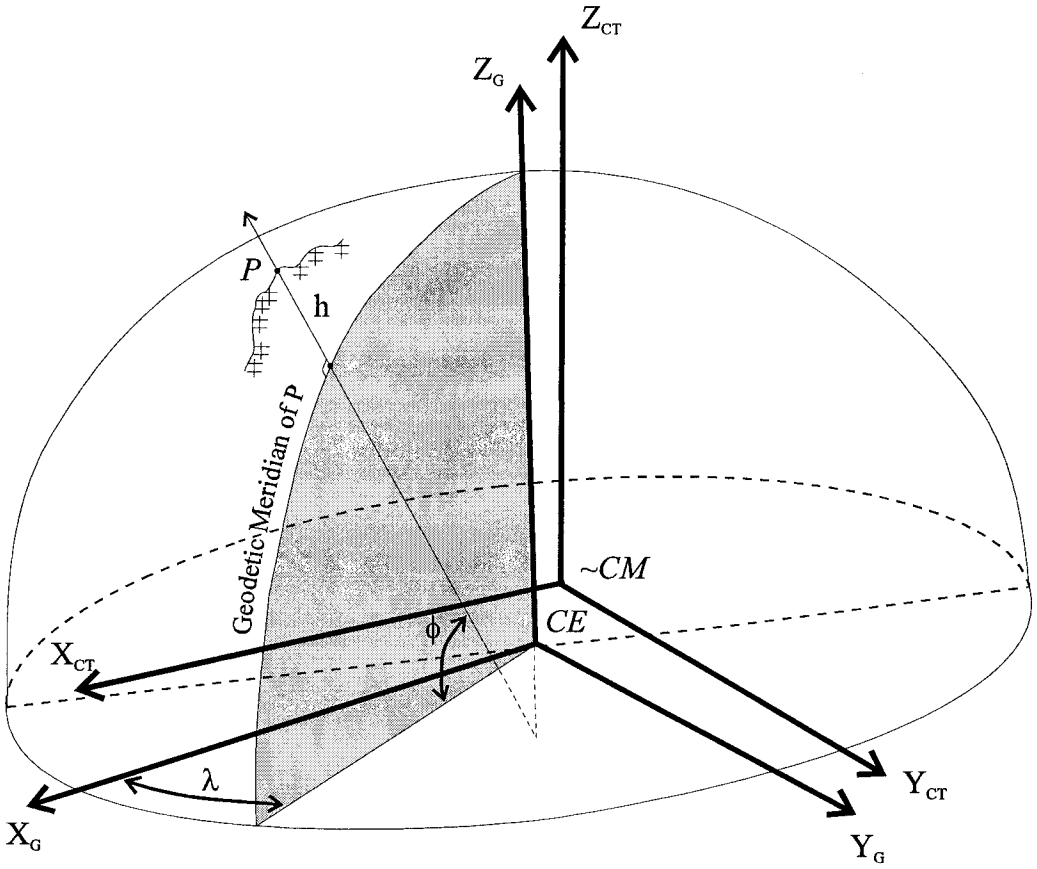

Figure 5 - 1 : Conventional Terrestrial (CT) and Geodetic (G) Reference Frames (adapted from Soler and Hothem, 1988)

In summary, a reference surface (datum) is realised by adjusting geodetic measurements, that have been reduced to a chosen reference ellipsoid, so as to fulfil the Laplace condition and to generate curvilinear geodetic coordinates for the physical ground marks. This process orientates the axes of the ellipsoid in the CTRS. The major error in this process is not the Laplace equation but the height of the stations above the ellipsoid. This is particularly so when heights are orthometric. The usual practice is to minimise

the residuals thereby aligning the ellipsoid to the geoid, which causes the centre of the ellipsoid (*CE*) to not be coincident with the Earth's centre of mass (*CM*).

5.2.4 Curvilinear Geodetic Coordinate System

It is often convenient to use curvilinear coordinates instead of spatial rectangular coordinates, especially when an ellipsoid has been adopted as a reference surface (datum). One reason is that most map projections, used for generating plane surface coordinates, require the ellipsoidal surface coordinates to commence the mapping. Curvilinear geodetic coordinates are defined by (Figure 5-1):

Geodetic longitude, λ : Angle between the plane containing both the Z_G axis (Earth's mean pole of rotation) and X_G axis (chosen to pass through Greenwich) and the geodetic meridian plane of point *P* measured positive toward the east; $0 \leq \lambda \leq 2\pi$.

Geodetic latitude, ϕ : Angle between the normal to the reference ellipsoid at *P* and the equatorial plane containing both the X_G and Y_G axes; $-\pi/2 \leq \phi \leq \pi/2$.

Geodetic (ellipsoidal) height, h : Distance along the normal to the reference ellipsoid between *P* and the surface of the ellipsoid (described further in Appendix L).

5.2.5 Geodetic Coordinate System

A unique geodetic coordinate system (and corresponding curvilinear geodetic coordinate system) is established each time a datum is defined (Figure 5-1). They are defined with the origin at the centre of the reference ellipsoid (*CE*) used for defining the specific datum. The Z_G-axis coincides with the semiminor axis of the reference ellipsoid. The X_G-axis passes through Greenwich (the point were $\lambda=0$ and $\phi=0$) and the Y_G-axis is chosen so as to form a right-handed system with the X_G- and Z_G-axes.

5.3 Transformation methods

There are a number of ways of defining the relationship between one reference system and another. The choice of the most appropriate network transformation model is influenced by:

i) the extents of the area for which it is to be applied
ii) the presence of distortion in either of the reference systems
iii) the dimensions of the reference systems (two- or three-dimensional), and
iv) the accuracy requirements.

This section focuses on those methods which have been applied to the New Zealand situation of converting between NZGD49 coordinates and global reference systems. It is noted that other theoretical transformation methods are available but parameters have not been developed for New Zealand.

Harvey (1986) outlined the properties of the affine, similarity, orthogonal and projection transformation as follows:

Affine transformation: An affine transformation transforms straight lines to straight lines and parallel lines remain parallel. Generally the size, shape, position and orientation of lines in a network are changed. The scale factor depends on the orientation of the line but not on its position within the network. Therefore it assumes that there are no systematic distortions within either network.

Similarity transformation: An affine transformation in which the scale factor is the same is all directions. A similarity transformation preserves the shape, so angles are not changed, but lengths of lines and the position of points may be changed.

Orthogonal transformation: A similarity transformation in which the scale factor is unity. The angles and distances within the network are preserved and only the positions of points change on transformation.

Projection transformation: An affine transformation where the scale factor is also dependent on the position of the line within the network. With this one can therefore attempt to model systematic distortions within the network.

The general similarity transformation is given by (Wolf, 1963):

$$\begin{bmatrix} \mathbf{X}_B \\ \mathbf{Y}_B \\ \mathbf{Z}_B \end{bmatrix} = s_F \mathbf{R} \begin{bmatrix} \mathbf{X}_A \\ \mathbf{Y}_A \\ \mathbf{Z}_A \end{bmatrix} + \begin{bmatrix} \mathbf{T}_X \\ \mathbf{T}_Y \\ \mathbf{T}_Z \end{bmatrix} \tag{5.4}$$

where

X_B, Y_B, Z_B	Cartesian coordinates in coordinate system B
X_A, Y_A, Z_A	Cartesian coordinates in coordinate system A
T_X, T_Y, T_Z	translations terms, are the coordinates of the origin of the XYZ_A coordinate system in the XYZ_B coordinate system, respectively
R	3 x 3 orthogonal rotation matrix (Section 5.3.1)
s_F	scale factor = 1 + Δs, where Δs is the differential scale

There are seven parameters which are usually associated with a similarity transformation; three rotation angles, three translation components and one scale factor. If the rotations are small, as is expected when both coordinate systems refer to the same CTRS, then (5.4) is approximately linear and the order of the rotations is unimportant.

Harvey (1994) states that it is presumptuous to assume that similarity transformations, rather than affine or projection transformations, correctly describe the differences between any two coordinate sets. However, the similarity transformation is popular due to:

i) the small number of parameters involved

ii) the simplicity of the model, which is more easily implemented into software, and

iii) the fact that it is adequate for relating two coordinate systems which are homogeneous (no local distortion in scale or orientation).

As a result similarity transformation parameters have been published to allow the conversion between coordinate systems used in New Zealand (Section 5.4). It is therefore necessary to outline some of the different models that are available for

determining similarity transformations, especially those used for establishing New Zealand transformation parameters.

Other transformation models besides those outlined in Sections 5.3.2 and 5.3.3 have been proposed and are reviewed by Krakiwsky and Thomson (1974), Adam *et al.* (1982) and Harvey (1985). Most models relate two sets of Cartesian coordinates but there are formulae that relate two sets of ellipsoidal coordinates. In addition to accounting for the difference in scale, origin and orientation between the two coordinate systems, they must also relate the results on different ellipsoids (due to a possible change in the size and shape of the ellipsoid). These formula are collectively referred to as the Molodenskii formula. The Molodenskii formula often assume that the deflections of the vertical are known (η and ξ). This is not generally the case for geometric systems such as GPS and EDM. They are not presented here as it is generally more convenient to convert ellipsoidal coordinates to Cartesian coordinates, and then use a Cartesian based model.

One disadvantage of the seven parameter similarity transformation method is that both networks are assumed to have only linear distortions (excluding shear components). Often older terrestrial networks do have non-linear distortions because of the adjustment and survey methodologies employed. One method to try and account for non-linear distortions uses Multiple Regression Equations (MRE), these are outlined in Section 5.3.4.

	Adopted	Harvey 1986	Boucher *et al.*, 1994	McCarthy 1992	DMA 1987a and 1987b
x axis translation	T_X	Tx	T1	Δx	$\overline{\Delta X}$
y axis translation	T_Y	Ty	T2	Δy	$\overline{\Delta Y}$
z axis translation	T_Z	Tz	T3	Δz	$\overline{\Delta Z}$
rotation about x axis	ε_x	ω	-R1	$\delta\varepsilon$	ε
rotation about y axis	ε_y	θ	-R2	$\delta\phi$	ψ
rotation about z axis	ε_z	k	-R3	$\delta\omega$	ω
differential scale	Δs	s-1	D	δs	ΔS
coordinate frame one	$X_A\ Y_A\ Z_A$	x y z	X Y Z	u v w	--
coordinate frame two	$X_B\ Y_B\ Z_B$	X Y Z	XS YS ZS	x y z	--

Table 5 - 1 : Seven parameter similarity transformation notation

As there appears to be no standard set of notation used in the literature to express the seven parameter similarity transformation parameters in geodesy, the notation used in this thesis has been summarised in Table 5-1, along with some of the references cited in this chapter.

5.3.1 Coordinate rotation methods

Before describing the different transformation models it is necessary to review some of the methods that are available for rotating a coordinate system. Harvey (1985) describes three of the methods for rotating a network. They are by Cardanian angles, Eulerian angles or Euler's Theorem.

The method of Cardanian angles is the most commonly applied and will be described further shortly. Georgiadou and Grafarend (1983) give conversion formula between the Cardanian angles and the Eulerian angles. They also note that if the Eulerian rotation angle about the X axis is zero then the other two Eulerian rotation angles are indeterminant. As rotation angles between GPS coordinates and NZGD49 coordinates are usually small (Table 5-4 & 5-5) then there will be instabilities in the solution of the transformation parameters if using Eulerian angles. Due to this instability Eularian angles will not be used in this research, but are described below.

Euler's theorem (eg. Thompson, 1969) states that provided one point of a body remains fixed the entire succession of rotations about each axis is equivalent to a single rotation about one axis. This one axis (Euler pole) does not necessarily coincide with either the X, Y or Z axis. Thomson also shows that for small rotations the single axis can be calculated from the Cardanian angles. Euler poles play a central role in plate velocity modelling (Cox and Hart, 1986).

The Cardanian rotation matrix is the most commonly applied method of rotating a coordinate system (Figure 5-2). If the rotation angles are small, the order of applying the Cardanian angles to their respective axes does not influence the result. One of the six possible combinations for the order of applying the Cardanian angles is:

$$\mathbf{R} = R_Z(\varepsilon_z) * R_Y(\varepsilon_y) * R_X(\varepsilon_x) \tag{5.5}$$

where

R_X, R_Y, R_Z rotation matrices about the X, Y, Z axes respectively.

$\varepsilon_x\ \varepsilon_y\ \varepsilon_z$ rotation angles in radians about the X, Y, Z axes respectively. Positive rotations are clockwise rotations as viewed looking from the origin to the positive end of the axis in a right handed coordinate system.

and

$$R_Z(\varepsilon_z) = \begin{bmatrix} \cos\varepsilon_z & \sin\varepsilon_z & 0 \\ -\sin\varepsilon_z & \cos\varepsilon_z & 0 \\ 0 & 0 & 1 \end{bmatrix} \qquad R_Y(\varepsilon_y) = \begin{bmatrix} \cos\varepsilon_y & 0 & -\sin\varepsilon_y \\ 0 & 1 & 0 \\ \sin\varepsilon_y & 0 & \cos\varepsilon_y \end{bmatrix}$$

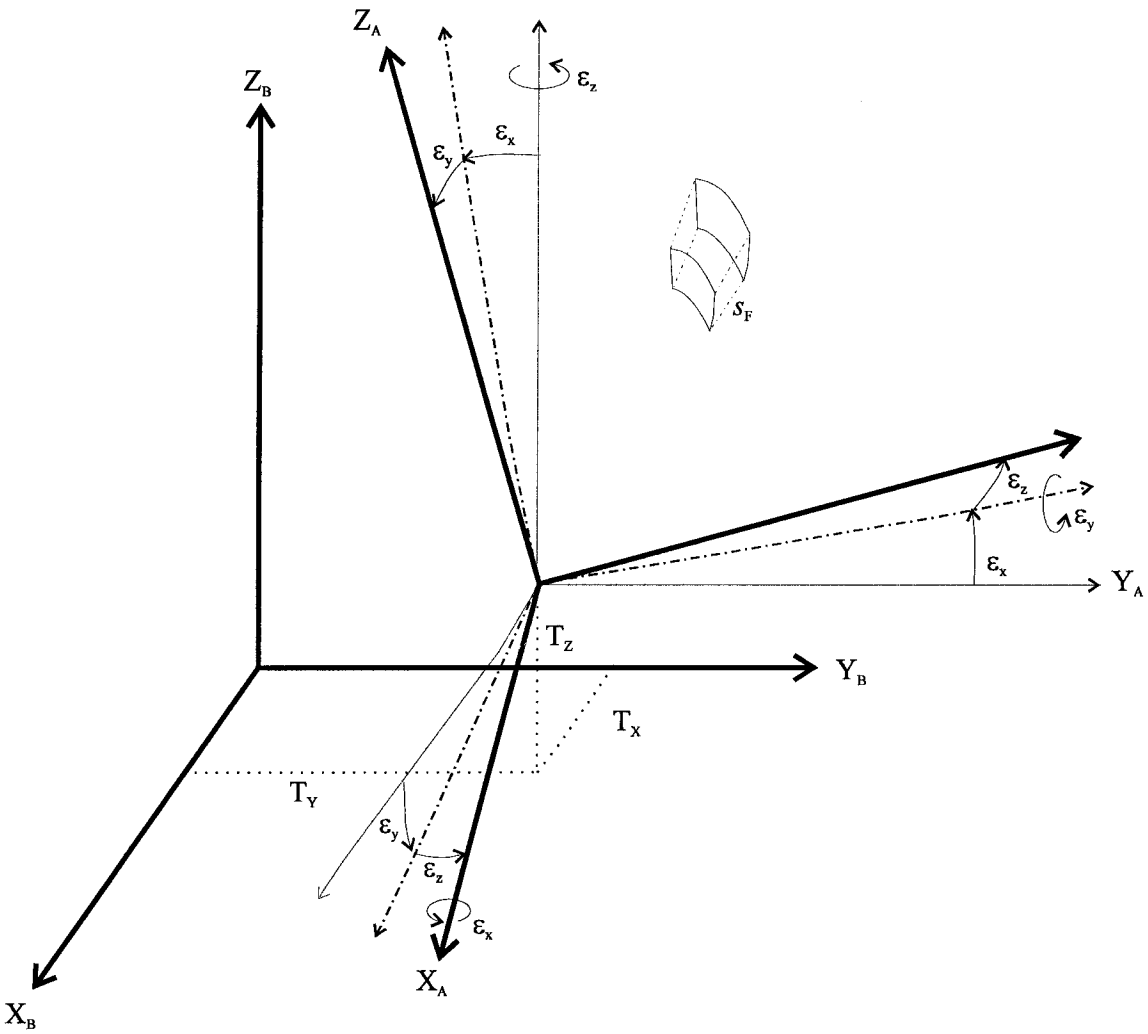

Figure 5 - 2 : Seven parameter transformation model using Cardanian Rotations, (adapted from Harvey, 1994)

$$R_X(\varepsilon_x) = \begin{bmatrix} 1 & 0 & 0 \\ 0 & \cos\varepsilon_x & \sin\varepsilon_x \\ 0 & -\sin\varepsilon_x & \cos\varepsilon_x \end{bmatrix}$$

Therefore **R** can now be written as:

$$\mathbf{R} = \begin{bmatrix} \cos\varepsilon_z \cos\varepsilon_y & \cos\varepsilon_z \sin\varepsilon_y \sin\varepsilon_x + \sin\varepsilon_z \cos\varepsilon_x & \sin\varepsilon_z \sin\varepsilon_x - \cos\varepsilon_z \sin\varepsilon_y \cos\varepsilon_x \\ -\sin\varepsilon_z \cos\varepsilon_y & \cos\varepsilon_z \cos\varepsilon_x - \sin\varepsilon_z \sin\varepsilon_y \sin\varepsilon_x & \sin\varepsilon_z \sin\varepsilon_y \cos\varepsilon_x + \cos\varepsilon_z \sin\varepsilon_x \\ \sin\varepsilon_y & -\cos\varepsilon_y \sin\varepsilon_x & \cos\varepsilon_y \cos\varepsilon_x \end{bmatrix} \quad (5.6)$$

For small rotation angles the rotation matrix (5.6) can be approximated by (5.7) when it is noted that the cosine of a small angle is approximately 1.0 and the sine of a small angle is the small angle.

$$\mathbf{R} \cong \begin{bmatrix} 1 & \varepsilon_z & -\varepsilon_y \\ -\varepsilon_z & 1 & \varepsilon_x \\ \varepsilon_y & -\varepsilon_x & 1 \end{bmatrix} \quad (5.7)$$

The assumption of small rotation angles is valid for rotation angles of up to about 3". However, considerably larger angles can be tolerated if the vectors being rotated are shorter than an earth radius. For example, rotating a 500 km baseline vector with each rotation angle equal to 10" will cause only 1 mm error in coordinates if (5.7) is used instead of (5.6) (Harvey, 1986).

5.3.2 Bursa-Wolf model

This model, presented by Bursa (1965) and Wolf (1963), solves for a seven parameter transformation - a scale factor, three rotation angles and three translation components. The Bursa-Wolf model is also known in Geodesy as the Seven Parameter Similarity model and takes the same form as the general similarity transformation of (5.4), repeated for completeness in (5.8).

$$\begin{bmatrix} \mathbf{X}_B \\ \mathbf{Y}_B \\ \mathbf{Z}_B \end{bmatrix} = s_F \mathbf{R} \begin{bmatrix} \mathbf{X}_A \\ \mathbf{Y}_A \\ \mathbf{Z}_A \end{bmatrix} + \begin{bmatrix} \mathbf{T}_X \\ \mathbf{T}_Y \\ \mathbf{T}_Z \end{bmatrix} \quad (5.8)$$

where the notation is as defined in (5.4).

One problem with the Bursa-Wolf model is that the adjusted parameters are very highly correlated when the network of points used to determine the parameters covers only a small portion of the earth (eg. Table 5-6).

5.3.3 Molodenskii-Badekas model

The Molodenskii-Badekas model (Badekas, 1969) removes the high correlation between parameters by relating the parameters to the centroid of the network.

$$\begin{bmatrix} \mathbf{X}_B \\ \mathbf{Y}_B \\ \mathbf{Z}_B \end{bmatrix} = \begin{bmatrix} \overline{\mathbf{X}}_A \\ \overline{\mathbf{Y}}_A \\ \overline{\mathbf{Z}}_A \end{bmatrix} + \begin{bmatrix} \mathbf{T}'_x \\ \mathbf{T}'_y \\ \mathbf{T}'_z \end{bmatrix} + s_F \mathbf{R} \begin{bmatrix} \mathbf{X}_A - \overline{\mathbf{X}}_A \\ \mathbf{Y}_A - \overline{\mathbf{Y}}_A \\ \mathbf{Z}_A - \overline{\mathbf{Z}}_A \end{bmatrix} \tag{5.9}$$

where

$\overline{\mathbf{X}}_A = \sum \mathbf{X}_{Ai} / n$ = centroid X coordinate for the points in coordinate system A

$\overline{\mathbf{Y}}_A = \sum \mathbf{Y}_{Ai} / n$ = centroid Y coordinate for the points in coordinate system A

$\overline{\mathbf{Z}}_A = \sum \mathbf{Z}_{Ai} / n$ = centroid Z coordinate for the points in coordinate system A

$T'_x\ T'_y\ T'_z$ Molodenskii-Badekas translations terms

remaining terms are as defined for the Bursa-Wolf model

The adjusted coordinates, baseline lengths, scale factor, rotation angles, their Variance Covariance (VCV) matrices and the *a posteriori* variance factor computed by this model are the same as those from the corresponding Bursa-Wolf solution. However, the translations are different and their precisions are generally an order of magnitude smaller (Harvey, 1986). The difference between the translation terms of the Bursa-Wolf and Molodenskii-Badekas models is due to the different scaling and rotating of the centroid of the network. This can be seen clearly by expanding (5.9) to give (5.10), where $\mathbf{P_c}$ is a constant term for all points and obviously affects the translation terms.

$$\begin{bmatrix} \mathbf{X}_B \\ \mathbf{Y}_B \\ \mathbf{Z}_B \end{bmatrix} = \mathbf{P_c} + \begin{bmatrix} \mathbf{T}'_x \\ \mathbf{T}'_y \\ \mathbf{T}'_z \end{bmatrix} + s_F \mathbf{R} \begin{bmatrix} \mathbf{X}_A \\ \mathbf{Y}_A \\ \mathbf{Z}_A \end{bmatrix} \quad \text{where } \mathbf{P_c} = \begin{bmatrix} \overline{\mathbf{X}}_A \\ \overline{\mathbf{Y}}_A \\ \overline{\mathbf{Z}}_A \end{bmatrix} - s_F \mathbf{R} \begin{bmatrix} \overline{\mathbf{X}}_A \\ \overline{\mathbf{Y}}_A \\ \overline{\mathbf{Z}}_A \end{bmatrix} \tag{5.10}$$

When transformation parameters from the Molodenskii-Badekas model are to be applied to transform coordinates of points, it is essential to know what values were used for the centroid ($\overline{\mathbf{X}}_A$ $\overline{\mathbf{Y}}_A$ $\overline{\mathbf{Z}}_A$) when deriving the parameters. However, in the past they have not always been published with the transformation parameters (eg. Mackie, 1982).

It should be noted that when working with a global network of points the Molodenskii-Badekas model has centroid coordinates that equal the centre of the ellipsoid (ie. $\overline{\mathbf{X}}_A = \overline{\mathbf{Y}}_A = \overline{\mathbf{Z}}_A = 0$) and therefore reduces to the Bursa-Wolf model.

5.3.4 Multiple Regression Equations (MRE)

Multiple Regression Equations have the advantage over either the Bursa-Wolf or the Molodenskii-Badekas models of being able to account for non-linear distortion in either of the networks. One significant disadvantage is that outside the area of the control points used to determine the MRE the results can be extremely unreliable. Therefore the control points need to extend to the boundaries of the datum for which the transformation is to apply.

There are various forms that an MRE can take, but only the form used by DMA(1987a) will be presented, as this form has been used to determine transformation parameters between WGS84 and NZGD49 (Section 5.4.2.1). For each coordinate component a difference between datum values ($\Delta\phi$, $\Delta\lambda$, Δh) is determined by an MRE, and this is then applied to the known datum coordinate component to obtain the unknown datum coordinate using:

$$\begin{aligned} \phi_B &= \phi_A + \Delta\phi \\ \lambda_B &= \lambda_A + \Delta\lambda \\ h_B &= h_A + \Delta h \end{aligned}$$

and where

$(\phi\lambda h)_A$	known curvilinear coordinates of a station in terms of datum A
$(\phi\lambda h)_B$	unknown datum B curvilinear coordinates of the same station

The general form of the difference between the two datum, using an MRE, for the latitude component is (DMA, 1987a, eqn. 7-14):

$$\Delta\phi = A_0 + A_1U + A_2V + A_3U^2 + A_4UV + A_5V^2 + ... + A_{54}V^9 + A_{55}U^9V + A_{56}U^8V^2 + ... + A_{64}U^9V^2 + A_{65}U^8V^3 + ... + A_{72}U^9V^3 + A_{73}U^8V^4 + ... + A_{99}U^9V^9 \quad (5.11)$$

where

$A_0, A_1, ..., A_{99}$ = 100 possible coefficients determined in a stepwise multiple regression procedure with U and V each limited to single digit exponents

$U = K(\phi - \phi_m)$ = normalised geodetic latitude of the computation point

$V = K(\lambda - \lambda_m)$ = normalised geodetic longitude of the computation point

K = scale factor and degree-to-radian conversion

ϕ, λ = local geodetic latitude and longitude, respectively, of the computation point (in degrees)

ϕ_m, λ_m = mid-latitude and mid-longitude values, respectively, of the local geodetic datum area (in degrees).

Similar equations are obtained for $\Delta\lambda$ and Δh by replacing $\Delta\phi$ in the left hand side of (5.11) by $\Delta\lambda$ and Δh, respectively.

The development of the MRE was performed by DMA (1987a, p. 7-18) using the following method. Prior to beginning the development process, individual $\Delta\phi$, $\Delta\lambda$, Δh coordinate differences are formed for each station within the datum area that has coordinates in terms of both datums. The multiple regression procedure of Appelbaum (1982) is then initiated to develop separate equations to fit the $\Delta\phi$, $\Delta\lambda$ and Δh coordinate differences. The first step of the procedure produces a constant and a variable. The variable will either be a function of ϕ or λ, or both. The procedure then sequentially adds one variable at a time to the equation. After a variable is added, all variables previously incorporated into the equation are tested and, if one is no longer significant, it is removed. This stepwise addition or removal of variables ensures that only significant variables are retained in the final equation. In keeping with (5.11), each variable consists of products of powers of normalised geodetic latitude (U), or normalised geodetic longitude (V), or both (ie. U^3V^4 is a single variable). The stepwise regression procedure continues until the precision desired for the equation is obtained.

The DMA derived MRE for transforming NZGD49 coordinates to WGS84 coordinates are contained in Section 5.4.2.1 for which the desired precision was that the rms difference be approximately less than 1.5 m (DMA, 1987a, p. 7-19).

5.3.5 Variance Covariance Matrices

As a least squares adjustment requires both the stochastic and mathematical model to be correct, there is the problem of "internal" and "external" accuracy. The elements of the VCV matrices of the coordinates may represent precision estimates. It is difficult to change these values to accuracies, especially the off-diagonal terms. Harvey (1985) states that the application of the covariance law (Jacobians) to add the effect of systematic effects to the VCV is the best method. Unfortunately, it is based on functional relationships between the parameters and the systematic errors, which may not be known. The VCV matrices can be diagonal, block diagonal or full matrices. However, as a coordinate of one point is usually correlated with another point in the network the full VCV matrices should be used in the computation of transformation parameters.

It is frequently the case that one may have ellipsoidal coordinates and the associated VCV matrix but it is necessary to convert these coordinates and VCV matrix to a Cartesian frame for use by either the Bursa-Wolf or Molodenskii-Badekas methods. The formula for conversion between ellipsoidal coordinates and Cartesian coordinates can be found in most Geodesy texts (eg. Heiskanen and Moritz, 1967, Section 5-3; or Vanicek and Krakiwsky, 1986, Section 15.4). The formula for conversion of a VCV matrix between ellipsoidal and Cartesian coordinates is not as widely published, though a clear presentation is given by Mikhail (1976). Harvey (1986) outlines the procedures, and where appropriate gives formula, for converting both the coordinates and VCV matrix between the ellipsoidal and Cartesian systems.

It should be noted that the VCV matrix of the transformed coordinates of a point is the combination of the VCV matrices of the original coordinates and the transformation parameters used. Therefore when the estimates of transformation parameters are

published it is also desirable that the VCV of the parameters be published. Alternatively the standard deviations and correlations of the parameters could be published as they provide a clear indication of the quality of the parameter estimates and from them the VCV can be formed (Harvey, 1986). One needs to remember that the rigorous application of least squares is only sensible if the underlying model (which includes the VCV) is believed to be correct.

5.3.6 Tests for parameter significance

Once transformation parameters have been determined using either the Bursa-Wolf or Molodenskii-Badekas method, they should be tested for significance using multi-variate tests, especially when parameters have high correlations. Vanicek and Krakiwsky (1986, Section 13.5) and Mikhail (1976, Section 11.5.2) both give the multi-variate tests for the cases when the *a priori* variance factor (σ_o^2) of the observations is either known or unknown. The two cases for the multi-variate test are (Harvey 1994):

i) known *a priori* variance

When the *a priori* variance (σ_o^2) is known reliably the multi-variate test is computed using:

$$t = (U - X)^T Q_X^{-1} (U - X) \tag{5.12}$$

where

- **X** vector of parameters being tested
- **U** vector of *a priori* values against which each X_i is being compared (often the null vector)
- $\mathbf{Q}_X$ estimated VCV matrix of the parameters being tested and it is assumed that $\mathbf{Q}_X = \sigma_o(A^T P A)^{-1}$.

The vectors **X** and **U** may contain either all the parameters or some subset of them. If a subset is being used then the corresponding portion of the VCV matrix of the parameters must be used. This test is rigorous and allows for correlations between the parameters.

The hypothesis that $X_i = U_i$ should be rejected if: $t > \chi^2_{k,\alpha}$. Where χ^2 is the Chi-squared distribution, k is the number of parameters being estimated and α is the significance level.

If only a single parameter is being tested, then it is obvious that (5.12) reduces to:

$$t = (u-x)^2 / \sigma_x^2 \quad > \quad \chi^2_{1,0.05} = 3.841 \quad \text{(at the 95\% confidence level)} \qquad (5.13)$$

where σ_x^2 is the *a posteriori* variance of the parameter being tested.

ii) unknown *a priori* variance

When the *a priori* variance (σ_o^2) is unknown or weakly determined the multi-variate test is computed using:

$$t' = \frac{(U - X)^T \hat{Q}_X^{-1} (U - X)}{k} \qquad (5.14)$$

where

k number of parameters being estimated

$\hat{\mathbf{Q}}_X$ estimated VCV matrix of the parameters, or relevant portion of it, multiplied by the estimated variance factor (VF)

U, **X** as defined in (5.12)

The hypothesis that $X_i = U_i$ should be rejected if: $t' > F_{k,r,\alpha}$, where F is the Fisher (or F) distribution, k is the number of parameters being estimated, r is the number of degrees of freedom in the adjustment and α is the significance level. The value of t' required to reject the hypothesis will be much larger than the value of t required in (5.12), unless r is very large (Harvey 1986).

If only a single parameter is being tested, then (5.14) reduces to:

$$t' = (u-x)^2 / (\sigma_x^2 * VF) > F_{1,r,\alpha}. \qquad (5.15)$$

If $r \rightarrow \infty$ and $\alpha = 0.05$, then $F_{1,\infty,0.05} = 3.841$. Therefore (5.13) and (5.15) are asymptotic.

For both of the multi-variate tests, if the tested parameters are not significantly different to their *a priori* values (**U**) then the parameter should be fixed at their *a priori* value and the transformation parameters recomputed.

5.3.7 The Generalised Method

In the Bursa-Wolf model (Section 5.3.2) and the Molodenskii-Badekas model (Section 5.3.3) a number of usually valid assumptions have been made. These are:

i) that the scale is uniform along each of the axial directions, and

ii) that there is no shearing process taking place.

These assumptions result in the transformation being of the similarity form as described by Harvey (1986) (Section 5.3).

The applicability of these assumptions is quite evident by the use of the Bursa-Wolf model in transforming between global systems such as the GPS and VLBI systems (Boucher *et al.*, 1994, Table T7).

However it is well known that terrestrial networks are not well behaved and as such it seems that the most appropriate models should include the provision for scale to vary along each axis and to admit shearing. This has the net effect of increasing the number of parameters to 12. Such models are not entirely new. Grant (1990) used shear terms to accommodate shearing that occurs between two plates but did not fully generalise the concept.

In the similarity transformation matrix (5.4) the translation is treated as an addition while the scale and rotation are treated as multiplication. A more general form of (5.4) can be written in such a way that the scale, rotation and translation terms can all be treated as a multiplication and combined into one single matrix, referred to as the Composite Matrix, $\boldsymbol{M}$. One of the basic purposes of composing transformations is to gain efficiency by applying a single compound transformation to a point, rather than applying a series of transformations, one after the other. In developing the generalised model it is appropriate to follow the concepts and notation of Computer Graphics (see Foley *et al.*, 1990, Chapter 5). This notation uses the homogeneous coordinate system

developed by Maxwell (1946, 1951). Its complete generality and compact form make it useful in many systems.

The first step in developing the Composite Matrix, ***M***, is to express points and transformation parameters in terms of homogeneous coordinates. That is instead of representing a point in space by the vector $(x,y,z)^T$ we represent it by the 4 tuple vector $(x,y,z,W)^T$. The critical parameter of choice is W which is often termed the "homogenising" parameter. When W=1 "conventional" 3-D space is a subspace of the more generalised 4-D space. The development which follows utilises W=1 which results in considerable similarity to the conventional 3-D space approach.

$$\boldsymbol{P} = \begin{bmatrix} X_A \\ Y_A \\ Z_A \\ 1 \end{bmatrix} \qquad \boldsymbol{P'} = \begin{bmatrix} X_B \\ Y_B \\ Z_B \\ 1 \end{bmatrix}$$

$$\mathbf{S}(s_X, s_Y, s_Z) = \begin{bmatrix} s_X & 0 & 0 & 0 \\ 0 & s_Y & 0 & 0 \\ 0 & 0 & s_Z & 0 \\ 0 & 0 & 0 & 1 \end{bmatrix} \qquad \mathbf{T}(T_X, T_Y, T_Z) = \begin{bmatrix} 1 & 0 & 0 & T_X \\ 0 & 1 & 0 & T_Y \\ 0 & 0 & 1 & T_Z \\ 0 & 0 & 0 & 1 \end{bmatrix}$$

$$\mathbf{R_Z}(\varepsilon_z) = \begin{bmatrix} \cos\varepsilon_z & \sin\varepsilon_z & 0 & 0 \\ -\sin\varepsilon_z & \cos\varepsilon_z & 0 & 0 \\ 0 & 0 & 1 & 0 \\ 0 & 0 & 0 & 1 \end{bmatrix} \qquad \mathbf{R_Y}(\varepsilon_y) = \begin{bmatrix} \cos\varepsilon_y & 0 & -\sin\varepsilon_y & 0 \\ 0 & 1 & 0 & 0 \\ \sin\varepsilon_y & 0 & \cos\varepsilon_y & 0 \\ 0 & 0 & 0 & 1 \end{bmatrix}$$

$$\mathbf{R_X}(\varepsilon_x) = \begin{bmatrix} 1 & 0 & 0 & 0 \\ 0 & \cos\varepsilon_x & \sin\varepsilon_x & 0 \\ 0 & -\sin\varepsilon_x & \cos\varepsilon_x & 0 \\ 0 & 0 & 0 & 1 \end{bmatrix} \tag{5.16}$$

where s_X, s_Y and s_Z are the scale factors for each axis. $\mathbf{R} = (\mathbf{R_Z}(\varepsilon_z) \bullet \mathbf{R_Y}(\varepsilon_y) \bullet \mathbf{R_X}(\varepsilon_x))$ can now be written, with the same first order approximations due to small angles used in (5.7), as:

$$\mathbf{R} \cong \begin{bmatrix} 1 & \varepsilon_z & -\varepsilon_y & 0 \\ -\varepsilon_z & 1 & \varepsilon_x & 0 \\ \varepsilon_y & -\varepsilon_x & 1 & 0 \\ 0 & 0 & 0 & 1 \end{bmatrix} \tag{5.17}$$

Utilising these homogeneous expressions for ***P'***, **S**, **R**, ***P*** and **T** it is possible to rewrite Harvey's transformation (5.4) utilising the homogeneous notation

$$\boldsymbol{P'} = \boldsymbol{M}\,\boldsymbol{P} = \begin{bmatrix} s_X & \varepsilon_z & -\varepsilon_y & T_X \\ -\varepsilon_z & s_Y & \varepsilon_x & T_Y \\ \varepsilon_y & -\varepsilon_x & s_Z & T_Z \\ 0 & 0 & 0 & 1 \end{bmatrix} \boldsymbol{P} \tag{5.18}$$

It is clear that under similarity, equal scale in all directions, $s_X = s_Y = s_Z = s_F$ (a constant), that this equation is equivalent to (5.4).

Indeed it is the ability of the homogeneous representation to incorporate the previously mentioned properties of similarity, orthogonality and projection that make it so useful.

The property of orthogonality is aligned with the concept of shear in that shearing systems are generally not orthogonal. In 3-D space there are three shears. Their homogeneous representations are:

$$\mathbf{SH_{XY}}\,(Sh_{XY}, Sh_{YX}) = \begin{bmatrix} 1 & 0 & Sh_{XY} & 0 \\ 0 & 1 & Sh_{YX} & 0 \\ 0 & 0 & 1 & 0 \\ 0 & 0 & 0 & 1 \end{bmatrix} \qquad \mathbf{SH_{YZ}}\,(Sh_{YZ}, Sh_{ZY}) = \begin{bmatrix} 1 & 0 & 0 & 0 \\ Sh_{YZ} & 1 & 0 & 0 \\ Sh_{ZY} & 0 & 1 & 0 \\ 0 & 0 & 0 & 1 \end{bmatrix}$$

$$\mathbf{SH_{XZ}}\,(Sh_{XZ}, Sh_{ZX}) = \begin{bmatrix} 1 & Sh_{XZ} & 0 & 0 \\ 0 & 1 & 0 & 0 \\ 0 & Sh_{ZX} & 1 & 0 \\ 0 & 0 & 0 & 1 \end{bmatrix}$$

The shear matrices behave in an analogous manner to the rotation matrices for small shears. The generalised form of the shear matrix is:

$$\mathbf{SH}\,(Sh_X, Sh_Y, Sh_Z) = \begin{bmatrix} 1 & Sh_{XZ} & Sh_{XY} & 0 \\ Sh_{YZ} & 1 & Sh_{YX} & 0 \\ Sh_{ZY} & Sh_{ZX} & 1 & 0 \\ 0 & 0 & 0 & 1 \end{bmatrix} \tag{5.19}$$

Finally the combination of the shear (5.19) and rotation (5.17) matrices yields, for small shears and small rotations:

$$\mathbf{SH} \bullet \mathbf{R} = \begin{bmatrix} 1 & Sh_{XZ} + \varepsilon_z & Sh_{XY} - \varepsilon_y & 0 \\ Sh_{YZ} - \varepsilon_z & 1 & Sh_{YX} + \varepsilon_x & 0 \\ Sh_{ZY} + \varepsilon_y & Sh_{ZX} - \varepsilon_x & 1 & 0 \\ 0 & 0 & 0 & 1 \end{bmatrix} \tag{5.20}$$

It is now seen that there are 6 independent linear coefficients in this matrix. The form of the composite matrix when scale and translation terms are added to (5.20) is:

$$\boldsymbol{M} = \begin{bmatrix} s_X & Sh_{XZ} + \varepsilon_z & Sh_{XY} - \varepsilon_y & T_X \\ Sh_{YZ} - \varepsilon_z & s_Y & Sh_{YX} + \varepsilon_x & T_Y \\ Sh_{ZY} + \varepsilon_y & Sh_{ZX} - \varepsilon_x & s_Z & T_Z \\ 0 & 0 & 0 & 1 \end{bmatrix} \tag{5.21}$$

The general form of (5.21) is:

$$\boldsymbol{M} = \begin{bmatrix} a_{11} & a_{12} & a_{13} & a_{14} \\ a_{21} & a_{22} & a_{23} & a_{24} \\ a_{31} & a_{32} & a_{33} & a_{34} \\ 0 & 0 & 0 & 1 \end{bmatrix} \tag{5.22}$$

Writing $\boldsymbol{M}$ in the general form of (5.22) emphasises the fact that there are 12 unknown parameters made up of:

- 3 scales s_X, s_Y, s_Z which effect the diagonal elements
- 3 translations T_X, T_Y, T_Z which effect the fourth column
- 3 rotations ε_x, ε_y, ε_z which effect the off-diagonal elements
- 6 shears Sh_{XY}, Sh_{YX}, Sh_{YZ}, Sh_{ZY}, Sh_{ZX}, Sh_{XZ} which linearly combine with the rotations to make for 6 unknowns involving rotations and shears

This generalised matrix contains all the deformations between the initial and final systems. That is it contains the classical deformation information although this information cannot be readily extracted due to the linear combinations in the presence of rotations. To demonstrate this fact it is noted that the shearing unit of deformation in the x-y plane is defined as:

$$\frac{\partial v}{\partial x} + \frac{\partial u}{\partial y}$$

where u and v are the deformations along the x and y axis respectively. The parameter Sh_{XZ} is the term $\frac{\partial u}{\partial y}$ while Sh_{YZ} represents $\frac{\partial v}{\partial x}$. Similarly the shearing unit deformation

in the y-z plane is $\frac{\partial w}{\partial y}+\frac{\partial v}{\partial z}$ which is Sh_{ZX} + Sh_{YX} while the shearing deformation in the x-z plane is $\frac{\partial u}{\partial z}+\frac{\partial w}{\partial x}$ which is Sh_{XY} + Sh_{ZY}.

It is possible to design (5.22) so as elements of $\boldsymbol{M}$ could be functions of position. The complexity that each elements equation could take is unlimited, though it is also possible to just solve for the numerical values of the elements of $\boldsymbol{M}$. Depending on whether you are interested in the underlying physical processes which influence the values of the elements or are only after a method to transform coordinates one may analyse the $\boldsymbol{M}$ elements further. The approach of only solving the numerical values of the elements of $\boldsymbol{M}$, rather than analysing the physical processes has been applied to the problem of converting between NZGD49 coordinates and ITRF93 coordinates (see Sections 5.4.3.5 and 5.4.3.6).

5.4 Transformation parameters

This section firstly outlines the transformation parameters used in this research to convert coordinates between the ITRS (Section 3.4.1) and WGS (Section 3.4.3) realisations. Then currently available transformation parameters to convert between NZGD49 and WGS84 are presented, along with the similarity transformation and generalised method parameters developed as part of this research, that convert directly between NZGD49 and ITRF93. Comparison of these transformation parameters are contained in Section 5.5.

5.4.1 Transformation parameters between ITRS and WGS realisations

The transformation parameters used in this thesis for converting between different realisations of ITRS and WGS are summarised in Table 5-2. The application of these parameters was performed using the seven-parameter similarity transformation (Bursa-Wolf) formula given in (5.8) using the simplified rotation matrix of (5.7).

The three sets of transformations parameters between ITRS realisations (ie. ITRF90-93), and between WGS84(G730) to ITRF92, in Table 5-2 refer to the epoch of 1988.0. The epoch to which the other sets of parameters refer was not clearly stated in their respective references.

From	To	Reference	T_X m	T_Y m	T_Z m	Δs $x10^{-8}$	ε_x mas	ε_y mas	ε_z mas
[1] ITRF90	ITRF91	Boucher *et al.*, 1992, p32	-0.001 *0.003*	0.004 *0.003*	0.016 *0.002*	-0.03 *0.03*	0.0 *0.1*	0.0 *0.1*	0.0 *0.1*
[2] ITRF91	ITRF92	Boucher *et al.*, 1993, p44	-0.011 *0.002*	-0.014 *0.002*	0.006 *0.002*	-0.14 *0.03*	0.00 *0.07*	0.00 *0.07*	0.00 *0.05*
[3] ITRF92	ITRF93	Boucher *et al.*, 1994, p80	-0.002 *0.001*	-0.007 *0.001*	-0.007 *0.001*	0.12 *0.02*	0.39 *0.06*	-0.80 *0.05*	0.96 *0.04*
[4] ITRF90	WGS84	McCarthy 1992	0.060	-0.517	-0.223	-1.1	-18.3	0.3	-7.0
[5] WGS84	WGS72	DMA 1987a	0.000	0.000	-4.500	-21.9	0.0	0.0	554.0
[6] WGS84	WGS84 (G730)	Swift 1994	-0.040	-0.010	-0.280	-21.8	4.2	-4.0	-15.6
[7] WGS84 (G730)	ITRF92	Swift 1994	-0.070 *0.030*	-0.130 *0.040*	0.150 *0.030*	-0.03 *0.01*	-6.0 *0.3*	2.0 *0.5*	-2.4 *0.7*

Table 5 - 2 : Transformation parameters between ITRS and WGS realisations. The first line contains the parameters, while the second line (in italics, when given) contains the formal uncertainty in the parameters at 1 sigma.

It is worth noting that the value given by DMA (1987a) for Δs, to convert WGS84 to WGS72 coordinates, is -21.9×10^{-8}. However, a preprint of DMA (1987a and b) stated that $\Delta s = -22.63 \times 10^{-8}$, which is the value quoted in Australia (eg. Higgins, 1987 and Steed, 1990) This difference of approximately 0.04 m at the Earth's surface can be considered insignificant when compared to the height accuracy obtainable by the Doppler method used to establish WGS72 and WGS84.

From Table 5-2 it is possible to derive another set of transformation parameters to convert from WGS84(G730) to ITRF92 by combining the parameters in lines 1, 2, 4 and 6 to compare with the direct parameters of Swift (1994) in line 7. The derived parameters are significantly different from Swift's direct determination (Table 5-3). This difference could be due to several sources. The most likely difference is due to uncertainties associated with the individual parameters and the mode that these uncertainties propagate. This cannot be tested as the necessary variance-covariance matrices are not available for all of the components.

From	To	Source	T_X m	T_Y m	T_Z m	Δs $x10^{-8}$	ε_x mas	ε_y mas	ε_z mas
WGS84 (G730)	WGS84		0.040	0.010	0.280	21.80	-4.2	4.0	15.6
WGS84	ITRF90		-0.060	0.517	0.223	1.10	18.3	-0.3	7.0
ITRF90	ITRF91		-0.001	0.004	0.016	-0.03	0.0	0.0	0.0
ITRF91	ITRF92		-0.011	-0.014	0.006	-0.14	0.00	0.00	0.00
WGS84 (G730)	ITRF92	derived	-0.032	0.517	0.525	22.73	14.1	3.7	22.6
WGS84 (G730)	ITRF92	Swift	-0.070	-0.130	0.150	-0.03	-6.0	2.0	-2.4

Table 5 - 3 : Derived transformation parameters between WGS84 (G730) and ITRF92.

5.4.2 Conversion between WGS and NZGD49

The two main determinations of transformation parameters for converting between WGS realisations and NZGD49 are Mackie (1982) and DMA (1987a & b). Both of these determinations of transformation parameters have been derived from Doppler observations at NZGD49 coordinated sites. There are however some distinct differences which will be summarised in the following sub-sections, along with an attempt to standardise the parameters for converting between WGS84 and NZGD49.

5.4.2.1 DMA derived parameters

DMA (1987a & b) contains three different methods of transforming between WGS84 and NZGD49. The first method uses the Seven Parameter Similarity Transformation formula (DMA, 1987a, Section 7.2.4.3.1), the second uses the Standard Molodenskii Datum Transformation formulas (DMA, 1987a, Table 7.8), while the third uses Multiple Regression Equations (MRE) (DMA, 1987a, Section 7.2.4.3.3).

The Molodenskii and MRE formulas are used for transforming between ellipsoidal coordinates. As was discussed in Section 5.3, transforming ellipsoidal coordinates to Cartesian (rectangular) coordinates is relatively simple. Therefore, the Molodenskii formulas will not be described further. However, as the MRE formula can take into account the non-linear distortion in either of the networks they will be analysed along with the Seven Parameter Similarity Transformation formula.

The similarity transformation parameters need to be applied to Cartesian coordinates. The local datum coordinates available to DMA consisted of orthometric heights rather than ellipsoidal heights. To convert orthometric height to ellipsoidal height the geoid height (N) needs to be known. DMA determined N values in terms of NZGD49 by assuming the local geoid height at each Doppler station was zero. Then using the Abridged Molodenskii Datum Transformation formula for ΔH (DMA, 1987a, Table 7.8), determined ΔH values ($\equiv \Delta N$). Then the ΔN values were subtracted from the WGS84 geoid height (degree and order 180) DMA (1987a).

Similarity Transformation Parameters

DMA (1987a) lists four different sets of similarity transformation parameters for converting from NZGD49 to WGS84, based on different combinations of parameters being solved for in the least squares solution. The values for the parameters (Table 5-4) were derived from 14 Doppler stations. No description of the location of these sites is contained in DMA (1987a or b).

The only indication of the accuracy of the transformation parameters in Table 5-4 was given by DMA (1987b, p. 10-9) for the three parameter solution. The accuracies for the T_X, T_Y and T_Z parameters were ± 5, 3 and 5 m, respectively, though the confidence interval was not specified.

Number of Parameters solved for	T_X m	T_Y m	T_Z m	ε_x "	ε_y "	ε_z "	Δs ppm
7*	55	-17	184	-0.773	0.122	-0.745	5.9218
6	83	-20	209	-0.773	0.122	-0.745	--
4*	56	-18	184	--	--	--	5.9218
3	84	-22	209	--	--	--	--

Table 5 - 4 : DMA Similarity Transformation Parameters to convert from NZGD49 to WGS84 (DMA, 1987a, p. 7-47). *: Δs possibly printed with wrong sign (see Section 5.5.2).

Multiple Regression Equations

The DMA (1987b, p. 20-20) MRE for the conversion of NZGD49 coordinates to WGS84 coordinates are in (5.23). The number of stations used to determine the MRE is

unclear as tests for determining the accuracy of the equations used either 14 points (DMA, 1987a, p. 7-51) or 31 points (DMA, 1987b, p. 20-20).

$$\begin{aligned}\Delta\phi = {} & 6.18012 + 0.18236U + 0.10785V - 0.15566UV + 1.36545U^3 - \\ & 0.44813UV^2 + 0.16518V^3 - 1.66408U^5 + 0.44854U^9 \\ \Delta\lambda = {} & 0.55131 + 0.18193U + 0.29501V - 0.36522UV - 0.12613U^3 - \\ & 1.13550U^2V^2 + 3.31705U^3V^3 + 3.40098U^9V^6 \\ \Delta h = {} & 8.630 + 13.910U + 7.007V + 3.463V^2 + 20.507U^3 - 16.813U^2V - \\ & 20.530U^6V - 11.602U^9 - 28.424U^9V^3 \end{aligned} \quad (5.23)$$

where

parameter definitions are the same as (5.11)

$\Delta\phi$ and $\Delta\lambda$ units are arc seconds, while Δh units are metres

$U = K(\phi + 41)$, with ϕ being the geodetic latitude in decimal degrees

$V = K(\lambda - 173)$, with λ being the geodetic longitude in decimal degrees

$K = 0.15707963$, the combined scale factor and degree-to-radian conversion

5.4.2.2 Mackie derived parameters

Mackie (1982) determined transformation parameters between WGS72 and NZGD49 based on 18 Doppler stations that were well distributed across both the North and South Islands of New Zealand. Mackie computed a geoid referenced to NZGD49, by integrating the components of the deviation of the vertical (ie. from Astro-geodetic levelling). This allowed the orthometric heights to be converted to ellipsoidal heights and when combined with the NZGD49 horizontal coordinates, provided a local three dimensional set of coordinates that were compared with the Doppler coordinates to establish the transformation parameters.

Mackie solved for what he termed a "3-parameter solution to the transformation vector" and also a 7-parameter solution. The seven parameter solution for the transformation parameters was obtained by a least squares solution based on the Molodenskii-Badekas method (Section 5.3.3). The parameters to transform from NZGD49 to WGS72 were stated by Mackie (*ibid.*, p. 22) as:

$$
\begin{aligned}
T'_x &= +83.217\text{ m} && \pm 0.27\text{ m} \\
T'_y &= -9.026\text{ m} && \pm 0.27\text{ m} \\
T'_z &= +202.024\text{ m} && \pm 0.27\text{ m} \\
\Delta s &= -4.8256 \times 10^{-6} && \pm 6.32 \times 10^{-7} \\
\varepsilon_x &= -2.2650 \times 10^{-6} && \pm 1.32 \times 10^{-6} && = -0.47'' \pm 0.27'' \\
\varepsilon_y &= +4.6660 \times 10^{-7} && \pm 1.06 \times 10^{-6} && = +0.10'' \pm 0.22'' \\
\varepsilon_z &= -2.2558 \times 10^{-6} && \pm 1.36 \times 10^{-6} && = -0.47'' \pm 0.28''
\end{aligned}
\qquad (5.24)
$$

Note that the sign of Δs as given by Mackie in (5.24) has the opposite sign to the Δs given by DMA (Table 5.4). The difference in sign for Δs is compared in Section 5.5.2.

The values that were used for the centroid ($\overline{\mathbf{X}}_A$ $\overline{\mathbf{Y}}_A$ $\overline{\mathbf{Z}}_A$) when deriving the parameters in (5.24) were not specifically stated. However if one assumes that the centroid was calculated using Mackie's equation 5 (*ibid.*, p. 22), which is equivalent to that given in (5.9), the coordinates of the centroid can be calculated from the Cartesian coordinates given in Mackie's table 1 (*ibid.*, p. 22) to be:

$$
\begin{aligned}
\overline{\mathbf{X}}_A &= -4774224.01\text{ m} \\
\overline{\mathbf{Y}}_A &= 545802.12\text{ m} \\
\overline{\mathbf{Z}}_A &= -4159198.36\text{ m}
\end{aligned}
\qquad (5.25)
$$

To compare the parameters derived by Mackie with parameters contained in Sections 5.4.2.1 and 5.4.3, the parameters need to be converted from the Molodenskii-Badekas method to the Bursa-Wolf method. This can be achieved by combining (5.7), (5.8) and (5.10) to give the Bursa-Wolf translation parameters:

$$
\begin{bmatrix} \mathbf{T}_X \\ \mathbf{T}_Y \\ \mathbf{T}_Z \end{bmatrix} = \begin{bmatrix} \overline{\mathbf{X}}_A \\ \overline{\mathbf{Y}}_A \\ \overline{\mathbf{Z}}_A \end{bmatrix} - s_F \begin{bmatrix} 1 & \varepsilon_z & -\varepsilon_y \\ -\varepsilon_z & 1 & \varepsilon_x \\ \varepsilon_y & -\varepsilon_x & 1 \end{bmatrix} \begin{bmatrix} \overline{\mathbf{X}}_A \\ \overline{\mathbf{Y}}_A \\ \overline{\mathbf{Z}}_A \end{bmatrix} + \begin{bmatrix} \mathbf{T}'_x \\ \mathbf{T}'_y \\ \mathbf{T}'_z \end{bmatrix} \qquad (5.26)
$$

Solving (5.26) using the values in (5.24) and (5.25) results in (the sense, from NZGD49 to WGS72):

$$\begin{aligned} T_X &= +59.47 \text{ m} \\ T_Y &= -5.04 \text{ m} \\ T_Z &= +182.94 \text{ m} \end{aligned} \tag{5.27}$$

As was discussed in Section 5.3.3 the scale and rotation parameters remain unchanged. Having now converted Mackie's Molodenskii-Badekas based parameters to Bursa-Wolf parameters it is now possible to convert these parameters so that they for transforming from WGS84 to NZGD49, rather than transforming from WGS72 to NZGD49. This is achieved, due to the small rotation angles, by adding algebraically the parameters for converting WGS84 to WGS72 (Table 5-2), with the rotation and scale parameters from (5.24) and the translation parameters from (5.27) (Table 5-5).

From	To	T_X m	T_Y m	T_Z m	Δs $x10^{-6}$	ε_x "	ε_y "	ε_z "
WGS84	WGS72	0.0	0.0	-4.50	-0.219	0.0	0.0	0.554
WGS72	NZGD49	-59.47	5.04	-182.94	4.8256	0.47	-0.10	0.47
WGS84	NZGD49	-59.47	5.04	-187.44	4.6066	0.47	-0.10	1.024

Table 5 - 5 : Seven parameter similarity transformation parameters derived from Mackie (1982) for conversion from WGS84 to NZGD49.

5.4.3 Solving for parameters between ITRF93 and NZGD49

The School of Geomatic Engineering has software (TRANS3D), that is based on Harvey (1985), to determine the seven Bursa-Wolf model transformation parameters by a least squares adjustment. Harvey (1985) lists the original program code and design matrices of the least squares adjustment that allow for rotation angles of any size. It should be noted that for solutions containing less than the seven parameters the adjustment was achieved by assigning very small variances (eg. $1.0x10^{-7}$) to the parameters being fixed (normally to zero). This technique will produce results that are similar to undertaking a least squares adjustment with less parameters, but is not identical. The solutions that solve for less than seven parameters still have seven parameters, it is just that some of the parameters are constrained to zero.

As part of this research software was written to implement a least squares solution to the generalised method described in Section 5.3.7.

Details of least squares adjustment are widely published and can be found in textbooks such as Cross (1983) and Mikhail (1976).

The sub-sections 5.4.3.1 through 5.4.3.4 contain the transformation parameters determined using the TRANS3D software. Sub-sections 5.4.3.5 and 5.4.3.6 contain the transformation parameters determined using the generalised approach software, LSQ12P. The ITRF93 GPS coordinates and associated VCV matrix for 26 stations were obtained from the output of the GLOBK adjustment (Section 3.5.2). The NZGD49 three dimensional coordinates for the same 26 stations were generated by combining the latitude and longitude coordinates for the stations with their orthometric heights. These coordinates were obtained from DOSLI's geodetic database. The orthometric heights were then converted to ellipsoidal heights by adding on the geoid heights. The geoid heights were determined firstly in terms of GRS80 using the OSU91A GGM to degree and order 360 with (4.46), then transformed using the parameters in Table 5-5 to obtain geoid heights with respect to the NZGD49 International (Hayford) ellipsoid. It is recognised that these GGM derived geoid heights are not ideal when compared to geoid heights determined by local gravimetric solutions and may have errors of up to -1.1 m (Section 4.6). However, a high resolution nationwide gravimetrically determined geoid had not been computed at this time.

The 26 stations ITRF93 and NZGD49 coordinates and VCV matrices used in the following sub-sections are contained in Appendix K.

Unfortunately the VCV matrix or even *a priori* standard deviations for the five separate blocks used in the original adjustment of the NZGD49 coordinates (Section 2.4.2.2) are not available. It should be noted that NZGD49 is only a two dimensional datum and even if the original VCV matrices were available the height variances would be zero. Therefore, only a diagonal VCV matrix was used for the NZGD49 network of stations, though this VCV matrix did distinguish between the differences in the accuracy of the

horizontal and vertical coordinates (see Appendix K). The variances for the NZGD49 network are estimated as part of the least squares adjustment. One could also argue that when a first order horizontal station is used to determine transformation parameters, the station should be held fixed as by the NZGD49 definition these first order stations are error free.

5.4.3.1 Seven parameter solution

The determination of seven transformation parameters to transform between ITRF93 and NZGD49 was undertaken using the TRANS3D software. Through an iterative process the *a priori* variance for the NZGD49 latitude, longitude and height was determined as 0.04" (approx. 1.2 m), 0.04" (approx. 0.9 m) and 1.0 m, respectively. These *a priori* variance estimates are reasonable when considering the likely deformation that has occurred between the original triangulation survey and the GPS survey (Section 2.2). The corresponding adjusted parameters and correlations are contained in Table 5-6. Due to the enforcement of the Laplace equations during the establishment of NZGD49 the rotation parameters are, as expected, small (< 1.5 sec). From Table 5-6 it can also be noted that there are high correlations (> 0.8) between the rotation and translation parameters. This is primarily due to the relatively small global extent of the NZGD49 network especially in the East-West direction which is longitude.

A condensed output listing of the TRANS3D solution is contained in Appendix K. Testing the combined significance of the three rotation parameters using the multi-variate test of (5.14) indicated that the combined rotations are significant (ie. t' = 39.69 > $F_{3,71,0.05}$ = 2.72).

Testing the significance of the individual parameters using (5.15) indicated that the rotation parameters about the X and Y axes are insignificant at the 95% confidence level (ie. t' = 0.09 < $F_{1,71,0.05}$ = 3.99 and t' = 0.05 < F = 3.99, respectively). The insignificance of the X and Y axes rotations can be expected based on the known quality of the Earth's polar motion determinations by the International Latitude Service (ILS) at the time NZGD49 was established. The results from redetermining the transformation parameters holding the rotations about the X and Y axes fixed at zero is contained in the following section.

A posteriori estimate of the variance factor (sigma sq) is 1.033
Approximate degrees of freedom = 71
The *a priori* weights on the parameters contribute 0.0% to the estimated variance factor.
These results HAVE passed the F test of the variance factor at the 95% confidence level

Adjusted transformation parameters (Bursa-Wolf model)

Parameter	Adjusted Value
Differential Scale (Δs)	4.562 +/- 0.514 ppm
Rotation about X axis (ε_x)	0.072 +/- 0.241 secs
Rotation about Y axis (ε_y)	-0.049 +/- 0.208 secs
Rotation about Z axis (ε_z)	1.344 +/- 0.242 secs
Translation along X axis (T_x)	-60.788 +/- 4.465 m
Translation along Y axis (T_y)	-9.188 +/- 10.035 m
Translation along Z axis (T_z)	-187.073 +/- 5.718 m

Correlations between adjusted parameters

	Δs	ε_x	ε_y	ε_z	T_x	T_y	T_z
Δs	1.000						
ε_x	0.063	1.000					
ε_y	-0.023	0.805	1.000				
ε_z	0.077	-0.831	-0.803	1.000			
T_x	0.556	-0.602	-0.838	0.653	1.000		
T_y	-0.042	0.949	0.840	-0.963	-0.674	1.000	
T_z	0.366	0.811	0.919	-0.738	-0.559	0.795	1.000

Table 5 - 6 : ITRF93 to NZGD49 seven parameter transformation solution.

5.4.3.2 Five parameter solution

In the previous section it was shown that not all rotation parameters were significant for the seven parameter solution due the quality of the ILS polar motion determinations. The results from redetermining the transformation parameters holding the rotations about the X and Y axes fixed at zero are contained in Table 5-7. The *a priori* variance for the NZGD49 latitude, longitude and height was the same as for the seven parameter solution (ie. 0.04", 0.04", 1.0m). One of the most noticeable differences of setting the X and Y rotations to zero in comparison to solving for them is that the correlations between the differential scale and each translation component has significantly increased.

Testing the significance of each of the five estimated parameters in Table 5-7, against zero, indicated all five parameters are significant at the 95% confidence level using (5.15). The residuals on transformed coordinates from applying the transformation

parameters determined by fixing ε_x and ε_y to zero (Table 5-7) is discussed in Section 5.5.4.

A posteriori estimate of the variance factor (sigma sq) is 1.014
Approximate degrees of freedom = 73
The *a priori* weights on the parameters contribute 28.6% to the estimated variance factor.
These results HAVE passed the F test of the variance factor at the 95% confidence level

Adjusted transformation parameters (Bursa-Wolf model)

Parameter	Adjusted Value
Differential Scale (Δs)	4.501 +/- 0.509 ppm
Rotation about X axis (ε_x)	0.000 +/- 0.000 sec
Rotation about Y axis (ε_y)	0.000 +/- 0.000 sec
Rotation about Z axis (ε_z)	1.360 +/- 0.123 sec
Translation along X axis (T_x)	-62.113 +/- 2.377 m
Translation along Y axis (T_y)	-10.979 +/- 2.899 m
Translation along Z axis (T_z)	-186.400 +/- 2.149 m

Correlations between adjusted parameters

	Δs	ε_x	ε_y	ε_z	T_x	T_y	T_z
Δs	1.000						
ε_x	0.000	1.000					
ε_y	0.000	0.000	1.000				
ε_z	0.202	0.000	0.000	1.000			
T_x	0.987	0.000	0.000	0.067	1.000		
T_y	-0.300	0.000	0.000	-0.993	-0.168	1.000	
T_z	0.995	0.000	0.000	0.200	0.980	-0.297	1.000

Table 5 - 7 : ITRF93 to NZGD49 five parameter transformation solution

5.4.3.3 Four parameter solution

For some applications (ie. mapping) the accuracy requirements for the transformed coordinates are sufficiently relaxed to allow the transformation to be represented by only a 4 parameter solution. The results of determining only 4 parameters (translations and scale) are contained in Table 5-8.

To satisfy the *F* test on the variance factor the *a priori* variance for the NZGD49 latitude and longitude were both increased to 0.083" (approx. 2.5 m and 1.9 m), while the *a priori* variance for height remained at 1.0 m. Using (5.14) all four parameters are significant at the 95% confidence level.

Results and discussion from applying the transformation parameters of Table 5-8 are contained in Section 5.5.4.

A posteriori estimate of the variance factor (sigma sq) is 1.116
Approximate degrees of freedom = 74
The *a priori* weights on the parameters contribute 42.9% to the estimated variance factor.
These results HAVE passed the F test of the variance factor at the 95% confidence level

Adjusted transformation parameters (Bursa-Wolf model)

Parameter	Adjusted Value	
Differential Scale (Δs)	3.296 +/-	1.035 ppm
Rotation about X axis (ε_x)	0.000 +/-	0.000 sec
Rotation about Y axis (ε_y)	0.000 +/-	0.000 sec
Rotation about Z axis (ε_z)	0.000 +/-	0.000 sec
Translation along X axis (T_x)	-64.372 +/-	4.933 m
Translation along Y axis (T_y)	20.785 +/-	0.723 m
Translation along Z axis (T_z)	-191.243 +/-	4.379 m

Correlations between adjusted parameters

	Δs	ε_x	ε_y	ε_z	T_x	T_y	T_z
Δs	1.000						
ε_x	0.000	1.000					
ε_y	0.000	0.000	1.000				
ε_z	0.000	0.000	0.000	1.000			
T_x	0.997	0.000	0.000	0.000	1.000		
T_y	-0.847	0.000	0.000	0.000	-0.844	1.000	
T_z	0.996	0.000	0.000	0.000	0.988	-0.839	1.000

Table 5 - 8 : ITRF93 to NZGD49 four parameter transformation solution

5.4.3.4 Three parameter solution

The minimum number of parameters that can be used to transform three dimensional coordinates is three. The choice of solving the three translation parameters is often referred to as a block shift. The results of determining only 3 translation parameters are contained in Table 5-9. To satisfy the *F* test on the variance factor the *a priori* variance for the NZGD49 latitude and longitude were both increased to 0.108" (approx. 3.25 m and 2.5 m), while the *a priori* variance for height remained at 1.0 m. Using (5.14) all four parameters are significant at the 95% confidence level.

Results and discussion from applying the transformation parameters of Table 5-9 are contained in Section 5.5.4.

A posteriori estimate of the variance factor (sigma sq) is 0.991
Approximate degrees of freedom = 75
The *a priori* weights on the parameters contribute 57.1% to the estimated variance factor.
These results HAVE passed the F test of the variance factor at the 95% confidence level

Adjusted transformation parameters (Bursa-Wolf model)

Parameter	Adjusted Value	
Differential Scale (Δs)	0.000 +/-	0.000 ppm
Rotation about X axis (ε_x)	0.000 +/-	0.000 sec
Rotation about Y axis (ε_y)	0.000 +/-	0.000 sec
Rotation about Z axis (ε_z)	0.000 +/-	0.000 sec
Translation along X axis (T_x)	-80.192 +/-	0.451 m
Translation along Y axis (T_y)	22.648 +/-	0.494 m
Translation along Z axis (T_z)	-204.969 +/-	0.500 m

Correlations between adjusted parameters

	Δs	ε_x	ε_y	ε_z	T_x	T_y	T_z
Δs	1.000						
ε_x	0.000	1.000					
ε_y	0.000	0.000	1.000				
ε_z	0.000	0.000	0.000	1.000			
T_x	0.000	0.000	0.000	0.000	1.000		
T_y	0.000	0.000	0.000	0.000	0.003	1.000	
T_z	0.000	0.000	0.000	0.000	-0.820	0.106	1.000

Table 5 - 9 : ITRF93 to NZGD49 three parameter transformation solution

5.4.3.5 Generalised model solution

In this section the approach of solving the numerical values for the elements of ***M*** (5.22) using least squares is applied to the problem of converting between NZGD49 coordinates and ITRF93 coordinates.

Software was developed as part of this research to determine the elements of the Composite Matrix (Section 5.3.7) by a least squares adjustment. This software, referred to as LSQ12P, does not currently utilise the VCV data of the coordinates as this was not available.

Using the tools of strain (Section 5.3.7) to help interpret the values of the parameters in Table 5-10 one needs to keep in mind that these strains are not only comprised of information about the physical strain (deformation) but also the differences between the reference systems and the observations that realised those datums.

The values for parameters a_{11}, a_{22} and a_{33} in Table 5-10 are statistically different and therefore indicate that there is different axial scales between NZGD49 and ITRF93. This is not unexpected as NZGD49 is a horizontal only datum and for the purpose of transforming to ITRF93 the orthometric heights were used to provide the third dimension.

Parameter	from NZGD49 to ITRF93	Units
a_{11}	1.00003051 ± 0.00000013	dimensionless
a_{12}	-0.00001140 ± 0.00000003	dimensionless
a_{13}	0.00003062 ± 0.00000011	dimensionless
a_{14}	359.2841 ± 1.1063	m
a_{21}	0.00000829 ± 0.00000013	dimensionless
a_{22}	0.99999567 ± 0.00000003	dimensionless
a_{23}	0.00000158 ± 0.00000011	dimensionless
a_{24}	25.5594 ± 1.1063	m
a_{31}	-0.00005054 ± 0.00000013	dimensionless
a_{32}	0.00000734 ± 0.00000003	dimensionless
a_{33}	0.99995045 ± 0.00000011	dimensionless
a_{34}	-246.3249 ± 1.1063	m

correlations	a_{11}	a_{12}	a_{13}	a_{14}	a_{21}	a_{22}	a_{23}	a_{24}	a_{31}	a_{32}	a_{33}	a_{34}
a_{11}	1.000											
a_{12}	-0.811	1.000										
a_{13}	0.993	-0.749	1.000									
a_{14}	0.999	-0.791	0.997	1.000								
a_{21}	0.000	0.000	0.000	0.000	1.000							
a_{22}	0.000	0.000	0.000	0.000	-0.811	1.000						
a_{23}	0.000	0.000	0.000	0.000	0.993	-0.749	1.000					
a_{24}	0.000	0.000	0.000	0.000	0.999	-0.791	0.997	1.000				
a_{31}	0.000	0.000	0.000	0.000	0.000	0.000	0.000	0.000	1.000			
a_{32}	0.000	0.000	0.000	0.000	0.000	0.000	0.000	0.000	-0.811	1.000		
a_{33}	0.000	0.000	0.000	0.000	0.000	0.000	0.000	0.000	0.993	-0.749	1.000	
a_{34}	0.000	0.000	0.000	0.000	0.000	0.000	0.000	0.000	0.999	-0.791	0.997	1.000

Table 5 - 10 : Derived generalised model parameters and correlations for conversion between NZGD49 and ITRF93

If parameter $a_{12} = -a_{21}$ then there would be no shear between NZGD49 and ITRF93 in the xz and yz planes. Table 5-10 shows that statistically $-a_{12} \neq a_{21}$ ($0.00001140 \neq 0.00000829$) therefore indicating shear is present in these planes. Since $a_{13} \neq -a_{31}$ and $a_{23} \neq -a_{32}$ this also indicates that shear is present in the remaining 4 planes (xy, zy, yx

and zx). The difference between the values of these parameters (a_{12}, a_{13}, a_{21}, a_{23}, a_{31}, a_{32}) indicates that the generalised method is able to account for additional signals than the seven parameter similarity transformation. The existence of shearing is to be expected between NZGD49 and ITRF93 due to the active tectonic processes taking place across New Zealand (see Section 2.2).

The a_{14}, a_{24} and a_{34} parameters in Table 5-10 represent primarily the translations in the X, Y and Z axes, respectively. Comparison of the values of a_{14}, a_{24} and a_{34} with the translations in Tables 5-6 through 5-10 shows that they are different, with the a_{14} and T_x parameters being significantly different ($a_{14} \approx 359$m and $T_x \approx 65$m). However the effect of this difference can only be determined after applying the parameters to a set of coordinates due to the high correlations between the parameters (Table 5-10). Results from applying the generalised model parameters to the conversion between NZGD49 and ITRF93 coordinates are contained in Section 5.5.5.

5.4.3.6 Generalised model solution using velocities

Since the establishment of NZGD49 in 1949 the effects of earth deformation have continued to shift the relative positions of the first order control marks. This effect could amount to 2.5m over the approximately 50 years that have elapsed between the original observations and the GPS observations of the first order network (Chapter 2).

The LSQ12P software currently assumes homogeneous strain (elements of $\boldsymbol{M}$ are considered to be constant across the region, ie. position independent). As Earth deformation effects vary across New Zealand (Figure 2-4) the application of a velocity model to remove the heterogeneous strain effects before solving for the elements of $\boldsymbol{M}$ is tested.

In the absence of other information the NUVEL1A (DeMets *et al.*, 1994) rates for 50 years were applied to the NZGD49 coordinates even though it is known that they are not fully applicable near plate boundaries. The NUVEL1A model is a surface only model (ie. contains no rates for changes in height) and therefore it is expected that the height component of transformed coordinates will be unaffected. No additional model was

used to model uplift. It is expected that in the near future more realistic three dimensional velocities will become available for New Zealand sites.

Sites were assigned to either the Pacific or the Australian plate based on which plate their principle motion most closely resembled as reported by Beavan *et al.*, 1996 (Figure 2-4). The sites were assigned to a tectonic plate as follows:

Tectonic Plate	Sites
Australian	D078, D100, D431, D072, D473, D143, D131, D452, D045, D026, D105, D158, D469, D309, D320
Pacific	WELL, D425, D191, D212, D233, D229, D253, D338, D286, D474, D302

As was the case in Section 5.4.3.5 the values for parameters a_{11}, a_{22} and a_{33} in Table 5-11 are statistically different and therefore indicate that there is still different axial scales between NZGD49 and ITRF93. This is expected as NUVEL1A rates do not affect the axial scales.

Table 5-11 shows that $a_{12} \neq -a_{21}$, $a_{13} \neq -a_{31}$ and $a_{23} \neq -a_{32}$ therefore indicating that the NUVEL1A rates were not able to account for all the shear signal that is present in each plane. This confirms that the NUVEL1A rates poorly model New Zealand sites that are near the plate boundary.

All the composite matrix parameters containing shear strain (a_{12}, a_{13}, a_{21}, a_{31}, a_{32}) except a_{23} have smaller numerical values when the NUVEL1A velocities have been applied (Table 5-11) compared to those generated by not applying velocities (Table 5-10). To be able to compare the different parameters in Tables 5-10 and 5-11, due to the effects of the correlations, one needs to apply them to a set of coordinates. Results from applying the generalised model parameters to the conversion between NZGD49 and ITRF93 coordinates after applying NUVEL1A plate velocities are contained in Section 5.5.6.

Parameter	from NZGD49 to ITRF93	Units
a_{11}	1.00002515 ± 0.00000013	dimensionless
a_{12}	-0.00001050 ± 0.00000003	dimensionless
a_{13}	0.00002661 ± 0.00000011	dimensionless
a_{14}	317.4818 ± 1.1063	m
a_{21}	0.00000807 ± 0.00000013	dimensionless
a_{22}	0.99999601 ± 0.00000003	dimensionless
a_{23}	0.00000450 ± 0.00000011	dimensionless
a_{24}	35.7007 ± 1.1063	m
a_{31}	-0.00004721 ± 0.00000013	dimensionless
a_{32}	0.00000660 ± 0.00000003	dimensionless
a_{33}	0.99995255 ± 0.00000011	dimensionless
a_{34}	-222.5551 ± 1.1063	m

correlations	a_{11}	a_{12}	a_{13}	a_{14}	a_{21}	a_{22}	a_{23}	a_{24}	a_{31}	a_{32}	a_{33}	a_{34}
a_{11}	1.000											
a_{12}	-0.811	1.000										
a_{13}	0.993	-0.749	1.000									
a_{14}	0.999	-0.791	0.997	1.000								
a_{21}	0.000	0.000	0.000	0.000	1.000							
a_{22}	0.000	0.000	0.000	0.000	-0.811	1.000						
a_{23}	0.000	0.000	0.000	0.000	0.993	-0.749	1.000					
a_{24}	0.000	0.000	0.000	0.000	0.999	-0.791	0.997	1.000				
a_{31}	0.000	0.000	0.000	0.000	0.000	0.000	0.000	0.000	1.000			
a_{32}	0.000	0.000	0.000	0.000	0.000	0.000	0.000	0.000	-0.811	1.000		
a_{33}	0.000	0.000	0.000	0.000	0.000	0.000	0.000	0.000	0.993	-0.749	1.000	
a_{34}	0.000	0.000	0.000	0.000	0.000	0.000	0.000	0.000	0.999	-0.791	0.997	1.000

Table 5 - 11 : Derived generalised model parameters and correlations for conversion between NZGD49 and ITRF93 after applying NUVEL1A plate velocities.

5.5 Comparison of transformation parameters

In Sections 5.4.2 and 5.4.3 both published and derived transformation parameters to convert between NZGD49 and either ITRF93 or WGS84 were presented. This section compares these transformations by applying them to a set of 26 stations that had both ITRF93 (as determined in Chapter 3) and NZGD49 coordinates (Appendix K). Comparison of coordinate differences between the known values and the transformed values was undertaken with WGS84 coordinates. The ITRF93 coordinates obtained by the application of the published and derived transformation parameters between

NZGD49 and ITRF93 were converted to WGS84 coordinates to allow the comparison between WGS84 coordinates derived from NZGD49-WGS84 parameters. The choice of comparing transformed coordinates in terms of WGS84 as opposed to ITRF93 did not influence the findings. The transformation parameters used to convert the ITRF93 coordinates into WGS84 coordinates were generated by combining parameters from Table 5-2, as shown in Table 5-12.

From	To	T_X m	T_Y m	T_Z m	Δs $x10^{-8}$	ε_x mas	ε_y mas	ε_z mas
ITRF93	ITRF92	0.002	0.007	0.007	-0.12	-0.39	0.80	-0.96
ITRF92	WGS84 (G730)	0.070	0.130	-0.150	0.03	6.0	-2.0	2.4
WGS84 (G730)	WGS84	0.040	0.010	0.280	21.8	-4.2	4.0	15.6
ITRF93	WGS84	0.112	0.147	0.137	21.71	1.41	2.8	17.04

Table 5 - 12 : ITRF93 to WGS84 Similarity Transformation Parameters

5.5.1 Results using the DMA Multiple Regression Equations

Applying the DMA MRE in (5.23) to the NZGD49 coordinates (Appendix K) generated WGS84 coordinates. These MRE-derived WGS84 coordinates were compared with those WGS84 coordinates obtained by transforming the ITRF93 coordinates (Appendix C) to WGS84 by the parameters in Table 5-12. The differences in the WGS84 coordinates are summarised in Table 5-13 (in the sense MRE minus ITRF93 determinations).

	Difference in North (m)	Difference in East (m)	Difference in Height (m)
minimum	-3.319	-2.882	-9.701
maximum	3.923	1.021	-2.868
mean	-0.323	-0.880	-6.271
rms	1.675	1.226	6.583

Table 5 - 13 : DMA Multiple Regression Equations Transformation results.

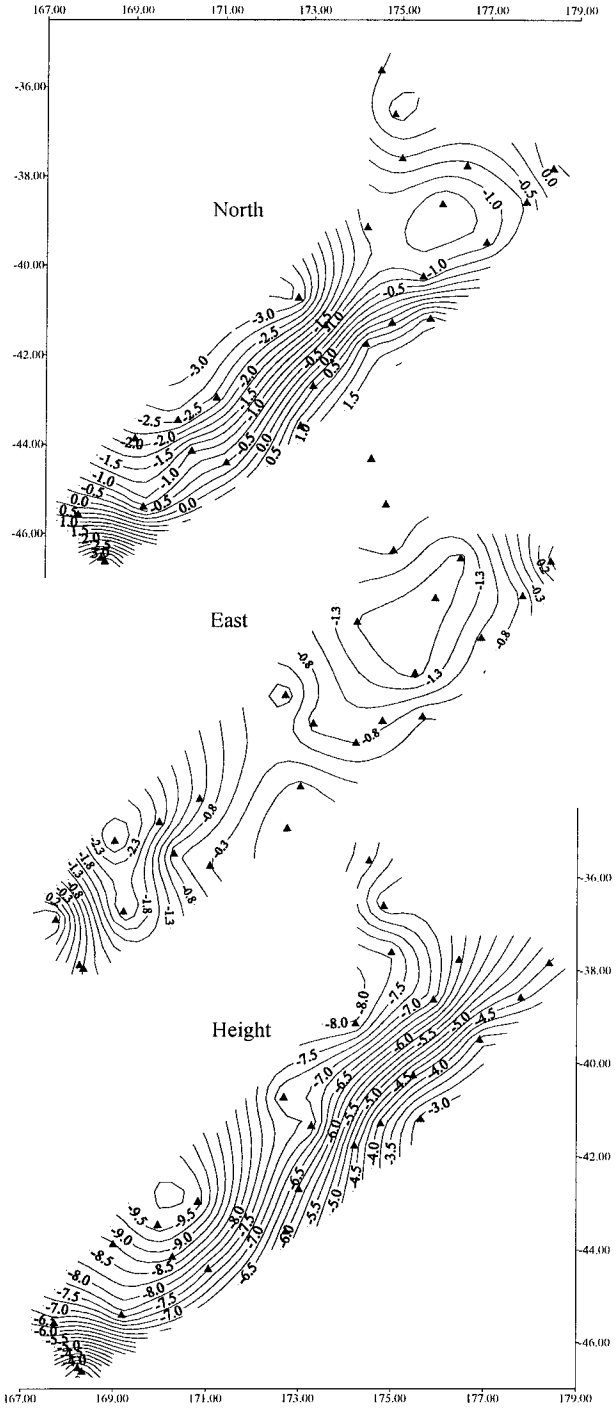

Figure 5 - 3 : DMA Multiple Regression Equations Transformation difference results as contour maps (units = metres). Triangles represent March 1993 GPS stations (see Figure 3-1)

From Table 5-13 it can be seen that the DMA MRE produces Northing differences that have a larger range, though a mean closer to zero, than the Easting differences. While the height component has a maximum difference of approximately 10.0 m. When one considers that at the MRE reference point (S41°, E173°) the conversion for ellipsoidal

height is 8.630 m (see 5.23), then the results in Table 5-13 indicate that this MRE height bias is too large, by approximately 6 m.

From Figure 5-3 it is clear that the differences in each component, between the MRE-derived WGS84 coordinates minus the ITRF93-derived WGS84 coordinates, have significantly different signatures. The north and height components have steep east - west gradients, while the east component has generally flatter gradients.

5.5.2 Results using the DMA Similarity Transformation Parameters

Applying each of the DMA Similarity Transformation parameters in Table 5-4 to the NZGD49 coordinates of Appendix K generated WGS84 coordinates. These DMA similarity transformation derived WGS84 coordinates were compared with those WGS84 coordinates obtained by transforming the ITRF93 coordinates (Appendix C) to WGS84 by the parameters in Table 5-12. The differences in the WGS84 coordinates are summarised in Table 5-14 (in the sense DMA minus ITRF93 determinations).

Difference	Number of Parameters					
in	Seven	Six	Four	Three	Seven *	Four *
North	metres					
minimum	-1.907	-2.898	-2.774	-3.990	-2.158	-3.027
maximum	2.645	4.580	3.535	5.935	2.392	3.290
mean	-0.011	0.014	0.125	0.069	-0.260	-0.124
rms	1.167	2.026	1.434	3.123	1.196	1.436
East	metres					
minimum	-2.766	-5.325	-4.534	-3.372	-2.766	-4.534
maximum	1.059	2.944	2.080	1.570	1.059	2.080
mean	-1.009	-1.393	-1.542	-0.937	-1.009	-1.542
rms	1.477	2.308	2.506	1.576	1.477	2.505
Height	metres					
minimum	67.120	-8.180	66.281	-9.147	-8.304	-9.144
maximum	71.176	-4.189	70.362	-5.060	-4.262	-5.078
mean	69.567	-5.722	68.733	-6.644	-5.870	-6.703
rms	69.579	5.869	68.746	6.776	6.017	6.832

Table 5 - 14 : DMA Similarity Transformation results. Note: * indicates that the differential scale with opposite sign to that in Table 5-4 was used.

When comparisons of the results in Table 5-14 are made, it would be expected that the similarity transformation results from using a larger number of parameters would produce superior results due to the extra parameters being able to account for additional differences between the datums. For the DMA similarity transformation results the rms of the differences does reduce as the number of parameters solved for increases. This indicates that the extra parameters are allowing the differences between the two datums to be better modelled.

It is clear from Table 5-14 that there is a significant problem with the ellipsoidal height differences, especially for the seven and four parameter results. The similarity transformation parameter most likely to cause differences in heights is the differential scale (Δs) due to this parameters main effect is to scale the radius. The Δs parameter is also present in both the seven and four parameter results. From comparing the mean height difference with the scale correction ($s_F * R$) it was found that the difference is twice the scale correction. This implies that Δs was used with the wrong sign. Transforming the NZGD49 coordinates to WGS84 coordinates using the DMA seven and four similarity transformation parameters but with the sign changed for Δs produced the results in columns labelled Seven* and Four* of Table 5-14. As can be clearly seen from Table 5-14, the new results from the seven and four parameter solutions produce ellipsoidal heights that agree well with those of the six and three parameter solutions, and those from the DMA MRE (Table 5-13) and Mackie-based seven parameter similarity transformation (Table 5-15).

Comparison of the similarity transformation formula for Cartesian coordinates given in DMA (1987a, eqn. 7-4) with the implementation in the TRANS3D software (Section 5.4.3.1) confirmed they were consistent, thus the conclusion drawn was that Δs has been printed with the wrong sign in DMA (1987a, p. 7-47).

Comparing the DMA similarity transformation parameter results (Table 5-14) against each other shows that the seven parameter result (corrected for scale sign) produces superior results to the other parameter sets for the north and east components. However,

the six parameter set produced height results that were superior to the seven parameter set by approximately 0.2 m, the significance of this height difference is unknown. Due to the significantly inferior north and east component results from the six parameter set, the seven parameter set was considered to be the overall superior DMA similarity transformation parameters.

Comparison of the DMA seven parameter similarity transformation results (Table 5-14) with the DMA MRE results (Table 5-13) reveals that the seven parameter similarity transformation results were significantly superior for the northing results, equivalent for the easting results and only marginally better for the height results. The three parameter set was assigned accuracies by the DMA (1987b, p. 10-9) for T_X, T_Y and T_Z of $\pm$ 5, 3, 5m, respectively, though the confidence interval was not stated. If a confidence interval of 95% is assumed, then the three parameter set results, in Table 5-14, satisfy these stated accuracies.

From Figure 5-4 it is clear that the differences in each component, between the DMA seven parameter-derived WGS84 coordinates minus the ITRF93-derived WGS84 coordinates, have significantly different signatures. When the DMA seven parameter similarity transformation difference results (Figure 5-4) are compared with the DMA MRE difference results (Figure 5-3) each of the respective components are practically uncorrelated. The north and east components no longer have steep east - west gradients and the east component minimum and maximum features have been shifted.

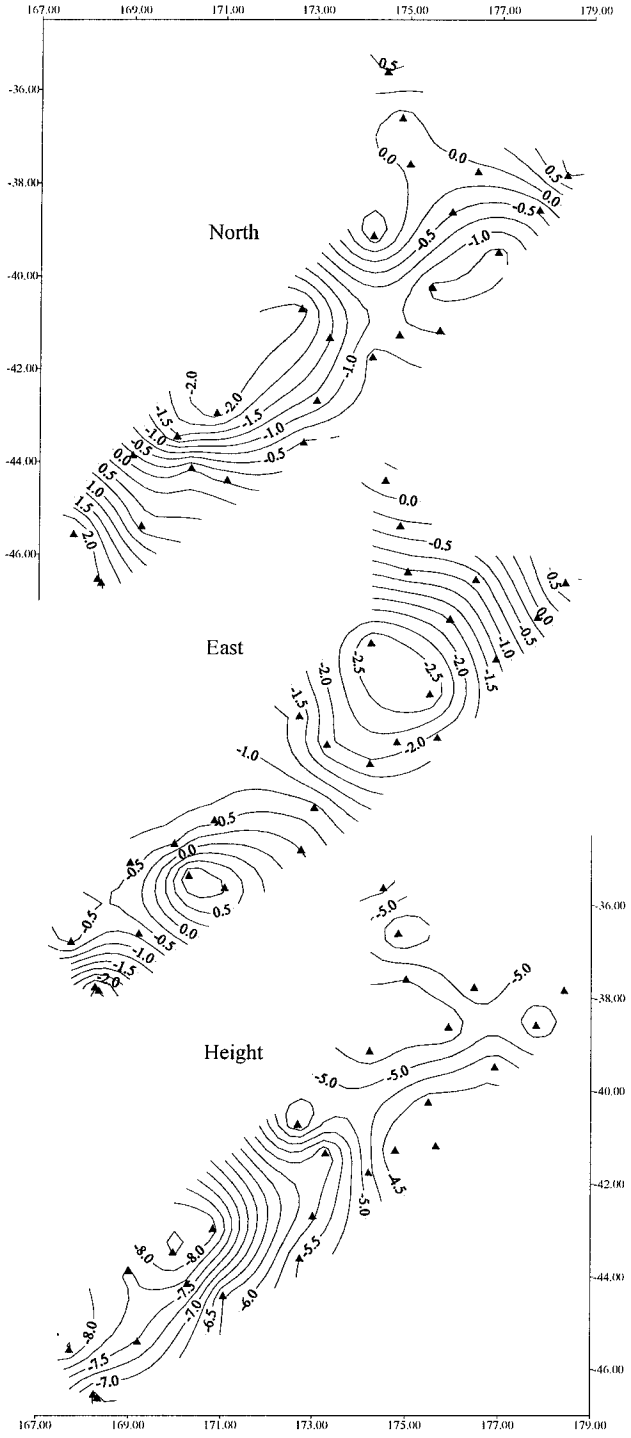

Figure 5 - 4 : DMA Seven Parameter Similarity Transformation difference results as contour maps (units = metres). Triangles represent March 1993 GPS stations (see Figure 3-1)

5.5.3 Results using the Mackie based Similarity Transformation Parameters

Applying the Mackie (1982) based parameters from Table 5-5 to the NZGD49 coordinates of Appendix K generated WGS84 coordinates. These derived WGS84

coordinates were compared with those WGS84 coordinates obtained by transforming the ITRF93 coordinates to WGS84 by the parameters in Table 5-12. The differences in the WGS84 coordinates are summarised in Table 5-15 (in the sense Mackie-based minus ITRF93 determinations).

	Difference in North (m)	Difference in East (m)	Difference in Height (m)
minimum	-2.142	-2.553	-3.950
maximum	2.200	1.198	-0.435
mean	-0.061	-0.775	-1.983
rms	1.133	1.327	2.216

Table 5 - 15 : Mackie-based Similarity Transformation results.

Comparison of the Mackie-based results (Table 5-15) shows that the north and east components of the differences produced similar quality results, with the maximum difference being approximately 2.5 m. Though the easting component does have a mean difference of approximately 0.8 m. This implies that the WGS84 coordinates derived from the ITRF93 coordinates are on average 0.8 m to the east of the WGS84 coordinates derived via the Mackie-based parameters from the NZGD49 coordinates. The difference in the east can be interpreted as a rotation about the Z axis. A possible cause of this rotation is that the angular rotation of the Earth as measured by UT1 was poorly defined when observations were made to establish NZGD49.

The mean difference in height of approximately 2.0 m (Table 5-15) indicates a possible problem in the generation of the ellipsoidal heights. The control ellipsoidal heights associated with the NZGD49 coordinates were determined by adding the OSU91A based geoid heights to the orthometric heights (see 4.1). These OSU91A based N values were obtained by transforming N values in terms of a geocentric GRS80 ellipsoid to the International (Hayford) ellipsoid (positioned through NZGD49) using the Mackie-based parameters from Table 5-5. Whether this method of generating geoid heights is inferior or superior to the geoid heights generated by Mackie (*ibid.*), using deflections of the vertical, is unknown.

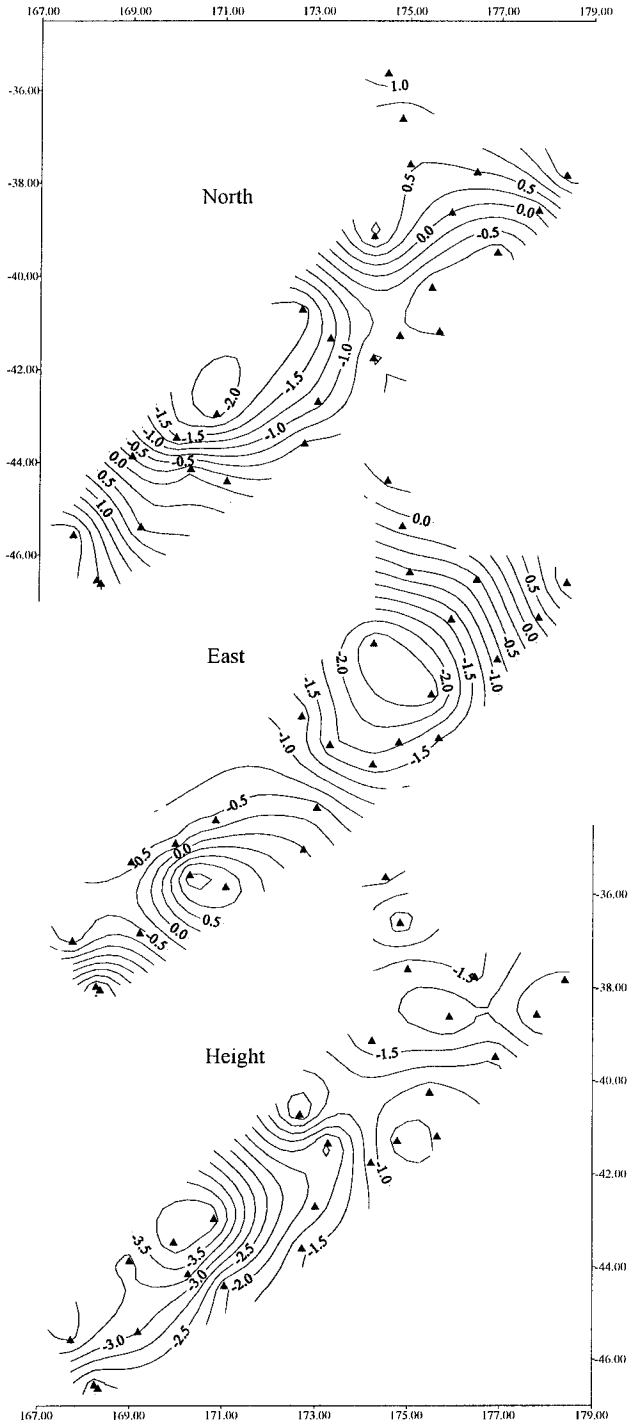

Figure 5 - 5 : Mackie-based Seven Parameter Similarity Transformation difference results as contour maps (units = metres). Triangles represent March 1993 GPS stations (see Figure 3-1).

The Mackie-based similarity transformation parameter results (Table 5-15) produce smaller differences than either the DMA similarity transformation parameter results (Table 5-14) or the DMA MRE results (Table 5-13).

From Figure 5-5 it is clear that the differences in each component, between the Mackie-based seven parameter derived WGS84 coordinates minus the ITRF93-derived WGS84 coordinates, have significantly different signatures. When the Mackie-based seven parameter similarity transformation difference results (Figure 5-5) are compared with the DMA seven parameter similarity transformation difference results (Figure 5-4) each of the respective components are showing high correlations.

5.5.4 Results using derived Similarity Transformation Parameters

For Sections 5.5.1 through 5.5.3, the transformation parameters were checked by analysing differences in the converted coordinates at 26 stations that were well distributed across the country.

In Section 5.4.3 all 26 stations were used in the determination of the similarity transformation parameters. Analysing the residuals from what was considered to be an over determined least squares adjustment (71 degrees of freedom for seven parameter solution - Table 5-6) indicated that the determined transformation parameters were realistic. Though to check the reliability of the derived parameters, six stations (three in each of the North and South Islands) were each in turn removed from a determination of the seven parameter similarity transformation parameters. This resulted in six sets of seven parameter similarity transformation parameters each determined from only 25 stations. The station removed from each determination of the parameters could then be used as a check station at which the transformation parameters could be applied and differences (in the sense of known NZGD49 minus ITRF93 transformed) between the known and transformed coordinate analysed (Table 5-16).

Check Station	Difference in North (m)	Difference in East (m)	Difference in Height (m)
D473	0.186	-0.870	-0.631
D143	-0.649	-0.791	0.846
D026	1.453	0.779	0.128
D158	-1.361	-0.952	-0.163
D229	-0.124	2.286	-0.951
D474	1.948	-1.680	0.885
minimum	-1.361	-1.680	-0.951
maximum	1.948	2.286	0.885

Table 5 - 16 : Results of derived similarity parameters at the six check stations

The parameter values for the six sets of transformation parameters were not different to the values in Table 5-6 at the 95% confidence interval. This indicates that each of the six stations were consistent with the other stations and also that the parameter solutions were stable.

With the reliability of the least squares determined seven parameter similarity transformation having been confirmed (at the six check stations), the four parameter sets derived during this research, from Sections 5.4.3.1 through 5.4.3.4, were applied to the NZGD49 coordinates (Appendix K). Each of these four derived ITRF93 coordinates sets were then converted to WGS84 coordinates using the parameters in Table 5-12. The ITRF93 coordinates (Appendix C) were also converted to WGS84 coordinates using the same parameters in Table 5-12, so as to enable the parameters derived by this research to be compared using WGS84 coordinates as was the case for the comparisons of the DMA (Sections 5.5.1 and 5.5.2) and Mackie (Section 5.5.3) based transformations.

In Table 5-17 the difference between the five (2 parameters fixed to zero) and seven parameter results only varied by a maximum of 0.1m in any component. Values for the ε_x and ε_y rotations of zero suggest that the polar motion was correctly applied to NZGD49 astronomic observations to convert these observations from being with respect to the Earth's instantaneous pole to the CIO. This is consistent with the known quality of the International Latitude Service which relied on crystal oscillators.

These original observations may indeed have been of high quality, though some small errors may exist. To reduce the effect of these small possible errors it is considered necessary to solve for all seven parameters, though the extra parameters could obscure small but important information.

From Table 5-17 it can be seen that, in general, the difference results deteriorate as the number of parameters solved for decreases. This also confirms the same finding with the DMA similarity transformations (Table 5-14). From the results in Table 5-17 it is interesting to note that as expected the mean difference for each component deteriorates as the number of parameters solved for decreases. It can be concluded that of the four derived sets of similarity transformation parameters, the seven parameter similarity transformation produces the superior results.

Difference in	Number of Parameters			
	Seven	Five	Four	Three
North	metres			
minimum	-2.201	-2.250	-3.651	-4.463
maximum	2.062	1.945	3.847	5.030
mean	-0.002	0.006	-0.397	-0.556
rms	1.136	1.141	1.953	2.944
East	metres			
minimum	-1.819	-1.863	-3.151	-2.889
maximum	2.132	2.197	2.899	2.282
mean	-0.008	0.001	-0.320	-0.371
rms	1.064	1.067	1.687	1.342
Height	metres			
minimum	-1.525	-1.431	-2.513	-2.507
maximum	1.652	1.653	1.654	1.632
mean	-0.003	0.000	-0.003	0.012
rms	0.786	0.795	1.360	1.342

Table 5 - 17 : Derived Similarity Transformation results NZGD49 and WGS84.

Comparing the derived seven parameter similarity transformation results (Table 5-17) with the DMA MRE (Table 5-13) and seven parameter similarity transformation (Table 5-14) results shows that the derived seven parameter similarity transformation produces the superior results. However, comparison of the derived seven parameter results with

the Mackie-based seven parameter results (Table 5-15) is not as clear. The Mackie-based minimum, maximum and rms results for the north and east components are approximately the same as the derived seven parameter results. When the height component is compared the derived seven parameter results are superior. What is interesting to note is that for each component the derived seven parameter results mean difference is basically zero, while the mean difference for the Mackie-based results reaches up to 2.0 m. It was therefore concluded that the derived seven parameter transformation parameters were able to convert NZGD49 coordinates to WGS84 coordinates more reliably than the Mackie-based parameters, though further investigation into the conversion of orthometric heights to ellipsoidal heights is required.

From Figure 5-6 it is clear that the differences in each component, between the derived seven parameter generated WGS84 coordinates minus the ITRF93-derived WGS84 coordinates, have significantly different signatures. When the derived seven parameter similarity transformation difference results (Figure 5-6) are compared with the DMA seven parameter similarity transformation difference results (Figure 5-4) and the Mackie-based seven parameter similarity transformation difference results (Figure 5-5), each of the respective components are showing high correlations. It should be noted that the mean residual coordinate difference reduces in magnitude between the DMA (Table 5-14), the Mackie-based (Table 5-15) and the Derived seven parameter similarity transformation (Table 5-17). For the derived seven parameter similarity transformation results the mean residual in each component is practically zero.

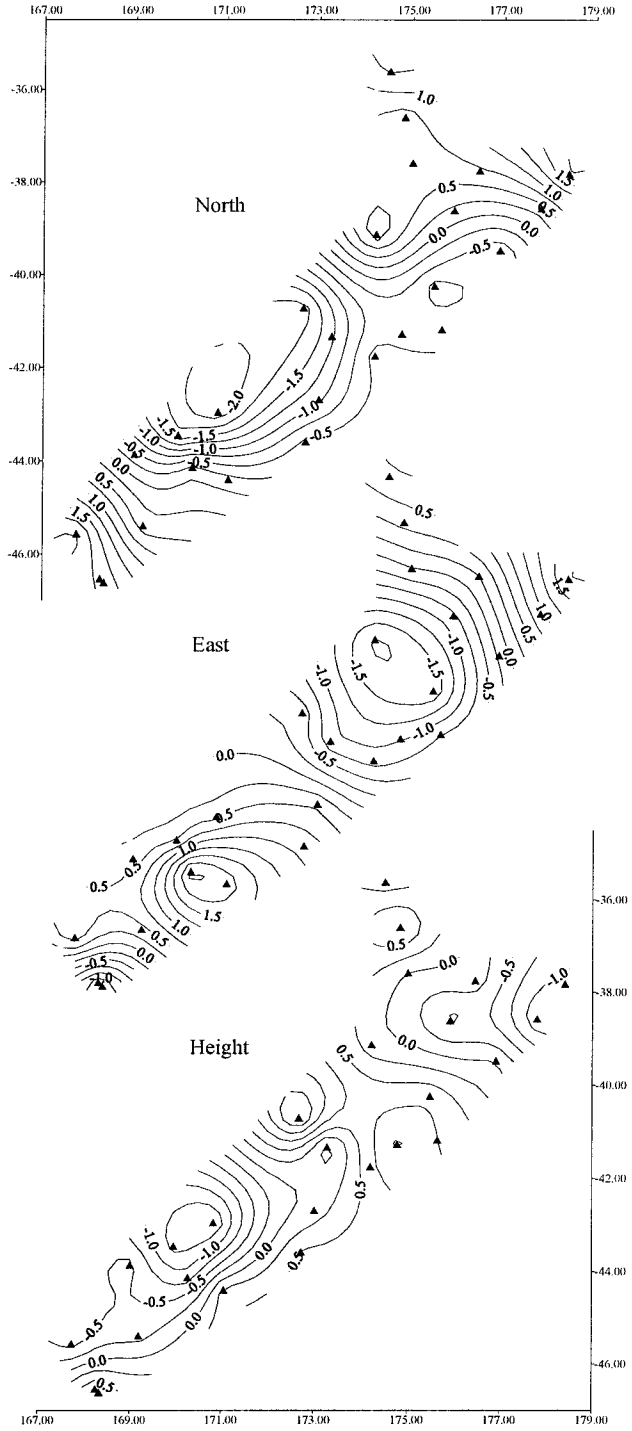

Figure 5 - 6 : Derived Seven Parameter Similarity Transformation difference results as contour maps (units = metres). Triangles represent March 1993 GPS stations (see Figure 3-1).

5.5.5 Results using the Generalised Model Parameters

Applying the Composite Matrix parameters from Table 5-10 to the NZGD49 coordinates of Appendix K generated ITRF93 coordinates. The derived ITRF93

coordinates were converted to WGS84 by the parameters in Table 5-12 to allow comparison between the other transformation techniques as was described in Section 5.5.4. The differences in the WGS84 coordinates are summarised in Table 5-18 (in the sense Generalised Model based minus ITRF93 determinations).

Difference in	Method			
	Mackie based 7 parameter	derived 7 parameter similarity	Composite Matrix	Composite Matrix (Nuvella)
North	metres			
minimum	-2.142	-2.201	-1.251	-0.956
maximum	2.200	2.062	1.621	1.632
mean	-0.061	-0.002	0.002	0.002
rms	1.133	1.136	0.586	0.521
East	metres			
minimum	-2.553	-1.819	-1.780	-2.109
maximum	1.198	2.132	2.183	1.880
mean	-0.775	-0.008	0.006	0.006
rms	1.327	1.064	1.075	1.109
Height	metres			
minimum	-3.950	-1.525	-1.684	-1.689
maximum	-0.435	1.652	1.535	1.528
mean	-1.983	-0.003	-0.006	-0.006
rms	2.216	0.786	0.799	0.798

Table 5 - 18 : Comparison of Derived 7 Parameter Similarity Transformation results and Generalised Method results for converting between NZGD49 and WGS84.

The range between the minimum and maximum difference, and magnitude of the rms, of the north component (Table 5-18) successively improves between using the Mackie-based parameters, the derived 7 parameters and the generalised model (Composite Matrix). For the east component the range is approximately the same between the three methods but the Mackie-based results have the largest bias. In the height component the derived 7 parameter similarity transformation and the generalised model produce equivalent results which are an improvement over the Mackie-based results. The probable reason why the height component does not improve by using the generalised model is that the random errors in the height are approximately 0.8 m. Reasons for the 0.8 m random error are probably the conversion of the orthometric heights to ellipsoid heights using the OSU91A GGM and the multiple independent height datums across

New Zealand. This effect is common to both the 7 parameter similarity transformation and the generalised model.

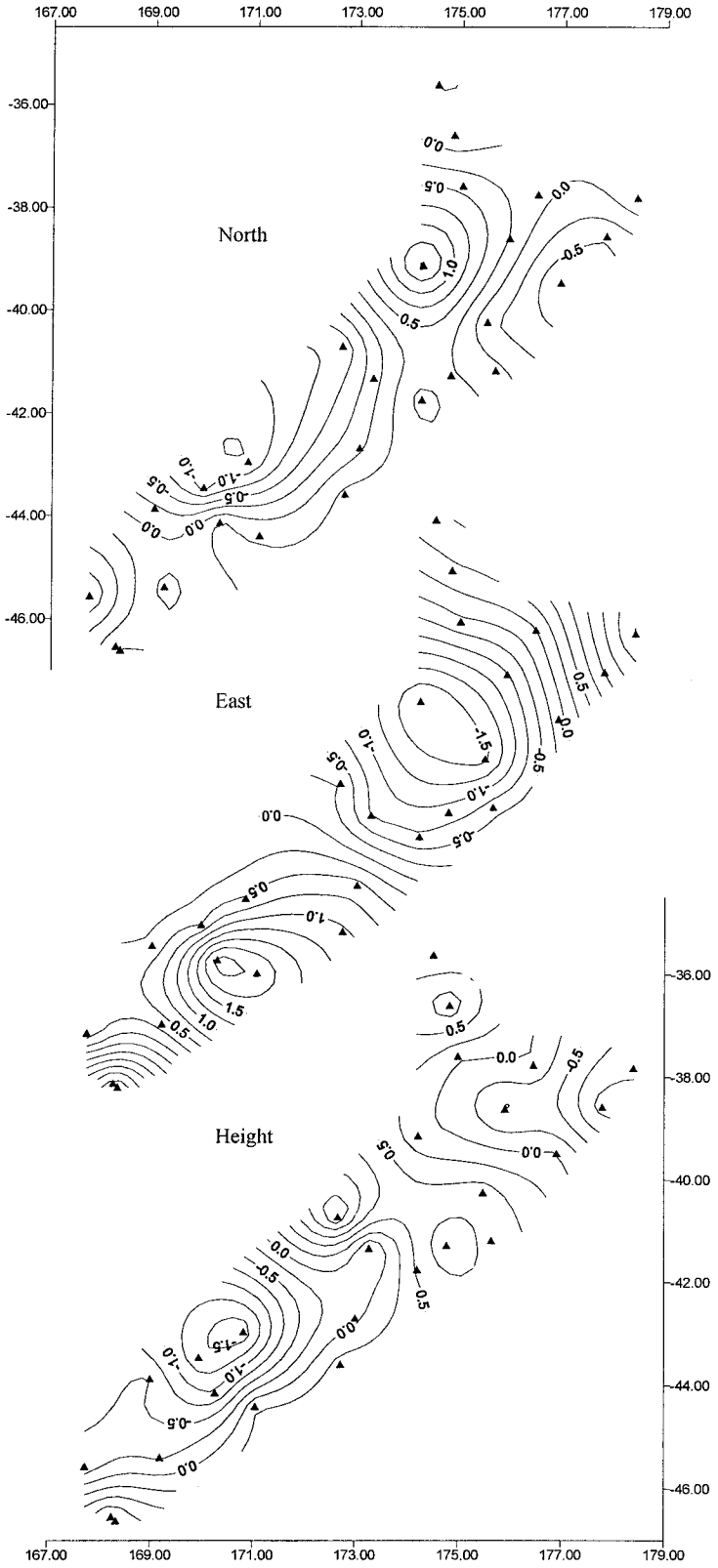

Figure 5 - 7 : Derived Generalised Method Transformation difference results as contour maps (units = metres). Triangles represent March 1993 GPS stations (see Figure 3-1).

Spatially comparing the differences between the generalised model (Figure 5-7) and the derived 7 parameter similarity transformation (Figure 5-6) show that there is high correlation between the east and height components. The north component of the generalised model still has the minimum and maximum differences in the same areas as the 7 parameter, except that now the range of the differences, has been reduced and the differences are a smoother field.

5.5.6 Results using velocities and the Generalised Model

The Composite Matrix parameters, determined after applying the NUVEL1A rates to the NZGD49 coordinates (Table 5-11), were applied to the NZGD49 coordinates of Appendix K after the NUVEL1A rates had been applied, resulting in ITRF93 coordinates. These derived ITRF93 coordinates were converted to WGS84 by the parameters in Table 5-12 to allow comparison between the other transformation techniques as was described in Section 5.5.4. The differences in the WGS84 coordinates are summarised in Table 5-18 (in the sense Generalised Model based minus ITRF93 determinations).

Table 5-18 shows that the north component rms improves by using the Generalised Model parameters determined with the NUVEL1A rates (Table 5-11) over those determined without the NUVEL1A rates (Table 5-10). There is negligible difference between either using or not using the NUVEL1A rates when comparing the east component. The relative motion between the Pacific and Australian Plates across New Zealand is primarily in the east/west component (Figure 2-4). The lack improvement in the east component therefore indicates that the velocity model of NUVEL1A is unable to remove the relative motion sufficiently to improve the accuracy of the transformed coordinates. When an improved velocity model for New Zealand is available then it is expected that the east component results generated by incorporating the velocity model will improve. As was predicted in Section 5.4.3.6 the height component does not change due to the application of the NUVEL1A velocities as the NUVEL1A model contains no rates for uplift.

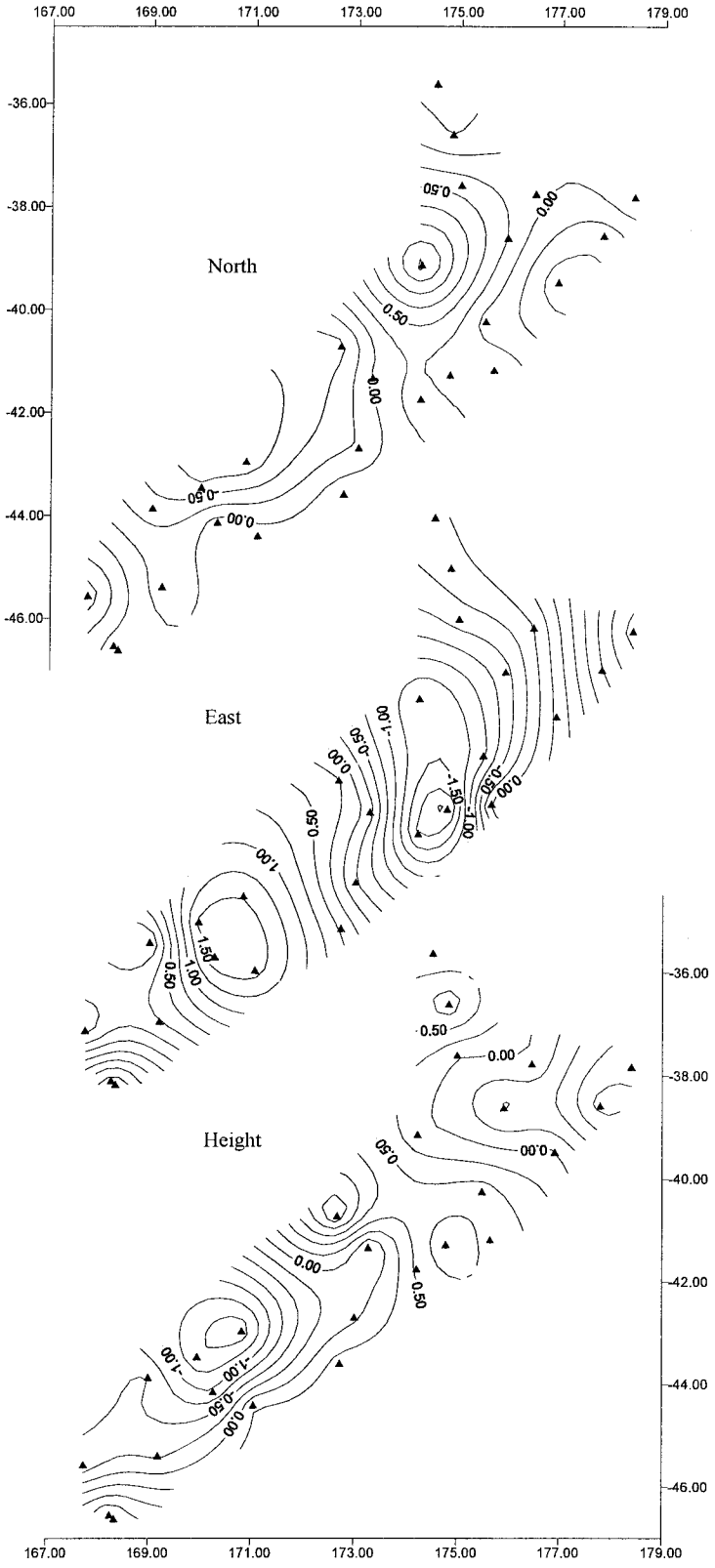

Figure 5 - 8 : Derived Generalised Method Transformation difference results as contour maps (units = metres) when Nuvel1a velocities for 50 years are applied to the NZGD49 coordinates. Triangles represent March 1993 GPS stations (see Figure 3-1).

Comparison of Figures 5-7 and 5-8 show that spatially the differences for the height component is unchanged. For the north component the minimum and maximum differences are in the same areas, except that by applying the velocities the lower half of the South Island has a considerably smoother field. The east component has been changed significantly through the middle east/west section of the country due to NUVEL1A assuming an abrupt plate boundary rather than a transition zone in this region.

The use of a velocity model to remove time dependant distortions in networks highlights the fact that transformation parameters are between two sets of coordinates at specific epochs. For coordinates that are not at the epoch used to determine the transformation parameters one should apply a velocity model to the coordinates to convert them to the transformation parameters reference epoch before applying the transformation parameters. If this is not done errors will appear in the shear terms of $\boldsymbol{M}$. If the transformed coordinates are not at the epoch required then a velocity model should be applied to the coordinates to convert them to the required epoch. As the transformation parameters are between fixed epochs they do not need to be updated if the velocity model is regularly maintained.

5.5.7 Discussion of results

In section 5.5 it was shown that different transformation options are available to convert ITRF93 and WGS84(G730) coordinates to NZGD49 coordinates. None of the parameter sets tested could produce coordinates that had all residuals less than 1.6 m, 2.1 m and 1.7 m in the north, east and height components respectively. This accuracy of approximately 2.0 m meets the requirements of classification (i) (Section 5.1) and is sufficient for many mapping applications and the GIS/LIS applications.

The application of a velocity model combined with the 12 parameter generalised model, developed during this research, produced the best transformation results when compared against the other parameters tested. The NUVEL1A velocities apply only to rigid plates. Their ability to accurately and sufficiently model the real motion occurring across New

Zealand must be questioned and therefore they are unable to remove the effects of heterogenous strain prior to the computation of the transformation parameters. Further improvements are expected when new velocity models are developed for New Zealand. It is therefore concluded that the generalised model combined with a new velocity model shows the most potential out of those methods tested in this research of meeting the sub-metre level accuracy requirements of classification (ii) (Section 5.1).

Of the previously published transformation options the Mackie-based parameters produce the smallest residuals at the test sites, with a maximum difference in the north and east components of 2.5 m and 2.2 m in height. The superiority of the derived seven parameter transformation results over the Mackie-based parameters is probably due to:

i) Mackie relied on lower quality Doppler observations and realization of WGS72 compared to the higher quality GPS observations and realization of WGS84(G730) available for this research.
ii) Mackie's results would be subjected to serious degradation by the continuing crustal deformation which has occurred since they were published in 1982.
iii) It was necessary to use supplementary work, which would increase errors, to bridge the WGS72 system used by Mackie and the ITRF93 system used for this research.

Since most surveying, geodesy and geophysical applications today require absolute positioning at a higher level of accuracy than ±2 m, it is recommended that new transformation parameters based on a new velocity model be developed to allow the transformation of coordinates between NZGD49 and an ITRF. When the velocity model and the transformation parameters can convert coordinates between NZGD49 and an ITRF with better than a 0.25 m accuracy this would provide a link between the old and new systems for all but the most demanding applications and meet the requirements of classification (iii) (Section 5.1).

It is worth commenting separately on the seven parameter similarity and MRE transformation methods tested in the previous sections.

The seven parameter similarity based transformation methods are not able to transform coordinates to better than approximately 2.2 m in the north component and 2.1 m in the east component (Table 5-18). This is most likely to be due to the magnitude of the non-linear distortions that are present in NZGD49, as reported by Bevin and Hall (1994), which cannot be modelled by the similarity transformation method. Therefore these nationwide derived parameters represent a mean transformation that are unable to account for local variations. Their value lies in their national applicability and that they are supported in most surveying, engineering and GIS/LIS software. The use of a velocity model prior to determining the seven similarity based transformation parameters may reduce the residuals on the transformed coordinates. It is not expected that these results would equal the twelve parameter generalised matrix method since it is able to account for strain between the networks.

The DMA MRE was developed using Doppler and NZGD49 coordinates, both of which have similar error budgets. The MRE method if developed with a better distribution of stations, with one system dominating the error budget and better consideration of the high order terms, may be able to accommodate the distortions of NZGD49 and yield a transformation system at the sub-metre level. One disadvantage of the MRE method when compared to the generalised method is that the software code for the MRE is very specific whereas the generalised method code can be written to also allow seven parameter similarity and block shift (three translation parameters) transformations.

A common feature between the DMA and Mackie based transformation results when used to convert between WGS84 and NZGD49 coordinates, is the mean easting difference of approximately 0.8 m. The main source of this bias is considered to be due to poorly defined UT1 values at both the time the NZGD49 astronomic observations were made and when the Doppler coordinates in terms of WGS72 were established. Another possible source of this error could be an error in any one of the sets of transformation parameters in Table 5-12. There is not a similar bias in the northing differences, which implies polar motion was known to sufficient accuracy during the establishment of NZGD49. The DMA transformations had a mean height difference of approximately 6.0 m, while the Mackie based transformation had approximately a 2.0 m

bias. These different ellipsoidal height biases are most probably due to the different geoid models used to convert the orthometric heights to ellipsoidal heights before determining the transformation parameters. In this thesis the geoidal heights were computed using the OSU91A GGM (Section 5.4.3) and when combined with the seven parameter transformation model and the generalised method of this research the height biases were not as apparent.

5.6 Review of transformation parameters

As already noted, the seven parameter similarity transformation method, on a New Zealand wide basis, is not able to transform coordinates (WGS84 / ITRF93 to NZGD49) with better than 2.2 m accuracy. This is primarily due to the inability of this method to account for non-linear distortions in either of the networks involved in the transformation, the crustal deformation that has occurred over the last 40 years and the difference in axial scales.

The MRE of Section 5.3.4 may be able to produce higher accuracy New Zealand wide transformed coordinates if redetermined equations were generated between a densified set of ITRF93 coordinates and NZGD49 coordinates. It should be noted that from a survey of the literature the MRE technique of transforming coordinates is currently not widely used, if at all, in New Zealand. The ability of the MRE to account for an average crustal motion over the period is implicit in the zero order offsets.

The derived 12 parameter generalised model combined with the NUVEL1A velocity model produced the smallest residual transform coordinates results when compared against the other parameters tested. The transformed coordinates had rms values of 0.5 m, 1.1 m and 0.8 m in the north, east and height components respectively (Table 5-18). When new parameters are computed based on the generalised method and incorporating an improved velocity model for New Zealand it is envisaged that higher accuracy New Zealand wide transformed coordinates will result. It is anticipated that the use of the generalised method with a new velocity model is the most likely approach which will enable coordinates to be transformed between NZGD49 and ITRF93 with residuals less than a metre. This approach is recommended over the development of new parameters

for an MRE as the generalised approach could be more readily incorporated into software packages to allow both the conventional similarity parameters and the composite matrix parameters to be used in the same computer code.

Reilly (1996) has investigated the application of polynomial interpolation, weighted-sum interpolation and least-squares collocation (LSC) for transforming between NZGD49 coordinates and any future geocentric Cartesian coordinate system. The investigations were based on theoretical data, for transforming coordinates within a small number of first order stations (between 3 and 12). The recommendation was that both weighted-sum interpolation and LSC both warrant further testing on real data. It is to be noted that there is a close similarity between Reilly's polynomial approach and the MRE methods of DMA. However, Reilly (*ibid.*) considers that there is no point in trying to develop large scale transformation parameters to cover the whole country. The generalised method would also produce smaller residuals if regional parameters were determined however a national parameter set is preferred for the following reasons.

i) If a single transformation technique and parameters can be developed to meet sub-decimetre coordinate accuracy across the whole country, then confusion about which parameters need to be applied in different regions would be avoided.
ii) Additionally one national set of parameters would eliminate the problem of discontinuities at the boundaries between regional parameters.

One problem with the transformation techniques discussed so far (especially for the MRE and similarity transformation, and to a less extent weighted-sum interpolation and LSC) is that they all rely on the fitting of data to a mathematical model which explicitly defines a continuous function in two space variables. Assumptions in the modelling are usually simplistic, precluding the analysis of highly variable data, as might be encountered with geodetic data gathered by different observers, with differing instruments and over various epochs (Dewhurst, 1990).

To overcome the need to define a model, Dewhurst (*ibid.*) has applied the technique of minimum curvature to the transformation of coordinates between various geodetic datums. This approach mathematically minimises the total curvature, or rate of bending,

associated with a smooth surface describing the shift values between datums. Besides the advantage of not having to define the exact form of the mathematical function, it is also unnecessary to have a complete knowledge of the systematic and random errors in the data. Dewhurst (*ibid.*) implemented this approach for transforming data between the North American Datum of 1927 (NAD27) and the North American Datum of 1983 (NAD83). Comparison of the accuracy of the transformations was reported to represent at least an order of magnitude improvement over the traditional methods of Molodenskii and the MRE as implemented by the DMA for transforming NAD27 to WGS84. WGS84 is a datum that is almost identical in ellipsoidal parameters and definition to NAD83 (DMA, 1987a). For the conterminous United States the minimum curvature approach introduced no more than approximately 0.15 m (1σ) of uncertainty.

The conterminous United States covers a significantly larger portion of the Earth's surface, with reasonably equal extents in Latitude and Longitude, when compared to New Zealand. These physical features and possibly the distribution of data used in applying the minimum curvature approach to transforming coordinates in the United States may not be suitable for the New Zealand situation. It was initially thought that the linear latitudinal nature of New Zealand coupled with its rather narrow longitudinal nature would preclude this approach. Indeed this limiting geometry was part of the rationale for adopting the rather broad regional fiducial network that was used to determine the ITRF93 coordinates from GPS, as discussed in Chapter 3.

However, the inability of simple models to account for the distortions that exist in NZGD49 either due to the observations themselves, or due to the differential deformation that has occurred since its adoption, means that models such as this should be considered if transformation rather than computation of coordinates is to be part of the adoption of a new reference system for New Zealand.

Chapter 6

Conclusions and Recommendations

This research has addressed geodetic issues associated with the establishment of a new three dimensional, homogeneous geodetic reference system for New Zealand, based on GPS data. The research was timely because of new positioning technology (eg. GPS) and the effect of earth deformation on New Zealand's horizontal geodetic datum (NZGD49) and multiple vertical datums.

Any new reference system adopted for New Zealand is likely to be based primarily on GPS data, which can be processed in terms of global geocentric reference frames. This will avoid most of the inter-system and inter-technique biases contained in the present horizontal and multiple vertical datums. As an important step in the process of defining a new reference system for New Zealand, this research sheds light on the problem of transforming between global geocentric reference systems and the non-geocentric NZGD49. This problem needs to be addressed because of the widespread use of GPS for positioning and navigation, and especially when used in conjunction with Geographic Information Systems.

6.1 Anticipated Future Geodetic Requirements

The history and state of the NZGD49 and anticipated future demands of NZGD49 users was investigated. This highlighted that a new homogeneous horizontal geodetic datum is required for New Zealand and that this new datum should be a geocentric reference system. Currently the highest quality global geocentric terrestrial reference frame is that produced by IERS. It is recommended that a new geodetic reference system for New Zealand have its relationship to an IERS terrestrial reference frame (ITRF) defined.

A new reference system based on GPS observations will be able to provide a three dimensional, homogeneous geodetic datum for New Zealand. One problem with a GPS-

based reference system is that the heights established will be ellipsoidal heights. Ellipsoidal heights bear no relationship to the direction that fluids naturally flow due to the influence of gravity. For this reason a consistent national orthometric height datum needs to be established in conjunction with the GPS based reference system, and a national geoid model should be defined with respect to GRS80.

New Zealand is situated across the active Australian and Pacific tectonic plate boundary, which is converging at approximately 50 mm/yr. If this crustal deformation is not accounted for in a new geodetic reference system then it can be expected that the reference system will be subjected to continually increasing distortion. It is recommended that a new geodetic reference system have mechanisms incorporated into the design, such as a velocity model, so that the deformation can be accounted for (ie. the reference system be dynamic).

To enable observations from different campaigns to be combined, the motion of each stations ground mark needs to be known. It is therefore recommended that an improved velocity model for New Zealand be developed, or at least the velocity of each station be estimated during the adjustment process.

6.2 Geocentric Coordinates

The New Zealand 1st order 2000 March 1993 GPS campaign was processed using the GAMIT/GLOBK software suite. The results provide ITRF93 coordinates, at the mid observation epoch of 1993.200 with formal uncertainties of 2 cm (1σ), for 26 sites distributed across New Zealand.

Sites that were observed with two four-hour occupations per day produced inferior results compared to sites with 9 hour continuous observations, although continuous 24 hour observations produced superior coordinate uncertainties. The sites with 24 hour observations were also the sites with the larger number of re-occupations; conversely the sites with two four-hour observations had less re-occupations. Establishing whether the improvement in coordinate uncertainties was due to the length of observation or the number of re-occupations was not possible. As one would expect, it was found that

increasing the observation period and the number of days a site was occupied resulted in improved coordinate uncertainties. It is recommended that 24 hour GPS data be collected for high precision geodetic surveys, and there should be a minimum of three days of consecutive observations.

The practice of switching off the GPS receiver and altering the antenna height (as was the procedure for the March 1996 campaign) to detect gross errors in the measurement of the antenna height above the ground mark, is not recommended. It is instead recommended that antenna heights be validated by check measurements. This recommended method minimises the number of times the receiver clock characteristics need to be resolved per day and allows the receiver clock to better stabilise with the longer operation periods. It also means that the biases between the days are constant.

To attach the New Zealand March 1996 GPS campaign to ITRF93, it was necessary to process the New Zealand data with GPS data from sites (which had previously determined ITRF93 coordinates) that surround New Zealand. Four sites, referred to as Regional Fiducial sites, were used for this attachment (two in Australia, one in Tahiti and one in Antarctica). One of the Australian regional fiducial sites (DS42) is an IGS core site. On DOY 070, when only 7 hours of data from DS42 was available, the quality of the results were inferior to the results on those days when one of the other three regional fiducial sites were unavailable. It is recommended that future processing of New Zealand GPS data in terms of an ITRF, maintain a minimum of four regional fiducial sites in the network. The sites should be chosen considering their distribution around New Zealand (ie. situated in neighbouring countries) and the reliability to which they are known in terms of an ITRF.

Since processing the New Zealand GPS data in the GAMIT/GLOBK suite there have been a number of new features incorporated into the software. These features include antenna phase centre modelling, full Earth and Ocean Tide Loading models, improved orbit modelling and multiple zenith delay parameters. It is recommended that these features be investigated in future processing of GPS data for New Zealand datum

maintenance or development as they have the potential to improve the coordinate accuracy, especially in the height component.

6.3 Geoid Model

The conversion between ellipsoidal and orthometric heights requires the geoid height to be known. Four global geopotential models (GGM) were used to compute the geoid height at control stations (ie. stations that have both ellipsoidal and orthometric heights defined) in the lower North Island test area. Comparison of results showed that the joint GSFC and DMA model (EGM96) produced superior results to the other GGM's including the commonly used OSU91A.

The geoid heights computed from a GGM can be improved upon by combining the GGM information with local gravity data. Investigations into the determination of a local geoid model, by combining a GGM with local gravity data for the New Zealand test area, were undertaken using the UNSW gravity (GRAV) software suite. The GRAV suite is based on the Ring Integration (RINT) technique. As part of this research significant improvements were made to the capabilities and efficiencies of the GRAV suite. Improvements included :

- removal of VAX specific fortran code to allow compilation on DOS and UNIX operating systems,
- converted from command line input to batch files to allow automation of the processing and the inclusion of on-line help files,
- improved data searching routines,
- new file formats to reduce the size of data files,
- option to use DEM's in the computation of the compartment height, and
- incorporation of kernel modifications designed to reduce truncation errors due to the integration limit.

RINT allows local gravity data surrounding the computation point to be varied based on the radius of the spherical cap of the data centred on the point where the geoid height is required. Tests revealed that as the radius was increased (from 0.0° up to either 1.5° or

2.0°), the RINT based results contained an oscillatory nature (W-curve in appearance) with respect to the control stations. That is, the inclusion of additional gravity data did not always result in improved geoid heights.

Investigations into the source of this W-curve indicated that it may be dependent on the GGM. This conclusion was supported by the reduction in magnitude of the W-curve when using recently released GGM. However, further investigations into the source of the W-curve are required and should include varying the radius for local gravity data inclusion in other gravimetric geoid techniques, such as Fast Fourier Transforms and Least Squares Collocation.

By comparing the gravimetrically-derived geoid heights with the geometrically-derived control values, it is possible to determine an optimum radius to which gravity data should be integrated for the analysed region. For the lower North Island test area the optimum radius of the spherical cap was determined to be 0.3° (≅ 30 km).

The RINT technique requires the mean compartment height to restore the free-air anomaly from the Bouguer anomaly. The RINT software was modified to allow either DEM heights or the heights of the seven closest gravity observations, to be used to calculate the mean compartment height. The use of the DEM heights produced superior geoid heights in the test area. It is therefore recommended that a DEM be used in the computation of geoid heights by the RINT technique.

One consequence of limiting the inclusion of local gravity data to a spherical cap is that the contribution of the gravity data beyond that radius is disregarded. The effect of neglecting this data is referred to as the "truncation error". The truncation error is theoretically reduced by modifying the Stokes' kernel. Investigations into the effect of modifying the Stokes' kernel to reduce the truncation error for the RINT technique were conducted. The effect of the tested modifications on the geoid heights in the New Zealand test area are inconclusive - any change is probably below the level of the noise in the control data. Until there is further testing of the effect of modifying the Stokes'

kernel to reduce truncation error in the RINT technique, it is recommended that the RINT technique be used without modification for truncation error.

The computation of a high resolution geoid model (eg. 5 km grid spacing) is required to enable ellipsoidal heights to be converted to orthometric heights. From the investigations in the lower North Island test area, the combination of GPS-derived ellipsoidal heights with RINT generated gravimetric geoid heights can produce orthometric heights which are capable of meeting New Zealand's third (and probably even second) order levelling specifications. It is therefore recommended that a gravimetric geoid model be computed for New Zealand once suitable DEM are available for the nation, with Land Information New Zealand probably being the correct organisation to undertake this task.

6.4 Transformation Methods

In New Zealand there are two main types of transformations available for use in transforming between NZGD49 and the more recent Cartesian systems, such as WGS84 and ITRF93. The first, or most common type, is the similarity transformation. It is commonly found as a seven parameter transformation. The second type is the MRE transformation.

Of the two types, the similarity transformation was the most extensively examined, as it is not only mathematically rigorous but has the potential of easily being encoded and used inside GIS/LIS and navigation applications. It was determined that the full seven parameter solution yielded the better results, with maximum differences of just over 2 m per component. Reducing the number of parameters, more specifically, equating the parameters to *a priori* estimates (zero for rotations about the X and Y axes), had negligible effect, indicating that the horizontal only NZGD49 was correctly orientated through astronomical observations.

Some older similarity transformations, especially that of Mackie (1982), were found to be still useable although non-optimal. The reduction in optimality being due to the passage of time and the accumulation of deformation during the ensuing period.

The DMA MRE was found to be deficient, especially in height. However, it is noted that this method, with updated positions and models, may have a role to play in either converting the bulk of GIS data from NZGD49 to the new, as yet undefined, reference system or in the conversion of real-time GPS positions to NZGD49.

The suitability of the Generalised model to transform between NZGD49 and WGS84 was investigated. It was found that the composite matrix determined parameters were able to convert between NZGD49 and WGS84 coordinates more accurately than the using the seven parameter similarity transformation. Further improvement in the transformed coordinates were obtained when the NUVEL1A velocity model was used to account for the deformation effects that will have occurred between NZGD49 and the 1993 GPS observations. However transformed coordinates still had rms values of 0.5m, 1.1m and 0.8m in the north, east and height components respectively. It is envisaged that with the inclusion of an improved velocity model for New Zealand the generalised method will be able to transform coordinates between NZGD49 and ITRF93 at the sub-metre accuracy level.

Since none of the investigated methods were able to provide transformation at the sub-metre level, a level necessary for the maintenance of the cadastre, further research into transformations is required. It is recommended that further research be conducted into the suitability of the minimum curvature approaches and the generalised model. It is also recommended that a nationwide velocity model be determined for New Zealand to allow the conversion of coordinates to a common epoch prior to applying a transformation method. The benefit of this work is that a single nationwide consistent transformation system would be available to transform all present NZGD49 values to the new reference system without the need to re-adjust all of the historic data.

References

Adam, J., F. Halmos and M. Varga, **1982**. On the concepts of combination of doppler and terrestrial geodetic networks. *Acta Geodaetica, Geophysica et Montanistica, Hungarian Academy of Sciences*, Vol. 17, No. 2, pp. 147-170.

Anderson, H., T. Webb and J. Jackson, **1993**. Focal mechanisms of large earthquakes in the South Island of New Zealand: implications for the Pacific-Australia plate motion. *Geophysical Journal International*, Vol. 115, No. 3, pp. 1032-1054.

Anderson, H. and T. Webb, **1994**. New Zealand seismicity: patterns revealed by the upgraded national seismograph network. *New Zealand Journal of Geology and Geophysics*, Vol. 37, pp. 477-493

Appelbaum, L.T., **1982**. Geodetic datum transformation by multiple regression equations. *Proceedings of the Third International Geodetic Symposium on Satellite Doppler Positioning*, New Mexico State University, Physical Science Laboratory, Las Cruces, New Mexico, USA, 8-12 February.

Balasubramania, N., **1994**. *Definition and Realisation of a Global Vertical Datum. Report No. 427*, Department of Geodetic Science and Surveying, Ohio State University, USA.

Bannister, A. and S. Raymond, **1984**. *Surveying*. 5th edition, Pitman Publishing, Bath, Great Britain.

Badekas, J., **1969**. *Investigations Related to the Establishment of a World Geodetic System. Report No. 124*, Department of Geodetic Science and Surveying, Ohio State University, USA.

Berryman, K.R., S. Beanland, A.F. Cooper, H.N. Cutten, R.J. Norris and P.R. Wood, **1992**. The alpine fault, New Zealand: variation in quaternary structural style and geomorphic expression. *Annales Tectonicae*, Supplement 6, pp. 126-163.

Beavan, J., M. Moore, C. Pearson, R. Walcott, G. Blick, C. Meertens and T. Koczynski, **1996**. An overview of GPS experiments in the New Zealand region. *Presented at the Western Pacific Geophysics Meeting*, Brisbane, Australia, July 23-27.

Bevin, A.J., P.M. Otway and P.R. Wood, **1984**. *Geodetic Monitoring of Crustal Deformation in New Zealand. Miscellaneous Series 7*, Royal Society of New Zealand, pp. 13-60.

Bevin, A.J. and J. Hall, **1994**. The review and development of a modern geodetic datum. *Proceedings of Commission 5, XX FIG Congress*, 5-12 March, Melbourne, Australia.

Blick, G., **1996**. *New Zealand Standards of Accuracy for Geodetic Surveys. Survey System - Immediate Report No. 96/1*, Department of Survey and Land Information, Wellington, New Zealand.

Bomford, G., **1980**. *Geodesy*, 4th edition., Claredon Press, Oxford, England.

Boucher, C. and Z. Altamimi, **1993**. Development of a Conventional Terrestrial Reference Frame, *in* D.E. Smith and D.L. Turcotte (Eds), *Contribution of Space Geodesy to Geodynamics: Earth Dynamics. Geodynamical series Vol. 24*, American Geophysical Union Books Board, Washington, USA.

Boucher, C., Z. Altamimi and L. Duhem, **1992**. *ITRF91 and its Associated Velocity Field. IERS Technical Note 12*, Central Bureau of IERS, Observatoire de Paris, Paris, France.

Boucher, C., Z. Altamimi and L. Duhem, **1993**. *ITRF92 and its Associated Velocity Field. IERS Technical Note 15*, Central Bureau of IERS, Observatoire de Paris, Paris, France.

Boucher, C., Z. Altamimi and L. Duhem, **1994**. *Results and Analysis of the ITRF93. IERS Technical Note 18*, Central Bureau of IERS, Observatoire de Paris, Paris, France.

Bracewell, R., **1986**. *The Fourier Transform and its Applications*. 2nd ed., McGraw-Hill, New York, USA.

Brouwer, F.J.J. and E.J. de Min, **1994**. On the Definition of a European Vertical Datum. Gubler E. and Hornik H. (Eds.), *Report on the Symposium of the IAG Subcommission for the European Reference Frame (EUREF) held in Warsaw 8-11 June*. pp 176-185. Veroffentlichungen der Bayerischen Kommission fur die Internationale Erdmessung, Heft 54, Munchen.

Bursa, M., **1965**. Fundamentals of the theory of geometric satellite geodesy. *Travaux de l'institut Geophysique de l'academie Teheco-slovaque des Sciences*, Vol. 241.

Cohen, E.R. and B.N. Taylor, **1990**. The fundamental physical constants. *Physics Today*, Vol. 43, No. 8, pp. 9-13.

Cole, J.W., **1990**. Structural control and origin of volcanism in the Taupo volcanic zone, New Zealand. *Bulletin of Vulcanology*, Vol. 52, No. 6, pp. 445-459.

Collins, J. and A. Leick, **1985**. Analysis of macrometer networks with emphasis on the montgomery (PA) County Survey. *Proceedings of the First International Symposium on Precise Positioning with the Global Positioning System*, Rockville, Maryland, 15-19 April, pp. 677-693.

Cox, A. and R.B. Hart, **1986**. *Plate Tectonics: How it Works*. Blackwell Scientific Publications, Victoria, Australia.

Crook, C., **1995**. *User Manual for SNAP - A Survey Network Adjustment Program.* version 2.1, September, Research and Development, Department of Survey and Land Information, Wellington, New Zealand.

Cross, P.A. 1983. *Advanced Least Squares Applied to Position-Fixing. Working paper No. 6*, Department of Land Surveying, North East London Polytechnic, Essex, England.

Darby, D.J., and C.M. Meertens, **1995**. Terrestrial and GPS measurements of deformation across the Taupo back arc and Hikurangi forearc regions in New Zealand. *Journal of Geophysical Research*, Vol. 100, No. B5, pp. 8221-8232.

Davis, J.L., T.A. Herring, I.I. Shapiro, A.E.E. Rogers and G. Elgered, **1985**. Geodesy by radio interferometry: effects of atmospheric modeling errors on estimates of baseline length. *Radio Science*, Vol. 20, pp. 1593-1607.

de Min, E., **1995**. A comparison of Stokes numerical integration and collocation and a new combination technique. *Bulletin Geodesique*, Vol. 69, pp. 223-232.

DeMets, C., R.G. Gordon, D.F. Argus and S. Stein, **1990**. Current plate motions. *Geophysical Journal International*, Vol. 101, pp. 425-478.

DeMets, C., R.G. Gordon, D.F. Argus and S. Stein, **1994**. Effect of recent revisions to the geomagnetic reversal time scale on estimates of current plate motions. *Geophysical Research Letters*, Vol. 21, No. 20, pp. 2191-2194.

Dewhurst, W.T., **1990**. *The Application of Minimum-Curvature-Derived Surfaces in the Transformation of Positional Data from the North American Datum of 1927 to the*

North American Datum of 1983. NOAA Technical Memorandum NOS NGS-50, Rockville, USA.

DMA, **1987a**. *Supplement to Department of Defense World Geodetic System 1984 Technical Report: Part I - Methods, Techniques, and Data Used in WGS84 Development. DMA TR 8350.2-A*, first edition, December 1.

DMA, **1987b**. *Supplement to Department of Defense World Geodetic System 1984 Technical Report: Part II - Parameters, Formulas, and Graphics for Practical Application of WGS84. DMA TR 8350.2-B*, first edition, December 1.

DMA, **1991**. *Department of Defense World Geodetic System 1984: Its Definition and Relationship with Local Geodetic Systems. DMA TR 8350.2*, second edition, September 1.

Dobrin, M.B., **1976**. *Introduction to Geophysical Prospecting*, 3rd edition. McGraw-Hill, USA.

Engelis, T., R.H. Rapp and C.C. Tscherning, **1984**. The precise computation of geoid undulations differences with comparison to results obtained from the global positioning system. *Geophysical Research Letters*, Vol. 1, No. 9, pp. 821-824.

Featherstone, W.E., **1992**. *A GPS Controlled Gravimetric Determination of the Geoid of the British Isles*. D.Phil thesis, Oxford University, England.

Featherstone, W.E., K.F. Zhang and M.P. Stewart, **1995**. A study of the behaviour of the Earth's gravity field in Australia. *Presented at GB11I-15, IUGG XXI General Assembly*, Boulder, Colorado, USA, July 2-14.

Featherstone, W.E. and J. Evans, **1996**. A Meissl-Molodenskii modified Stokes kernel for gravimetric geoid computations. Submitted to the *Journal of Geophysical Research*.

Foley, J. and A. van Dam, S. Feiner and J. Hughes, **1990**. *Computer Graphics: Principles and Practice*. 2nd ed., Addison-Wesley, New York, USA.

Georgiadou, Y. and E.W. Grafarend, **1983.** The small scale structure of geometry and gravity space I, *Bull. di Geod. e Sci. Aff.* Anno XLII No. 2.

Gilliland, J.R., **1986**. Heights and GPS. *The Australian Surveyor*, June, Vol. 33, No. 4, pp. 277-283.

Gilliland, J.R., **1987**. A review of the levelling networks of N.Z. *New Zealand Surveyor*, Vol. 32, No. 271, pp. 7-15.

Gilliland, J.R., **1988**. *Research Contract R87/496*. School of Surveying, South Australian Institute of Technology, Adelaide, Australia, unpublished project report.

Gilliland, J.R., **1990**. A gravimetric geoid for the New Zealand region. *New Zealand Surveyor*, Vol. 32, No. 276, pp. 591-595.

Gilliland, J.R., **1994**. Geoid undulations and GPS heights in the Melbourne region. *Australian Journal of Geodesy, Photogrammetry and Surveying*, Vol. 61, December, pp. 41-48.

Goring, D.G. and R.G. Bell, **1996**. Distilling information from patchy tide gauge records: the New Zealand experience. *Marine Geodesy*. Vol. 63, pp. 63-76.

GMS, **1996**. *User Interviews*, Geodetic Management System User Requirements, Land Information New Zealand, Wellington, New Zealand.

Grant, D.B., **1990**. *Combination of Terrestrial and GPS Data for Earth Deformation Studies. UNISURV S-32*, School of Geomatic Engineering (formerly Surveying), The University of New South Wales, Sydney, Australia.

Grant, D.B., **1995**. A dynamic datum for a dynamic cadastre. *Trans Tasman Surveyor*. Vol. 1, No. 1, pp. 22-28.

Grant, D.B. and M.B. Pearse, **1995**. Proposal for a dynamic national geodetic datum for New Zealand. *Presented at IUGG XXI General Assembly*, Boulder, Colorado, USA, July 2-14.

Groten, E. and T. Muller, **1990**. Combined sea surface determination based on various geometric and dynamic techniques. *Marine Geodesy*, Vol. 14, pp. 185-195.

Gruber, T. and M. Anzenhofer, **1993**. The GFZ 360 gravity field model, presented at *the European Geophysical Society meeting*, Wiesbaden.

Gubler, E. and D. Schneider, **1994**. Propositions for Defining a modern national geodetic reference frame. Gubler E. and Hornik H. (Eds.), *Report on the Symposium of the IAG Subcommission for the European Reference Frame (EUREF) held in Warsaw 8-11 June*. pp 162-164. Veroffentlichungen der Bayerischen Kommission fur die Internationale Erdmessung, Heft 54, Munchen,

Hammer, S., **1939**. Terrain corrections for gravimeter stations. *Geophysics*, Vol. 4, No. 3, pp. 184-194.

Harvey, B.R., **1985**. *The Combination of VLBI and Ground Data for Geodesy and Geophysics. UNISURV S-27*, School of Geomatic Engineering (formerly Surveying), The University of New South Wales, Sydney, Australia.

Harvey, B.R., **1986**. Transformation of 3D co-ordinates. *The Australian Surveyor*, June, Vol. 33, No. 2, pp. 105-125.

Harvey, B.R., **1994**. *Practical Least Squares and Statistics for Surveyors. Monograph No. 13*, Second Edition, School of Geomatic Engineering (formerly Surveying), The University of New South Wales, Sydney, Australia.

Heck, B., **1990**. An evaluation of some systematic error sources affecting terrestrial gravity anomalies. *Bulletin Geodesique*, Vol. 64, pp. 88-108.

Heiskanen, W.A. and H. Moritz, **1967**. *Physical Geodesy*. Freeman & Co., San Francisco, USA. (corrected reprint of 1993, Institute of Physical Geodesy, Technical University, Graz, Austria).

Herring, T.A., J.L. Davis and I.I. Shapiro, **1990**. Geodesy by radio interferometry: the application of kalman filtering to the analysis of very long baseline interferometry data. *Journal of Geophysical Research*, Vol. 95, pp. 12561-12581.

Herring, T.A., **1994**. *Documentation for the Global Kalman filter VLBI and GPS Analysis Program (GLOBK)*. Version 3.2, Massachusetts Institute of Technology, Cambridge, Massachusetts, USA.

Higgins, M.B., **1987**. *Transformation from WGS84 to AGD84 - An Interim Solution.* Internal report of the Department of Mapping and Surveying, Queensland, Australia.

Higgins, M.B., M.B. Pearse and A.H.W. Kearsley, **1996**. Using digital elevation models in the computation of geoid heights. *Geomatics Research Australasia*, No. 65, pp. 59-74.

Holloway, R.D., **1988**. *The Integration of GPS Heights into the Australian Height Datum. UNISURV S-33*, School of Geomatic Engineering (formerly Surveying), The University of New South Wales, Sydney, Australia.

IERS, **1996**. *1995 International Earth Rotation Service Annual Report*. Central Bureau of IERS, Observatoire de Paris, Paris, France.

Jekeli, C., **1981**. Modifying Stokes' function to reduce the error of geoid undulation computations. *Journal of Geophysical Research*, Vol. 86, No. B8, pp. 6985-6990.

Jones, B.M., **1981**. The origin of the New Zealand geodetic datum 1949. *New Zealand Surveyor*, Vol. 30, No. 1, pp. 8-10.

Kaplan, E.D. (Ed.), **1996**. *Understanding GPS Principles and Applications*. Artech House, Norwood, Massachusetts, USA.

Kearsley, A.H.W., **1984**. *Precision Limitations and Data Requirements for the Determination of Relative Geoid Heights from Gravimetry. Report No. 26*, Department of Geodesy, Institute of Geophysics, University of Uppsala.

Kearsley, A.H.W., **1985**. Towards optimum evaluation of the inner zone contribution to the geoidal parameters. *Australian Journal of Geodesy, Photogrammetry and Surveying*, Vol. 42, pp. 75-98.

Kearsley, A.H.W., **1986a**. Data requirements for determining precise relative geoid heights from gravimetry. *Journal of Geophysical Research*, Vol. 91, No. B9, pp. 9193-9201.

Kearsley, A.H.W., **1986b**. The determination of precise geoid height differences using ring integration. *Proceedings of the International Symposium on the definition of the Geoid*, Vol. 2, Florence, Italy, 26-30 May, pp. 433-476.

Kearsley, A.H.W., **1988**. Tests on the recovery of precise geoid height differences from gravimetry. *Journal of Geophysical Research*, Vol. 93, No. B6, pp. 6559-6570.

Kearsley, A.H.W. (ed.), **1993**. *Contributions to Geoid Evaluations and GPS Heighting. UNISURV S-43*, School of Geomatic Engineering, The University of New South Wales, Sydney, Australia.

King, R.W., J. Collins, E.G. Masters, C. Rizos and A. Stolz, **1985**. *Surveying with GPS. Monograph No. 9*, School of Geomatic Engineering (formerly Surveying), The University of New South Wales, Sydney, Australia.

King, R.W. and Y. Bock, **1994**. *Documentation for the GAMIT GPS Analysis Software*, Release 9.28, Massachusetts Institute of Technology (and Scripps Institution of Oceanography), Cambridge, Massachusetts, USA.

Krakiwsky, E.J. and D.B. Thomson, **1974**. Mathematical models for the combination of terrestrial and satellite networks. *Canadian Surveyor*, Vol. 28, No 5, pp 606-615.

Kumar, M., **1993**. World geodetic system 1984: A reference frame for global mapping, charting and geodetic applications. *Surveying and Land Information Systems*, Vol. 53, No. 1, pp. 53-56.

Lahmeyer, B., **1988**. Gravity field continuation of irregularly spaced data using least squares collocation. *Geophysical Journal International*, Vol. 95, pp. 123-134.

Lambeck, K., **1988**. *Geophysical Geodesy - The Slow Deformation of the Earth*. Claredon Press, Oxford, Great Britain.

Lambert, W.D. and F.W. Darling, **1936**. *Tables for Determining the Form of the Geoid and its Indirect Effect on Gravity. Special Publication 199*, U.S. Coast and Geodetic Survey, Washington, D.C., USA.

Lee, L.P., **1978**. *First-Order Geodetic Triangulation of New Zealand 1909-49 and 1973-74. Technical Series No. 1*, Dept. Lands and Survey, New Zealand.

Lemoine, F.G., D.E. Smith, R. Smith, L. Kunz, E.C. Pavlis, S.M. Klosko, D.S. Chinn, M.H. Torrence, R.G. Williamson, C.M. Cox, K.E. Rachlin, Y. M. Wang, S.C. Kenyon, R. Salman, R. Trimmer, R.H. Rapp and R.S. Nerem, **1996**. The development of the NASA GSFC and DMA joint geopotential model. *Proceedings of the International Symposium on Gravity, Geoid and Marine Geodesy*, Tokyo, Japan, September 30 - October 5.
available from: http://cddis.gsfc.nasa.gov/926/egm96/egm96.html

Li, Y.C. and M.G. Sideris, **1995**. Evaluation of 2-D and 3-D geodetic convolutions by the Hartley transform. *Geomatics Research Australasia*, No. 63, pp. 19-34.

Mackie, J.B., **1982**. *The relationship between the WGS72 doppler satellite datum and the New Zealand Geodetic Datum 1949. Report No. 178*, Geophysics Division, Department of Scientific and Industrial Research, New Zealand

Mackie, J.B., **1983**. Transformation of coordinates from the world geodetic system (WGS-72) doppler satellite datum to the New Zealand geodetic datum 1949 (NZGD-49). *New Zealand Surveyor*, Vol. 30, No. 4, pp. 412-420.

Malys, S. and J. Slater, **1994**. Maintenance and enhancement of the world geodetic system 1984. *Proceedings of ION GPS-94*, Salt Lake City, Utah, USA, 20-23 September.

Marsh, J.G., F.J. Lerch, B.H. Putney, T.L. Felsentreger, B.V. Sanchez, S.M. Klosko, G.B. Patel, J.W. Robbins, R.G. Williamson, T.L. Engelis, W.F. Eddy, N.L. Chandler, D.S. Chinn, S. Kapor, K.E. Rachlin, L.E. Braatz and E.C. Pavlis, **1990**. The GEM-T2 gravitational model. *Journal of Geophysical Research*, Vol. 95, No. B13, pp. 22043-22071.

Maxwell, E.A., **1946**. *Methods of Plane Projective Geometry Based on the Use of General Homogeneous Coordinates*, Cambridge University Press, Cambridge, England.

Maxwell, E.A., **1951**. *General Homogeneous Coordinates in Space of Three Dimensions*, Cambridge University Press, Cambridge, England.

McCarthy, D.D. (Ed.), **1989**. *IERS Standards (1989). IERS Technical Note 3*, Observatoire de Paris, Paris, France.

McCarthy, D.D. (Ed.), **1992**. *IERS Standards (1992). IERS Technical Note 13*, Observatoire de Paris, Paris, France.

McCarthy, D.D. (Ed.), **1996**. *IERS Conventions (1996). IERS Technical Note 21*, Observatoire de Paris, Paris, France.

Meissl, P., **1971**. *Preparations for the Numerical Evaluation of Second-Order Molodenskii-Type Formulas. Report No. 163*, Department of Geodetic Science and Surveying, Ohio State University, USA.

Merry , C.L., **1980**. A practical comparison of some methods for predicting point gravity anomalies. *Manuscripta Geodaetica*, Vol. 5, pp. 299-314.

Mikhail, E.M., **1976**. *Observations and Least Squares*. IEP, Dun-Donnelley, New York, USA.

Minster, J.B. and T.H. Jordan, **1978.** Present day plate motions. *Journal of Geophysical Research*, Vol. 83, pp. 5331-5354.

Molodenskii, M.S., V.F. Eremeev and M.I. Yurkina, **1962**. Methods for study of the external gravitational field and the figure of the Earth. *Israel Program for Scientific Translations*, Jerusalem.

Morgan, P., **1992**. An analysis of the Australian height datum: 1971. *The Australian Surveyor*, June, Vol. 37, No. 1, pp. 46-63.

Morgan, P., Y. Bock, R. Coleman, P. Feng, D. Garrard, G. Johnston, G. Luton, B. McDowall, M. Pearse, C. Rizos and R. Tiesler, **1996**. *A Zero Order GPS Network for the Australian Region. UNISURV S-46*, School of Geomatic Engineering, The University of New South Wales, Sydney, Australia.

Moritz, H, **1980a**. Geodetic reference system 1980. *Bulletin Geodesique*, Vol. 54, No. 3, pp. 395-405.

Moritz, H, **1980b**. *Advanced Physical Geodesy*. Abacus Press, England

Mueller, I.I., **1969**. *Spherical and Practical Astronomy as Applied to Geodesy*. Ungar Publications, New York, USA.

Mueller, I.I., **1985**. Reference coordinate systems and frames: concepts and realisation. *Bulletin Geodesique*, Vol. 59, pp. 181-188.

Nerem, R.S., C. Jekeli and W.M. Kaula, **1995**. Gravity field determination and characteristics: retrospective and prospective. *Journal of Geophysical Research*, Vol. 100, No. B8, pp. 15053-15074.

Nettleton, L.L., **1976**. *Gravity and Magnetics in Oil Prospecting*. McGraw-Hill, USA.

NZNCGG, **1991**. New Zealand Geodetic Operations 1987-90. *Report for the general assembly of the International Union of Geodesy and Geophysics*, Vienna, Austria, August. Complied by the Surveyor General for the New Zealand National Committee for Geodesy and Geophysics, Wellington, New Zealand.

Pavlis, N.K., **1988**. *Modelling and Estimation of a Low Degree Geopotential Model from Terrestrial Gravity Data. Report No. 386*, Department of Geodetic Science and Surveying, Ohio State University, USA.

Park, R.G., **1988**. *Geological Structures and Moving Plates*. Blackie Academic and Professional, Glasgow, United Kingdom.

Paul, M.K., **1973**. A method of evaluating the truncation error coefficients for geoidal height. *Bulletin Geodesique*, Vol. 47, pp. 413-425.

Pearse, M.B. and P.J. Morgan, **1995**. Dynamic coordinates for New Zealand: a progress report, *Proceedings of the NZIS Annual Conference*, Christchurch, New Zealand, 21-23 October.

Pearson, C.F., J. Beavan, D.J. Darby, G.H. Blick and R.I. Walcott, **1995**. Strain distribution across the Australian-Pacific plate boundary in the central South Island, New Zealand, from 1992 GPS and earlier terrestrial observations. *Journal of Geophysical Research*, Vol. 100, No. B11, pp. 22071-22081.

Peng, M., Li Y.C. and Sideris, M.G., **1995**. First results on the computation of terrain corrections by the 3D FFT method. *Manuscripta Geodaetica*, Vol. 20, pp. 475-488.

Rapp, R.H., **1961**. *The Orthometric Height*. M.S. Thesis, Department of Geodetic Science, Ohio State University, USA.

Rapp, R.H., **1981**. *The Earth's Gravity Field to Degree and Order 180 using SEASAT altimeter Data, Terrestrial Gravity Data and Other Data: OSU81. Report No. 322*, Department of Geodetic Science and Surveying, Ohio State University, USA.

Rapp, R.H. and R. Rummel, **1975**. *Methods for the Computation of Detailed Geoids and Their Accuracy. Report No. 233*, Department of Geodetic Science and Surveying, Ohio State University, USA.

Rapp, R.H., Y.M. Wang and N.K. Pavlis, **1991**. *The Ohio State 1991 Geopotential and Sea Surface Topography Harmonic Coefficient Models. Report No. 410*, Department of Geodetic Science and Surveying, Ohio State University, USA.

Rapp, R.H. and N. Balasubramania, **1992**. *A Conceptual Formulation of a World Height System. Report No. 421*, Department of Geodetic Science and Surveying, Ohio State University, USA.

Rapp, R.H. and R.S. Nerem, **1994**. A joint GSFC/DMA project for improving the model of the Earth's gravitational field. in: Sunkel and Marson (eds.) *Gravity and Geoid*, International Association of Geodesy Symposium No. 113, Springer-Verlag. pp. 413-422.

Rapp, R.H., **1995**. Are we ready for a degree 720 potential coefficient model? *Presented at IAG Symposium G3*, IUGG XXI General Assembly, Boulder, Colorado, USA, July 2-14.

Reilly, W.I., **1972**. New Zealand gravity map series. *New Zealand Journal of Geology and Geophysics*, Vol. 15, No. 1, pp. 3-15.

Reilly, W.I., **1973**. A conformal mapping projection with minimum scale error. *Survey Review*, Vol. 22, No. 168, pp. 57-71.

Reilly, W.I., **1990**. Horizontal crustal deformation on the Hikurangi margin. *New Zealand Journal of Geology and Geophysics*, Vol. 33, pp. 393-400

Reilly, W.I., **1996**. *Geodetic Datums in New Zealand: Transformation Between NZGD49 and a New Standard National Geodetic Datum at a Specified Epoch.* Report prepared for the Department of Survey and Land Information, Wellington, New Zealand, April

Reyners, M., **1989**. New Zealand seismicity 1964-87: an interpretation. *New Zealand Journal of Geology and Geophysics*, Vol. 32, No. 3, pp. 307-315

Rizos, C., R. Coleman and N. Ananga, **1991**. The Bass Strait GPS survey: preliminary studies of an experiment to connect Australian height datums. *Australian Journal of Geodesy, Photogrammetry and Surveying*, Vol. 55, Dec., pp. 1-25.

Roelse, A., H.W. Granger and J.W. Graham, **1975**. *The Adjustment of the Australian Levelling Survey 1970-71*. Department of National Development, Division of National Mapping, *Technical Report 12*, 2nd edition, Canberra, ACT, Australia.

Rowe, G.H., **1981**. The doppler satellite positioning technique. *New Zealand Surveyor*, Vol. 29, No. 6, pp. 608-624.

Saastamoinen, J., **1972**. Atmospheric correction for the troposphere and stratosphere in radio ranging of satellites. In *The Use of Artificial Satellites for Geodesy, Geophys. Monogr. Ser.*, Vol 15, edited by S.W. Henriksen *et al.*, pp. 247-251, American Geophysical Union, Washington, D.C., USA.

Sandwell, D.T., **1992**. Antarctic marine gravity field from high-density satellite altimetry. *Geophysical Journal International*, Vol. 109, pp. 437-448.

Sandwell, D.T., M.M. Yale and W.H.F. Smith, **1995**. Gravity anomaly profiles from ERS-1, Topex, and Geosat altimetry. 1995 Spring Meeting published as a supplement to *EOS - Transactions of the American Geophysical Union*, April 25, Vol. 76, No. 17, S89.

Seeber, G., **1993**. *Satellite Geodesy : Foundations, Methods and Applications*. Walter de Gruyter & Co., New York, USA.

Sideris, M.G., **1984**. *Computation of Gravimetric Terrain Correction Using Fast Fourier Transform Techniques. UCSE Report No. 20007*, Department of Surveying Engineering, The University of Calgary, Calgary, Alberta, Canada.

Sideris, M.G., **1990**. Rigorous gravimetric terrain modelling using Molodensky's operator. *Manuscripta Geodaetica*, Vol. 15, pp. 97-106.

Sideris, M.G., **1994**. Geoid determination by FFT techniques. Lecture Notes, *International School for the Determination and Use of the Geoid*, DIIAR, Politecnico di Milano, October.

Smith, D.A., **1992**. *The use of High Resolution Height Data in the Computation of High Precision Geoid Undulations on the Island of Maui. Report No. 424,* Department of Geodetic Science and Surveying, Ohio State University, USA.

Soler, T. and L.D. Hothem, **1988**. Coordinate systems used in geodesy: basic definitions and concepts. *Journal of Surveying Engineering*, Vol. 114, No. 2, May, pp. 84-97.

Steed, J., **1990**. A practical approach to transformation between commonly used reference systems. *The Australian Surveyor*, Vol. 35, No. 3, pp. 248-264.

Steed, J. and S. Holtznagel, **1994**. AHD heights from GPS using AUSGEOID93. *The Australian Surveyor*, Vol. 39, No. 1, pp. 21-27.

Stewart, M.P., **1990**. *Computation of a Gravimetric Geoid for the British Isles: An Assessment of Fourier and Classical techniques*. D.Phil thesis, University of Edinburgh, United Kingdom.

Sutherland, N.C., **1994**. The Sears ratio and its effect on coordinate transformations in New Zealand. *New Zealand Surveyor*, Vol. 34, No. 284, pp. 142-145.

Swift, E., **1994**. Improved WGS84 coordinates for the DMA and Air Force GPS tracking sites. *Proceedings of ION GPS-94*, Salt Lake City, Utah, USA, 20-23 September, pp. 285-292.

Tait, K., **1991**. *GPS Survey for Invercargill District Office of Fiordland Photocontrol, 24 Feb - 10 Mar. Internal report of GPS Operations Unit*, Head Office, Department of Survey and Land Information, Wellington, New Zealand.

Thompson, E.H., **1969**. *An Introduction to the Algebra of Matrices with some Applications*. Adam Hilger Ltd, London, England.

Torge, W., **1980**. *Geodesy : An Introduction*. Walter de Gruyter & Co., Berlin, Germany.

Tregoning, P., **1996**. *GPS Measurements in the Australian and Indonesian Region (1989-1993): Studies of the Java Trench Subduction Zone, the Sunda Strait and the Australian Plate. UNISURV S-44*, School of Geomatic Engineering, The University of New South Wales, Sydney, Australia.

Tscherning, C.C., **1979**. Comparison of some methods for the detailed representation of the Earth's gravity field. *Presented at the XVII General Assembly of the IUGG*, December, Canberra, Australia.

Tscherning, C.C. and R. Forsberg, **1992**. Harmonic continuation and gridding effects on geoid height prediction. *Bulletin Geodesique*, Vol. 66, No. 1, pp. 41-53.

Tsen, A., **1992**. *Determination of Geoidal Height Difference Using Ring Integration Method.* M.Sc.E. thesis, Department of Surveying Engineering, *Technical Report No. 158*, University of New Brunswick, Fredericton, New Brunswick, Canada.

Tsuei, G.C., D. Arabelos, R. Forsberg, M.G. Sideris, and I.N. Tziavos, **1995**. Geoid computations in Taiwan. in: Sunkel and Marson (eds.) *Gravity and Geoid*, International Association of Geodesy Symposium No. 113, Springer-Verlag. pp. 446-458.

Tziavos, I.N., **1996**. Comparisons of spectral techniques for geoid computations over large regions. *Journal of Geodesy*, Vol. 70, pp. 357-373.

Vanicek, P., **1991**. Vertical datum and NAVD88. *Surveying and Land Information Systems*, Vol. 51, No. 2, pp. 83-86.

Vanicek, P. and L.E. Sjoberg, **1991**. Reformulation of Stokes' theory for higher than second-degree reference field and modification of integration kernels. *Journal of Geophysical Research*, Vol. 96, No. B4, pp. 6529-6539.

Vanicek, P. and E.J. Krakiwsky, **1986**. *Geodesy : The Concepts*. second edition, Elsevier Science B.V., Amsterdam, The Netherlands.

Walcott, R.I., **1984**. The kinematics of the plate boundary zone through New Zealand: a comparison of short- and long-term deformations. *Geophysical Journal of the Royal Astronomical Society*, Vol. 79, pp. 613-633.

Wells, D.E., N. Beck, D. Delikaraoglou, A. Kleusberg, E.J. Krakiwsky, G. Lachapelle, R.B. Langley, M. Nakiboglu, K.P. Scharz, J.M. Tranquilla and P. Vanicek, **1986**. *Guide to GPS Positioning*. Canadian GPS Associates, Fredericton, New Brunswick, Canada.

Wellman, H.W., **1955**. New Zealand quaternary tectonics. *Geologische Rundschau*, Vol. 43, pp. 248-257.

Wessel, P. and W.H.F. Smith, **1991**. Free software helps map and display data. *EOS - Transactions of the American Geophysical Union*, Vol. 72, pp. 441.

Wichiencharoen, C., **1982a**. *The Indirect Effects on the Computation of Geoid Undulations. Report No. 336*, Department of Geodetic Science and Surveying, Ohio State University, USA.

Wichiencharoen, C., **1982b**. *Fortran Programs for Computing Geoid Undulations from Potential Coefficients and Gravity Anomalies. Internal Report of the Department of Geodetic Science and Surveying*, Ohio State University, USA.

Wolf, H., **1963**. Geometric connection and re-orientation of three-dimensional triangulation nets. *Bulletin Geodesique*, Vol. 68, pp. 165-169.

Wong, L. and R. Gore, **1969**. Accuracy of geoid heights from modified Stokes' kernels. *Geophysical Journal of the Royal Astronomical Society*, Vol. 18, pp. 81-91.

Woodward, D.J., **1982**. *Reduction of Gravity Observations on the Vax11/780 Computer. Technical Note No. 83*, Geophysics Division, Department of Scientific and Industrial Research, New Zealand.

Yokoyama, K., **1991.** Summary report of the International Earth Rotation Service for the period from August 1987 through July 1991. *Presented at the XX General Assembly of the IUGG*, 11-24 August, Vienna, Austria.

Zilkoski, D.B., J.H. Richards and G.M.Young, **1992**. Results of the general adjustment of the North American vertical datum of 1988. *Surveying and Land Information Systems*, Vol. 52, No. 3, pp. 133-149.

Zumberge, J.F., R. Liu and R.E. Neilan (Eds), **1995**. *International GPS Service for Geodynamics 1994 Annual Report*. IGS Central Bureau, Jet Propulsion Laboratory, California Institute of Technology, Pasadena, California, USA.

Appendix A

New Zealand GPS Observation Campaign

GPS data available for processing as the March 1993 New Zealand GPS campaign.

Station		Day of 1993												
		067	068	069	070	071	072	073	074	075	076	077	078	079
DS42	Tidbinbilla	•	•	•	x	•	•	•	•	•	•	•	•	•
HOB1	Hobart	•	•	•	•	•	.	x	•	•	•	•	•	•
MCMU	Mc Murdo	•	•	•	•	•	•	•	•	•	•	•	.	•
PAMA	Tahiti	•	•	•	•	•	.	•	•	•	•	.	.	.
D026	Pukearenga No. 2	.	.	.	.	.	.	.	.	.	.		•	.
D045	XVII Whangaparaoa	.	.	.	.	.	.	.	•	•	•	•	•	○
D072	F Maketu	.	.	.	.	.	.	.	.	.	.	•	.	*
D484	F Maketu Ecc.	.	.	.	.	.	.	.	.	.	.	.	.	○
D078	201 Te Pohue	.	.	.	.	.	.	.	.	.	.	.	•	•
D100	106 Okahuatiu	.	.	.	.	.	.	.	.	.	.	.	•	•
D105	A Huirangi	.	.	.	.	.	.	.	.	○	.	•	.	.
D131	Mt Stewart	.	.	.	.	.	.	.	.	•	•	.	.	.
D143	Eringa	.	.	.	.	.	.	.	•	.	•	.	.	.
D158	Jenkins Hill No. 2	.	.	.	.	.	.	•	.	.	.	.	.	.
D172	Mt Murchison	.	.	.	.	.	○	○	.	.	.	.	.	.
D191	Isolated Hill	.	.	.	.	.	•	.	○	.	.	.	.	.
D212	Mt Pleasant	.	.	.	.	•	•	.	.	.	.	.	.	.
D229	Mt Mary	.	•	.	•	•	.	.	.	.	.	.	.	.
D233	A Mt Horrible	.	•	.	.	○	.	.	.	.	.	.	.	.
D253	T Hyde Rock	•	•	•	.	.	.	.	.	.	.	.	.	.
D286	X The Bluff	•	.	.	.	.	.	.	.	.	.	.	.	.
D269	A North Taieri	○	○	.	.	.	.	.	.	.	.	.	.	.
D302	Mt York	•	.	○	.	.	.	.	.	.	.	.	.	.
D309	HB Mt Greenland	.	.	.	•	•	•	.	.	.	.	.	.	.
D320	JF (Gillespies S.D.)	.	.	•	•	.	.	.	.	.	.	.	.	.
D338	8741	.	.	•	○	.	.	.	.	.	.	.	.	.
D425	A (Cape Campbell S.D.)	.	.	.	.	.	.	•	•	.	.	.	.	.
D431	Bluff Hill No. 3	.	.	.	.	.	.	.	.	.	•	.	.	•
D452	79 (Rangiriri S.D.)	.	.	.	.	.	.	.	.	.	.	•	.	.
D469	I Parapara	.	.	.	.	.	.	•	.	•	.	.	.	.
D473	Marotiri No. 2	.	.	.	.	.	.	.	.	.	○	*	*	.
D481	Marotiri Ecc.	.	.	.	.	.	.	.	.	.	.	○	○	.
D474	Three Sisters	•	•	•	•	•	•	•	•	•	.	.	.	.
D482	HHR9	.	.	.	.	.	.	.	.	.	.	*	.	.
D483	HHR9A	.	.	.	.	.	.	.	.	.	.	.	*	*
WELL	HH GPS Pillar	○	○	○	•	•	•	•	•	•	•	•	•	•

The symbols used in the table have the following meaning:

- . indicates that no data was collected
- • data was collected and processed successfully in GAMIT and GLOBK.
- x data was collected and processed but did not coincide with Local NZ data.
- ○ data was collected but was **not** able to be processed successfully in GAMIT and GLOBK.
- * data was collected using the Leica system 200 receivers (to cover the faulty Ashtech receiver) and was processed successfully in GAMIT and GLOBK.

The shaded days (67,70,78)indicate processing in GAMIT used 2 sessions per 24 hours.

Appendix B

ITRF 93 Cartesian Coordinates and Rates

ITRF93 Cartesian Coordinates for the March 1993 GPS campaign stations. No velocities for the New Zealand stations were determined, due to only 13 consecutive days of data being processed. The coordinates and velocities for the IGS stations that were held fixed were obtained from Boucher *et al.* (1994). The Cartesian Coordinates are in terms of ITRF93 at the mean observation epoch of 1993.200.

CODE	X (metres)	Y (metres)	Z (metres)	$\dot{X}$ (m/yr)	$\dot{Y}$ (m/yr)	$\dot{Z}$ (m/yr)
New Zealand Local Fiducial stations						
D045	-5105842.454	461788.409	-3781953.476	0.000	0.000	0.000
D474	-4303267.210	894811.309	-4606633.497	0.000	0.000	0.000
WELL	-4780648.795	436507.231	-4185440.404	0.000	0.000	0.000
New Zealand stations						
D026	-5167214.341	496239.304	-3693852.393	0.000	0.000	0.000
D072	-5039298.830	311182.391	-3884430.300	0.000	0.000	0.000
D078	-5042731.101	140230.769	-3890300.390	0.000	0.000	0.000
D100	-4989460.513	191252.665	-3955756.665	0.000	0.000	0.000
D105	-4929040.099	498221.675	-4004033.393	0.000	0.000	0.000
D131	-4860522.592	383529.172	-4098473.679	0.000	0.000	0.000
D143	-4794050.785	364491.793	-4177890.343	0.000	0.000	0.000
D158	-4763996.341	561250.961	-4190671.505	0.000	0.000	0.000
D191	-4660964.463	571445.660	-4302316.463	0.000	0.000	0.000
D212	-4590224.191	585796.213	-4375478.592	0.000	0.000	0.000
D229	-4519608.888	774369.481	-4419877.158	0.000	0.000	0.000
D233	-4509242.432	709568.162	-4440279.054	0.000	0.000	0.000
D253	-4408673.420	841182.585	-4518904.885	0.000	0.000	0.000
D286	-4298488.086	887139.138	-4612663.040	0.000	0.000	0.000
D302	-4371448.615	950019.392	-4531599.188	0.000	0.000	0.000
D309	-4616400.244	745241.704	-4324328.443	0.000	0.000	0.000
D320	-4566344.445	808430.432	-4364476.946	0.000	0.000	0.000
D338	-4521641.788	878624.099	-4396964.540	0.000	0.000	0.000
D425	-4741512.998	480470.779	-4225018.634	0.000	0.000	0.000
D431	-4922647.803	265115.162	-4033578.967	0.000	0.000	0.000
D452	-5041355.081	441059.474	-3869624.756	0.000	0.000	0.000
D469	-4802026.165	617521.377	-4138428.040	0.000	0.000	0.000
D473	-4977955.202	355512.137	-3959577.681	0.000	0.000	0.000
D482	-4780645.012	436500.619	-4185441.880	0.000	0.000	0.000
D483	-4780653.193	436501.265	-4185431.728	0.000	0.000	0.000

continued on next page

CODE	X (metres)	Y (metres)	Z (metres)	$\dot{X}$ (m/yr)	$\dot{Y}$ (m/yr)	$\dot{Z}$ (m/yr)
IGS core stations held to define ITRF93 coordinates						
ALGO	918129.536	-4346071.161	4561977.768	-0.060	0.181	-0.185
DS42	-4460996.146	2682557.192	-3674444.025	0.137	-0.105	0.183
FAIR	-2281621.360	-1453595.750	5756961.937	-0.222	-0.125	0.479
KOKR	-5543838.060	-2054587.460	2387809.571	0.318	0.184	-0.113
KOSG	3899225.272	396731.782	5015078.249	0.041	-1.586	1.608
TROM	2102940.410	721569.372	5958192.105	0.800	0.189	1.296
YAR1	-2389025.503	5043316.861	-3078531.080	0.560	-1.270	0.821
Other IGS stations						
HOB1	-3950184.111	2522364.550	-4311588.520	0.671	0.013	0.673
MCMU	-1310696.452	310469.230	-6213368.487	0.238	-0.335	1.585
PAMA	-5245195.230	-3080472.239	-1912825.551	0.815	-0.472	-0.545
Additional SIO stations to help improve network adjustment						
DRAO	-2059164.654	-3621108.335	4814432.404	-0.103	-0.108	0.082
DS10	-2353614.158	-4641385.357	3676976.461	-0.158	-0.301	0.090
DS60	4849202.471	-360329.138	4114912.962	-0.240	-0.655	1.311
HART	5084625.094	2670366.577	-2768494.226	2.077	-0.387	2.025
JPL1	-2493304.147	-4655215.474	3565497.346	-0.099	0.306	-0.285
KOUR	3839591.279	-5059567.330	579956.704	-0.648	0.878	0.102
MASP	5439189.119	-1522054.782	2953464.099	-0.720	-0.222	1.098
ONSA	3370658.701	711877.011	5349786.797	0.194	-1.155	1.303
PIE1	-1640916.787	-5014781.133	3575447.134	-0.236	-0.011	-0.152
PIN1	-2369510.453	-4761207.143	3511396.154	-0.315	-0.050	-0.041
QUIN	-2517230.968	-4198595.134	4076531.259	0.021	0.260	-0.499
RCM2	961318.887	-5674090.867	2740489.515	-0.002	0.162	-0.493
SANT	1769693.061	-5044573.902	-3468321.291	-1.704	3.225	0.578
SIO2	-2455539.303	-4767224.042	3441628.898	-0.363	-0.317	-0.003
STJO	2612631.278	-3426806.954	4686757.715	-0.205	-0.279	0.626
TAIW	-3024781.853	4928936.913	2681234.440	-0.146	0.851	1.300
USU3	-3855263.020	3427432.567	3741020.403	0.252	0.094	0.444
VNDP	-2678089.853	-4525437.721	3597431.490	-0.061	-0.235	-0.844
WTZ1	4075578.608	931852.667	4801569.926	0.585	-0.743	2.006
YELL	-1224452.431	-2689216.042	5633638.264	-0.185	-0.289	0.488

The formal uncertainties for the above stations at 1σ (67% Confidence interval) are listed below. These uncertainties result from the adjustment of the daily GPS solutions together in GLOBK and are expressed in cartesian components.

CODE	Name	σX (metres)	σY (metres)	σZ (metres)
New Zealand Local Fiducial stations				
D045	Whangaparaoa	0.006	0.004	0.005
D474	Three Sisters	0.003	0.003	0.003
WELL	HH GPS Pillar	0.005	0.003	0.004
New Zealand stations				
D026	Pukearenga No2	0.011	0.007	0.008
D072	F Maketu	0.010	0.005	0.007
D078	201 Te Pohue	0.010	0.005	0.006
D100	106 Okahuatiu	0.009	0.006	0.007
D105	A Huirangi	0.012	0.007	0.009
D131	Mt Stewart	0.007	0.004	0.005
D143	Eringa	0.006	0.004	0.005
D158	Jenkins Hill	0.024	0.011	0.019
D191	Isolated Hill	0.016	0.012	0.012
D212	Mt Pleasant	0.008	0.007	0.008
D229	Mt Mary	0.007	0.006	0.006
D233	A Mt Horrible	0.011	0.006	0.010
D253	T Hyde Rock	0.006	0.004	0.005
D286	X The Bluff	0.010	0.013	0.010
D302	Mt York	0.008	0.006	0.007
D309	Mt Greenland	0.006	0.004	0.005
D320	JF Gillespies	0.007	0.005	0.006
D338	8741	0.010	0.006	0.009
D425	Cape Campbell	0.007	0.005	0.006
D431	Bluff Hill No3	0.008	0.004	0.005
D452	79 Rangiriri	0.017	0.008	0.012
D469	I Parapara	0.009	0.004	0.006
D473	Marotiri No2	0.008	0.005	0.006
D482	HHR9	0.014	0.007	0.011
D483	HHR9A	0.008	0.005	0.006
	mean	0.010	0.006	0.007

Appendix C

ITRF 93 Ellipsoidal Coordinates

The Ellipsoidal Coordinates for the March 1993 GPS campaign stations in terms of ITRF93 at the mean observation epoch of 1993.200 using the GRS80 ellipsoid.

CODE	Station Name	Latitude ° ' "	Longitude ° ' "	Height m
New Zealand Local Fiducial stations				
D045	Whangaparaoa	-36 36 0.79792	174 49 55.38203	141.907
D474	Three Sisters	-46 32 12.95276	168 15 12.38483	176.531
WELL	HH GPS Pillar	-41 16 29.61945	174 46 58.63422	37.820
New Zealand stations				
D026	Pukearenga No2	-35 37 2.08803	174 30 51.68873	174.519
D072	F Maketu	-37 45 34.08767	176 27 59.06815	95.930
D078	201 Te Pohue	-37 49 28.35458	178 24 25.56376	360.584
D100	106 Okahuatiu	-38 34 30.55239	177 48 17.46420	323.545
D105	A Huirangi	-39 8 2.40734	174 13 41.56402	263.237
D131	Mt Stewart	-40 14 24.72122	175 29 17.92014	143.727
D143	Eringa	-41 10 48.51725	175 39 7.79514	590.954
D158	Jenkins Hill	-41 19 53.84854	173 16 51.24351	791.897
D191	Isolated Hill	-42 41 14.71076	173 0 37.00609	405.657
D212	Mt Pleasant	-43 35 20.28698	172 43 38.37662	510.526
D229	Mt Mary	-44 8 19.85910	170 16 39.36538	1005.888
D233	A Mt Horrible	-44 24 2.05656	171 3 26.44548	397.352
D253	T Hyde Rock	-45 23 15.52656	169 11 51.73196	1681.042
D286	X The Bluff	-46 36 53.84558	168 20 19.66414	269.062
D302	Mt York	-45 33 43.61785	167 44 20.12969	411.445
D309	Mt Greenland	-42 57 11.69578	170 49 46.76520	919.511
D320	JF Gillespies	-43 27 20.86252	169 57 37.17061	114.831
D338	8741	-43 51 38.95148	169 0 12.92462	14.639
D425	Cape Campbell	-41 44 56.57259	174 12 49.71330	254.693
D431	Bluff Hill No3	-39 28 44.35242	176 55 2.08045	119.396
D452	79 Rangiriri	-37 35 21.79138	175 0 0.07893	319.113
D469	I Parapara	-40 42 46.81246	172 40 19.94940	169.677
D473	Marotiri No2	-38 36 57.77784	175 54 54.09199	760.488
D482	HHR9	-41 16 29.74882	174 46 58.90236	35.511
D483	HHR9A	-41 16 29.32603	174 46 58.90670	34.981

Appendix D

Station Coordinate Repeatability between GAMIT solutions

This appendix contains diagrams showing the individual daily GAMIT solution corrections to the *a priori* coordinates for each New Zealand station, plus a selection of global stations, after a forward and backward adjustment in GLOBK. The error bars indicate the formal uncertainty at 1σ. The 1σ (67%) standard deviation (sd) of the residuals has been computed for stations that contained data on six or more days.

Comments have been included on the possible cause of the larger corrections and uncertainties for some stations.

Identical *a priori* coordinates were maintained between days, with stochastic mode constraints of 0.05 m in the horizontal and vertical being applied to the four New Zealand regional fiducial sites to maintain a consistent reference frame. However, to obtain the repeatability information for HOB1, MCMU and PAMA, each site had to be independently set to stochastic mode in separate GLOBK solutions, so as to ensure a stable reference frame was maintained. DS42 was never run through GLOBK in stochastic mode as it is the closest IGS core site to the New Zealand network, thus was required to remain deterministic to position the reference frame.

The following table lists those figures that are contained in this appendix. The code in the square brackets indicates the stations status in this adjustment, where GF = Global Fiducial, RF = Regional Fiducial, LF = Local Fiducial and LS = Local Station.

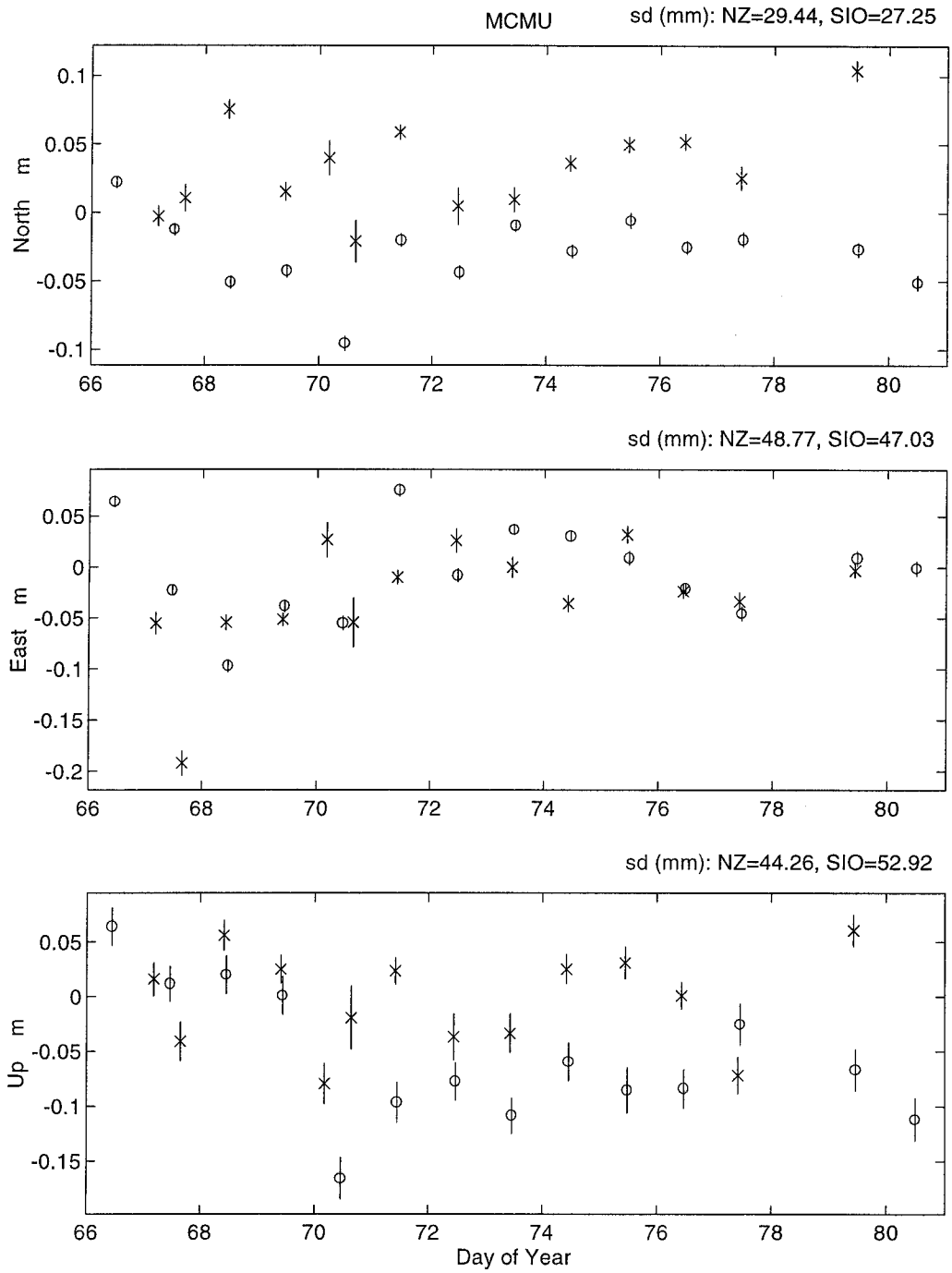

Figure D - 1 : MCMU - Mc Murdo [GF & RF]

MCMU, PAMA (Figure D-2) and DS42, are sites which were included in both the New Zealand regional network and the SIO global network. One is able to compare the variability and uncertainty for the daily solutions between the SIO solution (shown as **o**) and the New Zealand regional solution (shown as **x**). It is clear from the standard deviations (sd) that both solutions are almost identical. Notice that there is a tendency for systematic differences between the global SIO solution and the regional solution. These differences are thought to be due to the different weights and errors that each network brings to the combined least squares solution. The level of differences has since been lowered by improved modelling of the observables (Morgan *et al.*, 1996).

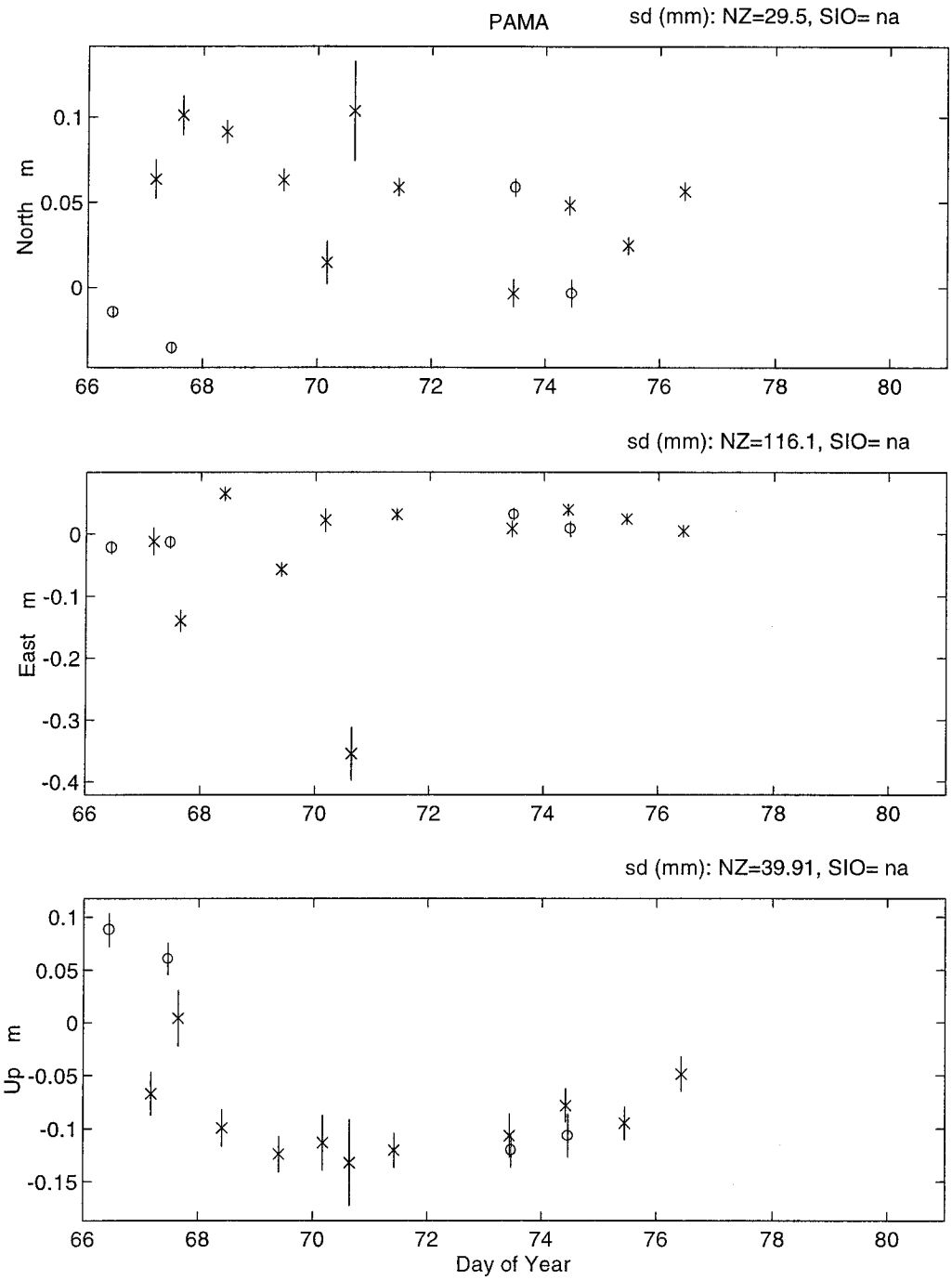

Figure D - 2 : PAMA - Tahiti [GF & RF]

For general details refer back to MCMU (Figure D-1) (**o** = SIO solution, **x** = New Zealand regional solution). As can be seen in Figure D-2, the SIO solution did not always run a fully consistent network when compared to the New Zealand regional solution. This could have been due to the data arriving after the SIO solution was computed or there were difficulties in processing the data, resulting in it being dropped from the solution. For the second session on DOY 070, the East component has what appears as an outlier. When PAMA was removed from the second session, the solution for all other sites in the second session became unstable. This was probably due to the fact that only HOB1 and MCMU were available as Regional Fiducial stations (see

Appendix A). Therefore PAMA was kept in the solution, though in hindsight this may have contaminated the results.

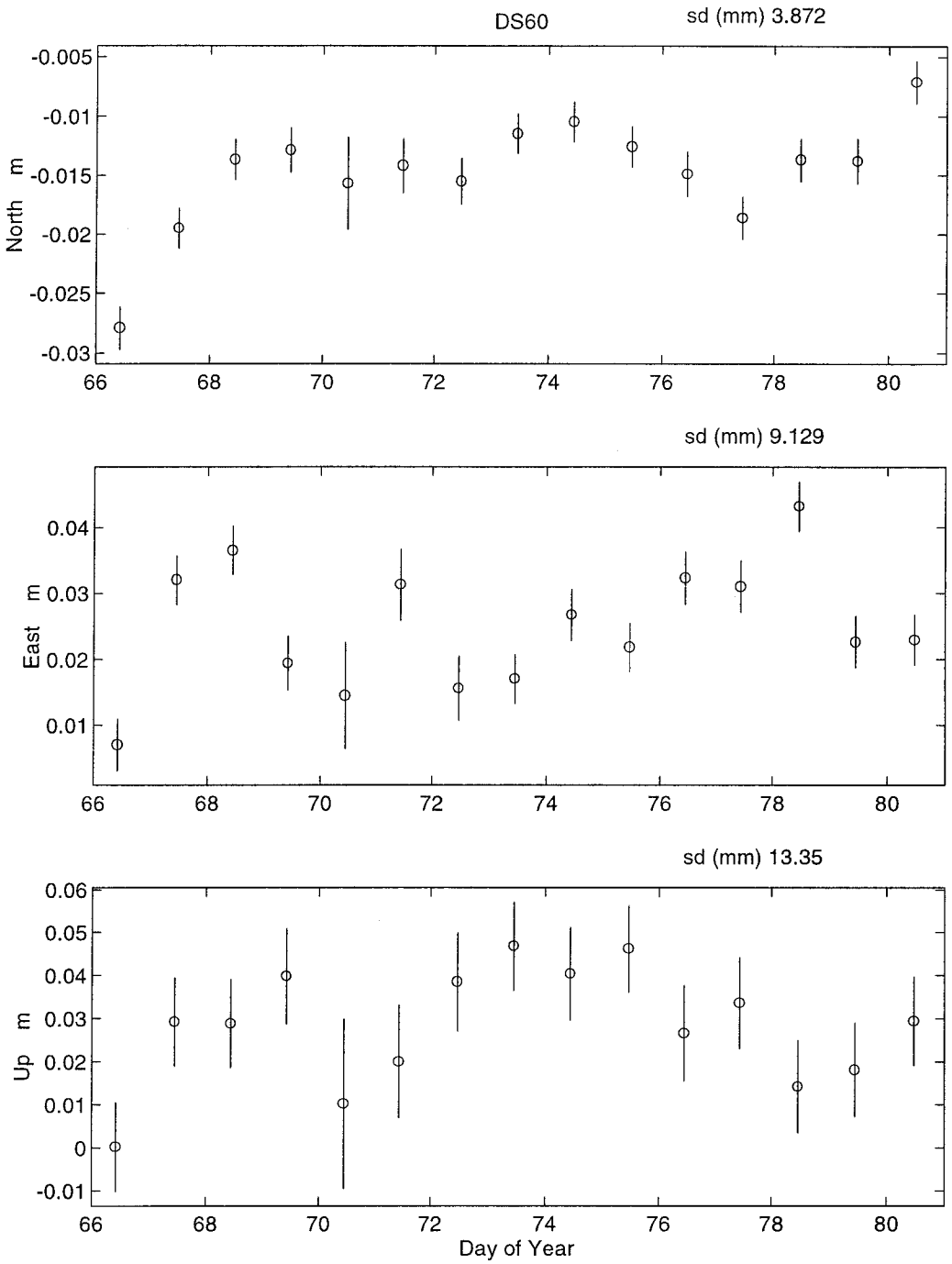

Figure D - 3 : DS60 - Madrid [GF]

DS60 is one of the IGS core sites and is located in the Northern Hemisphere. In comparison with MCMU (Figure D-1) or PAMA (Figure D-2), the variability at DS60, from the SIO processing, is approximately an order of magnitude smaller. This is probably due to the denser Northern Hemisphere permanent tracking network. Similar results are reported by Morgan *et al.* (1996).

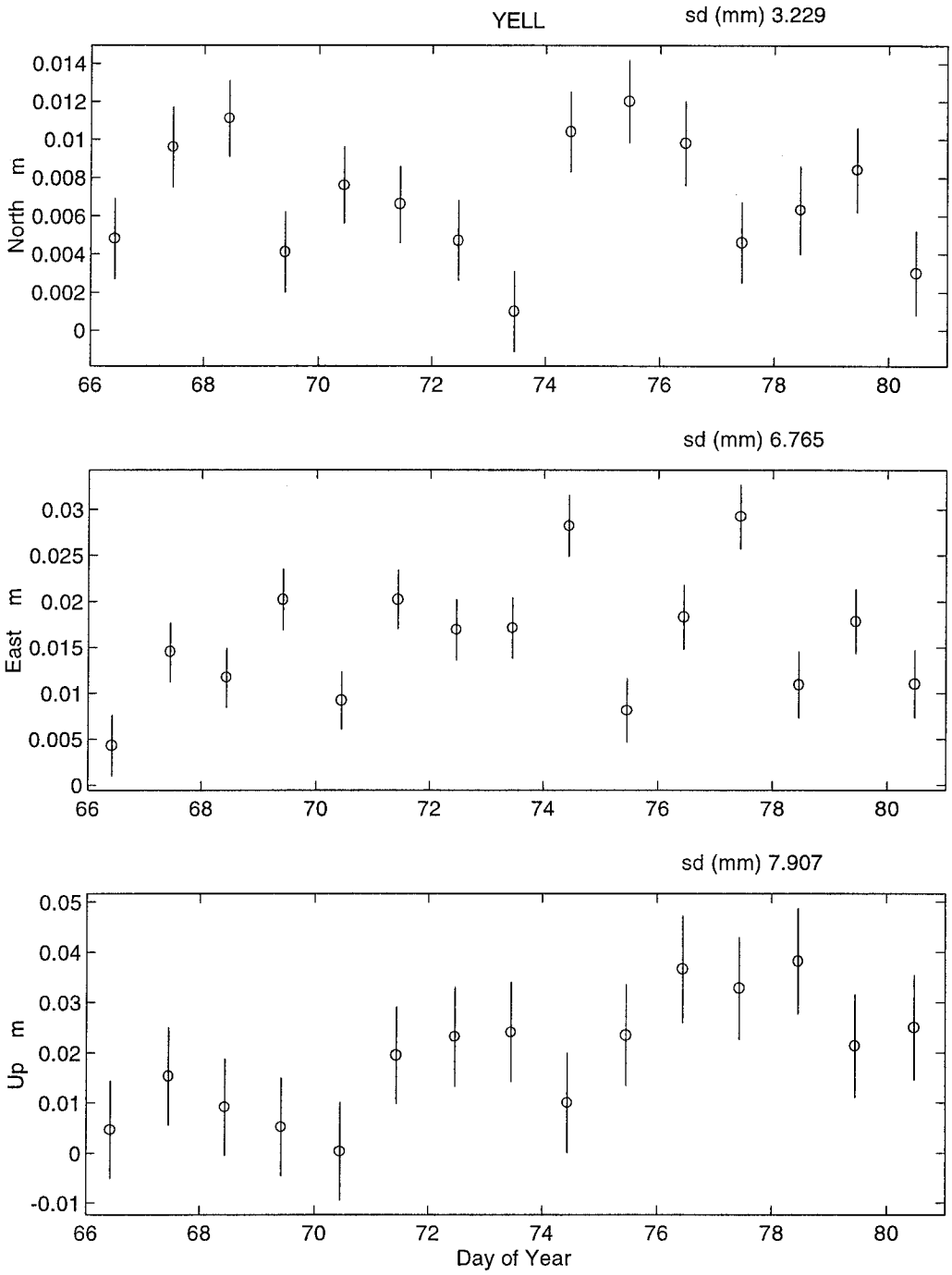

Figure D - 4 : YELL - Yellowknife [GF]

YELL, like DS60 (Figure D-3), is one of the IGS core sites located in the Northern Hemisphere which also shows variability that is approximately an order of magnitude smaller than MCMU (Figure D-1) or PAMA (Figure D-2).

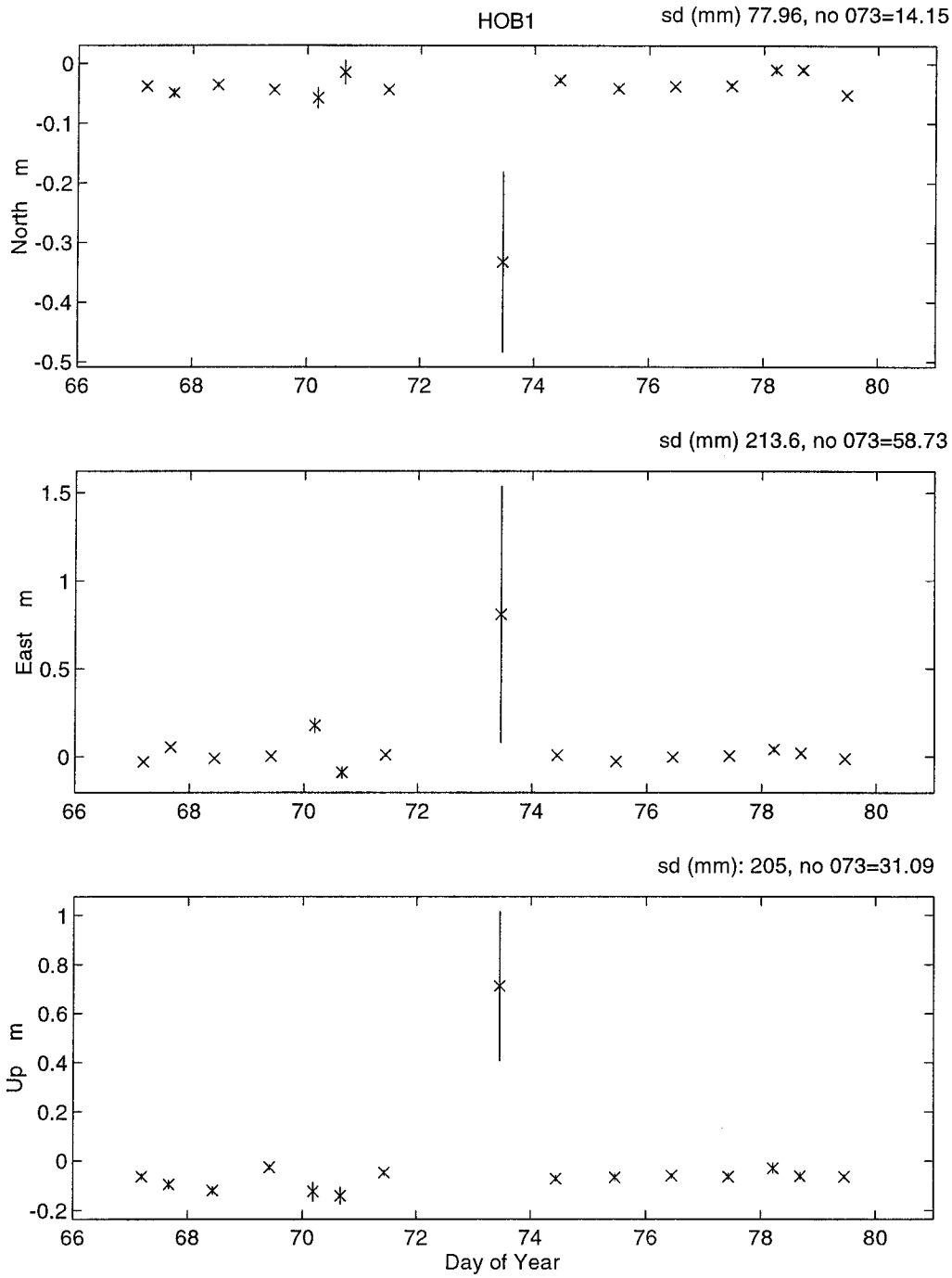

Figure D - 5 : HOB1 - Hobart CIGNET [RF]

On DOY 073 HOB1 only collected the last 1.5 hours of data. As is very obvious, the sd of HOB1 on this day is considerably larger than for the other days. HOB1 on DOY 073 was left in the solution as it was thought that the large sd will downgrade the contribution of this data in the GLOBK adjustment since the solution is a weighted solution. However, not removing the DOY 073 data for HOB1 may have contaminated the solution (see Figure D-16). When DOY 073 data is removed from the calculation of the sd, HOB1 is shown to perform at a similar level to MCMU (Figure D-1) and PAMA (Figure D-2).

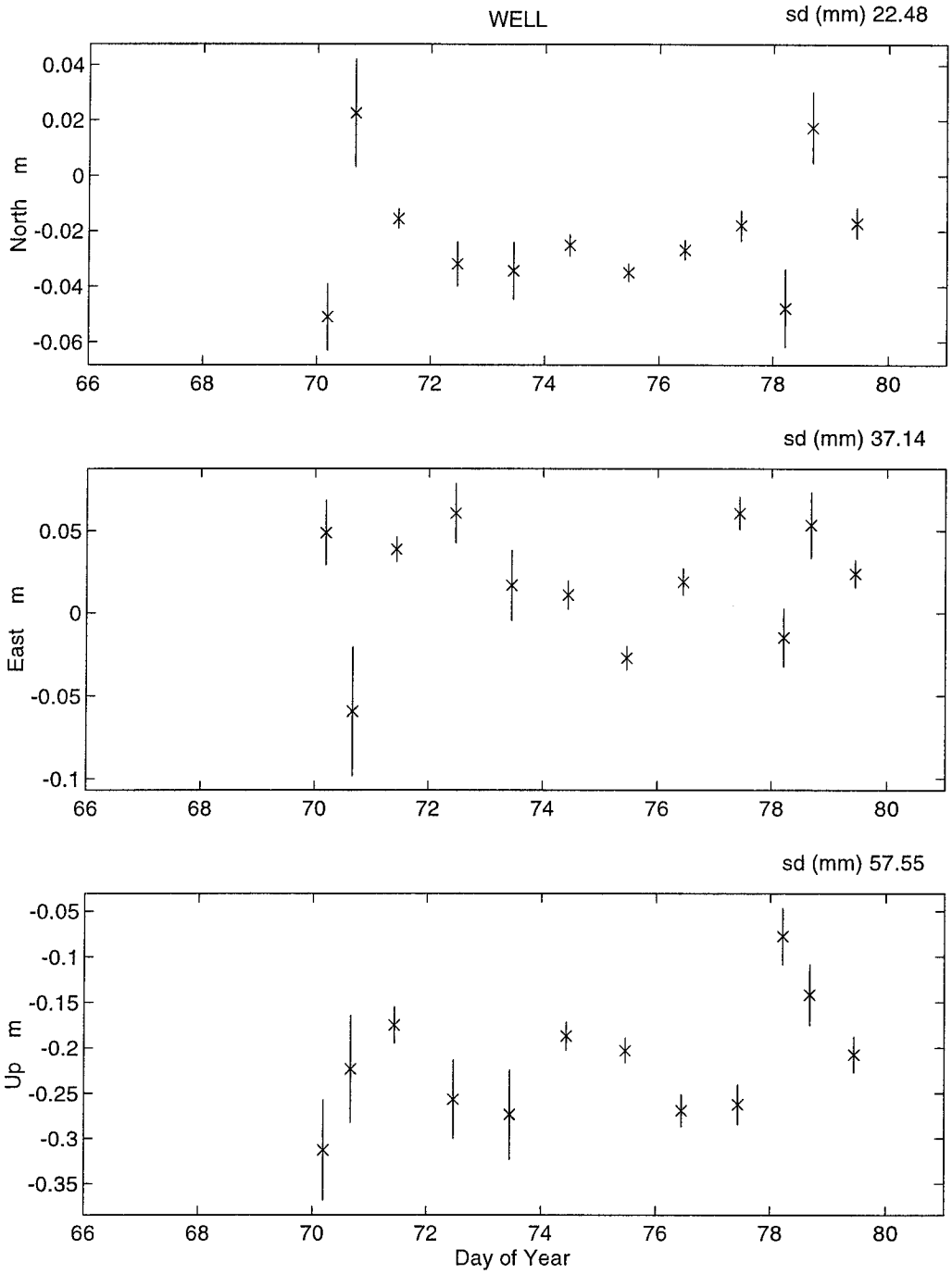

Figure D - 6 : WELL - Wellington CIGNET [LF]

The largest uncertainties for WELL occur on DOY 070. On DOY 070 DS42 only collected the first 7 hours of data, though HOB1, MCMU and PAMA collected a full 24 hours of data. The larger uncertainties on the second session of DOY 070 are is probably due to there being no data from DS42 in this session, resulting in a less desirable network geometry. Other large uncertainties occur on DOY 078, which contained no data from PAMA or MCMU and was split into two sessions. The smallest uncertainties occur on days 071, 074, 075 and 076 which contain data from all four regional fiducial sites. This illustrates the need for a well balanced external fiducial network.

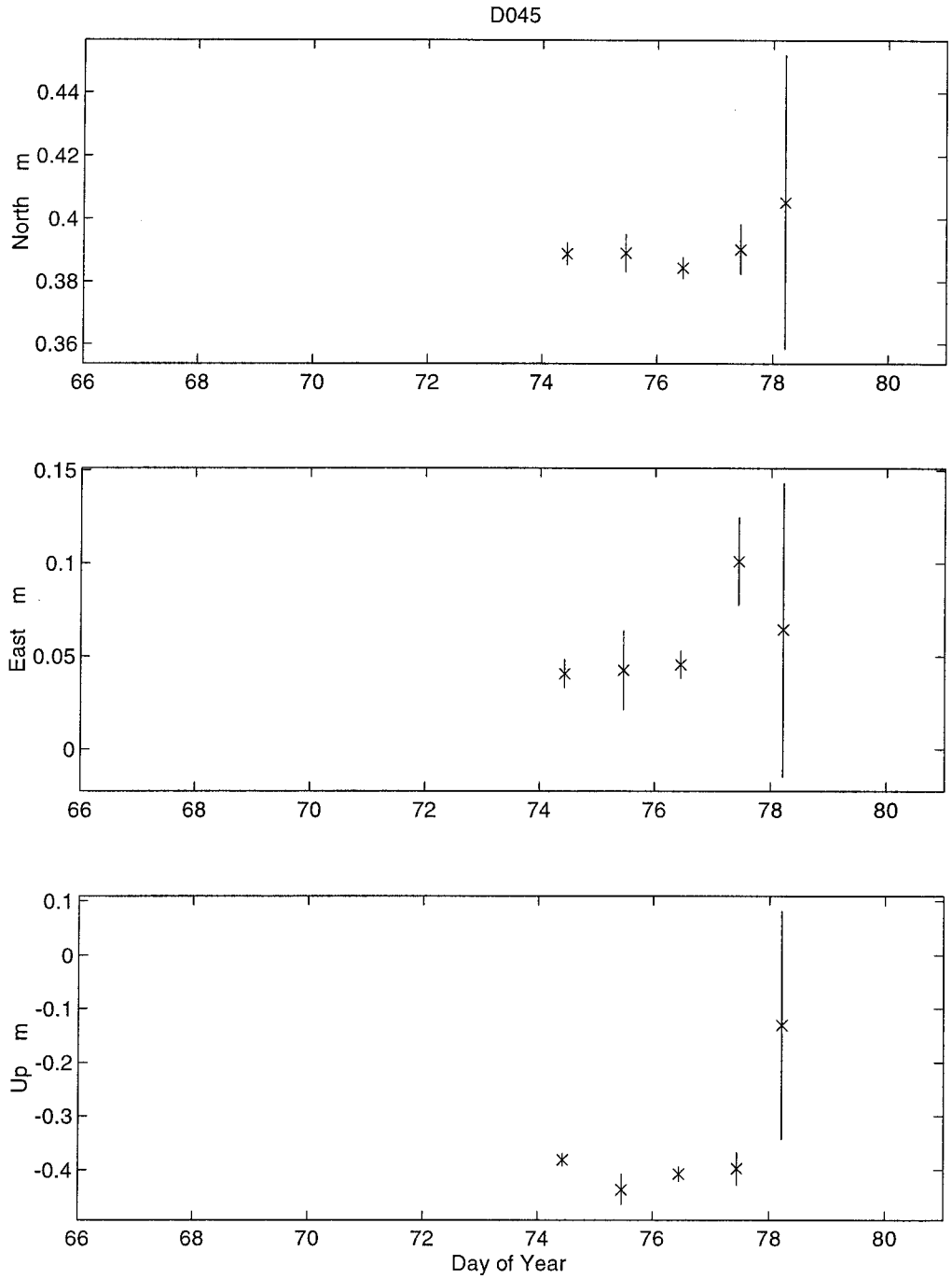

Figure D - 7 : D045 - XVII Whangaparaoa [LF]

The receiver stationed at D045 (alias Ashtech number 5) began to develop an unresolved problem on DOY 078. This resulted in only data for the first session on DAY 078 being able to be processed. No data from the second session or any of DOY 079 was able to be processed in GAMIT. As can be seen from the diagram the first session results for DOY 078 had significantly larger sd than other days. When the scatter (ie. $|x - \bar{x}|$)for D045 is compared with the known sd of the Ashtech receiver at WELL (Figure D-6), D045 results are within 3σ. Due to the large sd values on the DOY 078 result this data should not contribute significantly in the GLOBK adjustment.

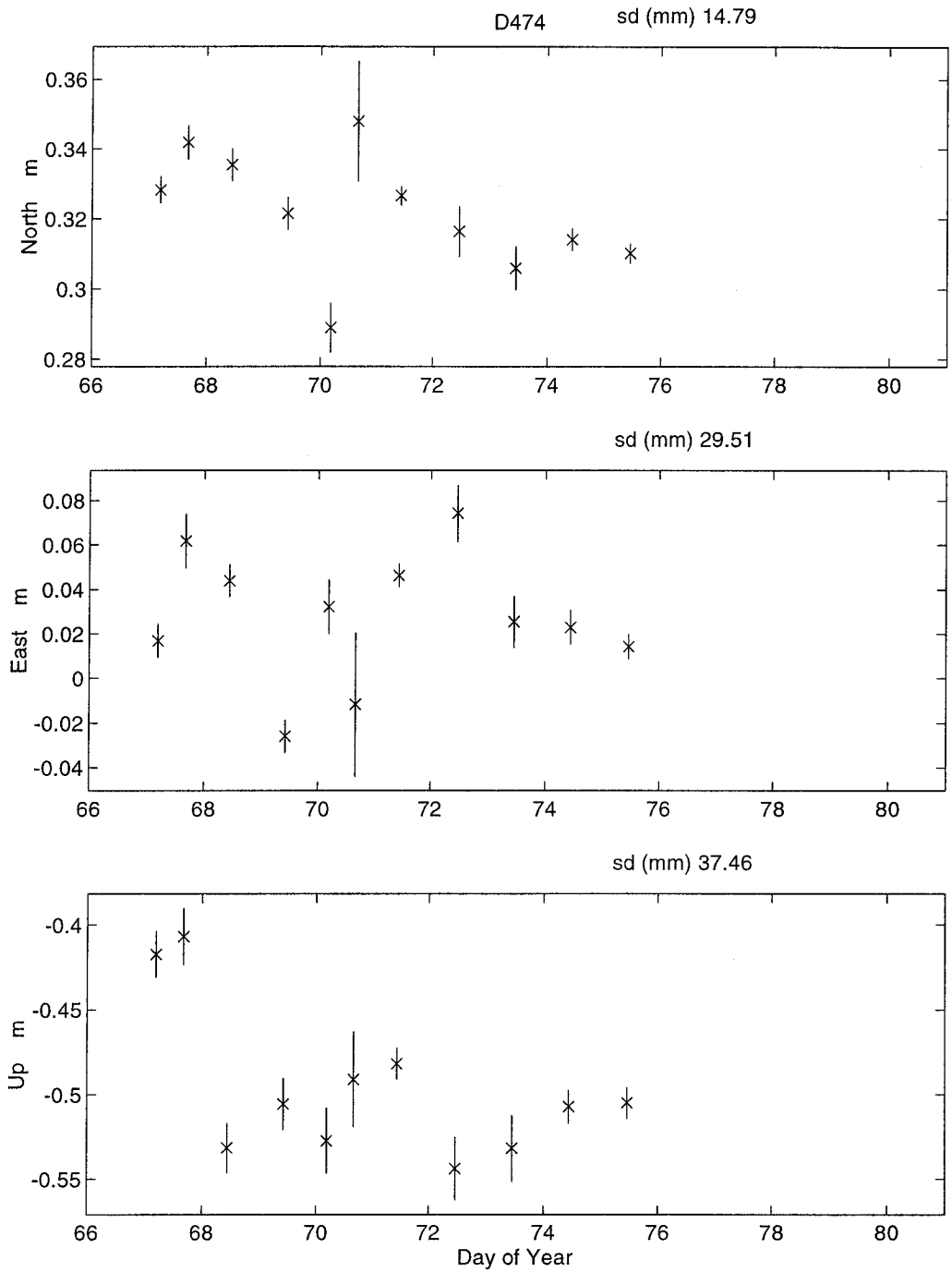

Figure D - 8 : D474 - Three Sisters [LF]

D474 site repeatability has been discussed in detail within Section 3.5.3.3. Most of the comments referring to WELL (Figure D-6) are also applicable to D474. Note that the sd on the North (N), East (E) and Up (U) components of D474 are 35%, 20% and 35% smaller than the respective components of WELL. This deterioration at WELL could be due to internal receiver quality, or more probable is that there is a larger chance of radio noise and interference at a WELL than D474. D474 sd values of 15, 30, and 38 mm for the N, E, U components are the lowest of any of the New Zealand local fiducial sites. These sd values represent approximately the level of coordinate recovery for any of the New Zealand sites, and have been used to validate the scatter on New Zealand sites that had less than six days of processable data.

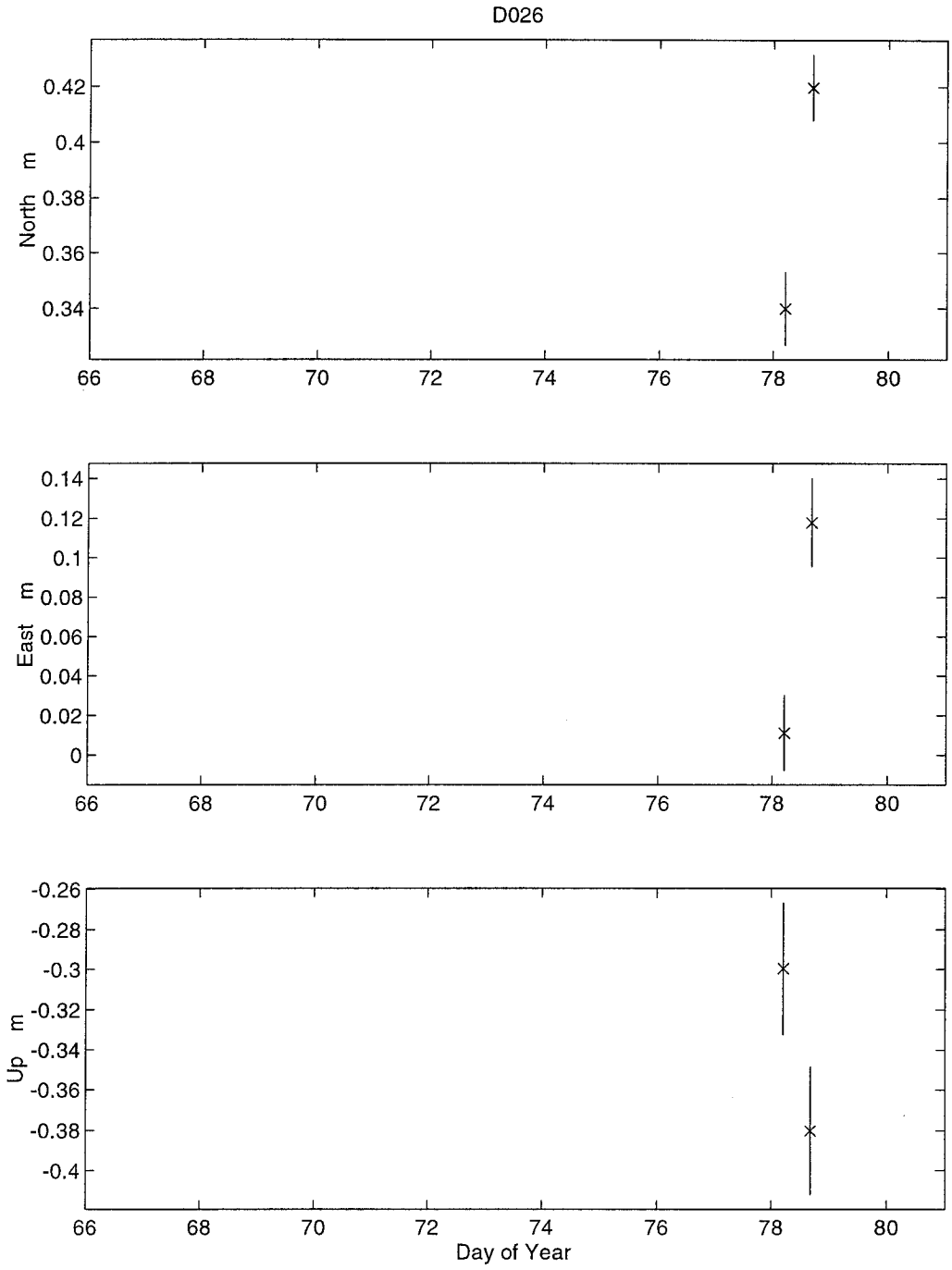

Figure D - 9 : D026 - Pukearenga No. 2 [LS]

Comparing the scatter of D026 results for each component against the respective sd values from D474 (Figure D-8) reveals that $N \leq 3\sigma$, $E \leq 2\sigma$ and $U \leq 1\sigma$.

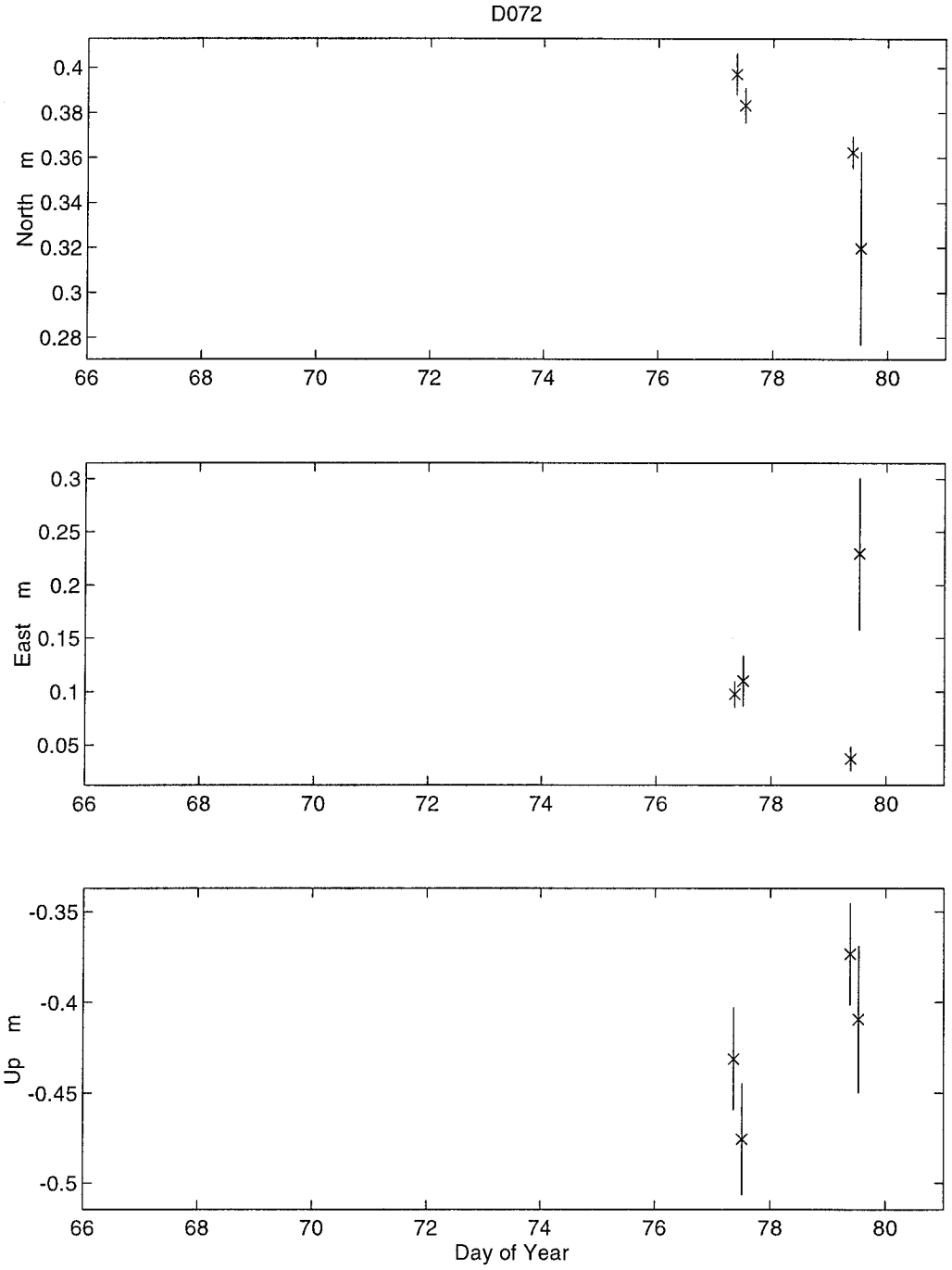

Figure D - 10 : D072 - F Maketu [LS]

D072 is the only site to be occupied by both an Ashtech (DOY 077) and Leica receiver (DOY 079). Both receivers appear to generate similar levels of variability and uncertainty, when the problem with the second session on DOY 079 is removed. Refer to D078 (Figure D-11) for comments on the second session of DOY 079. Comparing the scatter of D072 results for each component against the respective sd values from D474 (Figure D-8) reveals that $N \leq 3\sigma$, $E > 3\sigma$ and $U \leq 2\sigma$. Note that the problem with the second session on DOY 079 only seriously affected the East component.

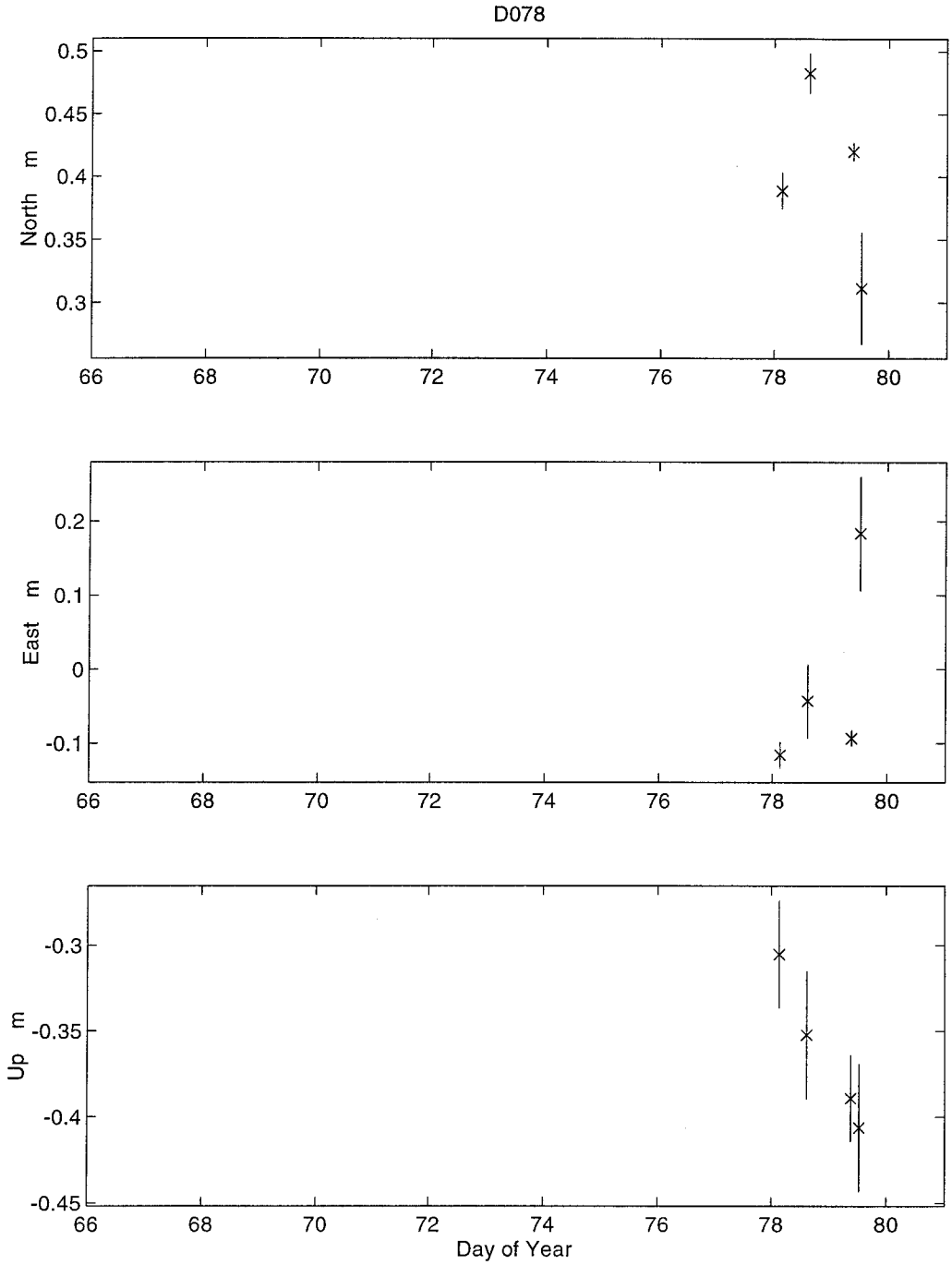

Figure D - 11 : D078 - 201 Te Pohue [LS]

The larger second session uncertainties for DOY 079 in the North and East components is clearly seen also at D072 (Figure D-10), D100 (Figure D-12), D431 (Figure D-28) and D483 (Figure D-33). The cause of this larger uncertainty has not been resolved. Though between sessions the number of double differences between the sites and satellites is not that dis-similar. The first session with 7 satellites has 27670 differences, while for the same sites in the second session with 8 satellites the total was 21546. Comparing the scatter of D078 results for each component against the respective sd values from D474 (Figure D-8) reveals that $N > 3\sigma$, $E > 3\sigma$ and $U \leq 2\sigma$.

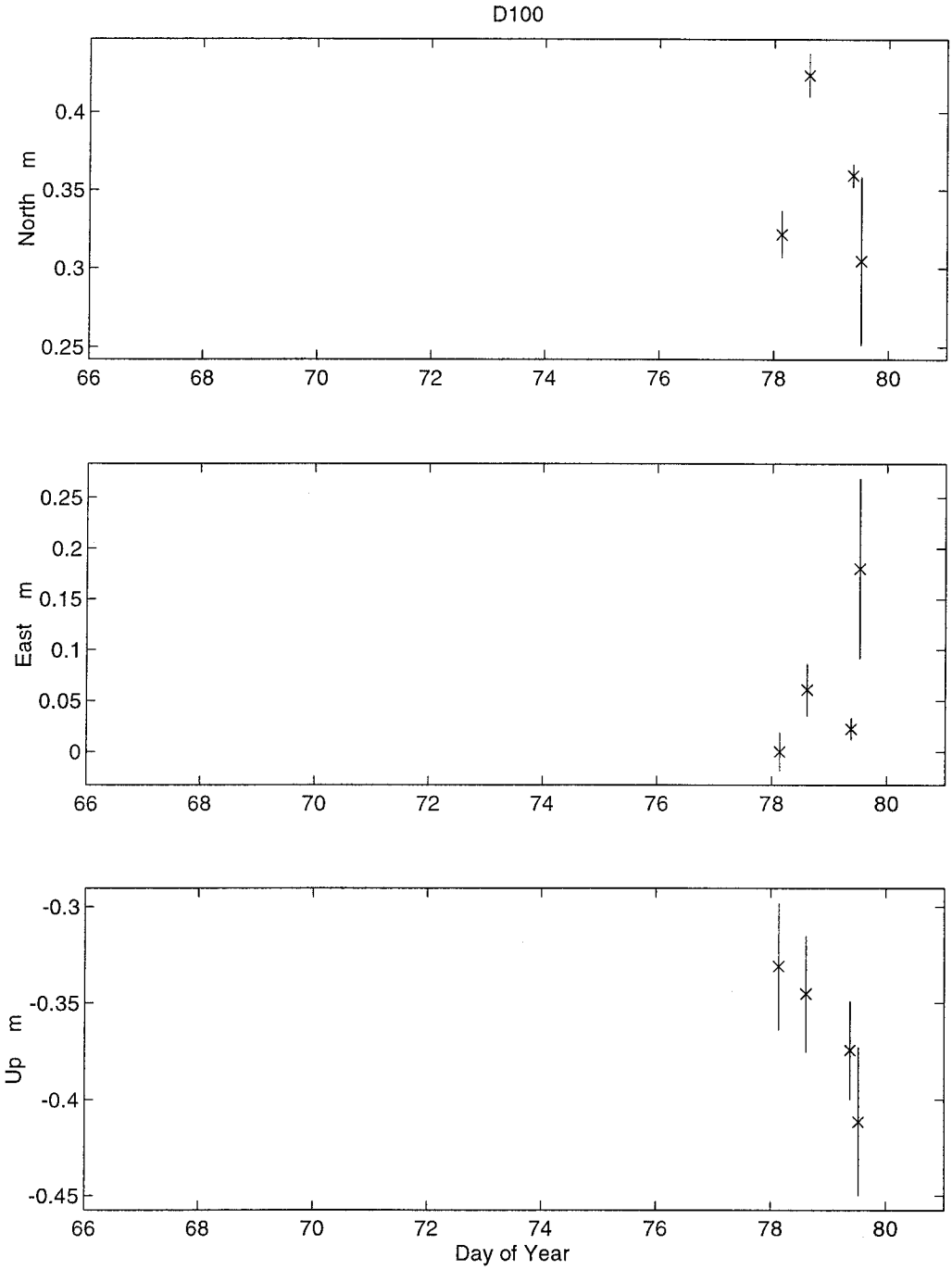

Figure D - 12 : D100 - 106 Okahuatiu [LS]

Refer to D078 (Figure D-11) for comments on the second session of DOY 079. Comparing the scatter of D100 results for each component against the respective sd values from D474 (Figure D-8) reveals that $N > 3\sigma$, $E > 3\sigma$ and $U \leq 3\sigma$. Note that as was the case for D078, the Up component is not effected by the second session of DOY 079.

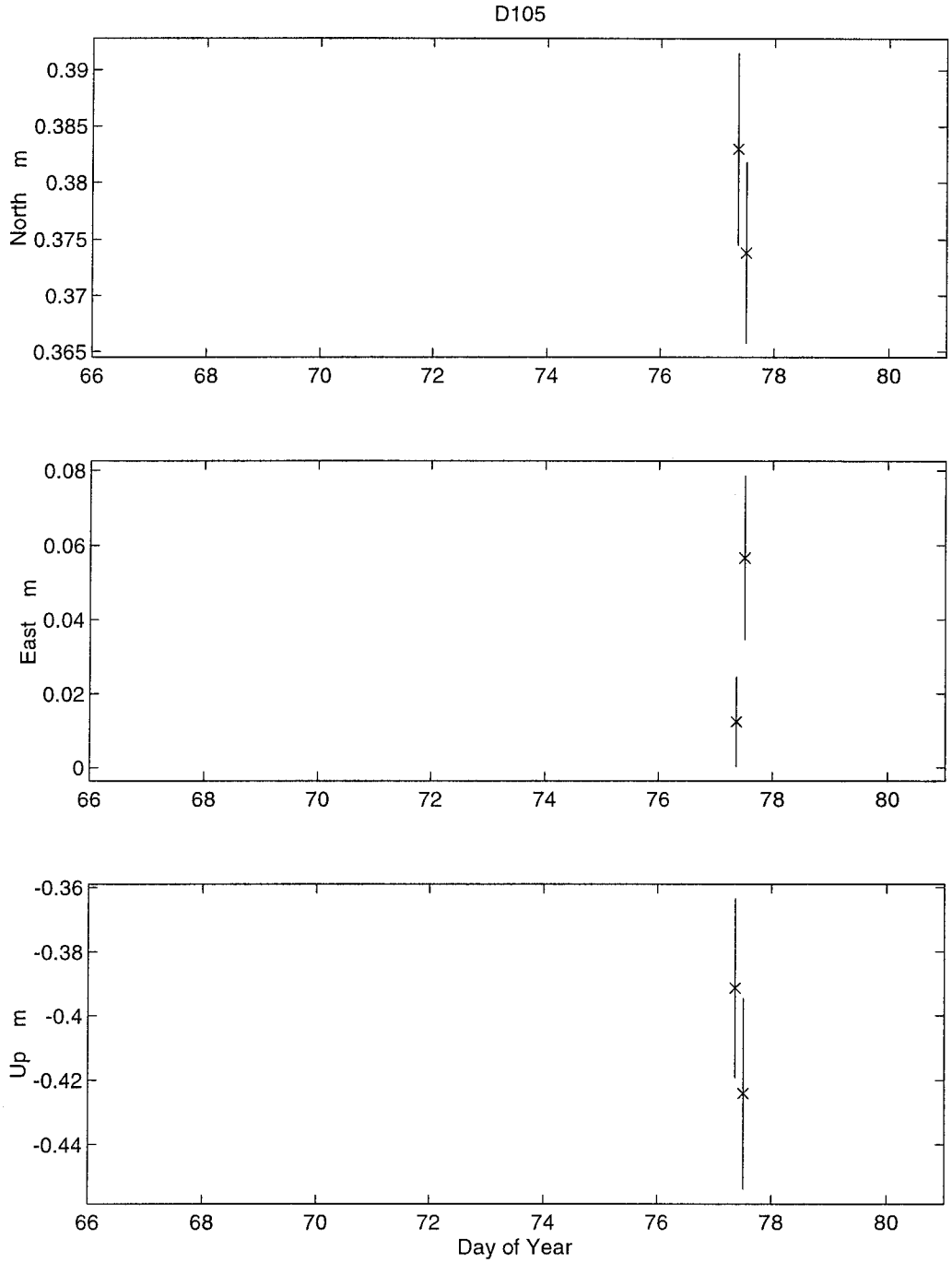

Figure D - 13 : D105 - A Huirangi [LS]

Comparing the scatter of D105 results for each component against the respective sd values from D474 (Figure D-8) reveals that N ≤ 1σ, E ≤ 1σ and U ≤ 1σ.

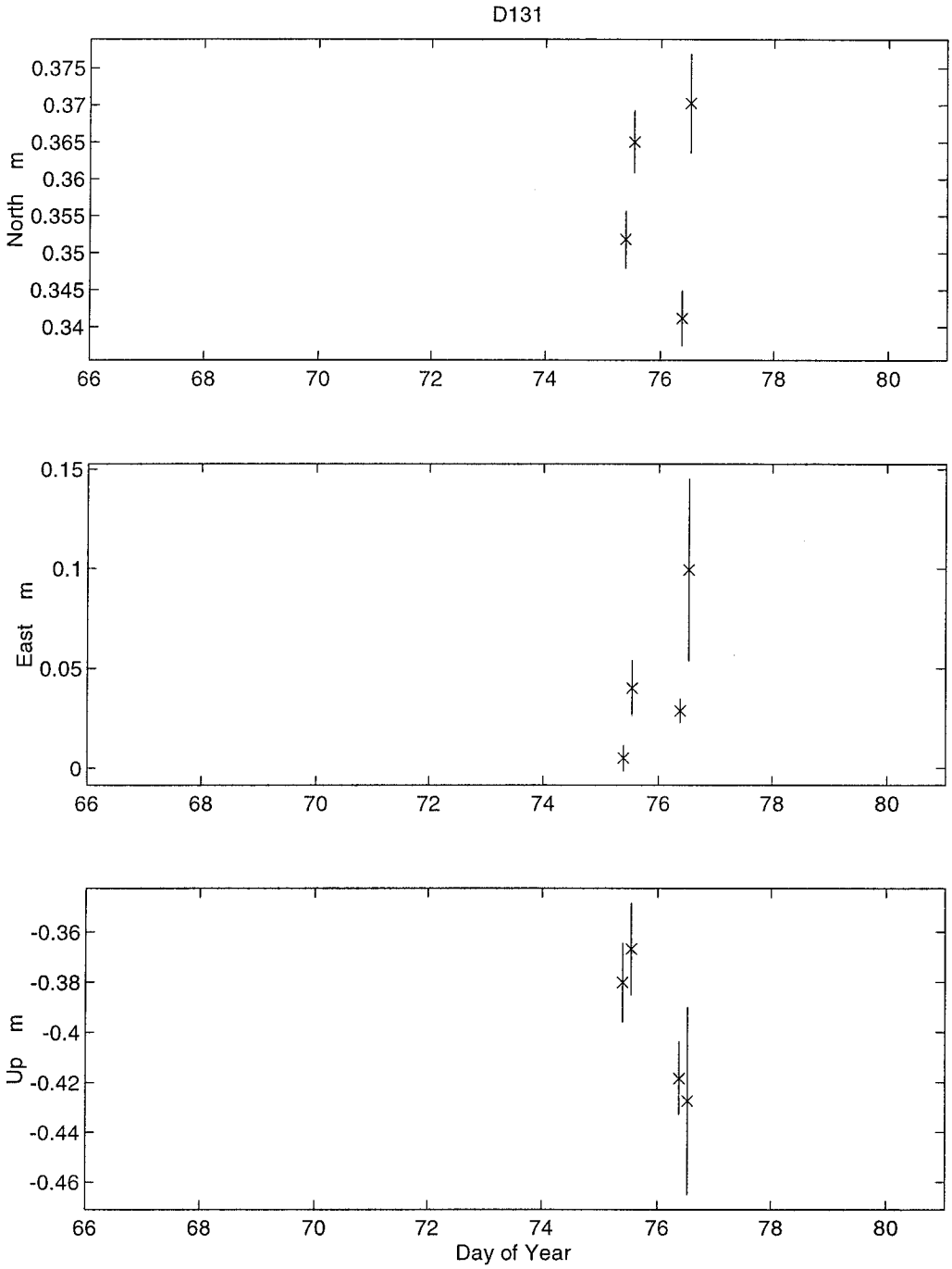

Figure D - 14 : D131 - Mt Stewart [LS]

Comparing the scatter of D131 results for each component against the respective sd values from D474 (Figure D-8) reveals that N $\leq 1\sigma$, E $\leq 2\sigma$ and U $\leq 1\sigma$.

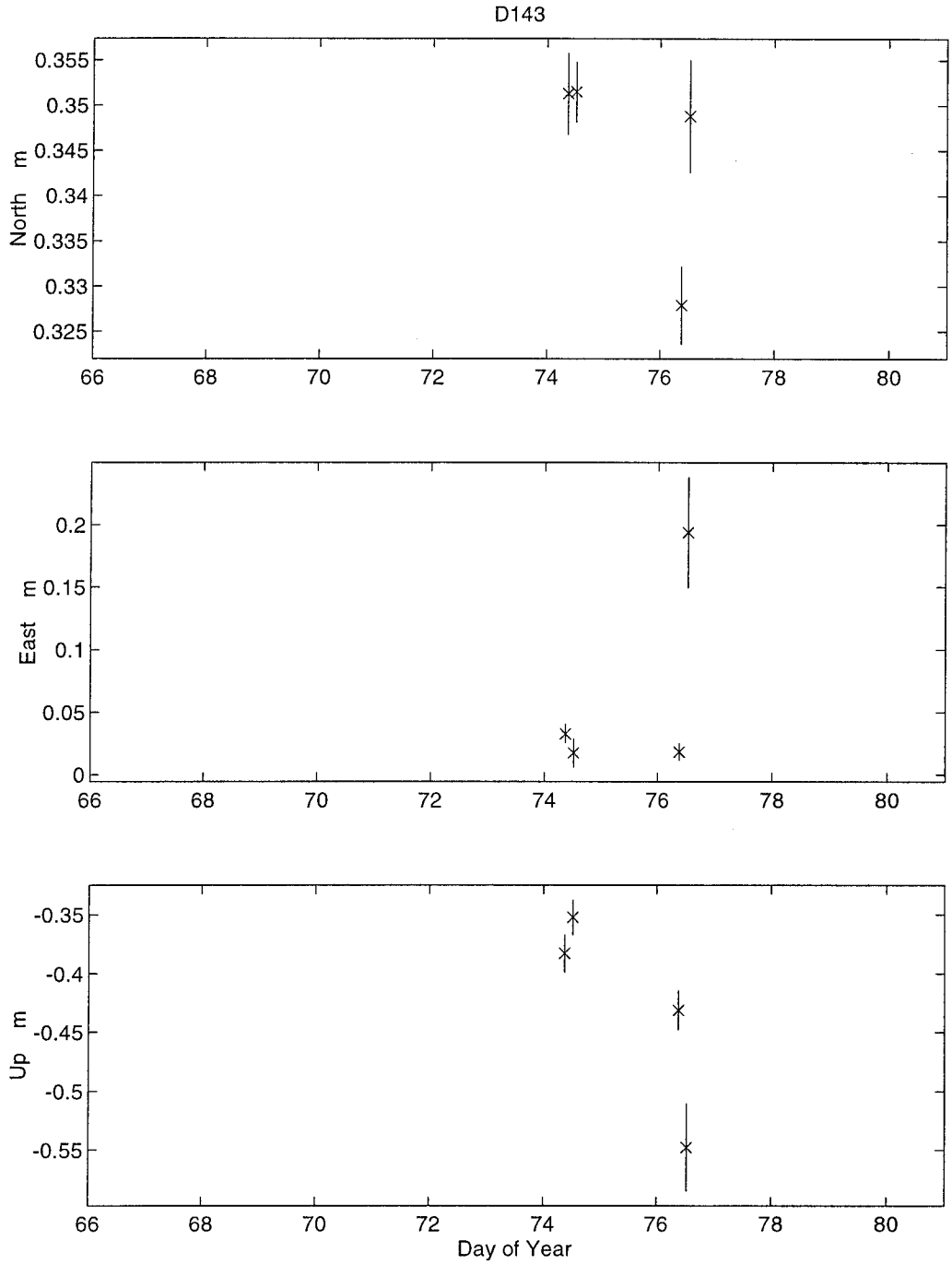

Figure D - 15 : D143 - Eringa [LS]

Comparing the scatter of D143 results for each component against the respective sd values from D474 (Figure D-8) reveals that N ≤ 1σ, E ≤ 3σ and U ≤ 3σ.

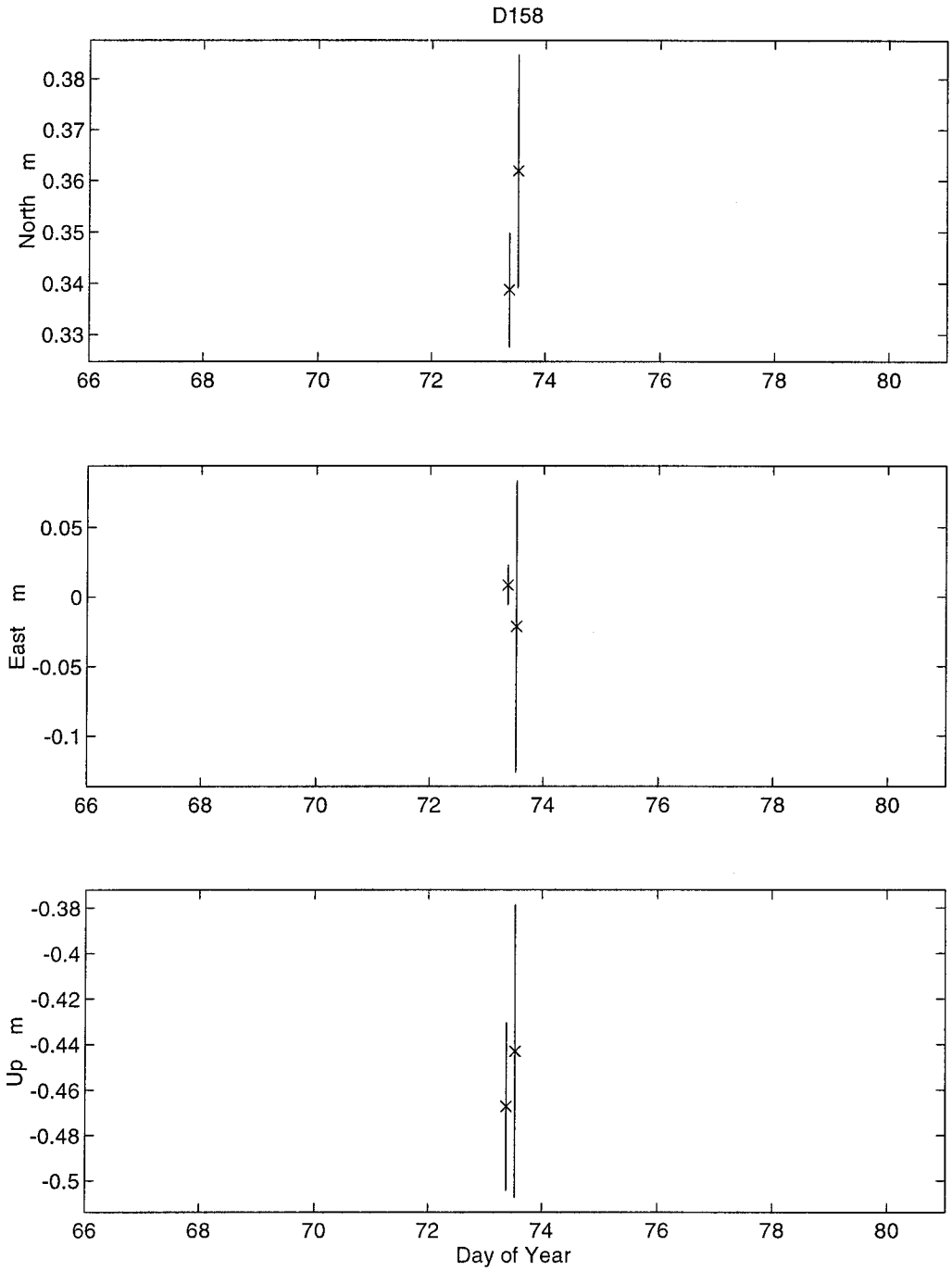

Figure D - 16 : D158 - Jenkins Hill No. 2 [LS]

The larger uncertainty in the second session of DOY 073 remains unexplained, though it is not problematic. This larger uncertainty does exists at all sites (D158; D425, Figure D-27; and D469, Figure D-30) that observed 2 four-hour data sets on DOY 073. One possible cause is that the larger than normal uncertainty for HOB1 (Figure D-5) on DOY 073 (due to only collecting data for 1.5 hours) has propagated through the solution. Comparing the scatter of D158 results for each component against the respective sd values from D474 (Figure D-8) reveals that $N \leq 1\sigma$, $E \leq 1\sigma$ and $U \leq 1\sigma$.

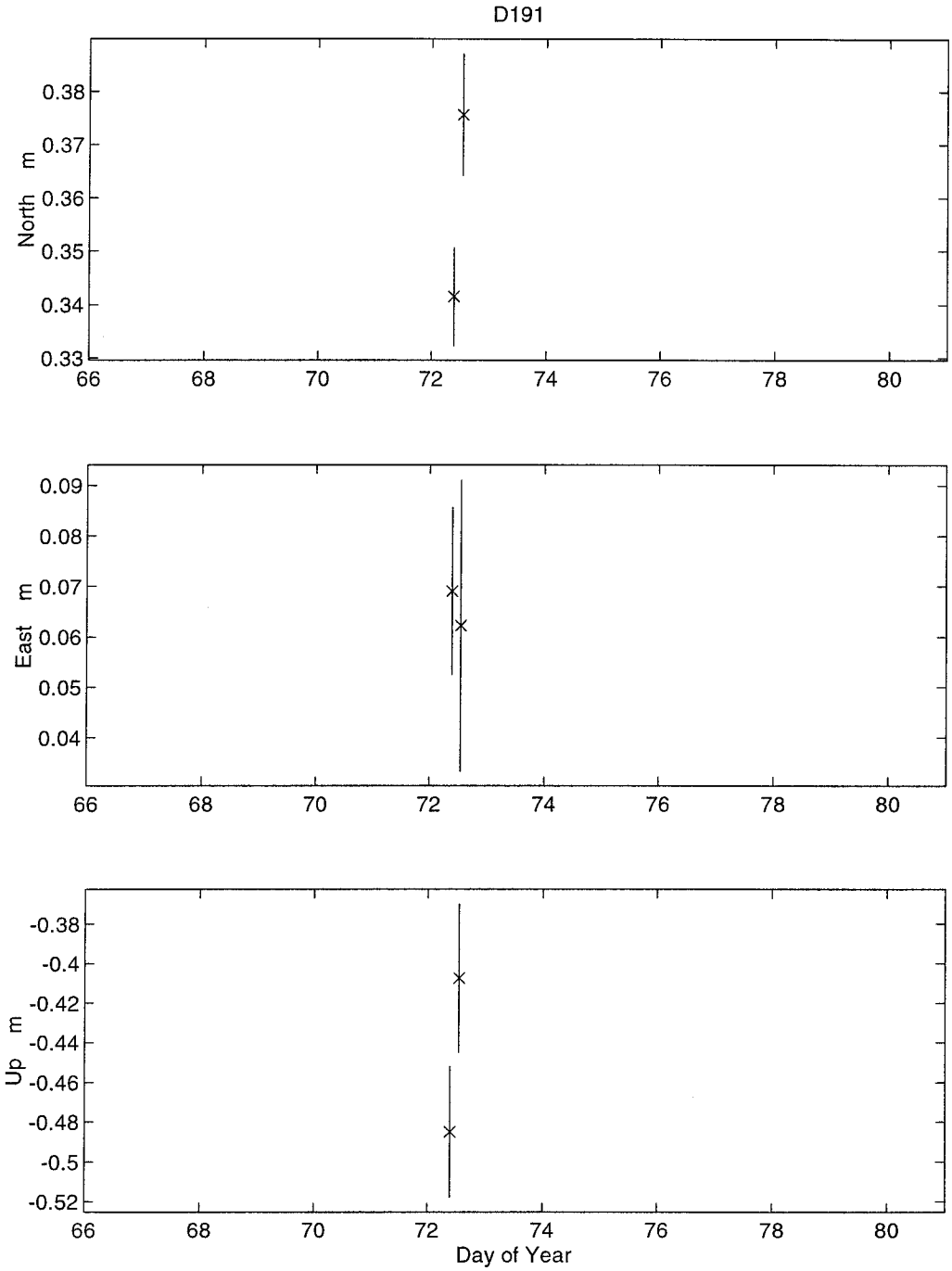

Figure D - 17 : D191 - Isolated Hill [LS]

Comparing the scatter of D191 results for each component against the respective sd values from D474 (Figure D-8) reveals that N ≤ 1σ, E ≤ 1σ and U ≤ 1σ.

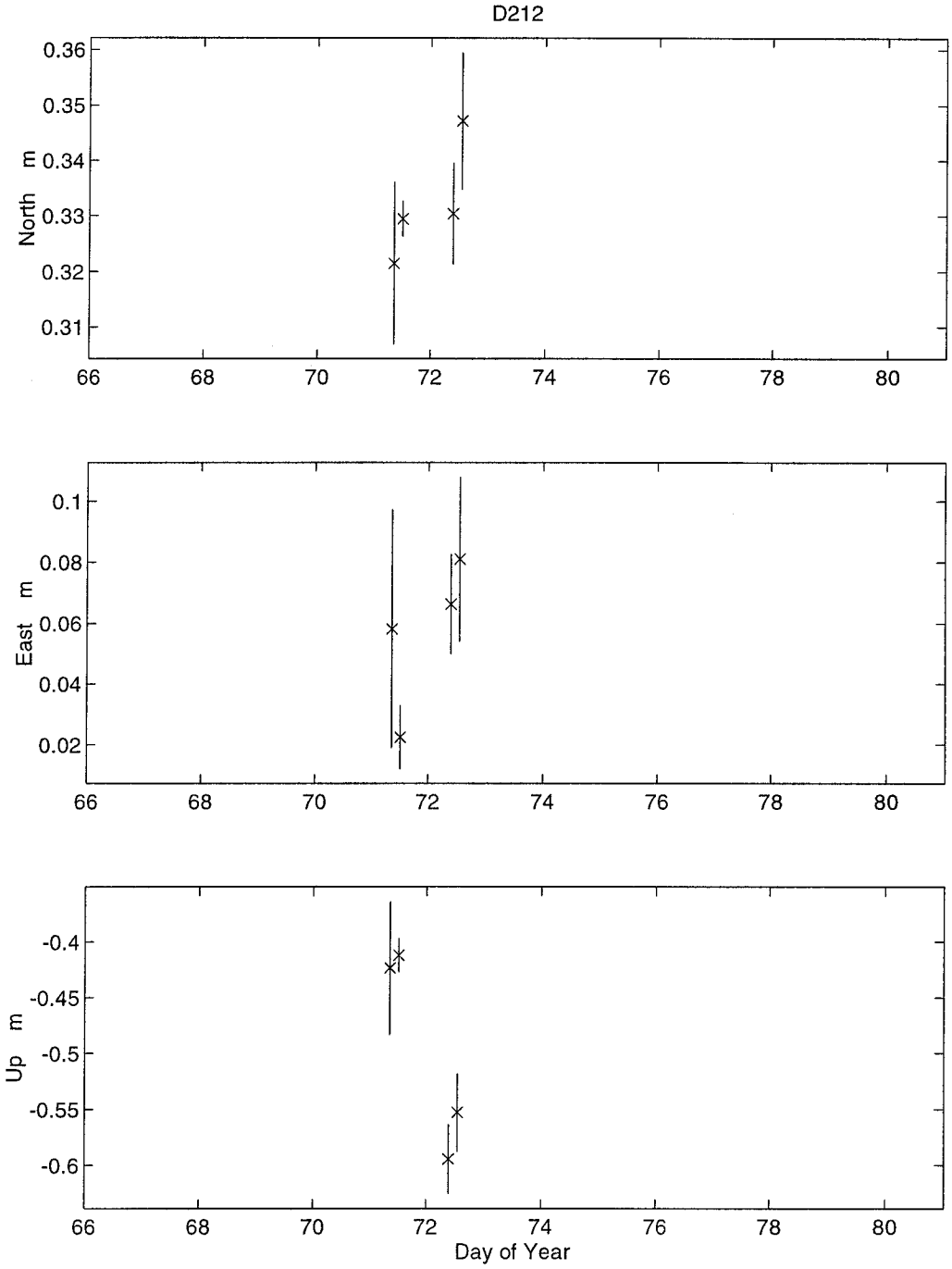

Figure D - 18 : D212 - Mt Pleasant [LS]

Comparing the scatter of D212 results for each component against the respective sd values from D474 (Figure D-8) reveals that N ≤ 1σ, E ≤ 1σ and U ≤ 3σ.

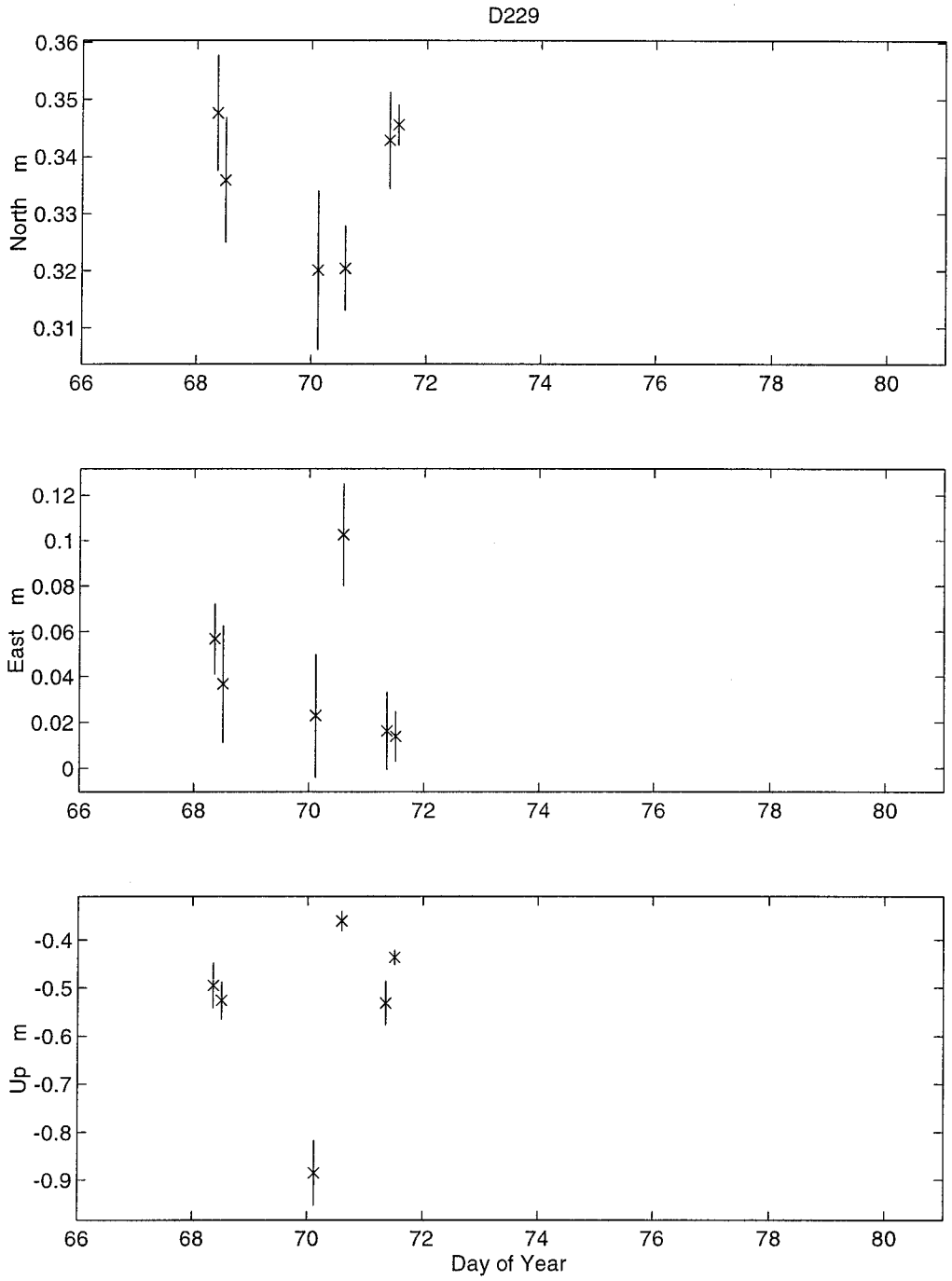

Figure D - 19 : D229 - Mt Mary [LS]

Comparing the scatter of D229 results for each component against the respective sd values from D474 (Figure D-8) reveals that N ≤ 2σ, E ≤ 2σ and U > 3σ. The first session on DOY 070 has an outlier in the Up component. This outlier was not detected during processing and in hindsight should have been investigated. The effect of the outlier would have been partially mitigated in GLOBK due to its larger uncertainty. The probable cause of the outlier is that the height of receiver was either incorrectly measured or entered. This is supported by the second session not being affected so it is unlikely to be due to network geometry problems due to no DS42 data being available. Also the North and East components remain unaffected.

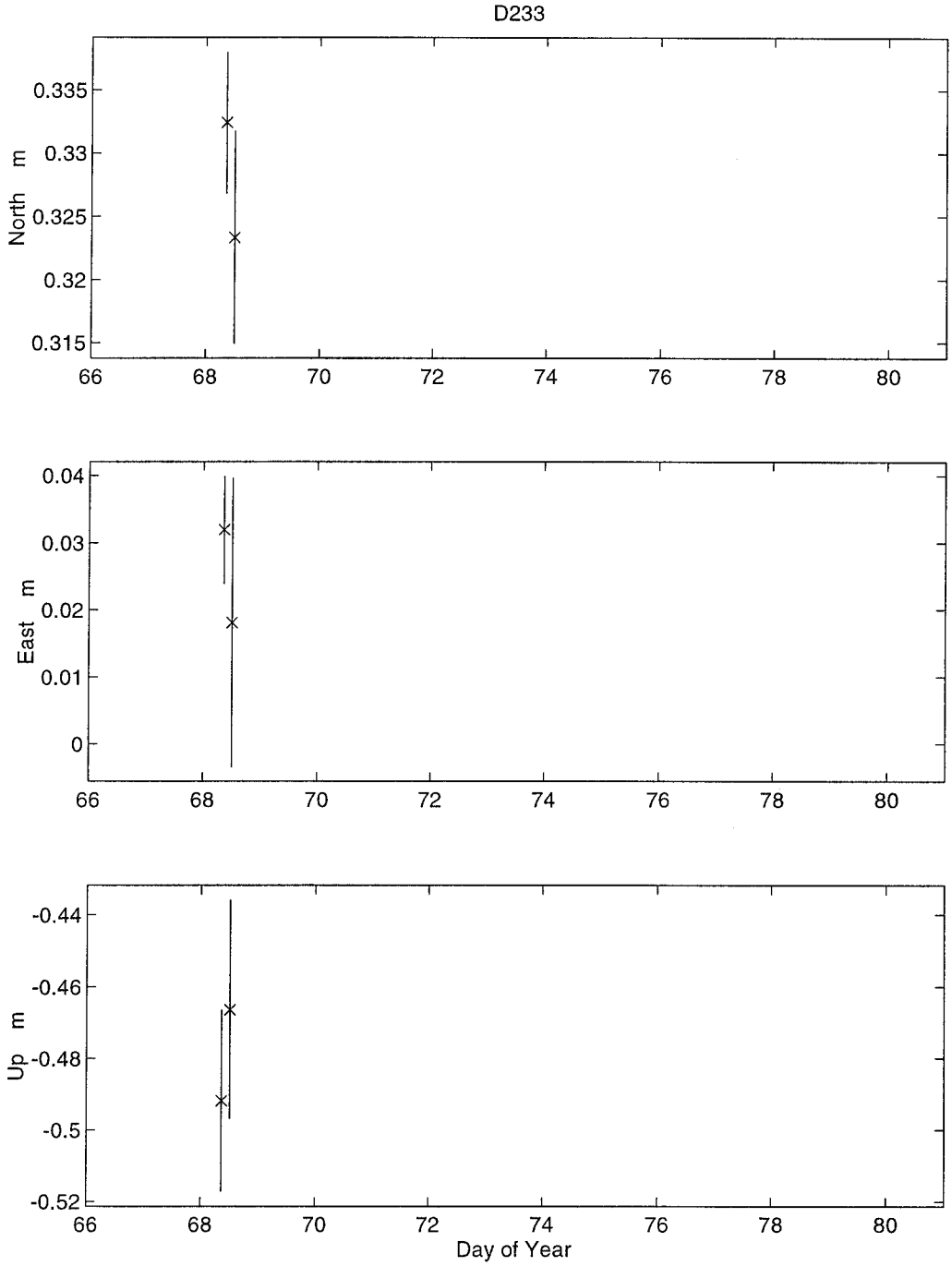

Figure D - 20 : D233 - A Mt Horrible [LS]

Comparing the scatter of D233 results for each component against the respective sd values from D474 (Figure D-8) reveals that N ≤ 1σ, E ≤ 1σ and U ≤ 1σ.

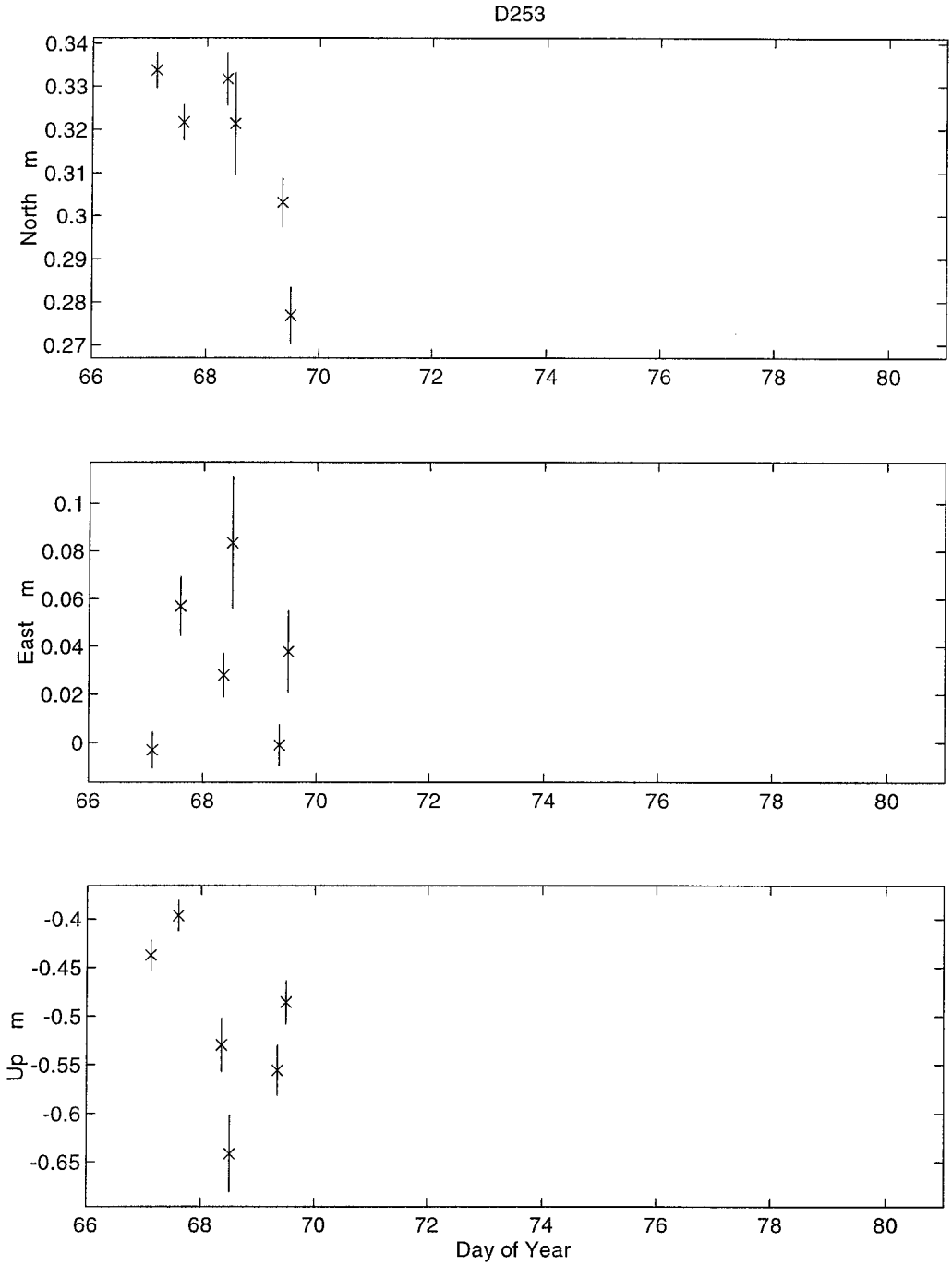

Figure D - 21 : D253 - T Hyde Rock [LS]

These three days of data show no distinct variation in variability or uncertainty even though DOY 067 was split into two sessions and SINCLN used, while DOY 068 and 069 used AUTCLN with one session. The regional and local fiducial network were consistent for all three days. Comparing the scatter of D253 results for each component against the respective sd values from D474 (Figure D-8) reveals that $N \leq 2\sigma$, $E \leq 2\sigma$ and $U \leq 3\sigma$.

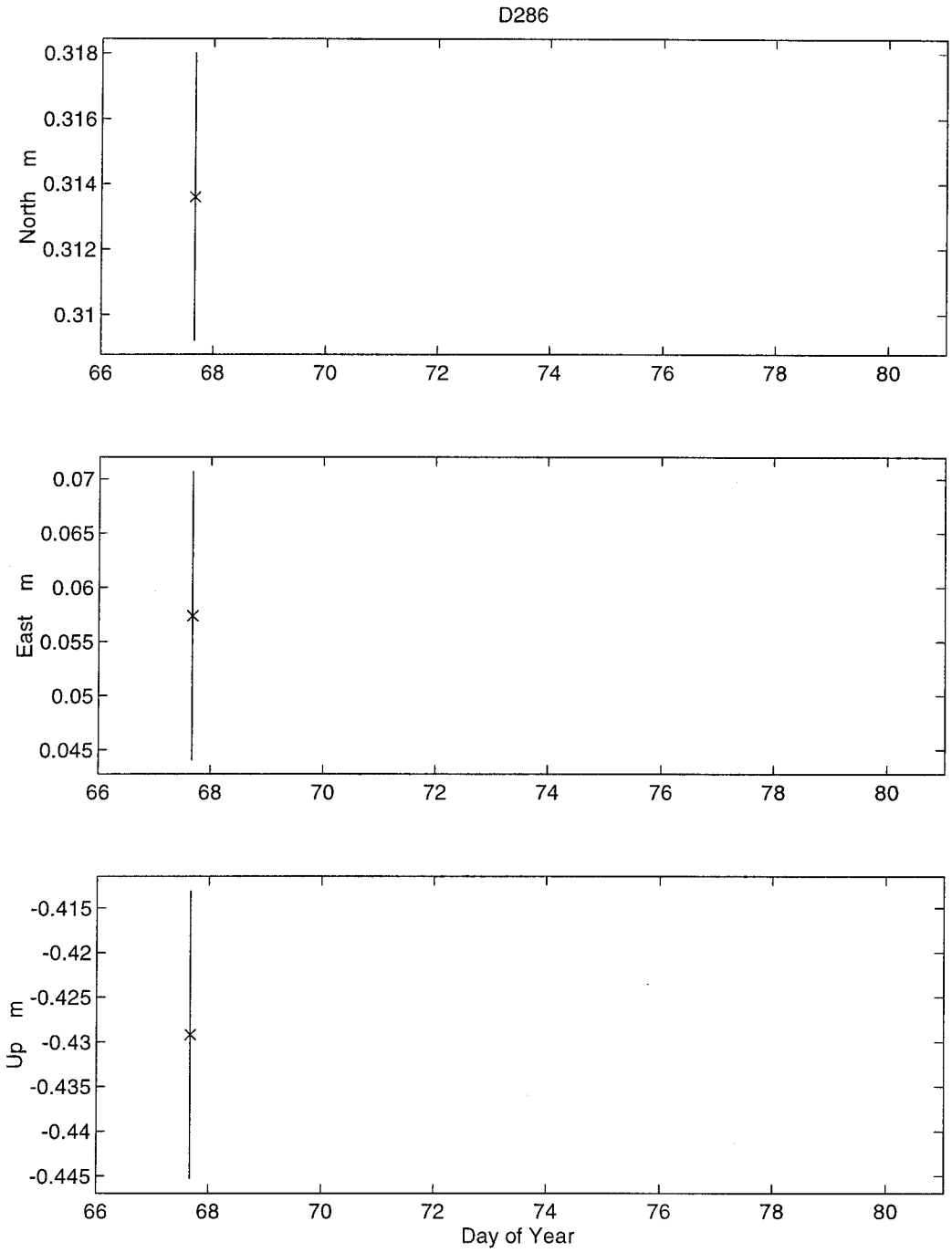

Figure D - 22 : D286 - X The Bluff [LS]

No data from D286 for the first session of DOY 067 was able to be processed in GAMIT. As a consequence the second session of DOY 067 is the only result for this station. Therefore there are no checks on D286 coordinates.

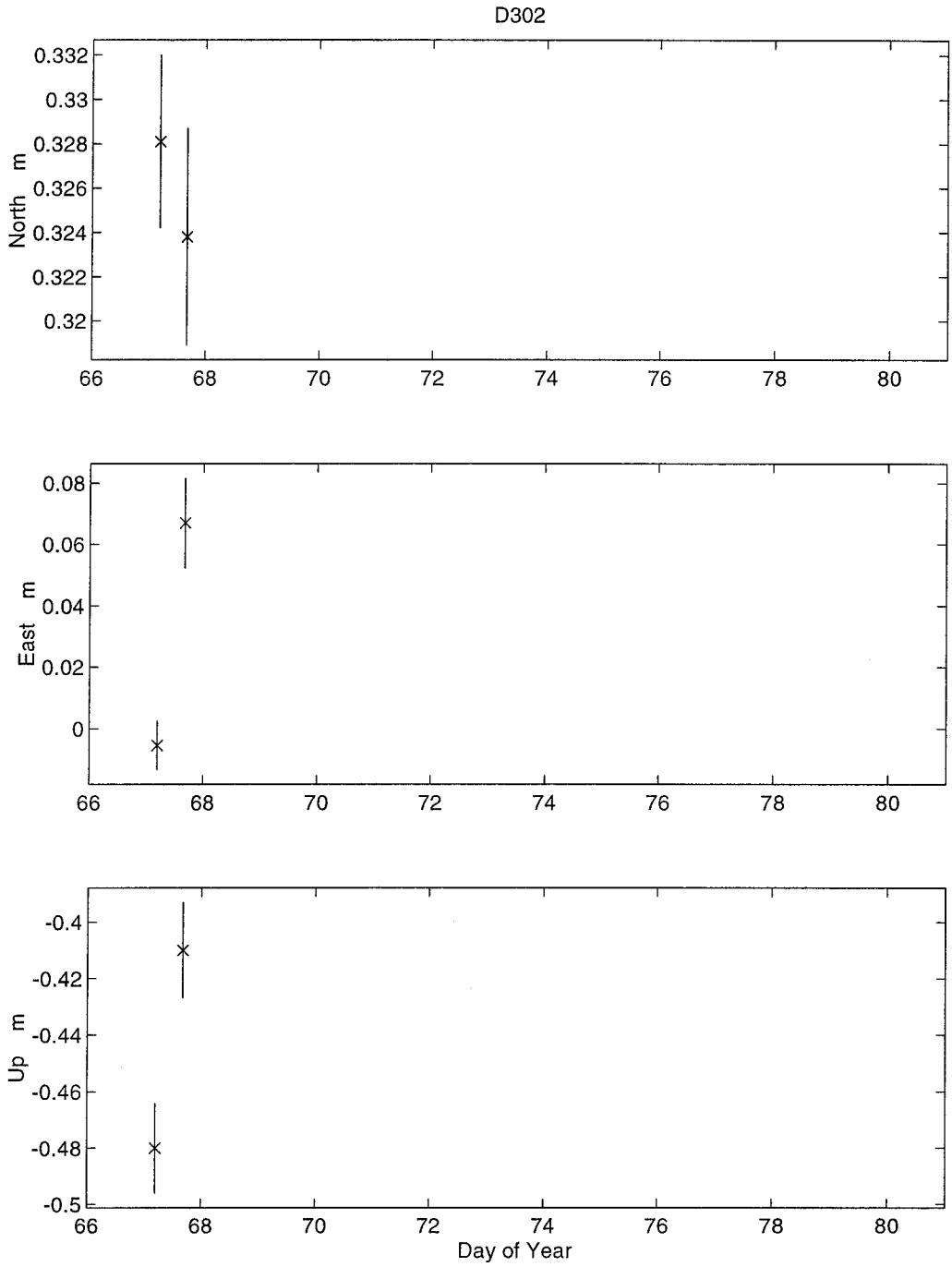

Figure D - 23 : D302 - Mt York [LS]

Comparing the scatter of D302 results for each component against the respective sd values from D474 (Figure D-8) reveals that N ≤ 1σ, E ≤ 2σ and U ≤ 1σ.

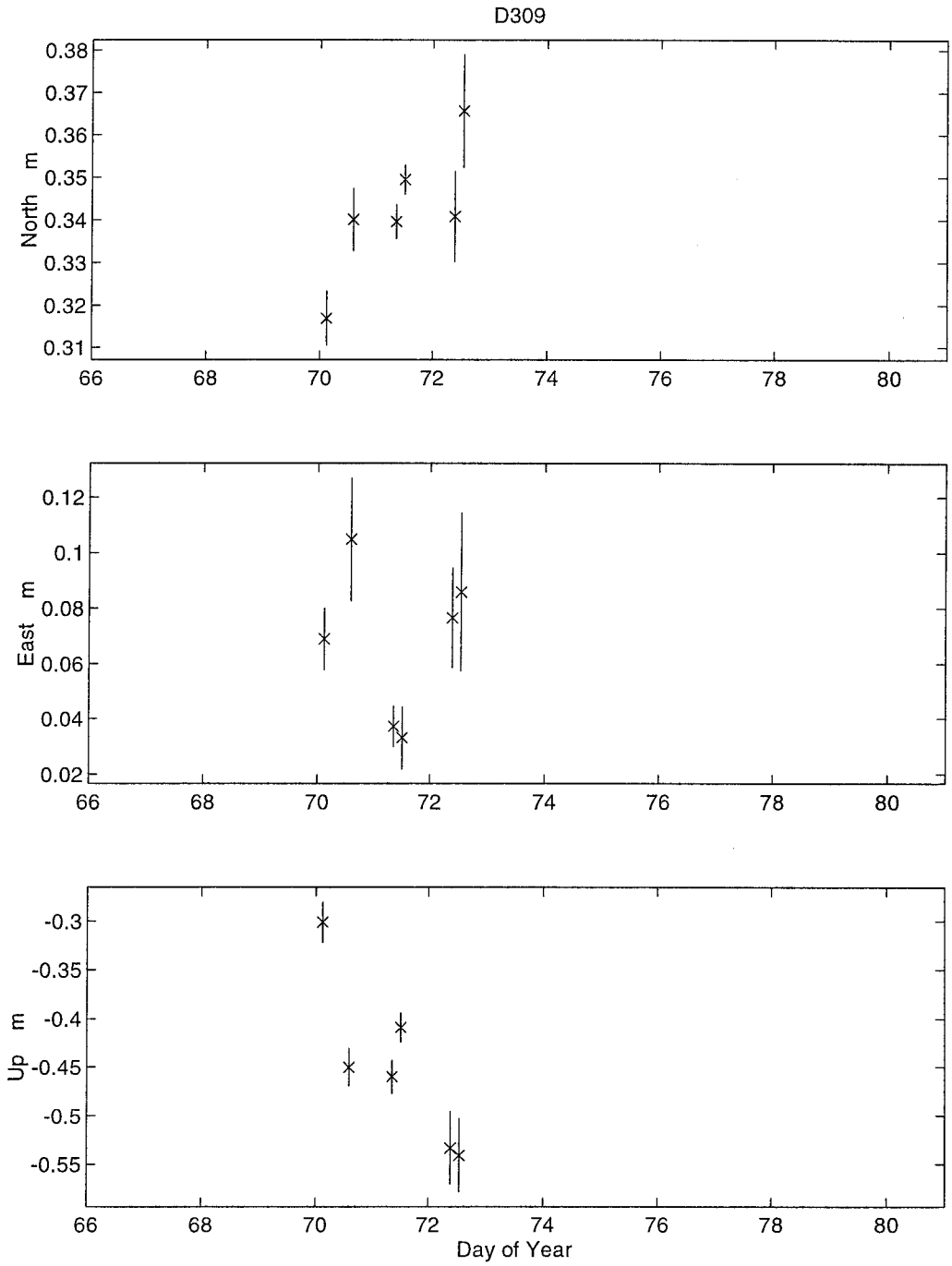

Figure D - 24 : D309 - HB Mt Greenland [LS]

Comparing the scatter of D309 results for each component against the respective sd values from D474 (Figure D-8) reveals that N ≤ 2σ, E ≤ 2σ and U ≤ 3σ.

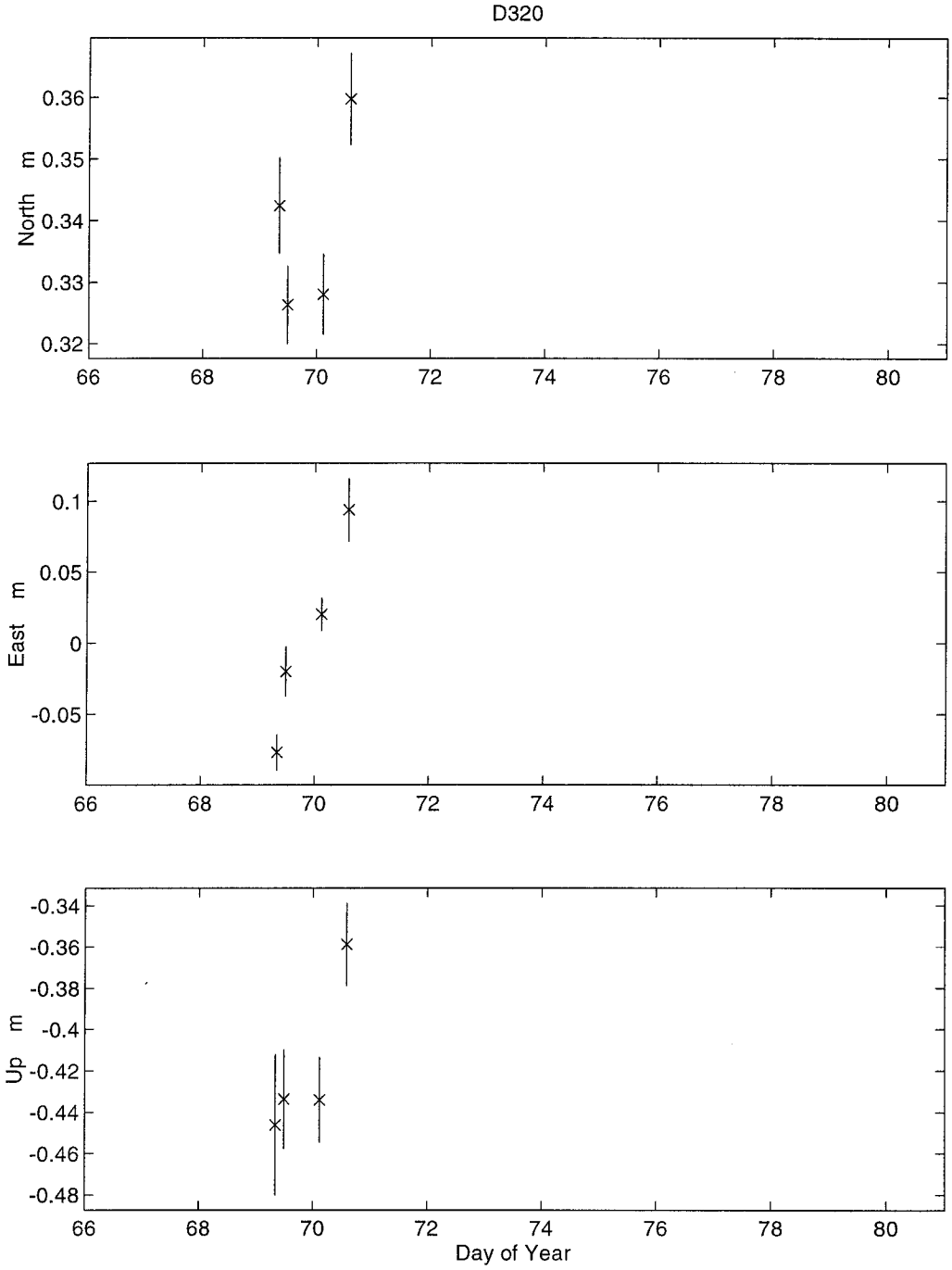

Figure D - 25 : D320 - JF (Gillespies Survey District) [LS]

Comparing the scatter of D320 results for each component against the respective sd values from D474 (Figure D-8) reveals that N ≤ 2σ, E ≤ 3σ and U ≤ 2σ.

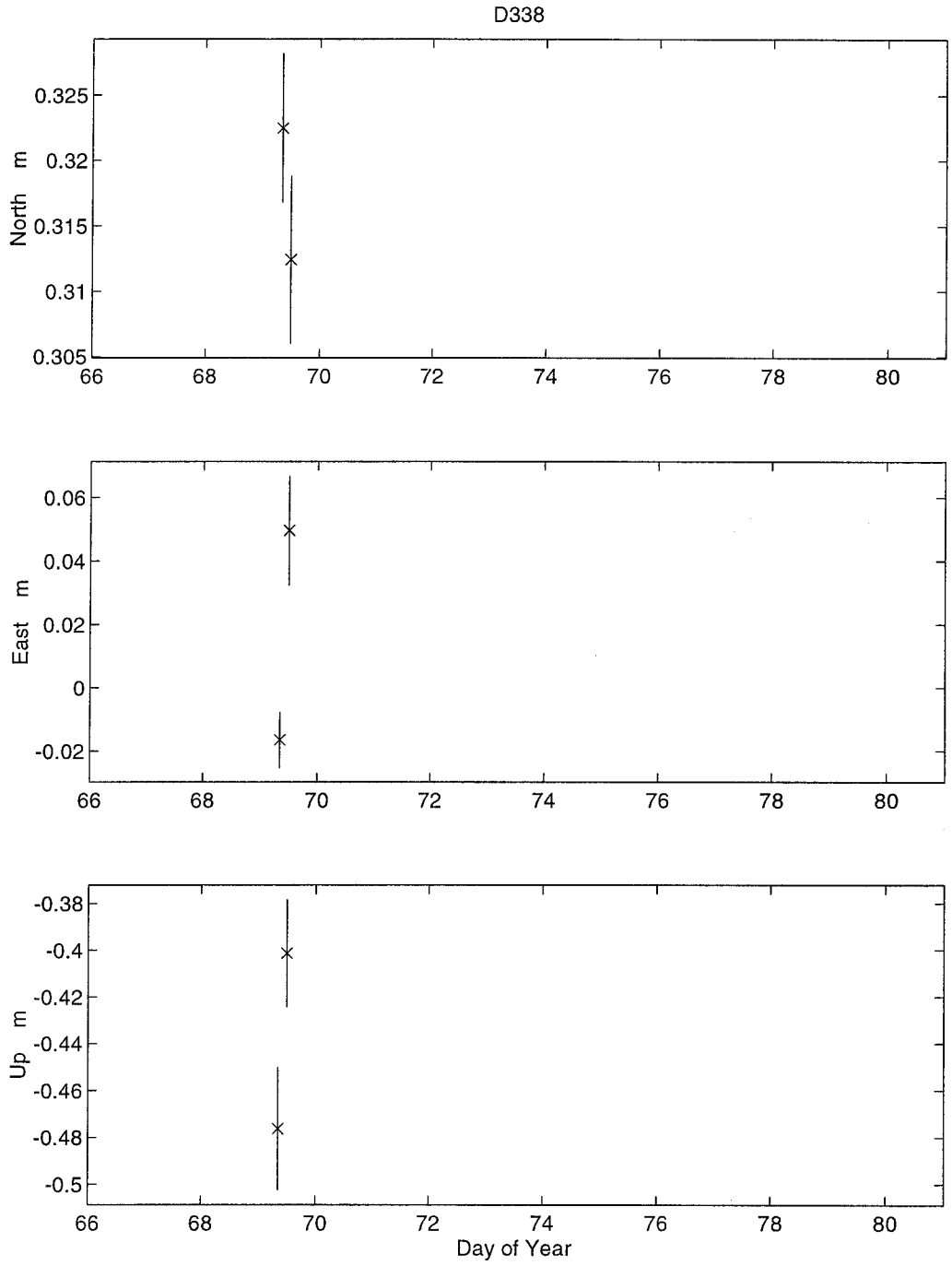

Figure D - 26 : D338 - 8741 [LS]

Comparing the scatter of D338 results for each component against the respective sd values from D474 (Figure D-8) reveals that N $\leq 1\sigma$, E $\leq 2\sigma$ and U $\leq 1\sigma$.

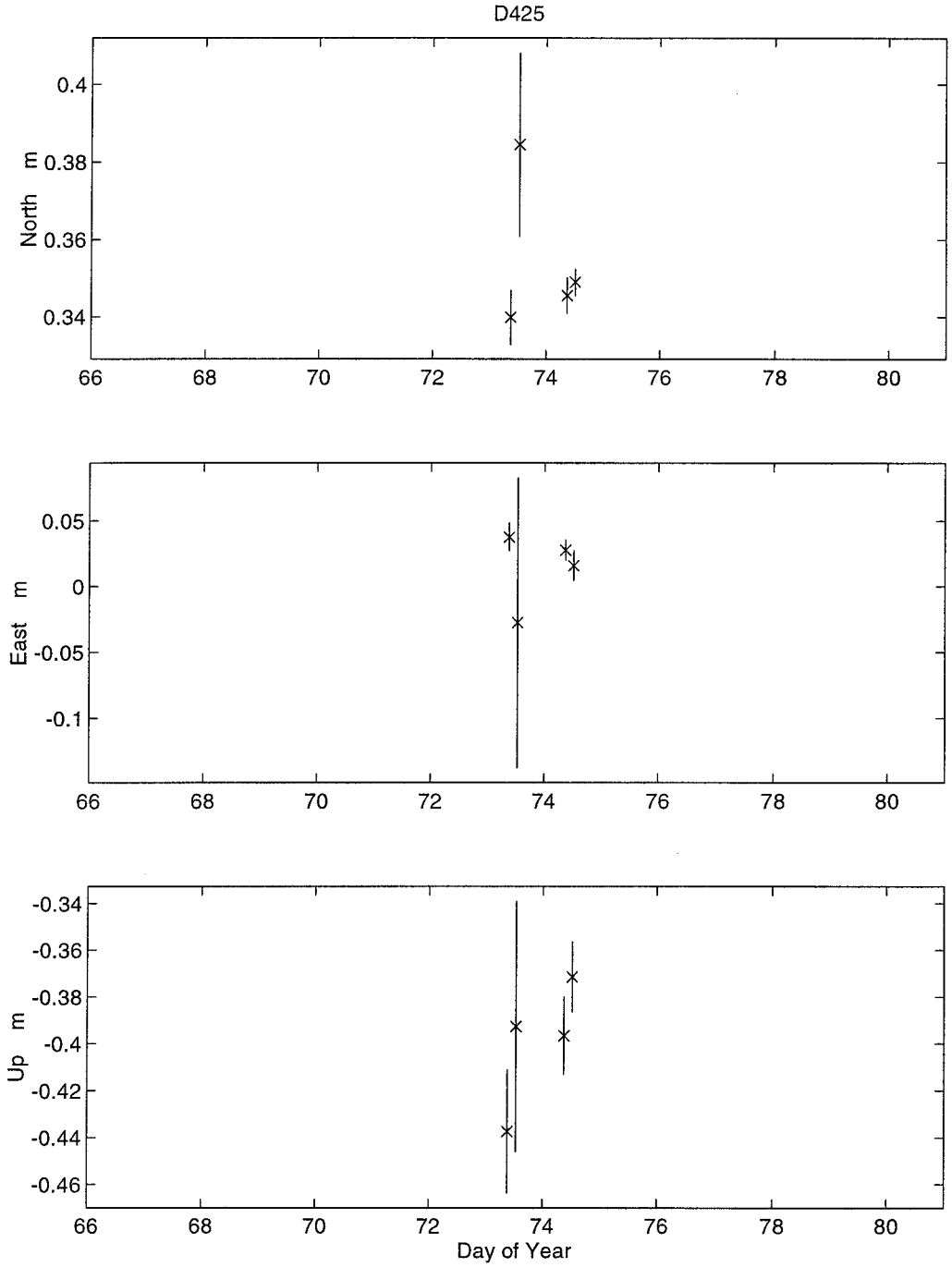

Figure D - 27 : D425 - A (Cape Campbell Survey District) [LS]

Refer to D158 (Figure D-16) for comments on the larger than normal uncertainty for the second session of DOY 073. Comparing the scatter of D425 results for each component against the respective sd values from D474 (Figure D-8) reveals that $N \leq 2\sigma$, $E \leq 2\sigma$ and $U \leq 2\sigma$.

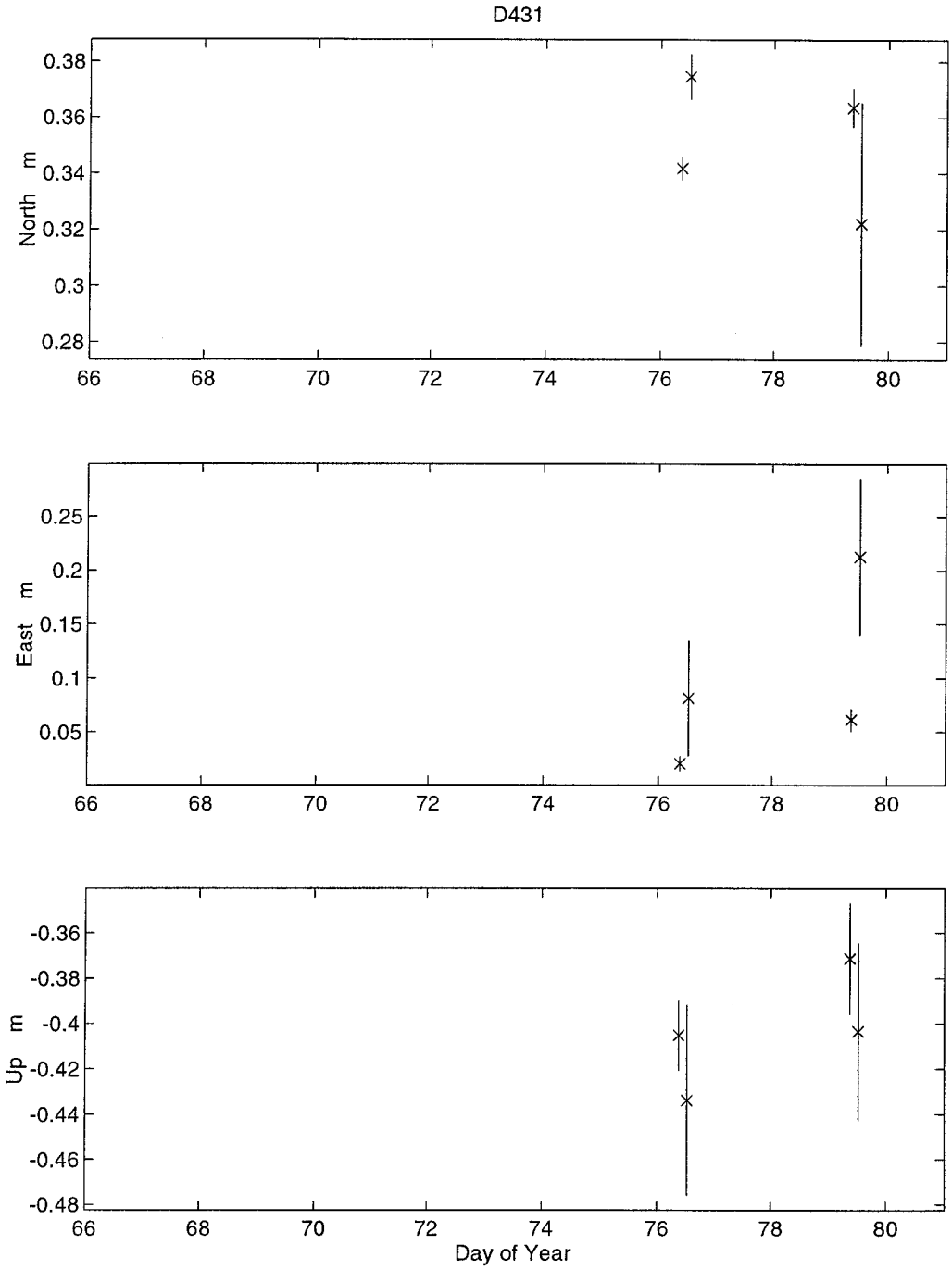

Figure D - 28 : D431 - Bluff Hill No. 3 [LS]

Refer to D078 (Figure D-11) for comments on the large uncertainty in the East component on the second session of DOY 079. Comparing the scatter of D431 results for each component against the respective sd values from D474 (Figure D-8) reveals that $N \leq 2\sigma$, $E > 3\sigma$ and $U \leq 1\sigma$.

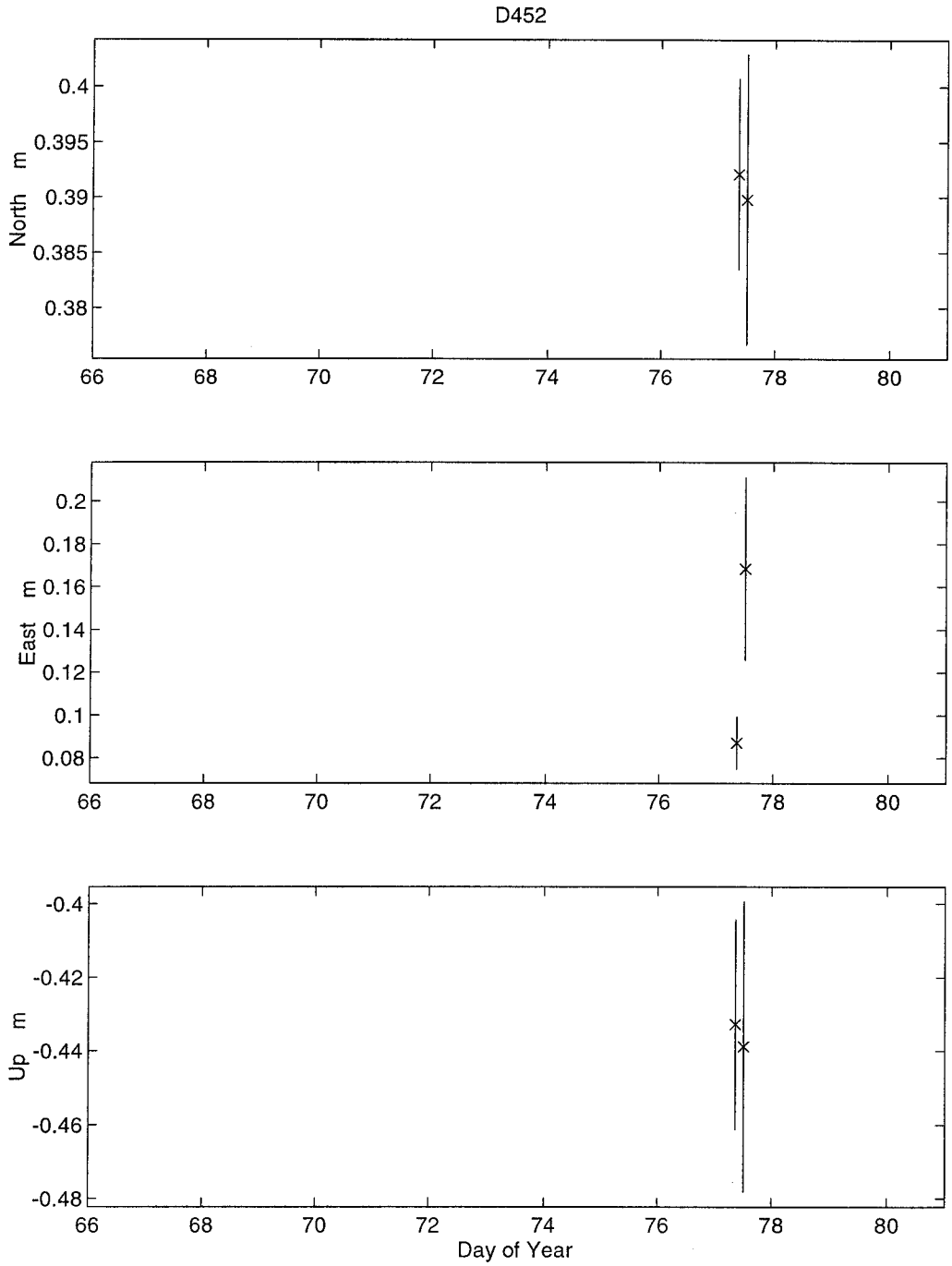

Figure D - 29 : D452 - 79 (Rangiriri Survey District) [LS]

Comparing the scatter of D452 results for each component against the respective sd values from D474 (Figure D-8) reveals that N $\leq 1\sigma$, E $\leq 2\sigma$ and U $\leq 1\sigma$.

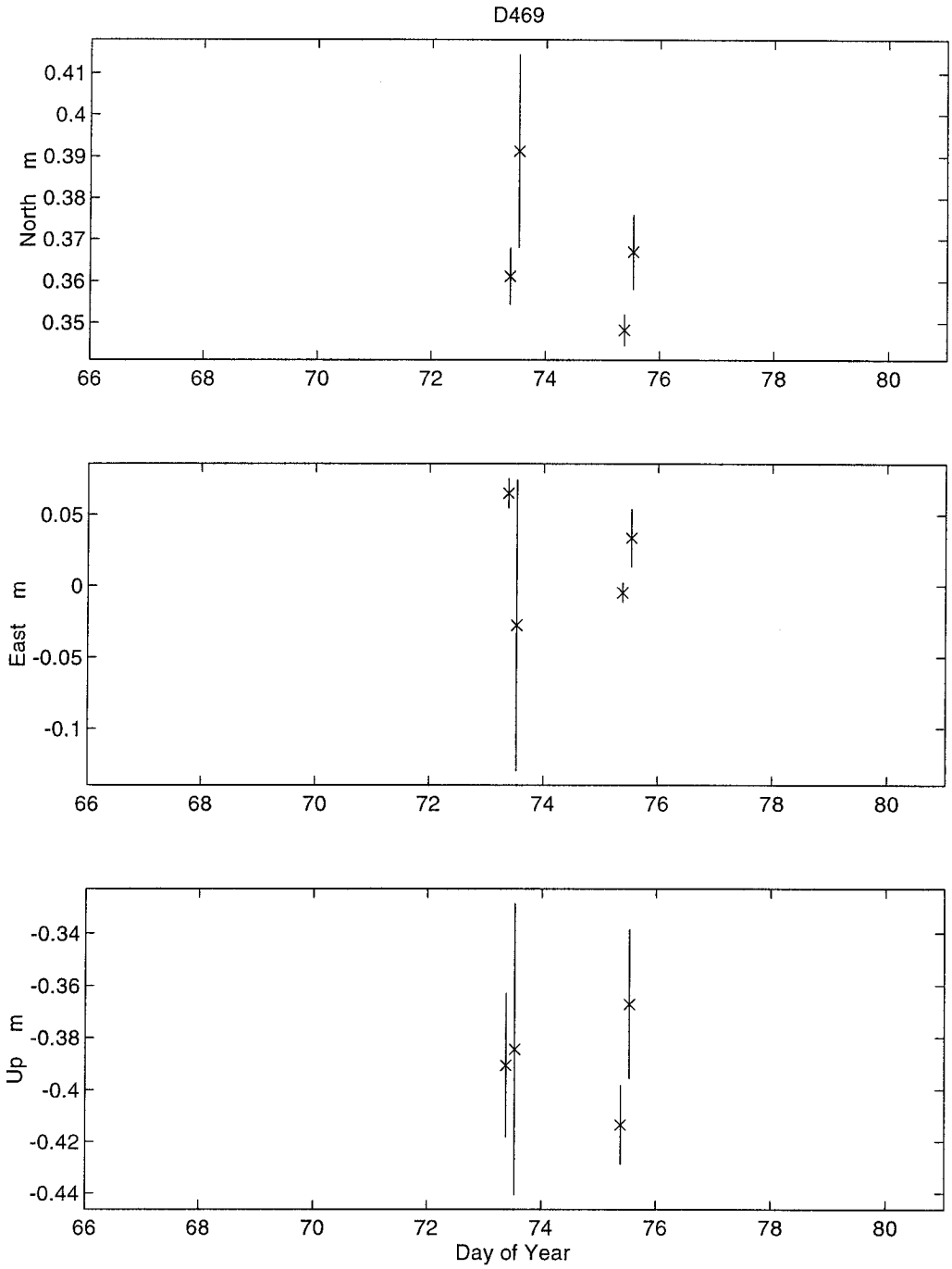

Figure D - 30 : D469 - I Parapara [LS]

Refer to D158 (Figure D-16) for comments on the larger than normal uncertainty for the second session of DOY 073. Comparing the scatter of D469 results for each component against the respective sd values from D474 (Figure D-8) reveals that N $\leq 2\sigma$, E $\leq 2\sigma$ and U $\leq 1\sigma$.

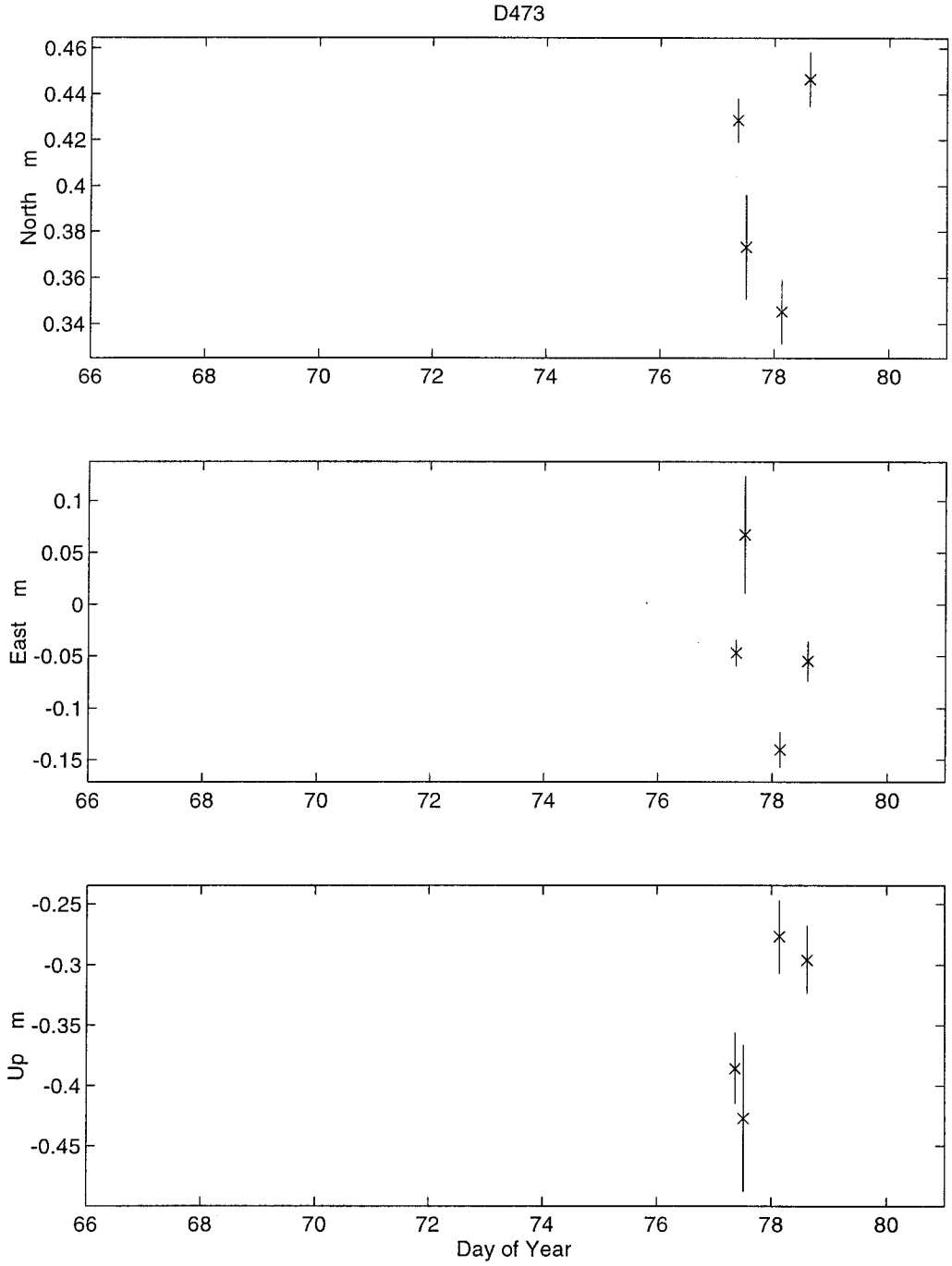

Figure D - 31 : D473 - Marotiri No. 2 [LS]

D473 was observed with a Leica system 200 receiver. Comparing the scatter of D473 results for each component against the respective sd values from the Ashtech receiver at D474 (Figure D-8) reveals that $N \leq 3\sigma$, $E \leq 3\sigma$ and $U \leq 2\sigma$. Therefore it can be concluded, with the supporting results at D072 (Figure D-10), D482 (Figure D-32) and D483 (Figure D-33), that the Leica system 200 receivers performed in a similar manner to the Ashtech LM-XII receivers.

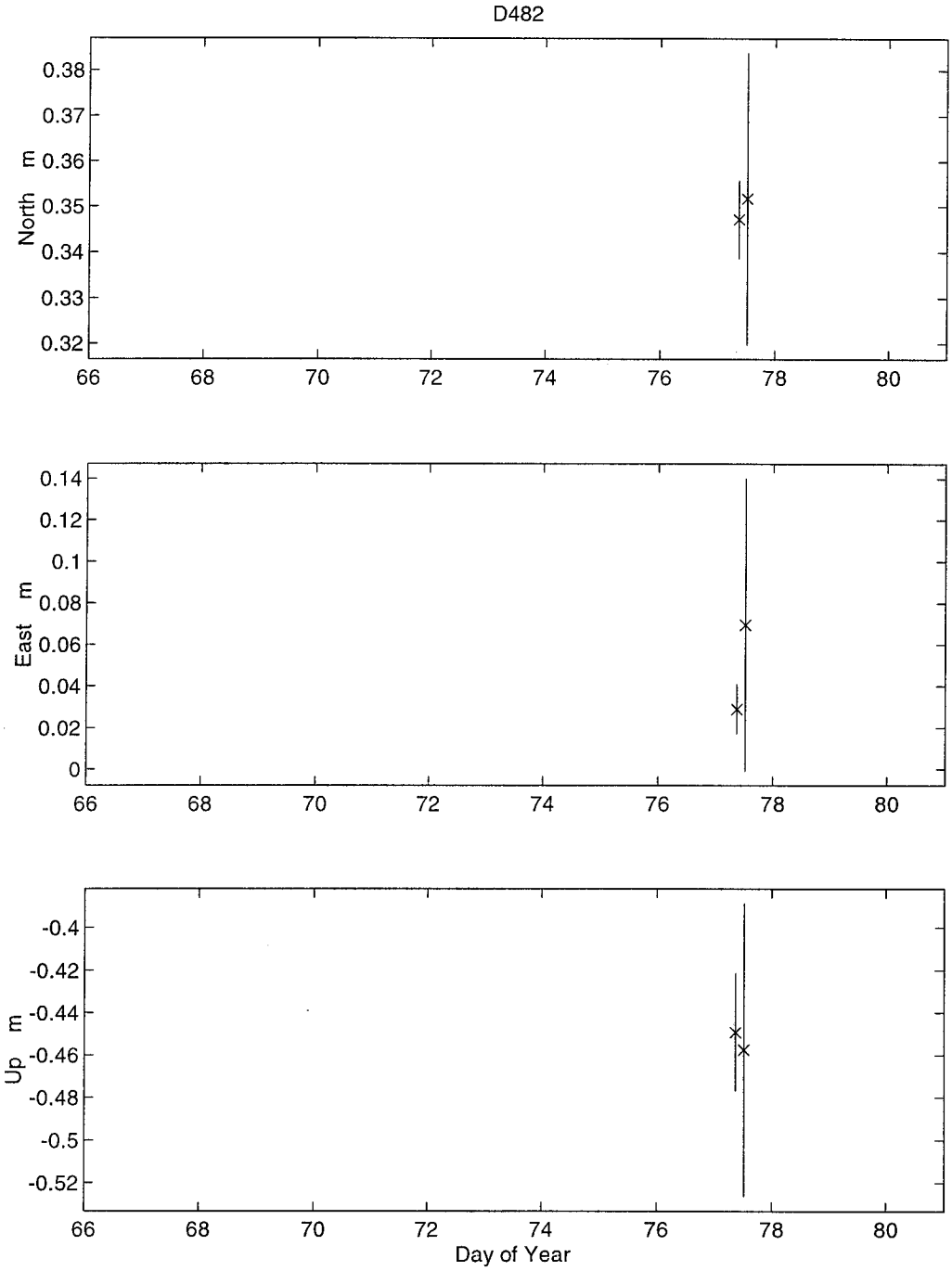

Figure D - 32 : D482 - HHR9 (Heaphy House Roof Mark 9) [LS]

D482 was observed with a Leica system 200 receiver. Comparing the scatter of D482 results for each component against the respective sd values from the Ashtech receiver at D474 (Figure D-8) reveals that N ≤ 1σ, E ≤ 1σ and U ≤ 1σ. Refer to D473 (Figure D-31) for further comments on the performance of the Leica and Ashtech receivers.

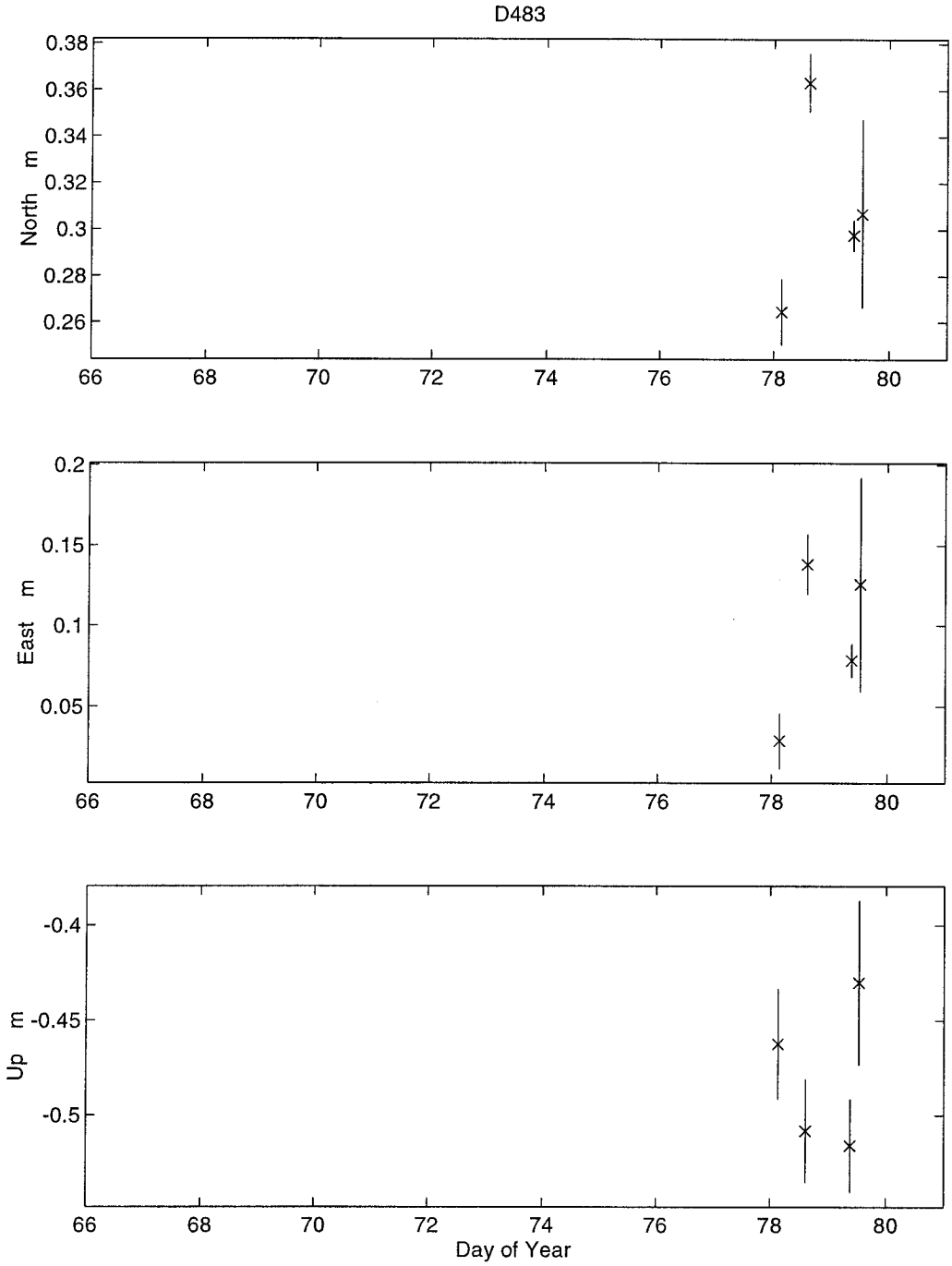

Figure D - 33 : D483 - HHR9A (Heaphy House Roof Mark 9A) [LS]

D483 was observed with a Leica system 200 receiver. Comparing the scatter of D483 results for each component against the respective sd values from the Ashtech receiver at D474 (Figure D-8) reveals that $N \leq 3\sigma$, $E \leq 2\sigma$ and $U \leq 2\sigma$. Refer to D473 (Figure D-31) for further comments on the performance of the Leica and Ashtech receivers.

Appendix E

GPS data quality plots from CVIEW

The diagrams contained in this Appendix were generated from CVIEW (the interactive data editing module) screen dumps for DOY 067. The data displayed in these following cviews diagrams is the residual phase data (ie. observed - computed) but the satellite orbits and station coordinates are at their a priori input level. As a result there is no orbit modelling. From the examples given in this appendix it can be seen that data collected by different receivers were influenced by a number of effects (ie. varying atmospheric conditions or type of hardware).

Figure E-1 is an example CVIEW screen dump which highlights those main features that need to be considered when analysing the remaining Figures. For all Figures the first four panels display the L1, L2, LC and LG combinations (Section 3.5.1). The fifth panel
displays either the WL combination (if a receiver records the P-code) or the elevation of the satellite at the site being considered. The mean (O@) and standard deviation (s - 95% confidence interval) statistics given for each panel are computed from the data displayed in that panel only. Each panel's vertical axis is in cycle units of the respective combination, while the horizontal axis is the UTC time for the span of data currently displayed.

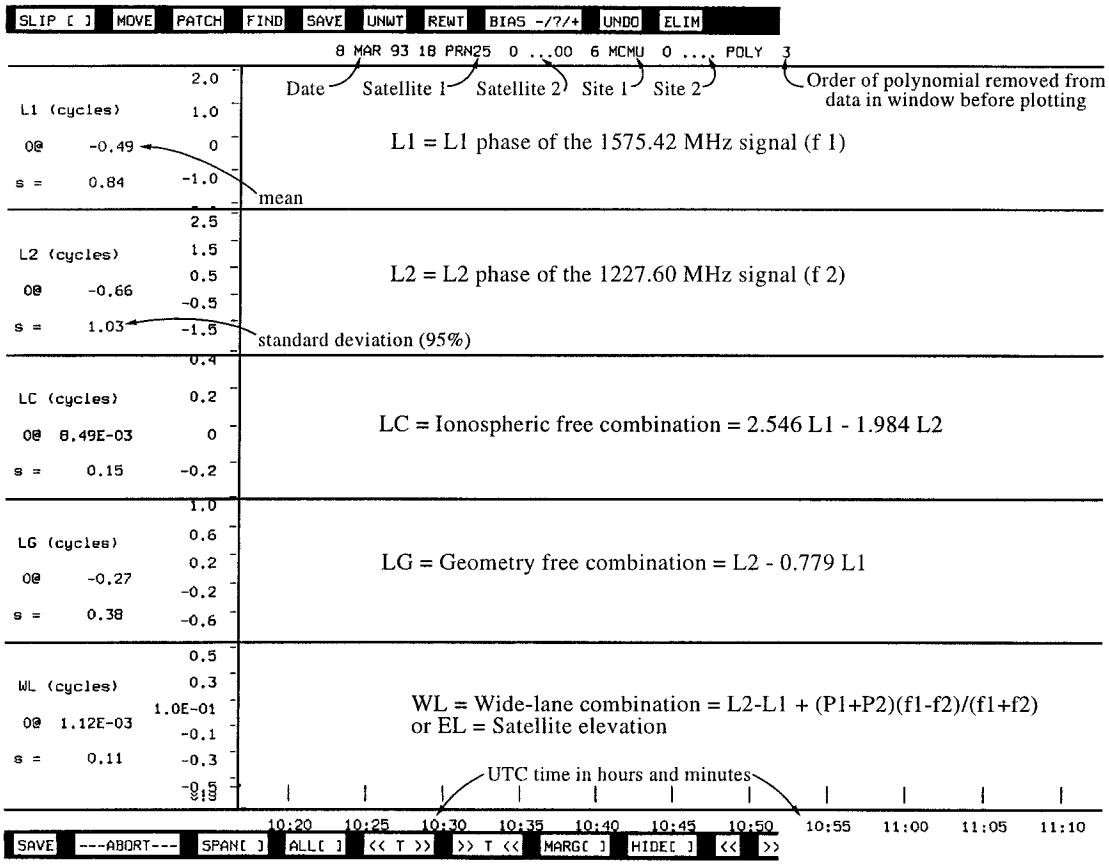

Figure E - 1 : Sample CVIEW screen dump

The following table lists those figures that are contained in this appendix.

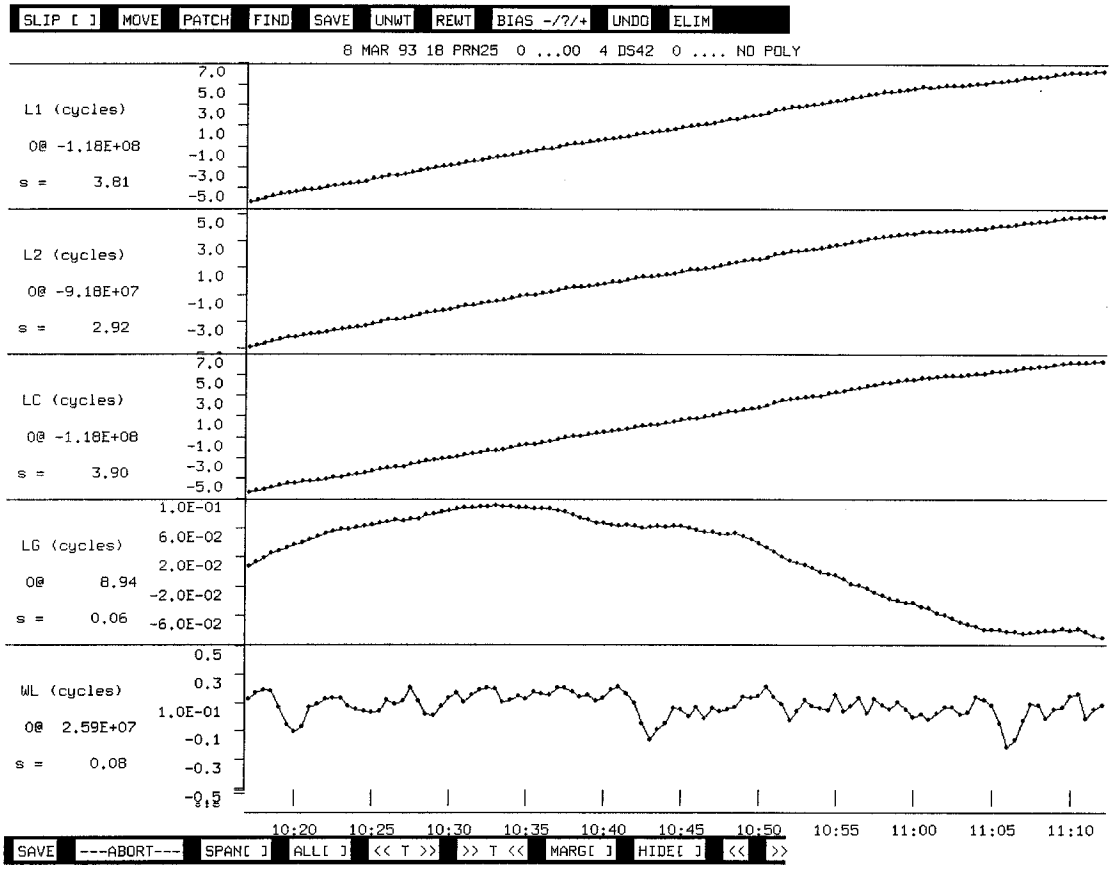

Figure E - 2 : One-way combination of DS42 and PRN25

The one-way combination of the mid-latitude station DS42 and satellite PRN 25 (Figure E-2) shows the lack of orbit modelling clearly as longer term features. These long term features have influenced the standard deviations and hide the true variability of the data.

It should be noted that there are no gaps in the data, which is indicated by each measurement of data (dots) being joined by a line.

The LG combination has a standard deviation of 0.06. This indicates that the L1 and L2 data is good, but is being hidden by the long term features.

DS42 had a Rogue receiver (which is capable of recording the P-code) so the wide-lane (WL) combination can be formed. Note that the WL is not affected by the lack of modelling and has a standard deviation of only 0.08 cycles. This is an example of high quality wide-lane data.

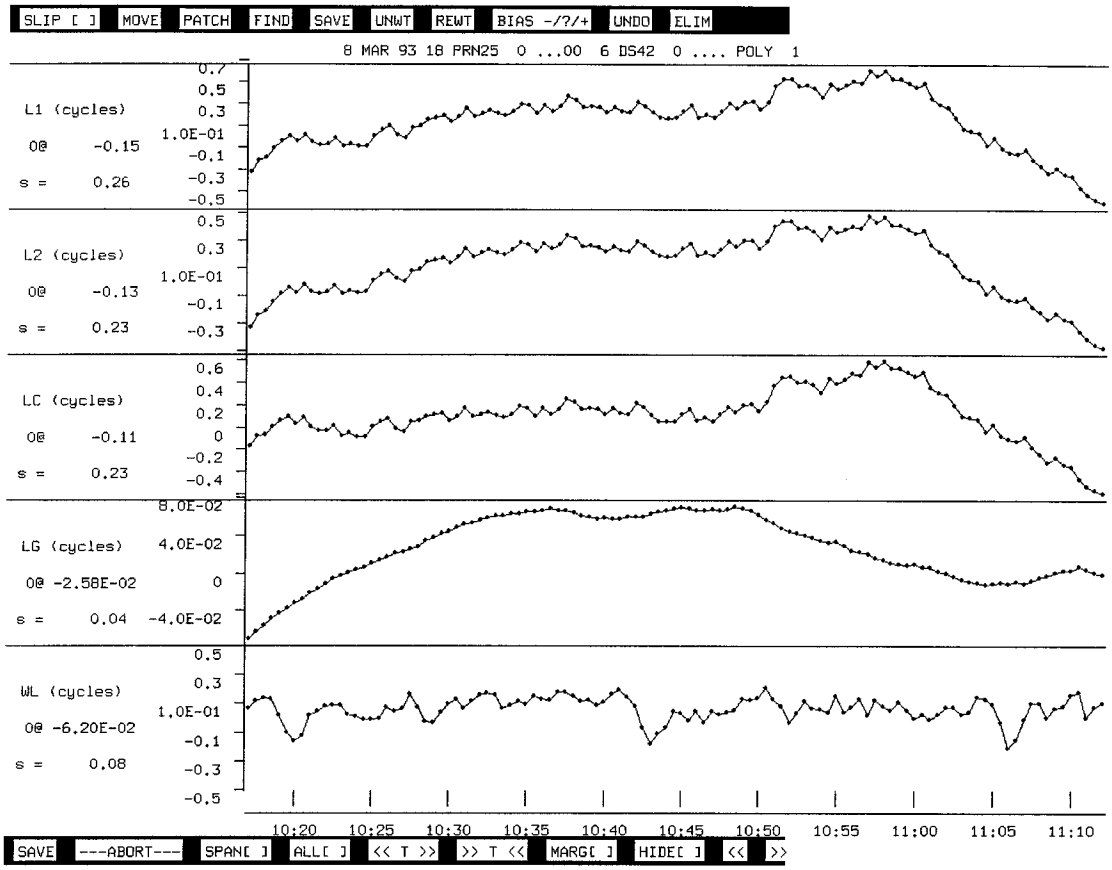

Figure E - 3 : One-way combination of DS42 and PRN25 with a first order polynomial removed.

Figure E-3 displays the same data as Figure E-2 except that a first order polynomial has been removed from the data. The statistics are now relative to the the first order polynomial. The small scale variations in the data are now visible in the L1, L2 and LC combinations (Figure E-3). This figure shows that no cycle slips exist in any of the combinations. Note that the data is very smooth, with jumps being generally less than 0.1 cycle for all combinations.

This is an example of well behaved data and will be used to compare other receivers and satellites against.

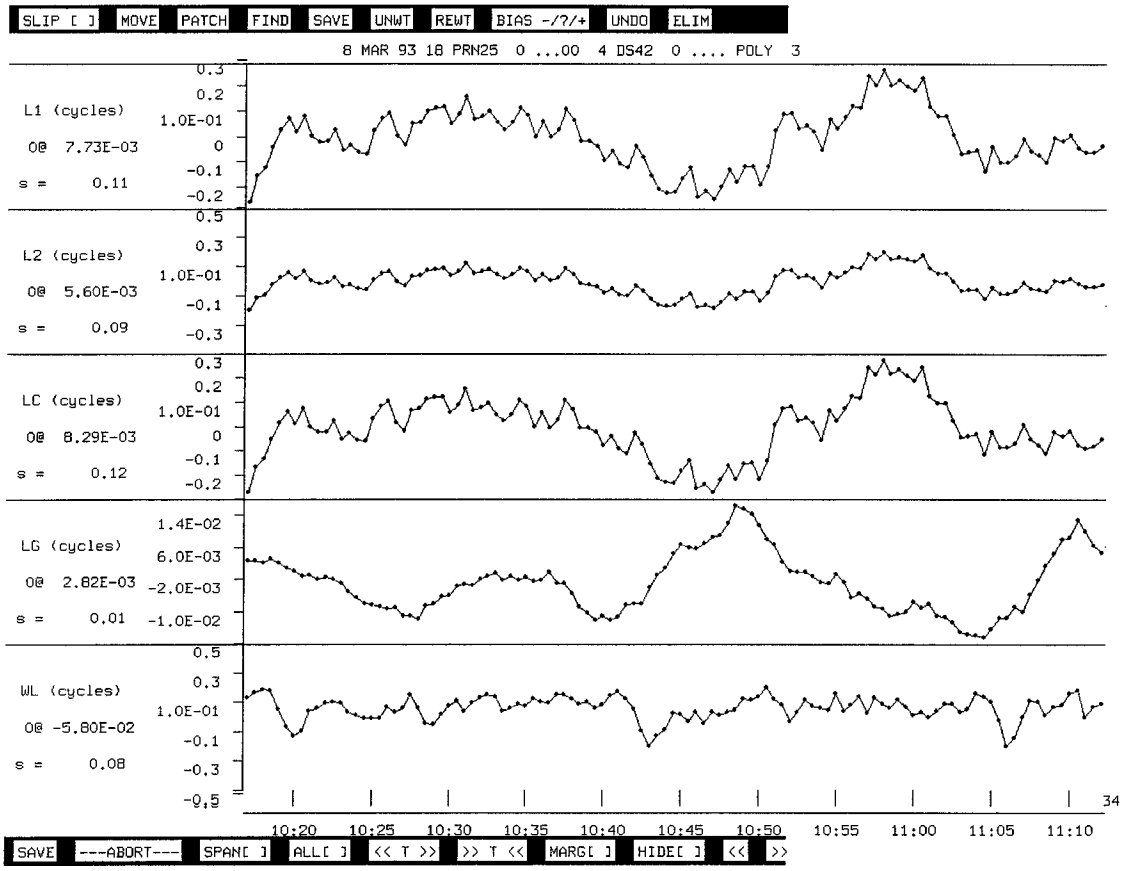

Figure E - 4 : One-way combination of DS42 and PRN25 with a third order polynomial removed.

Figure E-4 displays the same data as Figures E-2 and E-3, except that a third order polynomial has been removed from the data. The LC combination is relatively well behaved since the noise is commensurate with the L1 and L2 noise. The third order polynomial was removed from the DS42 to PRN25 combination to show its affect on well behaved data. Figure E-4 will be used as a reference data set against which other station and satellite combinations having a third order polynomial removed can be compared.

Note that the statistics are now in terms of the third order polynomial, which is introducing effects into the data which have wavelengths of approximately the data span.

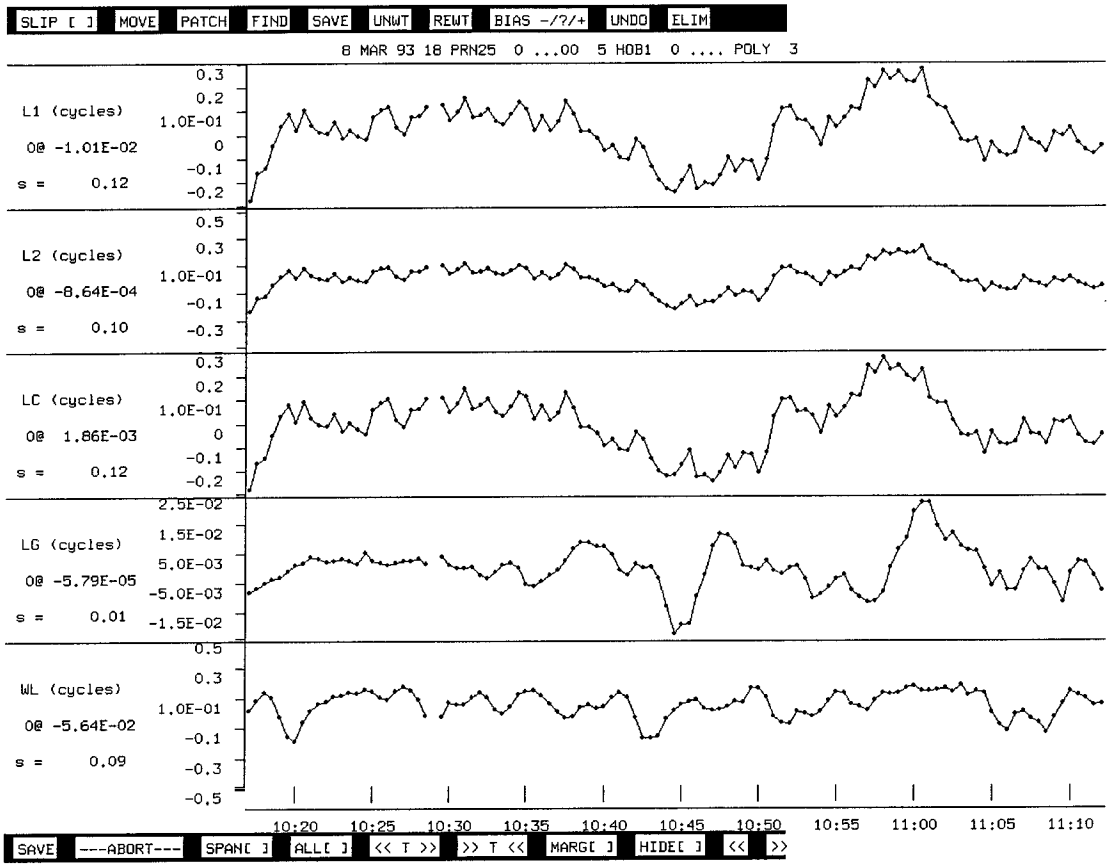

Figure E - 5 One-way combination of HOB1 and PRN25 with a third order polynomial removed.

The one-way combination of the mid-latitude station HOB1 and satellite PRN 25 (Figure E-5) has had a third order polynomial removed to reduce the influence of plotting the residual phase data without orbit modelling.

It is clearly seen by comparing Figures E-4 and E-5, that the Rogue receiver at HOB1 performed as reliably as the DS42 receiver for this period. Comparison of the LC and LG combinations for both HOB1 and DS42 show that both receivers experienced similarly low levels of atmospheric disturbance.

In Figure E-5, at approximately 10:30, no data was collected for both the L1 and L2 phase data. This data loss did not result in any cycle slips, due to no jumps being present in any of the combinations at the following epoch.

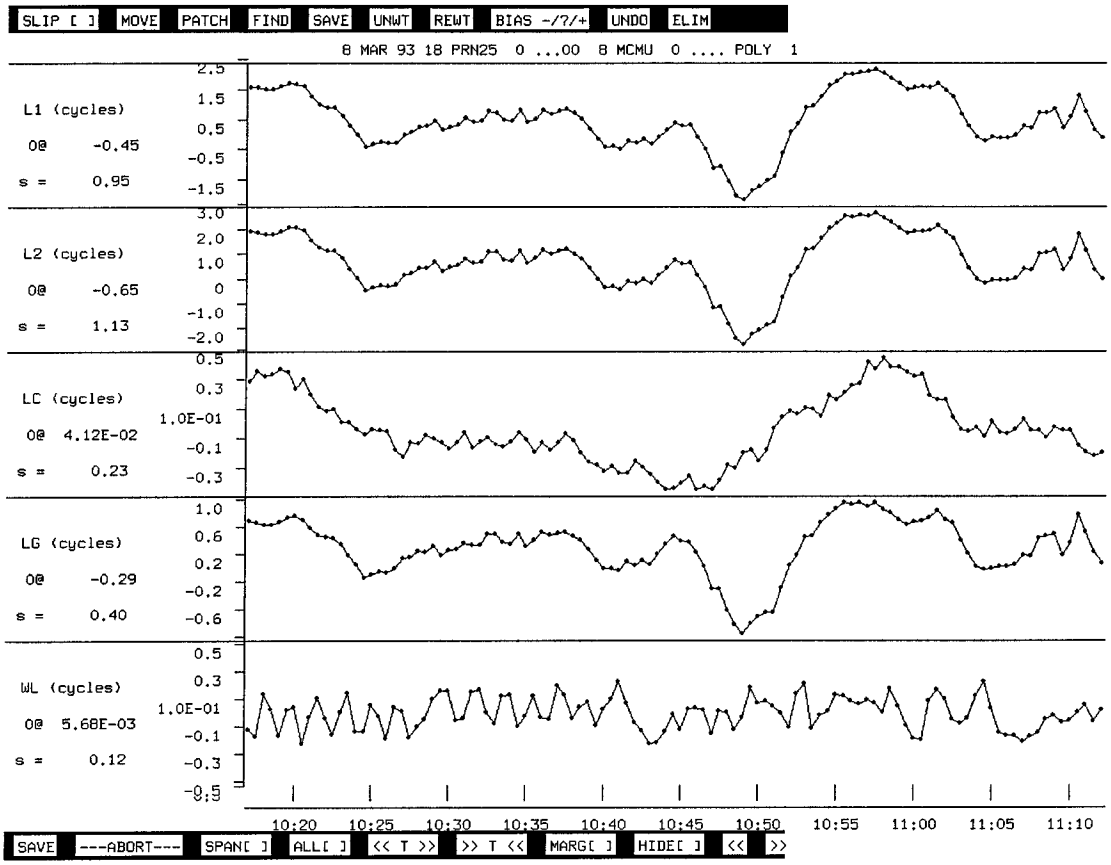

Figure E - 6 : One-way combination of MCMU and PRN25 with a first order polynomial removed.

The one-way combination of the Antarctic station MCMU and satellite PRN 25 (Figure E-6) has had a first order polynomial removed. What is first noticed with this combination is that the L1, L2 and LG combinations have a significantly larger standard deviations than those of DS42 with a first order polynomial removed (Figure E-3). Comparison of the LC combination (which is not sensitive to the ionospheric effect) reveals that its standard deviation has only been marginally affected.

Inspection of all combinations in Figure E-6 did not reveal the presence of any cycle slips. Closer inspection of the data between 10:45 and 10:55, shows that there is a medium wavelength effect influencing the L1, L2 and LG combinations, but not the LC combination. It is therefore concluded that since this medium wavelength effect is not apparent in the LC (or WL) combination, that it is an ionospheric disturbance at this Antarctic site.

The WL combination has decreased in quality by about 50% when compared to both the DS42 and HOB1 results (Figures E-3 and E-5, respectively). This highlights that different sites operating the same type of receiver (in this case Rogues) can produce varying quality data due to the combination of instrument and site effects.

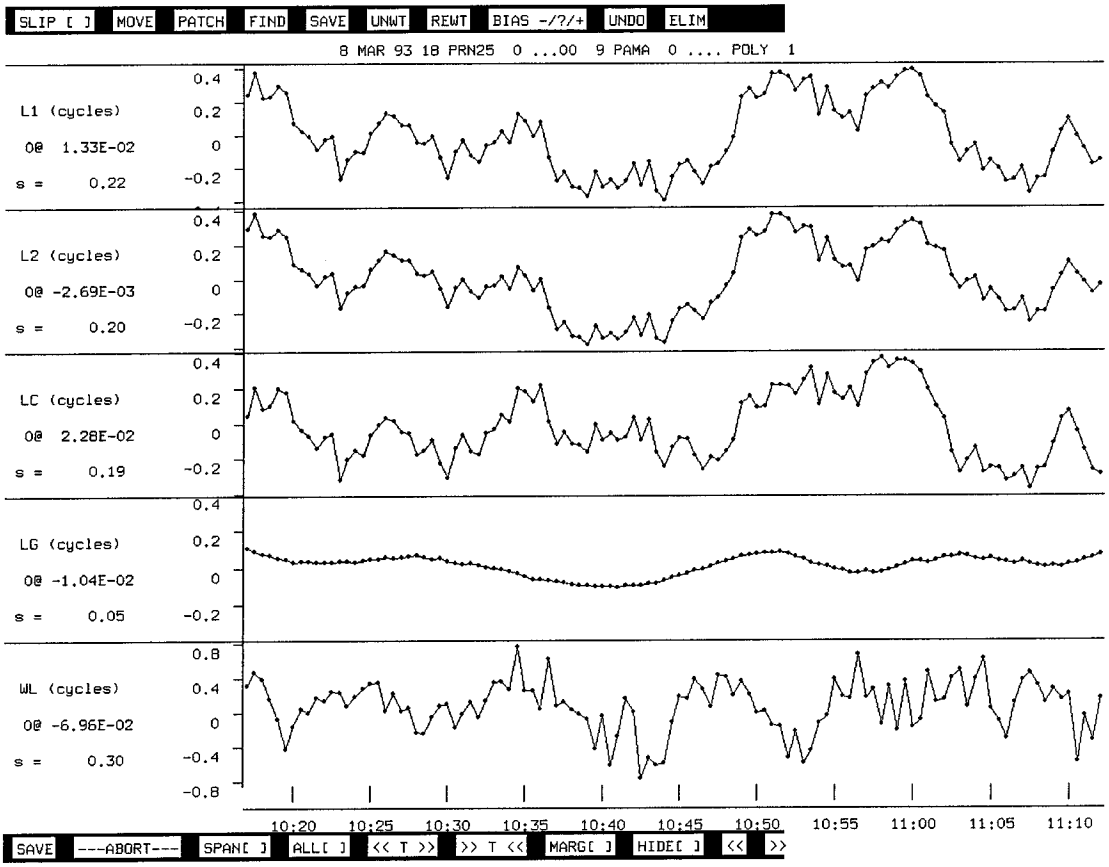

Figure E - 7 : One-way combination of PAMA and PRN25 with a first order polynomial removed.

The one-way combination of the equatorial station PAMA and satellite PRN 25 (Figure E-7) has had a first order polynomial removed.

The L1, L2 and LC combinations all have a similar standard deviations of about 0.2 cycles, with maximum differences between epochs in the order of only 0.2 cycles. The LG combination (which is insensitive to geometric effects) has a small standard deviation of 0.05. This indicates that PAMA was not experiencing varying geometric effects, such as tropospheric delay, during this period.

PAMA does not appear to have been affected by ionospheric disturbances during this period since L1, L2 and LC show similar features.

The WL combination of PAMA has further decreased in quality when compared to the DS42, HOB1 and MCMU results (Figures E-3, E-5 and E-6, respectively).

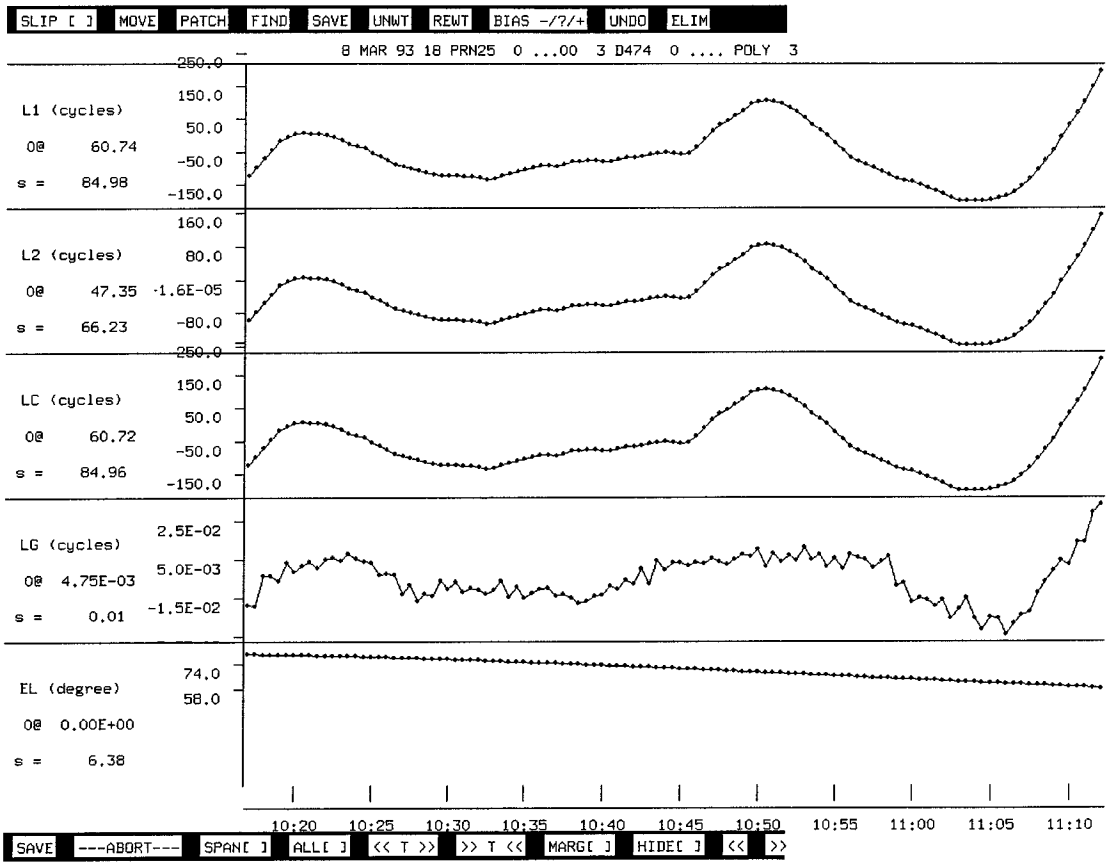

Figure E - 8 : One-way combination of D474 and PRN25 with a third order polynomial removed.

The one-way combination of the New Zealand station D474 and satellite PRN 25 (Figure E-8) has had a third order polynomial removed. As can be clearly seen from Figure E-8, the third order polynomial was unable to represent this data well and as a result the unmodelled changes due to sation coordinates and station clocks dominates the L1, L2 and LC combinations.

D474 was occupied by an Ashtech LM-XII receiver which was not capable of tracking the P-code. Consequently no WL combination could be plotted to help with cycle slip detection. In place of the WL, the fifth panel has been used to display the elevation (EL) of PRN25 with respect to D474 and shows that PRN25 has a minimum elevation of 58° for this displayed period with respect to the local horizon at D474 . Notice that the L1, L2 and LC combinations for D474 have significantly larger irregularities than those for the Rogue receiver sites (DS42, HOB1, PAMA and MCMU). Due to the fact that the LG combination shows no apparent cycle slips, it can be concluded that the L1, L2 and LC combinations are also likely to have no cycle slips.

The D474 and PRN 25 combination is typical of other Ashtech and Leica System 200 receivers that were operated during the campaign. The data collected at D474, as with the previously discussed sites of DS42, HOB1, PAMA and MCMU, was able to be processed in GAMIT and GLOBK.

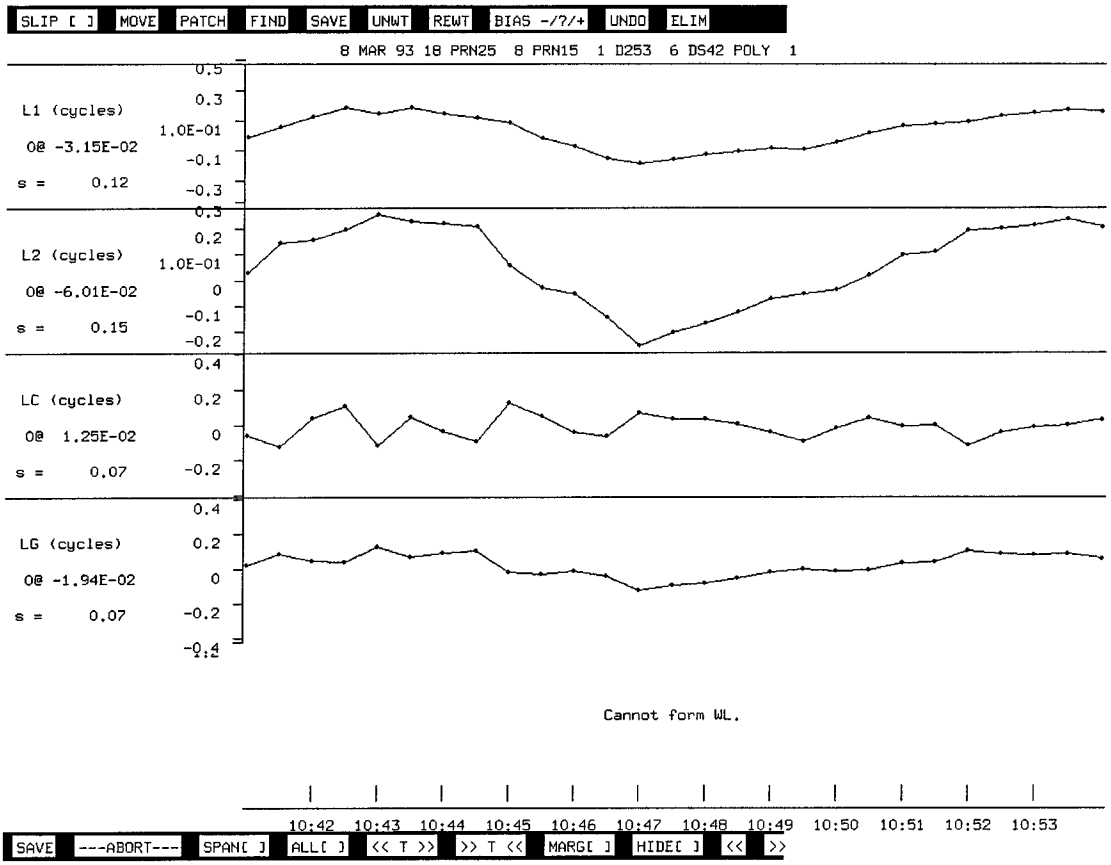

Figure E - 9 : Two-way combination between the sites of DS42 and D253, and the satellites of PRN15 and PRN25, with a first order polynomial removed.

The New Zealand station D253 was occupied by an Ashtech LM-XII receiver. The plot of the one-way combination of D253 and satellite PRN 25 (not included) with a third order polynomial removed showed very similar characteristics to those of D474 (Figure E-8). To remove what appeared to be mainly receiver effects (ie. clock effects), the two-way combination between the sites of D253 and DS42, and satellites PRN15 and PRN25, was formed and a first order polynomial removed (Figure E-9). The forming of the two-way combination cancels the between satellite and receiver differences.

In Figure E-3 it was shown that the data between DS42 and PRN25, for this same period, was free of cycle slips. From analysing the two-way combinations in Figure E-9 it can be safely concluded that since no cycle slips exist in any of these combinations, no cycle slips also exist in the D253 to PRN15 one-way combination.

A similar two-way combination plot using D474 instead of D253 (not included) produced similar good quality results on all combinations. The data collected at station D253 was able to be processed in GAMIT and GLOBK.

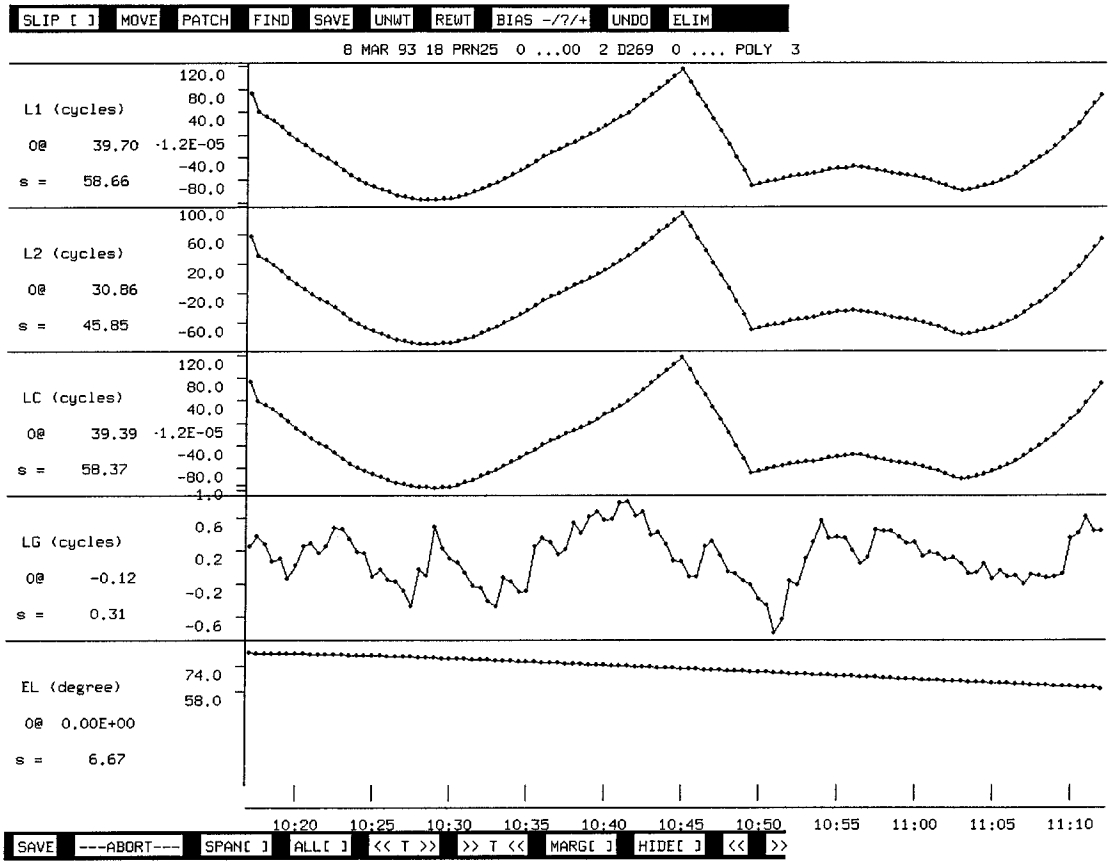

Figure E - 10 : One-way combination of D269 and PRN25 with a third order polynomial removed.

The one-way combination of the New Zealand station D269 and satellite PRN 25 (Figure E-10) has had a third order polynomial removed.

The L1, L2 and LC combinations all have a similar large abrupt changes at approximately 10:45 and 10:50. These abrupt changes are not expected in the data. The LG combination has no apparent cycle slips where the abrupt changes occur in the L1, L2 and LC combinations. However, the LG combination does have differences between epochs of approximately 0.5 cycles at a number of epochs (ie. approximately 10:29 and 10:35). As D269 was observed using an Ashtech LM-XII receiver (alias Ashtech number 4) the WL combination could not be formed to help in understanding the cause of these abrupt changes.

The two-way combination between the sites of D2269 and DS42, and satellites PRN15 and PRN25, was formed and a first order polynomial removed (Figure E-11). This two-way combination was formed in an attempt to understand the abrupt changes in Figure E-10 at approximately 10:45 and 10:50.

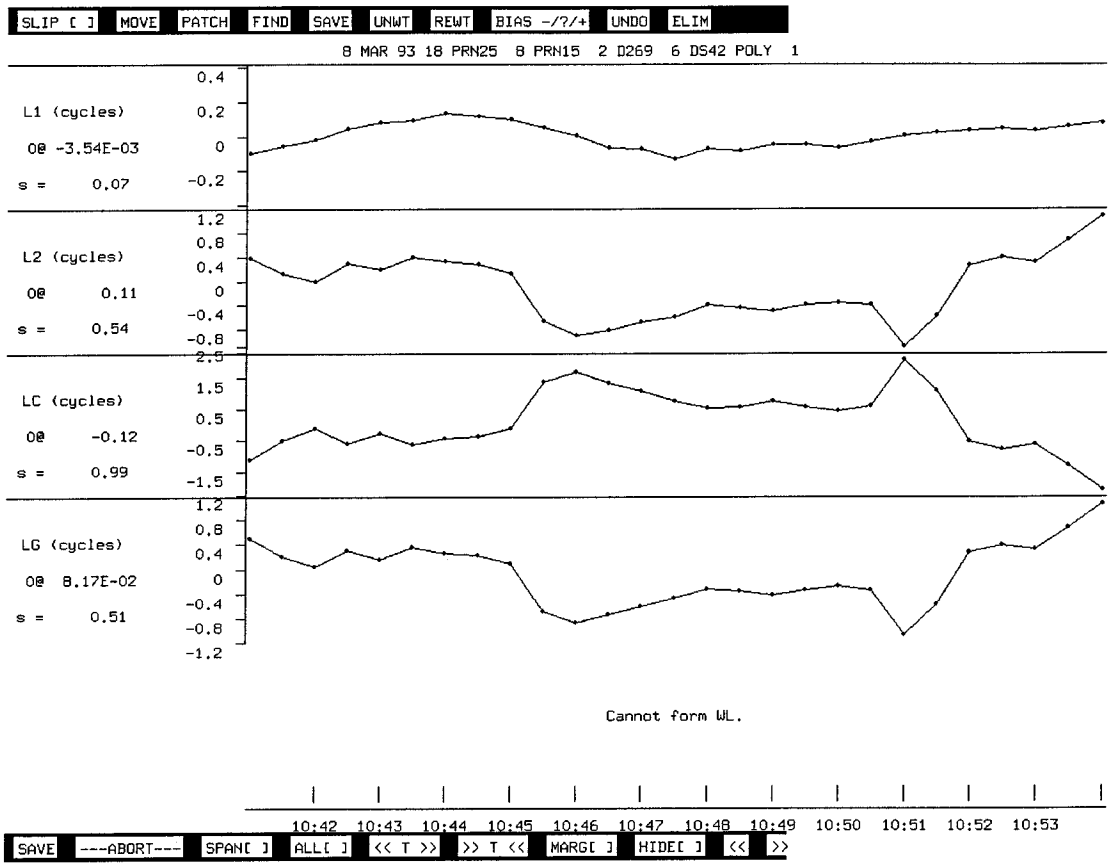

Figure E - 11 : Two-way combination between the sites of DS42 and D269, and the satellites of PRN15 and PRN25, with a first order polynomial removed.

The L1 combination (Figure E-11) shows no apparent cycle slips, however the L2 combination shows three cycle slips of approximately 1.0 cycles near 10:45 and 10:51. The effect of a single cycle slip in the L2 combination with no corresponding slip in the L1 combination would produce the following effect on the LC and LG combinations (when L1 = 0):

if L2 = -1, LC = 2.546*0.0 - 1.984*-1.0 = 1.984, LG = L2 - 0.779*-1.0 = -1.0
if L2 = +1, LC = 2.546*0.0 - 1.984*1.0 = -1.984, LG = L2 - 0.779*1.0 = 1.0

The L1 combination at 10:45.5 and 10:51.0 appears to have -1.0 cycle slips. This is confirmed by the LC combination having approximately +2.0 cycle slips and the LG combination having approximately -1.0 cycle slips. The L1 combination at 10:51.5 and 10:52.0 appears to have +1.0 cycle slips. This is confirmed by the LC combination having approximately -2.0 cycle slips and the LG combination having approximately +1.0 cycle slips. These cycle slips alone are not normally a problem to fix in GAMIT, but when they occur in successive epochs (ie. 10:51.0, 10:51.5 and 10:52.0) with the varying sign (ie L2 slips of ±1.0 cycle), detection becomes difficult.

The only difference between this two-way combination (Figure E-11) and the two-way combination in Figure E-9 (which had no apparent cycle slips) is that D269 is compared instead of D474. Therefore, it can be concluded that all cycle slips in Figure E-11 were caused by the receiver at D269. This data was not able to be processed in GAMIT/GLOBK. It was diagnosed by a high normalised rms in GAMIT.

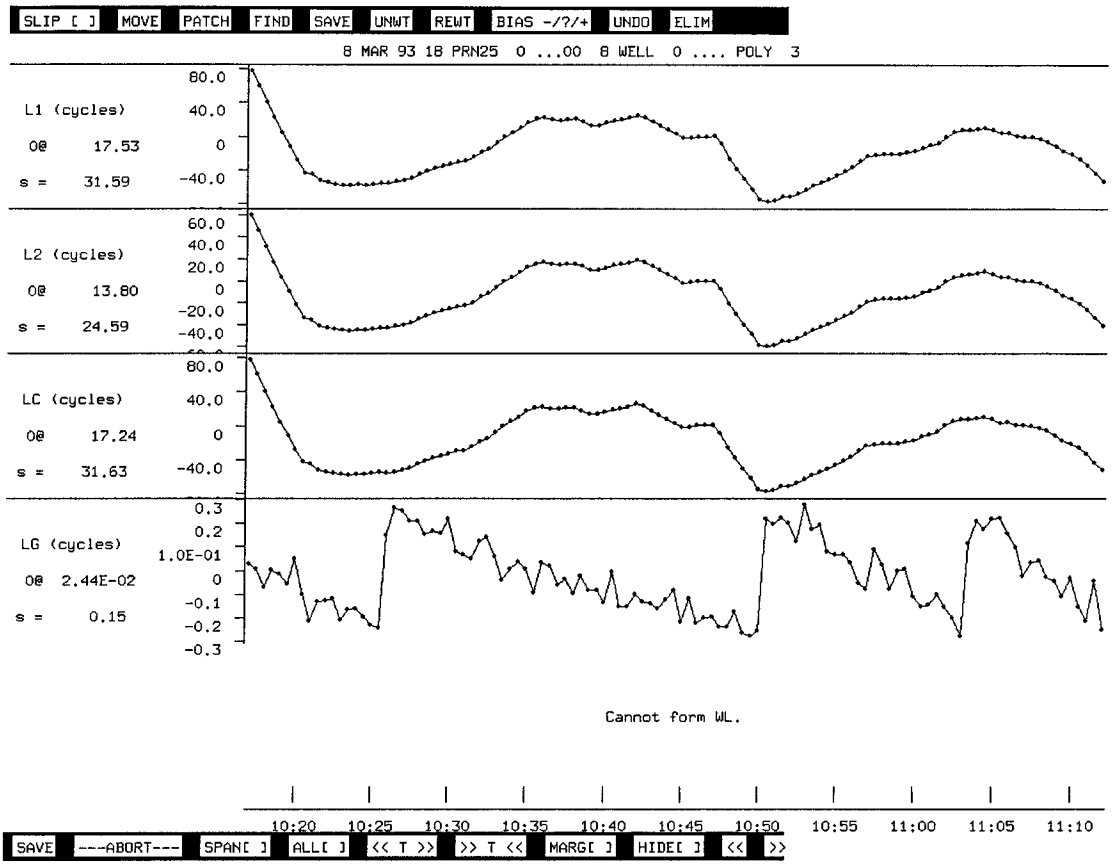

Figure E - 12 : One-way combination of WELL and PRN25 with a third order polynomial removed.

The one-way combination of the New Zealand station WELL and satellite PRN 25 (Figure E-12) has had a third order polynomial removed.

The L1, L2 and LC combinations all have a similar features, with the steep slopes near 10:20 and 10:45 being of concern. Of larger concern are the three approximately 0.5 cycle slips in the LG combination near 10:25, 10:50 and 11:03). As WELL was observed using an Ashtech LM-XII receiver (alias Ashtech number 4) the WL combination could not be formed to help in the cycle slip detection.

A cycle slip in LG of approximately +0.5 can be caused by a number of combinations of L1 and L2 cycle slips. Some of the combinations include:

if L1 = +3 and L2 = +3,	LC = 1.686,	LG = 0.663
if L1 = +2 and L2 = +2,	LC = 1.124,	LG = 0.442
if L1 = 0 and L2 = +0.5,	LC = -0.992,	LG = 0.5

Since the Ashtech LM-XII receiver is designed on the principle of squaring the incoming signal to extract the carrier beat phase it is possible to have 0.5 cycle slips on the L2 frequency. Closer inspection of the LG cycle slip at approximately 10:50 is contained in Figure E-13.

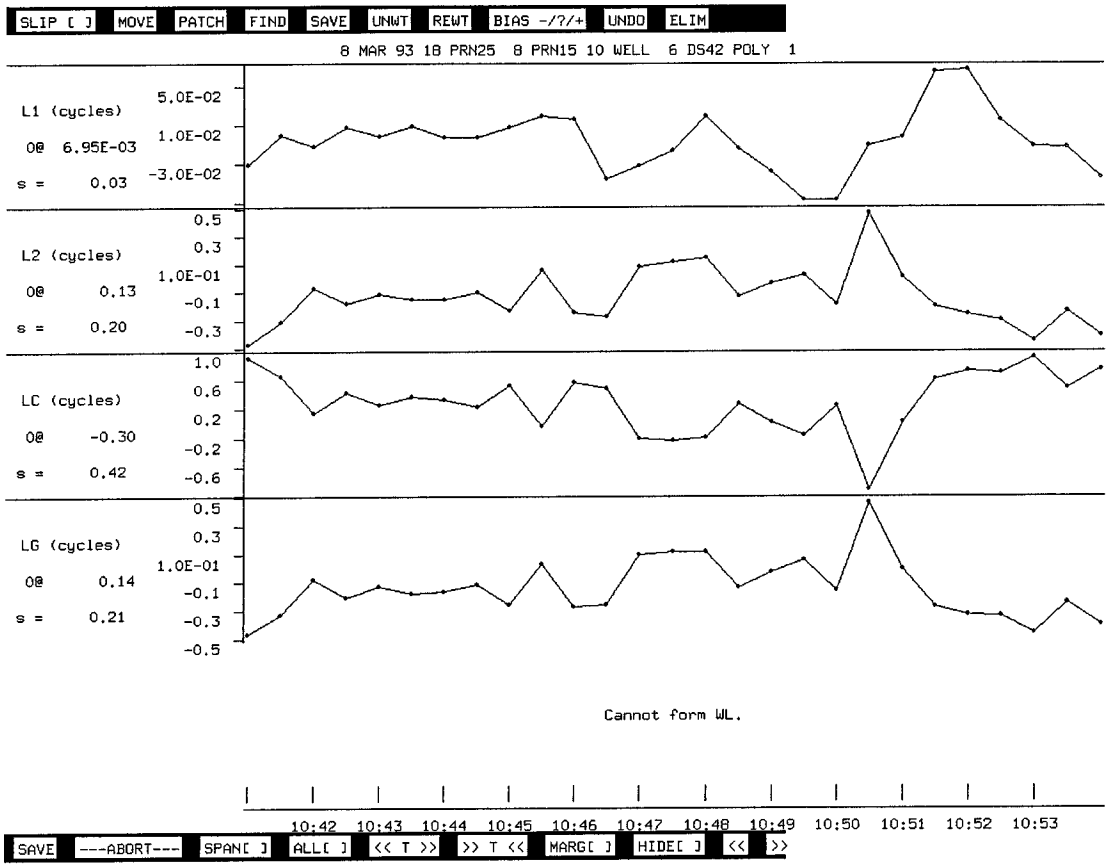

Figure E - 13 : Two-way combination between the sites of DS42 and WELL, and the satellites of PRN15 and PRN25, with a first order polynomial removed.

It is not possible to see cycle slips in L1 or L2 with a magnitude of 1-3 cycles in Figure E-12. It was therefore necessary to choose a smaller sample of data in an attempt to determine the cause of the LG cycle slips. Figure E-13 displays the data in the immediate vicinity of the LG cycle slip at approximately 10:50 through the two-way combination of stations DS42 and WELL and Satellites PRN15 and PRN25.

The LG combination (Figure E-13) clearly shows a cycle slip of approximately 0.5 cycles at 10:50.5. Inspection of the L1 combination at this epoch shows no apparent cycle slips, though the L2 combination shows a 0.5 cycle slip. If this +0.5 cycle slip exists then the LC and LG combinations should also show cycle slips of approximately -0.992 and +0.5, respectively. These LC and LG cycle slips can be seen in Figure E-13 and therefore it can be concluded that the 0.5 LG cycle slip in Figure E-12 at 10:50.5 was caused by a +0.5 cycle slip in the L2 data. The two other LG cycle slips of Figure E-12 were also confirmed to be due to +0.5 cycle slip on L2, through similar analysis as described above.

The inclusion of this data from WELL produced a large normalised rms in GAMIT solution for DOY 067.

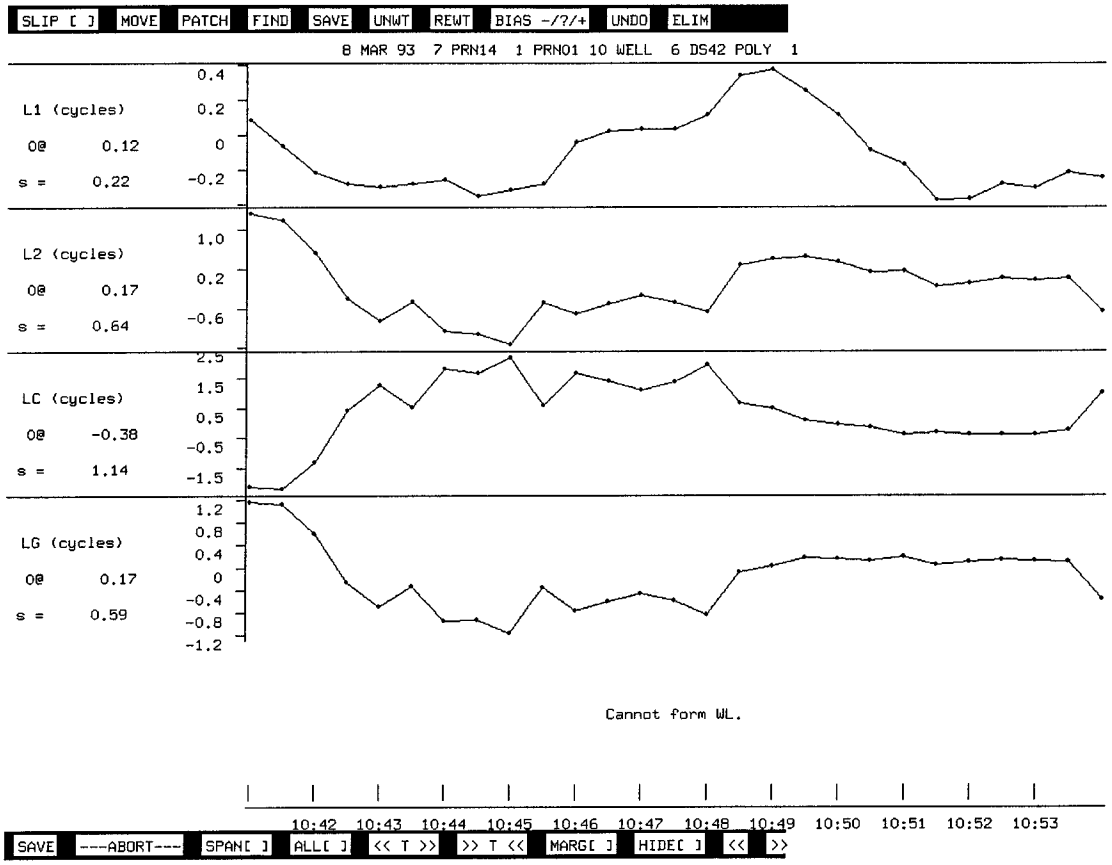

Figure E - 14 : Two-way combination between the sites of DS42 and WELL, and the satellites of PRN01 and PRN14, with a first order polynomial removed.

The two-way combination of Figure E-13 was changed to include two new satellites, PRN01 and PRN14 (Figure E-14). By changing the satellites it possible to show that the cycle slips in Figure E-13 are caused by the receiver at WELL.

One-way plots of DS42 to PRN01 and 14 (not included) revealed no cycle slips between this receiver and these satellites. From Figure E-14 it is clear that there are no cycle slips on L1, but L2 has +0.5 cycle slips at 10:45.5 and 10:48.5. Analysis of the LC and LG combinations show cycle slips of approximately -0.992 and +0.5, respectively, at 10:45.5 and 10:48.5. What cannot be determined from this plot alone is which satellite the cycle slip recorded by the receiver at WELL was between.

It is interesting to note that the cycle slip at 10:50.5, in Figure E-13, is not in the two-way combination of Figure E-14. This indicates that the receiver at WELL was able to maintain lock to some of the satellites at this epoch.

Due to the large number of cycle slips in the data from the receiver at WELL no data on DOY was able to be processed in GAMIT/GLOBK.

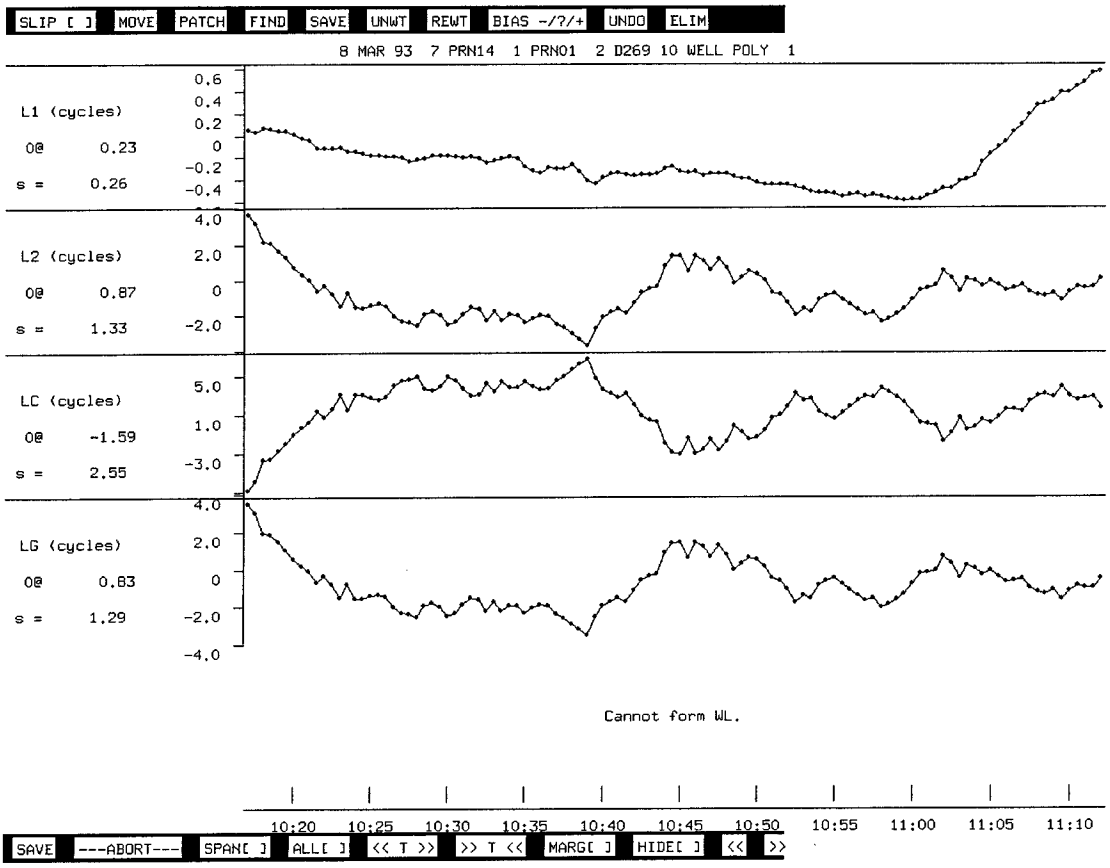

Figure E - 15 Two-way combination between the sites of D269 and WELL, and the satellites of PRN01 and PRN14, with a first order polynomial removed.

The two-way combination between the stations D269 and WELL and satellites PRN01 and PRN14 (Figure E-15) has been included as an example of the poor data collected by the Ashtech receivers located at these two sites.

From Figure E-15 it is clear that the L1 data for both stations contained apparently no cycle slips. The L2 data however contained an excessive number of cycle slips with a sample of these being shown in Figures E-11 and E-14. What should be noted in the L2 and LG combinations (Figure E-15) is the 0.5 cycle oscillatory nature throughout most of the displayed data; a particularly nasty segment is near 10:45. The LG combination shows similar oscillations though having the associated magnitude of 0.99 cycles. What is also a disturbing feature of Figure E-15 is that the LC combination is negatively correlated with the L2 and LG combinations.

No data collected at these two sites on DOY067 were able to be processed in GAMIT/GLOBK.

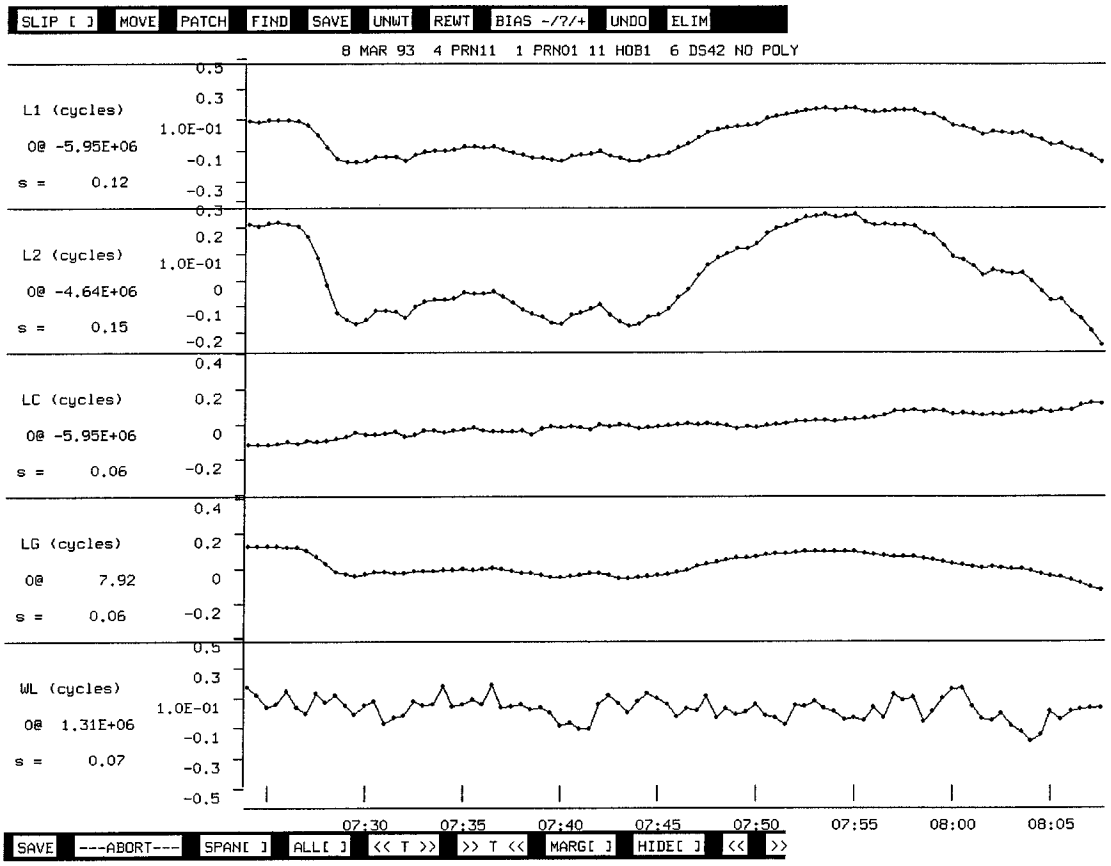

Figure E - 16 : Two-way combination between the sites of DS42 and HOB1, and the satellites of PRN01 and PRN11, with a first order polynomial removed.

The two-way combination between the stations DS42 and HOB1 and satellites PRN01 and PRN11 (Figure E-16) has been included as an example of some of the high quality data collected by receivers used in this GPS campaign.

It should be noted that all five combinations show low standard deviation values without the removal of a polynomial. The data is continuous and has small variations between epochs.

Appendix F

Flow diagram for UNSW Gravity software suite

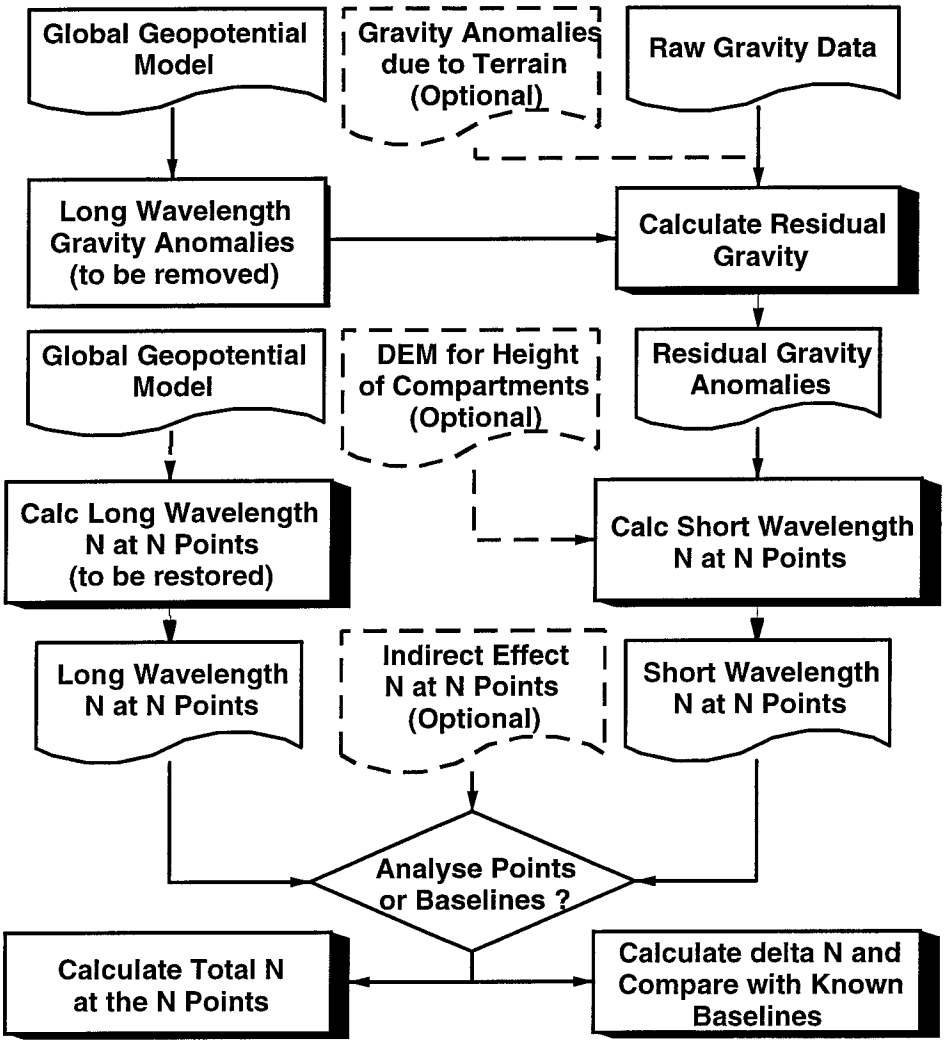

The above flow diagram outlines the main features of the GRAV suite of software held at The University of New South Wales. The Ring Intergration (RINT) module is represented by the box containing "Calc Short Wavelength N at N Points".

Appendix G

WGS84 coordinates of the lower North Island control stations

This appendix contains the summary of two emails from Jim Hall, DOSLI, describing the method used to obtain WGS84 coordinates for the GPS points used in the Wellington to Palmerston North horizontal control investigation. A selection of these GPS stations were used as control for the lower North Island geoid investigations of Chapter 4.

```
From:   IN%"JIM@hh.dosli.govt.nz" 20-JAN-1995 16:00:28.02
To:     IN%"P2143202@csdvax.csd.unsw.EDU.AU"
CC:
Subj:   GPS DATA FILES


The input station is H/H GPS Pillar (D475) where the
value 37.800 is the WGS84 ellipsoidal height in metres.

Regards
Jim Hall


From:   IN%"JIM@hh.dosli.govt.nz" 24-JAN-1995 14:23:31.20
To:     IN%"P2143202@csdvax.csd.unsw.EDU.AU"
CC:
Subj:   More GPS data

I have now done SNAP adjustment for GPS stations only on WGS84 with no geoid, holding
the WGS84 coordinates and ellipsoidal height of HH GPS Pillar fixed.


Coords for all stations wellington palmerston north investigation
wgs84
no_geoid
! Updated by SNAP version 2.0d at 24-JAN-1995 09:12:09
CODE       LATITUDE           LONGITUDE          ELLP HT  STATION NAME

D115     39 27 35.857506 S 175 11 53.005561 E   768.7261 WAIPUNA
D126     40 06 28.643231 S 175 16 54.002021 E   127.9957 MT SARAH
D131     40 14 24.726502 S 175 29 17.913817 E   143.7486 MT STEWART
D133     40 29 34.580202 S 175 15 31.231141 E    57.6080 E ORUARONGO
D134     40 30 36.531846 S 175 37 31.225694 E   781.3927 AA ARAWARU
D136     40 50 53.262154 S 174 54 55.542775 E   531.7349 KAPITI NO 2
D137     40 47 47.582018 S 175 26 36.112017 E  1561.2606 GIRDLESTONE
D138     41 11 00.318561 S 174 52 26.387142 E   469.4390 BELMONT
D139     41 07 08.574312 S 175 13 48.595721 E   740.1737 RIMUTAKA
D141     41 11 32.428274 S 175 23 55.991053 E   127.2275 BIDWILL
D143     41 10 48.524095 S 175 39 07.786816 E   590.8576 ERINGA
D145     41 16 35.665751 S 174 37 40.445384 E   470.3358 F TERAWHITI
D146     41 17 39.996452 S 174 49 42.544366 E   176.1517 MT CRAWFORD
D147     41 13 53.328270 S 174 46 40.708244 E   458.1703 KAUKAU
D150     41 20 27.991979 S 174 42 40.356358 E   496.8275 TE KOPAHOU
D151     41 19 02.716119 S 175 02 51.685659 E   915.9022 PAPATAHI
D427     41 00 45.804779 S 174 58 42.685884 E   735.1928 WAINUI NO 2
D428     41 09 01.247753 S 175 08 36.191846 E   876.0633 CLIMIE NO 2
D443     40 22 47.914149 S 175 45 29.910224 E   558.5754 B TARAKAMUKU
D446     40 50 57.929792 S 175 44 11.536216 E   620.4445 RANGITUMAU NO 2
D475     41 16 29.625950 S 174 46 58.625510 E    37.8000 HEAPHY HOUSE GPS PILLAR *
D482     41 16 29.755054 S 174 46 58.893965 E    35.3580 HEAPHY HOUSE HHR9       *
D483     41 16 29.332333 S 174 46 58.898335 E    34.8624 HEAPHY HOUSE HHR9A      *
D485     41 16 29.671587 S 174 46 59.129723 E    35.3227 HEAPHY HOUSE HHR6       *
D499     40 30 51.606135 S 175 27 35.451633 E    36.6464 BM LA81 NO 2
D500     40 35 19.486877 S 175 14 25.582688 E    96.2210 MOUTERE NO 2
D501     40 52 20.413395 S 175 01 15.941448 E    39.7136 WAIMEA NO 4
D502     40 58 55.603738 S 174 57 59.031640 E    30.2944 BM L25
D503     40 38 58.543219 S 175 20 50.119080 E   390.0654 E ARAPAEPAE NO 1
D504     40 44 16.397492 S 175 07 58.179297 E    50.3596 A WAITOHU
D505     40 48 42.351296 S 175 15 21.494133 E   926.5762 A TAUNGATA
D506     40 55 56.500454 S 175 09 43.457413 E  1115.8921 A KAPAKAPANUI
D507     40 52 30.202922 S 175 04 02.225923 E    42.2352 BM LA35                 *
D508     40 35 56.170920 S 175 42 53.988009 E   207.1887 BM KA66                 *
D509     41 02 18.678658 S 175 06 07.738249 E   641.0829 A MT BARTON
D510     41 04 44.381995 S 174 46 52.175756 E   134.1310 MANA
D511     41 06 45.155445 S 174 59 52.921985 E   445.1373 NABHRA
D512     41 14 07.592781 S 174 55 42.568580 E   361.6625 TOWAI
D513     41 13 09.786844 S 175 02 16.464567 E   645.6814 DEVINE
```

D514	41	24	19.358141	S	174	52	41.671907	E	179.5886	PARA			
D515	40	56	46.937099	S	175	40	01.990840	E	126.3674	15881			
D516	40	28	00.294951	S	175	49	37.304547	E	134.7858	BM KA80			*
D517	41	01	34.765357	S	175	31	38.902373	E	92.6498	16211			
D518	40	28	16.611053	S	175	17	05.559266	E	19.2082	BM L72 NO 2			*
D519	40	32	47.652979	S	175	16	22.677663	E	33.7582	BM L65			*
D520	40	37	59.348997	S	175	16	31.980228	E	48.3258	BM L57			*
D521	40	43	45.505839	S	175	12	21.014215	E	64.5149	BM L49			*
D522	40	48	57.513118	S	175	06	37.607507	E	32.3869	BM L40			*
D523	41	05	25.137077	S	175	26	58.717702	E	70.4316	BM KA9			*
D524	40	44	03.094104	S	175	37	15.813473	E	334.2317	BM KA49 NO 2			*
D525	41	17	09.314423	S	174	48	13.061784	E	15.8544	ORM 8 SO35860			*
D526	41	20	44.828748	S	174	47	29.666862	E	17.9763	BM6A SO35872			*
D527	41	08	54.285411	S	174	50	18.013561	E	23.7206	BM L9 NO 2			*
D528	41	06	14.332437	S	174	52	12.365700	E	17.7744	BM L14			
D529	41	01	52.224794	S	174	53	47.330491	E	58.6066	BM L20			*
D530	41	08	43.946785	S	174	59	57.136128	E	51.9560	BM KC2			*
D531	41	16	35.818067	S	174	37	40.641731	E	469.9209	TERAWHITI ECC			*
D532	41	09	19.060994	S	174	48	12.938073	E	472.1216	COLONIAL KNOB ECC			*
D533	41	11	01.103833	S	174	52	26.307236	E	466.6758	BELMONT ECC			*
D534	41	17	39.952440	S	174	49	42.419878	E	175.4286	CRAWFORD ECC			*
D535	41	20	27.887196	S	174	42	40.420289	E	496.3624	TE KOPAHOU ECC			*
D536	41	13	53.579511	S	174	46	40.909565	E	457.5597	KAUKAU ECC			*
D537	41	09	19.667864	S	174	48	13.537292	E	471.4636	COLONIAL KNOB NO 3			
D538	40	26	30.622597	S	175	24	39.425131	E	56.3570	HIMATANGI			
D539	40	19	23.493512	S	175	38	46.997046	E	78.5047	14943			
D540	40	25	43.272471	S	175	34	25.659529	E	62.1670	FITZHERBERT NO 2			
D541	40	30	03.659027	S	175	33	23.111602	E	687.1165	BB KAIHINU			
D542	40	27	18.919674	S	175	38	39.742426	E	570.7175	CC (ARAWARU SD)			
D543	40	27	16.626457	S	175	36	16.164489	E	464.6277	D TE MATA			
D544	40	28	49.503494	S	175	32	36.363976	E	392.2123	14972			
D545	40	29	22.791069	S	175	30	06.502769	E	58.5214	15311			
16063	41	06	14.364696	S	174	51	24.838061	E	105.7569	16063			
160813CC	41	08	39.227940	S	174	49	16.152684	E	302.8387	160813 Ecc			*
MT_COOPER	41	05	44.411839	S	174	50	22.514908	E	117.1009	MT COOPER			
PIKARERE	41	07	01.569071	S	174	49	14.894892	E	200.8949	PIKARERE			
PKRRN2	41	07	06.666710	S	174	49	36.361537	E	148.0769	PIKARERE NO 2			
16091	41	08	39.857913	S	174	52	36.386746	E	165.1795	16091			
BXTRSKNB	41	07	37.581374	S	174	51	43.844681	E	151.8782	BAXTERS KNOB			
160917	41	09	20.259236	S	174	51	14.650423	E	269.4576	160917			
RBRTSN2	41	09	34.633425	S	174	50	54.340373	E	261.7694	ROBERTS NO 2			
TIDEMAN	41	07	46.445674	S	174	53	12.775171	E	207.9656	TIDEMAN			
BRADEY	41	06	24.399121	S	174	53	44.972540	E	84.3116	BRADEY			
16031	41	03	14.630762	S	174	53	11.598185	E	178.7691	16031			
16032	41	02	19.087774	S	174	53	38.787319	E	159.5929	16032			
16064	41	04	19.122139	S	174	52	00.879646	E	128.3633	16064			
16065	41	03	48.852487	S	174	52	12.447638	E	127.1641	16065			
PORIRUA	41	03	10.361116	S	174	51	14.723038	E	274.5982	PORIRUA			
WRKN2	41	02	13.325892	S	174	52	40.932414	E	229.5801	WAIRAKA NO 2			
RM1	41	04	13.641631	S	174	51	14.305686	E	15.5426	RM1 (MOANA ROAD)			*
WLKRSHLLN2	41	05	22.201128	S	174	52	16.976669	E	110.0968	WALKERS HILL NO 2			
160610	41	07	22.981417	S	174	54	03.999017	E	155.9857	160610			
16062	41	06	53.618817	S	174	52	23.696090	E	169.7837	16062			
16069	41	06	36.849291	S	174	53	09.278736	E	121.3870	16069			
RTNPNTN2	41	05	43.899273	S	174	54	46.954179	E	39.3821	RATION POINT NO 2			
5307	41	06	16.566067	S	174	54	25.869363	E	14.3672	5307 (IGNS STATION)			*
BAKER	41	04	03.902246	S	174	55	05.131621	E	335.0292	BAKER			
DGGNGSN2	41	02	20.478551	S	174	55	11.705407	E	452.6912	DIGGINGS NO 2			
GRAYS_NO2	41	04	43.868900	S	174	53	36.005440	E	182.4653	GRAYS NO2			
PKKRK	41	00	24.106812	S	174	56	09.489893	E	287.3365	PAEKAKARIKI			
ABBOTT	41	04	21.475802	S	174	57	45.592782	E	446.9324	ABBOTT			
MLHRNN2	41	06	21.064884	S	174	57	25.274647	E	143.4934	MULHERN NO 2			
EE	41	03	01.247998	S	174	59	59.450954	E	565.0878	EE (PAEKAKARIKI SD)			
5502	41	06	50.477801	S	174	57	07.845488	E	53.1702	5502 (IGNS STATION)			*
EDSBLK	41	03	06.155607	S	175	00	03.807284	E	564.7182	EDS BLK EE (IGNS)			*
16033	41	01	46.876859	S	174	53	55.582859	E	74.6055	16033			
WAINUI	41	00	45.647891	S	174	58	42.832191	E	735.2229	WAINUI			
LNDNN2	41	06	34.796785	S	174	52	16.409531	E	134.9702	LONDON NO 2			
RLWYN2	41	03	09.602453	S	174	52	30.791925	E	70.4500	RAILWAY NO 2			

Appendix H

Orthometric heights of the lower North Island control stations

This appendix contains information extracted from two emails from Jim Hall, DOSLI, that listed the orthometric height and order of the stations in the Wellington to Palmerston North control investigation. A selection of these stations were used as control for the lower North Island geoid investigations of Chapter 4. It should be noted that besides the EDS survey points the last 3 sites (Ken, Fitzherbert, Mowlem No. 3) were also not occupied by GPS.

```
From:    IN%"JIM@hh.dosli.govt.nz" 20-JAN-1995 16:01:02.77
To:      IN%"P2143202@csdvax.csd.unsw.EDU.AU"
CC:
Subj:    GPS DATA FILES


Coords for all stations wellington palmerston north investigation

!Note this listing includes stations in the Wairarapa as well as points in the
!southern part of the New Plymouth - Castle Point EDS and the northern portion
!of the Wellington - Karamea EDS surveys.  Stations are listed in three groups
!first, second and third order as determined by WN DO (some points have been
!upgraded and others downgraded.  Except for eccentric marks, new stations and
!some bench that were very poorly fixed for position, latitudes, longitudes and
!heights agree with those shown in the geodetic data base.

!Stations marked with an * at the end of the name are not currently
!in the geodetic data base or in the case of bench marks the coordinates are
!not reliable and better values have been used to clarify the analysis of results

!All stations listed below are GPS stations except for the following which are
!EDS points for which the terrestial observations were included in the adjustment.
!D120,D123,D127,D135,D144,D152,D429,D430,D439,D440,D441,D442,D444,D445,D447,D448.

NZGD49

! Coordinate file created by SNGEOID version 1.0
```

STN ID	LATITUDE	LONGITUDE	ORTHO HEIGHT M	HT ORDER	GEOID UNDULATION M	STATION NAME
!First order stations						
D115	39 27 42.177800 S	175 11 52.269000 E	748.2900	3	-0.934	WAIPUNA
D120	39 43 22.789800 S	174 57 02.437600 E	558.3000	4	-3.859	RANGITATAU
D123	39 45 24.364300 S	175 28 51.869000 E	698.5700	3	-3.384	I MANGAMAHU
D126	40 06 34.937200 S	175 16 53.250800 E	116.4000	4	-5.370	MT SARAH
D127	40 12 44.091200 S	175 52 50.580200 E	1053.1100	3	-1.744	B ROSS
D131	40 14 31.009700 S	175 29 17.158600 E	131.3750	1	-4.194	MT STEWART
D133	40 29 40.852300 S	175 15 30.482200 E	45.8400	3	-3.785	E ORUARONGO
D134	40 30 42.799700 S	175 37 30.471700 E	767.1000	3	-1.568	AA ARAWARU
D135	40 34 54.539400 S	176 00 22.642200 E	763.5700	3	0.964	L PUKETOI
D136	40 50 59.509600 S	174 54 54.819000 E	521.2400	3	-2.063	KAPITI NO 2
D137	40 47 53.828300 S	175 26 35.379300 E	1545.9900	3	-0.219	GIRDLESTONE
D138	41 11 06.528100 S	174 52 25.693100 E	456.2900	3	0.024	BELMONT
D139	41 07 14.778700 S	175 13 47.884900 E	725.3200	3	1.075	RIMUTAKA
D141	41 11 38.626700 S	175 23 55.293100 E	112.0500	3	1.967	BIDWILL
D143	41 10 54.721200 S	175 39 07.077200 E	574.9000	3	2.566	ERINGA
D144	40 59 40.878200 S	175 59 27.884800 E	483.5000	3	2.568	FLAGSTAFF NO 3
D145	41 16 41.866400 S	174 37 39.769200 E	457.8000	4	-0.204	F TERAWHITI
D146	41 17 46.188400 S	174 49 41.864200 E	163.1000	4	0.272	MT CRAWFORD
D147	41 13 59.531100 S	174 46 40.024300 E	445.3000	4	-0.058	KAUKAU
D150	41 20 34.179700 S	174 42 39.684000 E	484.8000	4	0.078	TE KOPAHOU
D151	41 19 08.900000 S	175 02 51.000000 E	902.3000	4	0.995	PAPATAHI
D152	41 24 02.740300 S	175 19 54.987800 E	979.2600	3	1.813	S TE MAUNGA
!Second order stations						
D427	41 00 52.031700 S	174 58 41.976700 E	722.0000	4	-0.559	WAINUI NO 2
D428	41 09 07.451800 S	175 08 35.489600 E	861.8000	4	0.873	CLIMIE NO 2
D429	41 31 07.940700 S	175 29 35.735900 E	363.9500	3	1.559	PUKEMURI
D430	41 19 06.240700 S	175 46 00.147500 E	663.8500	3	2.557	MT ADAMS
D439	39 41 38.613800 S	175 12 44.847900 E	713.6000	4	-3.512	A TAUAKIRA
D440	39 55 54.626000 S	175 05 33.697900 E	128.1000	4	-5.350	BB IKITARA
D441	39 57 20.548200 S	175 29 31.970700 E	447.8000	4	-4.383	ASHCROFT NO 2
D442	40 07 42.311700 S	175 20 29.626700 E	143.2900	3	-5.158	14361
D443	40 22 54.190200 S	175 45 29.147900 E	544.2500	3	-1.642	B TARAKAMUKU
D444	40 34 09.262300 S	175 47 05.355000 E	349.5600	3	-0.204	MT HEALE NO 2
D445	40 46 50.144700 S	175 53 06.764800 E	531.3700	3	1.585	U TINTOCK
D446	40 51 04.162000 S	175 44 10.803700 E	604.2400	3	1.459	RANGITUMAU NO 2
D447	40 47 11.553300 S	176 11 16.082100 E	391.9500	3	2.300	MANGAHOEKA NO 3
D448	41 03 34.212900 S	175 58 54.303300 E	578.2100	3	2.704	REWA
D475	41 16 35.821800 S	174 46 57.945100 E	24.9800	2	0.113	HEAPHY HOUSE GPS PILLAR *
D482	41 16 35.950500 S	174 46 58.213700 E	22.5400	2	0.113	HEAPHY HOUSE HHR9 *
D483	41 16 35.528200 S	174 46 58.217900 E	22.0300	2	0.113	HEAPHY HOUSE HHR9A *
D485	41 16 35.867500 S	174 46 58.449500 E	22.5400	2	0.113	HEAPHY HOUSE HHR6 *
D499	40 30 57.867300 S	175 27 34.691200 E	23.3490	1	-2.550	BM LA81 NO 2

D500	40	35	25.747700	S	175	14	24.840900	E	83.9240	2	-3.096	MOUTERE NO 2	
D501	40	52	26.649700	S	175	01	15.221000	E	26.9000	4	-1.522	WAIMEA NO 4	
D502	40	59	01.831900	S	174	57	58.318500	E	17.2283	1	-0.928	BM L25	
D503	40	39	04.798300	S	175	20	49.371400	E	376.6600	3	-2.055	E ARAPAEPAE NO 1	
D504	40	44	22.643100	S	175	07	57.447900	E	37.7100	3	-2.315	A WAITOHU	
D505	40	48	48.592100	S	175	15	20.763200	E	912.4200	3	-0.995	A TAUNGATA	
D506	40	56	02.738700	S	175	09	42.729100	E	1101.6000	4	-0.506	A KAPAKAPANUI	
D507	40	52	36.438824	S	175	04	01.500366	E	29.0750	1	-1.332	BM LA35	*
D508	40	36	02.434678	S	175	42	53.246517	E	191.8130	1	-0.409	BM KA66	*
D509	41	02	24.896600	S	175	06	07.023400	E	626.6000	4	0.119	A MT BARTON	
D510	41	04	50.600900	S	174	46	51.474500	E	120.5800	3	-0.723	MANA	
D511	41	06	51.367000	S	174	59	52.218500	E	431.4000	4	0.112	NABHRA	
D512	41	14	13.794900	S	174	55	41.875300	E	348.2300	3	0.375	TOWAI	
D513	41	13	15.986600	S	175	02	15.769200	E	631.8800	3	0.736	DEVINE	
D514	41	24	25.536700	S	174	52	40.992900	E	166.7000	4	0.515	PARA	
D515	40	56	53.157800	S	175	40	01.264800	E	110.5168	1	1.759	15881	
D516	40	28	06.572681	S	175	49	36.564467	E	119.5303	1	-0.698	BM KA80	*
D517	41	01	40.977700	S	175	31	38.184600	E	77.1182	1	1.799	16211	
D518	40	28	22.886510	S	175	17	04.820727	E	7.4030	1	-3.830	BM L72 NO 2	*
D519	40	32	53.921461	S	175	16	21.942573	E	21.5320	1	-3.241	BM L65	*
D520	40	38	05.609088	S	175	16	31.243685	E	35.4680	1	-2.539	BM L57	*
D521	40	43	51.757380	S	175	12	20.286450	E	51.4040	1	-2.089	BM L49	*
D522	40	49	03.755282	S	175	06	36.881774	E	19.3700	1	-1.640	BM L40	*
D523	41	05	31.352373	S	175	26	57.988923	E	55.1287	1	1.806	BM KA9	*
D524	40	44	09.348672	S	175	37	15.068476	E	318.4660	1	0.100	BM KA49 NO 2	*
D525	41	17	15.507954	S	174	48	12.380470	E	2.9550		0.190	ORM 8 SO35860	*
D526	41	20	51.016306	S	174	47	28.985141	E	5.2210		0.271	BM6A SO35872	*
D527	41	09	00.497240	S	174	50	17.317547	E	10.7840	1	-0.228	BM L9 NO 2	*
D528	41	06	20.547700	S	174	52	11.668400	E	4.8376	1	-0.355	BM L14	
D529	41	01	58.449260	S	174	53	46.631540	E	45.8072	1	-0.704	BM L20	*
D530	41	08	50.160184	S	174	59	56.430120	E	38.2440	1	0.276	BM KC2	*
D531	41	16	42.015137	S	174	37	39.968655	E	457.2294	4	-0.204	TERAWHITI ECC	*
D532	41	09	25.270783	S	174	48	12.255162	E	459.0879	3	-0.289	COLONIAL KNOB ECC	*
D533	41	11	07.311500	S	174	52	25.617898	E	453.4048	3	0.025	BELMONT ECC	*
D534	41	17	46.147632	S	174	49	41.735436	E	162.3513	4	0.272	CRAWFORD ECC	*
D535	41	20	34.077822	S	174	42	39.742775	E	483.6126	4	0.078	TE KOPAHOU ECC	*
D536	41	13	59.781403	S	174	46	40.227008	E	444.5496	4	-0.058	KAUKAU ECC	*
D537	41	09	25.881200	S	174	48	12.842600	E	458.5400	3	-0.288	COLONIAL KNOB NO 3	
D538	40	26	36.891000	S	175	24	38.662200	E	44.0100	3	-3.437	HIMATANGI	
D539	40	19	29.772600	S	175	38	46.237600	E	65.0300	3	-2.726	14943	
D540	40	25	49.541000	S	175	34	24.894200	E	48.8000	2	-2.544	FITZHERBERT NO 2	
!Third order stations													
D541	40	30	09.922500	S	175	33	22.349700	E	673.1800	3	-2.044	BB KAIHINU	
D542	40	27	25.187100	S	175	38	38.980300	E	556.6000	3	-1.936	CC(ARAWARU SD)	
D543	40	27	22.894300	S	175	36	15.401400	E	450.8900	3	-2.182	D TE MATA	
D544	40	28	55.768500	S	175	32	35.602300	E	378.5900	3	-2.363	14972	
D545	40	29	29.054700	S	175	30	05.742400	E	45.2410	2	-2.539	15311	
16063	41	06	20.581100	S	174	51	24.139600	E	92.9300	3	-0.393	16063	
160813CC	41	08	45.435368	S	174	49	15.475720	E	289.9970	3	-0.293	160813 Ecc	*
MT_COOPER	41	05	50.628900	S	174	50	21.815700	E	104.4000	4	-0.486	MT COOPER	
PIKARERE	41	07	07.784200	S	174	49	14.195500	E	188.1000	4	-0.425	PIKARERE	
PKRRN2	41	07	12.882000	S	174	49	35.663300	E	135.3000	4	-0.402	PIKARERE NO 2	
16091	41	08	46.069300	S	174	52	35.689200	E	152.1000	4	-0.136	16091	
160917	41	09	26.470800	S	174	51	13.955100	E	256.4300	3	-0.151	160917	
BXTRSKNB	41	07	43.795900	S	174	51	43.144700	E	138.9300	3	-0.261	BAXTERS KNOB	
RBRTSN2	41	09	40.845200	S	174	50	53.645600	E	248.7300	3	-0.150	ROBERTS NO 2	
TIDEMAN	41	07	52.658200	S	174	53	12.077800	E	194.9000	4	-0.176	TIDEMAN	
BRADEY	41	06	30.614700	S	174	53	44.274000	E	71.2000	4	-0.264	BRADEY	
16031	41	03	20.853000	S	174	53	10.895500	E	165.7800	3	-0.590	16031	
16032	41	02	25.311700	S	174	53	38.082900	E	146.6000	4	-0.663	16032	
16064	41	04	25.342000	S	174	52	00.178400	E	115.4900	3	-0.541	16064	
16065	41	03	55.073800	S	174	52	11.746300	E	114.2700	3	-0.581	16065	
PORIRUA	41	03	16.583100	S	174	51	14.022500	E	261.8200	3	-0.690	PORIRUA	
WRKN2	41	02	19.551100	S	174	52	40.229000	E	216.7700	3	-0.720	WAIRAKA NO 2	
RM1	41	04	19.856569	S	174	51	13.623130	E	2.6810		-0.586	RM1 (MOANA ROAD)	*
WLKRSHLN2	41	05	28.420100	S	174	52	16.276900	E	97.2000	4	-0.430	WALKERS HILL NO 2	
160610	41	07	29.194800	S	174	54	03.300800	E	142.8000	4	-0.165	160610	
16062	41	06	59.833500	S	174	52	22.997300	E	156.8000	4	-0.290	16062	
16069	41	06	43.064200	S	174	53	08.579800	E	108.3000	4	-0.276	16069	
RTNPNTN2	41	05	50.116000	S	174	54	46.252500	E	26.3000	4	-0.270	RATION POINT NO 2	
5307	41	06	22.775914	S	174	54	25.184728	E	1.3033		-0.240	5307 (IGNS STATION)	*
BAKER	41	04	10.123100	S	174	55	04.429100	E	321.9000	4	-0.411	BAKER	
DGGNGSN2	41	02	26.702500	S	174	55	11.001200	E	439.6000	4	-0.581	DIGGINGS NO 2	
GRAYS_NO2	41	04	50.088400	S	174	53	35.303800	E	169.3000	4	-0.424	GRAYS NO2	
PKKRK	41	00	30.333400	S	174	56	08.781900	E	274.3000	4	-0.745	PAEKAKARIKI	
ABBOTT	41	04	27.694300	S	174	57	44.888100	E	433.4000	4	-0.234	ABBOTT	
MLHRNN2	41	06	27.278300	S	174	57	24.572300	E	130.1000	4	-0.069	MULHERN NO 2	
EE	41	03	07.467800	S	174	59	58.742200	E	551.5000	4	-0.234	EE (PAEKAKARIKI SD)	
5502	41	06	56.685761	S	174	57	07.158457	E	39.9457		-0.043	5502 (IGNS STATION)	*
EDSBLK	41	03	12.367951	S	175	00	03.113694	E	551.3885		-0.185	EDS BLK EE (IGNS)	*
16033	41	01	53.101500	S	174	53	54.878700	E	61.6000	4	-0.706	16033	
WAINUI	41	00	51.874800	S	174	58	42.123000	E	722.1000	4	-0.559	WAINUI	
LNDNN2	41	06	41.012300	S	174	52	15.710500	E	122.0	4	-0.323	LONDON NO 2	
RLWYN2	41	03	15.823800	S	174	52	30.090000	E	57.82	3	-0.631	RAILWAY NO 2	
KEN	41	12	11.702300	S	174	58	56.749100	E	391.4	4	0.443	KEN	
FTZHRBRT	41	13	12.595500	S	174	57	32.385200	E	376.82	3	0.421	FITZHERBERT	
MWLMN3	41	15	17.401400	S	174	57	51.239800	E	386.00	4	0.566	MOWLEM NO 3	

```
From:   IN%"JIM@hh.dosli.govt.nz" 20-JAN-1995 16:00:28.02
To:     IN%"P2143202@csdvax.csd.unsw.EDU.AU"
CC:
Subj:   GPS DATA FILES

The orthometric heights in the above file are followed by the
accuracy code which has the following meaning
1   Precise levelling
2   Good levelling or simultaneous verticals from reliable fixed
    points
3&4 Heights derived from vertical angles where the relative accuracy
    is dependent on the strength of the adjustment network and
    reliability of the fixed points.

Regards
Jim Hall
```

Appendix I

GPS surveys for New Zealand datum investigation studies

The March 1993 GPS survey was the first campaign undertaken specifically by DOSLI for datum investigations within New Zealand. Listed in the table below are further GPS surveys that have been undertaken by DOSLI (since July 1996 Land Information New Zealand) for datum investigation studies.

Date	Coverage	Network [1]	Stations	Sessions
March 1993	All NZ	1st Order 2000	28	2 of 4 hours
Feb-March 1994	All NZ	1st Order 2000	30	1 of 24 hours
Feb+April 1995 [2]	All NZ	1st Order 2000	29	3 of 24 hours
January 1995	Gisborne, Taupo	2nd Order 2000	52 [3]	8 hours
February 1995	Canterbury	2nd Order 2000	69 [3]	8 hours
February 1995	West Coast	2nd Order 2000	47 [3]	8 hours
March-April 1995	Otago, Southland	2nd Order 2000	83 [3]	8 hours
March-April 1995	Wellington	2nd Order 2000	100 [3]	8 hours
February 1996	All NZ	1st Order 2000	29	3 of 24 hours

Notes

1. The "Order 2000" networks are described in Blick, 1996.
2. Observations from one station were lost in the February campaign. It was brought in to the network by re-observation of 7 stations in April.
3. Includes all NZGD49 1st order stations in the area plus new 2nd Order 2000 stations with better access.

Appendix J

W-curve investigations

Following the new emphasis given to determining the origin of the W-curve after the Western Pacific Geophysical Meeting in Brisbane, a number of tests were trialed during the visit by Jon Kirby, from Curtin University, to UNSW during 5 - 16 August 1996.

In Kearsley (1988) the W-curve was first noted and was thought that curve approximated half the wavelength recovered in theory by the GGM when summed to n_{max} (ie. $180/n_{max}$). Test using OSU81 (n_{max} = 180) showed that this was not the case for the lower North Island test area (Section 4.5.2.1). Further tests using OSU91A as the reference GGM in RINT with n_{max} being set to 180 and 360 showed insignificant variation in the W-curve wavelength, though the amplitude of the n_{max} = 180 results were larger than the n_{max} = 360 results. The other name given to the W-curve was a bi-modal curve. However results found in this study show that the curve has more than two maximum and therefore should not be referred to as bi-modal, when using model gravity.

AIM

To try and develop an understanding of how the W-curve was generated based on model data as input to the Ring Integration software held at UNSW. Two different types of data sets were used. The first was using the higher degree and order terms of the OSU91A model (ie. 180 to 360). The second type of data sets were generated by sine functions.

TESTING WITH OSU91A DATA

This test is emulating a residual gravity field in terms of OSU91A computed to n_{max} = 180 (ie. degree and order 180).

Method

1) generate a gravity anomaly field for input to RINT using only the coefficients from degree and order 181 to 360 inclusive of the OSU91A GGM.
2) compute the geoid height values using RINT for a grid of stations using as input the data from 1. The contribution per compartment (C_N) in m/mGal was set at 0.0003 and compartments had a fixed 10.0° apex angle ($d\alpha$) which results in approximately a 0.1° (≅10km) step between the rings.
3) generate geoid height values for the same grid of stations as in 2 using only the coefficients from degree and order 180 to 360 inclusive of the OSU91A GGM.
4) compare the difference between the N values generated directly from the model (ie. step 3) with the N values obtained by using RINT on the gravity anomalies (ie. step 2).

Results for Southern NSW

A grid of gravity anomalies was generated for an area in south eastern NSW (S34° to S38°, E146° to E150°). The 4°x4° block was generated with a 0.1° grid spacing. The 1681 gravity anomalies generated had the following statistics (units = mGal): Average 0.240, Standard Deviation (1σ) 12.411, Minimum -37.248 and Maximum 38.487

By choosing Ring 12 (approx 1.2° or 120 km) as the maximum cap size allowed a grid of computation points for testing that consisted of 14 by 18 (252) points with a spacing of 0.1° over the area of S35.2° to S36.9° and E147.3° to E148.6°. (Note there is a 0.5° border added to the maximum cap size for the required data.)

Then by subtracting the model N value for each grid point from the RINT N value a difference was obtained, ie. $N_{diff} = N_{Rint} - N_{GGM}$. Statistical analysis of all these differences for each ring were then computed and are shown in Table 1 and plotted in Figure 1.

	ring1	ring2	ring3	ring4	ring5	ring6
std dev (1σ)	0.2023	0.0774	0.0676	0.1384	0.1851	0.2021
min	-0.435	-0.160	-0.188	-0.323	-0.408	-0.429
max	0.399	0.167	0.097	0.241	0.335	0.370
mean	-0.038	-0.037	-0.037	-0.037	-0.038	-0.039
	ring7	ring8	ring9	ring10	ring11	ring12
std dev (1σ)	0.1965	0.1726	0.1419	0.1142	0.0973	0.0938
min	-0.401	-0.342	-0.271	-0.230	-0.216	-0.208
max	0.353	0.295	0.264	0.251	0.220	0.176
mean	-0.040	-0.040	-0.040	-0.041	-0.041	-0.041

Table 1 : Difference of Model generated N values and RINT generated N values in metres for each ring at all 252 grid points in the Southern NSW area.

From Table 1 the Ring 3 cap size (approx 30 km) has the smallest standard deviation for the N_{diff} values. Varying the cap size also varied the mean N_{diff} but only by 0.004m.

Results for Western SA

A grid of gravity anomalies was generated for an area in western South Australia (S26° to S30°, E130° to E134°). The 4°x4° block was generated with a 0.1° grid spacing. This grid had the same dimensions and spacing as the Southern NSW grid. The 1681 gravity anomalies generated had the following statistics (units = mGal): Average 0.442, Standard Deviation (1σ) 17.993, Minimum -51.981 and Maximum 50.145.

The new grid of testing points consisted of 14 by 18 (252) points with a spacing of 0.1° over the area of S27.2° to S28.9° and E131.3° to E132.6°.

Statistical analysis of all these differences, $N_{diff} = N_{Rint} - N_{GGM}$, for each ring were then computed and are shown in Table 2 and Figure 1.

	ring1	ring2	ring3	ring4	ring5	ring6
std dev (1σ)	0.4685	0.2518	0.0717	0.1120	0.2242	0.2977
min	-0.641	-0.361	-0.137	-0.319	-0.536	-0.641
max	0.929	0.451	0.135	0.164	0.321	0.427
mean	0.099	0.053	0.013	-0.021	-0.045	-0.061
	ring7	ring8	ring9	ring10	ring11	ring12
std dev (1σ)	0.3307	0.3274	0.2934	0.2365	0.1663	0.0983
min	-0.645	-0.603	-0.546	-0.443	-0.309	-0.171
max	0.484	0.487	0.448	0.376	0.280	0.181
mean	-0.067	-0.066	-0.059	-0.046	-0.031	-0.014

Table 2 : Difference of Model generated N values and RINT generated N values in metres for each ring at all 252 grid points in the Western SA area.

From Table 2 the Ring 3 cap size (approx 30 km) has the smallest standard deviation for the N_{diff} values. Varying the cap size also varied the mean N_{diff} by up to 0.166m. The mean value closest to zero occurs at rings 3 and 12.

Examining the effect of data density

The grid of gravity anomalies that was generated for the area in south eastern NSW (S34° to S38°, E146° to E150°) at a spacing of 0.1° was thinned and densified to form two new data sets. These data sets were generated as follows:

Thinned input data

Every third data point was extracted from the 0.1° data set to give an input file for RINT that had a 0.3° grid spacing.

Densified input data

The method of triangulation with linear interpolation was used to densify the 0.1° data set to obtain a 0.02° grid. By using triangulation with linear interpolation the chance of introducing new gridding induced features to the data should be minimised.

Geoid height's were then computed using RINT at the same 252 grid points that were used for the Southern NSW test. For these tests, on the effect of varying the input data density, the intention was to try and minimise the chance of introducing any new features to the data structure. For this reason the input data was not recomputed from the GGM coefficients.

Results from using thinned input data

	ring1	ring2	ring3	ring4	ring5	ring6
std dev (1σ)	0.2154	0.0970	0.0478	0.1027	0.1463	0.1640
min	-0.470	-0.221	-0.151	-0.260	-0.322	-0.346
max	0.411	0.202	0.056	0.159	0.253	0.286
mean	-0.038	-0.037	-0.037	-0.037	-0.037	-0.038
	ring7	ring8	ring9	ring10	ring11	ring12
std dev (1σ)	0.1608	0.1429	0.1200	0.1023	0.0972	0.1023
min	-0.336	-0.291	-0.227	-0.228	-0.221	-0.257
max	0.270	0.261	0.271	0.269	0.239	0.201
mean	-0.039	-0.039	-0.040	-0.040	-0.040	-0.040

Table 3 : Differences of Model generated N values and RINT generated N values in metres using as input the thinned (0.3° spacing) for each ring at all 252 grid points in the Southern NSW area.

Results from using densified input data

	ring1	ring2	ring3	ring4	ring5	ring6
std dev	0.2143	0.0956	0.0485	0.1046	0.1485	0.1662
min	-0.441	-0.207	-0.151	-0.260	-0.322	-0.346
max	0.411	0.202	0.069	0.235	0.334	0.368
mean	-0.037	-0.036	-0.036	-0.036	-0.036	-0.036
	ring7	ring8	ring9	ring10	ring11	ring12
std dev	0.1628	0.1448	0.1215	0.1033	0.0976	0.1022
min	-0.336	-0.291	-0.227	-0.228	-0.221	-0.257
max	0.348	0.291	0.271	0.269	0.239	0.201
mean	-0.037	-0.038	-0.038	-0.039	-0.039	-0.039

Table 4 : Differences of Model generated N values and RINT generated N values in metres using as input the densified (0.02° spacing) for each ring at all 252 grid points in the Southern NSW area.

Summary of input data density

When Tables 1, 3 and 4 are compared (NSW area) it is clear that ring 3 in all cases produces the minimum standard deviation (Figure 1). It should also be noted that the thin and dense input grids (0.3° and 0.02°, respectively) produce approximately equivalent results that are significantly different to the original grid with the 0.1° spacing. This may indicate that the amplitude of the W-curve could be influenced by the RINT input data density.

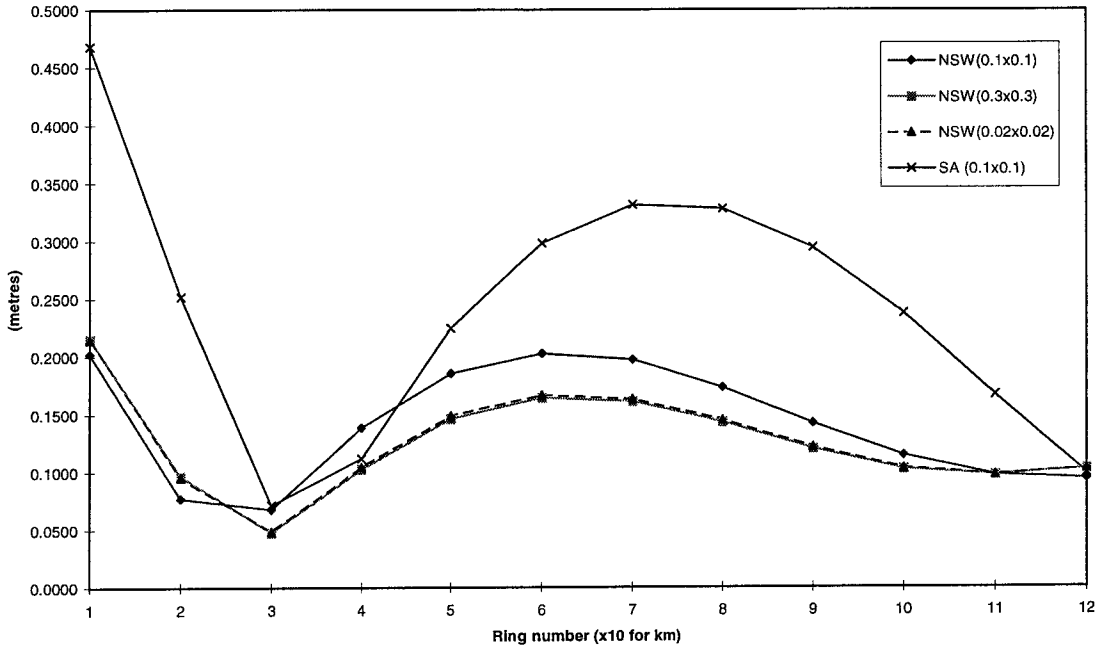

Figure 1 : Standard deviations (1σ) for all 4 tests using OSU91A gravity anomalies from degree and order 180 to 360

TESTING WITH DATA GENERATED BY A SINE FUNCTION

Method

1) generate a hypothetical residual gravity anomaly field for input to RINT using only a sine function.

2) compare the difference between the known wavelength features of the sine function with the wavelength of the N values generated by using RINT on the hypothetical gravity anomalies.

Two different sine functions were used. One was dependant only on the longitude of the grid point for generating the gravity anomaly field (ie. 1D sine function). The second was dependant on both the latitude and longitude of the grid point (ie. 2D sine function).

Results for a Longitude only dependant sine function

A grid of hypothetical anomalies were generated using the respective longitude dependant (1D) sine function for an area of 20°x20° (S10° to S30°, E150° to E170°). This gave a corrugated iron effect with the ridges and troughs running from north to south. The following input sine functions were tested.

Amplitude of Zero, Wavelength of Infinity (ie constant horizontal field)

A constant horizontal field of 1.0 mGal anomalies was generated. Once each mid-compartment anomaly value is determined RINT merely computes the sum of each compartment value and multiplies the total by the pre-defined contribution per compartment to the residual geoid height. As for all these tests the contribution to the geoid height per compartment (C_N) was 0.0003 m. Therefore using a constant input field to RINT results in an ever increasing geoid height the higher the maximum ring (cap) size used. RINT was run on the centre point of the grid using 120 rings (approx 12° maximum cap size).

Figure 2 shows that for each ring consisting of 36 compartments the geoid height increases by 0.0108 m for an input field of 1.0 mGal. This can be clearly seen with equation 1. If the constant horizontal field was changed to 2.0 instead of 1.0 then the contribution to N would double to 0.0216 per ring. When a constant residual anomaly field is input into RINT there is no oscillation (W-curve) in the results.

$$N_{RINT} = C_N \sum_{i=1}^{I} \sum_{j=1}^{J} \Delta\hat{g}_{ij} \qquad \text{ie. } 0.0003\text{x}1\text{x}36\text{x}1=0.0108 \qquad (1)$$

where $\Delta\hat{g}_{ij}$ is the residual mean free-air gravity anomaly, assumed in practice to equal the value at the mid point of compartment *i,j*.

i is the index for the rings.

I is the upper limit of the index for the rings ($I \equiv \psi_0$).

j is the index for the sectors, apex angle $d\alpha$.

$J = 2\pi/d\alpha$, ie. maximum number of compartments per ring.

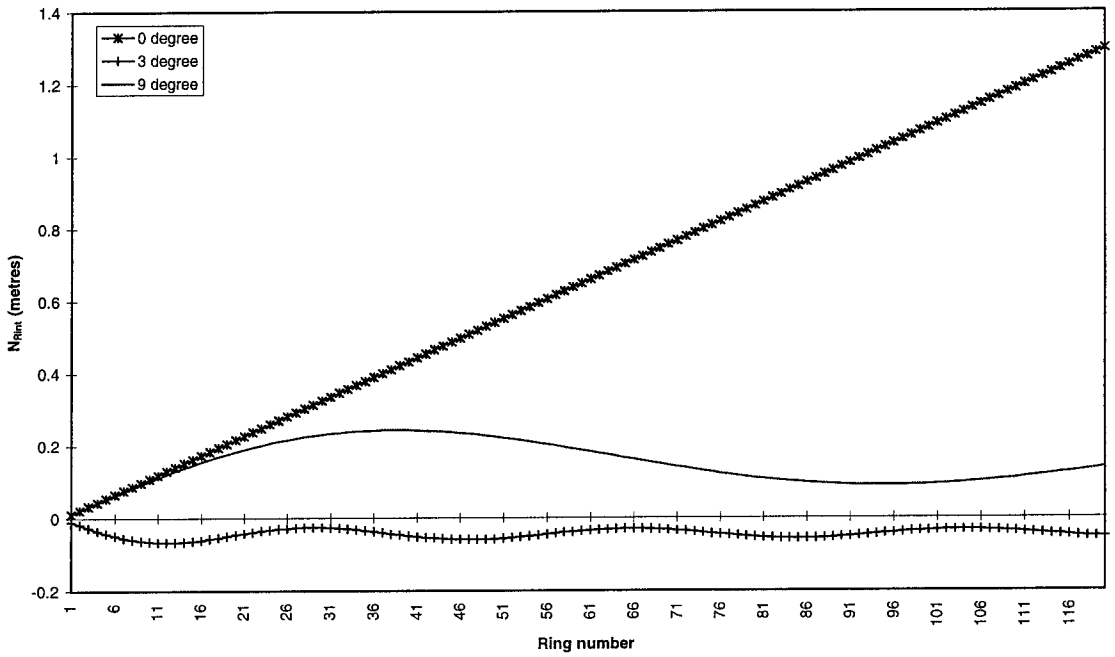

Figure 2 : Results from running RINT on the mid grid point out to 120 rings using as input **a)** a constant residual anomaly of 1.0 mGal (0 degree), **b)** a longitude dependant sine function with a 3° wavelength and amplitude of 1 mGal (3 degree), and **c)** a longitude dependant sine function with a 9° wavelength and amplitude of 1 mGal (9 degree).

Amplitude of One, Wavelength of Three degrees

Instead of generating a constant residual gravity field a hypothetical one was generated using a longitude dependant sine function with a wavelength of 3° and an amplitude of 1. The results are shown in Figure 3 for RINT being run on the centre point of the grid for 120 rings (approx 12° maximum cap size). The oscillation has clearly returned to the results. Analysing the wavelength in terms of distance rather than ring number shows that the wavelength is approximately 312 km. This agrees well with the distance that 3° represents on the ground at a Latitude of S20° (ie. cos(20) x 111 x 3 = 313 km).

Amplitude of One, Wavelength of Nine degrees

A hypothetical residual gravity field was generated using a longitude dependant sine function with a wavelength of 9 degrees and an amplitude of 1. The results are shown in Figure 3 for RINT being run on the centre point of the grid for 120 rings (approx 12° maximum cap size). The oscillation has remained in the results. Analysing the wavelength in terms of distance rather than ring number shows that the wavelength is approximately 942 km. This agrees well with the distance that 9° represents on the ground at a Latitude of S20° (ie. cos(20) x 111 x 9 = 938 km).

Amplitude of Two, Wavelength of Three degrees

A hypothetical residual gravity field was generated with an amplitude of 2 and a wavelength of 3°. The results are shown in Figure 3 for RINT being run on the centre point of the grid for 120 rings (approx 12° maximum cap size). The oscillation has clearly doubled in amplitude from the 3° wavelength with an amplitude of 1, but the wavelength remains at 3°. Note also that the oscillations are dampened with increasing ring number.

Effect of vary the computation point location within the grid

When comparing the 3° and 9° wavelength results (Figure 3) it is interesting to note that they have different signs. The sign of the results from RINT appeared to be directly related to the sign of the residuals at the computation point. To test this hypothesis a set of 27 computation points were used as input to RINT. The 27 points all had the same latitude but the longitude incremented in steps of 0.1°.

Results of computing N values out to ring number 70 using as input the 3° wavelength, amplitude of 1 data for the 27 points are summarised in Figure 4. It is obvious from this figure that the location of the computation point in the residuals affects the amplitude of the oscillations but not the wavelength. On inspecting the location of the computation points in the residuals grid it was confirmed that the sign of the N values from RINT were directly related to the magnitude of the surrounding residuals. This is of course want one expected and requires. However the important point to realise from Figure 4 is that if all your control points for determining the optimum ring size were to be located at residual minimums then no optimum ring size can be determined. Also the location of the control points with respect to residual gravity anomaly minima and maxima affects the amplitude of the oscillations.

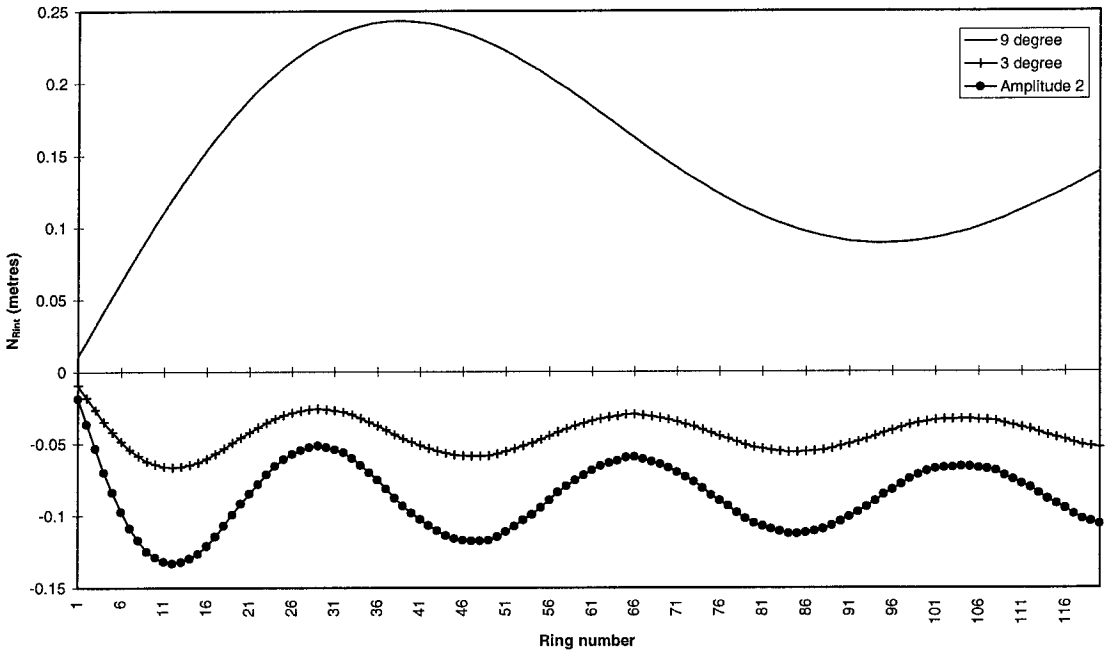

Figure 3 : Results from running RINT on the mid grid point out to 120 rings using as input **a)** a longitude dependant sine function with a 9° wavelength and amplitude of 1 mGal (9 degree), **b)** a longitude dependant sine function with a 3° wavelength and amplitude of 1 mGal (3 degree), and **c)** a longitude dependant sine function with a 3° wavelength and amplitude of 2 mGal (Amplitude 2).

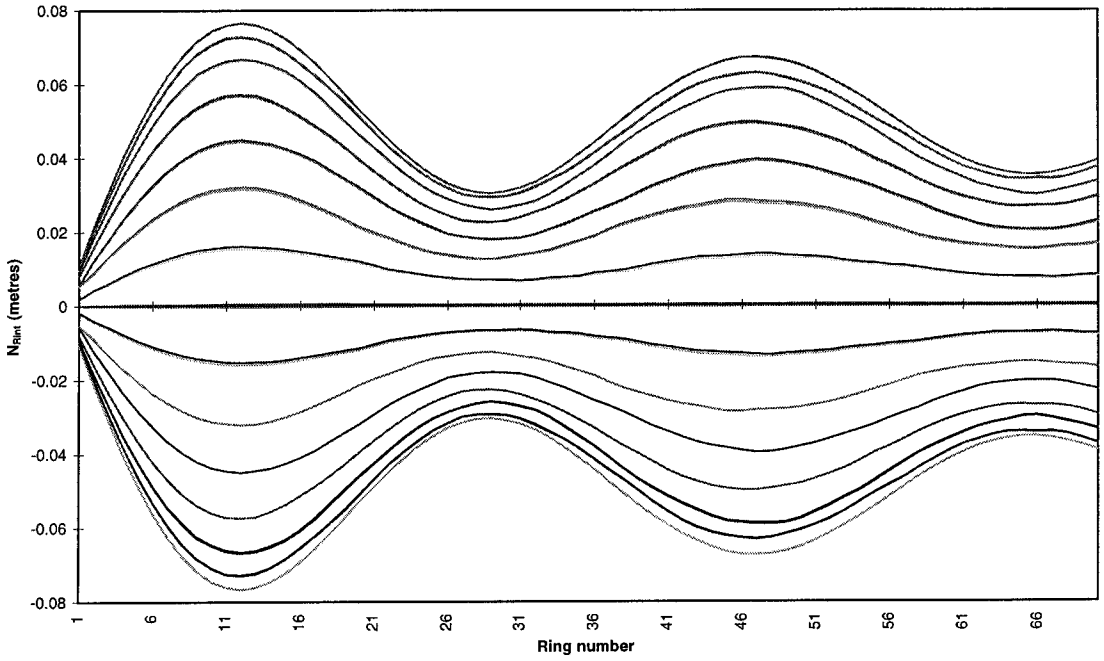

Figure 4 : Results from running RINT on a line of points out to 70 rings using as input a longitude dependant sine function with a 3° wavelength and amplitude of 1 mGal. Each line represents a separate computation point, that vary only in longitude.

Results for a Latitude and Longitude dependant sine function

A grid of hypothetical anomalies were generated using two latitude and longitude dependant (2D) sine functions for an area of 20°x20° (S10° to S30°, E150° to E170°). This gave an egg carton type effect for the residuals. The two latitude and longitude dependant sine functions were generated so as to have an amplitude of 1mGal though to vary the wavelength. One data set had a 2° wavelength while the other had a 3° wavelength. The computation point was chosen so as to be coincident with an area of maximum positive residuals. This results in maximum W-curve amplitude but does not affect the wavelength.

Two degree wavelength

Analysing the N_{Rint} wavelength for the 2° wavelength (Figure 5) in terms of distance rather than ring number shows that the wavelength is approximately 153 km. This is 25% less than the distance that 2° represents on the ground at a Latitude of S20° (ie. cos(20) x 111 x 2 = 208 km).

Three degree wavelength

Analysing the N_{Rint} wavelength for the 3° wavelength (Figure 5) in terms of distance rather than ring number shows that the wavelength is approximately 227 km. This is 25% less than the distance that 3° represents on the ground at a Latitude of S20° (ie. cos(20) x 111 x 3 = 313 km).

The reason for the 25% reduction in the wavelength is not fully understood.

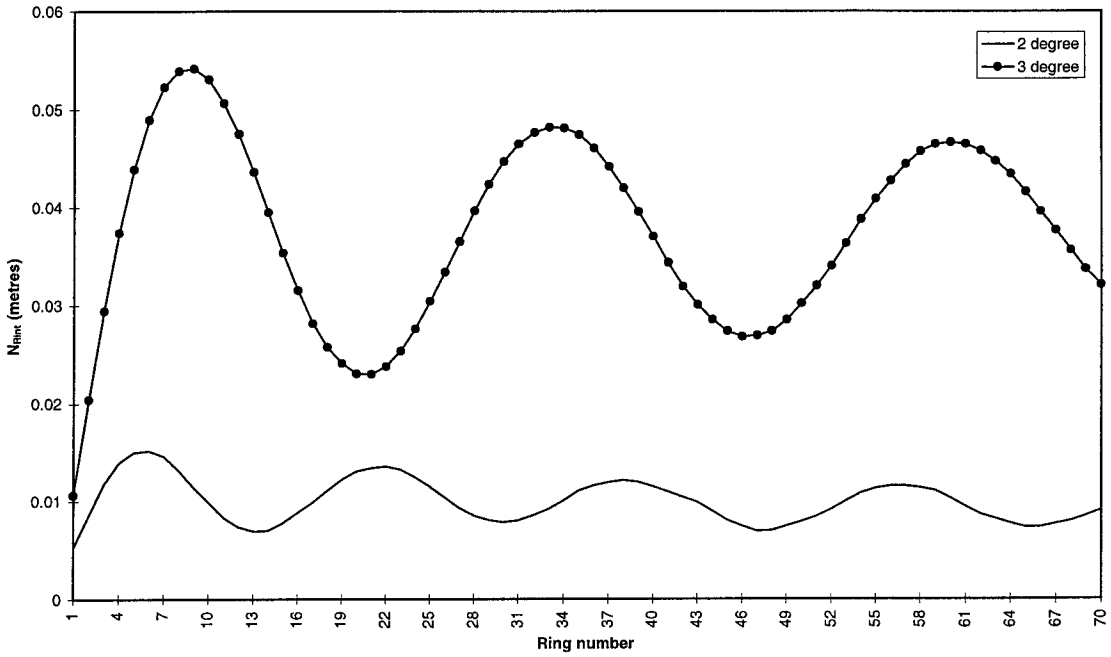

Figure 5 : Results from running RINT at a the maximum residual point out to 70 rings using as input **a)** a latitude and longitude dependant sine function with a 2° wavelength and amplitude of 1 mGal (2 degree), and **b)** a latitude and longitude dependant sine function with a 3° wavelength and amplitude of 1 mGal (3 degree).

Summary

Tests using the higher degree and order coefficients (180 to 360) of OSU91A showed that the W-curve still is present in this data. Determining whether the W-curve is a feature of RINT or OSU91A was attempted using hypothetical residual gravity anomalies that were of a known wavelength and amplitude. The tests using the 1D and 2D sine functions indicate that the W-curve is a feature of the input residual data used by RINT. Determining whether the oscillations in the real residual data are caused by the GGM or the observation of the gravity data (or possibly the orthometric or ellipsoidal height control) requires further work.

Final comments and possible next steps

In Figure 1 it is hard to determine where the actual minimum value occurs between 20 and 30 km (ie. Ring 2 & 3). If RINT were to be run using a C_N value of say 0.00015m then it may highlight that the minimum occurs at about 25 km (what would be ring 5). Now if this were the case then the diameter of the cap used be RINT would be approximately 50 km which approximates half the resolution of OSU91A when n_{max} = 180 (1.0°). From the tests with the simulated data the W-curve is a feature that is influenced by the input residual data characteristics. Therefore tests on the residual gravity auto-correlation function or possibly the power at different wavelengths in a Fourier analysis of the residual gravity may help to understand further the cause of the W-curve.

It would be unlikely that a residual anomaly field would only have a structure similar to the 1d sine functions. The reason why the 2D function data input to RINT results in an output that is 25% smaller , than the 1d sine function, needs to be understood. Once this is understood it may be possible to estimate the wavelengths that are driving the W-curve on real data.

Finally, it is worth noting that the amplitude of the W-curve is reduced between using OSU81, OSU91A and EGM96. This indicates that the residual gravity features driving the W-curve are being generated from the GGM, rather than the physical gravity observations.

Appendix K

Seven parameter Transformation output

An example of an output file from the School of Geomatic Engineering TRANS3D software, which was used in this research for determining transformation parameters between ITRF93 and NZGD49. This 7 parameter example has had some less critical information removed to save space.

The units are: metres for XYZ coordinates; Ellipsoidal latitude and longitude coordinates are in degrees, minutes and seconds, with ellipsoidal height in metres; VCV matrix has radians^2 for latitudes and longitudes, and km^2 for the X, Y, Z and height coordinates.

The input ITRF93 GPS coordinates and associated VCV matrix for NET A was obtained from the output of the GLOBK adjustment (Section 3.5.2). The NZGD49 three dimensional coordinates were generated by combining the latitude and longitude coordinates for the stations with their orthometric heights. These coordinates were obtained from DOSLI's geodetic database during October 1994. The orthometric heights were converted to ellipsoidal heights by adding on the geoid heights. The geoid heights were determined firstly in terms of GRS80 using the OSU91A GGM to degree and order 360, then transformed using the parameters in Table 5-5 to obtain geoid heights with respect to the NZGD49 International (Hayford) ellipsoid.

```
BURSA WOLF TRANSFORMATION OF 3D COORDINATES WITH FULL VCV MATRIX.
   THIS CALCULATION WAS DONE ON - DATE :  9-OCT-96     TIME : 12:13:52

INPUT DATA FOR 26 COMMON SITES.


NET A DATA DESCRIPTION -
      The New Zealand sites from GAMIT processing without WELL eccentrics
DATA TYPE / ELLIPSOID = XYZ         FLAT = 1/  0.00 RADIUS =    0.000

A PRIORI XYZ COORDINATES OF NET A
      X             Y             Z          SITE
 -5042731.013    140230.725  -3890300.801    D078
 -4989460.436    191252.616  -3955757.082    D100
 -4922647.699    265115.124  -4033579.382    D431
 -5039298.744    311182.353  -3884430.722    D072
 -4977955.114    355512.095  -3959578.095    D473
 -4794050.688    364491.748  -4177890.760    D143
 -4860522.481    383529.132  -4098474.090    D131
 -5041354.991    441059.442  -3869625.181    D452
 -5105842.378    461788.364  -3781953.900    D045
 -4780648.721    436507.180  -4185440.834    WELL
 -5167214.257    496239.264  -3693852.811    D026
 -4929040.021    498221.640  -4004033.826    D105
 -4741512.895    480470.733  -4225019.053    D425
 -4763996.242    561250.914  -4190671.927    D158
 -4660964.326    571445.603  -4302316.858    D191
 -4590224.056    585796.161  -4375478.977    D212
 -4802026.061    617521.335  -4138428.458    D469
 -4509242.339    709568.105  -4440279.479    D233
 -4616400.151    745241.656  -4324328.876    D309
 -4519608.804    774369.429  -4419877.604    D229
 -4566344.357    808430.382  -4364477.378    D320
 -4408673.332    841182.535  -4518905.322    D253
 -4521641.647    878624.057  -4396964.934    D338
 -4298487.995    887139.084  -4612663.478    D286
 -4303267.131    894811.260  -4606633.939    D474
 -4371448.523    950019.339  -4531599.627    D302

THE A PRIORI VARIANCE COVARIANCE MATRIX OF NET A
 0.172D-09
 0.197D-09  0.714D-08
 0.557D-10  0.103D-10  0.361D-09
 0.915D-10  0.247D-09  0.194D-10  0.161D-09
 0.179D-09  0.704D-08  0.524D-11  0.257D-09  0.699D-08
 0.197D-10  0.530D-11  0.328D-09  0.505D-10  0.842D-11  0.361D-09
 0.662D-10  0.309D-09  0.218D-11  0.675D-10  0.305D-09  0.186D-11
 0.166D-09
```

```
 0.170D-09  0.693D-08  0.110D-11  0.234D-09  0.686D-08  0.110D-11
 0.328D-09  0.679D-08
 0.685D-11  0.346D-11  0.312D-09  0.650D-11  0.342D-11  0.312D-09
 0.534D-10  0.123D-10  0.346D-09
 0.876D-10  0.412D-09  0.136D-10  0.889D-10  0.406D-09  0.129D-10
 0.811D-10  0.399D-09  0.814D-11  0.324D-09
 0.178D-09  0.710D-08  0.337D-11  0.244D-09  0.703D-08  0.321D-11
 0.310D-09  0.692D-08  0.330D-11  0.463D-09  0.714D-08
 0.137D-10  0.473D-11  0.325D-09  0.128D-10  0.435D-11  0.326D-09
 0.364D-11  0.264D-11  0.314D-09  0.120D-09  0.248D-10  0.400D-09
           [...Removed 22 stations VCV information...]

NET B DATA DESCRIPTION -
      NZGD49 coordinates of all stations with Gamit ITRF coords
DATA TYPE / ELLIPSOID = Hayford    FLAT = 1/297.00 RADIUS = 6378.388

A PRIORI COORDINATES OF NET B. ELLIPSOID IS Hayford
     LATITUDE           LONGITUDE      ELLIPSOIDAL HEIGHT   SITE
  -37  49  34.71660   178  24  24.79430        334.551    D078  201 TE POHUE
  -38  34  36.91160   177  48  16.69550        299.902    D100  106 OKAHUATIU
  -39  28  50.68510   176  55   1.31150         99.914    D431  BLUFF HILL NO
  -37  45  40.49930   176  27  58.31010         70.353    D072  F MAKETU
  -38  37   4.15020   175  54  53.33350        737.283    D473  MAROTIRI NO 2
  -41  10  54.72120   175  39   7.07720        577.755    D143  ERINGA
  -40  14  31.00970   175  29  17.15860        127.265    D131  MT STEWART
  -37  35  28.22590   174  59  59.37350        292.717    D452  79 (Rangiriri
  -36  36   7.29690   174  49  54.69760        112.881    D045  XVII WHANGAPAR
  -41  16  35.82180   174  46  57.94510         25.107    D475  H HOUSE GPS PI
  -35  37   8.62500   174  30  51.02240        141.207    D026  PUKEARENGA NO
  -39   8   8.72990   174  13  40.84230        242.187    D105  A HUIRANGI
  -41  45   2.73200   174  12  49.06250        243.068    D425  A (CAPE CAMPBE
  -41  20   0.07910   173  16  50.62690        777.841    D158  JENKINS HILL N
  -42  41  20.81970   173   0  36.48020        396.272    D191  ISOLATED HILL
  -43  35  26.29530   172  43  37.89690        504.451    D212  MT PLEASANT
  -40  42  53.11690   172  40  19.37660        155.208    D469  I PARAPARA
  -44  24   7.99330   171   3  26.10300        393.398    D233  A MT HORRIBLE
  -42  57  17.83510   170  49  46.34090        908.933    D309  HB MT GREENLAN
  -44   8  25.82620   170  16  39.06460        999.699    D229  MT MARY
  -43  27  26.94790   169  57  36.79660        105.864    D320  JF (GILLESPIES
  -45  23  21.36610   169  11  51.42730       1679.117    D253  T HYDE ROCK
  -43  51  44.96720   169   0  12.59570          7.621    D338  8741
  -46  36  59.52590   168  20  19.33550        271.739    D286  X THE BLUFF
  -46  32  18.64140   168  15  12.06220        179.085    D474  THREE SISTERS
  -45  33  49.40000   167  44  19.91020        409.402    D302  MT YORK

THE A PRIORI VARIANCE COVARIANCE MATRIX OF NET B
 0.376D-13
 0.000D+00  0.376D-13
 0.000D+00  0.000D+00  0.100D-05
 0.000D+00  0.000D+00  0.000D+00  0.376D-13
 0.000D+00  0.000D+00  0.000D+00  0.000D+00  0.376D-13
 0.000D+00  0.000D+00  0.000D+00  0.000D+00  0.000D+00  0.100D-05
 0.000D+00  0.000D+00  0.000D+00  0.000D+00  0.000D+00  0.000D+00
 0.376D-13
 0.000D+00  0.000D+00  0.000D+00  0.000D+00  0.000D+00  0.000D+00
 0.000D+00  0.376D-13
 0.000D+00  0.000D+00  0.000D+00  0.000D+00  0.000D+00  0.000D+00
 0.000D+00  0.000D+00  0.100D-05
 0.000D+00  0.000D+00  0.000D+00  0.000D+00  0.000D+00  0.000D+00
 0.000D+00  0.000D+00  0.000D+00  0.376D-13
 0.000D+00  0.000D+00  0.000D+00  0.000D+00  0.000D+00  0.000D+00
 0.000D+00  0.000D+00  0.000D+00  0.000D+00  0.376D-13
 0.000D+00  0.000D+00  0.000D+00  0.000D+00  0.000D+00  0.000D+00
 0.000D+00  0.000D+00  0.000D+00  0.000D+00  0.000D+00  0.100D-05
           [...Removed 22 stations VCV information...]

THE A PRIORI VCV MATRIX OF THE PARAMETERS
 0.100E+06
 0.000E+00  0.100E+06
 0.000E+00  0.000E+00  0.100E+06
 0.000E+00  0.000E+00  0.000E+00  0.100E+06
 0.000E+00  0.000E+00  0.000E+00  0.000E+00  0.100E+06
 0.000E+00  0.000E+00  0.000E+00  0.000E+00  0.000E+00  0.100E+06
 0.000E+00  0.000E+00  0.000E+00  0.000E+00  0.000E+00  0.000E+00  0.100E+06

THE APRIORI ESTIMATES OF THE TRANSFORMATION PARAMETERS
  SCALE FACTOR      0.000 ppm +/- 0.316E+09
ROTN ABT X AXIS     0.000 SECS +/- 0.652E+08
ROTN ABT Y AXIS     0.000 SECS +/- 0.652E+08
ROTN ABT Z AXIS     0.000 SECS +/- 0.652E+08
TRANS ALONG X AXIS     0.000 m +/- 0.316E+06
TRANS ALONG Y AXIS     0.000 m +/- 0.316E+06
TRANS ALONG Z AXIS     0.000 m +/- 0.316E+06

THERE ARE 325 BASELINES

APRIORI BASELINE LENGTHS BETWEEN NET A SITES
           [...Removed...]
APRIORI BASELINE LENGTHS BETWEEN NET B SITES
           [...Removed...]
```

```
 ITERATION NUMBER  1 OF  1

 The a posteriori estimate of the variance factor (sigma sq) is  1.03284
 vtPv = 73.3318  DxtPxDx = 0.387758E-06  Ux = 0.153343E-08  Approx degs free = 71
 A priori weights on the parameters contribute 0.0% to the estimated variance factor.
 Results HAVE passed the F test of the variance factor at the 95% confidence level

 ADJUSTED BASELINE LENGTHS BETWEEN NET A SITES
             [...Removed...]

 ADJUSTED BASELINE LENGTHS BETWEEN NET B SITES
             [...Removed...]

THE ADJUSTED PARAMETERS
 PARAMETER           ADJUSTED VALUE     SIGMA      ADJUSTMENT
     SCALE FACTOR (ppm)     4.562 +/-  0.514      4.562
 ROTN ABT X AXIS (secs)     0.072 +/-  0.241      0.072
 ROTN ABT Y AXIS (secs)    -0.049 +/-  0.208     -0.049
 ROTN ABT Z AXIS (secs)     1.344 +/-  0.242      1.344
 TRANS ALONG X AXIS (m)   -60.788 +/-  4.465    -60.788
 TRANS ALONG Y AXIS (m)    -9.188 +/- 10.035     -9.188
 TRANS ALONG Z AXIS (m) -187.073 +/-  5.718   -187.073

 CORRELATIONS OF ADJUSTED PARAMETERS

 CORRELATION & STANDARD DEVIATION MATRIX
 1)  0.5141E-06
 2)  0.6330E-01  0.1170E-05
 3) -0.2260E-01  0.8047     0.1007E-05
 4)  0.7713E-01 -0.8312    -0.8033     0.1174E-05
 5)  0.5557     -0.6021    -0.8377     0.6533     0.4465E-02
 6) -0.4182E-01  0.9487     0.8398    -0.9633    -0.6736     0.1004E-01
 7)  0.3660      0.8110     0.9188    -0.7375    -0.5591     0.7948     0.5718E-02

 ADJUSTED XYZ COORDINATES OF NET A
             [...Removed...]

 NET A
 CORRELATION & STANDARD DEVIATION MATRIX
             [...Removed...]
 ADJUSTED COORDINATES OF NET B. ELLIPSOID IS Hayford
             [...Removed...]
 NET B
 CORRELATION & STANDARD DEVIATION MATRIX
             [...Removed...]

 ALL REQUESTED ITERATIONS COMPLETED
 NORMAL PROGRAM END - NO FATAL ERRORS DETECTED
```

Appendix L

Commonly used heights in Geodesy

There are a number of different vertical reference systems available in geodesy, with some being able to detect which direction water will flow due to the height being referred to a natural equipotential surface, while others are simply mathematical approximations of the Earth. A brief summary of different vertical reference systems that are commonly used in geodesy is contained in the following subsections, which were adapted from Heiskanen and Moritz (1967) and Vanicek and Krakiwsky (1986).

L.1 Geopotential Number

Since only one equipotential surface (W_i) passes through any point (P_i), the gravity potential represents one possible way of defining a unique vertical position. The negative potential difference between the point P_i and the geoid is referred to as the geopotential number, C_i (Vanicek and Krakiwsky, 1986, eqn. 16.85).

$$C_i = -(W_i - W_o) = \int_P^{P_i} g \, dl \tag{L.1}$$

As was described in Section 4.2.2 the geoid is the equipotential surface (W_o) that approximates mean sea level. g is the value of gravity at P_i and dl is the continuous function of height difference along the terrain from a point on the geoid. dl is approximated in reality by δl, being the observed (levelled) height difference. C is measured in geopotential units (gpu), where 1 gpu = 1 kGal m.

Its Advantages are:

i) independent of levelling path used
ii) points with the same height are on the same potential surface
iii) no hypothesis needed about the composition of the Earth's interior
iv) independent of reference ellipsoid or reference gravity

Its Disadvantages are:

i) not expressed in length units
ii) requires the potential at the geoid

The geopotential number is used by height datums of the world (eg. NAVD 88) as the basic quantity for the definition and computation of the vertical reference system.

L.2 Dynamic Height

To overcome the intuitive problem of geopotential numbers not being expressed in length units, the dynamic height (H^D) was developed. Dynamic height is obtained by dividing the geopotential number by a constant reference gravity, often chosen to be the value of the current normal gravity (γ_Q) formula adopted by the IAG (Section 4.2.1) at a standard latitude (usually 45°, γ_o) (Heiskanen and Moritz, 1967, eqn. 4-9).

$$H_i^D = \frac{C_i}{\gamma_o} \tag{L.2}$$

Dynamic heights are numerically about 2% less than orthometric heights.

Its Advantages are:

i) independent of levelling path used
ii) points with the same height are on the same potential surface
iii) no hypothesis needed about the composition of the Earth's interior
iv) expressed in length units

Its Disadvantages are:

i) height can be wrongly interpreted as the geometrical distance between the geoid and P_i, when P_i not at the reference latitude.
ii) its dependant on chosen reference gravity
iii) it requires the potential at the geoid

The dynamic height difference (ΔH^D) between two points P_i and P_j can be expressed as a summation of the levelled height difference (Δl_{ij}) plus a correction referred to as the dynamic correction (DC_{ij}) (Vanicek and Krakiwsky, 1986, p. 370)

$$\Delta H^{D} = \Delta l_{ij} + DC_{ij} = \Delta l_{ij} + \sum_{k=i}^{j} \frac{g_k - \gamma_0}{\gamma_0} \delta l \qquad \text{(L.3)}$$

The dynamic correction can be very large because gravity varies from the equator to pole by about 5000 mGal (Heiskanen and Moritz, 1967). For a levelling line with a difference in height of 1000 m at the equator, g ≅ 978.0 Gal, computed with $\gamma_o = \gamma_{45°} = 980.6$ Gal then DC = -2.7 m.

L.3 Orthometric Height

The orthometric height (H_i) of a point P_i is defined as the geometrical distance between the geoid (P) and the point P_i, measured along the plumb line (Figure 4-2) (Vanicek and Krakiwsky, 1986, p. 371).

$$H_i = \frac{1}{\overline{g}} \int_{P}^{P_i} g \, dl = \frac{C_i}{\overline{g}} \qquad \text{(L.4)}$$

where $\overline{g}$ is the mean value of gravity along the plumb line between the geoid (P) and the point P_i. Since it is not practically possible to measure g along the plumb line between P and P_i, some assumption has to be made as to the behaviour of the density of the Earth in this region. Heiskanen and Moritz (1967) show that a density error of 0.6 g/cm^3, which corresponds to the maximum variation of rock density in practice, introduces an error in H_i = 1000m of only 0.025 m.

There are a number of different approaches to approximate $\overline{g}$, each of which result in a different kind of orthometric height usually referred by the name of the proponent, eg, Helmert, Niethammer or Mader. The Helmert orthometric height is one of the most commonly used in practice (Vanicek and Krakiwsky, 1986, p. 371) and is defined as:

$$H_i^H = C_i / g_i^H = C_i / (g_i + 0.0424 H_i) \qquad \text{(L.5)}$$

where g_i is the gravity at P_i on the Earth's surface (in Gal). The numerical coefficient (0.0424) follows directly from the use of Poincare-Pray's gravity gradient considered to be constant along the plumb line between the geoid and terrain, thus allowing $\overline{g}$ to be directly computed for the midpoint of the plumb line of P_i. H_i is the observed height in km.

The Helmert orthometric height is used in the USA to convert the NAVD88 geopotential numbers to an orthometric height.

Its Advantages are:

i) it is independent of levelling path used
ii) its expressed in length units

Its Disadvantages are:

i) it requires observed gravity data at the Earth's surface
ii) that a hypothesis is needed about the composition of the Earth's interior
iii) that points with the same orthometric height are not necessarily on the same equipotential surface, especially at high altitudes because of the uncertainty of the Earth's density and equipotential surfaces not being parallel to each other.

The orthometric height difference (ΔH) between two points P_i and P_j can be expressed as a summation of the levelled height difference (Δl_{ij}) plus a correction referred to as the orthometric correction (OC_{ij}) (Heiskanen and Moritz, 1967, p. 168)

$$\Delta H = \Delta l_{ij} + OC_{ij} \qquad \text{(L.6)}$$

where

$$OC_{ij} = \sum_{k=i}^{j} \frac{g_k - \gamma_0}{\gamma_0} \delta l + \frac{\overline{g}_i - \gamma}{\gamma_0} H_i - \frac{\overline{g}_j - \gamma}{\gamma_0} H_j \qquad \text{(L.7)}$$

In reality, as mean gravity along the plumb line unknown, OC is approximated by equations based on normal gravity (See Rapp, 1961). Therefore in theory, since the levelling differences have been corrected using an orthometric correction based on normal gravity rather than observed gravity the heights should be referred to as normal orthometric heights. In practice if g_i - γ_i is 10 mGal, an error of only 0.001 m in

100 m of measured height difference (δl) will result. This is trivial unless it accumulates systematically (Bomford, 1980).

The Australian Height Datum and the New Zealand levelling networks are based on normal orthometric heights (Roelse *et al.* 1975 and Gilliland 1987).

L.4 Normal Height

The normal height (H^N) of a point P_i was proposed in 1954 by Molodenskii et al. (1962) to overcome the problem in orthometric heights of having to determine the mean value of gravity along the plumb line. The normal height is obtained by dividing the geopotential number by the mean normal gravity along the normal plumb line of P_i (Vanicek and Krakiwsky, 1986, p. 372):

$$H_i^N = \frac{C_i}{\bar{\gamma}_i} \tag{L.8}$$

where $\bar{\gamma}_i$ is computed between the reference ellipsoid surface and the telluroid (Section 4.2.3)

As no gravity observations or assumptions for the Earth's density are made, some countries (eg. France, Germany and some Eastern European countries) use normal heights for their national vertical reference system.

Its Advantages are:

i) it is independent of levelling path used
ii) it is expressed in length units
iii) it does not require observed gravity data at the Earth's surface
iv) there is no hypothesis needed about the composition of the Earth's interior

Its Disadvantages are:

ii) it is dependant on the chosen reference gravity and ellipsoid
iii) that points with the same normal height are not on the same equipotential surface.

L.5 Ellipsoidal Height

The ellipsoidal height (h) is the distance along the normal to the reference ellipsoid between P_i and the surface of the ellipsoid (Section 5.2.4).

Its Advantages are:

i) it is independent of the levelling path used
ii) it is expressed in length units
iii) it does not require observed gravity data at the Earth's surface
iv) there is no hypothesis needed about the composition of the Earth's interior
v) it can be directly measured in terms of a geocentric reference ellipsoid using satellite techniques (ie. Satellite Altimetry or GPS)

Its Disadvantages are:

i) it is dependant on reference ellipsoid
ii) that points with the same ellipsoidal height bear no common relationship with the actual gravity field of the Earth.

Ellipsoidal height when combined with the geoid height using 4.1 provides orthometric heights. However, the determination of geoid heights when combined with ellipsoidal heights are not currently accurate enough to satisfy first order levelling standards (Table 2-3) to be met (Section 4.8).

L.6 Summary of Vertical reference systems

Out of the five different vertical reference systems described above, the ellipsoidal height is least able to predict the direction water will flow. A reference ellipsoid can be chosen to minimise the difference between the ellipsoid surface and the geoid for a portion of the Earth, but a geocentric reference ellipsoid surface (ie WGS84) can vary by up to 100 m from the geoid (DMA 1987a). This variation makes ellipsoidal heights unsuitable for topographic mapping and for use in general. With the introduction of space based techniques, such as Satellite Altimetry, Satellite Laser Ranging and GPS, absolute ellipsoidal heights in terms of the Earth's geocentre are attainable in a globally consistent reference system. These ellipsoidal heights are useful, since being a directly determinable quantity, to monitor the relative change of a station with respect to the chosen reference system (eg. monitoring the crustal deformation).

The geopotential number is of great scientific importance since it uniquely defines an equipotential surface, and is the most direct result from spirit-levelling (Heiskanen and Moritz, 1967). However, it is not a height in a geometrical or practical sense.

The difference between dynamic, normal or orthometric height is only in the choice of scaling the geopotential number. Dynamic heights are not suitable as practical heights due to the large dynamic corrections. Normal heights have less obvious physical and geometrical meaning than orthometric heights, due to the dependence on the reference ellipsoid used, but can be easily computed rigorously. Orthometric heights are the natural height above the geoid and thus have an unequalled geometrical and physical significance. However, orthometric heights have relatively involved computations due to requiring surface gravity data, unless Helmert orthometric heights are used (Heiskanen and Moritz, 1967, p. 172.)

Table L-1 compares the different vertical reference systems described in the preceding sections. Considering the geometrical and physical significance of orthometric heights, this system is recommended for the development of any national vertical datum in New Zealand. It should be remembered that, due to the definition of orthometric heights, points on the same equipotential surface (except on the geoid) do not generally have the same orthometric height; water may appear to flow "up hill" - from a lower to higher orthometric height (Vanicek and Krakiwsky, 1986).

	Geopotential Number	Dynamic Height	Orthometric Height	Normal Height	Ellipsoidal Height
independent of levelling path	yes	yes	yes	yes	yes
hypothesis required for Earth's crust density	no	no	yes	no	no
dependant on reference ellipsoid	no	no	no	yes	yes
small reductions	no	no	yes	yes	no
same height on same potential surface	yes	yes	no	no	no
in length units	no	yes	yes	yes	yes

Table L - 1 : Comparison of vertical reference systems (adapted from Brouwer and De Min, 1994)

The problem with all the heights discussed above, except ellipsoidal height, is that the position of the geoid is not directly measurable.

Appendix M

An alternative analysis technique for the RINT solutions

This Appendix outlines an alternative method, referred to as the 'power of prediction', to evaluate the RINT solutions and compares it against the method described in Section 4.3.5.1.

The power of prediction (ρ) statistic to compare different methods of computing gravity anomalies is stated by Tscherning (1979) as

$$\rho = \frac{\text{root mean square variation (observed - computed)}}{\text{root mean square variation of the observations}} \tag{M.1}$$

The terminology 'root mean square variation' is somewhat confusing in that it could be interpreted in a number of ways, three of these being: i) the square root of the sum of the data squared divided by the number of observations, ie. root mean square (rms), ii) the rms of the data with the mean removed, ie. standard deviation (sd), or iii) the variance of the data, ie. standard deviation squared (var).

If each different integration cap radius of RINT is thought of as a different method then it is possible to use the power of prediction to analyse the results. Stating (M.1) in terms of geoid heights (N) one obtains

$$\rho = \frac{\text{rms variation of } \delta N}{\text{rms variation of } N_{GEO}} \tag{M.2}$$

where δN is defined in (4.64) and N_{GEO} is defined in (4.1a). Depending on how the term rms variation is interpreted then (M.2) can be written as

$$\rho_{rms} = \frac{\text{rms of } \delta N}{\text{rms of } N_{GEO}} = \frac{\sqrt{\frac{1}{n}\sum_{i=1}^{n}(\delta N)^2}}{\sqrt{\frac{1}{n}\sum_{i=1}^{n}(N_{GEO})^2}} \tag{M.3}$$

or

$$\rho_{sd} = \frac{\text{sd of } \delta N}{\text{sd of } N_{GEO}} = \frac{\sqrt{\frac{1}{n}\sum_{i=1}^{n}\left(\delta N_i - \frac{1}{n}\sum_{j=1}^{n}\delta N_j\right)^2}}{\sqrt{\frac{1}{n}\sum_{i=1}^{n}\left(N_{GEO\,i} - \frac{1}{n}\sum_{j=1}^{n}N_{GEO\,j}\right)^2}} \tag{M.4}$$

or

$$\rho_{var} = \frac{\text{variance of } \delta N}{\text{variance of } N_{GEO}} = \frac{\frac{1}{n}\sum_{i=1}^{n}\left(\delta N_i - \frac{1}{n}\sum_{j=1}^{n}\delta N_j\right)^2}{\frac{1}{n}\sum_{i=1}^{n}\left(N_{GEO\,i} - \frac{1}{n}\sum_{j=1}^{n}N_{GEO\,j}\right)^2} \tag{M.5}$$

Merry (1980) has also evaluated different methods of computing gravity anomalies by applying (M.1) in the following form

$$\rho = \frac{\delta}{\Delta g^*} = \frac{\sqrt{\frac{1}{n}\sum_{i=1}^{n}\left(\Delta g_i - \Delta\tilde{g}_i\right)^2}}{\sqrt{\frac{1}{n}\sum_{i=1}^{n}\left(\Delta\tilde{g}_i - \frac{1}{n}\sum_{j=1}^{n}\Delta\tilde{g}_j\right)^2}} \qquad \text{(M.6)}$$

where Δg is the observed free-air gravity anomaly and $\Delta\tilde{g}$ predicted free-air gravity anomaly. In (M.6) Merry has the denominator being in terms of computed values rather than being observed values as described by Tscherning. As the computed values can vary depending on the method used it is more appropriate to have the denominator in terms of the observed values which are constant. When (M.6) is written in terms of geoid heights (N) one obtains

$$\rho = \frac{\text{rms of } \delta N}{\text{sd of } N_{GEO}} \qquad \text{(M.7)}$$

The version of (M.1) which is used to test the RINT solution will depend on what use is to be made of the results. If absolute geoid heights are required one can argue that (M.3) should be applied so that any bias in the solution is included in the analysis. However, for relative geoid heights the bias can be removed so (M.4) or (M.5) could be used.

Testing of (M.3), (M.4), (M.5) and (M.7) was undertaken using the same data that was used in Section 4.5.2.2 with the new results in Table M-1 and Figure M-1. That data being the reference GGM of OSU91A to n_{max} = 360, δN values computed for 14 first order control stations using the DEM to calculate the mean compartment height.

The rms of N_{GEO} is an order of magnitude larger than any of the other statistics (Table M-1) and therefore (M.3) is an order of magnitude smaller than the other ρ variations (see Table 5-1 and Figure 5-1).

As the denominator for M.3, M.4, M.5 and M.7 is constant for each cap size then the variations between the different cap sizes is due only to the changes in the computed geoid heights.

Comparison of the results from using (M.3) and (M.7) show that the inclusion of gravity data for cap sizes of 10 through 70 km produces approximately the same result which is a marginal improvement over the GGM only solution (0 km cap size). For cap sizes of 80 through 110 km there is a steady improvement. For cap sizes from 120 to 150 km the results are approximately the same as the 110 km cap size which is approximately an 80% improvement over the GGM only solution.

If one compares the standard deviation of δN with (M.7) then the major difference is that δN produces a minimum at the 30 km cap size as well as the 110 km cap size. The minimum using the 30 km cap size is an improvement over the GGM only solution of approximately 65%. Comparison of (M.4) against the standard deviation of δN shows that both statistics produce approximately equal results. As was described in Section

4.5.2.3, there are considerable savings in both computer time and data requirements by choosing the 30 km as opposed to the 110 km cap size.

Cap size (km)	sd N_{GEO} (m)	rms N_{GEO} (m)	sd δN (m)	rms δN (m)	ρ_{rms} (M.3) (unitless)	ρ_{sd} (M.4) (unitless)	ρ_{var} (M.5) (unitless)	ρ (M.7) (unitless)
0	1.267	14.012	0.303	0.548	0.039	0.239	0.057	0.432
10	1.267	14.012	0.231	0.437	0.031	0.182	0.033	0.345
20	1.267	14.012	0.167	0.428	0.031	0.132	0.017	0.338
30	1.267	14.012	0.110	0.472	0.034	0.087	0.008	0.372
40	1.267	14.012	0.148	0.473	0.034	0.117	0.014	0.374
50	1.267	14.012	0.239	0.461	0.033	0.189	0.036	0.363
60	1.267	14.012	0.303	0.459	0.033	0.239	0.057	0.362
70	1.267	14.012	0.298	0.422	0.030	0.235	0.055	0.333
80	1.267	14.012	0.235	0.353	0.025	0.185	0.034	0.278
90	1.267	14.012	0.156	0.265	0.019	0.123	0.015	0.209
100	1.267	14.012	0.098	0.190	0.014	0.078	0.006	0.150
110	1.267	14.012	0.071	0.112	0.008	0.056	0.003	0.089
120	1.267	14.012	0.075	0.076	0.005	0.060	0.004	0.060
130	1.267	14.012	0.094	0.102	0.007	0.074	0.006	0.080
140	1.267	14.012	0.092	0.111	0.008	0.073	0.005	0.088
150	1.267	14.012	0.103	0.130	0.009	0.081	0.007	0.103

Table M-1 : Comparison of using the standard deviation of δN (sd δN) against the 'power of prediction' (p) for determining the optimum cap for the RINT solution. Test data used was OSU91A to n_{max} = 360 as the reference GGM with the DEM mean compartment heights and ΔN values at the first order control stations.

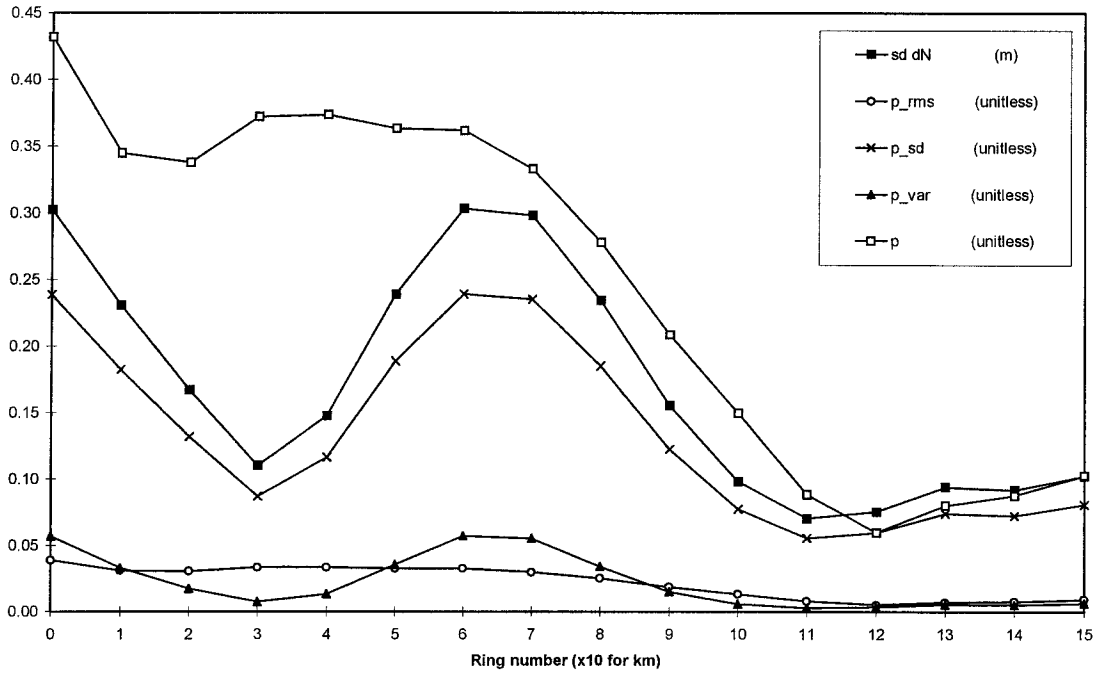

Figure M-1 : Comparison of using the standard deviation of δN (sd dN) against the 'power of prediction' (p) for determining the optimum cap for the RINT solution. Test data used was OSU91A to n_{max} = 360 as the reference GGM with the DEM mean compartment heights and ΔN values at the first order control stations. [Notation used: the standard deviation of δN (sd dN); power of prediction using (M.3), (M.4), (M.5) and (M.7) (p_rms, p_sd, p_var, and p)]

For relative geoid heighting the use of either (M.4), (M.5) or the standard deviation of δN does not alter the two cap sizes (30 km and 110 km) which produce optimum geoid heights. It is therefore concluded that the use of the power of prediction statistic in the form of (M.4) or (M.5) would result in the same conclusions being reached as those based on the use of the standard deviation of δN as used in Chapter 4.

From the results presented in Table 5-1 and Figure 5-1 it is clear that the choice of optimum cap size for use in the RINT solution can be influenced by whether the geoid height results are to be used for absolute or relative heighting purposes. If absolute heights are required and results are compared using (M.3) then the optimum cap size would be 120 km. However for relative heights using (M.4) or (M.5) to analyse the results one would chose either the 30 km or 110 km cap size as optimum.

Appendix N

Papers either published or presented during this research

Published

Higgins, M.B., M.B. Pearse and A.H.W. Kearsley, **1996**. Using Digital Elevation Models in the computation of Geoid Heights. *Geomatics Research Australasia*, No. 65, pp. 59-74.

Pearse, M.B., **1996**. PC-based software for gridding and validating randomly spaced data: - A consumer's review of Surfer and Transform. *The Australian Surveyor*, March, Vol. 41, No. 1, pp. 53-58.

Presented

Grant, D.B. and M.B. Pearse, **1995**. Proposal for a Dynamic National Geodetic Datum for New Zealand. *Presented at IUGG XXI General Assembly*, Boulder, Colorado, USA, July 2-14.

Higgins, M.B., A.H.W. Kearsley and Pearse, M.B., **1996**. Using digital elevation models for Terrain Effects and Gravity Interpolation in computation of geoid ellipsoid separation. *Presented at the Western Pacific Geophysics Meeting*, Brisbane, Australia, July 23-27.

Pearse, M.B., A.H.W. Kearsley and P. Morgan, **1995**. Height comparisons on the Australian National GPS Network (ANN): First results. in: Sunkel and Marson (eds.) *Gravity and Geoid*, International Association of Geodesy Symposium No. 113, Springer-Verlag. pp. 439-445.

Pearse, M.B. and P.J. Morgan, **1995**. Dynamic Coordinates for New Zealand: A Progress Report, *Proceedings of the NZIS Annual Conference*, Christchurch, New Zealand, 21-23 October.

Pearse, M.B. and A.H.W. Kearsley, **1996**. Progress towards the determination of a relative geoid for New Zealand using Ring Integration. *Presented at the Western Pacific Geophysics Meeting*, Brisbane, Australia, July 23-27.

Publications from

THE SCHOOL OF GEOMATIC ENGINEERING

(Formerly School of Surveying)

THE UNIVERSITY OF NEW SOUTH WALES

All prices include postage by surface mail. Air mail rates on application. (Effective March 1998)

To order, write to Publications Officer, School of Geomatic Engineering
The University of New South Wales, Sydney 2052, AUSTRALIA

NOTE: ALL ORDERS MUST BE PREPAID

UNISURV REPORTS - S SERIES

S8 - S20	Price (including postage) :		$10.00
S29 onwards	Price (including postage) :	Individuals	$25.00
		Institutions	$30.00

S8 A. Stolz, "Three-D Cartesian co-ordinates of part of the Australian geodetic network by the use of local astronomic vector systems", Unisurv Rep. S8, 182 pp, 1972.

S10 A.J. Robinson, "Study of zero error & ground swing of the model MRA101 tellurometer", Unisurv Rep. S10, 200 pp, 1973.

S12. G.J.F. Holden, "An evaluation of orthophotography in an integrated mapping system", Unisurv Rep. S12, 232 pp, 1974.

S14. Edward G. Anderson, "The Effect of Topography on Solutions of Stokes` Problem", Unisurv Rep. S14, 252 pp, 1976.

S16. K. Bretreger, "Earth Tide Effects on Geodetic Observations", Unisurv S16, 173 pp, 1978.

S17. C. Rizos, "The role of the gravity field in sea surface topography studies", Unisurv S17, 299 pp, 1980.

S18. B.C. Forster, "Some measures of urban residential quality from LANDSAT multi-spectral data", Unisurv S18, 223 pp, 1981.

S19. Richard Coleman, "A Geodetic Basis for recovering Ocean Dynamic Information from Satellite Altimetry", Unisurv S19,332 pp, 1981.

S20. Douglas R. Larden, "Monitoring the Earth's Rotation by Lunar Laser Ranging", Unisurv Report S20, 280 pp, 1982.

S29 Gary S Chisholm, "Integration of GPS into hydrographic survey operations", Unisurv S29, 190 pp, 1987.

S30. Gary Alan Jeffress, "An investigation of Doppler satellite positioning multi-station software", Unisurv S30, 118 pp, 1987.

S31. Jahja Soetandi, "A model for a cadastral land information system for Indonesia", Unisurv S31, 168 pp, 1988.

S33. R. D. Holloway, "The integration of GPS heights into the Australian Height Datum", Unisurv S33, 151 pp.,1988.

S34. Robin C. Mullin, "Data update in a Land Information Network", Unisurv S34, 168 pp. 1988.

S35. Bertrand Merminod, "The use of Kalman filters in GPS Navigation", Unisurv S35, 203 pp., 1989.

S36. Andrew R. Marshall, "Network design and optimisation in close range Photogrammetry", Unisurv S36, 249 pp., 1989.

S37. Wattana Jaroondhampinij, "A model of Computerised parcel-based Land Information System for the Department of Lands, Thailand," Unisurv S37, 281 pp., 1989.

S38. C. Rizos (Ed.), D.B. Grant, A. Stolz, B. Merminod, C.C. Mazur "Contributions to GPS Studies", Unisurv S38, 204 pp., 1990.

S39. C. Bosloper, "Multipath and GPS short periodic components of the time variation of the differential dispersive delay", Unisurv S39, 214 pp., 1990.

S40. John Michael Nolan, "Development of a Navigational System utilizing the Global Positioning System in a real time, differential mode", Unisurv S40, 163 pp., 1990.

S41. Roderick T. Macleod, "The resolution of Mean Sea Level anomalies along the NSW coastline using the Global Positioning System", 278 pp., 1990.

S42. Douglas A. Kinlyside, "Densification Surveys in New South Wales - coping with distortions", 209 pp., 1992.

S43. A. H. W. Kearsley (ed.), Z. Ahmad, B. R. Harvey and A. Kasenda, "Contributions to Geoid Evaluations and GPS Heighting", 209 pp., 1993.

S44. Paul Tregoning, "GPS Measurements in the Australian and Indonesian Regions (1989-1993)", 134 + xiii pp, 1996.

S45. Wan-Xuan Fu, "A study of GPS and other navigation systems for high precision navigation and attitude determinations", 332pp, 1996.

S46. Peter Morgan et al, "A zero order GPS network for the Australia region", 187 + xii pp, 1996.

S47. Yongru Huang, "A digital photogrammetry system for industrial monitoring", 145 + xiv pp, 1997.

S48. Kim Mobbs, "Tectonic interpretation of the Papua New Guinea Region from repeat satellite measurements", 256 + xc pp, 1997.

S49. Shaowei Han, "Carrier phase-based long-range GPS kinematic positioning", 185 + xi pp, 1997.

S50. Mustafa D Subari, "Low-cost GPS systems for intermediate surveying and mapping accuracy applications", 179 + xiii pp, 1997.

S51. Lao-Sheng Lin, "Real-time estimation of ionospheric delay using GPS measurements", 199 + xix pp, 1997.

S52. Merrin B Pearse, "A modern geodetic reference system for New Zealand", 324 +xviii pp, 1997.

S53. David B Lemon, "The nature and management of positional relationships within a local government Geographic Information System", 273 + xvi pp, 1997.

S54. Catherine Ticehurst, "Development of models for monitoring the urban environment using radar remote sensing", 282 + xix, 1998.

MONOGRAPHS

Prices include postage by surface mail

		Price
M1.	R.S. Mather, "The theory and geodetic use of some common projections", (2nd edition), 125 pp., 1978.	$15.00
M2.	R.S. Mather, "The analysis of the earth's gravity field", 172 pp., 1971.	$8.00
M3.	G.G. Bennett, "Tables for prediction of daylight stars", 24 pp.,1974.	$5.00
M4.	G.G. Bennett, J.G. Freislich & M. Maughan, "Star prediction tables for the fixing of position", 200 pp., 1974.	$8.00
M8.	A.H.W. Kearsley, "Geodetic Surveying", 96 pp, (revised) 1988.	$12.00
M11.	W.F. Caspary, "Concepts of Network and Deformation Analysis",183 pp., 1988.	$25.00
M12.	F.K. Brunner, "Atmospheric Effects on Geodetic Space Measurements", 110 pp., 1988.	$16.00
M13.	Bruce R. Harvey, "Practical Least Squares and Statistics for Surveyors", (2nd edition), 319 pp., 1994.	$30.00
M14.	Ewan G. Masters & John R. Pollard (Ed.), "Land Information Management", 269 pp., 1991. (Proceedings LIM Conference, July 1991).	$20.00
M15/1	Ewan G. Masters & John R. Pollard (Ed.), "Land Information Management - Geographic Information Systems - Advance Remote Sensing Vol 1" 295 pp., 1993 (Proceedings of LIM & GIS Conference, July 1993).	$30.00
M15/2	Ewan G. Masters & John R. Pollard (Ed.), "Land Information Management - Geographic Information Systems - Advance Remote Sensing Vol 2" 376 pp., 1993 (Proceedings of Advanced Remote Sensing Conference, July 1993).	$30.00
M16.	A. Stolz, "An Introduction to Geodesy", 112 pp., 1994.	$20.00
M17	Chris Rizos, "Principles and Practice of GPS Surveying", 565 pp., 1997.	$50.00